

DESIGN REPORT TEVATRON 1 PROJECT

SEPTEMBER 1983

**FERMI NATIONAL ACCELERATOR LABORATORY
BATAVIA, ILLINOIS**

**FERMILAB
LIBRARY**

**Operated by Universities Research Association Inc.,
under contract with the U.S. Department of Energy**

TABLE OF CONTENTS

1.	Introduction and Overview	1-1
2.	Proton Acceleration and Extraction for Antiproton Production	2-1
2.1	Proton Acceleration	2-1
2.2	Extraction at F17.....	2-3
3.	Antiproton Production	3-1
3.1	Antiproton Yields and Targeting	3-1
3.1.1	Antiproton Production Cross Sections	3-1
3.1.2	Proton Energy	3-1
3.1.3	Antiproton Momentum	3-1
3.1.4	Antiproton Longitudinal Acceptance	3-2
3.1.5	Antiproton Transverse Acceptance	3-2
3.1.6	Targeting Limitations	3-2
3.2	Antiproton Target System Components	3-3
3.2.1	Antiproton Production Target	3-4
3.2.2	Antiproton Collection; the Lithium Lens	3-5
3.2.3	Antiproton Selection	3-6
3.3	Target Hall	3-6
4.	Debuncher Ring	4-1
4.1	Purpose of the Debuncher	4-1
4.2	Requirements of the Design	4-1
4.3	Choice of Transition Energy	4-2
4.4	Lattice	4-3
4.5	Magnets	4-3
4.6	Tuning	4-4
4.7	Sextupoles	4-5
4.8	Magnet Power Supplies	4-6
4.9	Bunch Rotation and Other RF Manipulation	4-7
4.10	RF Systems for Bunch Rotation and Debunching	4-9
4.11	Gap-Preserving RF	4-11
4.12	Beam Injection and Extraction	4-11
4.12.1	Injection from the Target Station	4-11
4.12.2	Debuncher to Accumulator Transfer	4-12
4.12.3	Injection from the Booster	4-12
4.13	Betatron Cooling	4-12
4.13.1	Design Goal	4-12
4.13.2	Design Considerations	4-13
4.13.3	Hardware	4-13
4.13.4	Computer Simulation	4-15
5.	Accumulator Ring	5-1
5.1	Accumulator-Functional Summary	5-1
5.2	Design Requirements	5-2
5.3	Accumulator Lattice	5-3
5.4	Tuning	5-7
5.5	Chromaticity Corrections	5-7
5.6	RF Stacking System	5-8
5.7	Accumulator Magnets	5-9
5.8	Accumulator Vacuum System	5-11
5.8.1	Vacuum Requirements	5-11
5.8.2	Vacuum System Layout and Characteristics	5-11

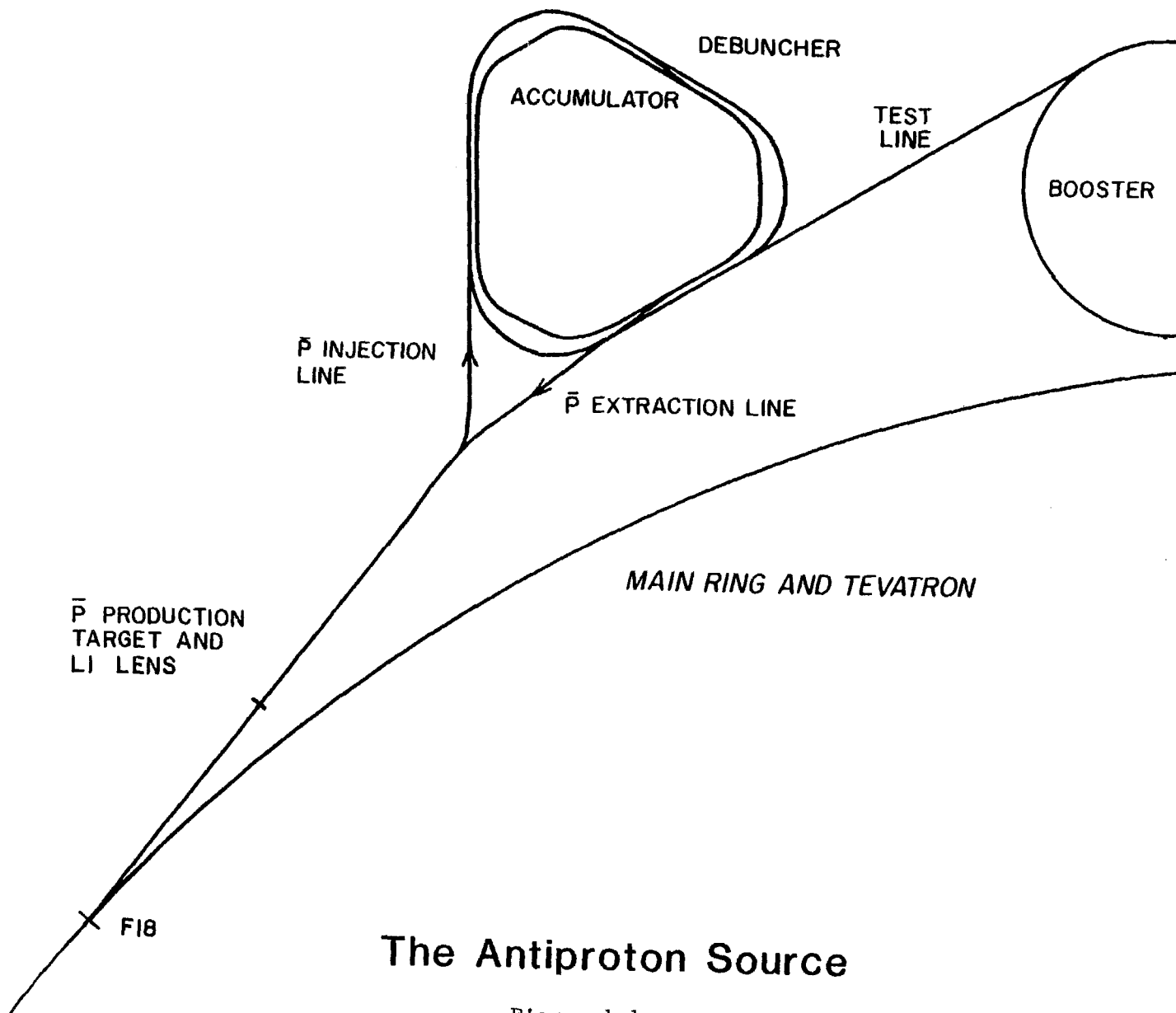
5.9	Momentum Cooling	5-12
5.9.1	Introduction to Stochastic Stacking	5-12
5.9.2	Summary of Design Considerations	5-16
5.9.3	Building the Exponential Gain Profile	5-16
5.9.4	Signal Suppression and Stability	5-18
5.9.5	Core Cooling	5-20
5.9.6	Numerical Calculations of Momentum Cooling	5-21
5.10	Betatron Cooling	5-21
5.10.1	Introduction	5-21
5.10.2	Betatron Cooling in the Core	5-23
5.10.3	Stack-Tail Betatron Cooling	5-23
5.10.4	Operation of Betatron Cooling Systems	5-24
5.11	Stochastic-Cooling Hardware	5-24
5.11.1	Pickup Electrodes	5-24
5.11.2	Preamplifiers	5-27
5.11.3	Notch Filters	5-28
5.11.4	Traveling Wave Tubes (TWT's)	5-30
5.11.5	Kicker Electrode Assemblies	5-31
5.11.6	Other Considerations	5-31
5.11.7	Accumulator Stochastic Cooling System Layout	5-32
6.	Extraction of Antiprotons from the Accumulator to the Main Ring	6-1
6.1	Accumulator Beam Manipulation and Extraction	6-1
6.2	Main Ring RF Capture and Acceleration	6-3
6.2.1	Introduction	6-3
6.2.2	Injection and Rebunching	6-3
6.2.3	Bunch Recombination at 150-GeV	6-4
7.	The Main Ring in Tevatron I	7-1
7.1	Functions of the Main Ring in Tevatron I	7-1
7.2	Antiproton Injection	7-2
7.3	Main Ring Acceleration and Rebunching Hardware	7-2
7.4	Main Ring Overpass	7-2
7.5	Main Ring Diagnostics	7-5
7.6	DO Overpass	7-5
8.	The Energy Saver in Tevatron I	8-1
8.1	Functions of the Energy Saver in Tevatron I	8-1
8.2	Energy Saver Lattice	8-1
8.2.1	Ring Location and Normal Lattice	8-1
8.2.2	Normal and High - Beta Long Straight Section	8-2
8.2.3	Lattice Elements	8-3
8.2.4	Low Beta Long Straight Section	8-3
8.3	Correction Systems	8-4
8.3.1	Types of Correction Elements	8-4
8.3.2	Correction Magnet Circuits	8-5
8.3.3	Coil Strength Requirements	8-6
8.3.4	Excitation	8-10
8.3.5	Power Supplies	8-10
8.4	Main Ring Extraction and Energy Saver Injection and Abort	8-11
8.5	Acceleration of Protons and Antiprotons	8-14
8.5.1	Energy Saver RF Requirements for Colliding Beams	8-14
8.5.2	Failure modes	8-15

8.6	Energy Saver Diagnostics	8-16
8.6.1	Energy Saver Position Detectors	8-16
8.6.2	Beam-Loss Monitors	8-17
8.6.3	Diagnostics for the Energy Saver Collider Operation	8-17
9.	Interaction Regions and Experimental Facilities	9-1
9.1	Experimental Areas	9-1
9.1.1	B0 Experimental Areas	9-1
9.1.2	D0 Experimental Areas	9-2
9.2	B0 Low-Beta Design	9-2
9.2.1	Lattice Design	9-2
9.2.2	Transition to Low Beta	9-2
9.3	Hardware Modifications	9-3
9.3.1	Magnets	9-3
9.3.2	Power Supplies and Bus	9-4
9.3.3	Refrigeration	9-4
9.3.4	Vacuum	9-4
9.4	D0 Low-Beta Design	9-4
10.	Performance and Luminosity	10-1
10.1	Beam Geometry	10-1
10.2	Beam Cross Section at the Collision Point	10-1
10.3	Beam - Beam Effects	10-2
10.4	Beam - Beam Tune Shift	10-3
10.5	Single - Beam and Luminosity Lifetime	10-3
10.5.1	Effects of Residual Gas	10-3
10.5.2	Intrabeam Scattering	10-4
10.5.3	Luminosity	10-6
10.5.4	Total Cross Section	10-6
10.5.5	Luminosity Lifetime	10-7
10.6	Collider Filling Strategy	10-8
11.	Beam-Transport Lines	11-1
11.1	120-GeV Proton Transport from F17 to Target (Line AP-1)	11-1
11.2	8-GeV Antiproton Transport to Debuncher (Line AP-2)	11-3
11.3	Debuncher to Accumulator Transfer (Line D To A)	11-5
11.4	Accumulator to Main Ring Transport (Line AP-3)	11-6
11.5	Booster Test Beam Line (Line AP-4)	11-7
11.6	Beam-Line Vacuum Systems	11-9
12.	Magnets and Magnet Power Supplies	12-1
12.1	Magnets	12-1
12.2	Magnet Power Supplies	12-1
12.2.1	Debuncher	12-1
12.2.2	Accumulator	12-2
12.2.3	Beam Lines	12-3
13.	Controls	13-1
13.1	General Requirements and Architecture	13-1
13.2	Computer Configuration	13-1
13.3	Software	13-2
13.4	Communications	13-2
13.5	Magnet Controls	13-3
13.6	Vacuum Controls	13-4
13.7	RF Control System	13-4
13.8	Stochastic Cooling Controls and Monitoring	13-5
13.9	Tev I Beam Diagnostics Interface to the Controls System	13-7

13.9.1	Beam Position Monitors	13-7
13.9.2	Beam Loss Monitors	13-8
13.9.3	Beam Current Monitors	13-8
13.9.4	Beam Profile Measurements	13-8
14.	Conventional Construction	14-1
14.1	Antiproton Source Construction	14-1
14.1.1	F18 Extraction Hall	14-2
14.1.2	Pretarget Enclosure	14-3
14.1.3	Antiproton Target Hall and 120-GeV Transport System ..	14-3
14.1.4	Antiproton Transport Enclosure	14-5
14.1.5	Debuncher-Accumulator Ring Enclosure	14-6
14.1.6	Antiproton Service Buildings	14-7
14.1.7	Booster Beam Enclosure and 8-GeV Target Station	14-8
14.1.8	Radiation Shielding	14-9
14.1.9	Survey and Alignment Control	14-11
14.1.10	Roads, Hardstands, and Parking	14-12
14.1.11	Underground Utilities	14-13
14.1.12	Primary Power, Switchgear, and Substations	14-14
14.1.13	Secondary Power and Distribution	14-15
14.1.14	Process-Water Systems	14-15
14.1.15	Finished Site Drainage	14-16
14.1.16	Landscaping	14-17
14.2	B0 Colliding Beam Area	14-17
14.2.1	B0 Colliding Beam Experimental Area	14-18
14.2.2	200-GeV Vertical Beam Bypass	14-21
14.2.3	Experimental-Equipment Foundations	14-21
14.2.4	Radiation Shielding	14-22
15.	Options for Future Improvements	15-1
15.1	Momentum Cooling	15-1
15.2	Target Development	15-3
15.3	Improvements in Stochastic Cooling	15-3
15.4	Electron Cooling of the Core	15-3

Appendices

- A. Beam Line, Accumulator and Debuncher Notation
- B. Parameters
- C. Site Coordinates
- D. Debuncher SYNCH
- E. Accumulator SYNCH



The Antiproton Source

Figure 1-1

CHAPTER 1

INTRODUCTION AND OVERVIEW

This report describes the design of the Tevatron I Project, which will enable Fermilab to produce proton-antiproton collisions in the Tevatron accelerator. Center-of-mass energies near 2 TeV, by far the highest available anywhere in the world for high-energy physics research until at least the decade of the 1990's, will provide enormous opportunities for exciting new physics.

After the energy, the most important parameter determining the utility of a colliding-beam facility is the luminosity, or interaction rate per unit cross section. The first goal of the Tevatron I project is to achieve a peak luminosity of $10^{30} \text{cm}^{-2} \text{sec}^{-1}$ for proton-antiproton collisions at the maximum energy in the Tevatron.

The luminosity depends on the intensity and phase space density of the interacting beams. The design luminosity of $10^{30} \text{cm}^{-2} \text{sec}^{-1}$ can be achieved with as few as 1.8×10^{11} protons and 1.8×10^{11} antiprotons of appropriate phase space density. The number and phase-space density of antiprotons produced by bombarding a dense target with one pulse of protons from the Main Ring are too small by orders of magnitude to achieve the design luminosity. Thus it is necessary to collect many pulses of antiprotons in an accumulator ring and to increase their phase-space density, i. e. to cool them, by roughly six orders of magnitude. To minimize user frustration and maximize the average luminosity, the accumulation time should be as short as possible, at least short compared to the luminosity lifetime, which is expected to be larger than twenty hours. The second goal of the project is to accumulate and cool the required number of antiprotons in five hours or less, starting with no antiprotons in the Accumulator.

The design presented here to meet these goals is based on the method of stochastic cooling developed by van der Meer, Thorndahl, and coworkers.¹ This method generates a non-uniform phase-space density distribution of the accumulated antiprotons, with only the high-density core useful for colliding beams. Thus the source has been designed to accumulate a total of 4.3×10^{11} antiprotons in 4 hours, of which typically 1.8×10^{11} antiprotons from the high-density core will be injected into the Tevatron. Subsequent accumulation cycles starting with the antiprotons left from the previous cycle will require considerably shorter times to achieve the necessary core density.

The amount of cooling to be done depends on the phase-space density at production. The higher the initial density, the easier it is to achieve the final density. The yield of antiprotons per incident proton is proportional to the product of the spatial solid angle and the momentum spread accepted by the beam-transport system, and the initial phase-space density can therefore be increased only by decreasing the spot size and

time spread of the antiprotons. The initial protons that produce the antiprotons determine these parameters and it is therefore useful to reduce the proton spot size and time spread.

The proton rms spot size will be reduced to 0.38 mm by the use of standard quadrupole lenses. Further reduction would provide little gain because the apparent spot size is ultimately dominated by the large antiproton beam divergence and the finite length of the target.² The first collection lens must match the large angular divergence of the antiproton beam at the target into the small angular admittance that is characteristic of a beam-transport system or a storage ring. This is achieved by using a lithium lens of the type developed by the Institute of Nuclear Physics at Novosibirsk.³

The time spread can be minimized by rf manipulation of the proton beam in the Main Ring just prior to extraction. The narrow time spread and large energy spread of the resulting antiproton bunches can be transformed into bunches with a much lower energy spread by rf phase rotation in a separate ring called the Debuncher. The rf phase-rotation system⁴ makes it possible to start with a large momentum spread from the target, thereby increasing the antiproton flux. The reduced energy spread also greatly simplifies the design of the magnets and cooling systems of the Accumulator ring.

The design thus uses two fixed energy rings, the Debuncher and the Accumulator, located south of the Booster as shown in Fig. 1-1. The Accumulator has the same circumference as the Booster; the Debuncher is slightly larger. Both rings operate at a kinetic energy of 8 GeV, the Booster energy. The sequence of operations leading to colliding beams involves seven steps:

1. Proton Acceleration for Antiproton Production. Every two seconds, one Booster batch containing 2×10^{12} protons in 82 rf bunches is accelerated in the Main Ring to 120 GeV and held at that energy while the rf manipulation described in the next step is carried out.
2. Preparation of Protons for Targeting. The 53-MHz rf voltage is lowered to cause each proton bunch to spread in time to 9 nsec. The rf voltage is suddenly increased to 4 MV per turn and each proton bunch rotates by 90° in phase space in 1.3 msec to a short bunch of less than a nanosecond in width, but with an energy spread of about 0.4%. This train of short bunches is extracted from the Main Ring at F17 as soon as the bunch rotation is completed.
3. Antiproton Production and Transport. The short proton bunches strike a tungsten target, producing a train of 82 equally short antiproton bunches. The peak energy deposition in the target is the same as that used successfully at CERN. 7×10^7 8.9-GeV/c antiprotons are collected by the lithium lens and transported to the Debuncher.

The momentum spread of the beam is 3% and the transverse beam emittances are 20π mm-mrad in each plane.

4. Bunch Rotation in the Debuncher. The antiprotons are injected into 53-MHz rf buckets in the Debuncher. The rf voltage is large enough that the antiproton bunches rotate just as the proton bunches rotated in the previous step. After a quarter of a synchrotron oscillation, the narrow time structure and large momentum spread have been transformed into a small momentum spread and a broad time structure. The rf voltage is then rapidly lowered to match the bucket to the rotated bunch, and finally adiabatically lowered to reduce the momentum spread to 0.2%.

5. Transverse Cooling in the Debuncher. After the rf manipulations, the horizontal and vertical transverse emittances are stochastically cooled in the Debuncher from 20π mm-mrad to 7π mm-mrad during the almost two seconds before the next antiprotons are to be injected.

6. Antiproton Accumulation and Cooling. The antiprotons are extracted from the Debuncher and injected into the Accumulator. Successive batches are accumulated by rf stacking each batch at the edge of the stack. Between injection cycles, the stack is stochastically cooled using a combination of longitudinal and transverse cooling systems similar to the types developed by CERN for the AA ring.⁵ A new batch of antiprotons with a density of about 7 antiprotons per eV is deposited at the stack tail every 2 sec. The fresh batch is moved by the coherent force of the stochastic-cooling system away from the injection channel and toward the center of the stack. The strength of the coherent force diminishes exponentially as the particles move away from the edge of the tail, causing the particle density to increase. Diffusion forces resulting from the Schottky noise of the antiproton stack and the thermal noise of the amplifiers cause the antiprotons to migrate from the high-density region toward the low-density region. As long as the coherent force is greater than the diffusion forces, the stack builds up in intensity until it reaches the core region where the coherent force is zero. Some antiprotons are lost during transfer and rf stacking and some diffuse away from the stack into the chamber walls. Allowing for losses, 6×10^7 antiprotons are stacked in each pulse. In 4 hours, the core will grow to a density of 1.0×10^5 antiprotons per eV. The total number of antiprotons in the core will be 4.3×10^{11} . During this time the transverse cooling systems will have reduced the horizontal and vertical emittances to 2π mm-mrad.

7. Filling the Tevatron. After accumulation is complete, antiproton bunches of the desired intensity are individually extracted from the core, transferred to the Main Ring, accelerated to 150 GeV and injected into the Tevatron. The same number of proton bunches of similar intensity are prepared in the Main Ring and injected into the Tevatron. Whether it is better to inject the protons or antiprotons

first will be determined empirically. Both beams are then simultaneously accelerated to the desired energy.

Sufficient antiprotons for a luminosity of $10^{30}\text{cm}^{-2}\text{sec}^{-1}$ can be produced in 4 hours by this sequence, even with reasonable losses in production, cooling, and beam transfer. The project includes Main Ring beam overpasses at B0 and D0 to allow antiproton accumulation to proceed in parallel with colliding beams in the Tevatron. The design luminosity can be achieved without exceeding a beam-beam tune shift of 0.0018 per crossing. As the Tevatron and the Antiproton Source become more reliable, longer collection times will become practical, resulting in higher luminosity.

Beam-accumulation techniques are developing rapidly and it seems highly advisable to design an antiproton source that can accommodate future improvements. Accordingly, the third goal of this design is to incorporate flexibility for future improvements so that the Antiproton Source may ultimately achieve a luminosity of $10^{31}\text{cm}^{-2}\text{sec}^{-1}$. The potential for luminosity of the proposed source is exhibited in Table 1-1, which shows the relationship between the number of accumulated antiprotons and the luminosity.

The peak luminosity and accumulation rate are limited not by the antiproton production rate but by the cooling systems of the Accumulator Ring. Higher luminosities may be achieved through improvements in these cooling systems. The present design uses less than a half of the total number of particles collected in each accumulation cycle to reach its design luminosity of $10^{30}\text{cm}^{-2}\text{sec}^{-1}$. If future improvements can increase the final density by a factor of three, it will be possible to approach a luminosity of $10^{31}\text{cm}^{-2}\text{sec}^{-1}$. The design of the rings therefore includes provisions (aperture and straight-section space) for:

- (i) Momentum precooling in the Debuncher.
- (ii) Improved stochastic cooling in the Accumulator.
- (iii) Improved Main Ring extraction for antiproton production.
- (iv) Intermediate energy electron cooling in the Accumulator.

These features are not part of the initial design because it is difficult to foresee which improvements will be most feasible and cost-effective. The most beneficial choices will be clear only after some experience in operating the collider.

The design of each system are described in greater detail in the following sections.

TABLE 1-I LUMINOSITY PROGRESSION

$N_{\bar{p}}$ (10^{11})	N_p (10^{11})	N_B	N_T (10^{11})	L ($10^{30} \text{cm}^{-2} \text{sec}^{-1}$)
0.8	0.8	1	0.8	0.65
0.6	0.6	3	1.8	1.0 (design goal)
0.8	0.8	3	2.4	2.0
1.0	1.0	3	3.0	3.0
1.0	1.0	6	6.0	6.0

$N_{\bar{p}}$ and N_p are the numbers of antiprotons and protons per bunch, N_B is the number of bunches, N_T is the total number of antiprotons, $\beta^* = 1 \text{ m}$ is the value of β at the center of the interaction region, and L is the luminosity.

References

1. S. van der Meer, Stochastic Damping of Betatron Oscillations in the ISR CERN/ISR-PO/72-31 (1972) (unpublished).
D. Mohl, G. Petrucci, L. Thorndahl, and S. van der Meer, Physics Reports 58, p. 73 (1980).
2. C. Hojvat and A. Van Ginneken, Fermilab \bar{p} Note 139, July 16, 1981 (unpublished).
3. B. F. Bayanov et al., Nucl. Inst. Methods 190, 9 (1981).
4. A. G. Ruggiero, Fermilab \bar{p} Note 102, January, 1981 (unpublished).
5. S. van der Meer, Stochastic Stacking in the Antiproton Accumulator CERN/PS/AA/78-22 (1978) (unpublished).

CHAPTER 2

PROTON ACCELERATION AND EXTRACTION FOR ANTIPROTON PRODUCTION

The production of antiprotons is done by bombarding a target with protons that have been accelerated to 120 GeV in the Main Ring. This chapter describes the acceleration of protons in the Main Ring and their subsequent extraction at F17.

2.1 Proton Acceleration

The accumulation cycle begins by accelerating a single Booster batch of protons in the Main Ring to 120 GeV with the existing rf system. This Booster batch consists of a string of 82 bunches spaced 5.6 m apart; its total length is 457 m. A single batch fills less than one-thirteenth of the Main Ring circumference. The Booster intensity record for a single batch is 3.4×10^{12} . For the purpose of this report, it is assumed that an intensity 2.0×10^{12} protons per Booster batch will be standard operating intensity for \bar{p} production. The minimum time needed to accelerate a single batch to 120 GeV in the Main Ring can be reduced to 1.87 seconds. A flat-top of 0.13 sec is added to provide time for the rf beam manipulation before extraction. The cycle time is 2 seconds. The major beam properties are given in Table 2-I.

TABLE 2-I MAIN RING BEAM PARAMETERS

Proton Beam Kinetic Energy @ Extraction	120 GeV
Relativistic Factors: β	0.99997
γ	128.9318
$B\rho$, magnetic rigidity	4035.506 kG-m
Momentum, p	120.9347 GeV/c
Number of Booster batches accelerated	1
Number of Proton Bunches	82
Total number of protons per Batch	2.0×10^{12}
Main Ring Cycle Time	2.0 sec
Betatron Emittance, 95% of beam, (H and V)	0.2π mm-mrad
Longitudinal Emittance, 95% of beam at 120 GeV	0.3 eV-sec
RF harmonic number (h)	1113
RF Frequency @ 120 GeV	53.1035 Mhz
Revolution Period @ 120 GeV	20.96 μ sec
Booster Batch Time Length	1.56 μ sec
Transition Energy (γ_t)	18.75
Betatron tune number (H and V)	19.4
$\eta = \gamma^{-2} - \gamma_t^{-2}$	-0.0028
Maximum RF voltage	4.0 MV
Average Radius	1000 m

A reasonable estimate for the normalized betatron emittance, based on measurements,¹ is 24π mm-mrad. This value includes 95% of the beam. If $\sigma_{H,V}$ denotes the rms beam size and $\beta_{H,V}$ the lattice amplitude function, the emittance can be expressed in terms of these quantities as

$$\epsilon_{H,V} = 6\pi \frac{\sigma_{H,V}^2}{\beta_{H,V}} .$$

The longitudinal phase-space area S of individual bunches in a Booster batch has been measured to be 0.3 eV-sec or less.² If the particle distribution is biGaussian in these variables, this value includes 95% of the beam. There is reason to believe this number can be reduced to 0.2 eV-sec in the future when improvements are made to the Main Ring and the Booster rf systems.

For energies well above the transition energy, a bunch area S half as large as the bucket area, and a bunch shape matched to the rf bucket, the rms bunch length σ_e and rms momentum spread σ_p/p are

$$\sigma_e = (142\text{cm}) \frac{S}{\sqrt{VE}} \quad \sigma_p/p = (0.0112) \frac{S}{\sqrt{E^3/V}} .$$

The bunch area can be expressed in terms of these quantities as

$$S = 6\pi\beta E \frac{\sigma_e}{c} \frac{\sigma_p}{p} .$$

The bucket area of a stationary bucket B and the phase-oscillation period T_s are respectively

$$B = (0.34 \text{ eV-sec}) \sqrt{VE} \quad T_s = (1\text{msec}) \sqrt{E/V} .$$

In all these equations E is in GeV, V in MV and S in eV-sec.

For a fixed antiproton momentum spread, the bunch area of the antiprotons is minimized by making the time spread of the extracted proton bunches as narrow as possible. At the end of acceleration when the rf voltage is 4 MV the relevant beam parameters are $T_s = 5.6$ msec, $\sigma_e = 16$ cm, $\sigma_p/p = 2.4 \times 10^{-4}$.

The rf voltage is slowly reduced from 4 MV to 30 kV so that the bunch motion remains matched to the rf bucket shape. At 30 kV, the beam parameters are $T_S = 65$ msec, $\sigma_e = 56$ cm, and $\sigma_D/p = 6.8 \times 10^{-4}$. The adiabatic reduction of the rf voltage is accomplished in 100 msec. At that moment the synchrotron phase of the bunch extends to $\pm 90^\circ$.

The rf voltage is then raised abruptly to 4 MV within two revolutions or 42 μ sec. The bunches are no longer matched to the buckets, so they start to rotate as in Fig 2-1. After a quarter of a phase oscillation or 1.4 msec, the time spread of the beam has been reduced by more than an order of magnitude. At that moment the beam parameters are $T_S = 5.6$ msec, $\sigma_e = 5.0$ cm, and $\sigma_D/p = 8.4 \times 10^{-4}$. After these operations are completed, a momentum spread of $\pm 0.4\%$ contains 95% of the beam.

The results of recent bunch-narrowing experiments in the Main Ring at 120 GeV, March 1982,² are shown in Fig. 2-2. In these experiments the maximum rf voltage was limited to 3.6 MV. Shorter bunches can be obtained by using the full available 4 MV.

Measurements made in the Main Ring³ have shown that the available momentum aperture is $\pm 0.27\%$ for 90% beam transmission at 120 GeV with extraction equipment for the Tevatron in place. The loss of beam due to the 0.4% momentum spread is expected to be small, since very little of the beam will extend into the bad-field region of the aperture. As soon as the bunch rotation is complete, all 82 bunches are ejected at F17 into the 120-GeV transport line.

2.2 Extraction at F17*

Extraction of 120-GeV protons from the Main Ring for the production of antiprotons takes place at location F17. Two Lambertson magnets deflect the extracted beam vertically by 32.2 mrad into the transport line, which is located just above the Main Ring magnets. The geometry and expected beam sizes at the Lambertsons are shown in Fig. 2-3 and 2-4. The horizontal beam size at 120 GeV includes the contribution of the $\pm 0.2\%$ momentum spread of the tightly bunched proton beam. The large horizontal size of the bunched beam uses most of the available Main Ring aperture to the inside of the Ring at the extraction point. As seen in Figs. 2-3 and 2-4, the septum of each Lambertson will be located well within the Main Ring aperture, preventing parasitic extraction at F17 during the slow-extraction fixed target program. The Lambertsons will be withdrawn from the aperture during this operation.

The relevant parameters of the Main Ring lattice are in TABLE 2-II.

*This design is being extensively revised at the time of writing.

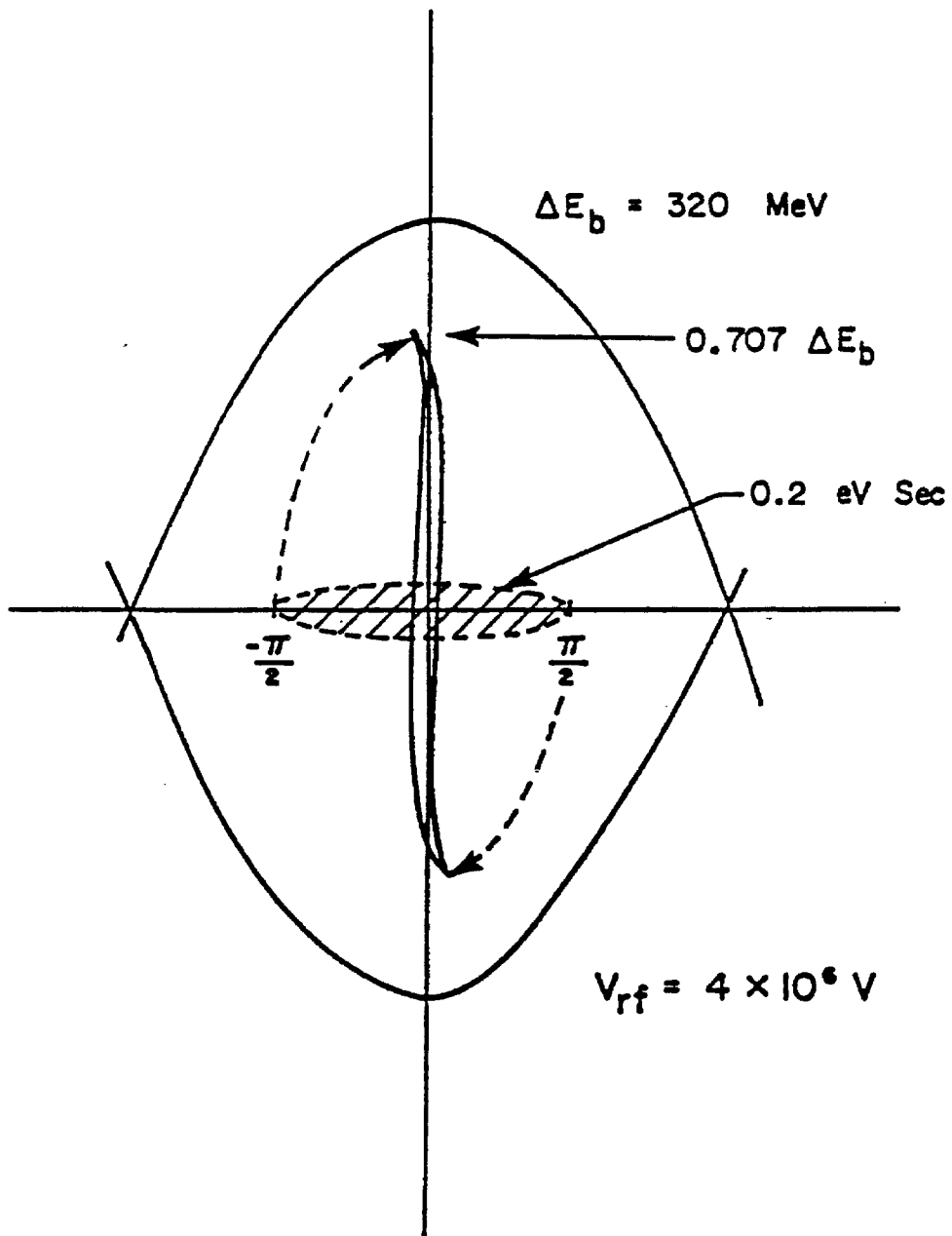
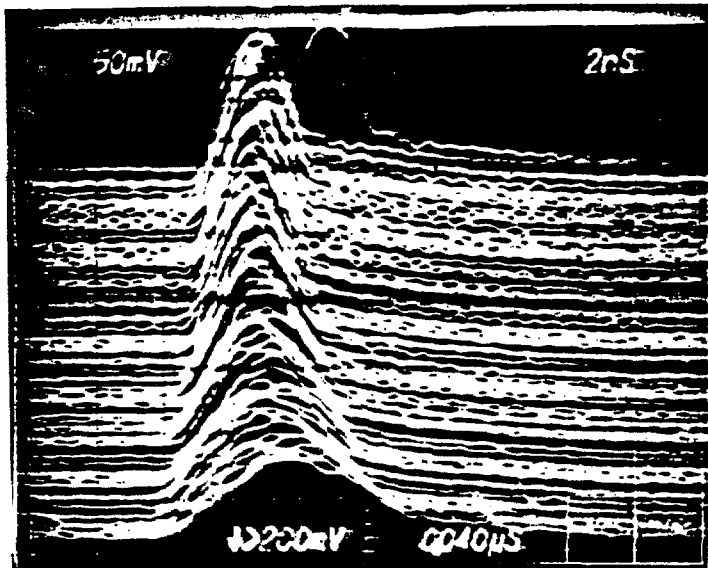
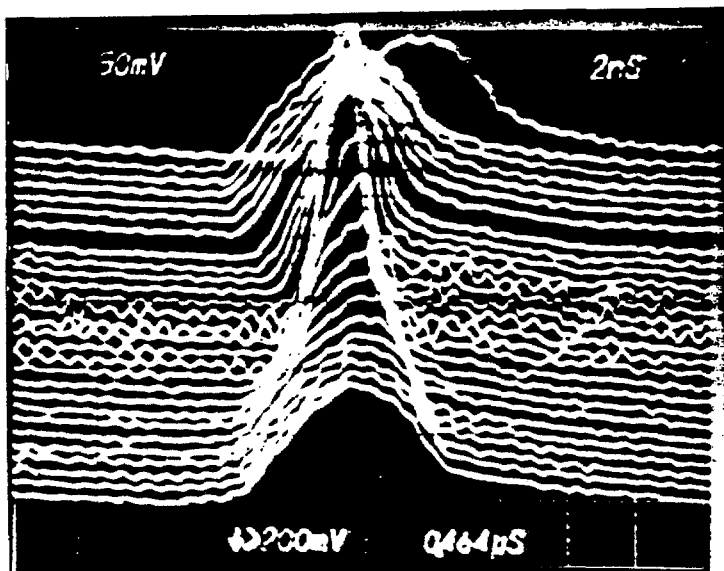


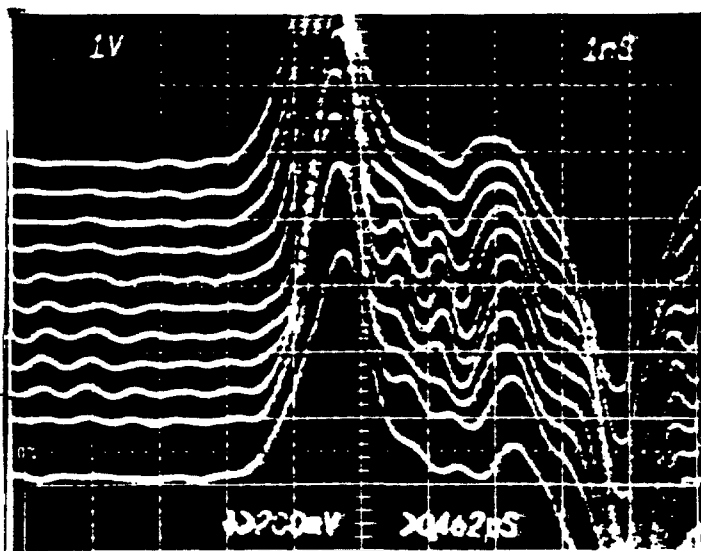
Figure 2-1



- a) Bunch broadening. Time progresses downward, and total debunching time is 100 ms. The final bunch length is about 9 ns.



- b) Rotation of mismatched bunch following sudden increase of the RF voltage to 1 MV. Time progresses downward, and traces are separated by about 100 ms. The topmost trace results from a mistrigger.



- c) Bunch lengths near the time of narrowest bunches. Traces are taken at the beam rotation frequency, every 20.9 μ s. The bunch pickup is a broadband transmission line, so inverted reflections from the downstream end of the pickup also appear. In this experiment the maximum RF voltage was 3.6 MV. Narrower bunches would be obtained with nominal 4 MV. A bunch with a 95% full time width of 1 ns has a length of 7.5 cm rms.

Figure 2-2 Debunching and Bunch Rotation.
Time base is 20 ms per major division.

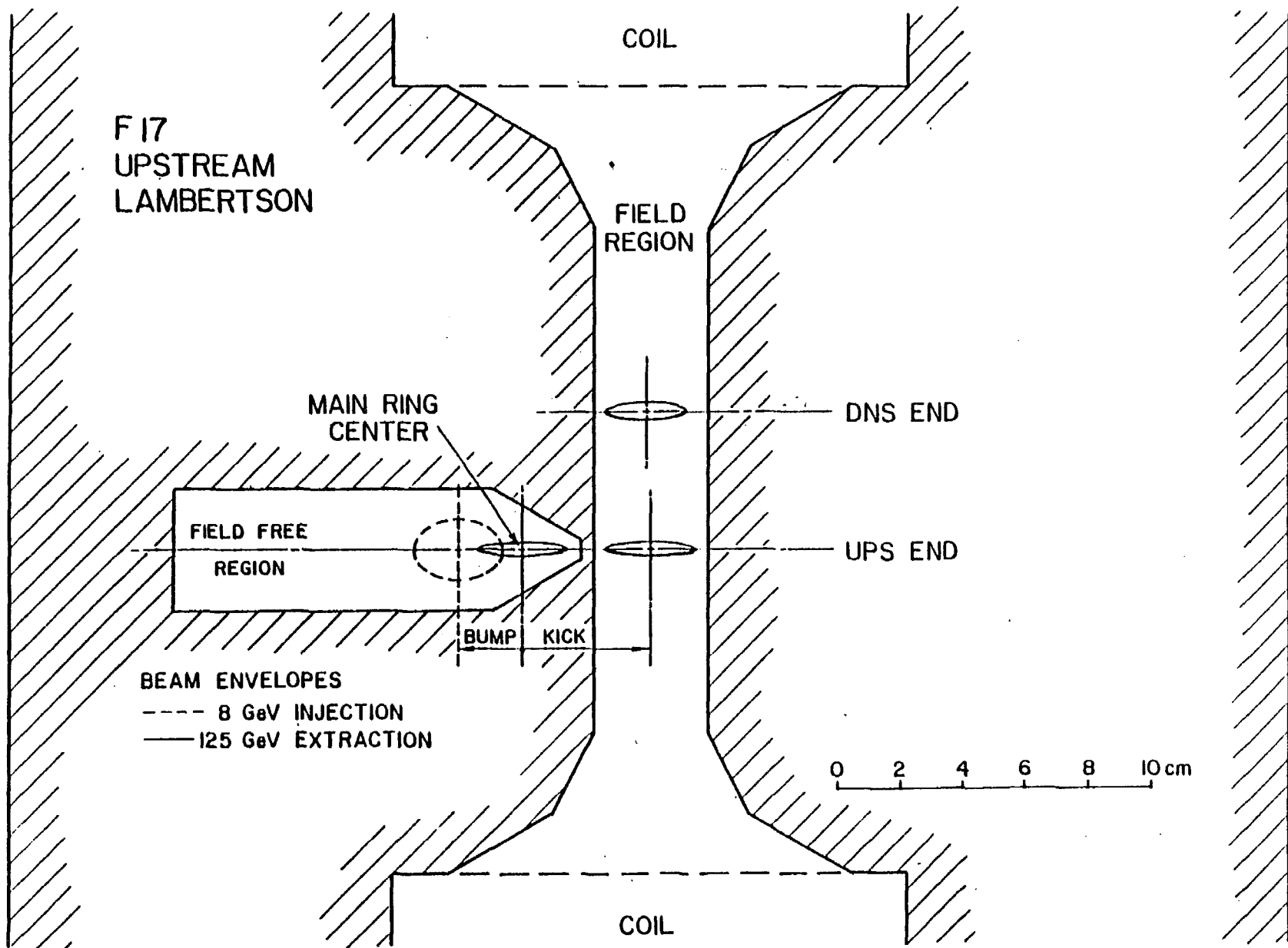


Fig 2-3

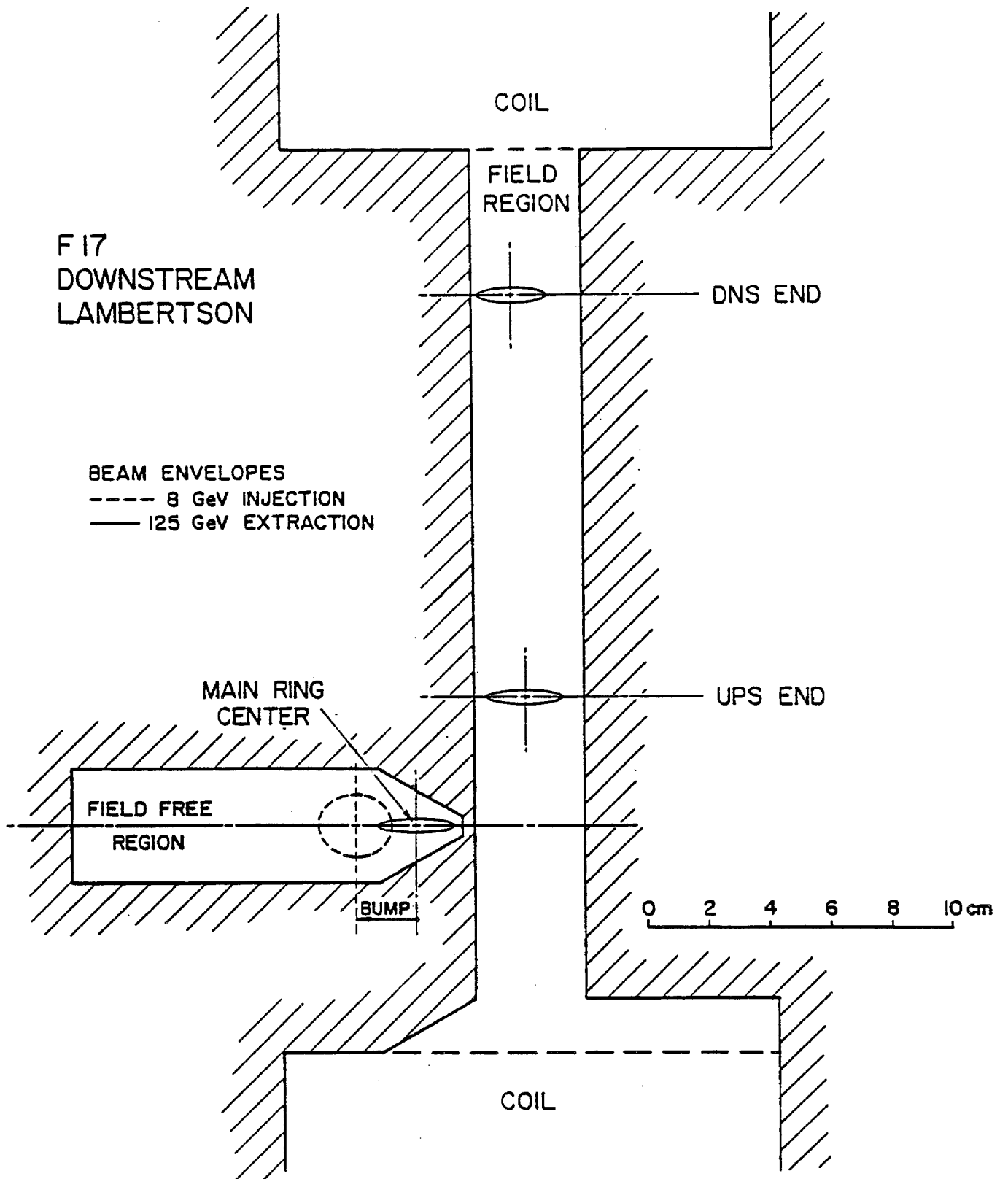


Figure 2-4

TABLE 2-II PROPERTIES OF SELECTED MAIN RING MINISTRAIGHTS

Horizontal-Plane Lattice Functions

Location	β (m)	α	Phase Relative to F17 (Modulo 360°)	Space Available (in.)
C48 Kicker	102.4	0.467	-90.11°	(Existing)
F12	29.6	-0.573	-168.30°	0.0
F13	95.4	1.858	-135.74°	0.0
F14	28.4	-0.589	-99.29°	34.0
F15 (Bump 1)	97.3	1.839	-66.32°	42.5
F16	30.1	-0.624	-31.47°	42.0
F17 (Bump 2) (Extraction)	99.7	1.939	0.00°	32.0
F18 (Bump 3)	28.9	-0.558	35.20°	52.0
F19	94.3	1.816	68.42°	0.0
F21	28.9	-0.618	104.71°	28.0
F22 (Bump 4)	99.5	1.893	136.92°	27.5
F23	30.1	-0.598	171.32°	35.0
F24	97.4	1.906	203.21°	0.0
F25	28.4	-0.567	239.23°	35.0
F26	95.2	1.810	272.60°	43.5

The kicker at location C48 causes a -43 mm horizontal displacement at F17, which is sufficient to cross the Lambertson septum. The required angular deflection at C48 is obtained with a voltage of 60.0 kV, well within the present operating range of the device. Given the Main Ring lattice characteristics, the kick at C-48 results in an angular displacement of +0.847 mrad at F17 as well as the horizontal displacement. This residual angle can be cancelled with a 3° rotation of the first Lambertson extraction magnet.

A local four-magnet orbit bump at F17 is used to position the closed orbit during 8-GeV injection in the center of the restricted aperture at F17 and to move the orbit close to the Lambertson septa during 120-GeV extraction. Four standard 35-in. long bump magnets are placed at F15, F17, F18 and F22. The closed orbit at 120 GeV can be adjusted over a range of ±37 mm at location F17.

Vertical extraction was chosen since it allows the extracted proton beam to clear the Main Ring magnet, F17-1, just downstream of the Lambertsons with a minimum deflection. The return coil on the upstream end

of F17-1 has been modified to permit the beam pipe containing the extracted 120-GeV to be as close to the magnet steel as possible. The length of the medium straight section at F17 limits the maximum energy that can be extracted to 120 GeV.

The Lambertson magnets are 204 in. long and are excited to less than 13 kG at 120 GeV. The second Lambertson accommodates a vertical beam translation of 5 in.

Transport of the 120-GeV protons to the target is discussed in Sec. 11.1.

References

1. C. Moore et al., Fermilab EXP Note 101, February 1980 (unpublished).
2. J. Griffin (unpublished).
3. J. Griffin, Fermilab Report, 7, July 1982.

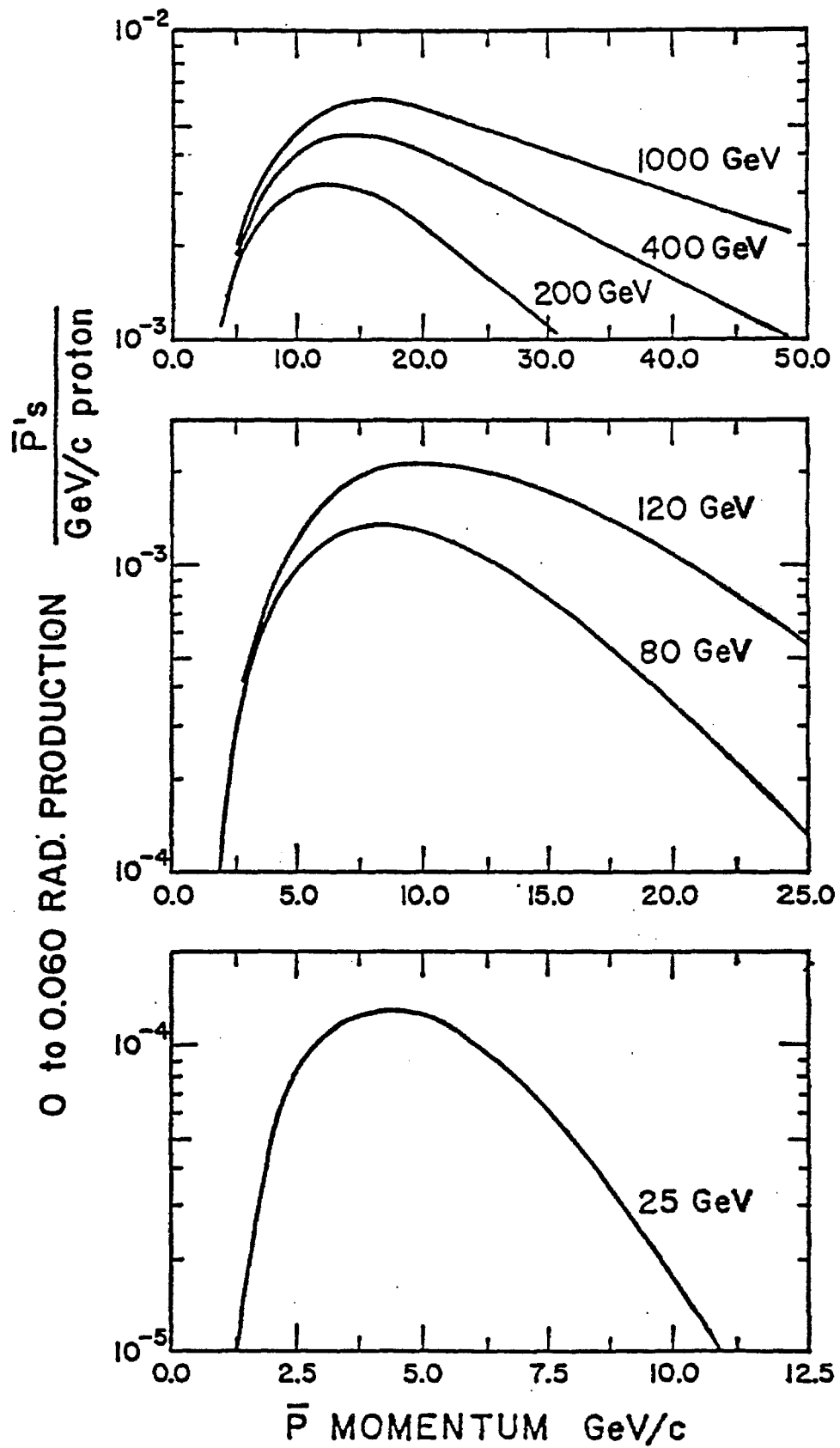


Figure 3-1

CHAPTER 3

ANTIPROTON PRODUCTION3.1 Antiproton Yields and Targeting

The choice of the antiproton energy and that of the protons for their production depend on the production cross sections and practical considerations relative to the existing facilities at the Laboratory. This section describes the present targeting scenario for the production of antiprotons, based on the discussion of the three following topics:

1. details of the production cross sections obtained from existing experimental data;
2. the choice of primary proton energy, antiproton momentum, antiproton longitudinal acceptance and antiproton transverse acceptance; and
3. limitations introduced by targeting and the antiproton collection system.

3.1.1 Antiproton Production Cross Sections. The available experimental data on the cross sections for the production of antiprotons have been described by a phenomenological formula that includes the dependence on the incident proton energy, the antiproton momentum and the target nucleus.¹ For example, the yields of antiprotons from a tungsten target collected within a laboratory angle of 60 mrad for various proton energies are shown in Fig. 3-1. It can be seen that there is a plateau at 120 GeV for the production of antiprotons between 8 and 13 GeV/c.

3.1.2 Proton Energy. The yield of antiprotons per unit volume of phase space per unit time changes very slowly with proton energy above 150 GeV, when the Main Ring cycle time is taken into consideration. Although some gain in yield could be obtained by going to a higher energy, a proton energy of 120 GeV was chosen because it is the maximum energy that can be extracted from a medium straight section such as F17. F17 provides a convenient location for the Antiproton Source. The choice was also influenced by the rapid increase in operating cost as the energy of the Main Ring is increased. The energy of 120 GeV is also compatible with the Colliding Beams Detector overpass. The B0 overpass is described in Chapter 7.

3.1.3 Antiproton Momentum. The optimum antiproton momentum is 10.0 GeV/c for an incident proton energy of 120 GeV. The yield is more than 90% of the optimum yield throughout the range from 7.5 GeV/c to 13.0 GeV/c. Since the normal injection momentum of the Main Ring, 8.89 GeV/c, is within this range of momenta, it is a reasonable choice. It has the advantage of

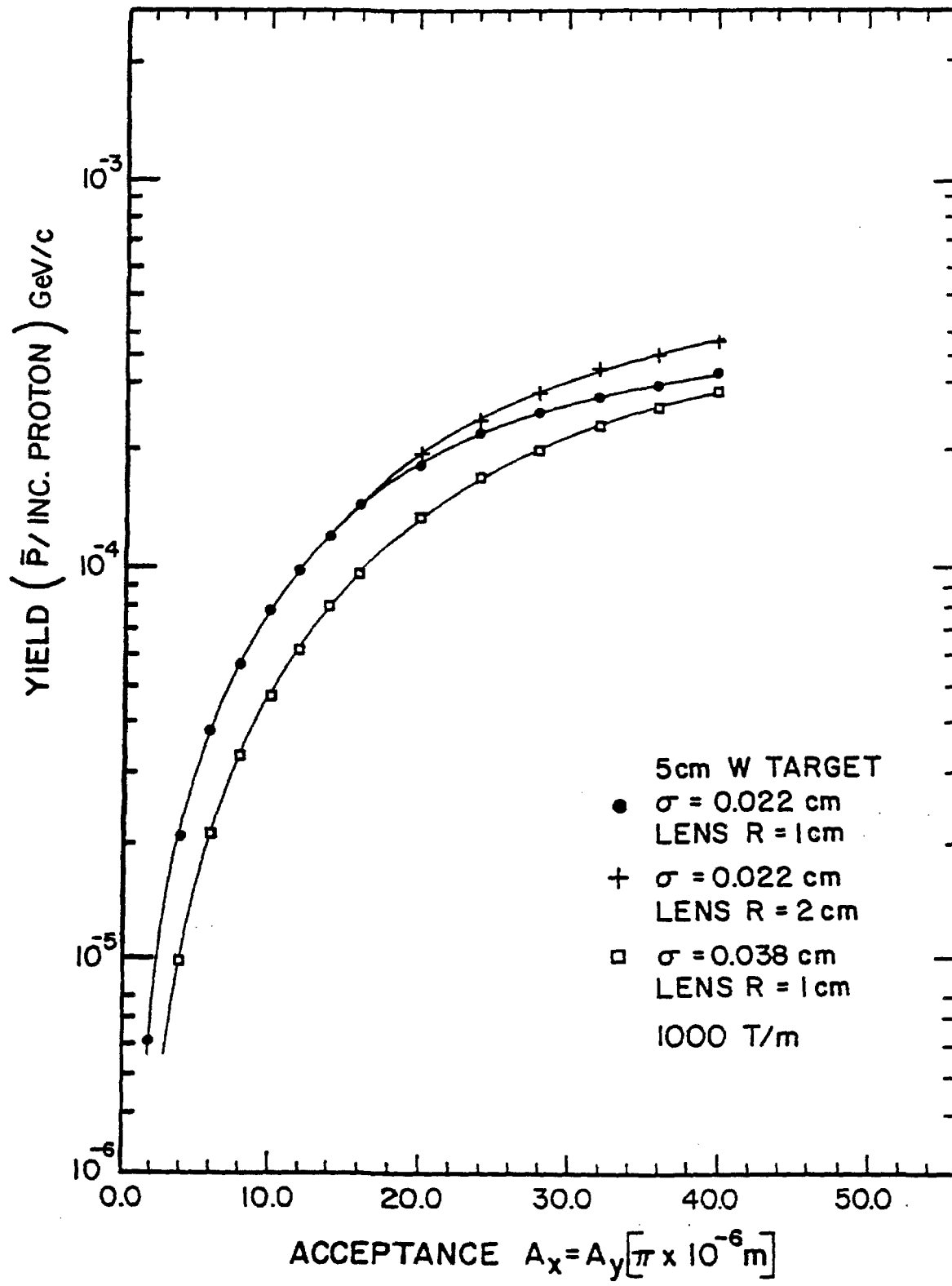


Figure 3-2

permitting the transfer of antiprotons directly from the Accumulator to the Main Ring. In addition, it opens the possibility of utilizing protons directly from the Booster as an alternative source of particles during commissioning of the source.

3.1.4 Antiproton Longitudinal Acceptance. Stochastic-cooling performance depends critically on the flux of \bar{p} 's injected into the Accumulator and on the particle density per unit of energy spread. This density, which is inversely proportional to the longitudinal emittance of the antiprotons, is determined in part by the time spread of the \bar{p} 's at production, as discussed in Chapter 2.

In the Debuncher, a total momentum spread of approximately 3% can be reduced to a momentum spread that can be accommodated by the Accumulator. Although a larger momentum spread will result in a larger flux the Accumulator is not able to cool the larger flux. The \bar{p} collection and transport system is designed to accept 4% total momentum spread. The momentum spread of the \bar{p} 's transported to the Debuncher will be adjusted by collimation in the beam transport.

3.1.5 Antiproton Transverse Acceptance. The calculation of expected antiproton yields depends crucially on the collection system downstream of the target. A comparison of different collection systems has been performed², taking into account the large momentum spread of the antiproton beam. The advantages of a device such as the lithium lens that was developed at the INP in Novosibirsk³ are clear. It has a very short focal length and it focuses in both transverse planes. Based on the INP experience, the parameters of the lithium lens collector were chosen to be: Radius = 1 cm, Gradient = 1000 T/m, Length = 15 cm. Within the present technology developed at Novosibirsk, a repetition rate of 1 Hz is feasible. The lens has a focal distance of 14.5 cm. The short focal distance requires the use of a dense target.

Antiprotons yields have been calculated with a Monte Carlo program¹ that includes the phenomenological description of the production cross section, the development of hadronic showers in the target and \bar{p} production by secondaries, multiple scattering and absorption. The result of these calculations is shown in Fig. 3-2 for two different rms proton beam spot sizes, $\sigma_x = \sigma_y = 0.038$ cm and $\sigma_x = \sigma_y = 0.22$ cm. The number of antiprotons increases approximately linearly with the transverse acceptance above 20π mm-mrad for $\sigma = 0.038$ cm. For the smaller beam size, the departure from linearity above 20π mm-mrad is caused by the finite lithium lens radius and the variation of field gradient. The optimum target length is approximately 5 cm.

3.1.6 Targeting Limitations. Decreasing the proton beam size at the target increases the transverse phase-space density of the produced

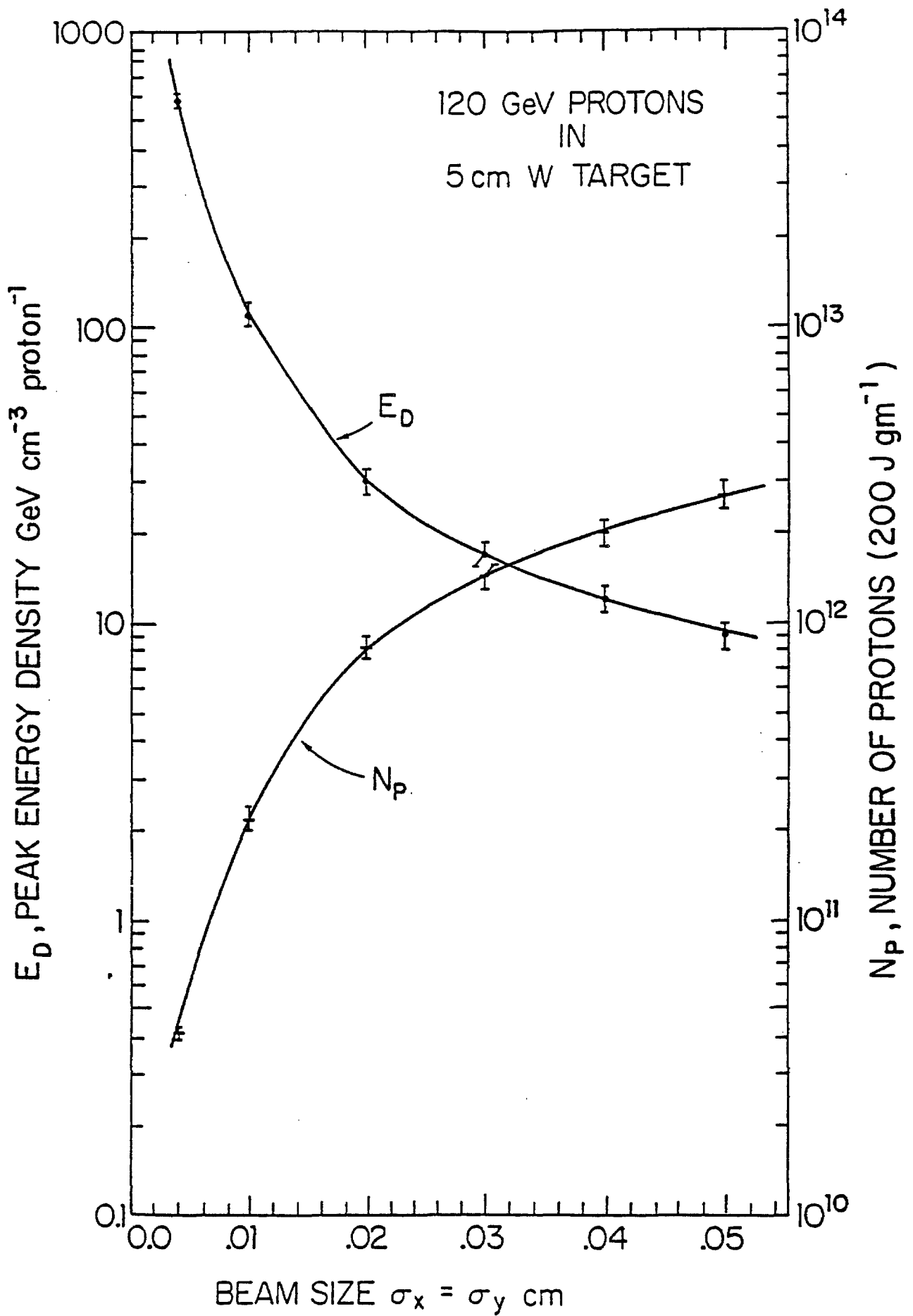


Figure 3-3

antiprotons, resulting in a larger yield within a given acceptance. The diameter of the proton beam cannot be reduced arbitrarily because the energy deposited by the beam per unit volume increases as the beam area decreases, causing the target to overheat.

The subject of high energy density deposition in targets was the subject of a Fermilab Workshop⁵. It was generally agreed that metal targets can sustain energy density deposition up to 200 Joules gm⁻¹ before the apparent onset of shock waves that could result in the destruction of the target. Calculations indicate that the CERN Antiproton Accumulator target sustains a maximum energy deposition of approximately 185 Joules/gm for tungsten. Both copper and rhenium (instead of tungsten) have been used at CERN for some time with no failures. The energy density deposited by a 120-GeV proton beam in tungsten has been calculated using the program MAXIM⁴. The maximum energy density deposited within a 5-cm long target is shown in Fig. 3-3 versus the rms size of the proton beam, σ . Within the errors of the calculation, it varies as σ^{-2} . Also shown is the maximum number of protons per pulse vs rms beam size, under the condition that the maximum allowable energy density is 200 Joules/gm.

Table 3-I shows the expected number of antiprotons per pulse as a function of beam size and maximum permissible proton intensity.

A feasibility study was carried out⁶ on sweeping the proton beam across the target to decrease the energy density deposited in the material. The antiproton acceptance must be simultaneously swept to track the proton beam spot. If the sweeping covers several proton-beam diameters, it is possible to target 3×10^{12} protons on beam spots corresponding to $\beta < 3$ m, which will give an increased number of antiprotons accepted per proton. The design of the target area makes it possible to incorporate a beam-sweeping system in the future.

TABLE 3-I NUMBER OF ANTIPROTONS PER PULSE

$\beta^*(m)^+$	$\sigma_x = \sigma_y$ (cm)	N_p Max	\bar{p}/p^{++}	\bar{p}/pulse
1.55	0.023	6.0×10^{11}	5.1×10^{-5}	3.1×10^7
3.07	0.032	1.2×10^{12}	4.3×10^{-5}	5.2×10^7
4.62	0.039	1.8×10^{12}	3.7×10^{-5}	6.7×10^7
8.00	0.052	3.0×10^{12}	2.5×10^{-5}	7.5×10^7

Notes: + $\psi\theta^*$ is for the proton beam at the center of the target
($\beta_x = \beta_y = \beta^*$)

++ The yield in \bar{p}/proton is for 3% $\Delta p/p$ and 20π mm-mrad.

3.2 Antiproton Target System Components

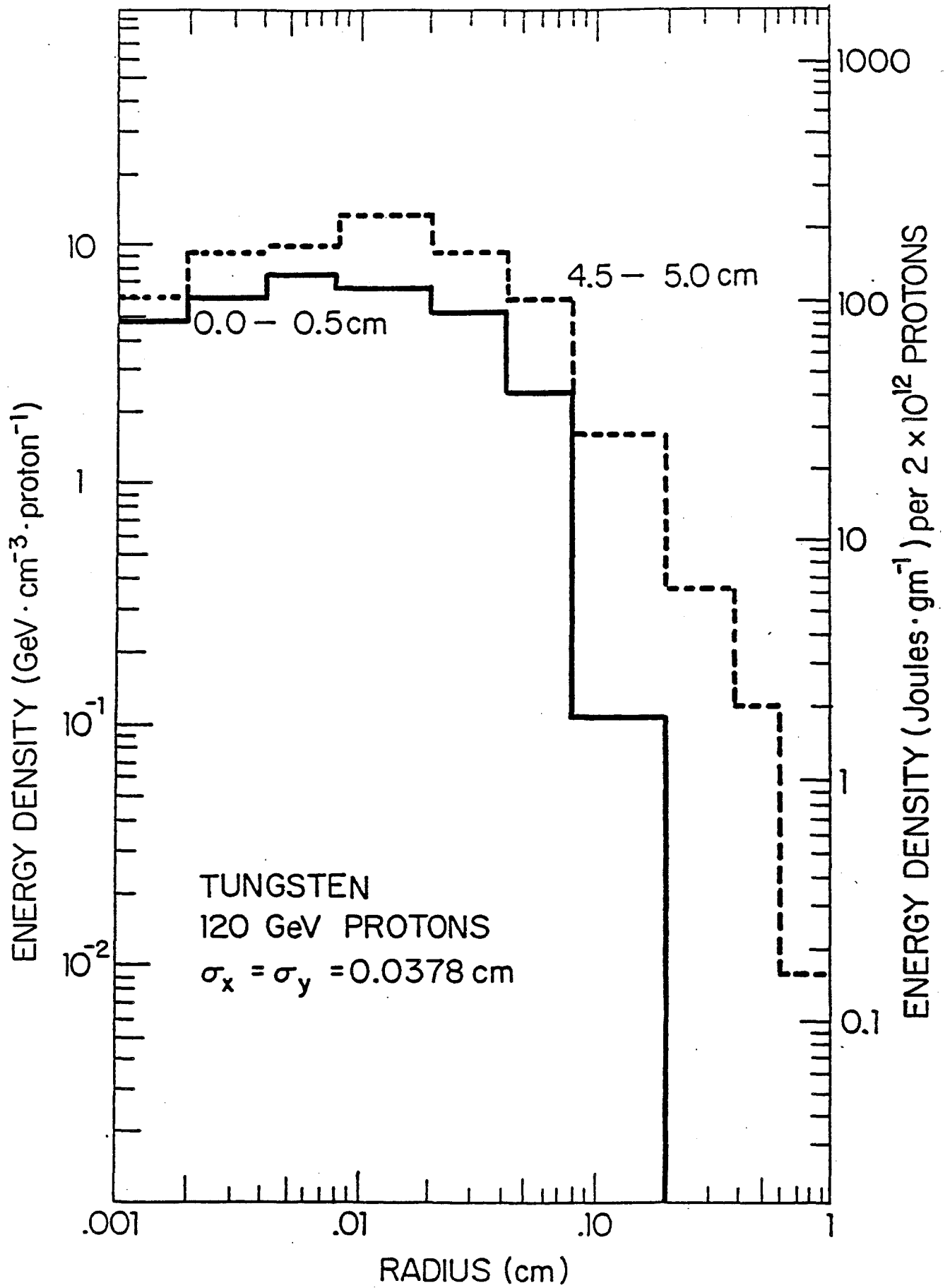


Figure 3-4

The principal components of the target system are the target itself and the antiproton collection device. This section discusses the design and limitations of these two components.

3.2.1 Antiproton Production Target The computer code MAXIM⁴ has been used to calculate radial and longitudinal energy density distributions in a stationary tungsten target for an rms beam size of 0.038 cm. The results are plotted in Fig. 3-4. The temperature rise of tungsten corresponding to an energy deposition in Joules/gm may be estimated from the enthalpy reserve curve given in Fig. 3-5. As is shown in Fig. 3-4, it is expected that local peak energy densities will be approximately 200 Joules/gm for the present design parameters $\sigma = 0.038$ cm and 2×10^{12} protons per pulse. To decrease the number of thermal and stress cycles in the volume of material struck by the beam, the target will be rotated continuously, exposing a new volume of material to each beam pulse. Two possible configurations are shown in Figs. 3-6 and 3-7. During the target development stage the wedges shown in Fig. 3-6 will contain different materials to allow for comparative testing. Provision is also being made to test stationary targets of the CERN design.

The target must have a high density and high melting point. A compilation of mechanical properties for different materials was performed. A figure of merit to compare the mechanical properties is given by the yield stress divided by the coefficient of thermal expansion and the modulus of elasticity. On this basis rhenium, tungsten and tungsten-rhenium alloys are in increasing order for this figure of merit. The coefficient of heat conductivity could also be included in the figure of merit without significantly altering the choice of material.

The high-temperature behavior of tungsten-rhenium alloys shows considerable increase of yield stresses with respect to tungsten, but little change in the coefficient of thermal expansion or the modulus of elasticity. Tungsten-rhenium alloys are utilized in industry for high-temperature applications such as incandescent-lamp wire and targets for high-power x-ray tubes. A significant amount of experience with the technology for their fabrication exists. Tungsten has been used for all β yield calculations, although a number of target configurations will be tested during the R & D phase of the target-station development. A summary of the target parameters is given in Table 3-II.

TABLE 3-II TARGET PARAMETERS

Target Material	Tungsten/Tungsten Alloys
Length	5 cm
120 GeV protons/pulse	2.0×10^{12}
Total Beam Energy	3.46×10^4 Joules
Repetition Rate	0.5 Hz
Beam Pulse Duration	1.6×10^{-6} sec
Energy Deposited/proton	1.26 GeV (1.81×10^{-10} Joules)

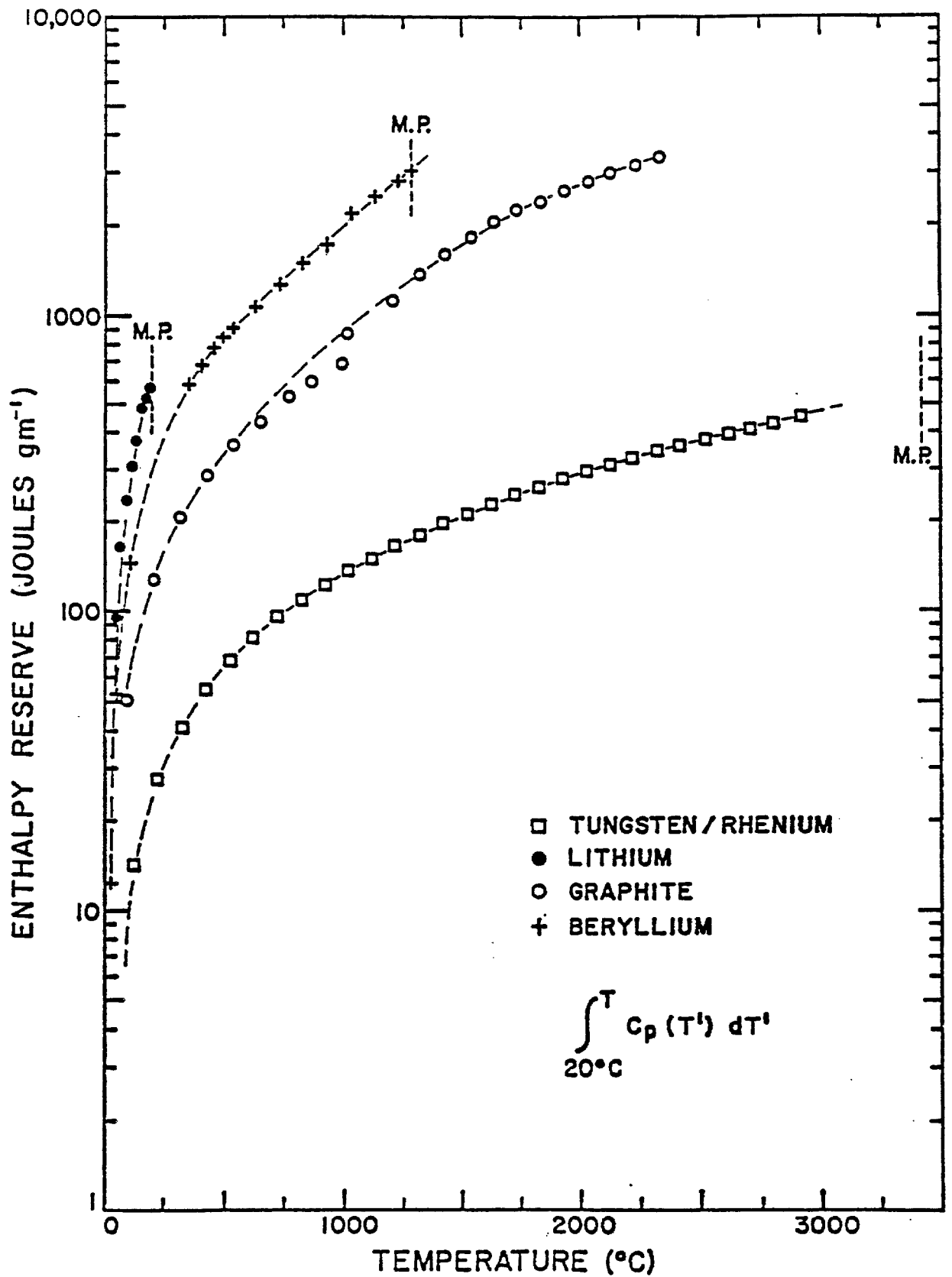
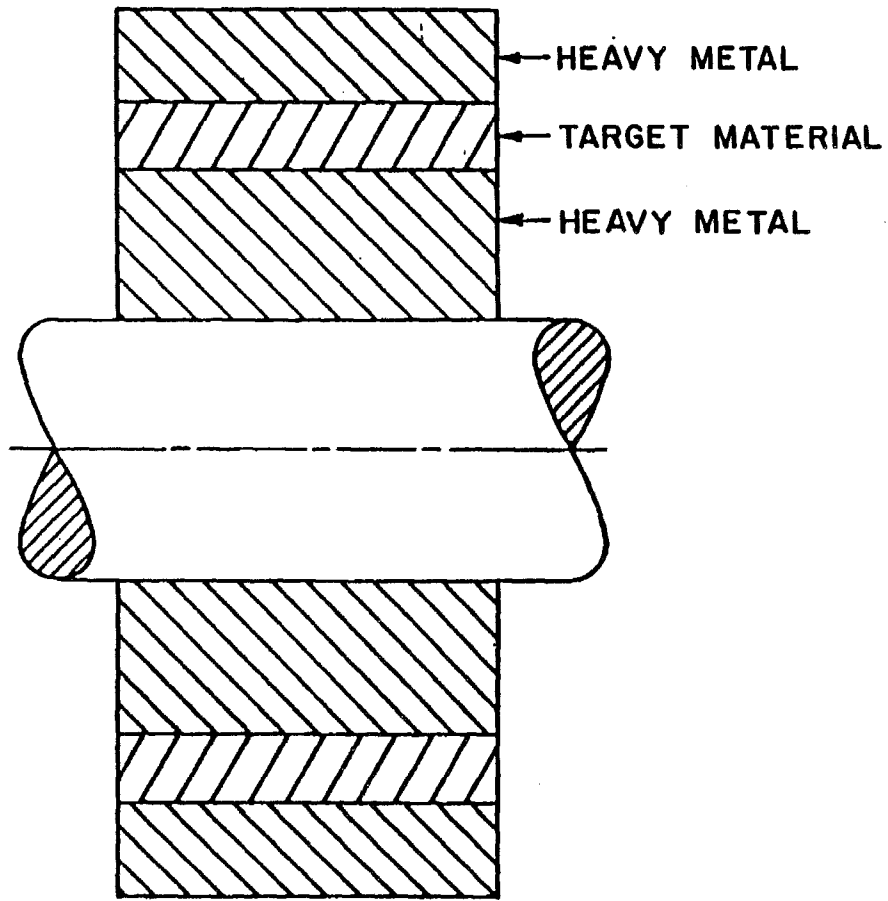


Figure 3-5



0 1 2 3 4 5 cm

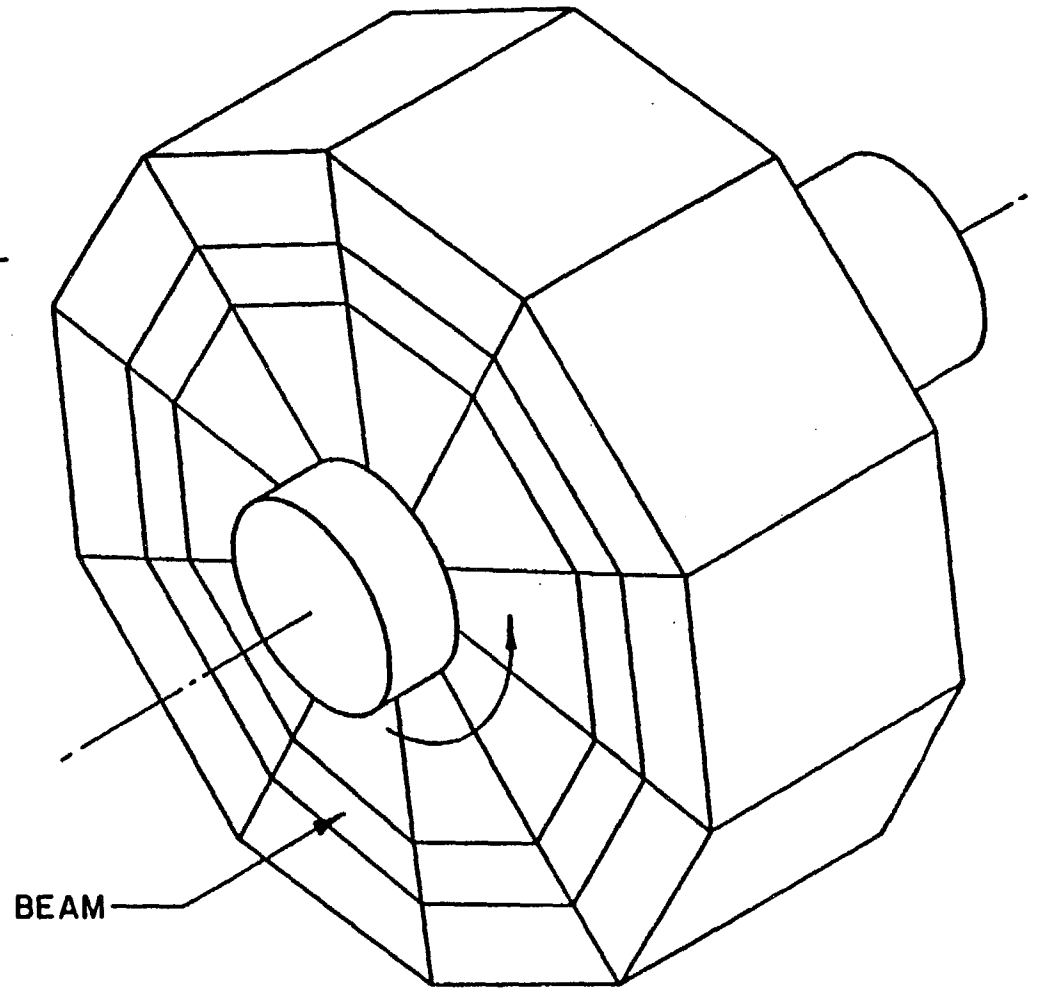


Figure 3-6

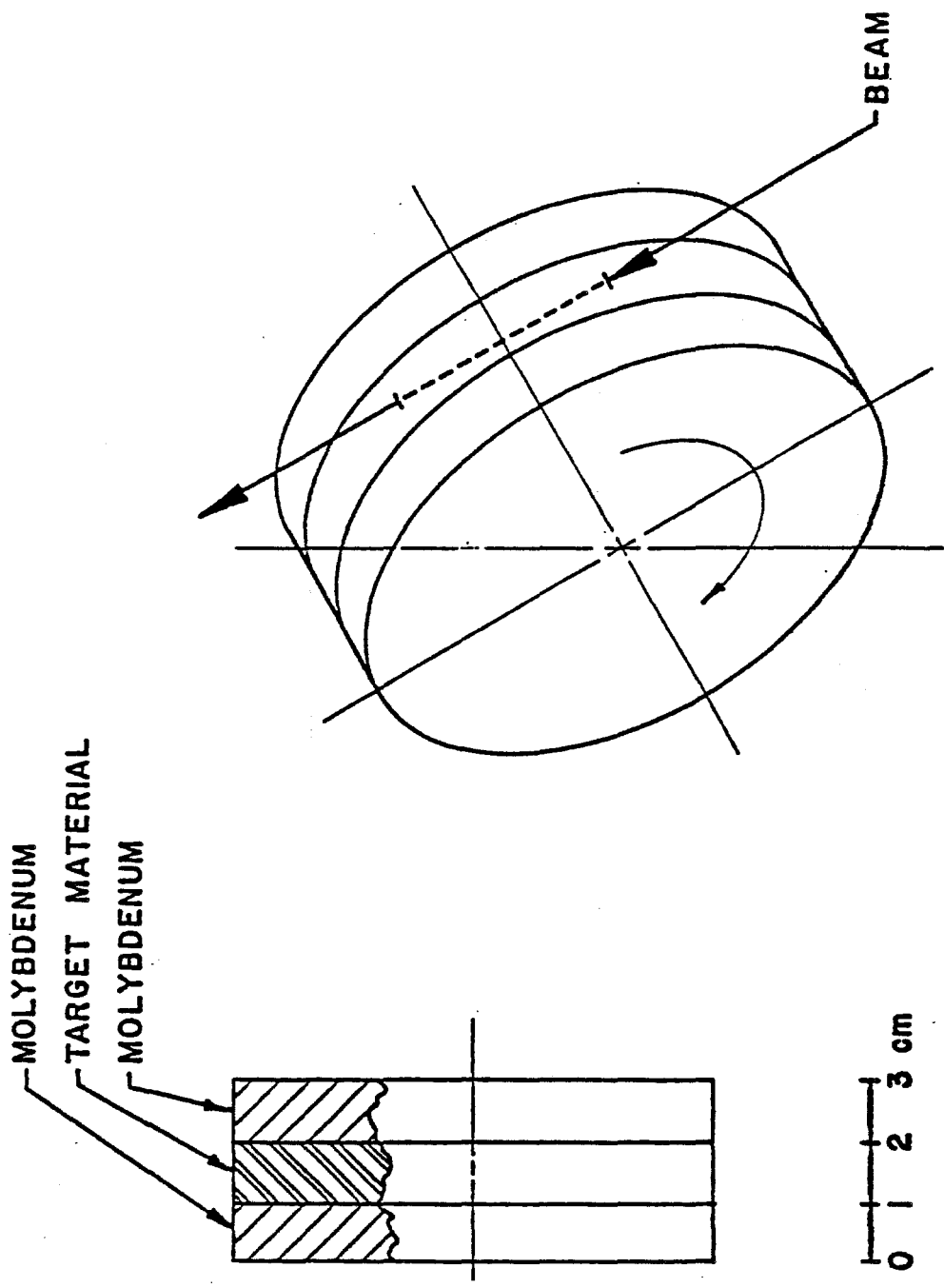


Figure 3-7

Energy Deposited/pulse	346 Joules
Power Deposited	173 Watts
Average Temperature	100°C
Beam Size ($\sigma_x = \sigma_y$)	0.038 cm
Peak Energy Density/proton	13.4 GeV/cm ³
Peak Energy Density/pulse	200.0 Joules/gm
Peak Temperature Rise	<1500.0°C

CERN

Peak Energy Density ⁺	>185 Joules/gm
Peak Temperature Rise	1500°C
Average Temperature	800°C

⁺This rhenium target has been used for some time with no failures.

3.2.2 Antiproton Collection; the Lithium Lens. A study has been made of the relative merits of \bar{p} collection schemes that utilize a lithium lens, a pulsed quadrupole multiplet, or a conventional quadrupole triplet.² Since it was found that the lithium lens is far more efficient for the collection of \bar{p} 's, this section concentrates on the lens. The other options that are discussed will be pursued if the lens development lags.

The basic physical principle of the lithium lens is that a uniformly distributed electric current in a cylindrical conductor produces an azimuthal magnetic field with a constant radial gradient. Charged beam particles traversing the length of such a conductor experience a force that focuses them toward the axis. Lithium is an appropriate material for such a focusing device because it is the least-dense solid conductor, thereby minimizing \bar{p} absorption and multiple scattering.³ The lens under development uses a 15-cm long lithium cylinder of radius 1 cm and requires a current of 0.5 MA to produce the desired gradient of 1000 T/m. Joule heating caused by direct current in the lithium is prohibitively large, so a 0.6 msec full-width unipolar sine-like pulse of amplitude 0.5 MA will be applied every 2 sec. Each pulse will generate about 6000 Joules of heat and the problem of removing this heat dominates the mechanical design of the lens. It is desirable to keep the average temperature well below the 180°C melting point of lithium because the 1.5% volume expansion that occurs upon melting could shorten the lifetime of the lens. The magnetic induction H created by the pulsed current does not have a constant radial gradient, due to the skin effect. Fig. 3-8 shows the variation of H/H_{\max} during one pulse.⁷

Energy deposition in a lithium lens located 14.5 cm (one focal length) downstream of a 5-cm tungsten target was calculated using the program MAXIM. Contributions from secondaries emerging from the target as well as from non-interacting 120 GeV protons were included. The heating due to the beam was found to be small compared to Joule heating.⁸

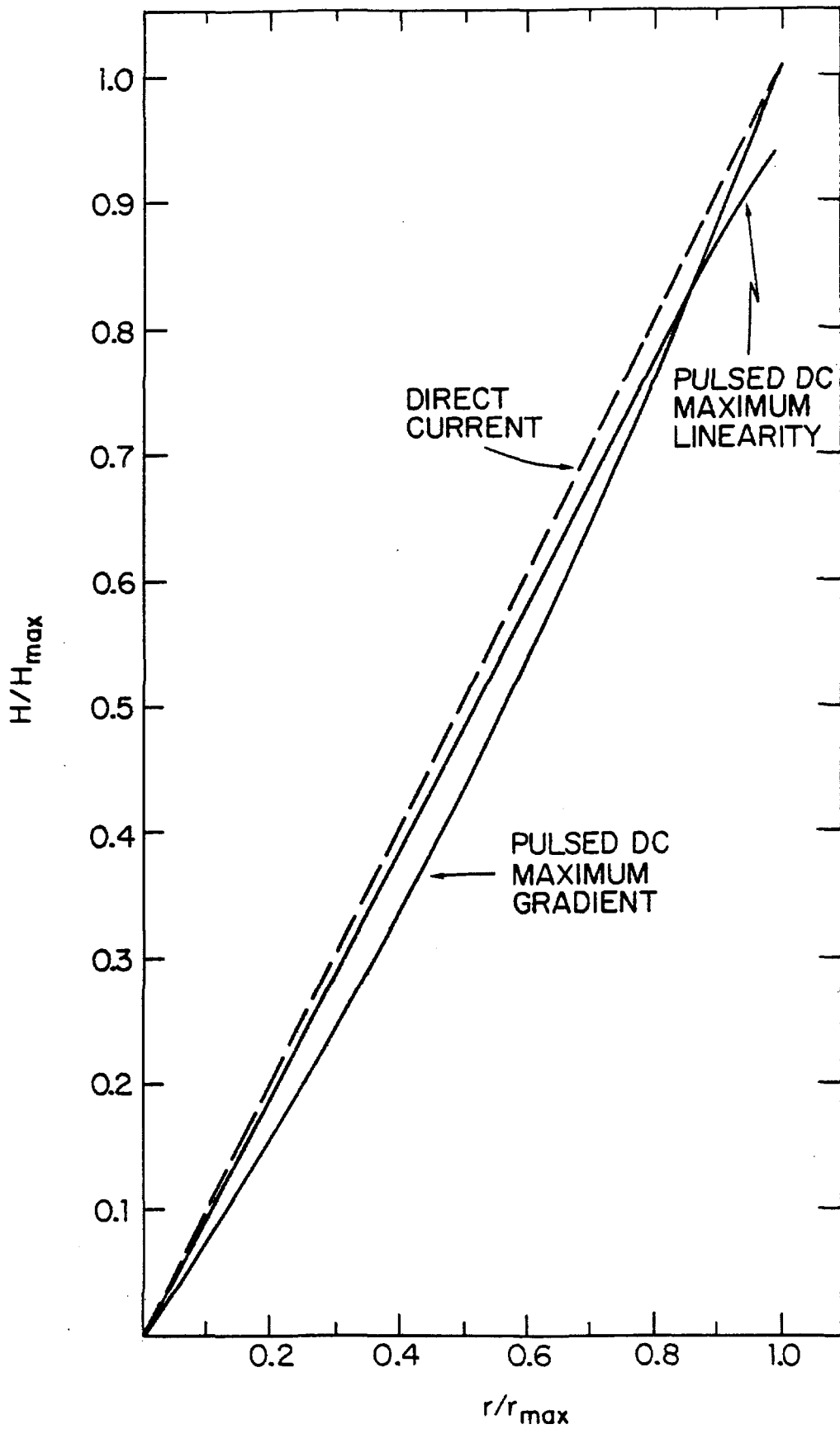


Figure 3-8

In case the lithium-lens development lags, linear and non-linear horns of the types developed for the CERN AA ring could be utilized. To optimize the \bar{p} rate, they require significantly longer targets. Preliminary results indicate that horns would not provide as good a collection efficiency as the proposed lithium lens at our p energy. The larger currents required for the 8.89 GeV/c \bar{p} 's, as compared with 3.5 GeV/c at CERN, may make the horn construction very difficult. Another option would be to install a 5Q36 triplet.² This would limit the \bar{p} production system to small momentum spreads and emittances, but could be useful in the early stages of running.

3.2.3 Antiproton Selection. Downstream of the lithium lens, a pulsed dipole magnet will be used to select negative particles of energies near 8 GeV. Particles not selected, the remnants of the 120 GeV proton beam and other interaction products, continue towards the beam dump. The 8 GeV antiprotons pass through a channel in the beam dump and then into the transport line to the debuncher ring.

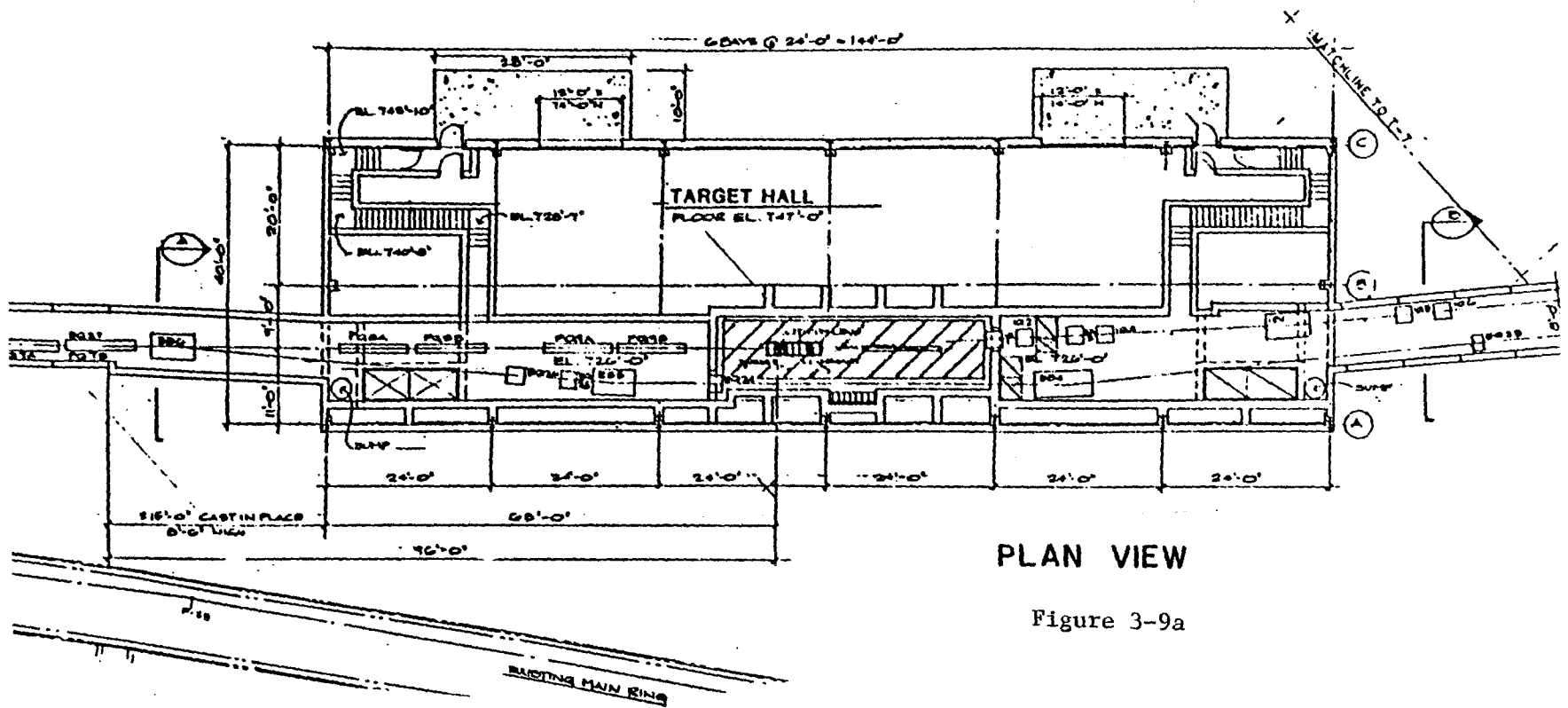
The pulsed magnet will be a dipole powered by a capacitive discharge supply similar to that of the lithium lens. The current pulse will be a half sine wave with $\omega = 1200$ hz. The magnet aperture will be 3 x 3 cm, and the field integral will be 1.55 Tesla-meter. This will provide a 3° bend in the antiproton beam.

3.3 Target Hall

The antiproton production target, proton beam dump and the lithium lens for antiproton collection will be located in a vault downstream of the final quadrupole focusing system in the 120-GeV proton line. The dimensions of this vault are planned to be 7 ft by 33 ft with the floor located at 17 ft below grade, as shown in Fig. 3-9a, and 3-9b.

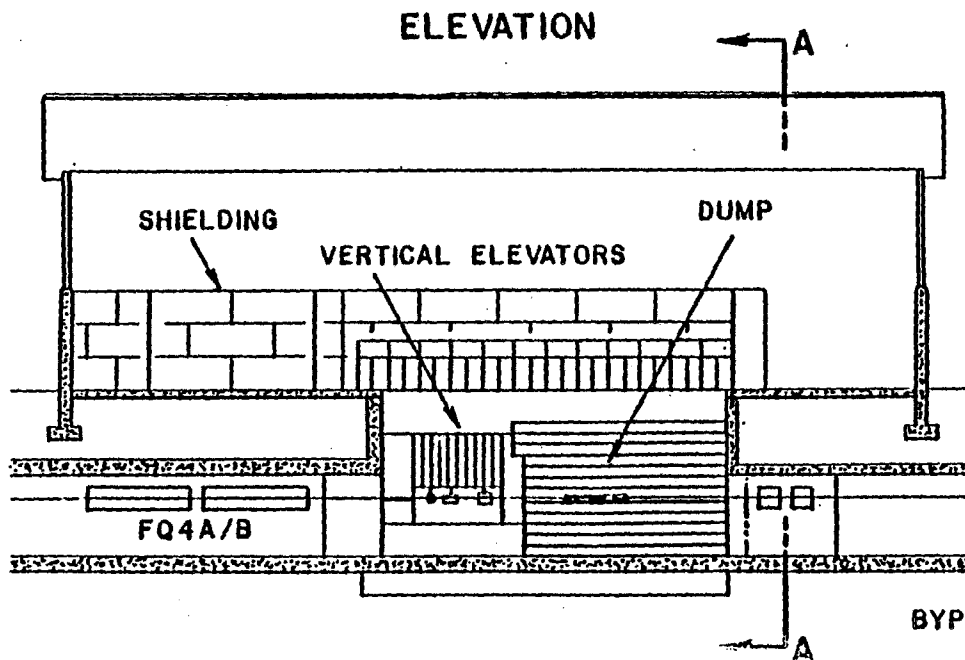
The upstream end of the hall is separated from the proton-beam transport tunnel by 3 ft of steel shielding. Further shielding is placed around the external walls of the vault in the earth. Below the vault two separate impermeable membranes are used to collect irradiated ground water. Shielding configurations that limit the irradiations of the soil and the above-ground fluxes to permissible values have been designed to allow operation at an intensity of 10^{13} protons per second.

Downstream of the upstream end of the shield, within the target vault, a 3 ft high by 8 ft long and 2 ft wide volume of space is available for components. The space between this volume and the concrete walls and floors of the vault is filled with steel shielding. Access to the target station components is accomplished by raising one of a set of solid steel elevators into the Target Service Building. Each elevator segment extends 10 in. along the beam direction and 24 in. transverse to the beam. Each is 7 ft long in the vertical direction. The components are suspended from the bottom of the elevator. The 7 ft length makes it possible to place electronics and control systems immediately above each elevator segment without danger of radiation damage. An additional 3 ft of concrete is

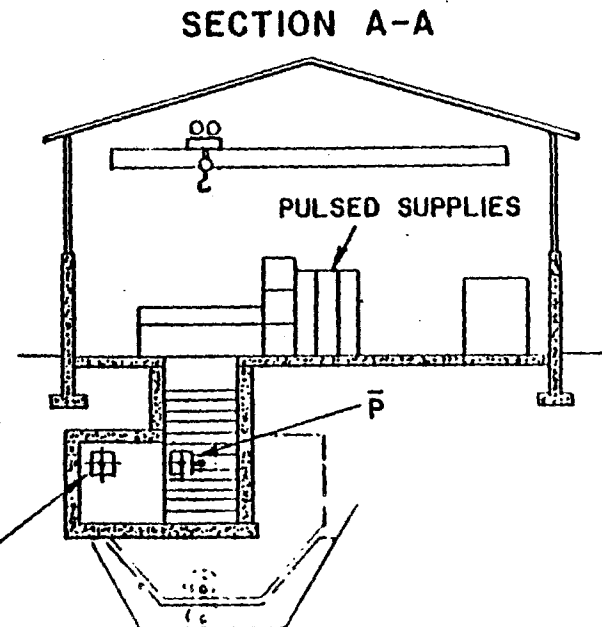


PLAN VIEW

Figure 3-9a



ELEVATION



SECTION A-A

Figure 3-9b

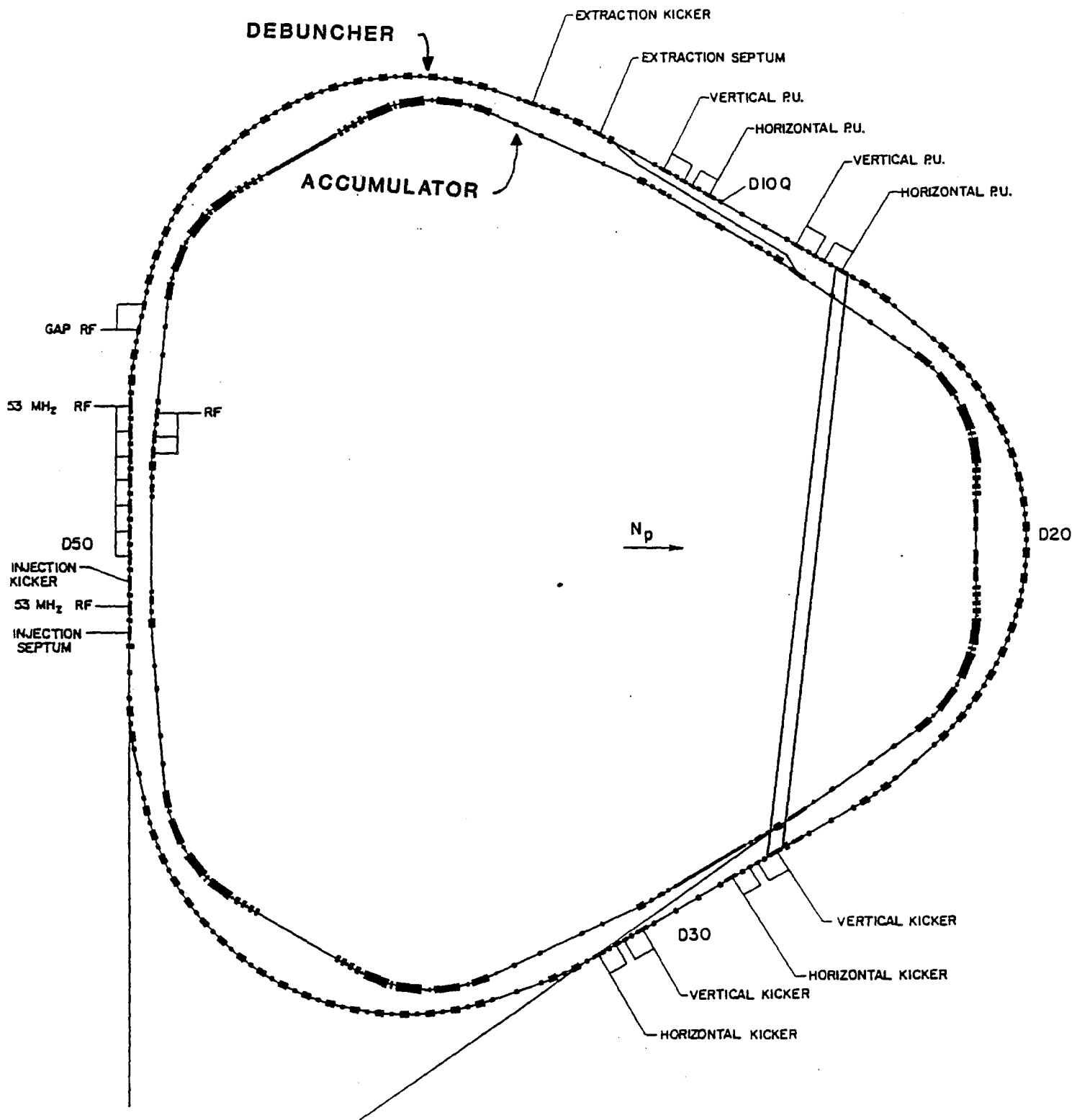
required to keep the above-ground radiation levels within the Target Service Building below the maximum permissible level. Within the Target Service Building and surrounding the vault, a shielded area incorporating thick windows will be used to exchange elevator segments remotely. Work will be performed on components with remote manipulators. The manipulators will be used to exchange targets routinely. Access to the electronics at the top of the elevator segments will be possible when beam is not being delivered to the target station.

The last component in the beam before the dump is a pulsed magnet to bend the \bar{p} 's to the right by 3° , in order to separate them from the protons. The dump is a water-cooled graphite core 6 ft long surrounded by a steel jacket which fills the inside of the vault. The steel extends for 22 ft along the proton beam. The construction is similar to the dump developed for the Tevatron abort system.

Transport of the 8-GeV antiprotons to the Debuncher is discussed in Sec. 11.2.

References

1. "Calculation of Yields for the Fermilab Antiproton Source" Carlos Hojvat and A. Van Ginneken, Fermilab-Pub-82/43, 1982 (submitted to Nucl. Inst. Meth.)
2. E. Colton, "More on Antiproton Collectors," \bar{p} note #120, Fermilab (unpublished).
3. B. F. Bayanov et al., "A Lithium Lens for Axially Symmetric Focusing of High Energy Particle Beams," Nuc. Inst. Meth., 1909(1981).
4. "MAXIM - Program to Simulate Cascades in Bulk Matter." A. Van Ginneken, Fermilab FN-272 (January 1975).
5. "High Intensity Targeting Workshop," Fermilab April 28-30, 1980.
6. F. Krienen and F. Mills, Spreading the Hot Spot on the Target, \bar{p} Note 70. E. Colton, \bar{p} Note 107.
7. "Skin Effect in Electrically Pulsed Cylindrical Conductors used as Focusing Devices," A.J. Lennox, Fermilab Report FN-379, January, 1983. "Optical Properties of Cylindrical Lenses," T.A. Vsevolozhskaya et al, Sov. Phys. Tech. Phys., Volume 20, No 12, 1556 (1976).
8. "Energy Deposition in the Lithium Lenses," A.J. Lennox, \bar{p} Note 204, Fermilab 1982 (unpublished).



DEBUNCHER LAYOUT

Figure 4-1

CHAPTER 4

DEBUNCHER RING4.1 Purpose of the Debuncher

The primary purpose of the Debuncher is to reduce the large momentum spread of the 8-GeV \bar{p} beam at production to 0.2% or less prior to injection into the Accumulator. This reduction is done by rf bunch rotation and adiabatic debunching after the \bar{p} beam is injected into stationary 53-MHz buckets in the Debuncher. The debunching time is only slightly longer than 10 msec, and there are therefore nearly two seconds available for cooling before the beam is transferred to the Accumulator. Stochastic cooling of betatron amplitudes has been shown to be feasible, and a betatron cooling system to reduce the emittance by a factor of 3 in both planes in 2 sec is included in the design.

A possible addition that is still being examined is a fast momentum stochastic precooling step to reduce even further the momentum spread by a factor of 2 or possibly 3, in 2 sec.

Table 4-I gives parameters of the Debuncher.

TABLE 4-I THE DEBUNCHER RING

Kinetic Energy	8.0 GeV
γ_t , transition energy	7.6482
$\eta = 1/\gamma_t^2 - 1/\gamma^2$	0.00608
Average Radius	80.42 m
RF Frequency	53.103 MHz
Maximum rf voltage	5 MV
Number of \bar{p} bunches injected	80
Harmonic number	90
Beam Gap for Injection Kicker	200 nsec
Momentum Aperture, $\Delta p/p$	4%
Betatron Acceptance, h and v	20π mm-mrad
Betatron Tunes, h and v	9.75
Natural Chromaticity, h and v	-10
Periodicity	3, each with mirror symmetry
Max amplitude function β	20 m
Max dispersion value	2.1 m
Phase Advance per Cell, h and v	60°

4.2 Requirements of the Design

As shown in Fig. 4-1, the Debuncher ring surrounds the Accumulator. Because of the triangular shape of the latter, a periodicity of three was chosen for the Debuncher, each period with mirror symmetry.

The Debuncher operates at a kinetic energy of 8 GeV. Its circumference must be at least as long as each antiproton pulse, made of 80 narrow bunches with a separation frequency of 53.1 MHz. The circumference was chosen to be 505 m, which corresponds to an rf harmonic number of 90. This arrangement allows a separation of 12 ft between the Debuncher and the Accumulator in the long straight sections so that these portions of the two rings can be accommodated in the same wide tunnel.

Each superperiod includes a long straight section. These accommodate: (i) injection, (ii) extraction, (iii) rf cavities for the bunch rotation, (iv) pickups and kickers for stochastic cooling. The phase advance between pickups and kickers should be an integer number of betatron waves $\pm 90^\circ$. This gives only a few possible choices for betatron tunes, which we take to be approximately the same in the two planes. The value 9.75 was finally chosen.

Another requirement is that the three long straight sections must have zero dispersion, an important requirement for the performance of stochastic cooling and for avoiding betatron-synchrotron coupling.

Finally the Debuncher is capable of accepting a momentum spread of $\pm 2\%$ and has a betatron acceptance of at least 20π mm-mrad in both planes.

4.3 Choice of Transition Energy

The most important parameter in the design of the Debuncher is the dispersion

$$\eta = 1/\gamma_t^2 - 1/\gamma^2$$

where γ is the relativistic energy factor and γ_t corresponds to the transition energy. The rf voltage needed for bunch rotation is proportional to $|\eta|$. If $|\eta|$ is less than 0.002, the variation of η with momentum will degrade the final momentum spread. On the other hand, a larger value of $|\eta|$ helps betatron cooling and is needed if momentum precooling is to be done in the future. We have reached a compromise by setting $\eta = 0.006$, which corresponds to $\gamma_t = 7.65$, a solution which gives $\nu_H \approx 9.75$. This choice corresponds to operating the Debuncher Ring above the transition energy.

We could also have chosen to operate below the transition energy (larger value of γ_t) because only the absolute value of η enters. We considered this possibility at the beginning of the design, but rejected it for the following reasons. A larger value of γ_t , and therefore of the strength of the lattice focusing, is desirable because it makes the dispersion and betatron amplitude functions small, which would also make the physical aperture of the magnets smaller. But larger values of γ_t would also lead to an unfortunately large natural chromaticity. To correct this, too much sextupole correction was required considering the smaller

dispersion around the ring. To eliminate problems intrinsic to sextupoles and chromaticity, we had to decrease the focusing of the ring to the present value of $Y_t=7.65$. When this was done, the dispersion of the ring doubled, but we could still manage to achieve the required momentum and betatron acceptance with reasonably small-aperture magnets.

With this choice of η , one still requires 5 MV peak rf voltage at 53 MHz for bunch rotation.

4.4 Lattice

We have opted for a smooth lattice to help stability of the ring against sextupoles and chromatic effects. The ring is divided into 57 FODO cells, each with a phase advance of 60° in each plane. One half a superperiod is shown in Fig. 4-2 with beta- and dispersion-function plots. In the curved sections of the ring, the cells are regular; bending magnets are placed exactly halfway between quads. The long straight sections are made of 6 cells, each without bending magnets. A "dispersion-killer" cell is located at each end of the long straight section. Zero dispersion is achieved by eliminating the two bending magnets just before the last regular cell. A regular cell is shown in Fig. 4-3.

Two fortunate features are obtained with this lattice: (i) the beta functions never exceed 20 m in either plane. This makes the beam size in the long straight sections small enough to fit in the aperture of stochastic-cooling pickups and kickers, which have a gap between plates of 30 mm (suitable for 2-4 GHz bandwidth). (ii) The chromaticity of the ring is reduced to a minimum of -10. In an earlier design, each long straight section was made of three consecutive low-beta insertions. To do this, four quadrupole triplets were required to provide room for stochastic-cooling devices, rf cavities and injection and extraction equipment. It has been found that these triplets added substantially to the natural chromaticity and it was therefore decided to bridge the long straight sections with regular FODO cells.

The beam envelope is shown in Fig. 4-4 for half of a superperiod. It corresponds to a momentum spread of 3% and an emittance of 20π mm-mrad in both planes.

4.5 Magnets

There is only one kind of each dipole in the design. The dipoles are 1.66 m long (effective length), have a full gap of 6 cm and have a strength of 17 kG. There are three kinds of quadrupoles. The dipole and quadrupoles are described in Table 4-II. There is one kind of sextupole. The sextupoles are discussed in Sec. 4.7.

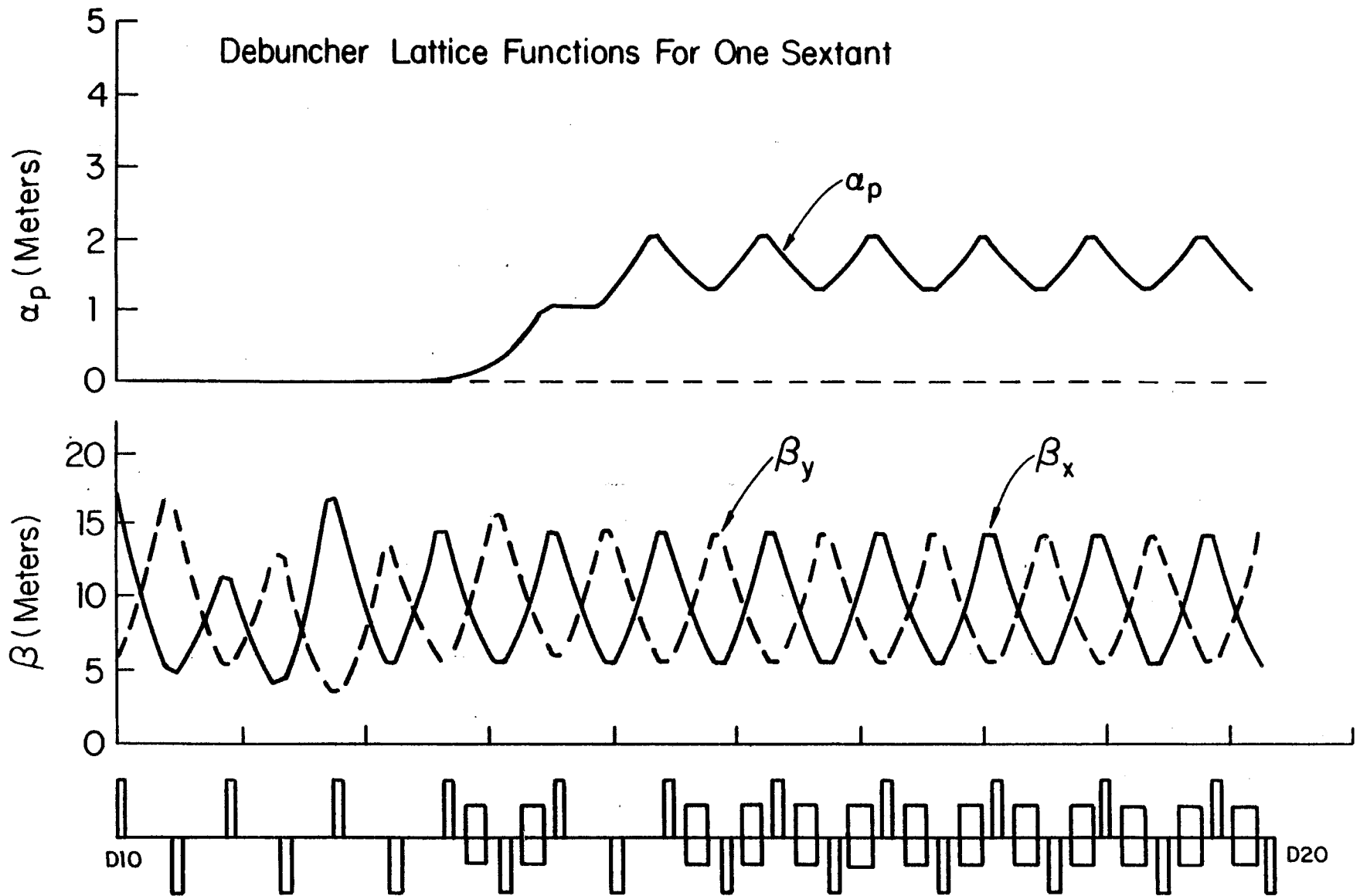


Figure 4-2

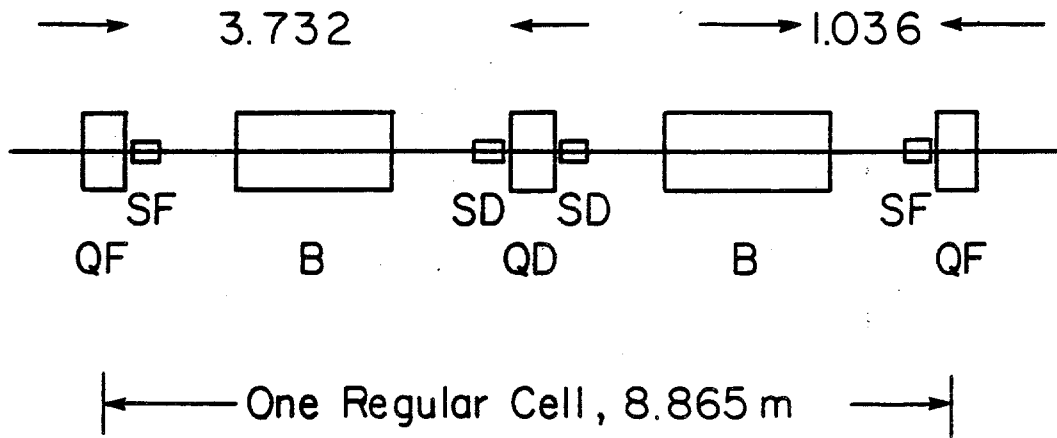
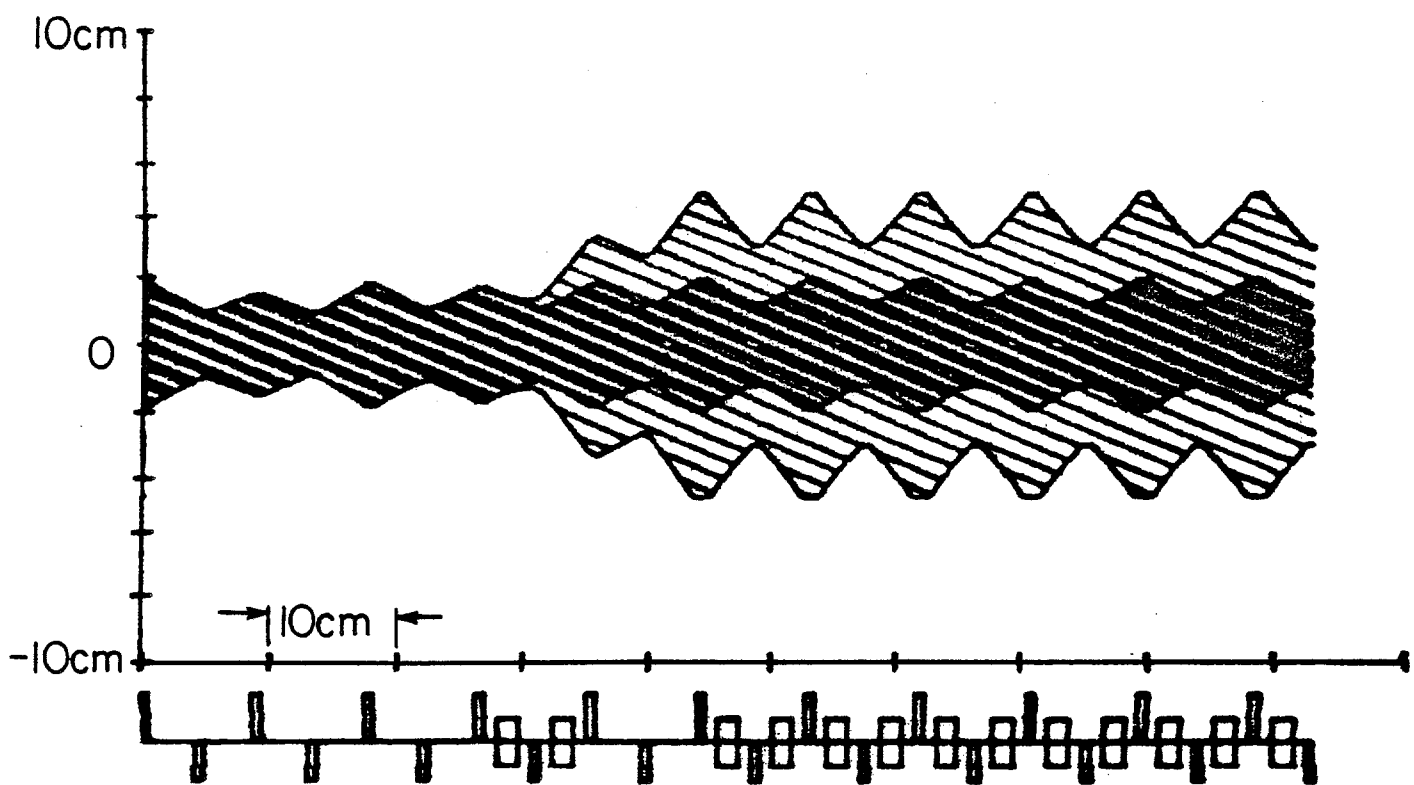
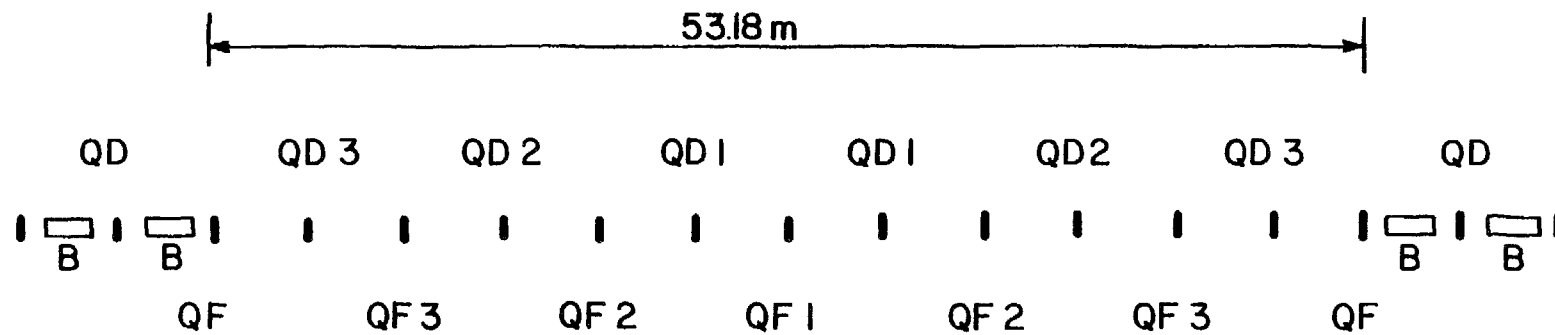


Figure 4-3



Beam Envelopes for $\Delta P/P = 3\%$ and $E = 20\pi$ mm-mrad



QUADRUPOLE LENGTHS: QF1, QF 2, QD1, QD 2 = 27.6 in
 QF 3, QD3 = 32.6 in
 DISTANCE BETWEEN QUADRUPOLE CENTERS = 4.43 m

DEBUNCHER LONG STRAIGHT SECTION

Figure 4-5

TABLE 4-II DEBUNCHER MAGNETS

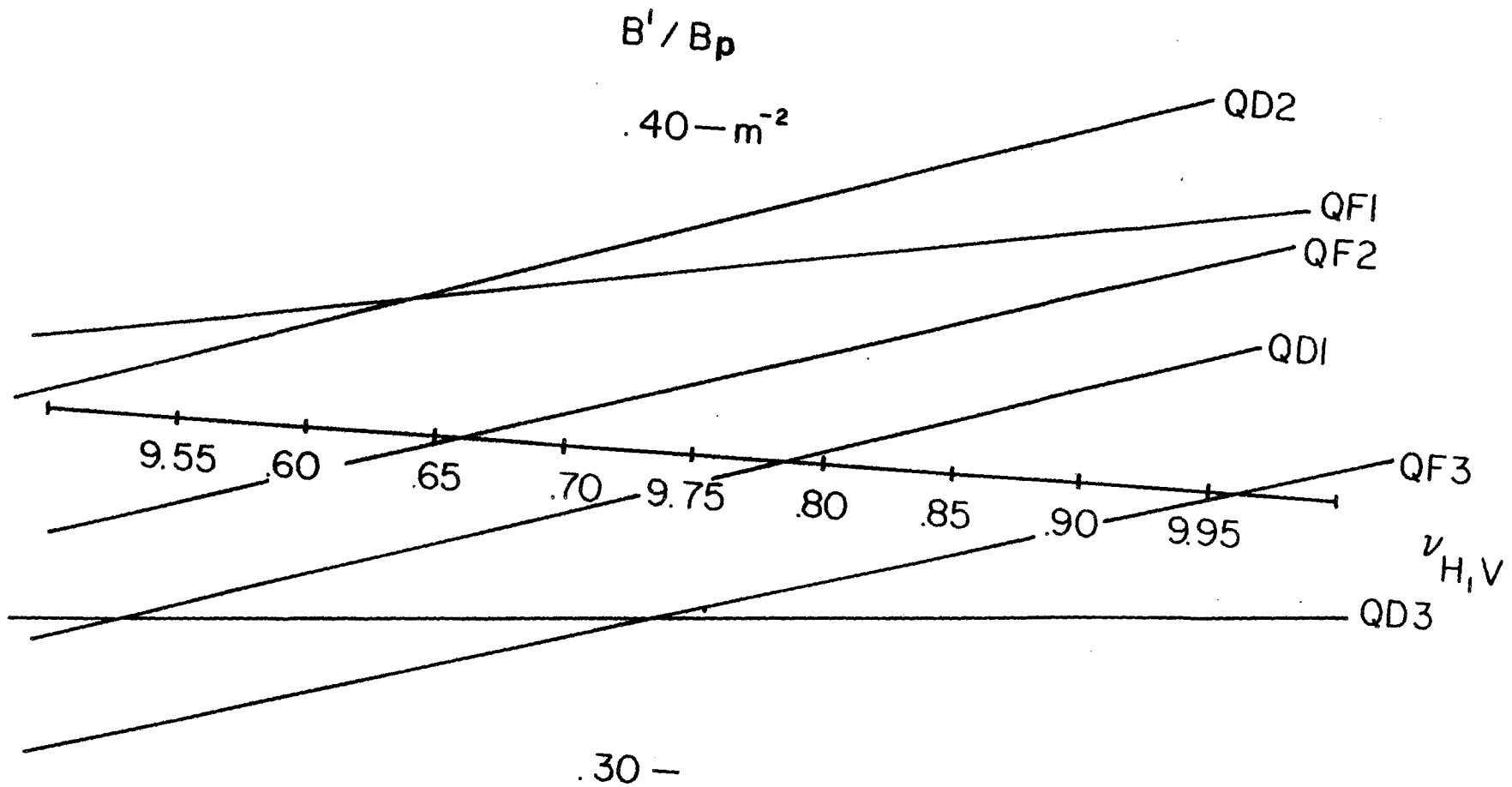
	<u>Number</u>	<u>Effective Length</u>	<u>Strength</u>	<u>Gap or Poletip Radius</u>
Dipoles:				
B	66	1.6604 m	1.7 T	66 mm
Quadrupoles:				
I. QF, QD QF1, QD1 QF2, QD2	102	27.6 in.	12 T/m	44.5 mm
II. QF3, QD3 small aperture	9	32.6 in.	10.5 T/m	44.5 mm
III. QF3, QD3 large aperture	3	32.6 in.	10.5 T/m	84.1 mm

There are two effective quadrupole lengths: 27.6 in. and 32.6 in. The longer quadrupoles are located in pairs at both ends of each long straight section as shown in Fig. 4-5 which shows a long straight section with the neighboring regular cells. All the other quadrupoles are shorter. All quadrupoles have the same aperture, with a poletip radius of 44.5 mm, except for three special ones that have a poletip radius of 84.1 mm. These quadrupoles are marked with an L in Fig. 4-1 and are also used in conjunction with beam transfer from and to several directions. The maximum gradient required is 12 T/m and somewhat less for the large aperture quadrupoles. The total magnet power to operate the ring at 8 GeV is 1.1 MW.

A detailed set of specifications for the magnets is given in Chapter 12.

4.6 Tuning

A nominal tuning mode has been worked out with betatron numbers $\nu_H=9.73$ and $\nu_V=9.77$. To obtain this, the regular cells have exactly 60° phase advance in both planes to give zero dispersion in the long straight sections. The quadrupoles in the long straight sections have been adjusted to get the required tune values with proper matching at the transition between the curved and straight sections. A waist is introduced in the middle of each long straight section and curved sector. The settings for all the magnets are given in Table 4-III for the nominal tune.



Variation Of B' / B For Each Type Of Quadrupole

Figure 4-6

TABLE 4-III MAGNET SETTING FOR THE TUNING MODE: $\nu_H=9.73$, $\nu_V=9.77$

B = 1.7 T
 $B\rho = 29.6501$ T-m

<u>Quadrupoles</u>	<u>$B_0/B\rho$</u>	<u>Current</u>	<u>Voltage</u>
QF	0.33652 m ⁻²	240 A	9.7 V
QD	0.32928	235	9.5
QF1	0.37747	270	10.9
QD1	0.34714	248	10.0
QF2	0.35881	256	10.3
QD2	0.38679	276	11.1
QF3 large	0.32494	1313	10.5
QD3 aperture	0.32459	1311	10.5
QF3 small	0.32494	232	10.4
QD3 aperture	0.32459	232	10.4

To achieve other betatron tune values, the strength of the regular quadrupoles QF and QD in the bending section is left unchanged, so that the phase advance/cell will remain 60°. With this mode of operation, the "dispersion killer" is always effective and the dispersion in the long straight section is always cancelled. To change the betatron tune, only the strengths of the six quadrupoles QF1, QD1, QF2, QD2, QF3 and QD3 in the long straight sections are varied. The search for the quadrupole setting is done by imposing the condition of matching between the long straight sections and the curved sections and of waists in the middle of both of them. It is possible to vary both tunes over the range from 9.5 to 10.0 by keeping them equal. The variation of $B_0/B\rho$ for each quad is shown in Fig. 4-6. The transition energy remains unchanged in this range. The variation of β_H and β_V , the maximum values of the horizontal and vertical beta functions in the space occupied by the pickups and kickers for the stochastic cooling, is given in Fig. 4-7. In the same figure, we give the variations of the natural horizontal and vertical chromaticities.

4.7 Sextupoles

Sextupoles are located next to each quadrupole, usually on both sides, as shown in Fig. 4-2. They are divided in two groups: those next to the horizontally focusing quads (SF) and those next to the vertically focusing quads (SD). The main purpose of these sextupoles is to correct and adjust the natural chromaticity of the ring. They are therefore elements of primary importance and are on an equal footing with the dipoles and quadrupoles. They are not intended to correct magnet errors and imperfections.

Their strength has been calculated with PATRIS, a particle tracking code that is a heavily modified version of PATRICIA suitable for protons.

Variation Of Lattice Functions Across A Cooling Straight Section

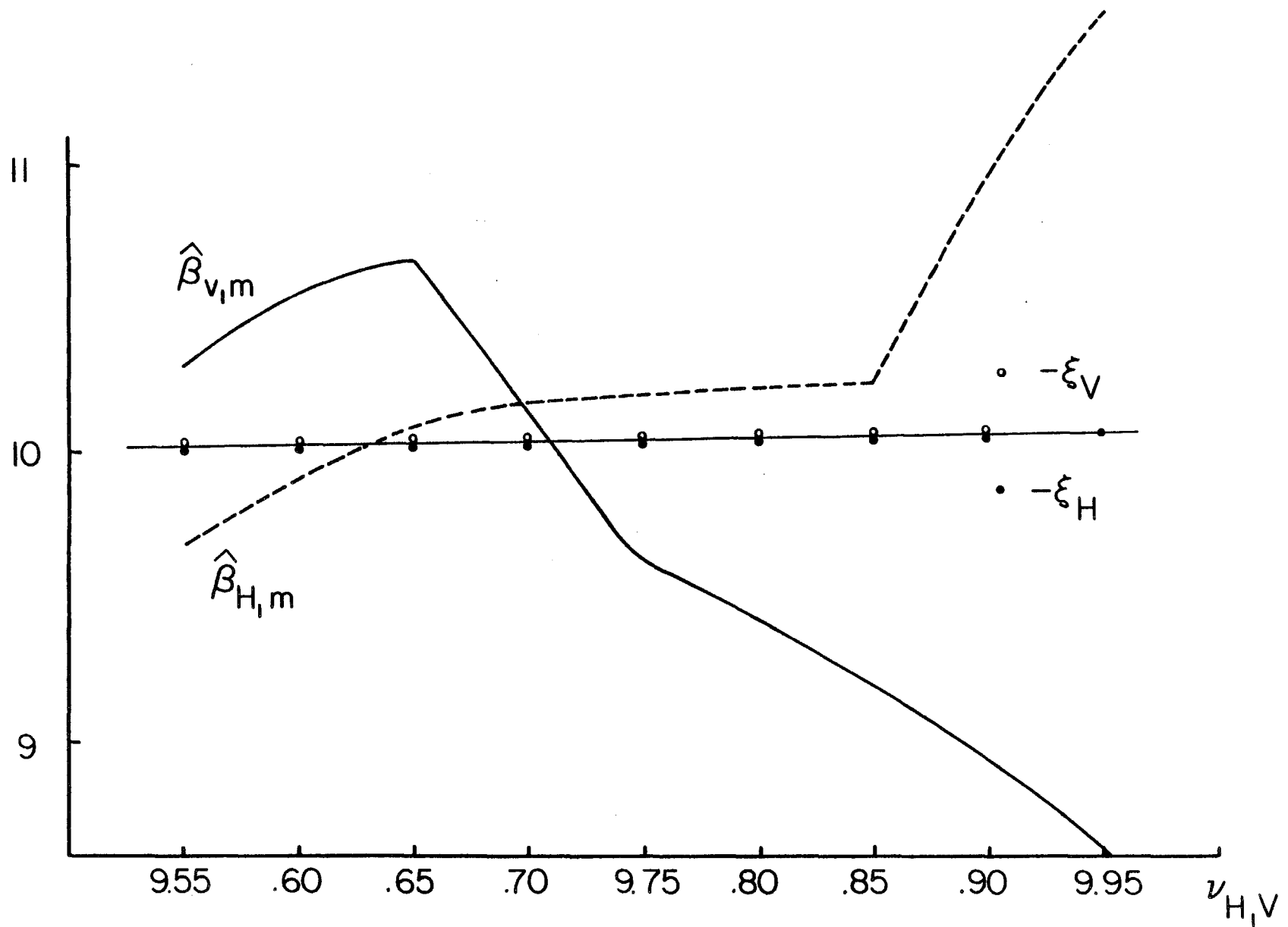
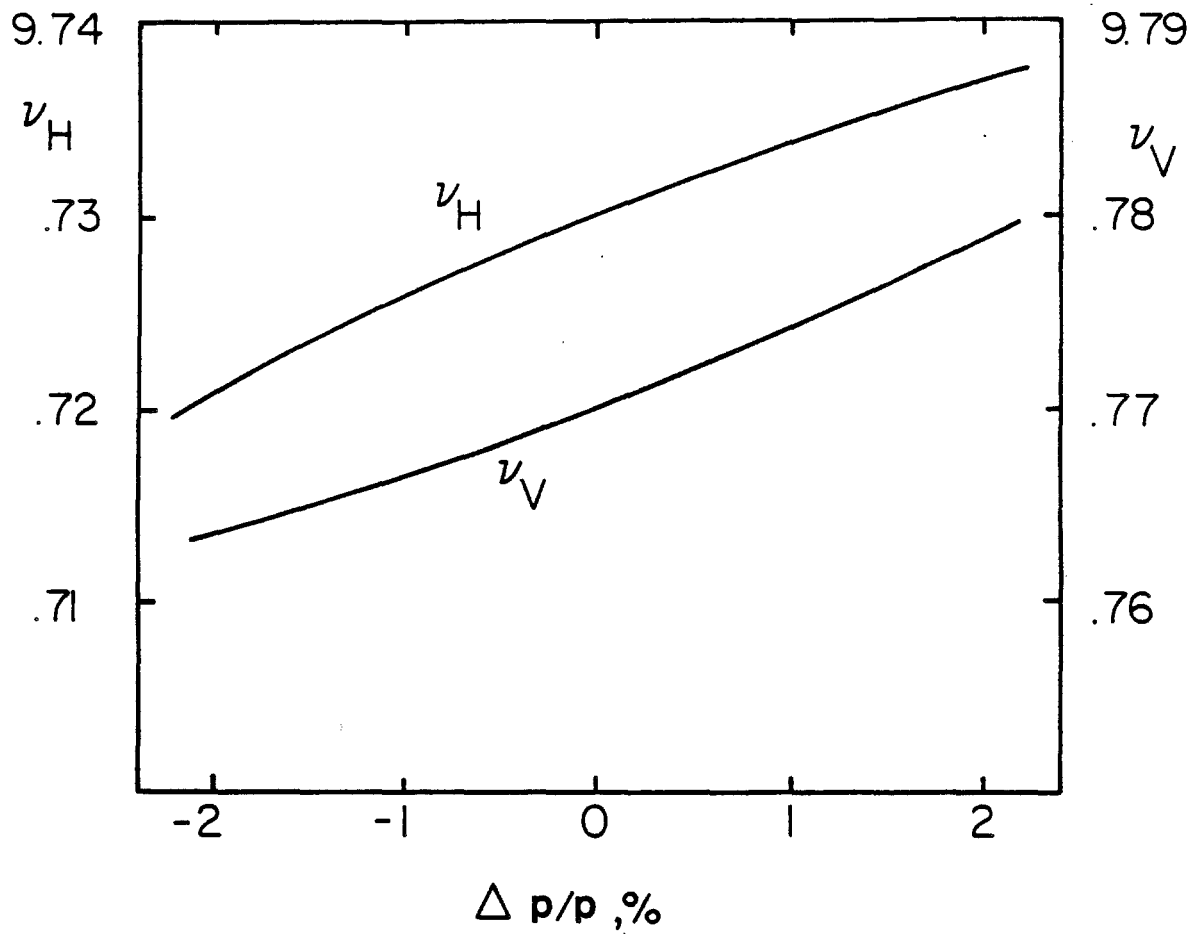


Figure 4-7



Variation Of Tunes With Momentum

The thin-lens approximation has been used. The sextupole strength given in Table 4-IV corresponds to zero chromaticity. The lattice variations with momentum have then been calculated with SYNCH. The results are shown in Fig. 4-8, which gives the variation of the betatron tunes with momentum, Fig. 4-9, which gives the change of $\alpha=1/\gamma_c^2$, the momentum compaction factor, and Fig. 4-10 which gives β_H , β_V and α_p versus $\Delta p/p$ at the downstream end of the injection kicker. Figure 4-11 gives the tune diagram with the working point for the reference tuning mode and the tune spread for $\pm 2\%$ beam momentum spread. Finally, Fig. 4-12 gives the variation of β with momentum along the ring circumference for half of a superperiod. As one can see, the variations are very modest, less than 10%.

TABLE 4-IV DEBUNCHER SEXTUPOLE DISTRIBUTION

Type	SF	SD
Number	72	66
B'' ℓ	0.141 m \geq^2	-0.213 m \geq^2

The design specifications for the sextupoles are given in Table 4-V. The power per magnet is so small that no water cooling is needed.

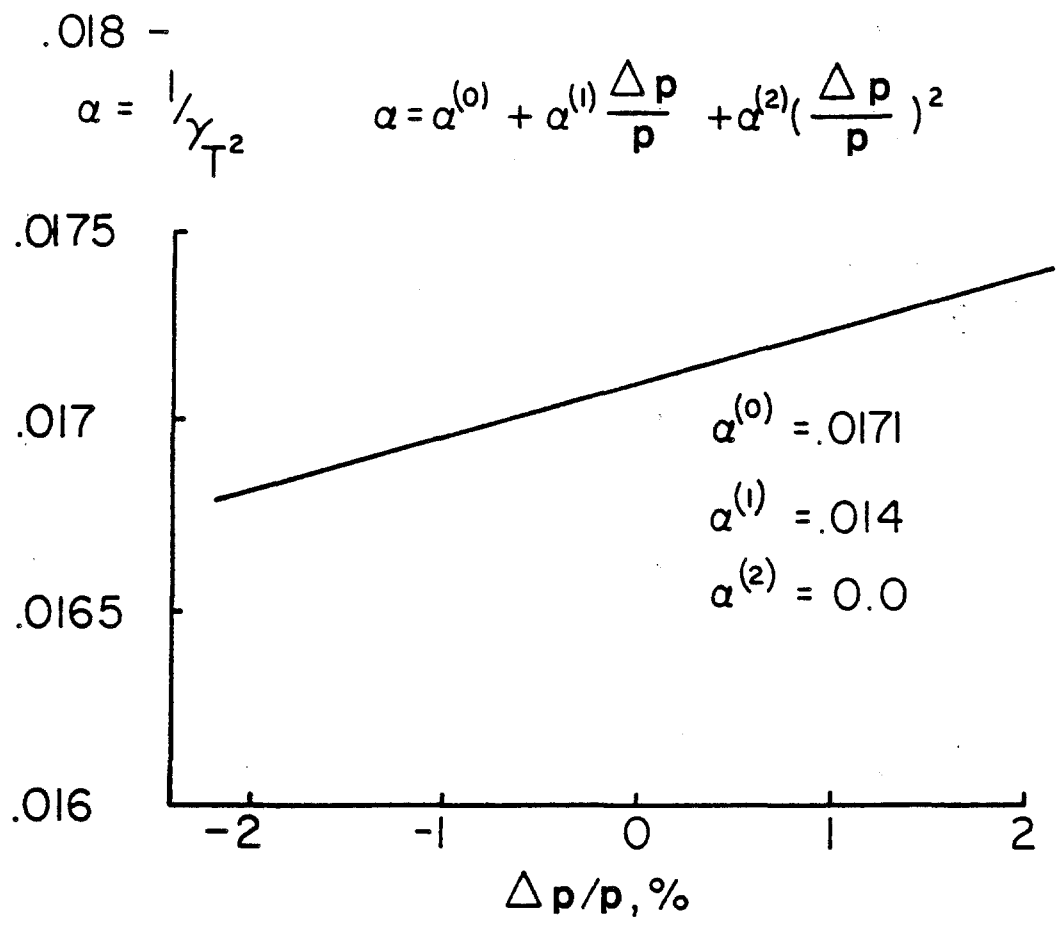
TABLE 4-V DEBUNCHER SEXTUPOLE MAGNETS

Maximum strength, B'' $\ell/B\rho$	0.22 m $^{-2}$
Bore radius	70 mm
Effective length	0.2 m
Maximum field, B''	33 T/m 2
Ampere-turns	1555 AT/pole
Current	256 A
Turns	6 turns/pole
Conductor size	0.3294" square, 0.18" hole dia., area 0.07723 in. 2
Current density	3.35 kA/in. 2
Resistance	5 m Ω /magnet
Voltage Drop	1.45 V/magnet
Thermal loss	375 W/magnet

4.8 Magnet Power Supplies

The layouts of the magnet power supplies and their circuits are dictated by the operating mode of the Debuncher Ring. The situation can be summarized as follows

- i) There will be one individually controlled power supply bus for each family of sextupoles, SF and SD. The current is 80 A and 120 A respectively with a regulation of 0.1%. A tunability range of $\pm 10\%$ is desirable for chromaticity control over a wider range.



Variation Of Momentum-Compaction Factor With Momentum

Variation Of Lattice Functions With Momentum At The Injection Kicker

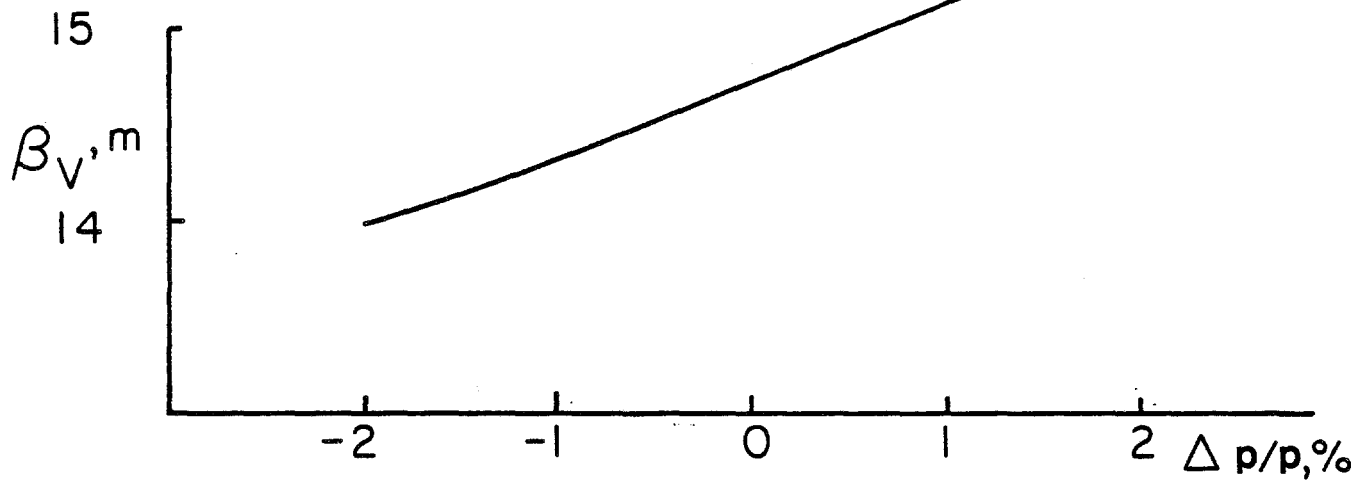
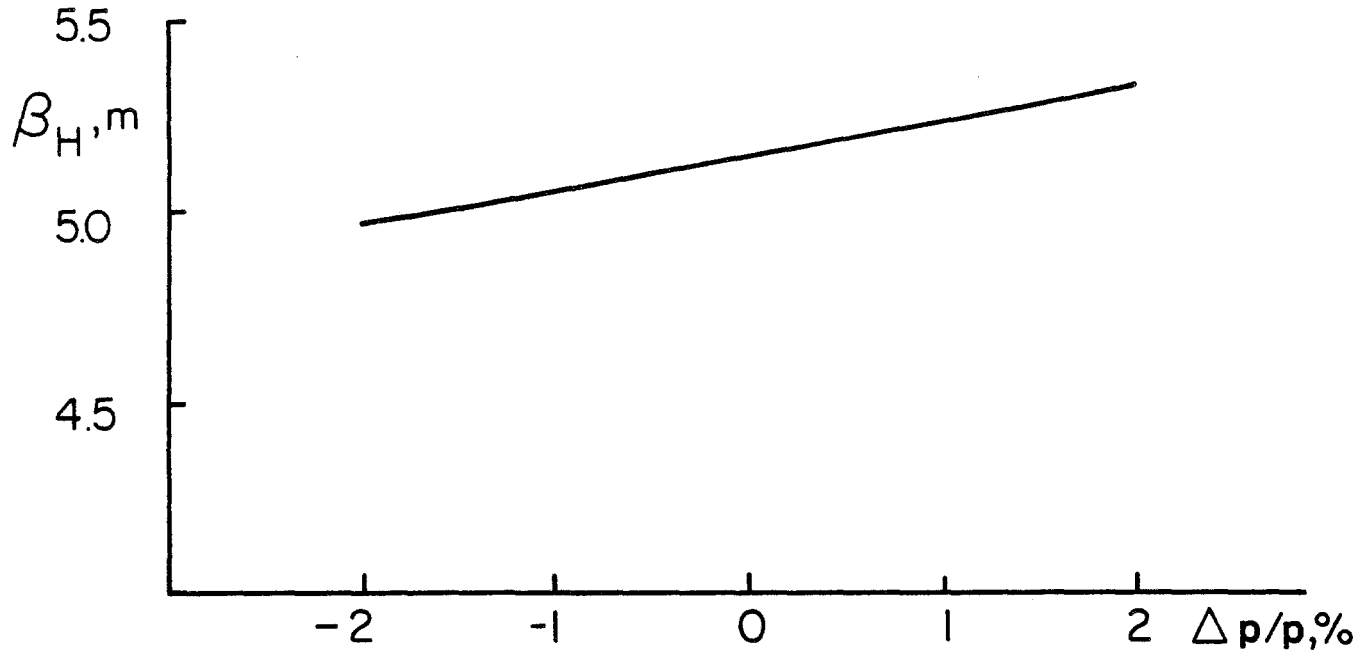
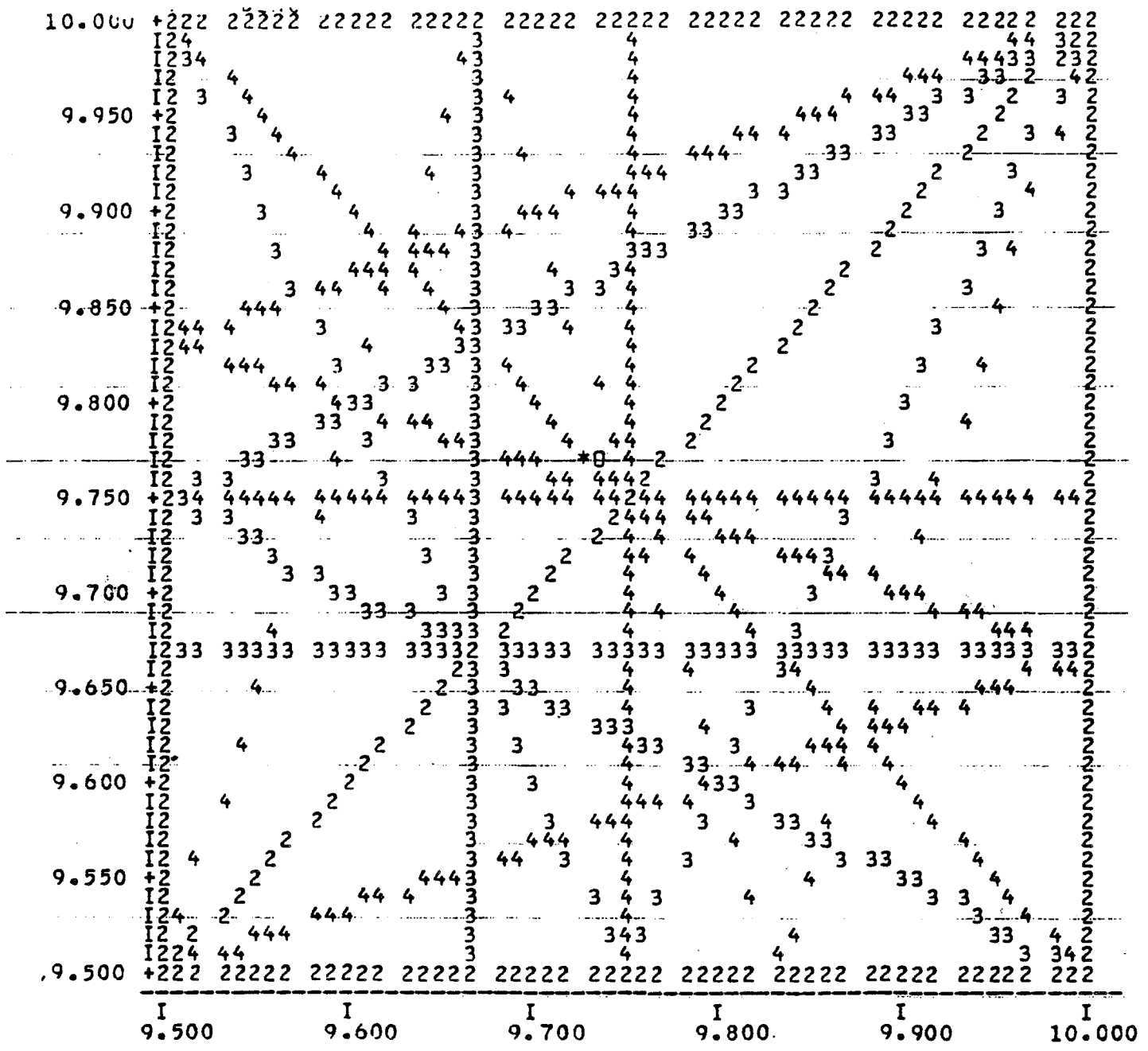


Figure 4-10



QX = 9.7300 QY = 9.7700

Tune Diagram

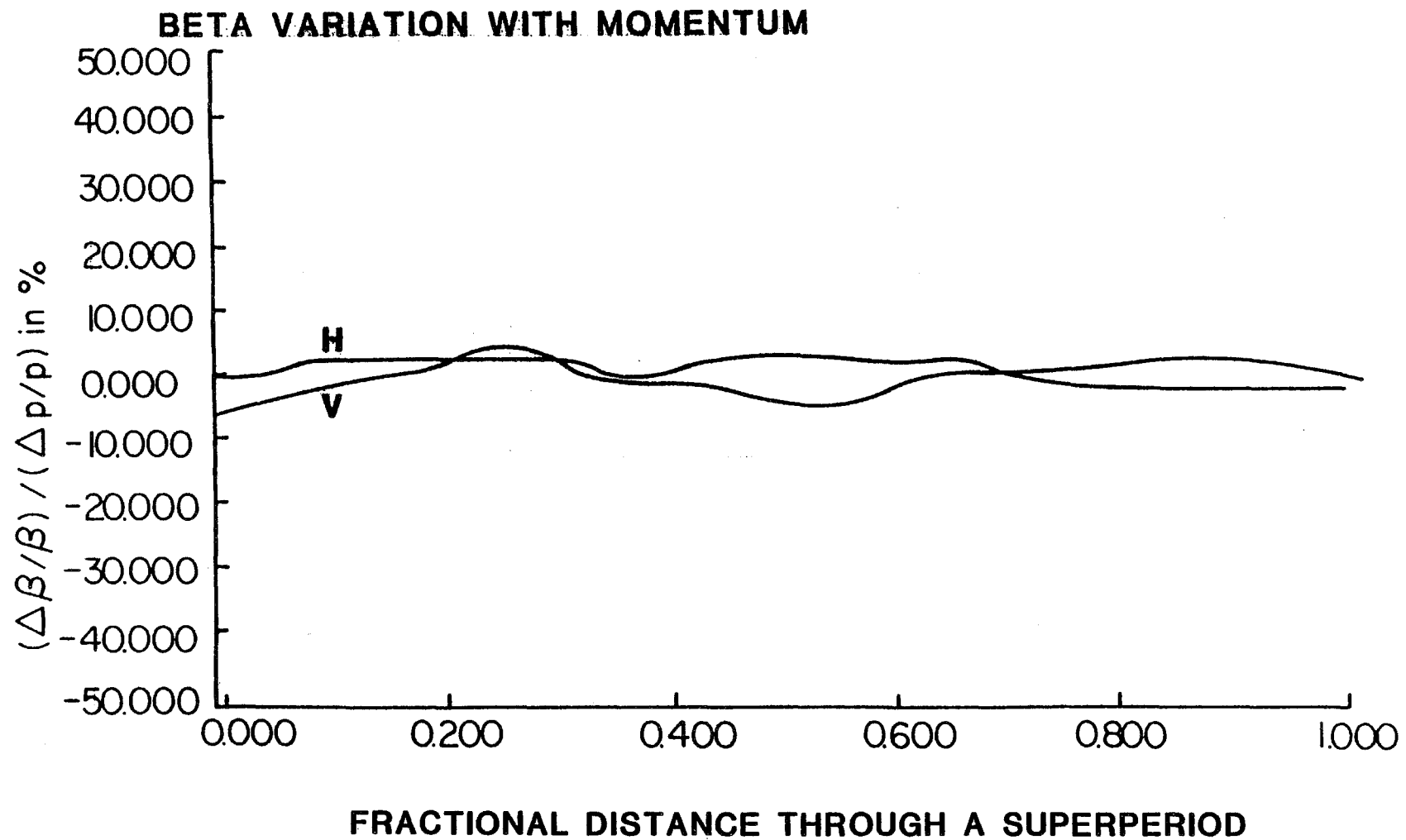


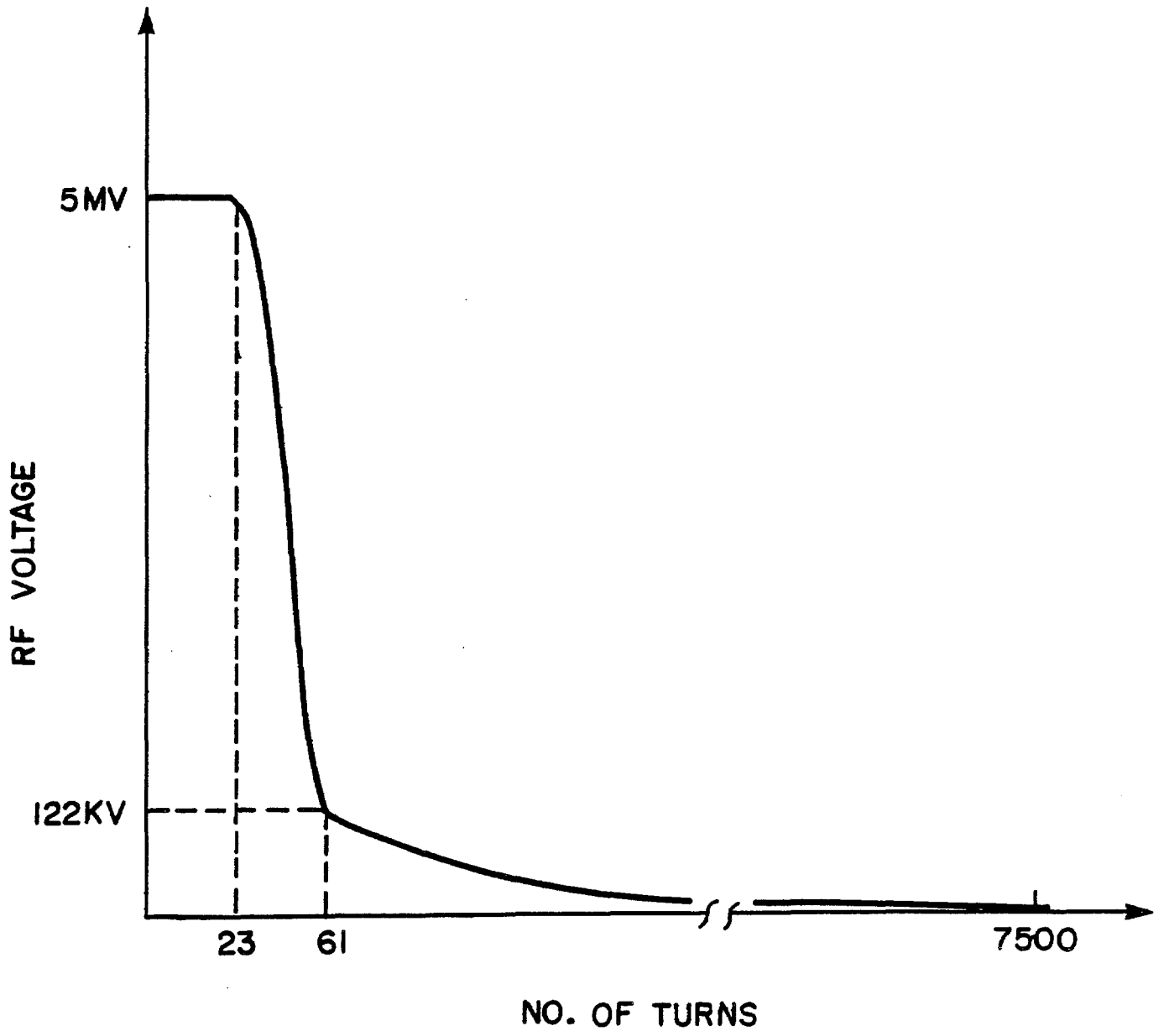
Figure 4-12

- ii) Only one current bus is required for all the dipoles. The current is 1175.6 A and a regulation of 0.01%. No shunts are needed, even for closed-orbit correction.
- iii) There is one bus for the regular horizontally focusing quads (QF) and one for the vertically focusing quads (QD). The two buses are individually controlled. The current is 240 for QF and 235 for QD. Power supply regulation is 0.01%. No shunts are required. Once the 60° phase advance/cell has been empirically obtained during the early days of operation, these quadrupole settings should remain unchanged.
- iv) The special quadrupoles QF1, QF2, QD1 and QD2 in the long straight sections are connected together to a common power supply bus with a maximum current of 290 A; each of them has a shunt to drive the current down 55 A. The regulation is, as usual, 0.01% in current.
- v) The special large-aperture quadrupoles QF3 and QD3 are connected to the dipole bus, which provides 1175.6 A, but on top of this individual power supplies for the range -50 to 100 A are added. The regulation requirement for this addition is 0.05%.
- vi) The small aperture quads QF3 and QD3 in the long straight sections are connected respectively to the QF and the QD buses, but each of them carries an individual shunt with a current range of -40 A and a regulation of 0.05%.

4.9 Bunch Rotation and Other RF Manipulation

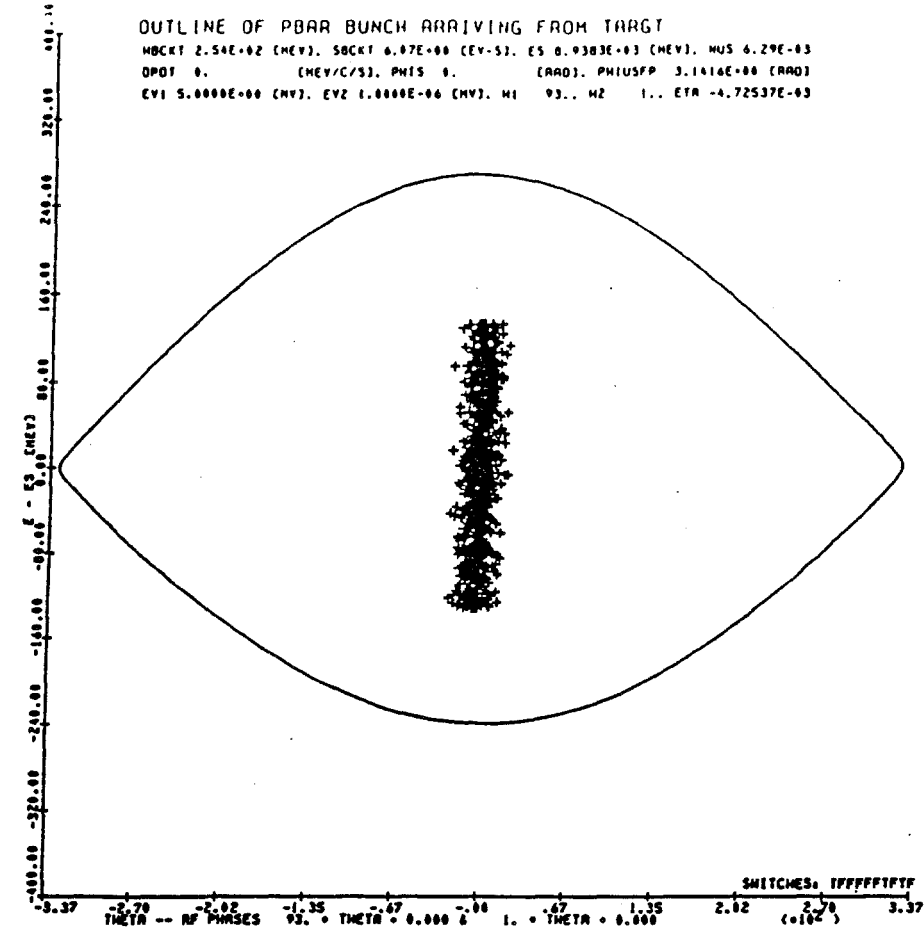
In order to evaluate the effectiveness of the debunching process and thus to determine the momentum spread of \bar{p} 's that can be accepted at production, extensive computer simulations of the rotation and debunching sequences have been carried out. The following features have been included:

- (i) The antiproton bunches, at the moment they have been generated at the target, have the same longitudinal distribution as the proton bunches, that is, an rms bunch length of 5 cm.
- (ii) The \bar{p} 's traverse a dispersionless drift of 100 to 400 m between the target and the first rf cavity. The rf voltage is to be generated by a single cavity located immediately following injection to the Debuncher.
- (iii) Three values of η were used to test the dependence of the rotation effectiveness versus the magnitude of η . Any value of -0.002 was used with an rf voltage of 2 MV and a value of -0.004 was used with an rf voltage of 4 MV. For these two



PHASE SPACE DURING DEBUNCHING

OUTLINE OF PBAR BUNCH ARRIVING FROM TARGT
 HBCKT 2.54E+02 (MEV), SBCKT 6.07E+00 (EV-S), ES 0.9303E+03 (MEV), MUS 6.29E-03
 DPOT 0. (MEV/C/S), PHIS 0. (RAD), PHISFP 3.1416E+00 (RAD)
 EV1 5.0000E+00 (MV), EV2 1.0000E+06 (MV), M1 93., M2 1., ETR -4.72537E-03



BUNCH ROTATION $\nu = \text{CONST STAGE}$ TURN # 27
 HBCKT 2.54E+02 (MEV), SBCKT 6.07E+00 (EV-S), ES 0.9303E+03 (MEV), MUS 6.29E-03
 DPOT 0. (MEV/C/S), PHIS 0. (RAD), PHISFP 3.1416E+00 (RAD)
 EV1 5.0000E+00 (MV), EV2 1.0000E+06 (MV), M1 93., M2 1., ETR -4.72537E-03

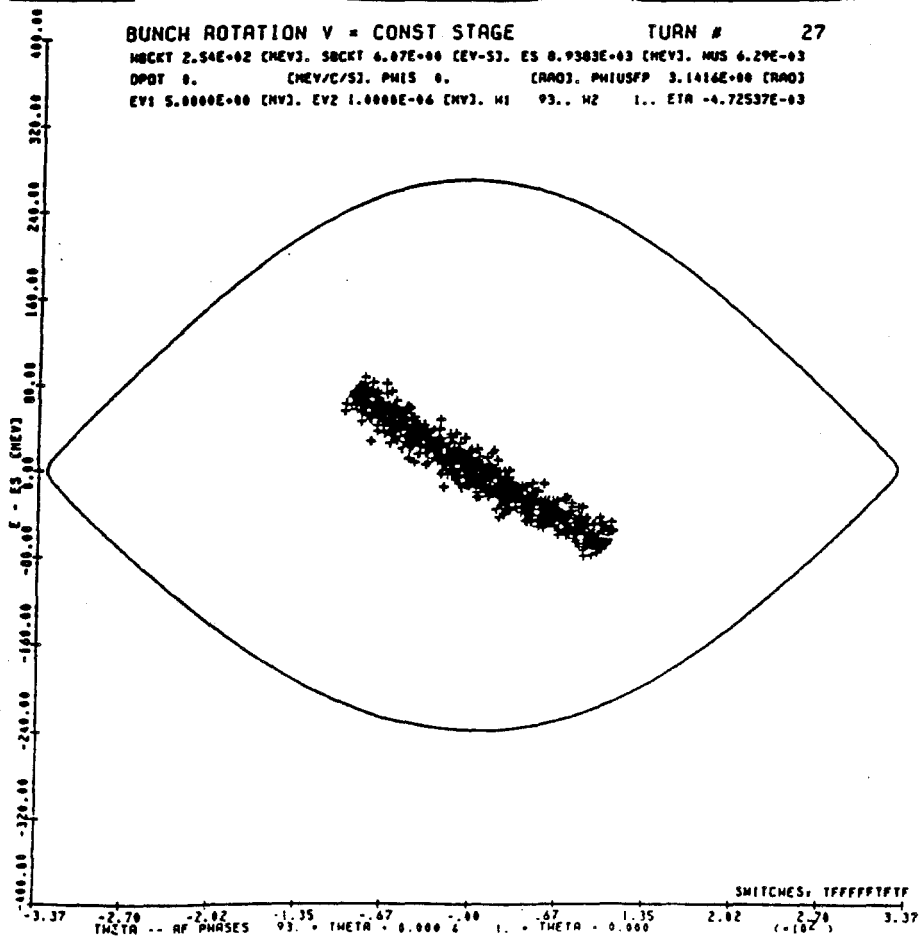


Figure 4-14 a&b

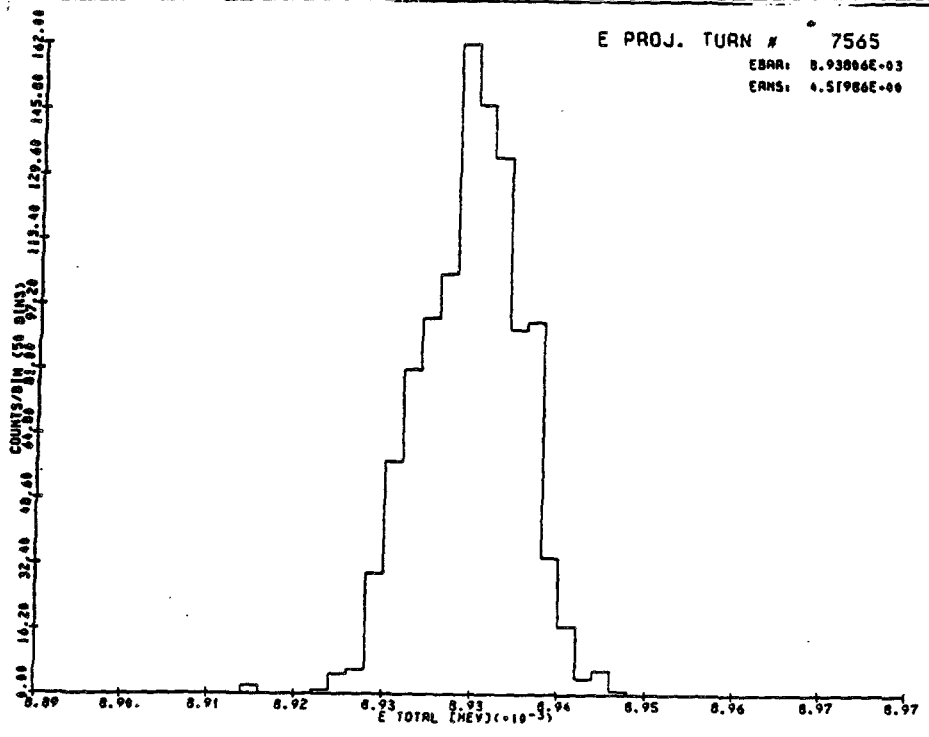
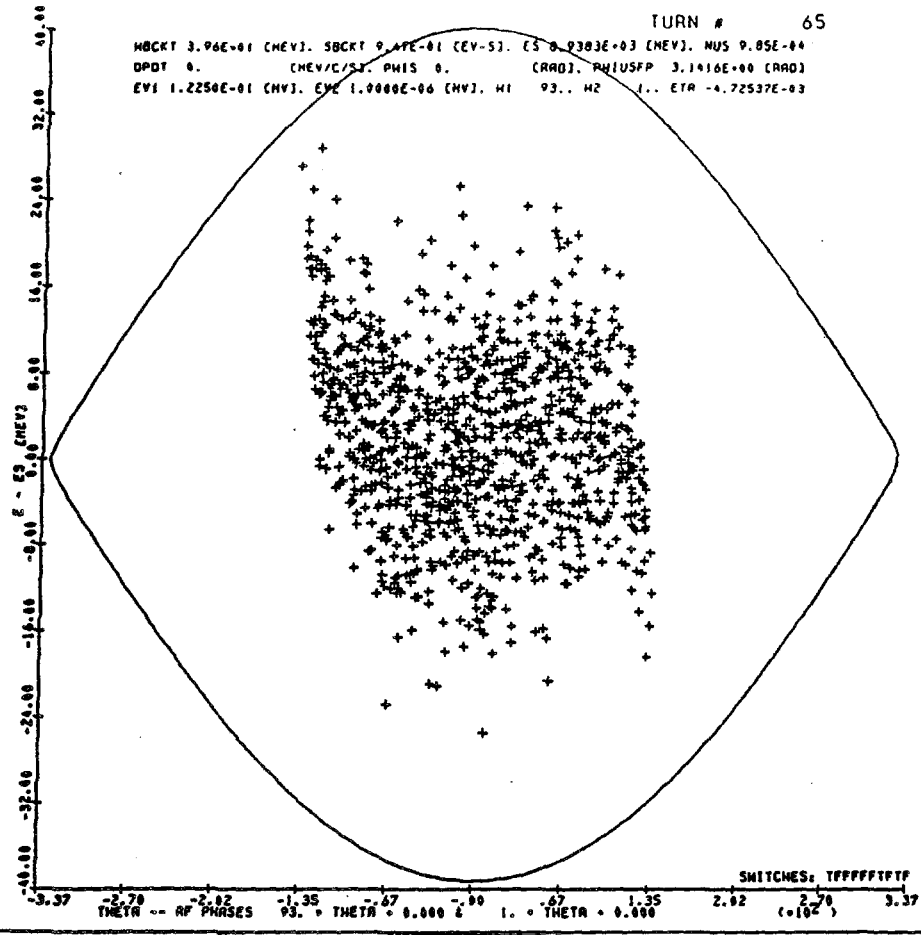


Figure 4-14 c&d

cases an initial $\Delta p/p=4\%$ was assumed. The simulation for the actual design case has $\eta=0.006$ and an initial momentum spread of 3%; the maximum rf voltage was taken to be 5 MV. The results do not depend very much on the value of η although the case of $\eta=-0.002$ is somewhat worse.

- (iv) The bunches are allowed to rotate for 20-35 turns while the voltage is kept constant. The rotation was about $45-60^\circ$.
- (v) The voltage is then dropped to $\sim 100-120$ kV in 30-35 turns (1 turn = 1.6 μsec) to form a bucket matched in shape to the beam bunch, which has evolved into a grossly distorted S-shape that extends over $\pm 90^\circ$ in synchrotron phase.
- (vi) The voltage is slowly reduced to 5 kV and then abruptly turned off.

A debunching time of 12 msec was chosen, since longer times did not significantly reduce the momentum spread, while shorter times did increase the momentum spread. The final momentum spread is not sensitive to the other details of the time dependence of the rf voltage except during the early stage of rotation. The rf voltage program for the rotation and debunching operations is shown in Fig. 4-13 for the actual design case of $\eta=0.006$ and $\Delta p/p=3\%$. Figures 4-14 shows the beam shape at the end of some of the steps for $\Delta p/p=3\%$. If the debunching could be done without dilution, 95% of the beam would be contained within a momentum spread of 0.17%. Computer simulations show that the debunched momentum spread is 0.23%. The 30% factor of dilution has several causes. It is caused in part by nonlinearities of phase oscillations of particles captured within an rf bucket and in part by the variations of γ^{-2} of the particles and the momentum compaction factor γ_t^{-2} with energy. These variations and the presence of sextupole corrections in the ring lattice were taken into account in the simulations (see Fig. 4-9).

Calculations were done with other initial momentum spreads for the design case. The initial rf voltage of 5 MV and the final rf voltage of 5 kV were kept fixed for these calculations. These results are shown in Fig. 4-15. The numbers in brackets are a measure of the dilution. The choice of 5 MV seems to be optimal for $\Delta p/p=3\%$. The momentum spread of the \bar{p} beam will be limited to 3% by collimation prior to injection into the Debuncher. The Debuncher itself has a momentum aperture of over 4%. It may be possible to reduce the debunched beam momentum spread further if the rf voltage can be reduced adiabatically to a value much less than 5 kV.

Harmonics of twice and three times the fundamental frequency were added in the simulations. Significant improvement was found only for larger initial momentum spread.

A summary of the rf parameters is given in Table 4-VI.

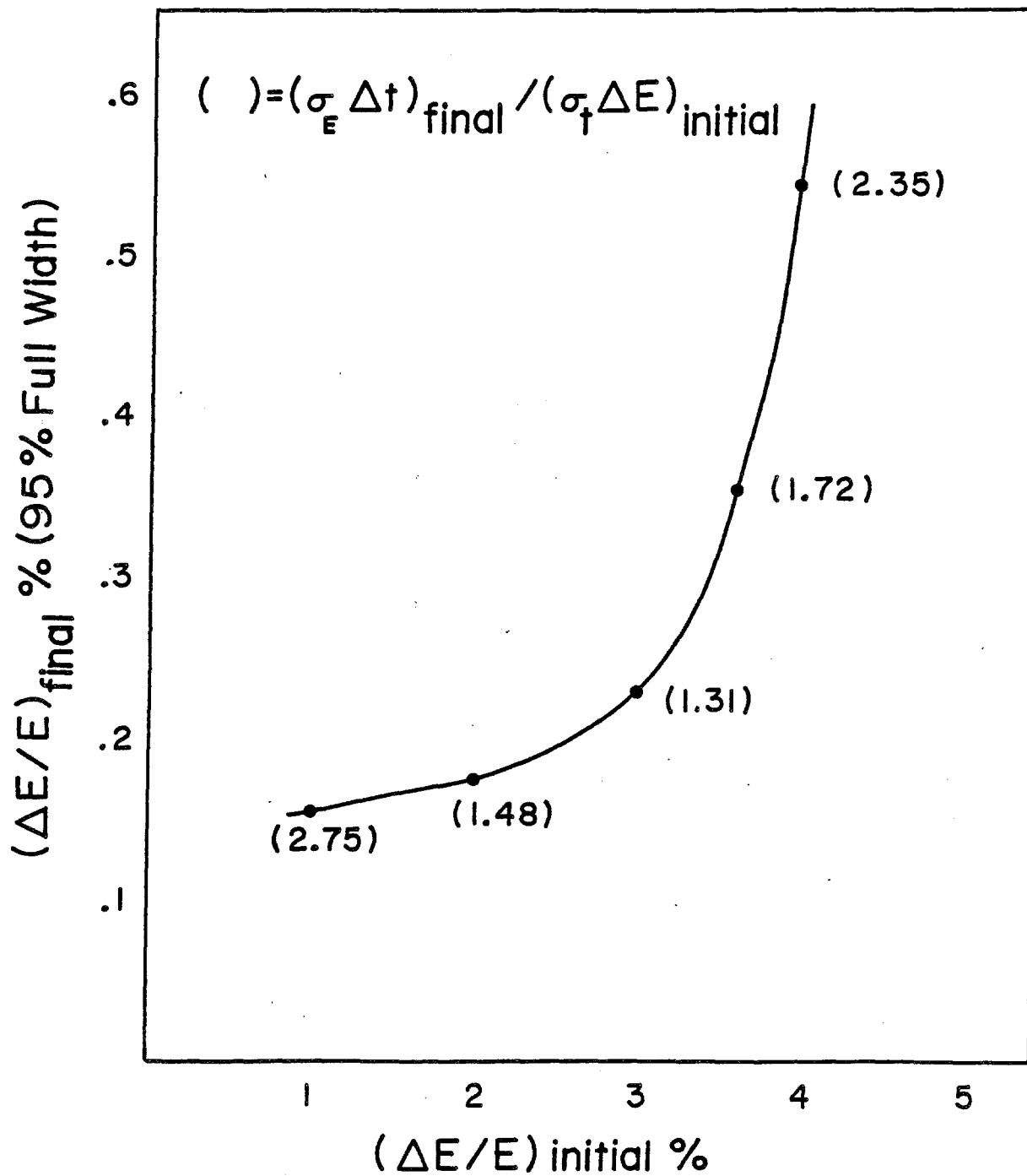


Figure 4-15

TABLE 4-VI DEBUNCHER RF PARAMETERS

Kinetic Energy	8.0 GeV
Number of antiproton bunches	80
Total number of antiprotons ($\Delta p/p=3\%$)	7×10^7
Momentum aperture, $\Delta p/p$ (full width)	4%
Bunch width (full)	<1 nsec
Transition γ (γ_t)	7.65
Mixing factor, $\eta = \gamma_t^{-2} - \gamma^{-2}$.006
RF frequency	53.1035 MHz
RF harmonic number (h)	90
Revolution period	1.695 μ sec
Maximum voltage	5.0 MV
RF voltage, end of rotation	122.5 kV
RF voltage, end of debunching	5.0 kV
Time required for rotation	.103 MSEC
Time required for debunching	12.712 msec

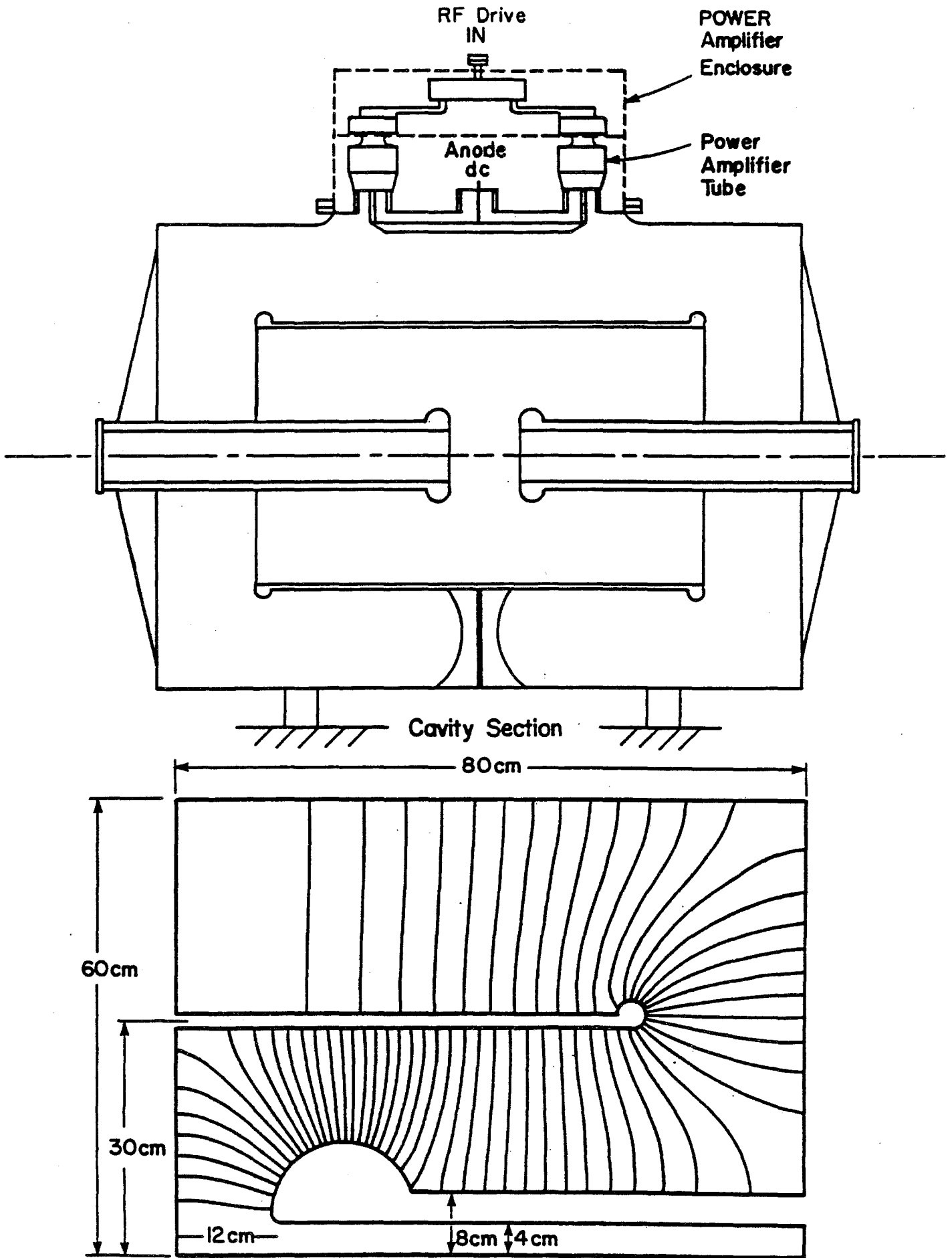
During the final debunching process, a broad-band, low-frequency rf system is operated to preserve a gap in the otherwise debunched beam. A 200 nsec gap is needed if the beam is to be transferred to the smaller Accumulator without loss. The rf system to make such a gap is described in Section 4.11.

4.10 RF Systems for Bunch Rotation and Debunching

The design criteria for the antiproton Debuncher rf are:

- (i) Voltage gain per turn approximately 5 MV.
- (ii) Maximum pulse length 100 μ sec (duty factor 5×10^{-5}).
- (iii) RF voltage pulse fall time from 5.0 MV to 120 kV, 50 μ sec.
- (iv) Pulse repetition rate 0.5 Hz.
- (v) Minimum voltage gain per turn ≤ 5 kV.
- (vi) Adiabatic reduction of voltage from 120 kV to ≤ 5 kV in a time of 5 to 20 msec under program control.

A representative rf voltage waveform was shown in Fig. 4-13. The design is simplified by the fact that the beam intensity will not exceed 10^{10} particles when the rf voltage is on. Of the particles that emerge from the production target when it is struck by 2×10^{12} 120-GeV protons, approximately 2×10^{10} are within the acceptance of the beam transport and the Debuncher. Some 90% of these particles are mesons, of which 50% decay before reaching the injection straight section. After each successive turn, 63% of the remaining mesons decay. The remainder of the particles



Superfish Computation of Fields

Figure 4-16

that reach the center of the injection straight section consist of muons, principally from pion decay, and electrons produced in showers in the target. The electrons lose 30 MeV per turn through synchrotron radiation and spiral out of the vacuum chamber within 20 turns.

The large rf voltage, low beam loading and small duty factor favor an accelerating cavity with a very high Q, hence a high shunt impedance, which requires very little rf drive power. But the short fall time of the rf voltage pulse is not obtained easily with a high-Q structure. Moreover, the physical size of high Q structures operating in the 53-MHz region would require much larger enclosures than are under consideration.

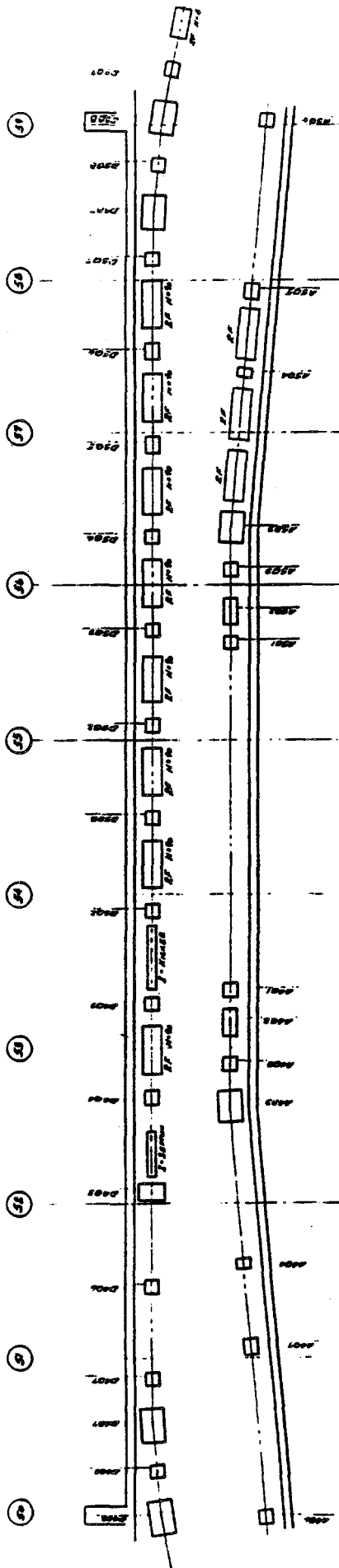
A compromise structure, which contains an intermediate cylinder that reduces both the Q and the physical size, is shown in Fig. 4-16a. Fig. 4-16b shows a SUPERFISH plot of the electric fields within one-quarter of the structure. The entire volume of each cavity will be evacuated, with rf power coupled through two small ceramic windows at the top. The plate through which rf power is introduced serves as a bedplate for the high-power driver amplifiers, which are mounted directly on top of the cavity and are completely enclosed. Thus high-power rf transmission lines are not needed and rf leakage is less likely. This may be important because rf noise could adversely affect stochastic cooling. Each cavity is driven by two relatively small 10-kW triodes operating in a cathode-driven grounded-grid configuration. In this configuration, the tubes are capable of delivering very large peak rf currents during the short pulse. Because the pulse is short and the duty factor is low, the average anode dissipation is only a few hundred watts.

The rf voltage is reduced quickly by reversing the phase of the power-amplifier excitation and raising the excitation amplitude to a very high level. The high peak-power capability of the tubes is used to "drive" the cavities off, even though the cavity time-constant is longer than the required turn-off time of 50 μ sec.

The peak rf voltage that each cavity can develop has been calculated to be larger than 650 kV. Eight of these 1.8 m long cavities provide the required 5 MV. They are located in the long straight section immediately following injection from the target. The location of these cavities is shown in Fig. 4-17.

In order to reduce the rf voltage down to 5 kV or less during the adiabatic-debunching part of the rf program, six of the cavities are turned off and two of the cavities are held at 50 kV and their relative phases each changed by 90° in opposite directions. The resultant rf voltage gradually reaches a small value. This is done to avoid instabilities at low rf voltage that might arise from multipactoring.

In order to provide the structural rigidity necessary for complete evacuation and to reduce material costs, the cavities will be constructed from aluminum.



PLAN — BUILDING # 50

Injection Straight Section Of The Debuncher

Figure 4-17

4.11 Gap-Preserving RF

Because the Debuncher circumference is larger than that of the Accumulator, antiprotons will be lost in the transfer to the Accumulator unless there is a gap in the Debuncher beam. Given the difference in circumference between the two rings and the need to allow for the fall time of the injection kicker, a gap greater than 200 nsec is needed.

An adequate gap can be created in the beam by a "barrier bucket" that excludes particles from its interior. It is created by a voltage that traces out a single complete sinusoidal oscillation for one-quarter of the rotation period and then becomes zero for the remaining three-quarters of the period. A sketch of this waveform is shown in Fig. 4-18. The voltage waveform repeats itself every turn. The phase of the voltage is chosen so that it establishes an unstable fixed point between two back-to-back half-bucket separatrixes. If the bucket height exceeds the beam energy spread, the beam will be forced away from the unstable fixed point by a distance determined by the ratio of the bucket height to the energy spread. The rf voltage is chosen so that the beam is excluded from a region between $\pm\pi/2$ radians in the "barrier bucket". This will create a gap of 221 nsec, as shown in Fig. 4-18. The peak amplitude required is 890 V. The Fourier series expansion of such a voltage waveform is given by

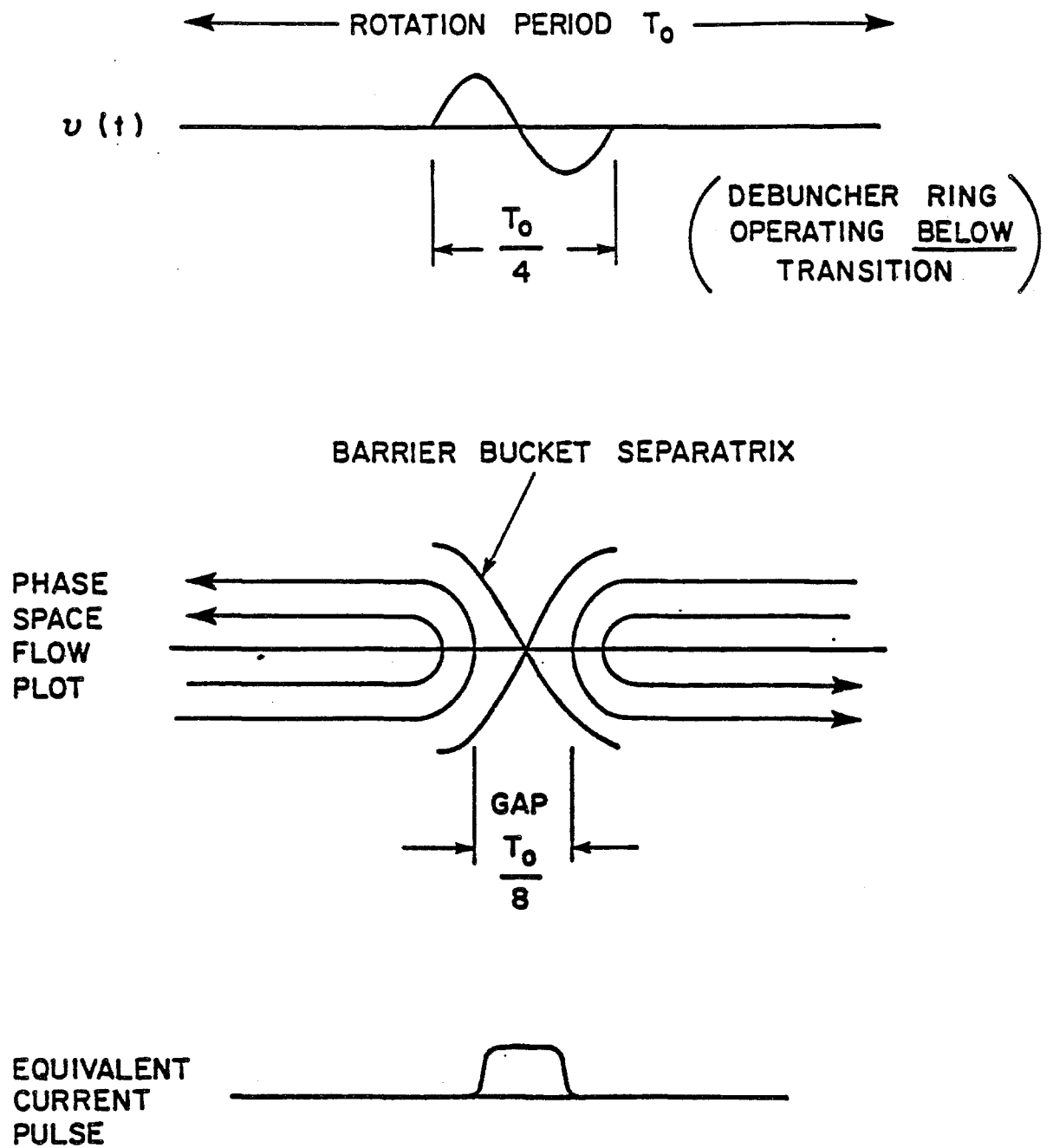
$$V(t) = 890 \frac{2h}{\pi} \sum_{n=1}^{\infty} \frac{\sin \pi n/h}{h^2 - n^2} \sin(n\omega_0 t),$$

where $\omega_0 = 2\pi f = 3.59 \times 10^6$ rad/sec and $h=4$. At frequencies above the 31st harmonic (17.7 MHz) the required amplitudes are reduced by more than three orders of magnitude. Amplifiers with a bandwidth between 0.1 and 30 MHz which are capable of delivering 300 W in a 50-ohm load are readily available. The required rf system can be broken into 450-V units, each consisting of a ceramic gap loaded with a 50-ohm resistor and surrounded by a shielding enclosure containing about ten large MnZn ferrite rings. The average power delivered to this system is very small. Since the physical size of each unit is dictated by the volume of ferrite required, each unit is 0.5 m in length. Their location is shown in Fig. 4-17.

An additional bonus associated with installation of the "barrier bucket" rf system is that it can be used in the "normal" $h=4$ mode to accelerate or decelerate 8-GeV protons across the ring aperture in tune-up testing of closed orbits and stochastic-cooling systems.

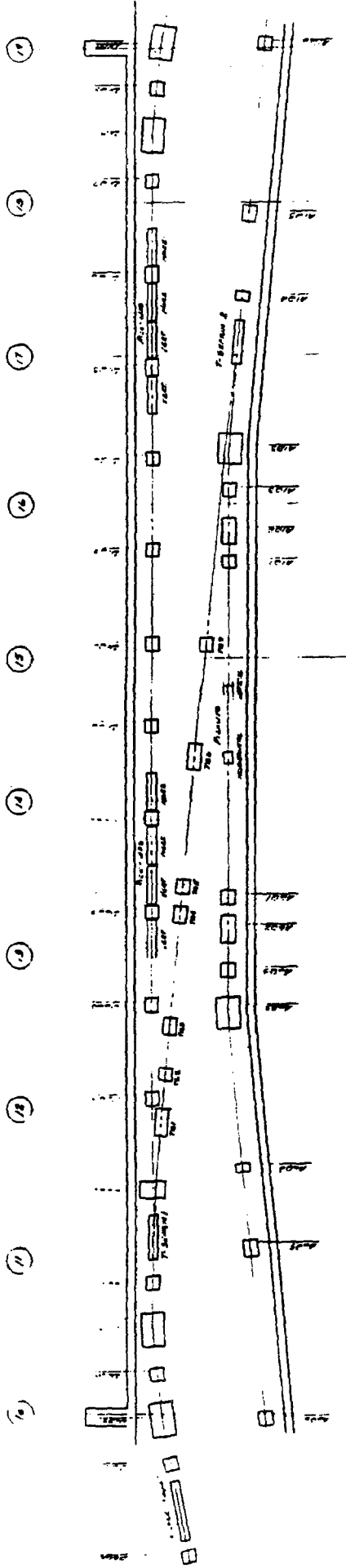
4.12 Beam Injection and Extraction

4.12.1 Injection from the Target Station. The beam enters the Debuncher in the vertical plane at an angle of 50 mrad to the closed orbit. The injection path is exactly aligned with the central closed orbit of the



Gap Preserving RF

Figure 4-18



Plan - Drawing #10

Beam Transfer From Debuncher To Accumulator

Figure 4-19

Debuncher. The beam first enters QF3, which has a large aperture to accommodate both the injected and the circulating beam. The circulating beam goes through the center of the quad, but the injected beam enters the quad with a vertical displacement of 5 in. at the upstream end and an angle of 50 mrad. A septum magnet located after QF3 brings the beam down to a vertical separation of 2 in. and parallel to the ring orbit. A kicker magnet between QF2 and QD1 brings finally the beam onto the reference orbit. The kicker and septum magnets parameters are given in Table 4-VII and are shown in Fig. 4-17. The injection channel has been designed to accommodate a beam with momentum spread of 4% and transverse emittances of 20π mm-mrad.

4.12.2 Debuncher to Accumulator Transfer. The beam transfer between the Debuncher and the Accumulator is a horizontal transfer taking place in the 10 straight section. Extraction from the Debuncher is accomplished with a kicker and a septum magnet, as shown in Fig. 4-19. The quadrupole after the septum magnet, QD3, has a large aperture to accommodate both the circulating and the extracted beam. This quad kicks the beam further to the inside of the ring toward the Accumulator. The horizontal displacement of the extracted beam from the magnet axis is 5 in. After extraction, the beam is transported to the Accumulator with no further bending through a string of 6 quadrupoles. At the Accumulator, the beam is injected onto a path displaced from the central momentum by $\Delta p = +0.93\%$ with an 12-kG 7-ft long pulsed septum placed between A1B3 and A1S3. Finally the beam is kicked onto the proper orbit in the Accumulator with a 500-G, 7-ft long shutter kicker placed in the A20 straight section. The elements are discussed in more detail in Sec. 11.3. A plot of the lattice functions of the transfer line is shown in Fig. 11-5 and the list of elements is given in Table 11-IV.

4.12.3 Injection from the Booster. Injection into the Debuncher from the Booster is exactly the same as injection from the Target Hall. The beam is transported to the upstream end of the 30 straight section and injected downward into the Debuncher at an angle of 50 mrad, again passing through a large-aperture quadrupole D2Q5 and then into a septum magnet. Finally a kicker located between D2Q3 and D2Q2 puts the beam onto the reference orbit.

4.13 Betatron Cooling

4.13.1 Design Goal. The goal of the stochastic cooling in the Debuncher is to cool the beam emittance from 20π mm-mrad to 7π mm-mrad in both the horizontal and vertical planes. An emittance of 7π mm-mrad is the assumed beam size that can be reliably transferred into the 10π mm-mrad acceptance Accumulator ring with negligible beam loss. In addition to cooling the beam to fit into the Accumulator, it is desirable to make the beam injected into the Accumulator as small as possible. In the Accumulator the momentum stacking is done in part by a pickup that senses a particle's momentum by observing its position in a region of high dispersion. Betatron oscillations add undesired noise to this process.

4.13.2 Design Considerations. The betatron-cooling system is conceptually simple. It consists of a pickup that senses the positions in a zero-dispersion region and therefore measures only the betatron amplitudes of the particles. The signal is amplified and applied to a kicker an odd multiple of 90° away in betatron phase. At the kicker, the position displacement that was sensed has been converted into an angular displacement. This angular displacement is decreased by a correcting kick, which thus decreases the betatron amplitude. As is well known, the cooling of a single particle is hampered by the presence of the other particles, that create a noise signal (Schottky noise) that heats the particle. For a properly designed system, the net effect over many turns is that cooling is achieved.

The process of betatron cooling is conventionally described by the equation

$$\frac{d\epsilon}{dt} = - \frac{W}{N}(2g-g^2(M+U))\epsilon, \quad (4.1)$$

where ϵ is the betatron amplitude, W the amplifier bandwidth, N the number of particles, g the system gain, M the mixing factor and U the ratio of noise to signal power. The mixing factor M is given by

$$M = \frac{f^2\psi(f)\Lambda}{2WN}, \quad (4.2)$$

where $\psi(f)$ is the density of particles (number per Hz), f is the revolution frequency, and Λ is a constant of order unity ($\Lambda=\ln 2$ if the gain is independent of frequency).

Stochastic cooling during the 2-sec Debuncher cycle is difficult because the mixing factor M is large compared to 1. M is inversely proportional to the dispersion η , where

$$\frac{\Delta f}{f} = \eta \frac{\Delta p}{p}, \quad (4.3)$$

The choice of the value of η was a compromise between the rf requirement for the bunch rotation (which favors a small η) and stochastic cooling (which favors a large η). The choice of $\eta = +0.006$ leads to a mixing factor M of about 10 for the particles near the central momentum of the Debuncher, assuming a parabolic momentum distribution with a full width of $\Delta p/p=0.3\%$.

Another problem is that the noise-to-signal ratio U tends to be large. The techniques to make U small are: 1) increase the beam signal as much as possible by using a large number of high-impedance pickups and 2) decrease the noise temperature by cooling the pickup terminating resistors and the preamplifiers.

The criterion for the thermal noise to be negligible is $U \ll M$. With the parameters of Table 4-VII below,

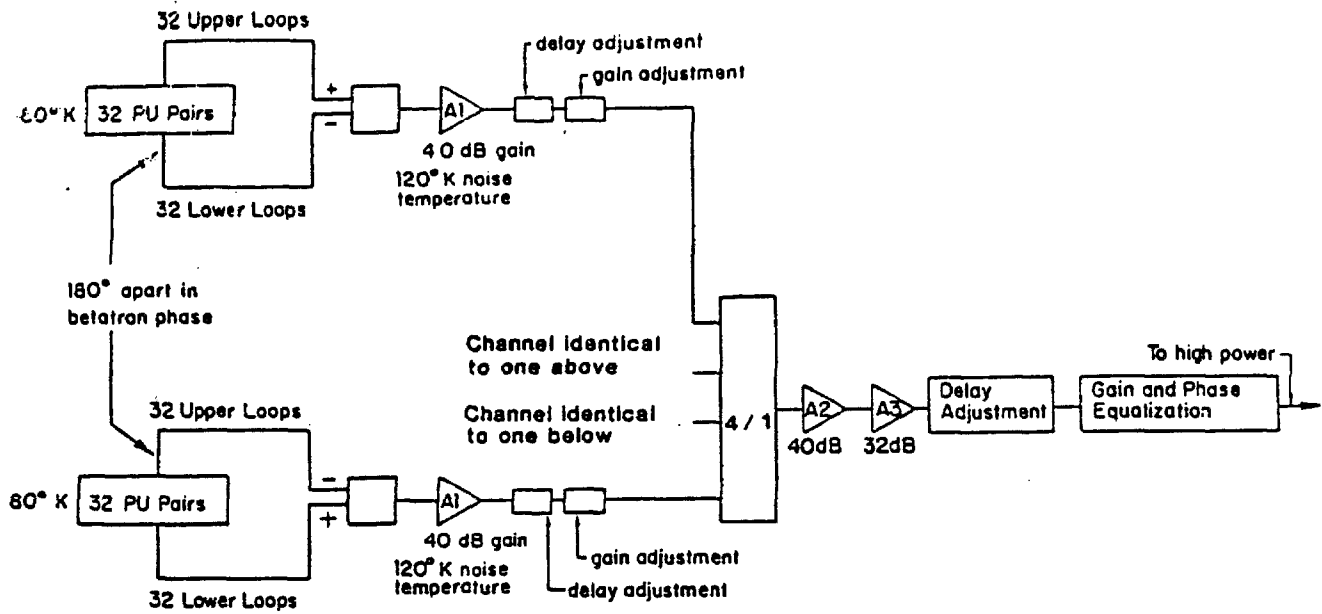
$$U = \frac{2K (\theta_R + \theta_A) h^2}{d^2 Z_0 e^2 f_0 n_p N \beta_p \bar{\epsilon}} \quad (4.4)$$

$$= 1.8 \text{ (initially) } ,$$

where $K = 1.38 \times 10^{-23}$ Joules/°K, $f_0 = 1/T =$ revolution frequency, $\bar{\epsilon} =$ average beam size $= 8\pi$ mm-mrad initially. But, as the beam is cooled to $\bar{\epsilon} = 0.8\pi$ mm-mrad, U will grow to 18, twice the value of M , the mixing factor. Thus cooling will initially proceed not limited by thermal noise, but as the beam cools, the effect of the Schottky and thermal noise become comparable (note that the cooling equation (4.1) is written in a deceptive form because it does not explicitly show the dependence of U on $\bar{\epsilon}$).

A practical problem that occurs in fast stochastic cooling is that the power requirements are often very high. In the Debuncher, the best cooling rate is obtained for a power level of 1800W. But, as can be seen from Eq. (4.1), the gain can be decreased by a factor of 2 and the cooling rate will be only $2g - g^2 = 3/4$ of the optimum rate. In the absence of suppression, the power will decrease by a factor of 4. In the case that signal suppression is important, the decrease in power can be even greater, because the system gain g increases more slowly than linearly with the amplifier gain. In a system with bad mixing like the Debuncher, most of the thermal power is between Schottky bands and is largely unaffected by signal suppression. In this case, the thermal power is therefore more nearly proportional to amplifier gain squared than to system gain squared (g^2).

4.13.3 Hardware. For each of the two betatron-cooling systems, 4 sets of 32 pickup pairs are installed in straight section D10, and a similar set of kickers are installed in straight section D30. Both straight sections have zero dispersion. The pickup arrays are spaced out between the quadrupoles in a manner such that 2 sets are roughly 180° out of phase with the other two. These signals are therefore combined with inverted phase. The signal is then amplified and sent to the kicker region which is $3\frac{1}{4}$ betatron oscillations away. The pickup termination resistors are cooled to 77°K, as are the preamplifiers. A block diagram of the betatron cooling system is shown in Fig. 4-20. In brief, the pickup signal from 32 upper plate pickups is combined with 32 lower plate signals to provide a difference



Debuncher Betatron Cooling Systems

2-4 GHz Horizontal and Vertical Systems are Identical.

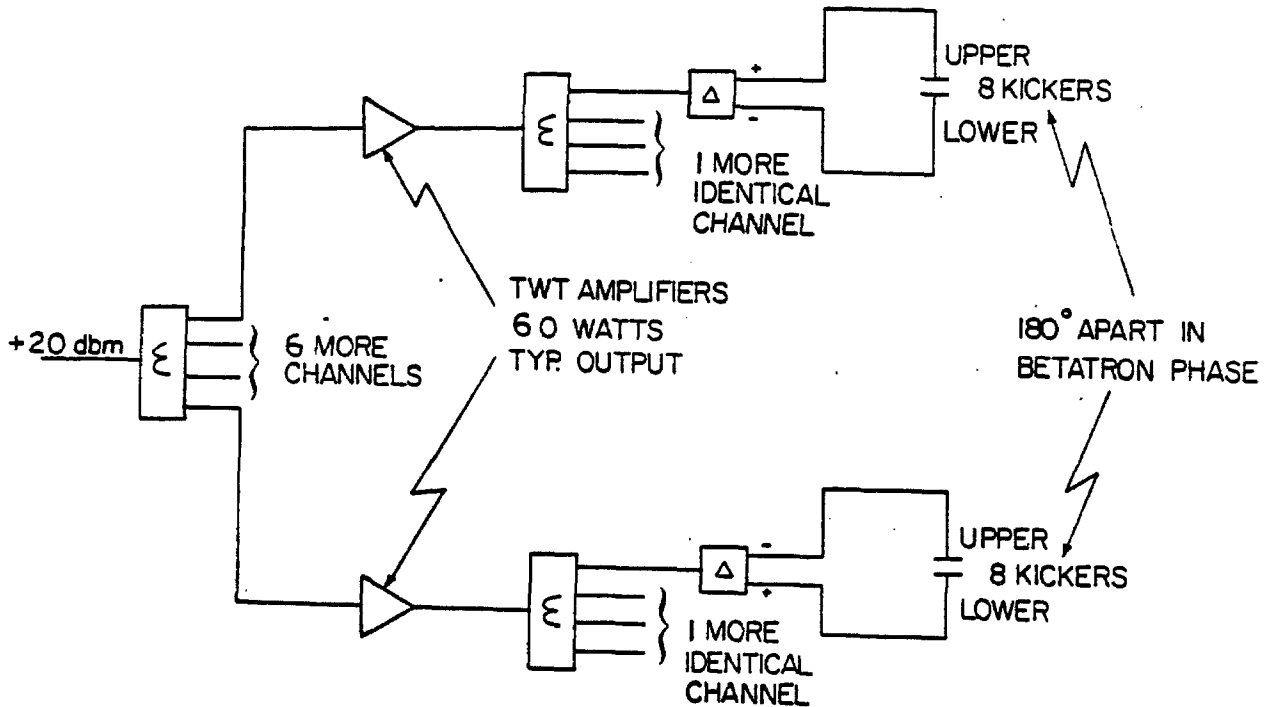


Figure 4-20

signal proportional to the position displacement of the beam. The signals from each set of 32 pickups amplified 40 dB are combined in an 4-fold combiner. Each combiner input has an adjustment for amplitude and delay. After combination the signal is further amplified by 72 dB to a level of about 25 dBm. An overall delay adjustment is followed by a gain and phase compensating circuit, to partially cancel the variations in the TWT (traveling wave tube) gain characteristics. The power is then split to drive two sets of TWT's, each of which drives an array of 16 kickers.

Table 4-VII lists some of the parameters of the betatron cooling systems. The characteristics of the hardware components are similar to those in the Accumulator, these characteristics are discussed in more detail in Section 5.4. The overall layout of the stochastic cooling system in one straight section was shown in Fig. 4-7.

4.13.4 Computer Simulation⁵. A simulation of the betatron cooling in the Debuncher was made to calculate the expected system performance. Included in the simulation were the pickup and kicker response functions, transit-time differences of the electrical signal and particles between pickup and kicker, and signal suppression. The amplifier was modeled as a physically unrealizable ideal amplifier having a gain g_A from 2 to 4 GHz and zero elsewhere. It was assumed that g_A was purely real. While the amplifier model was not realistic, measurements of the TWT tube amplifiers in the 1-2 GHz range show that, when externally phase compensated, these tubes can provide gain and phase characteristics that lead to cooling rates equal to or better than the 1-2 GHz "ideal" amplifier model used above. The initial \bar{p} distribution was taken from Fig. 3-4. It was assumed that the Debuncher had an acceptance of 25π mm-mrad but that the transport line had already limited the beam size to 20π mm-mrad. The total output power was limited to 500W. The gain was continually adjusted to provide the best cooling within the 500W limit.

Figure 4-21 shows the initial and final beam distributions for particles at the central momentum. Ninety-nine per cent of the particles fall within an emittance of 7π mm-mrad. Also shown is the final curve for particles with a momentum offset of 0.075%, or halfway to the edge of the distribution. The cooling of these particles is somewhat better since they have a somewhat lower density, i.e., less Schottky noise. Since the noise figure assumed is somewhat speculative, Fig. 4-22 compares the final spectrum for design case $\theta_A + \theta_R = 200^\circ\text{K}$. If the noise figures were worse because of the pickup sensitivity being less than supposed, the kickers would presumably be less sensitive in the same ratio. In this case, the total dissipated power would be larger than the design case of 500W. Figure 4-23 is a comparison of the final distribution for different power levels assuming the design case noise figure ($\theta_A + \theta_R = 200^\circ\text{K}$). As previously stated, there is little advantage in running at power levels corresponding to the optimum gain.

As designed, the stochastic cooling system for the Debuncher will cool the beam emittance by about an order of magnitude. If the system fails to

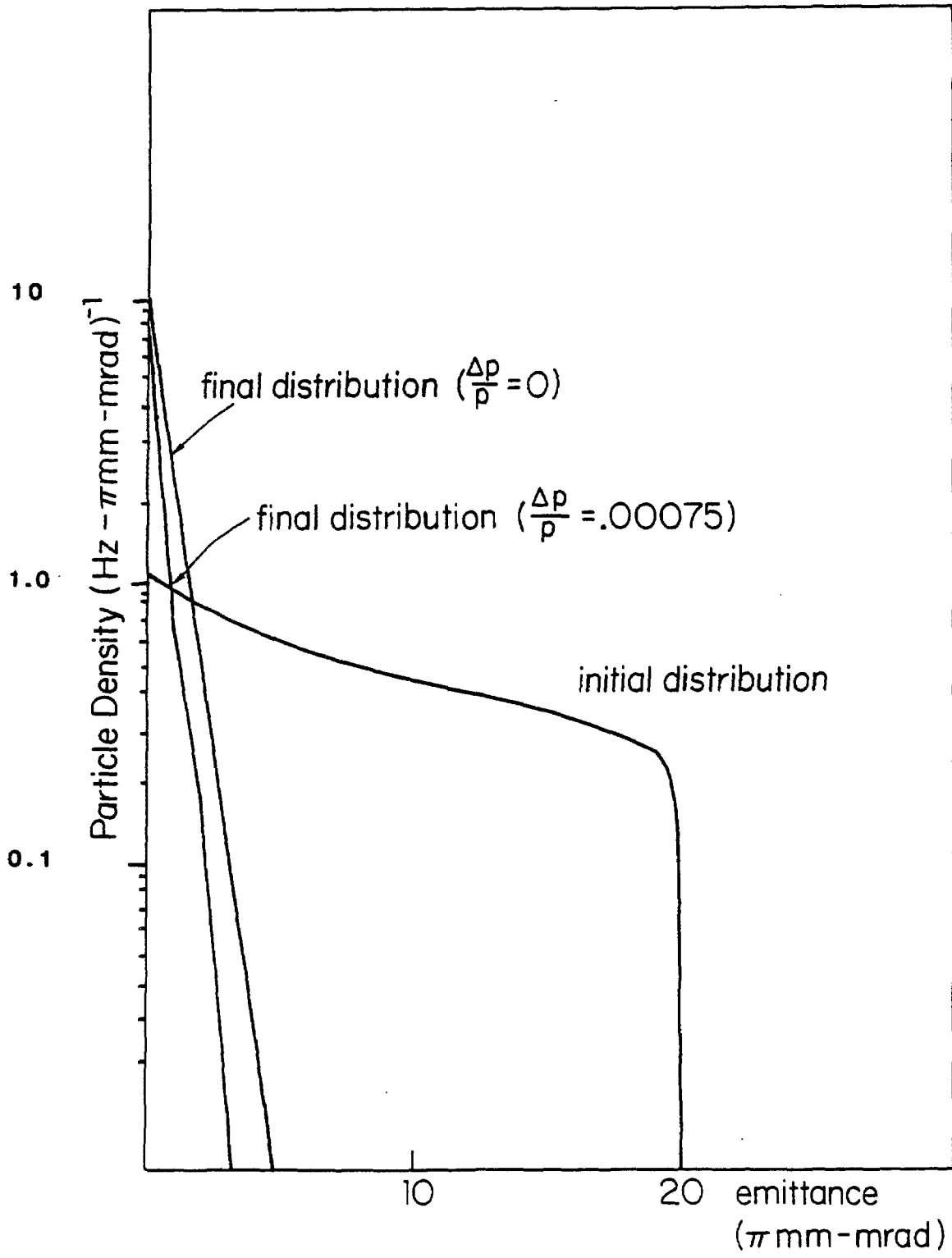


Figure 4-21

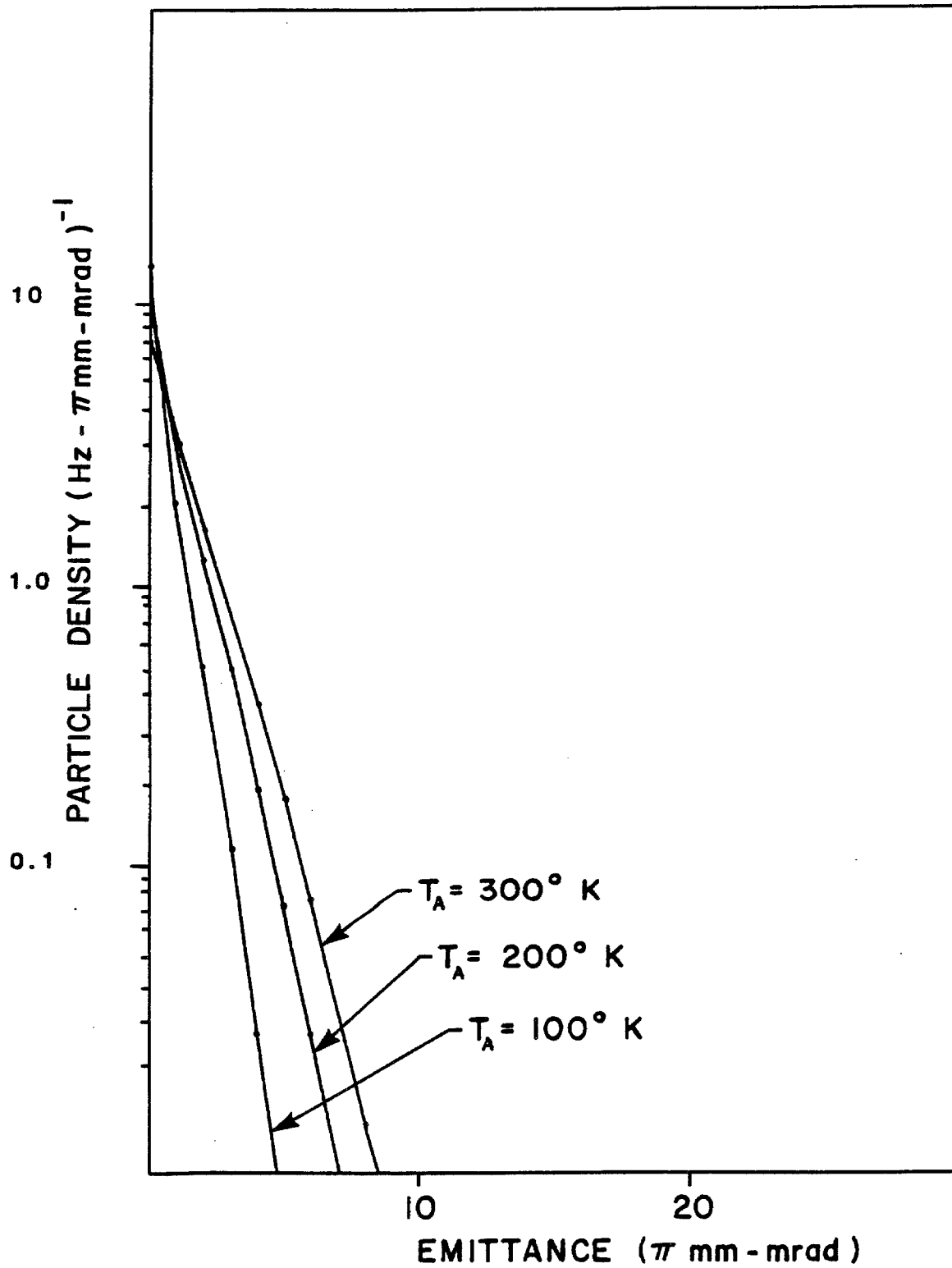


Figure 4-22

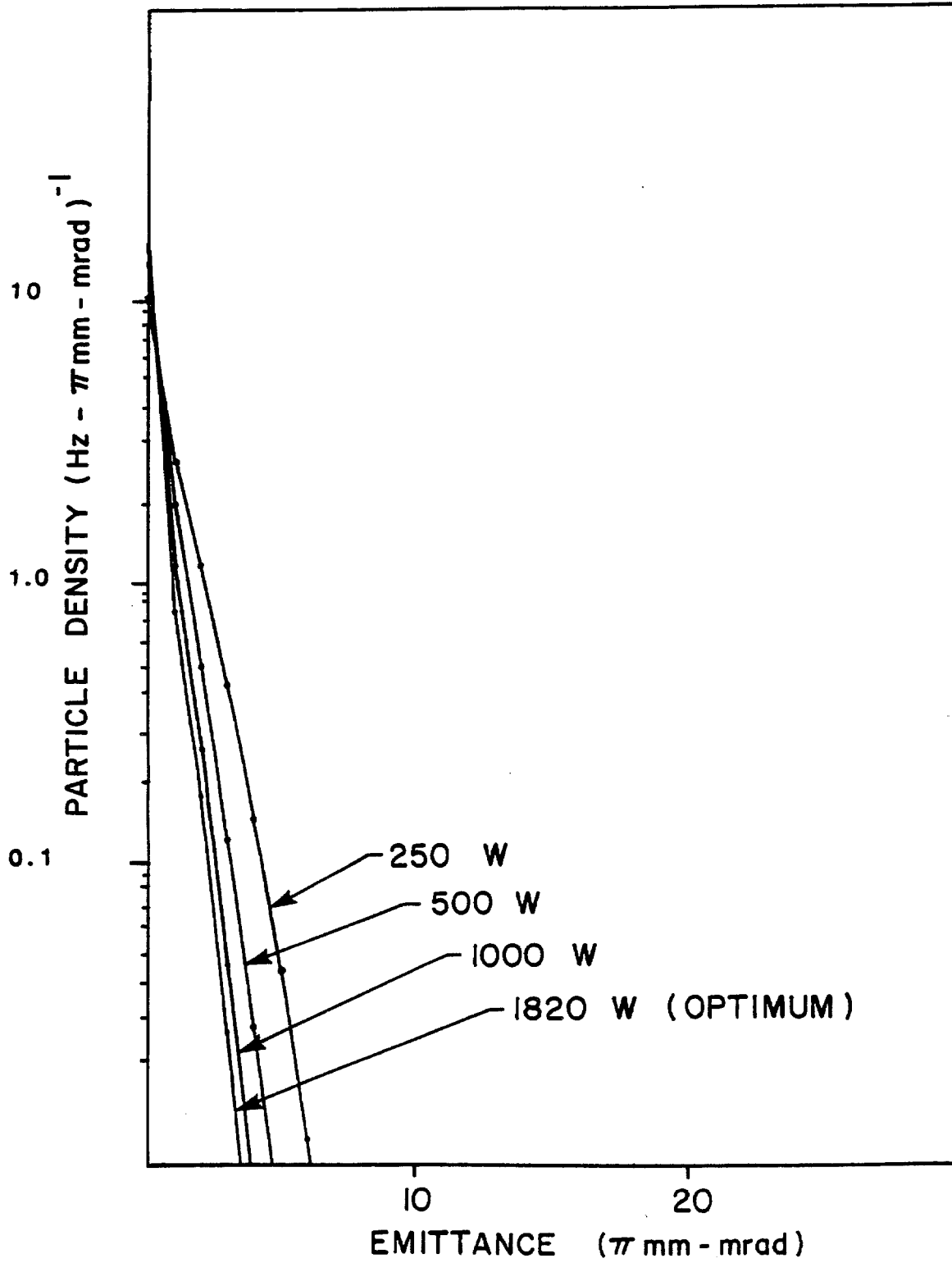


Figure 4-23

perform as designed, there is a substantial margin of safety in getting the beam to 7π mm-mrad for transfer into the accumulator.

TABLE 4-VII BETATRON-COOLING SYSTEM PARAMETERS (EACH SYSTEM)

Frequency band	2-4 GHz
Number of pickup pairs (loops)	128
Pickup Characteristic Impedance	75 Ω
Pickup Sensitivity d(0,0)	1.73
Pickup resistor noise temperature (θ_R)	80°K
Amplifier equivalent noise temperature (θ_A)	120°K
Amplifier gain (net) (variable)	138 dB (variable)
Output Power	
-Schottky	100 W (typical)
-Thermal	400 W (typical)
-Total	500 W
Number of TWT's	8
Number of kicker pairs (loops)	128
Kicker characteristic impedance	75 Ω
Kicker sensitivity d(0,0)	1.73
Spare time delay with foam heliax ($\beta=0.89$)	45 ns

CHAPTER 5

ACCUMULATOR RING5.1 Accumulator - Functional Summary

The first function of the Accumulator is to accept a pulse of \bar{p} 's every 2 seconds. In order to make room for this pulse, the \bar{p} 's must be compressed (cooled) into a smaller area of phase space. A technique to accomplish the continuous \bar{p} accumulation and compression has been developed at CERN and is the basis of this design. The technique consists of establishing a stack of \bar{p} 's with an energy density that rises approximately exponentially from the injection density (the low-density end is referred to as the "stack tail") and then culminates in a roughly Gaussian high-density region (the "core"). Betatron amplitudes are also cooled during the stacking process. The design criteria for the accumulation process are given in Table 5-1, and the parameters of the Accumulator are given in Table 5-II.

TABLE 5-I ANTIPROTON STACK PARAMETERS

Injected Pulse

Number of \bar{p} 's	8×10^7
$\Delta p/p$	0.2%
Horizontal and vertical emittance	$<10\pi$ mm-mrad
Time between injections	2 sec
Fraction of beam accepted	>85% of injected pulse
Flux	4×10^7 \bar{p} /sec

Final Stack

Number of \bar{p} 's	5×10^{11}
$\Delta p/p$	0.05%
Horizontal and vertical emittance	2π mm-mrad
Peak density	1×10^5 eV ⁻¹
Core width (Gaussian part)	1.7 MeV (rms)
Total stacking time	5 hours

TABLE 5-II ACCUMULATOR RING PARAMETERS

Kinetic energy	7.9 GeV
γ_t , transition energy	5.43
$\eta = 1/\gamma_t^2 - 1/\gamma^2$	0.023
Average radius	75.45 m
RF frequency	6.287 MHz

Maximum rf voltage	16.1 KV
Harmonic number	10
Beam gap for injection kicker	115 nsec
Momentum aperture, $\Delta p/p$	2.5%
Betatron acceptance, h and v	10π mm-mrad
Betatron tunes, ν_H	6.611
	ν_V 8.611
Natural chromaticities ζ_H	-8.48
	ζ_V -12.88
Periodicity	3, each with mirror symmetry
Maximum amplitude function, β	33 m
Maximum dispersion value, α_p	8.9 m

5.2 Design Requirements

The lattice of the Accumulator has been designed to accept the injection of antiprotons every few seconds at an energy of 8 GeV, momentum stack and stochastically cool the antiprotons, accumulate over a period of several hours a very dense core of antiprotons, and, finally extract a high-intensity beam to re-inject into the Main Ring and Tevatron. The requirements on the lattice are twofold. The Accumulator must be a high-class storage ring capable of reliable operation, and it must accommodate all the conditions imposed by the stochastic-cooling systems. The second set of requirements has led to the design of this ring and its somewhat unusual appearance, while those of the first set have also been incorporated. These conditions are:

- (i) The momentum mixing factor must be correct.

$$|1/\gamma_t^2 - 1/\gamma^2| = 0.023$$

where γ_t is the transition gamma of the ring and γ is the relativistic factor of the particle. Thus for 8-GeV kinetic energy the ring must have

$$\gamma_t = 5.41$$

- ii) There must be several long straight sections, some 16 m long, with very small transverse beam sizes. Some of these must have zero dispersion, and the rest dispersion of approximately 9 m. This requirement leads to the choice of transition gamma below rather than above the γ of the particles.
- (iii) Betatron-cooling straight sections must be an odd multiple of $\pi/2$ apart in betatron phase. Pickup and kicker straight sections must be far enough apart physically so that a chord will be at least 75 nsec shorter than the arc for signal-transfer purpose.

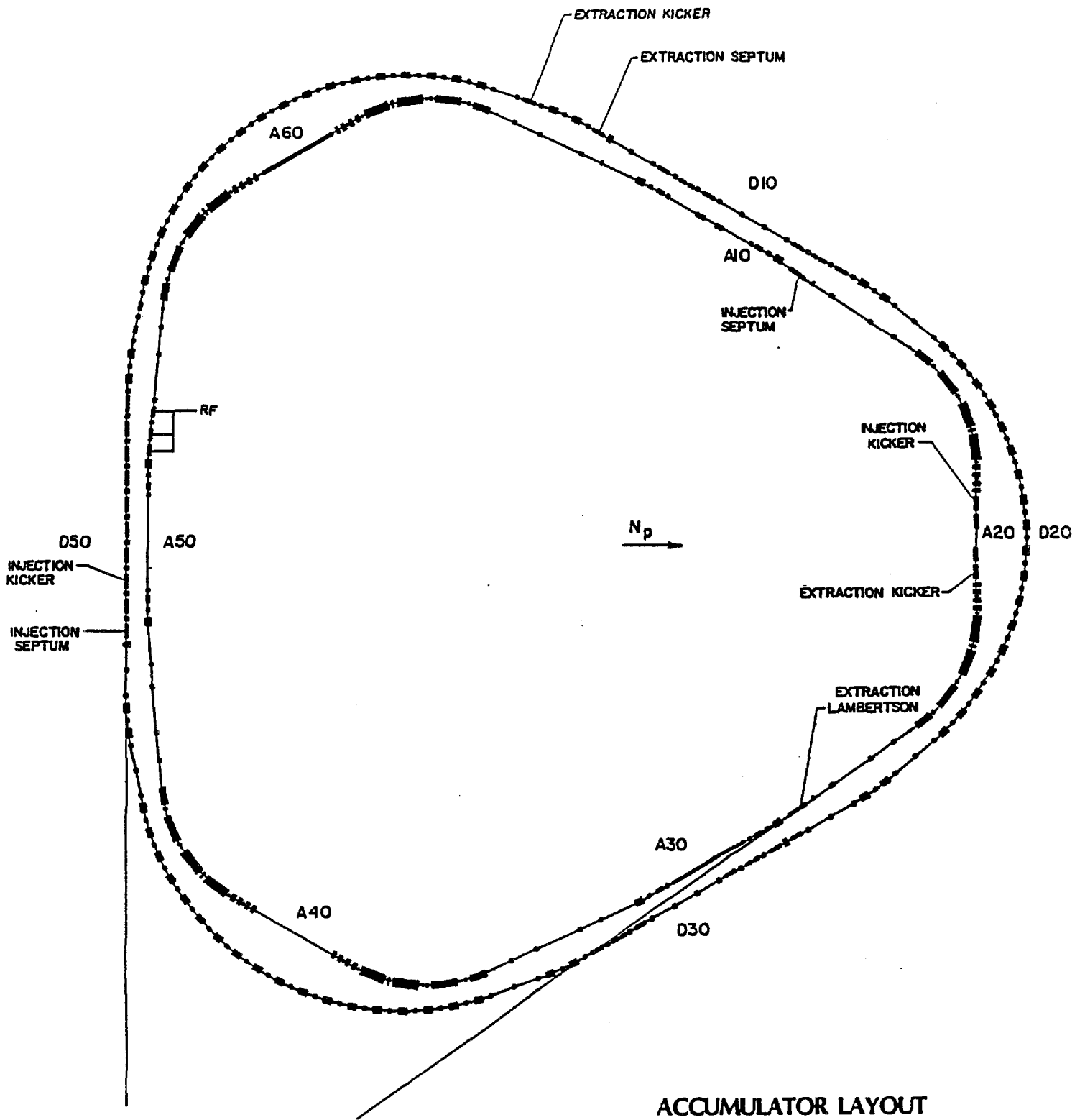


Figure 5-1

- (iv) The β values of the lattice should be about the same for the horizontal and vertical planes in the straight sections.
- (v) The ring should match the Booster circumference.
- (vi) There should be easy injection and extraction schemes.
- (vii) The beam everywhere should be as small as possible, consistent with the large-dispersion straight sections.
- (viii) The ring must have very good chromaticity corrections, be situated far from any resonances, have tuning flexibility, and generally be a good storage ring.

5.3 Accumulator Lattice

The lattice chosen is a six-sided ring with six 16-m long straight sections placed between optical triplets. The dispersions of the straight sections alternate between zero and 9 meters. The lattice has mirror symmetry about the straight sections and periodicity three. The middle quadrupole of the triplets near the high dispersion straight sections has been split in order to allow space for orthogonal chromaticity correction and to reduce the required sextupole fields. A plan view of the ring is shown in Fig. 5-1. The triangular shape was chosen as the most efficient in terms of the stochastic-cooling requirements. A ring with four straight sections and periodicity two will not allow a signal to be propagated from a high-dispersion to a zero-dispersion region fast enough relative to the beam. Lattices with eight and ten straight sections were considered, but had several drawbacks, including the fact that they severely limited the amount of non-straight section free space in which to put trim and correction elements.

Table 5-III lists the lattice structure and parameters for the Accumulator. The lattice functions for one sixth of the ring are plotted in Fig. 5-2.

TABLE 5-III DETAILED ACCUMULATOR PARAMETERS

1. General

Kinetic Energy (central orbit)	7.94779 GeV
Bend field	16.84 kG
Magnetic bend radius (ρ)	17.46 m
Circumference	474.07 m
Revolution time	1.59 μ sec
Superperiodicity	3
Focusing structure	Separated function FODO normal cell
Nominal working point	

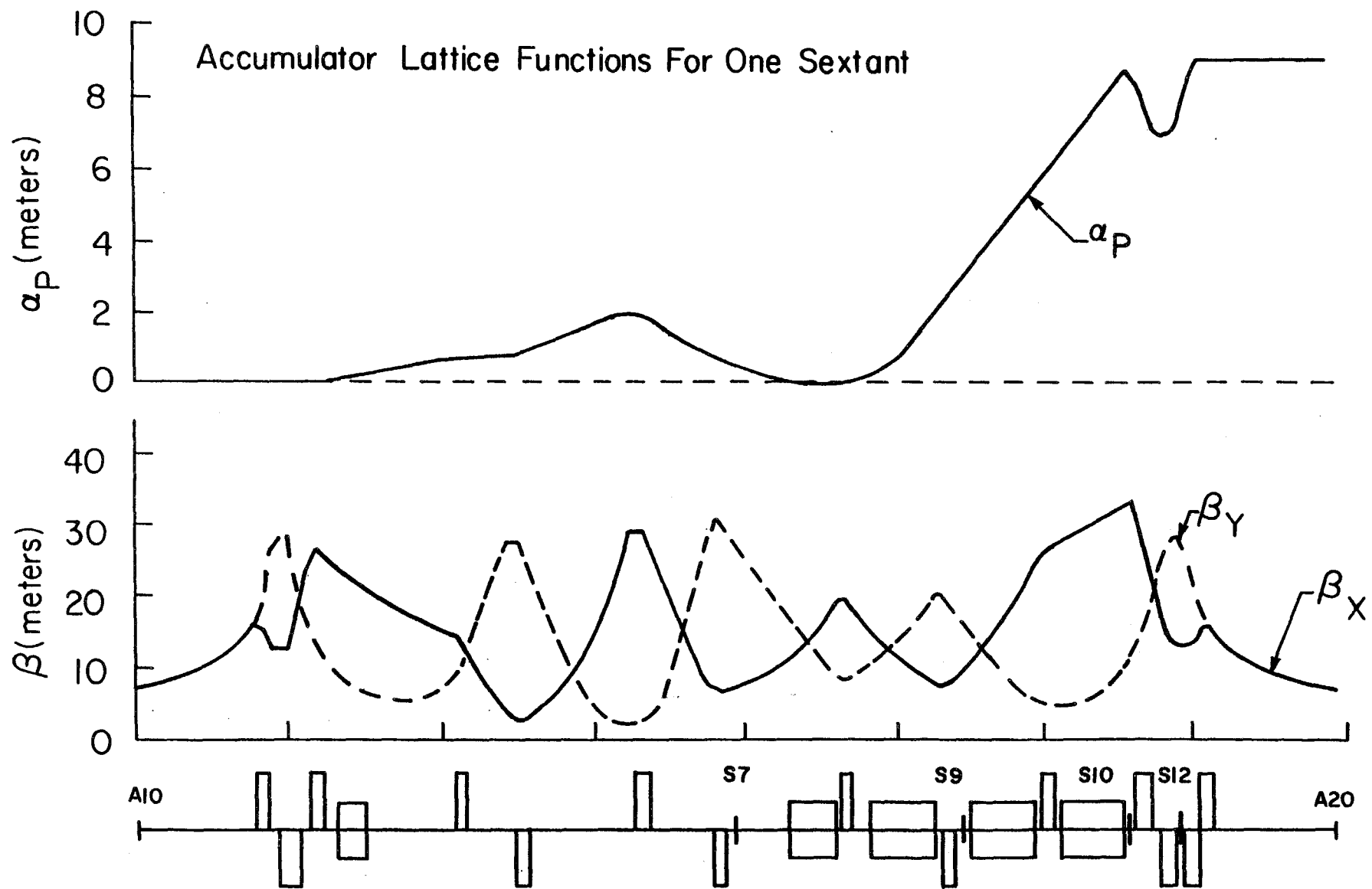


Figure 5-2

ν_x	6.61
ν_y	8.61

Nominal chromaticity

ξ_x	-8.52
ξ_y	-12.93

Chromaticity-Corrected Parameters

	Injection Orbit	Stacking Orbit	Core Orbit	Central Orbit
Kinetic Energy (GeV)	8.02951	7.96229	7.89068	7.94779
$\Delta p/p$ (%)	+0.930	+0.165	-0.690	
ν_x	6.616	6.611	6.614	
ν_y	8.611	8.611	8.611	
ξ_x	2.05	1.13	-0.22	
ξ_y	0.21	0.32	0.33	
γ_t	5.37	5.42	5.50	
$1/\gamma_t^2 \rho - 1/\gamma^2$	0.023	0.023	0.022	

2. Magnets

Number of dipoles 30
 Number of quadrupoles 84
 Number of sextupoles 24
 A. Small-aperture dipoles

	<u>Length</u>	<u>Field</u>	<u>Number</u>
(B3)	5.0 ft.	16.84 kG	6
(B7)	10.0 ft.	16.84 kG	6
(B8)	15.0 ft.	16.84 kG	6

B. Large-aperture dipoles

(B9)	15.0 ft.	16.84 kG	6
(B10)	15.0 ft.	16.84 kG	6

C. Small-aperture quadrupoles

(Q1)	25.2 in.	103.81 kG/m	6
(Q2)	51.6 in.	-103.81 kG/m	6

(Q3)	27.6 in	103.81 kG/m	6
(Q4)	18.0 in	96.63 kG/m	6
(Q5)	32.6 in	-97.41 kG/m	6
(Q6)	27.6 in	96.63 kG/m	6
(Q7)	27.6 in	-97.41 kG/m	6
(Q8)	18.0 in	96.63 kG/m	6
(Q9)	18.0 in	-97.41 kG/m	6

D. Large-aperture quadrupole

(Q10)	18.0 in	40.88 kG/m*	6
(Q11)	34.4 in	89.40	6
(Q12)	30.4	-89.40	6
(Q13)	30.4 in.	-89.40	6
(Q14)	25.3 in.	89.40	6

*Q10 will be built with missing turns to run in series with the other large aperture quadrupoles.

E. Sextupoles

(S7)	8.0 in.	53.58 kG/m ²
(S9)	8.0 in.	-329.28
(S10)	10.0 in.	162.16
(S12)	10.0 in.	-205.01

F. Octupoles

(O10)	10.0 in.	-390.33 kG/m ³
(O12)	10.0 in.	325.12 kG/m ³

3. Structure

A. Drift Lengths

LS	7.9465 m
LS*	7.8449
01	0.5124
02	0.9606
03	0.9042
0B3	6.4237
04	3.2610
05	7.3478
06	4.1872
07	0.3556
0S7	3.8866
0B7	0.5080
08	1.2192
0B8	0.5080
09	0.3556
0S9	0.6604

OB9	0.5080
O10	0.5080
OB10	0.3173
OS10	0.3173
O11	0.5210
O12	0.2432
OS12	0.2432
O13	0.4972

B. Sextant Structure (S)

LS (Q1)	O1 (Q2)	O2 (Q3)	O3 (B3)	
OB3 (Q4)	O4 (Q5)	O5 (Q6)	O6 (Q7)	
O7 (S7)	OS7 (B7)	OB7 (Q8)	O8 (B8)	
OB8 (Q9)	O9 (S9)	O9 (B9)	OB9 (Q10)	
O10 (B10)	OB10	(S10)	OS10 (Q11)	O11 (Q12)
O12 (S12)	OS12	(Q13)	O13 (Q14)	LS*

C. Ring Structure

S(S)S(S)S(S)

Length of central orbit 474.0702 m
 1555.348 ft

4. Aperture and Acceptance

Maximum Lattice functions (central orbit)

	β_x	β_y	α_p
Center of LS1	7.565 m	7.268 m	0.000 m
End of LS1	15.912	15.956	0.000
Center of LS2	7.577	7.520	8.946
End of LS2	15.699	15.704	8.946

Required beam

Emittance $\epsilon_x = \epsilon_y < 10\pi$ mm-mrad
 Momentum aperture $\Delta p/p \pm 1.25\%$

<u>Beam Size</u>	<u>A_x</u>	<u>A_y</u>
Small-aperture dipole	52.4 mm	29.2 mm
Large-aperture dipole	219.6	17.3
Small-aperture quadrupole	68.3	36.9
Large-aperture quadrupole	246.3	33.1
Small-aperture sextupole	54.9	34.1
Large-aperture sextupole	245.4	33.2

Injection into and extraction from this ring are done in a similar manner. The injection orbit is displaced radially outward by approximately 0.9% in $\Delta p/p$. The shuttered kicker in the high-dispersion straight section is closed just before the \bar{p} 's are injected. The momentum displacement is enough to allow the injected beam to clear the shutter. Beam is transferred from the Debuncher ring via two 2 m long, 6-kG current septum magnets located near the upstream end of a zero-dispersion straight section. It arrives at the kicker and is kicked onto the injection orbit. The kicker is 2 m long and has a field of 500 G. The shutter is then opened and the beam is rf stacked. A drawing of the injected, stacked and accumulated beams at the position of the shuttered kicker is shown in Fig. 5-3. The injection and extraction positions are shown on Fig. 5-4.

The beam envelope for one half of a superperiod is shown in Fig. 5-5. Four orbits have been superposed, corresponding to the rf-displaced injection orbit, the stacking orbit, the accumulated antiprotons, and the very dense core.

5.4 Tuning

The Accelerator ring is designed to have a nominal tune of 6.61 horizontally and 8.61 vertically for the central orbit. This puts the working point in a region clear of all resonances up to 15th order. It is easily tunable over a large range using the four existing quadrupole buses - QF, QD in the "regular" part of the lattice and QT, QL, the triplet buses for the zero and high dispersion straight sections, respectively. The tuning properties of the Accumulator are totally linear over a large range of values. While the beta and dispersion values vary as a function of tune in the straight sections, the variation is very small and causes no problems up until the structural stop band $\nu_y = 9.0$. A list of the tuning parameters is given in Table 5-III and is plotted in Fig. 5-6. The natural chromaticity vs. tune is shown in Fig. 5-7 and the zero-dispersion straight section lattice functions vs. tune are plotted in Fig. 5-8.

5.5 Chromaticity Corrections

The Accumulator has a momentum aperture of about 2%, 1% for stochastic accumulation and 1% for rf stacking. The largest part of the beam stays near the edge of the aperture for several hours. It must be noted that the equilibrium orbit for an off-momentum beam is changed so drastically in the curved section that the octupole tune shift coming from edge effects of the quadrupole magnets becomes very significant in the vertical plane. In principle, we can reduce this octupole tune shift by a suitable configuration of sextupoles, which gives large second-order sextupole fields. We avoid such a configuration for the stability of betatron oscillations. We take care to minimize the distortion of transverse emittance coming from nonlinear kicks in sextupoles, because the geometry of the pickups and kickers is very tight. We use four families of sextupoles and two families of octupoles, where each two families of sextupoles and octupoles correct the chromaticity and the additional two

ACCUMULATOR BEAM AT END OF HIGH DISPERSION STRAIGHT (at kicker)

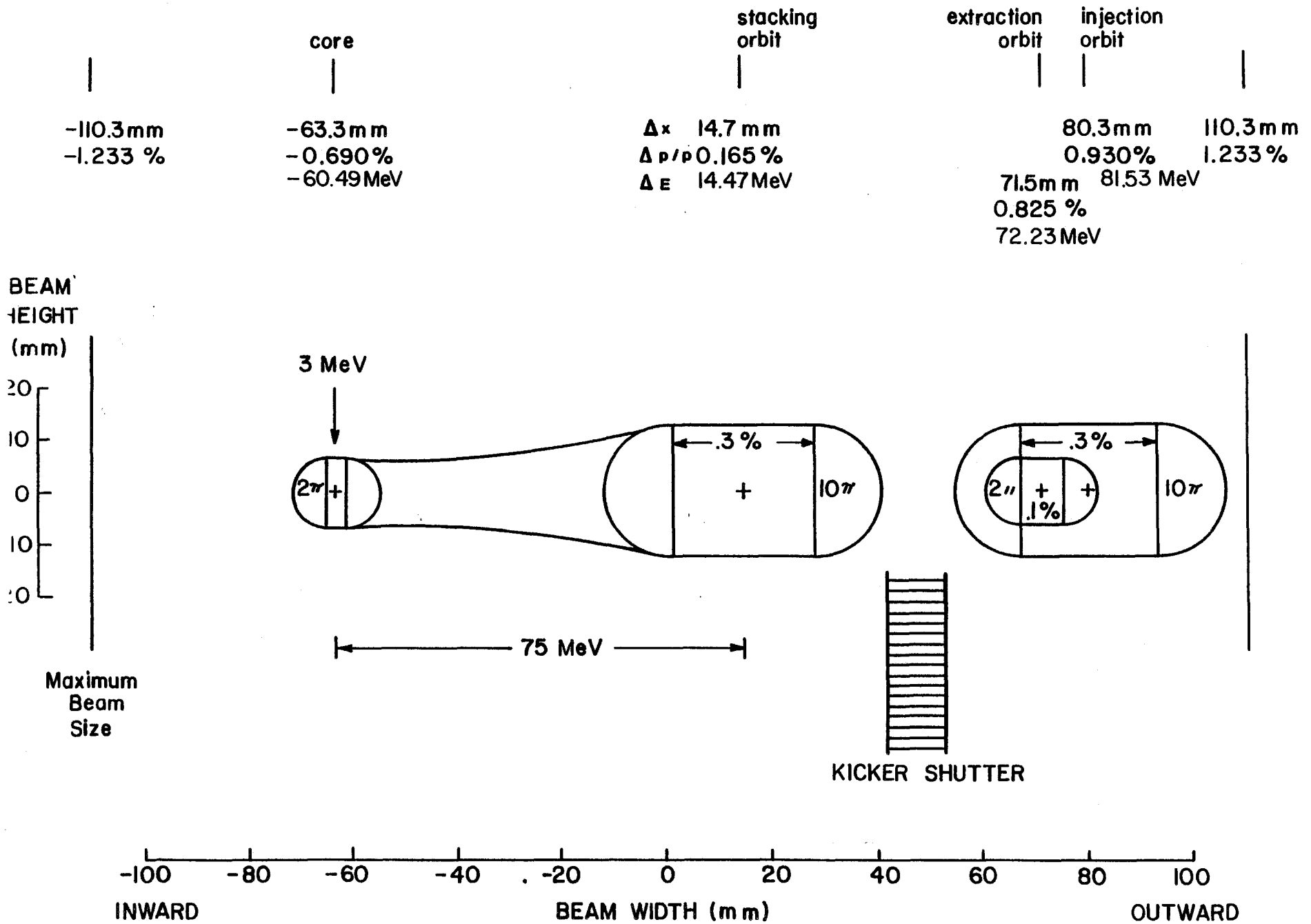
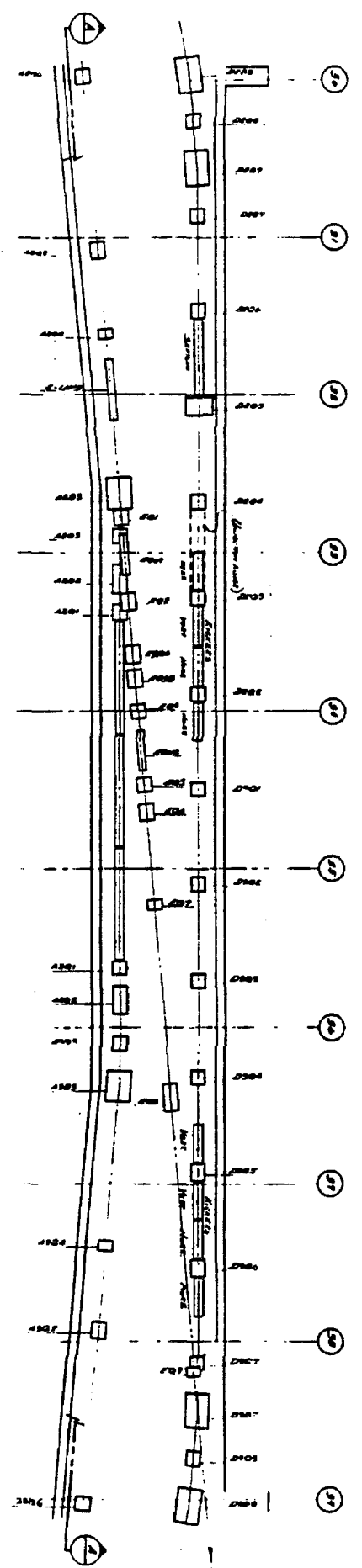
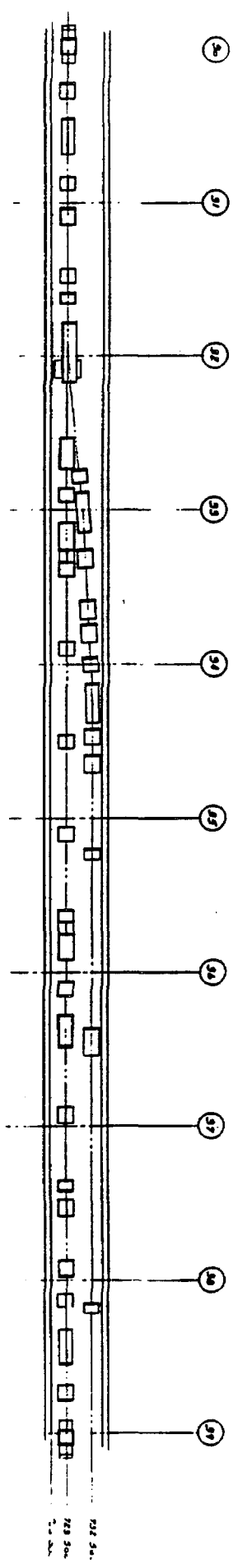


Fig. 5-



Injection Straight Section



Extraction Straight Section

Figure 5-4

100.00 MM
MAX.

100.00

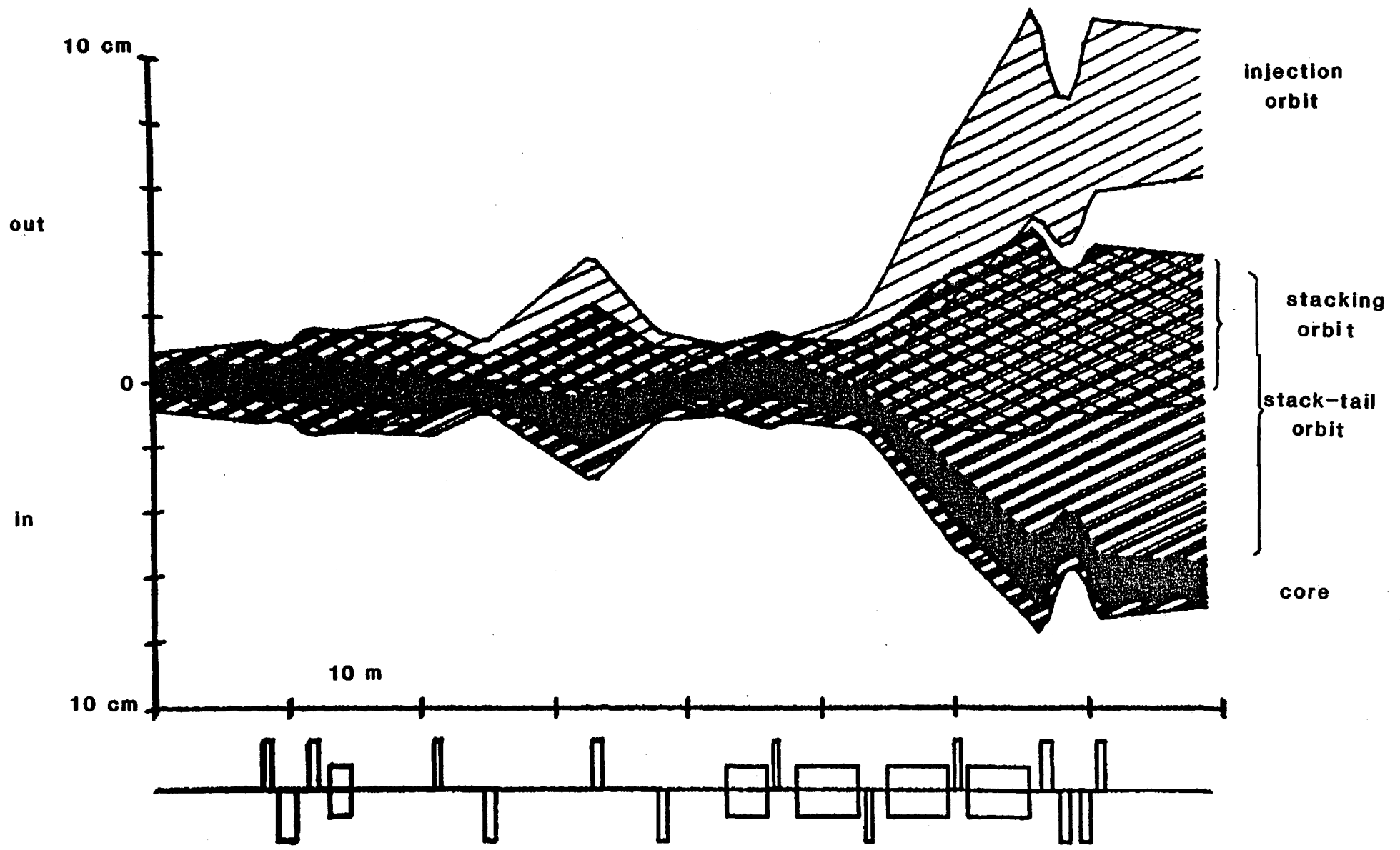


Figure 5-5

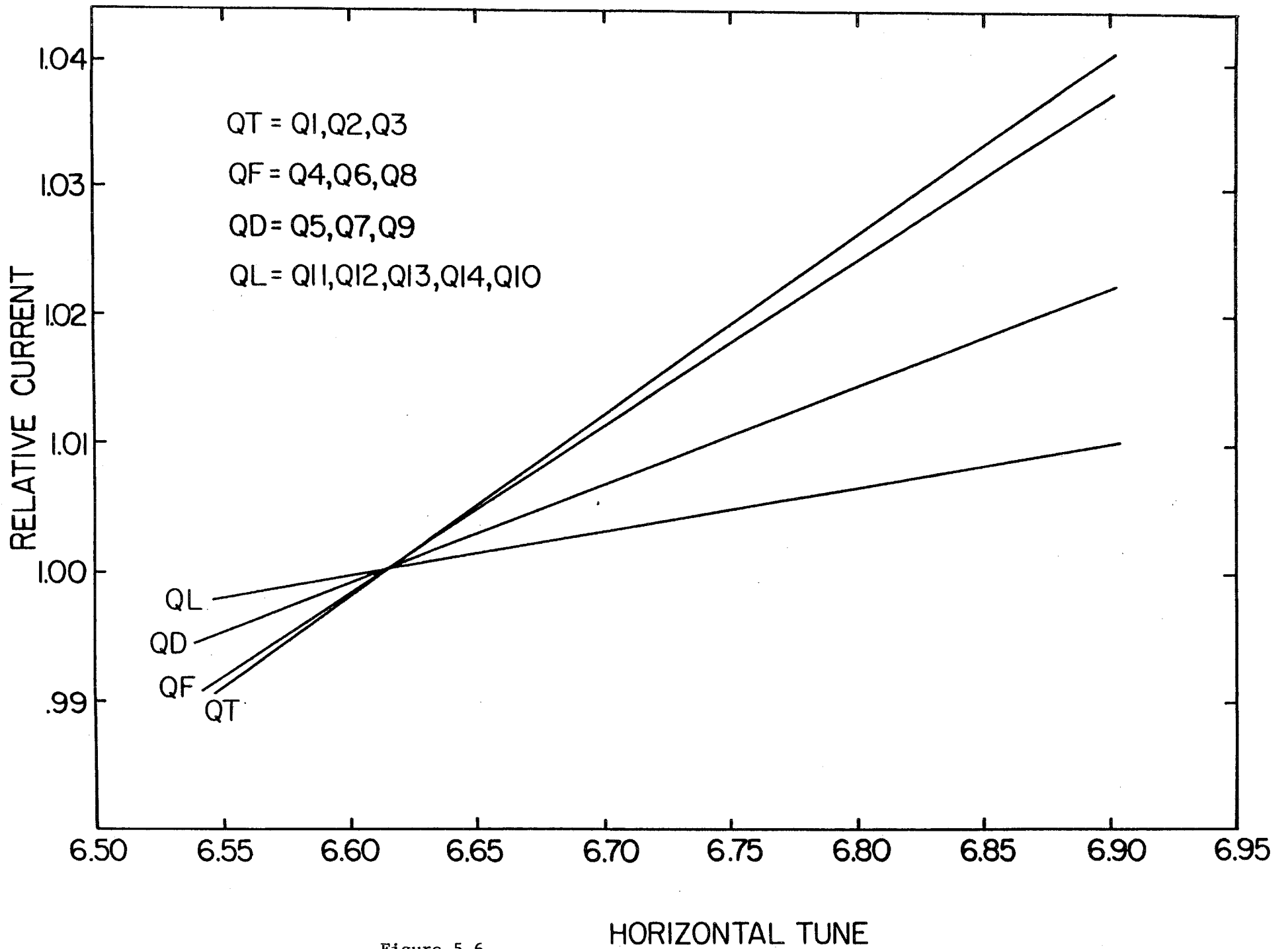


Figure 5-6

Accelerator Natural Chromaticities vs. Tune

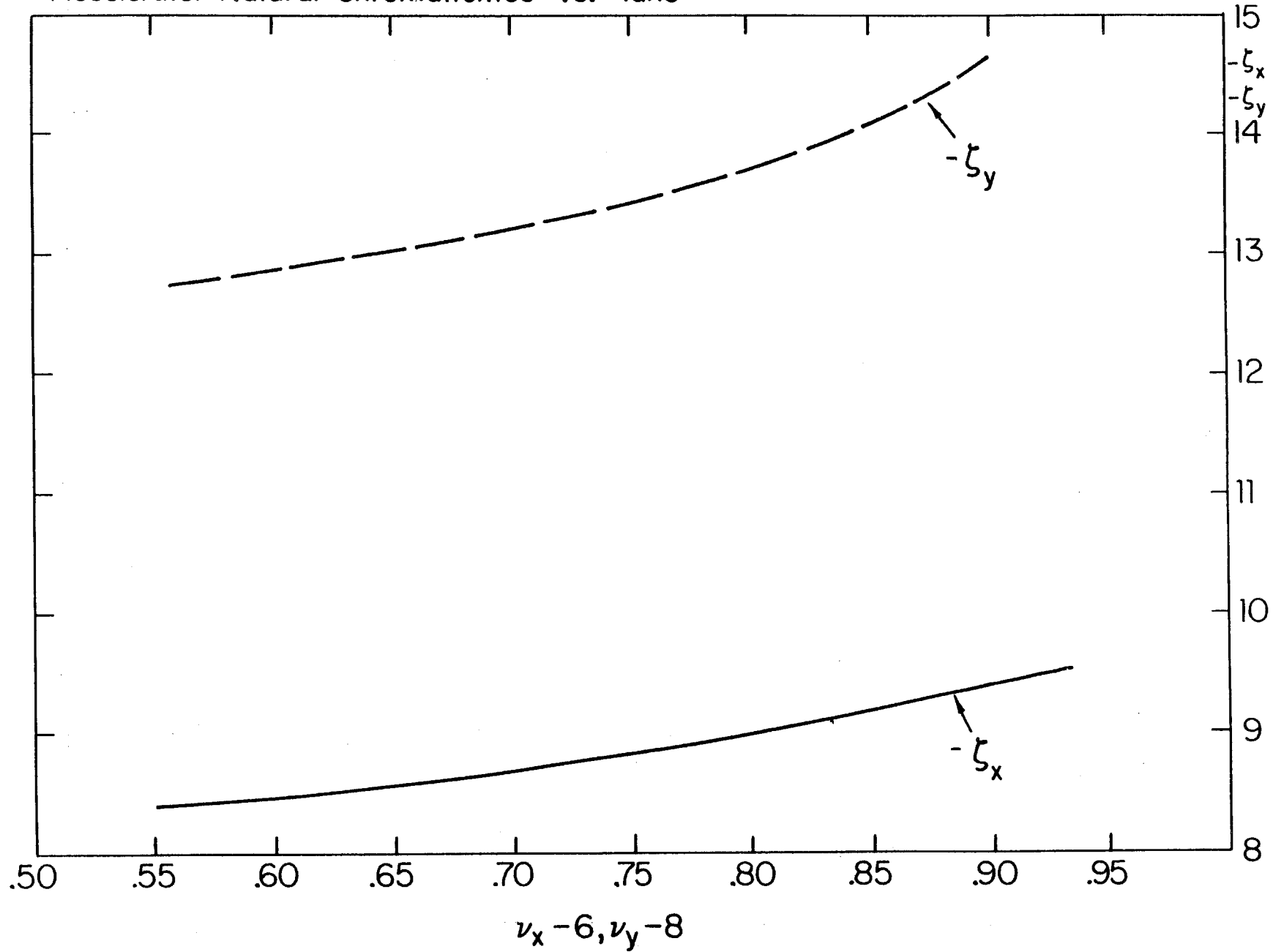


Figure 5-7

Accumulator Lattice Functions in Zero Dispersion S.S.

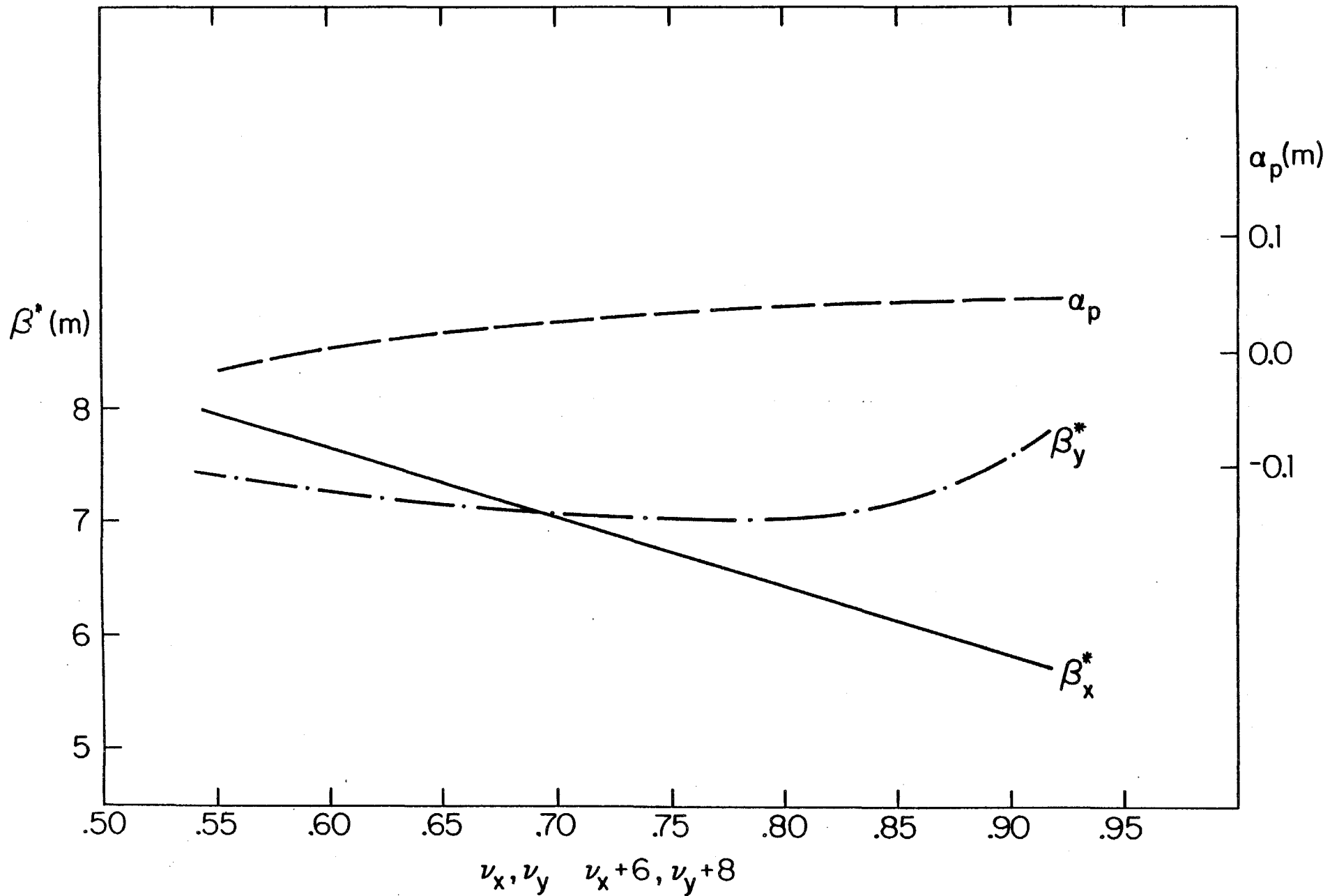


Figure 5-8

families of sextupoles compensate the emittance distortion. The locations and strengths of these multipoles are given in Table 5-III. The lattice also has enough space to install more sextupoles or any multiples if they are necessary for more correction.

5.6 RF Stacking System

With the injection shutter closed, antiprotons are injected from the Debuncher ring with a total momentum spread of about 0.2%. The energy spread (18 MeV) and the Accumulator revolution period (1.59 μ sec) result in an injected longitudinal emittance of about 29 eV-sec. This beam is bunched adiabatically and decelerated by 0.7% to the end of the tail of the previously stacked antiprotons where it is released by adiabatic debunching. Adiabatic capture can begin and can be completed within about 50 msec.

The phase-oscillation period is 10 msec and the deceleration time is 30 msec. The entire operation of establishing a moving bucket, deceleration, and adiabatic debunching can be accomplished within 0.1 seconds after the beam is injected.

At frequencies well below the GHz cooling band, the cooled core may be subject to longitudinal instabilities induced by the shunt impedance of the stacking rf cavity. The rf voltage required to establish a given phase-space area increases linearly with the harmonic number and, because the power required is $V^2/2R_{sh}$, the required rf power increases linearly, given the stability limit^{sh} on the shunt impedance. Consequently, to minimize the cost, size, and complexity, it would appear that rf stacking should be done at the lowest possible harmonic number. On the other hand, very low harmonic numbers and very low voltages result in excessively long synchrotron periods that are not consistent with the rapid production cycling rate. An adequate compromise appears to be $h = 10$, 6.289 MHz. An rf system at this frequency with an effective shunt impedance of 5 k Ω meet the requirement that $Z/h = 500 \Omega$. The parameters associated with rf stacking at $h = 10$ are listed in Table 5-IV. The shunt impedance of the bunching cavity is in agreement with this stability requirement for harmonics of interest.

TABLE 5-IV RF STACKING PARAMETERS

Injected Longitudinal Emittance	30 eV sec
Stacking rf Total Bucket Area	33 eV sec
Stationary Bucket RF Voltage	10 kV
Stationary Bucket Phase Oscillation Period	8.1 msec
$\Delta p/p$ Required for Stacking	0.77%
Δ (cp)	69.2 MeV
Deceleration Synchronous Phase Angle	10 degrees
$\Gamma = \sin \phi_s$	0.1736
Moving Bucket Factor $\alpha(\Gamma)$	0.6964

RF Voltage During Deceleration	16.1 kV
Time Required for Deceleration	30.2 msec
Number of Cavities	1
Cavity Structure	40 NiZn Ferrite Cores
Cavity Small Signal Shunt Impedance	5 k Ω
Peak RF Power Requirement	10 kW
Average RF Power Requirement (Cooling, etc)	1 kW
Harmonic Number	10
RF Starting Frequency	6.28695 MHz
$\eta = \gamma_t^{-2} - \gamma^{-2}$	0.023
$\beta = v/c$	0.99447
Injection Orbit Circumference	474.202 m
Stacking Efficiency*	98%

*Based on computer simulation

5.7 Accumulator Magnets

The main magnet system consists of 30 dipoles and 84 quadrupoles. In Table 5-III is shown a list of magnets, lengths, strengths and required apertures. The required apertures were calculated assuming construction tolerances of 2.5×10^{-4} (relative standard deviation) for dipole strengths, dipole level angles (radians), and quadrupole random position errors (meters). Sufficient space is allowed for at least 4σ , where σ is the standard deviation of the expected orbit position error, or the beam emittance plus momentum spread plus 10 mm whichever is larger. In addition, space is left for 4-mm (thickness plus deflection) vacuum chamber thickness and 5-mm insulation thickness. Several mm must be included also for heating tapes to bake the chamber (dipoles). The specification of these magnets are listed in the tables of Chapter 12.

There are three lengths of dipoles, all with field strengths of 1.689 T. There are 2 different apertures, 3 different lengths in the smaller aperture, in the larger. Because of the large sagitta, these magnets will be curved. The coils will be made of four pancakes plus two single-layer saddle coils.

There are 13 different quadrupoles, of two different profiles. Q1-Q9 have poletip radii of 1.75 mm and 5 different lengths. Q10-Q14 have poletip radii of 3.312 in and four different lengths. Each quadrupole will have a shunt with capability of about 10% of the quadrupole strength. The coils are fabricated in individual layers and assembled on the quad half cores, which are then assembled as a complete magnet.

There are 24 sextupoles of two types. S7 and S9 have a poletip radius of 71.4 mm and a length of 20.3 cm. The (maximum required strength is 33.0T/m². These sextupoles will be the same as those used in the Debuncher

and will be constructed with parallel-sided poles and a single-layer 6-turn winding. S10 and S12 are located in the high dispersion region and require an aperture of 96.5 mm x 300.0 mm (vertical and horizontal). These magnets will have a rectangular aperture with a variable current density across the upper and lower poles to produce the desired field. Octupole and vertical (correction) dipole windings will also be incorporated. The maximum required strengths are 20.5 T/m² (s), 39.0 T/m³ (O), and .064 T (D). The sextupoles are divided into four families each with its own power bus. There are two families of octupoles. These magnets are described in Tables 5-V and 5-VI.

TABLE 5-V ACCUMULATOR SEXTUPOLES

Max. B"	205	330 T/m ²
l eff	0.25	0.20 m
poletip radius	96.5x300.	71.4 mm
NI	6420	1550 AT/pole
Max. I.	430	2560 A
N	15	6 Turns/pole
Conductor		
Current density	5.2	5.0 A/mm ²
R	8.6	5.6 mΩ
Max. voltage drop	3.7	1.5 V
Max. ohmic loss	1575	375 W
Weight, cu	63	16 lbs
Fe	590	200 lbs

TABLE 5-VI ACCUMULATOR OCTUPOLES

Max. B"	39.0	T/m ³
Length	0.25	m
Aperture	96.5x300	mm
Current	15	A
Current Density	2.3	A/mm ²
Turns	120	
R	0.22	Ω
Voltage	3.2	V
Power	47.0	W
Number of magnets	12	

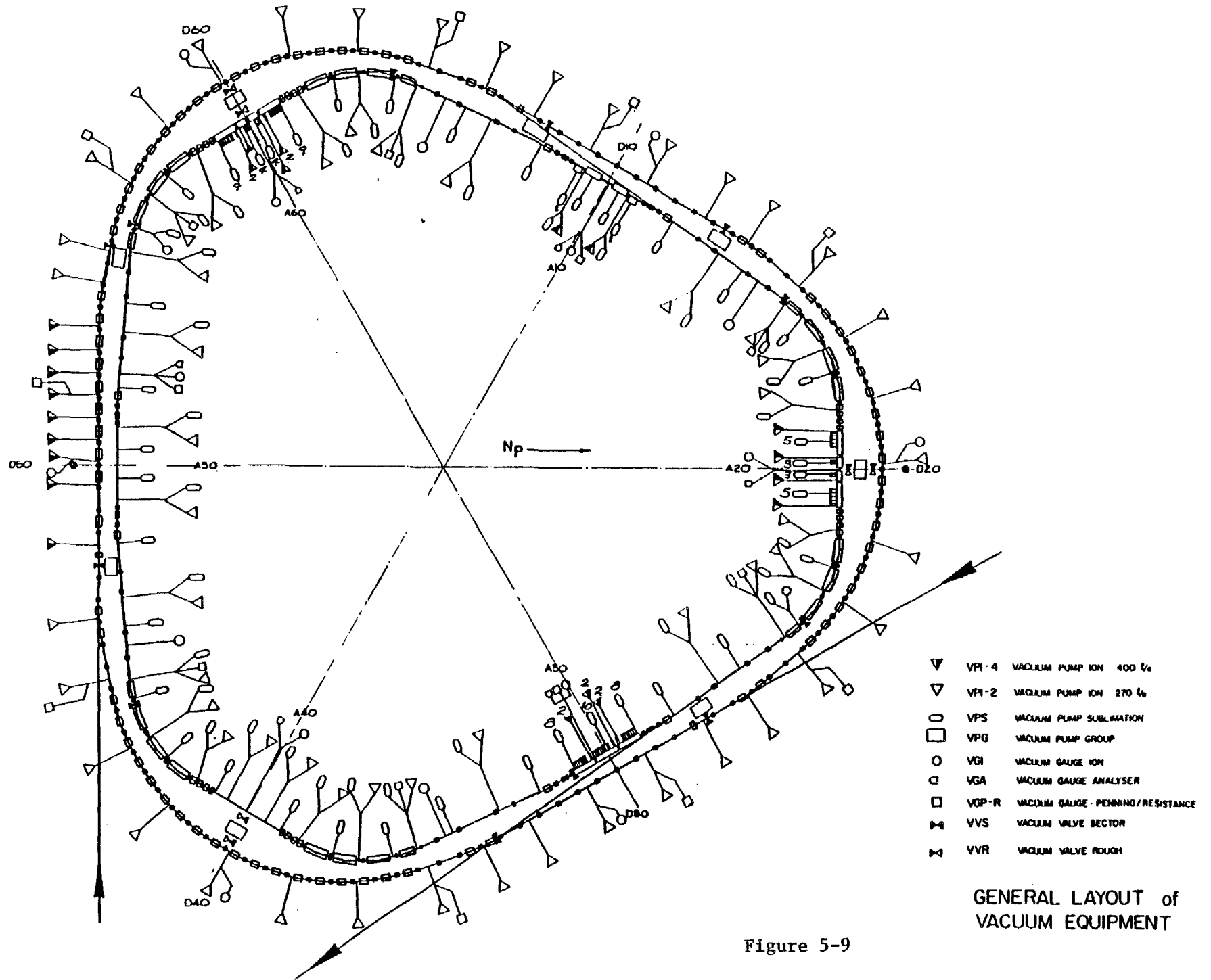


Figure 5-9

5.8 Accumulator Vacuum System

5.8.1 Vacuum Requirements. The base pressure is determined by the effects of the residual gas on the accumulated antiproton beam. These effects include particle loss by single Coulomb scattering and nuclear interactions, beam heating by multiple Coulomb scattering, energy loss by ionization, and effects of neutralization by positive ions attracted to the negative beam.

A detailed analysis has been made¹ of these effects. As a result, the system is designed for a nominal pressure of 3×10^{-10} Torr (nitrogen equivalent). At this pressure, the single-scattering lifetime will be 240 hr and the nuclear-interaction lifetime will be 2000 hr. Thus these effects are negligible. The heating rate for the final stack from multiple scattering will be 2×10^{-5} /sec, 10 times less than the cooling rate. (Here a gas composition of 50% H₂, 50% N₂ or CO is assumed). The energy loss per antiproton will be 20 keV/hr. Both the heating and energy loss can be easily compensated by the stochastic-cooling systems. We will keep the nominal design value of the neutralization factor $H < 0.03$. With this value, the scattering by positive ions trapped in the beam will be increased less than 2%. The vertical space-charge tune shift will be reduced by 10^{-3} . Thus these neutralization effects are negligible.

5.8.2 Vacuum System Layout and Characteristics. The pressure requirement can be met with a combination of sublimation sputter ion-pumps. Furthermore, vacuum-annealed austenitic high-tensile stainless steel will be used for the chambers so that specific degassing rates of better than 1×10^{-12} Torr-ℓ/cm²-sec can be attained. The maximum design bakeout temperature is 300°C.

Figure 5-9 shows the vacuum-system layout over one-sixth of the Accumulator ring. The sputter ion pumps should have a speed of 200 ℓ/sec. The stochastic-cooling pickups and kickers will be isolated with all metal valves, during the bakeout to prevent any vacuum contamination. These valves will divide the ring into approximately 5 irregular vacuum sectors.

The baking equipment (heaters, controls, thermal insulation) will be installed in a permanent fashion to allow bakeout to proceed without major preparations. Exceptions are areas that cannot tolerate the high temperature e.g. pump magnets, cable feed throughs and special devices.

Pump-down during bakeout will be carried out using mobile turbopump carts. This will allow the use of a large number of pumps in any given section being baked. These carts will be connected to metal valves distributed for that purpose throughout the system. Tests indicate that the pressure during bakeout has little effect on the success of the bake.

Vacuum gauges include 6 Pirani gauges to monitor pumpdown, 36 Bayard-Alpert ionization gauges, and 6 mass-analyzer heads, located near areas of complex equipment to monitor leaks and contamination.

The stochastic-cooling equipment will be capable of being baked at a maximum temperature of 150°C and materials compatible with the high-vacuum requirements will be used. Sublimation and ion pumping will be used to provide a pumping speed of up to 2000ℓ/sec/m.

Clearing electrodes will be installed to remove low-energy positive ions and thus keep the neutralization factor $H < 0.03$. There will be a pair of electrodes at the downstream end of each magnet. Ions move longitudinally to the electrodes by $E \times B$ drifting caused by the beam electric field and the ring guide field. This kind of system has been used successfully in the ISR.

The straight sections between magnets will also need clearing electrodes to avoid trapping ions in the cool-beam potential of 5 V. We plan to apply a dc potential of more than 5 V to the clearing electrodes and to the beam-position detector electrodes whenever these are in a suitable location.

All devices and ring sections will undergo a preliminary bake and low-pressure test before being installed. Their design will conform with strict rules of choice of material and will be subject to approval by the vacuum coordinator.

The vacuum control system will be constructed along the design evolved for the Tevatron. It is highly modular and economical. Many of the required modules and device controls have already been developed, including ion-pump supplies and ion-gauge controllers. A card cage containing all control modules will interface to the host computer through a CAMAC module. Much of the necessary software can be used or adapted.

5.9 Momentum Cooling

5.9.1 Introduction to Stochastic Stacking. The stochastic stacking system consists of pickup electrodes, an amplifier system with electronic filters and phase-compensation networks, and kicker electrodes. Each particle produces an electronic signal that, when applied to the kicker, changes its momentum in the direction of the core. The signal of each given particle thus produces a kick that tends to cool the beam into a small momentum width around the core. Other particles in the beam with approximately the same revolution frequency produce random kicks on the given particles and cause diffusion or heating. The interesting systems, of course, are those in which cooling dominates over heating.

Momentum cooling is usually described in terms of the Fokker-Planck equation

$$\frac{\partial \psi}{\partial t} = \frac{\partial}{\partial E} [-F\psi + (D_0 + D_1 + D_2\psi) \frac{\partial \psi}{\partial E}] \quad (5.1)$$

where $\psi = \partial N / \partial E$ is the particle density, F is the coefficient of the cooling term, D_0 is the coefficient of the heating term due to intrabeam scattering (described later), D_1 is the coefficient of the heating term due to thermal noise, and D_2 is the coefficient of the heating due to other particles. A derivation and discussion of this equation are given by Mohl et al.²

A simplified version of the Fokker-Planck equation has been used by van der Meer³ to describe the stacking process. It is assumed that the voltage on the kicker is exactly in phase with the particles that created it, that there is no amplifier thermal noise or intrabeam scattering, the feedback gain is independent of harmonic number, and that there are no beam-feedback effects. A more general approach, including thermal noise, is possible.* While none of these assumptions is justified in the proposed system, the simplified discussion yields semi-quantitative results that can form the basis of a design. Following van der Meer, the flux can be written as

$$\dot{\Phi} = - \frac{V}{T} \psi - AV^2 \psi \frac{\partial \psi}{\partial E}, \quad (5.2)$$

cooling term heating term

where $N(E,t)$ is the number of particles with energy less than E and

$$\dot{\Phi} = \frac{\partial N}{\partial t}$$

$$\psi = \frac{\partial N}{\partial E},$$

from which the Fokker-Planck equation

$$\frac{\partial \psi}{\partial t} = \frac{\partial \phi}{\partial E} \quad (5.3)$$

follows. Here $V = V(E)$ is the average energy loss per turn and T is the revolution period. The constant A describes the strength of the heating term and is given by

$$A = \frac{\beta p \Lambda}{4T^3 W^2 |\eta|} \quad (5.4)$$

where $\beta = v/c$, p is the momentum, T is the revolution period, W is the bandwidth $= f_{\max} - f_{\min}$, $\Lambda = \ln(f_{\max}/f_{\min})$, and $\eta = \gamma_t^{-2} - \gamma^{-2}$. If the amplifier gain is not independent of frequency, Λ is modified. The ideal gain profile, in fact, rises linearly with frequency, but the exact value of Λ is not important for this discussion.

The Fokker-Planck equation is nonlinear in ψ and it is therefore usually solved numerically. Stationary solutions, $\phi(E,t) = \phi_0 = \text{constant}$, can often be found by elementary methods. These solutions are useful because in the stack tail between the core region and the injection region, the actual time-dependent solution is normally very close to the steady-state solution.

Consider $\phi_0 = \text{constant}$ and $\psi(E,t) = \psi(E)$, and ask what the shape of the voltage profile $V(E)$ should be. The answer, as given by van der Meer, is to maximize $d\psi/dE$ everywhere and thus minimize the energy aperture which is required. This choice also minimizes the total Schottky power in the amplifier. The solution is

$$V(E) = -\frac{2\phi_0 T}{\psi(E)} = -\frac{2\phi_0 T}{\psi_1} e^{-(E_1 - E)/E_d} \quad (5.5)$$

where ψ_1 is the initial stack-tail density at E_1 and E_d is the characteristic energy

$$E_d = -4A\phi_0 T^2 = -\frac{\beta p \Lambda \phi_0}{TW^2 |\eta|} \quad (5.6)$$

This equation exhibits the major design consideration. We know that $d\psi/dE$

is maximized by a gain profile $V(E)$ that is exponential in energy. The exponential slope $d\psi/dE$ is maximized by minimizing E_d . In the stack tail, we want a density increase of 1000, so we require a minimum momentum aperture of $\Delta p/p = \ln(1000) E_d/p = 6.9 E_d/p$. If we want to limit the aperture ($\Delta p/p$) required for the stack tail to 0.75%, then $E_d = 0.001 p \approx 10$ MeV for $p = 8.9$ GeV/c. Since we want to have Φ_0 as large as possible, we must make E_d small by choosing $TW^2|\eta|$ to be as large as possible. The density profile is shown in Fig. 5-10.

We have chosen to work with a maximum frequency of 4 GHz for the purposes of this report, but we intend to use frequencies up to 8 GHz for core cooling if our research program indicates that 8 GHz cooling systems are practical. The stack-tail system was chosen to have a maximum frequency of 2 GHz. As described below, the choice of frequency dictates the choice of η . By limiting the stack-tail system to 2 GHz, we are able to use a relatively high η ($\eta = 0.02$). The high value of η is useful for the core-cooling systems, where the core cooling times are inversely proportional to η .

The maximum value of η is limited once we choose f_{\max} . For a number of reasons, it is required that $\eta(\Delta p/p) f_{\max} T < \delta$, where δ is some number of order unity. The reasons that determine the value of δ are:

- (i) The Schottky bands must not overlap in a system that uses electronic filters for gain shaping. In such a system, the particle energy is sensed in the electronics by the connection between energy and the harmonics of the revolution frequency. If the relationship is not unique, it is difficult and probably impossible to design appropriate filters. In this case, $\delta = 1$ and $\Delta p/p = 1\%$ so $\eta = 0.03$ with $T = 1.6$ μ sec.
- (ii) The phase shift between PU and kicker must not vary across the momentum band more than about $\pm 45^\circ$. If PU and kicker are exactly opposite in the Accumulator Ring, then $\delta = 0.5$. If the stack-tail system is divided into subsystems with $\Delta p/p = 1/3\%$, then this constraint applies to each system individually, so $\eta = 0.05$.
- (iii) For reasons described below, the filters must have the peak of their response at the tail end and a notch in the core. Between Schottky bands, of course, the response must rise from the notch in the core back to the peak value. Since the rise back to the peak value cannot be done infinitely sharply, at least without undesirable phase characteristics, this requirement is more severe than 1) above. We have found that $\eta = 0.02$ is a suitable value for a maximum frequency of 2 GHz.

We have chosen a Booster-sized ring ($T = 1.6$ μ sec) because it is large enough to accommodate the cooling-system hardware and can run at 8 GeV, a good energy for production of \bar{p} 's and their injection into the Main Ring.

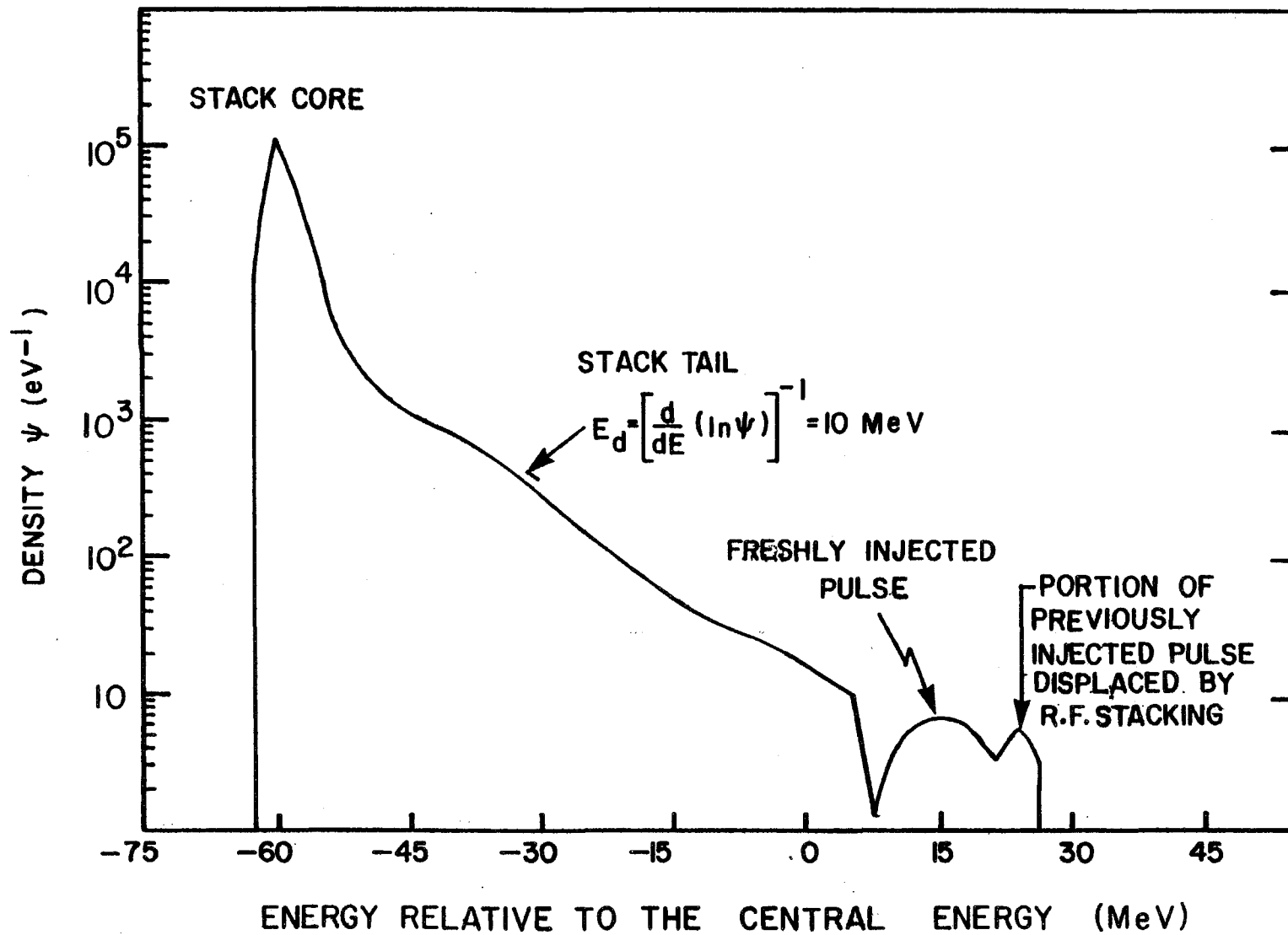


Figure 5-10

5.9.2 Summary of Design Considerations. We have chosen $E_d = 0.001p = 10$ MeV to keep the required momentum aperture sufficiently small. The product $Tf_{\max} \eta$ is fixed by the requirement of a minimum spacing between Schottky bands. We have chosen $W = 1$ GHz with $f_{\max} = 2$ GHz to yield a somewhat higher value of η (0.02) than would be the case if we chose a higher frequency. Higher frequencies also have the disadvantage that it is somewhat more difficult to build the quality of hardware that is required.

5.9.3 Building the Exponential Gain Profile. Once the parameters of the stack tail have been chosen, the next step is to build the required gain profile. We use a combination of two techniques. The first technique is to sense the particle momentum by sensing its position in a region of high momentum dispersion. The position sensitivity of the strip-line pickups we plan to use is given in Section 5.11.1. For large horizontal displacement x the sensitivity of these pickups becomes

$$s(x,0) \propto e^{-\pi x/h}, \quad (5.7)$$

where h is the gap between plates. In our case, the momentum dispersion is $\alpha_p = 9$ m and we have chosen $h = 3$ cm. Thus for large ΔE ,

$$V(E) \propto e^{-|\Delta E|/E^*}, \quad (5.8)$$

$$\text{where } E^* = \frac{\beta^2 E h}{\pi \alpha_p}$$

where $V(E)$ is the average (coherent) particle voltage gain per second, ΔE is the difference between energy E and the energy where the pickup response is centered, and $E^* = 10$ MeV. In our system we use the pickups in the region where the falloff is not truly exponential, but the system can be characterized roughly by an E^* of approximately 15 MeV for the pickup response.

The second method of gain shaping is with filters. However, the main purpose of the filters is to reduce the thermal noise in the core. In order to maintain a flux of $3 \times 10^7 \text{ sec}^{-1}$ into the stack tail, an amplifier system with very high gain (150dB) is required. Even with preamplifiers with low noise temperatures (80°K), the thermal noise produces an rms voltage of approximately 1500 V/turn. This noise voltage is (perhaps surprisingly) tolerable in the tail where the average (cooling) voltage gain is about 10 V/turn. In the core region, where the cooling voltage is a few mV/turn, this noise voltage must be reduced to a tolerable level. The filter does this by making a notch at all harmonics of the revolution frequency of the particles in the core. The filter also does some gain shaping in the tail region. The filters used are composed of a series of

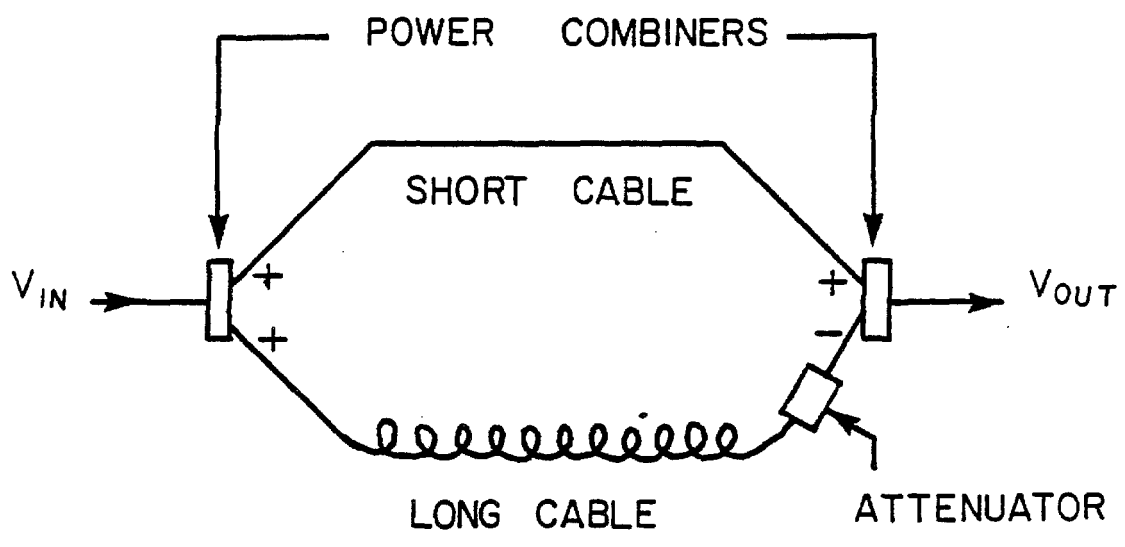


Figure 5-11

notch filters similar in concept to those used at CERN. A schematic diagram of the individual component filters is given in Fig. 5-11. The response of these filters is given by⁵

$$\frac{V_{\text{out}}}{V_{\text{in}}} = (e^{-i\gamma_1 \ell_1} - \xi e^{-i\gamma_2 \ell_2})/2, \quad (5.9)$$

where γ_1 , γ_2 and ℓ_1 , ℓ_2 are the propagation constants and lengths of cables and ξ is a variable attenuation of order unity. To get a clearer picture of the operation of this filter, consider the approximation $\xi = 1$, $\ell_1 = 0$, $\gamma_2 = \omega T_c / \ell_2$, where ω is the applied frequency electrical length of the cable. In this case,

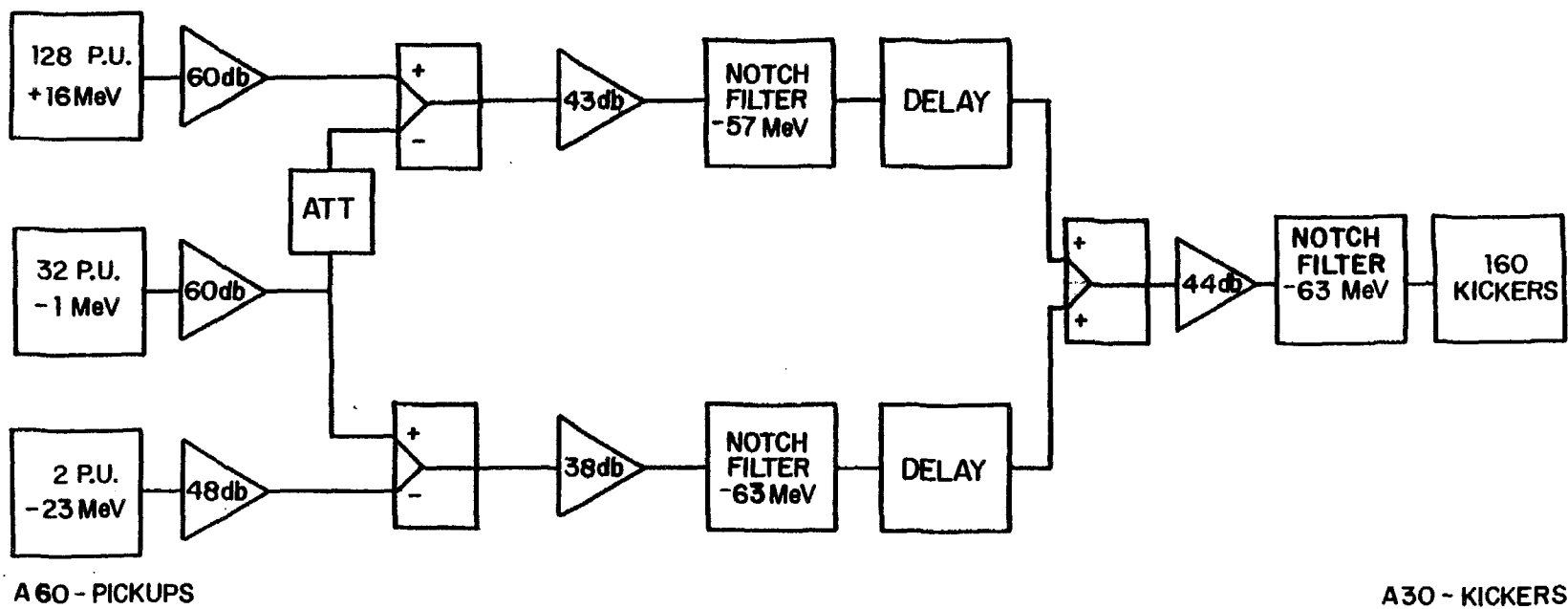
$$\left| \frac{V_{\text{out}}}{V_{\text{in}}} \right|^2 = (1 - \cos \omega T_c) / 2, \quad (5.10)$$

and the phase changes linearly with frequency except at the transmission zero, where it takes a discontinuous jump of 180° .

The absence of amplifier noise would not necessarily eliminate the need for filters. Nonlinearities in the pickups, amplifiers and other components cause frequency mixing, as is well known to rf engineers. The input power at frequencies corresponding to the stack tail, where the power density is high, will mix in a nonlinear device and produce output power at frequencies corresponding to the core where the power density must be low. The filters suppress the most dangerous part of the unwanted distortion because of the notch at the frequency of the core particles. (These particles are cooled by a separate system without filters, as will be described later.) It will be advantageous to place some of the filtering after the final amplifier to reduce the sensitivity to the nonlinear distortions from that source.

The shape of the gain curve at the injection end is purposely different from the ideal exponential curve, becoming flat in the injection region because of several practical considerations:

- (i) It is desirable to keep the electronic gain between Schottky bands as low as possible. The gain between Schottky bands does not affect the cooling process, but the thermal power between Schottky bands is significant.



STACK TAIL MOMENTUM COOLING SYSTEM 1-2 GHz

Figure 5-12

- (ii) To maximize the ratio of Schottky signal to thermal noise, it is desirable to place the pickups so they have maximum sensitivity to the freshly injected beam, i.e., so they operate in the non-exponential region.
- (iii) The exponential gain profile minimizes Schottky power only in the approximation that beam is injected in a steady state manner. In fact, each newly injected pulse substantially alters this picture since the density of particles will differ by factors of 2 or 3 from the steady state situation. By making the gain profile flatter in the injection region, we can reduce the required Schottky power immediately after a new pulse is injected.

The stack-tail system we have designed consists of two sections of pickups and associated amplifiers and filters. The two sections make it possible to control undesirable phase shifts and thermal noise in the tail. A block diagram of the system is shown in Fig. 5-12. The number of pickups was chosen to be as large as possible to minimize the thermal-noise to Schottky-signal ratio and to minimize the total thermal power. In order to keep the betatron oscillations from substantially affecting the momentum cooling, the betatron amplitudes must be limited. To achieve the desired gain profile, the pickups have a plate separation of 3 cm. Calculations indicate that the beam size should be less than 2.4 cm to avoid trouble with betatron motion. For an emittance of 10π mm-mrad, the β function at the pickup must be 15 m or less. This requirement limits the pickup straight section to 15 m in length and a total of 200 pickups. The function of the subtracting pickups is discussed in the next section. The number of kickers was chosen to fill the straight section across from the pickups to minimize total power (inversely proportional to the number of kickers). The gain profile achieved with this system is shown in Fig. 5-13 abc for the Schottky bands at 1.1, 1.5 and 1.9 GHz.

5.9.4 Signal Suppression and Stability. An important aspect of the cooling process, when using high-gain cooling systems, is signal feedback via the beam. A signal of frequency ω will modulate the beam at frequency ω , and this modulation will be sensed at the pickup. Thus the cooling system forms a closed-loop feedback system. This feedback system is analogous to amplifier systems with conventional electronic feedback. An expression for the beam feedback has been given by van der Meer⁶ and independently by Ruggiero.⁷ An approximate expression is

$$F = \frac{I_p}{V} = jef_0^2 \bar{p} \int \frac{CP}{nk(E-E')} \frac{d\psi}{dE'} dE' - \frac{\pi ef_0^2}{n|k|} CP \frac{d\psi}{dE}, \quad (5.11)$$

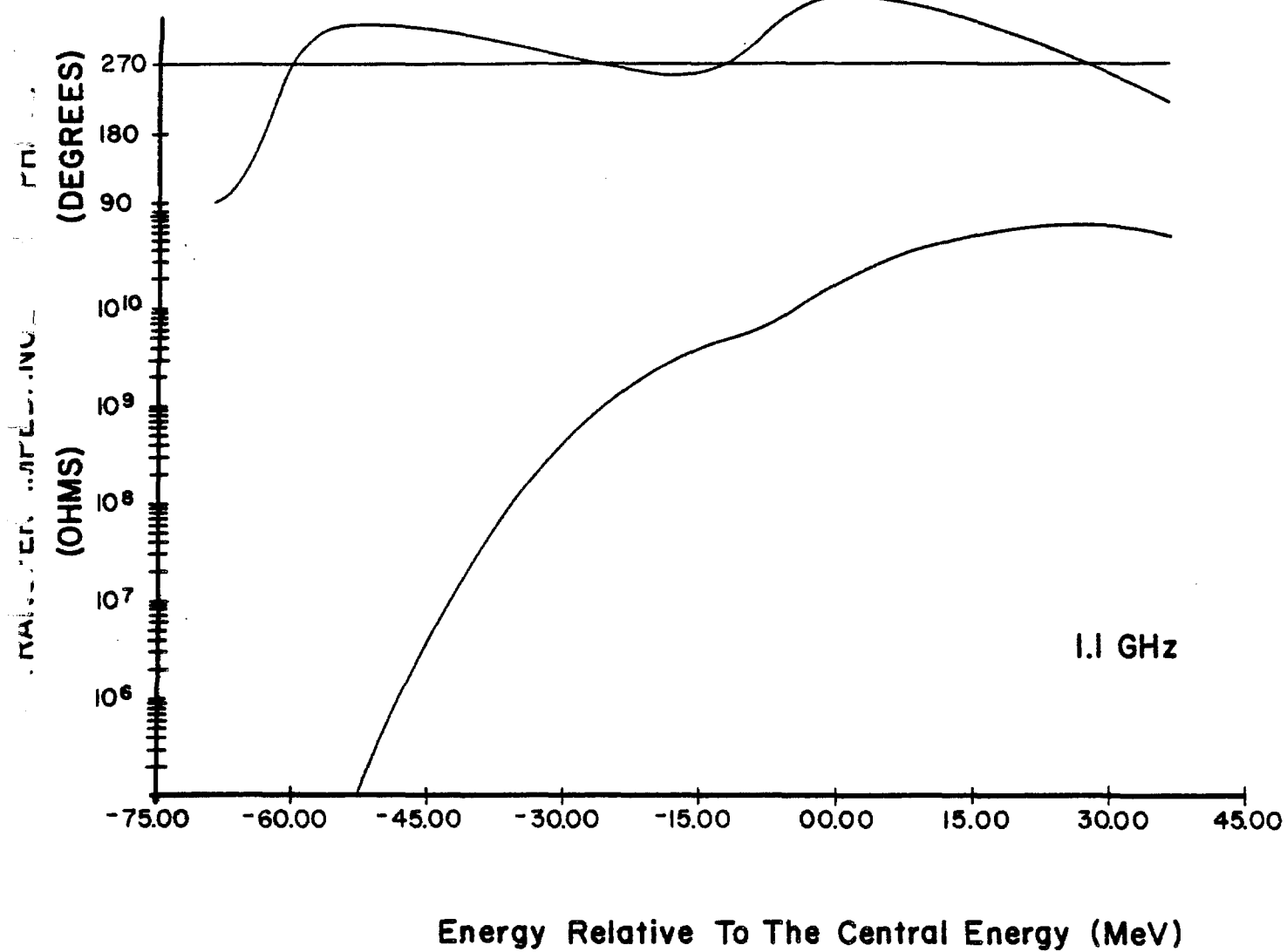


Figure 5-13a

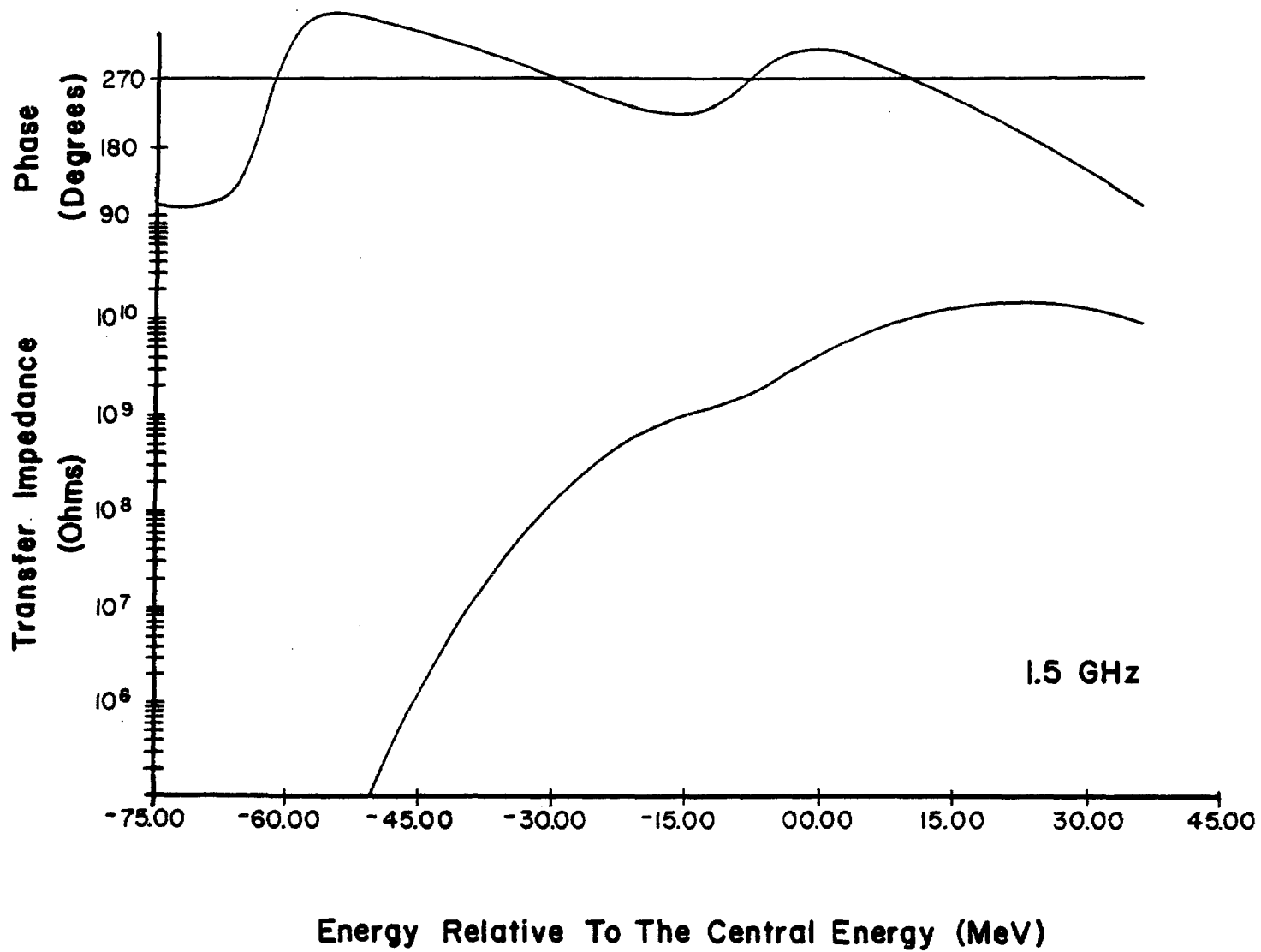


Figure 5-13b

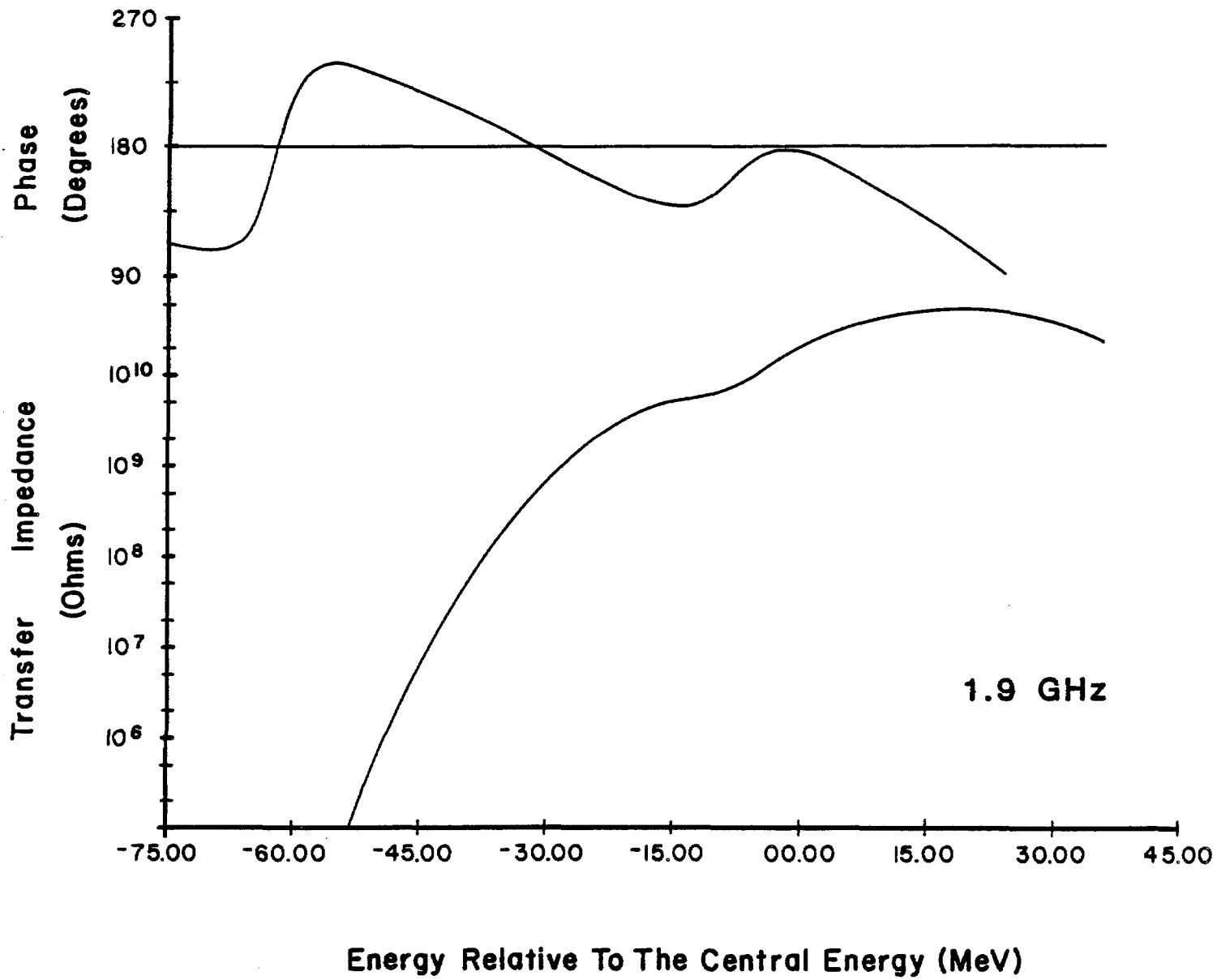


Figure 5-13c

where \bar{p} denotes the principal value of the integral, $I_p =$ induced current at the frequency $f = nf_0$ in the pickup due to modulation caused by voltage V on the kicker, f_0 is the revolution frequency corresponding to energy E , n is the harmonic number, e is the unit charge, $j = \sqrt{-1}$, $k = 2\pi df_0/dE$, C is the phase factor due to transit time differences between pickup and kicker, and $P = P(f, E')$ is the pickup sensitivity. P depends on E' because P depends on particle position, which depends on E' (usually exponentially). The dependence of P on f comes from electrical properties and is usually weak.

This approximation is valid when the Schottky bands are well separated, but is a poor approximation for quantitative results for the system described here. Nonetheless, it is sufficient to show the main features of the physical process.

The closed-loop gain of the system is given by $G' = G/(1-FG)$, where G is the open-loop gain ($G = V/I_p$) of the electronics going from pickup to kicker. If the real part of FG is less than zero, then $G' < G$ and the cooling signal is suppressed. If the real part is greater than zero, the signal may be enhanced. If the real part of $FG > 1$, when the imaginary part is zero, the system is unstable. (This situation is completely analogous to the case of conventional electronic circuits with feedback).

In the approximate expression for F , one sees that there is a resistive (energy-absorbing) component of the beam response proportional to the gradient of the density at the driving frequency and a reactive component that depends on the asymmetry of the gradient about the driving frequency. It would be wrong to conclude, however, that the resistive term is the more important when looking at system stability. Both terms must be considered because the open-loop gain function G is a complex quantity; it unavoidably contains phase shifts from the filters and differences in time delays between pickup and kicker.

In fact, in the stack tail, the feedback can be dominated by the contribution from the particles in the core where $d\psi/dE$ is very large - 10^4 times larger than in the tail. Fortunately, $d\psi/dE$, which is increasing exponentially, is multiplied by the pickup response, which is decreasing exponentially. The rate of exponential increase of $d\psi/dE$ depends on the total gain profile, i.e., the product of pickup and filter response. The damping of $d\psi/dE$ in the feedback integral, however, depends only on the pickup response. Thus, it is important that the filter gain profile not be too sharp compared with the pickup in order to avoid severe problems with stability and signal suppression. The importance of the relative amounts of the gain profile derived from filters and pickups has been pointed out previously by Sacherer.⁸

An additional suppression of signal from particles in the core is provided by the subtracting pickups in each section. These pickups are placed closer to the core and normalized so that their sensitivity to the core region is equal and opposite to the sensitivity of the main pickups.

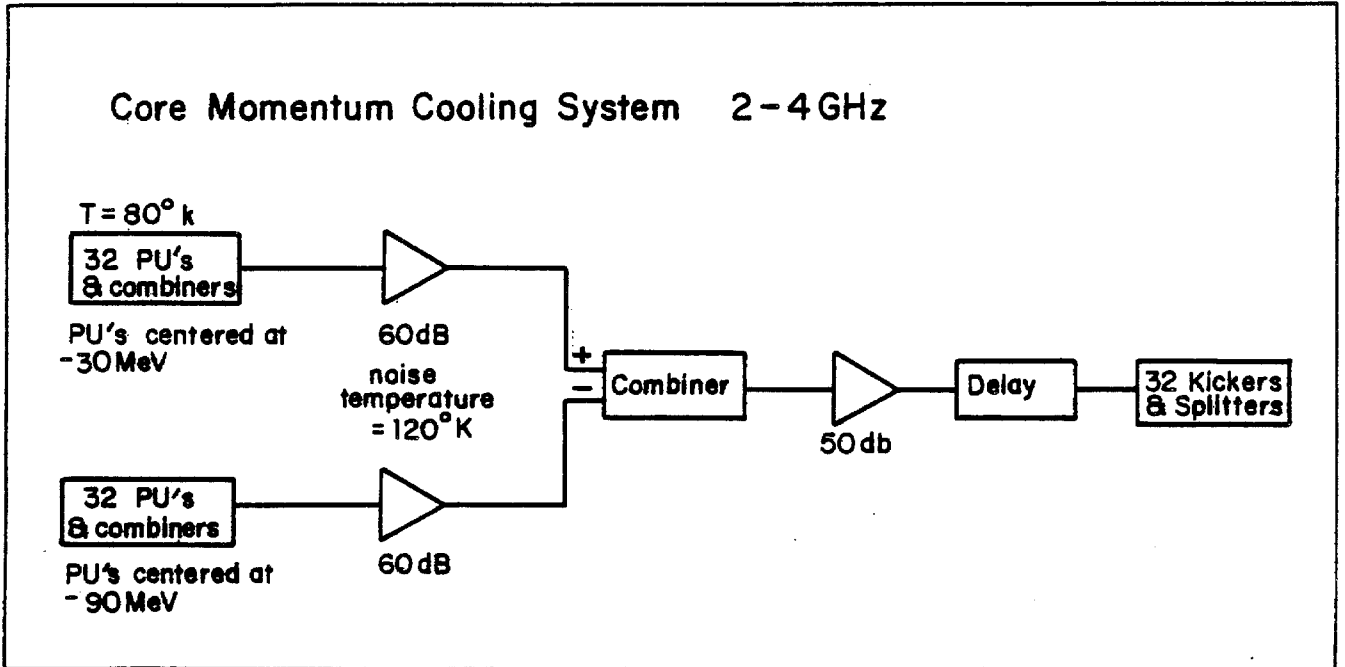


Figure 5-14

In the stack tail, however, they subtract less than 10% of the signal. Several subtracting pickups followed by substantial attenuation are required to avoid having the subtracting pickups appreciably affect the amount of thermal noise in the pickups. Immediately after injection, the signal suppression is substantially larger because of the large values of $d\psi/dE$ created by the RF stacking process. The gradients quickly (after 200 msec) smooth out because of the diffusion terms in the Fokker-Planck equation. It appears that during the first 200 msec of the injection cycle, it may be necessary to reduce the amplifier gain in order to maintain beam stability. This gain reduction has been taken into account in computer simulations and, in any event, is only of minor importance.

5.9.5 Core Cooling. The same Fokker-Planck equation that describes the stack-tail system also describes the core system. In fact, the distinction between core and tail cooling systems is somewhat arbitrary. The asymptotic distribution is given by

$$\phi = F\psi + (D_0 + D_1 + D_2\psi) \frac{\partial \psi}{\partial E} = 0 \quad (5.12)$$

The cooling coefficient F has a zero at the peak of the core and a slope proportional to $g(E-E_c)$ where g is the electronic gain and E_c is the energy at the peak of the core. The other terms are heating terms. D_0 is the contribution of intrabeam scattering (via the Coulomb force) to the diffusion and has been calculated by Ruggiero⁹ to be $D_0 = 0.0015 N_D^{-1} (eV)^2/\text{sec}$, where N_D is the total number of antiprotons in the Accumulator. This value of D_0 corresponds to a momentum heating time of 2 hr. D_0 is independent of both g and E . D_1 is the contribution of thermal noise and is proportional to g^2 . D_2 is the Schottky heating term and is proportional to $g^2 (E-E_c)^2$. In our system D_1 is small compared with D_0 . Optimum performance occurs when g is adjusted so that intrabeam scattering dominates in the central part of the core and the Schottky heating term dominates at the edges of the core. Smaller values of g leave the cooling term F less than optimum ($g = 0$ means no cooling) and larger values of g mean that Schottky heating is larger than the cooling. Computer calculations show that densities in excess of $1 \times 10^5/\text{eV}$ can be reached.

The choice of 1 - 2 GHz bandwidth (and $\eta = 0.02$) for the tail system was made because of the desire to optimize core cooling. Since D_2 is proportional to $1/\eta$, a larger gain can be used to counteract intrabeam scattering in the core. Choosing a higher maximum frequency and the same momentum width for the stack tail system would have required a lower η for the lattice. This would have reduced the core cooling effectiveness.

A block diagram of the core cooling system is shown in Fig. 5-14. The zero in gain is obtained by subtracting the signals from two sets of

pickups placed in a region of high momentum dispersion. One set of pickups is centered above the core energy and one is centered below. The signal is then applied to a kicker placed in a region of zero momentum dispersion. The gain profile for the core system Schottky bands at 2.2, 3.0, and 3.8 GHz is shown in Fig. 5-15 abc.

5.9.6 Numerical Calculations of Momentum Cooling. A computer simulation of the combined core and stack-tail momentum cooling systems has been made. These calculations use the full theory developed by van der Meer et al and not the simplified models given here. It has been found that a core density of $1 \times 10^5/\text{eV}$ can be obtained after 4 hours of stacking with an average flux of $4 \times 10^7 \text{ sec}^{-1}$. Figure 5-16 shows the stack profile as a function of time. Figure 5-17 shows the cooling term (F) including the effects of beam feedback after 3 hours. Figures 5-18 and 5-19 show the heating term coefficients $D_0 + D_1$ and D_2 . Figures 5-20 and 5-21 are stability plots: the real versus the imaginary part of the cooling system gain G times the beam feedback F. In this plot the system is stable if the curve does not enclose the point (1,0).

5.10 Betatron Cooling

5.10.1 Introduction. Betatron cooling is accomplished by using a pickup sensitive to the transverse displacement of the particles. In going from pickup to kicker the particle oscillates in betatron phase by an odd multiple of $\pi/2$, converting the position displacement to an angle displacement. Each given particle creates a signal in the pickup which, when applied to the kicker, decreases the angle displacement. Other particles with similar revolution frequencies contribute noise that tends to increase the betatron amplitude. This situation is similar to the momentum-cooling discussed earlier.

Betatron cooling is conventionally described in terms of the time decrease of the betatron emittance¹⁰

$$\frac{d\bar{\epsilon}}{dt} = -\frac{W}{N} (2g - g^2(M+U)) \bar{\epsilon} \quad , \quad (5.13)$$

where W is the system bandwidth, N is the number of particles being cooled, g is the system gain, M is the mixing factor, and U is the ratio of noise to signal power. The rms beam size is the square root of the beta function times $\bar{\epsilon}$. Equation (5.13) can be an exact result if the definition of g is given by a sum over Schottky bands of a gain function including signal suppression. Some algebraic license is also required to define g^2 as something different than g times g. However, the approach taken here will be that the gain function is constant, independent of frequency. The sum over Schottky bands is therefore trivial.

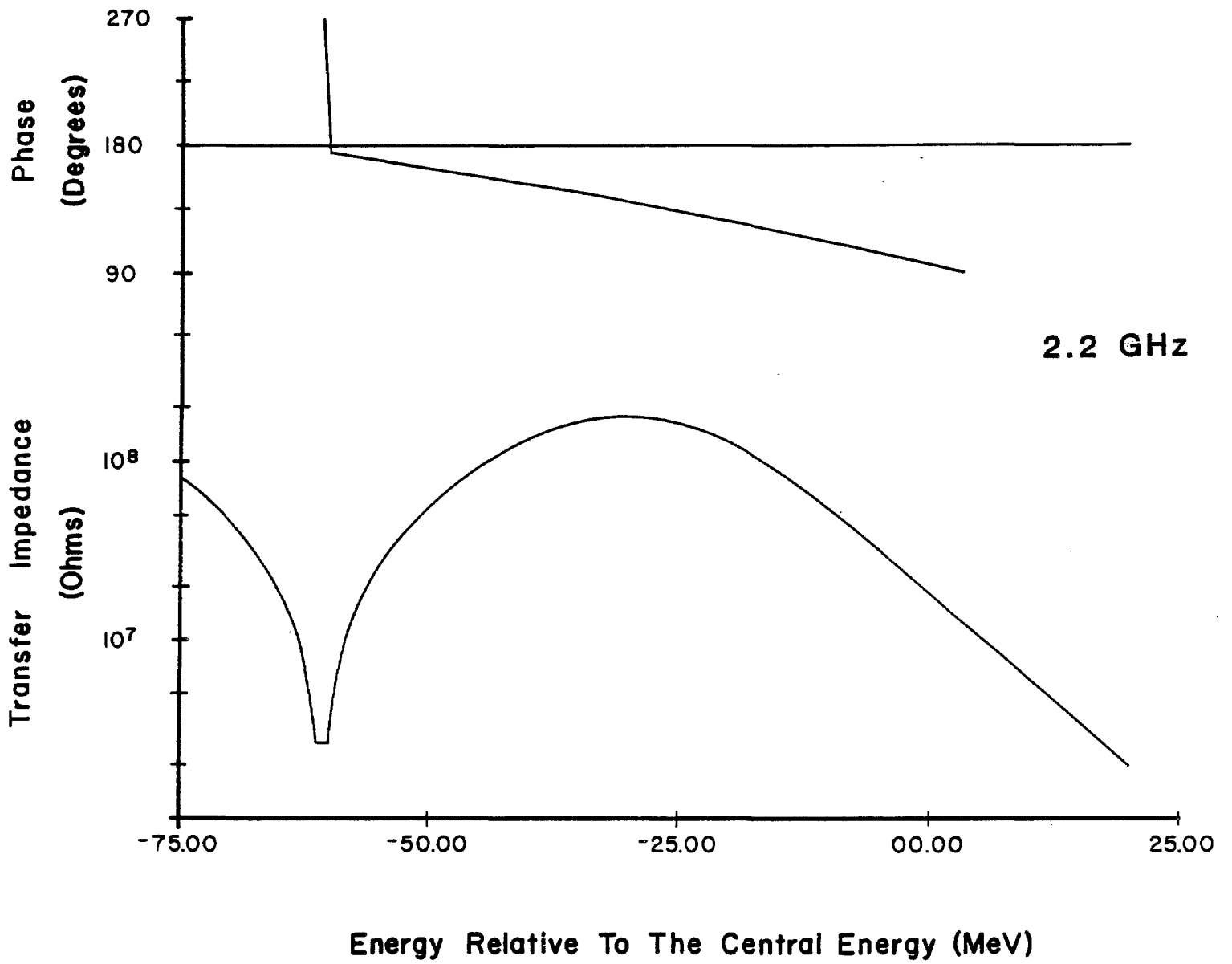


Figure 5-15a

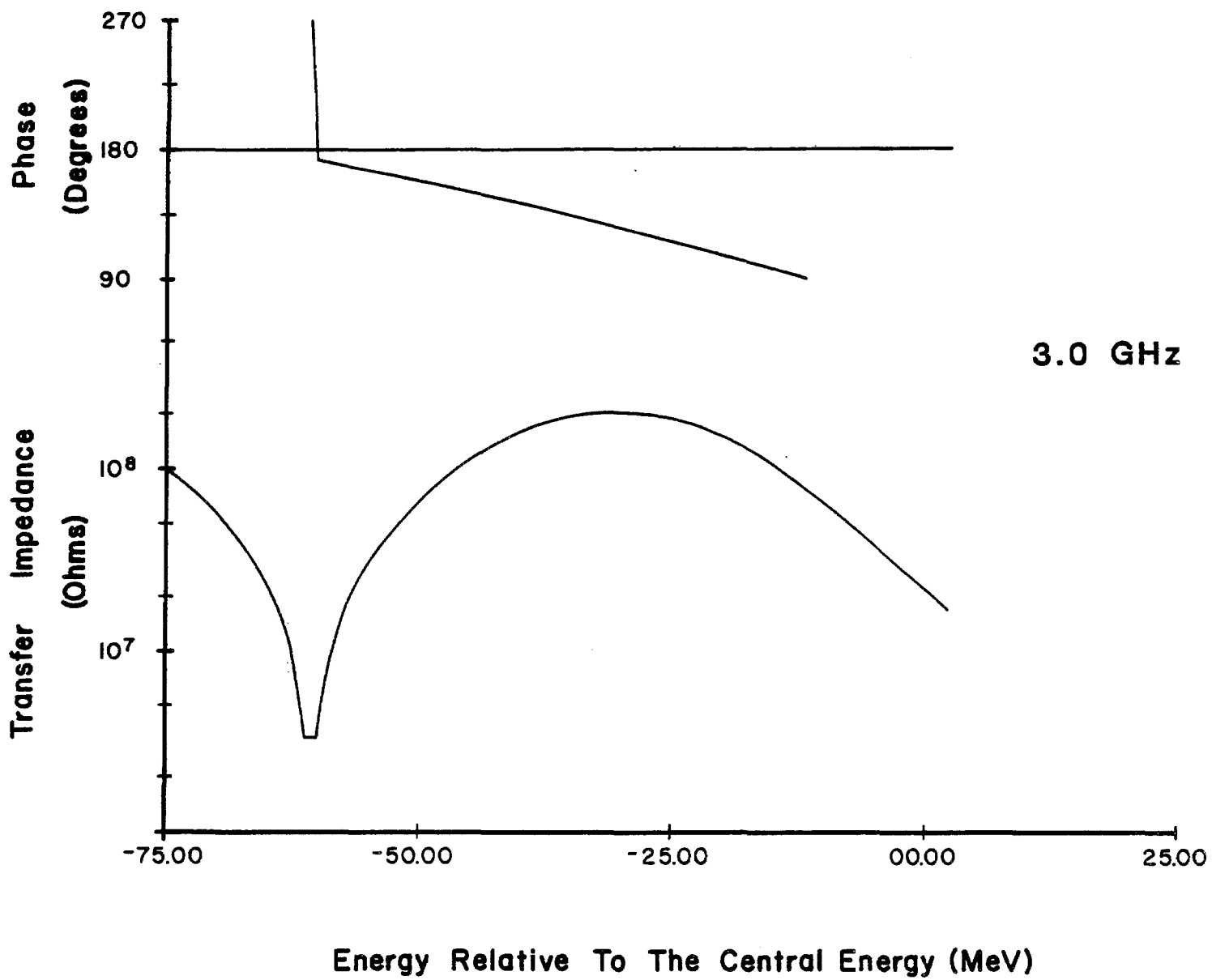


Figure 5-15b

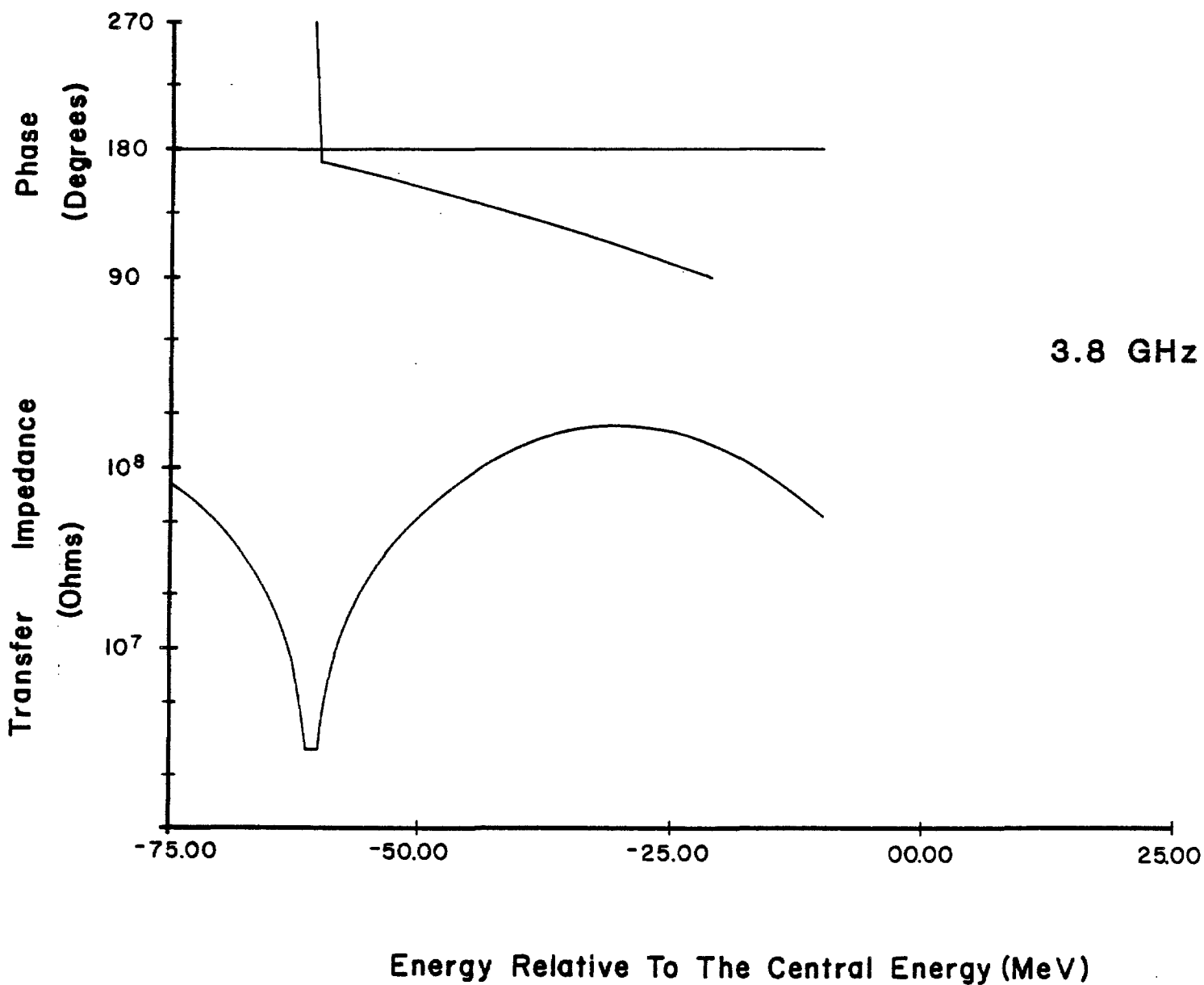


Figure 5-15c

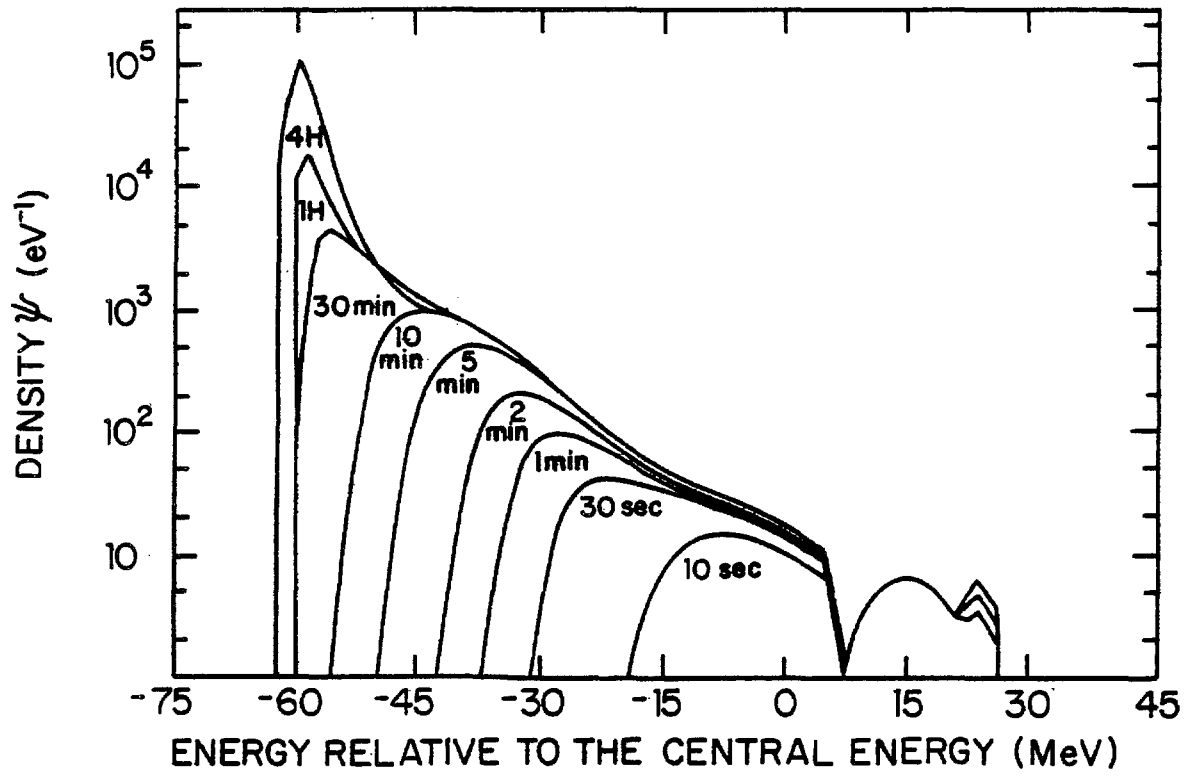


Figure 5-16

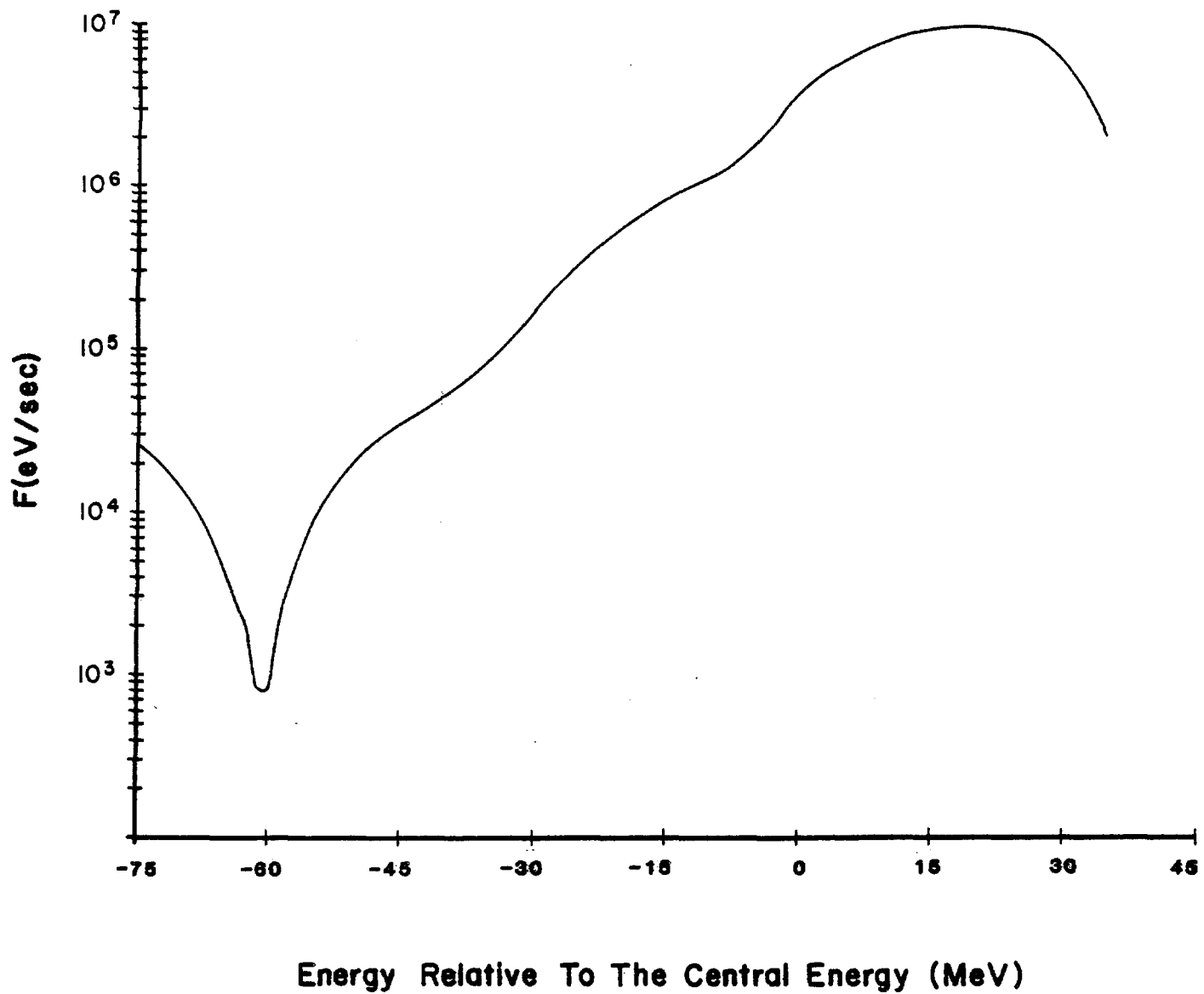


Figure 5-17

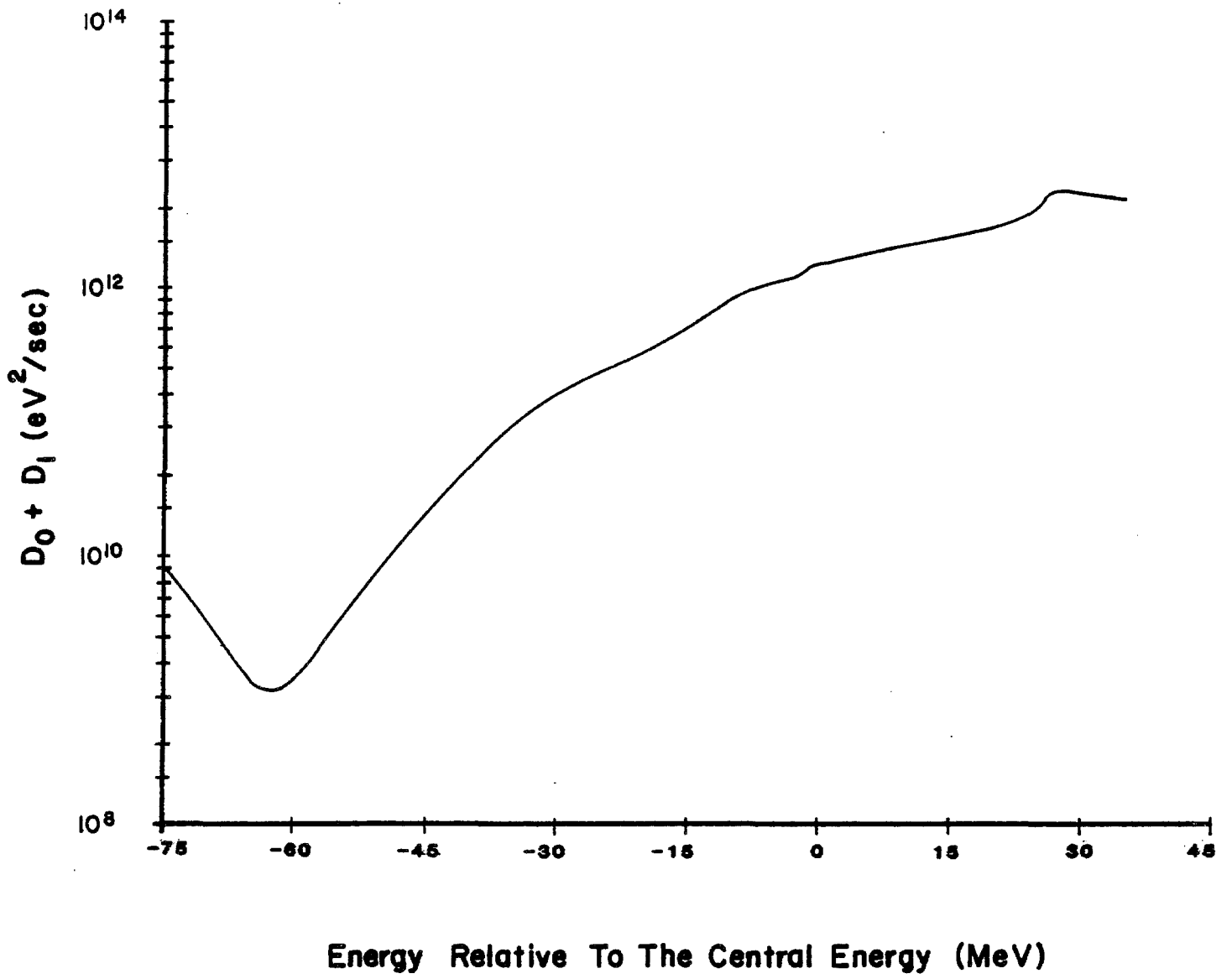


Figure 5-18

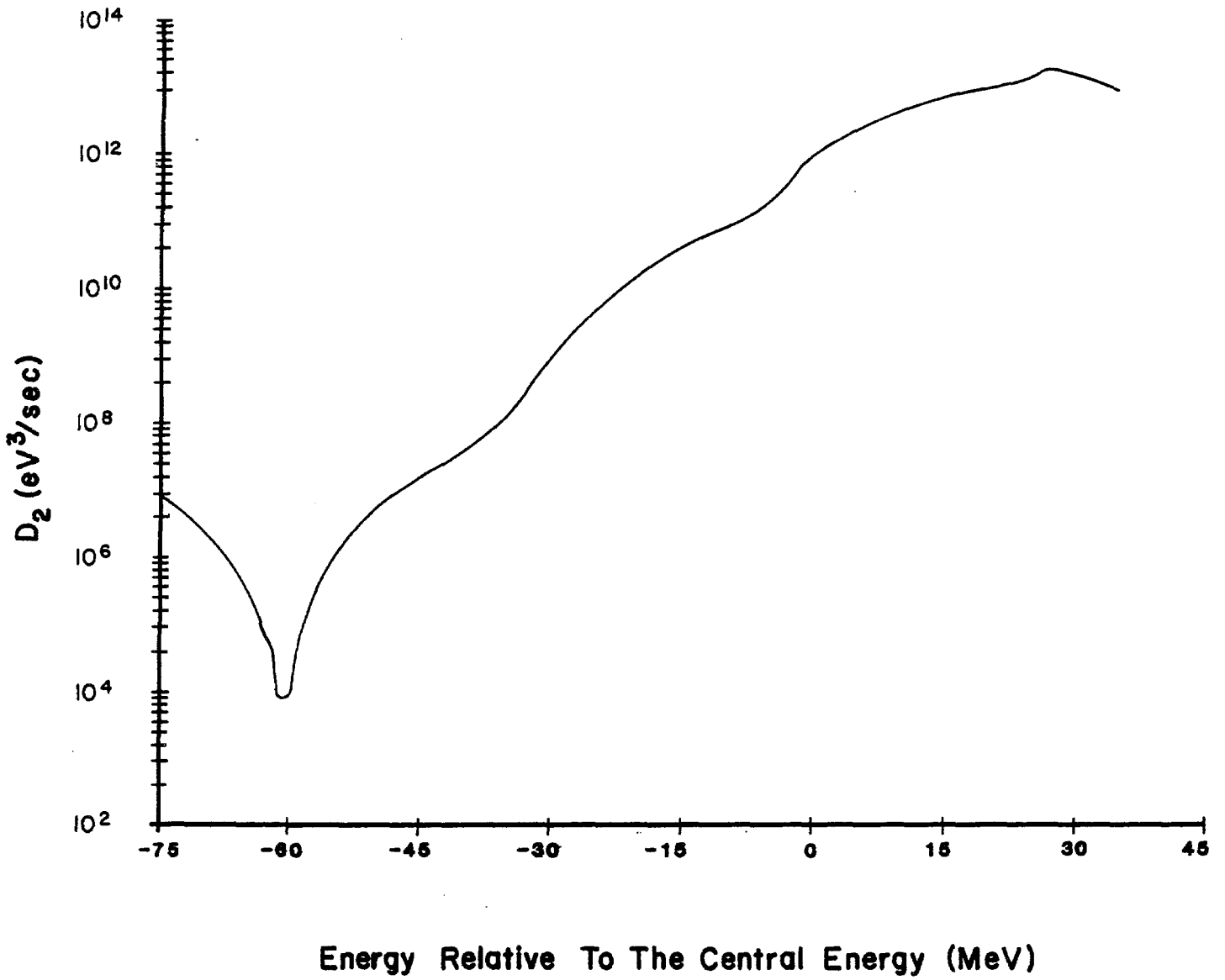


Figure 5-19

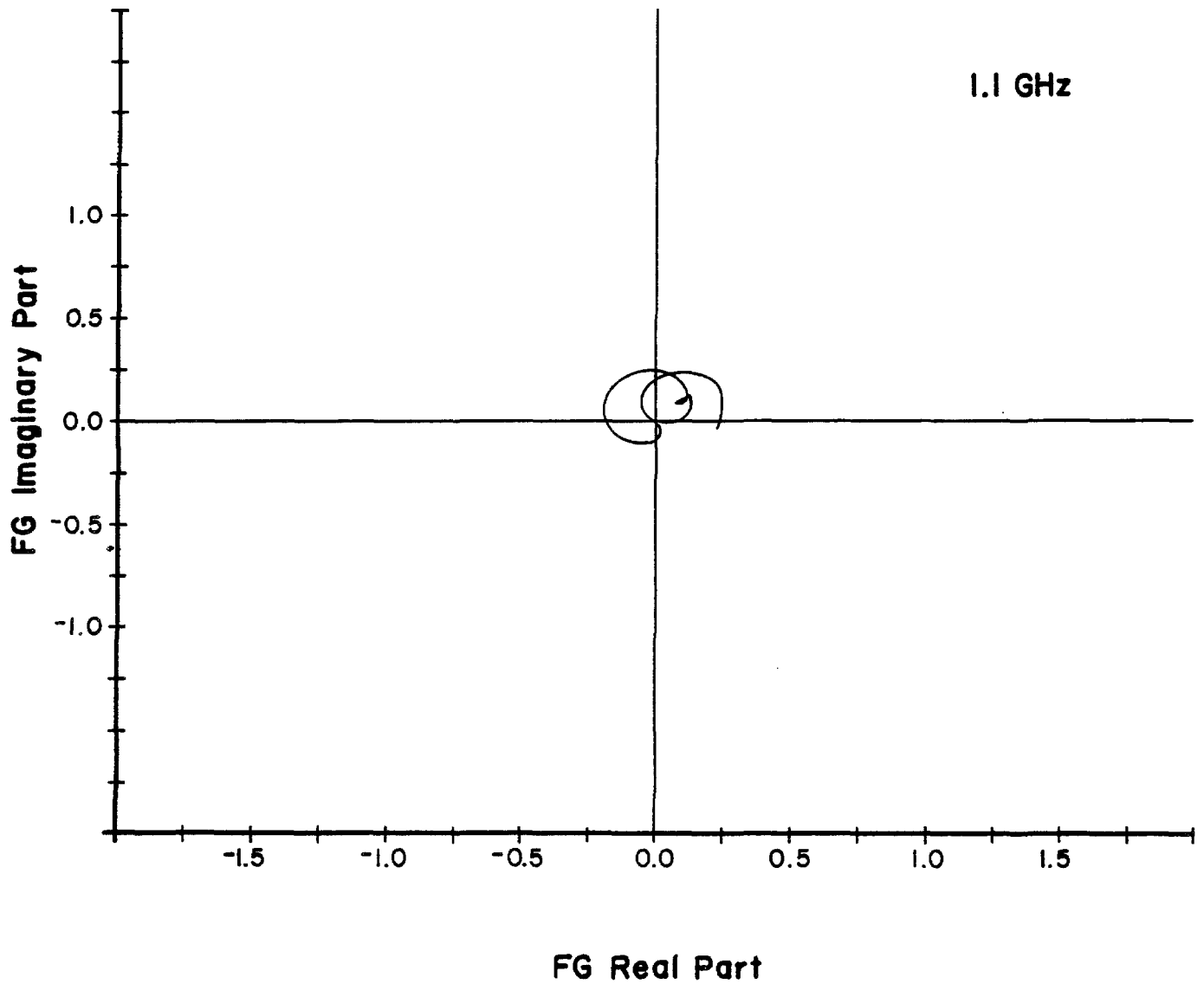


Figure 5-20a

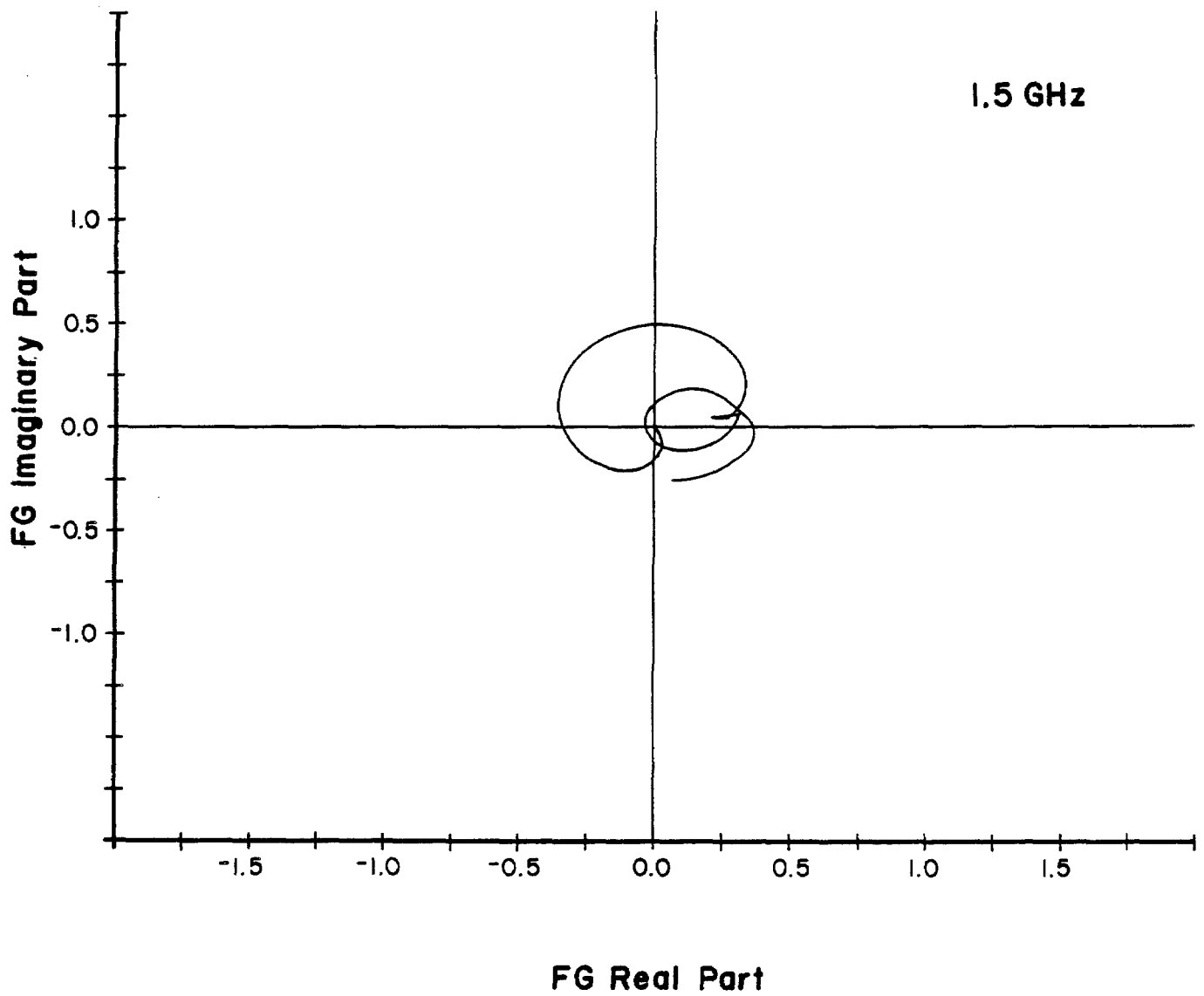


Figure 5-20b

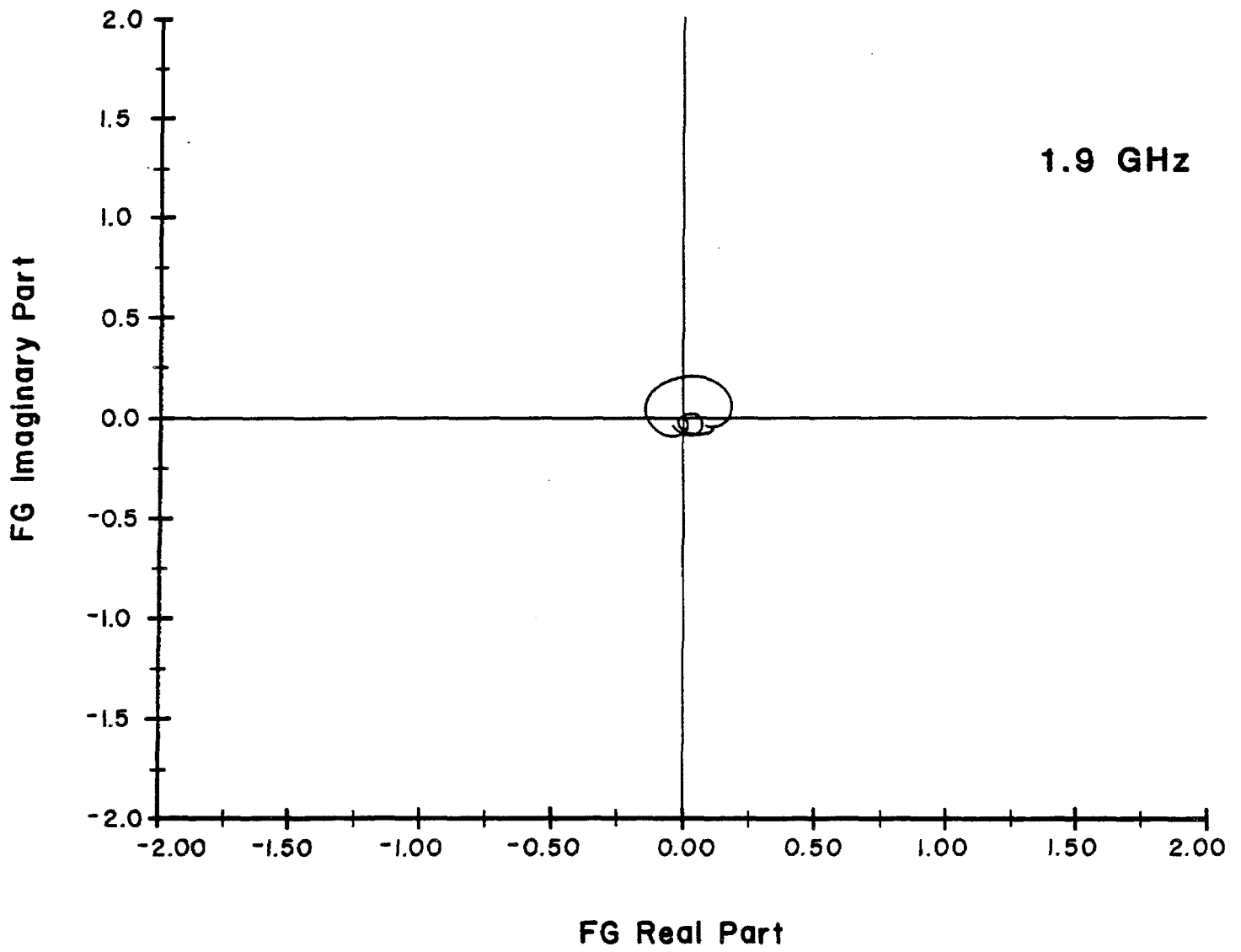


Figure 5-20c

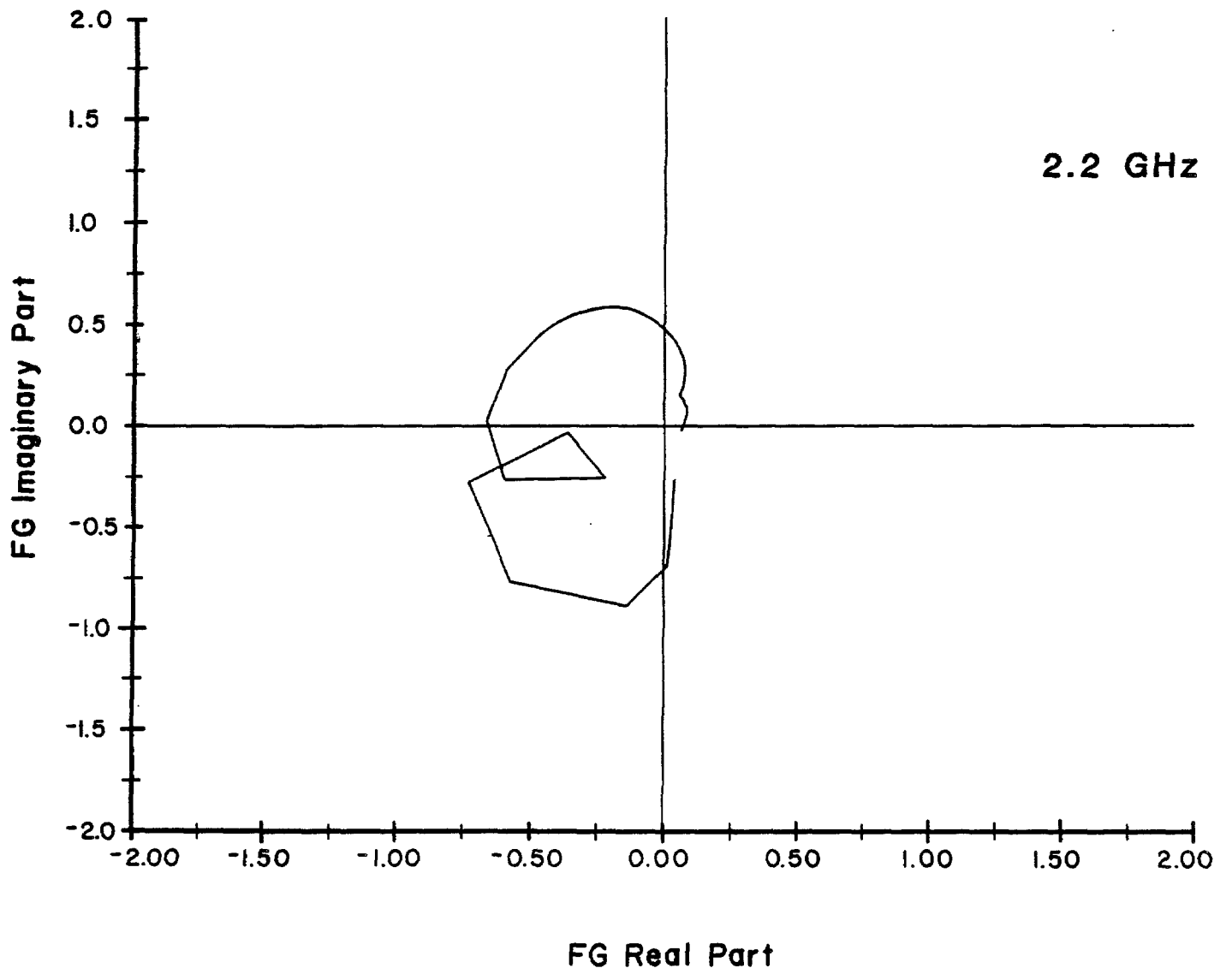


Figure 5-21a

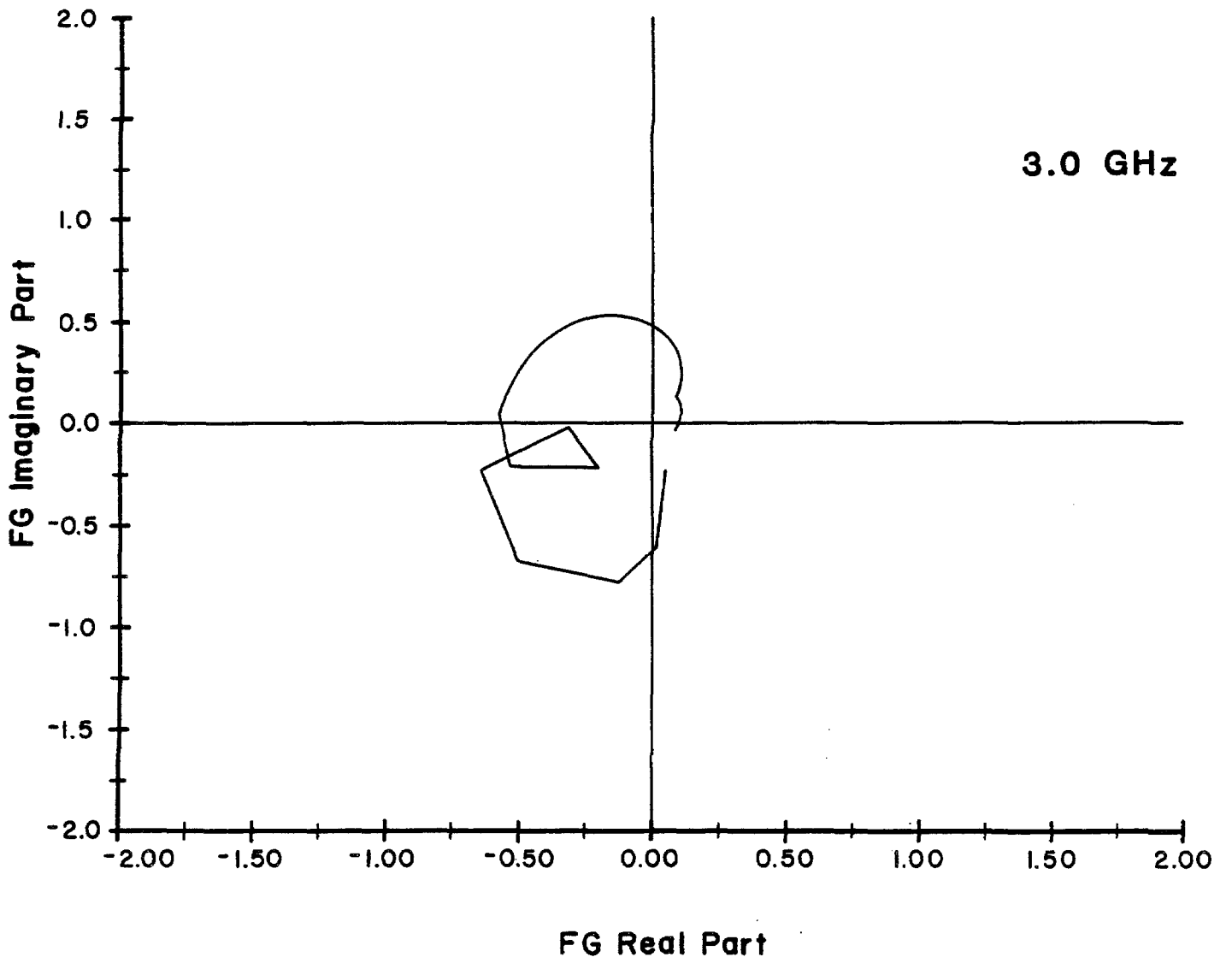


Figure 5-21b

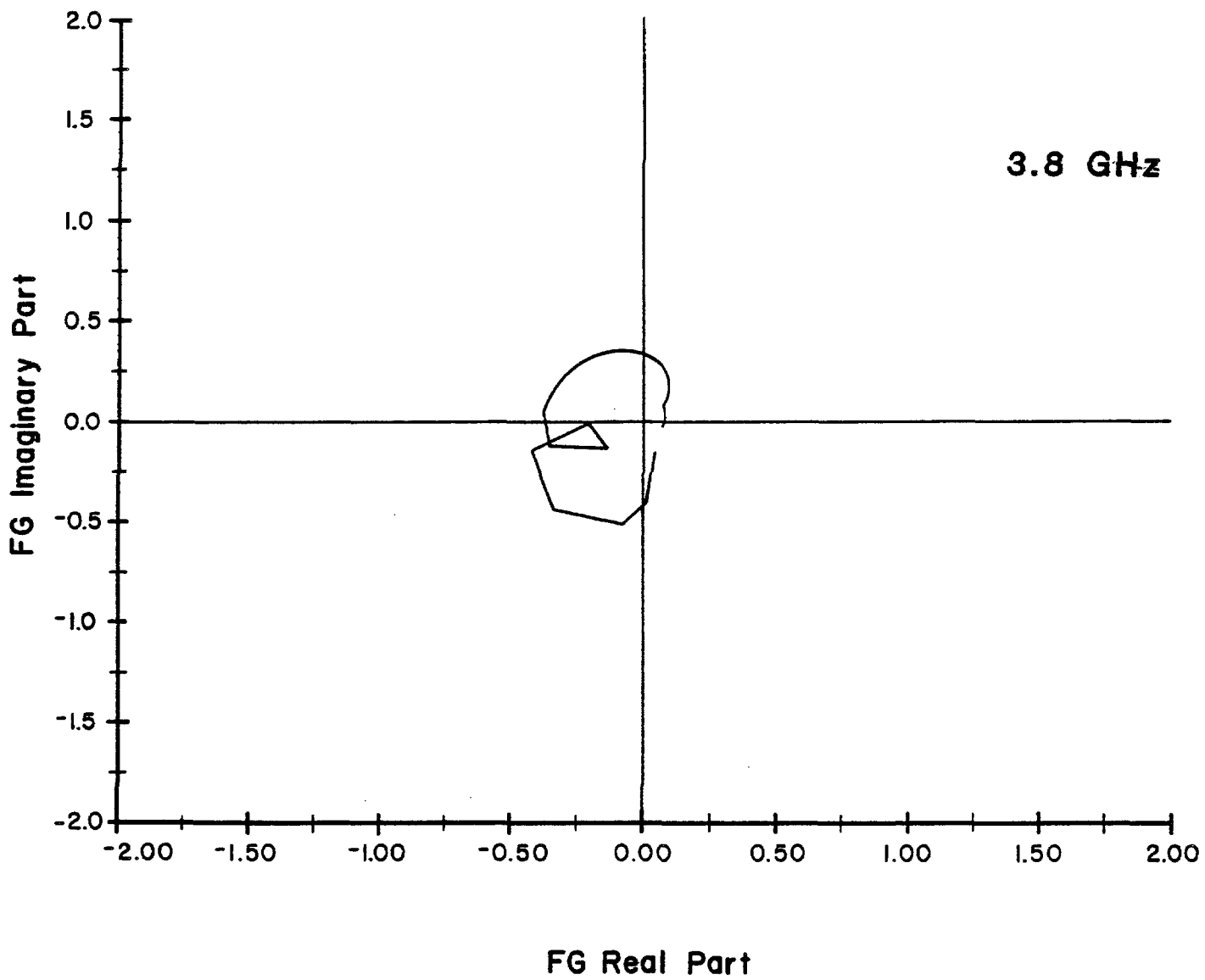


Figure 5-21c

For the loop pickups and kickers that we plan to use, g is defined by

$$g = N \beta_p \beta_k n_p n_k \left(\frac{d}{h} \right)^2 \frac{e f_o Z_{pu} g_A}{(\beta^2 E/e) k} \quad , \quad (5.14)$$

where β_p (β_k) is the function at the pickup (kicker), n_p (n_k) is the number of pickups (kickers), d is the pickup and kicker sensitivity defined in section 5.11.1, h is the pickup and kicker gap, g_A is the amplifier gain, and $k = \omega/\beta c$. In order for g to be independent of frequency, g_A must increase linearly with frequency. The optimum gain profile would be for g to increase with frequency and therefore for g_A to increase with frequency squared. The effect of signal suppression is to modify 5.2. At small values of amplifier gain, such as exist in the stack tail betatron cooling system, the signal suppression is small and can be ignored. As the gain is increased to obtain the optimum cooling the beam feedback reduces the effective gain of the system by a factor of 2 at the center of a symmetric distribution that is peaked at the center. Off center, the value of the suppression factor depends on the shape of the distribution, but it is generally true that the cooling is slowest at the peak of the distribution. For a system like the core betatron cooling system, it is sufficient to perform calculations ignoring signal suppression, remembering that the actual amplifier gain required is $2 g_A$.

The mixing factor M is the ratio of the peak power density in the Schottky band to a uniform power density of the same power. For a system with constant gain g ,

$$M = \frac{f^2 \psi(f) \Lambda}{2WN} = \frac{f \beta^2 E \psi(E) \Lambda}{2WN \eta} \quad , \quad (5.15)$$

where f is the revolution frequency, $\psi(f)$ is the particle density (number/Hz), $\psi(E)$ is the particle density (number/eV), $\Lambda = \ln 2$, and $\eta = 1/\gamma_t^2 - 1/\gamma^2$.

The total thermal power in the system is

$$P_T = k_B (\theta_R + \theta_A) g_A^2 W \quad , \quad (5.16)$$

where k_B is Boltzman's constant (1.38×10^{-23} Joules/K), θ_R is the temperature of the pickup terminating resistor, θ_A is the equivalent noise temperature of the amplifier. Strictly speaking, g_A^2 should be averaged over the system bandwidth, but it suffices to take the g_A^2 value at midband. The Schottky power is

$$P_S = \frac{1}{2} N e^2 f_o Z_{pu} \left(\frac{d}{h} \right)^2 \beta_p n_p \bar{\epsilon} g_A^2 W; \quad (5.17)$$

U is the ratio of noise to signal power

$$U = \frac{P_T}{P_S} \quad (5.18)$$

5.10.2 Betatron Cooling in the Core. Betatron cooling in the core is limited by the relatively large density of particles. The cooling is therefore necessarily a slow one, accomplished with low power and a large signal to noise ratio. The core betatron cooling is accomplished with two identical systems. A schematic of one system is given in Fig. 5-22. Both pickups and kickers are located in zero dispersion straight sections. The betatron phase advance between pickup and kicker is $2-3/4 \times 2\pi$ in the horizontal and $2-3/4 \times 2\pi$ in the vertical. After 4 hours of stacking there are 5×10^{11} particles in the core, with a peak density of $10^5/\text{eV}$. For $W=2$ GHz and $\tau=0.02$ the mixing factor M is equal to 10. Other relevant parameters are $\beta_D = \beta_K = 6$, $n_D = n_K = 8$, $h=3$ cm, $d=1.73$, $Z_{DU} = 75\Omega$, $\theta_A = \theta_R = 373$ K. With these parameters $U=0.5$ for the final emittance $\epsilon = 0.5\pi$ mm-mrad. From Eq. (5.13) it can be seen that the maximum cooling rate is obtained when

$$g = \frac{1}{M+U} \quad (5.19)$$

For this value of g the amplifier gain at midband according to Eq. (5.16) is $g_A = 100$ dB. If the signal suppression effect is included the required gain will become 106 dB. The Schottky power is given approximately by Eq. (5.3) with $g_A = 100$ dB and is about 1 watt. The thermal power is given approximately by Eq. (5.16) with $g_A = 106$ dB (most of the thermal power is between Schottky bands and not greatly affected by the suppression). The thermal power is also about 1 watt.

5.10.3 Stack-Tail Betatron Cooling. The stack tail betatron cooling system uses the same pickups as the second section of the tail momentum-cooling system. The pickup plates are centered at -1 MeV relative to the central energy. For horizontal signals the pickup is most sensitive at its edges at +21 MeV and -19 MeV. Most of the cooling takes place at the -19 MeV edge because the momentum cooling system is pushing particles much more slowly past the -19 MeV edge than the +21 MeV edge. The pickup is most sensitive at its center (-1 MeV) for signals in the vertical direction. The kickers are also placed at -1 MeV in a region with high dispersion. A block diagram of the system is shown in Fig. 5-23.

Approximate calculations of the system performance have been made with Eq. (5.13) except that the time variable has been replaced with the energy variable, using the relationship

CORE BETATRON COOLING SYSTEM 2-4 GHz

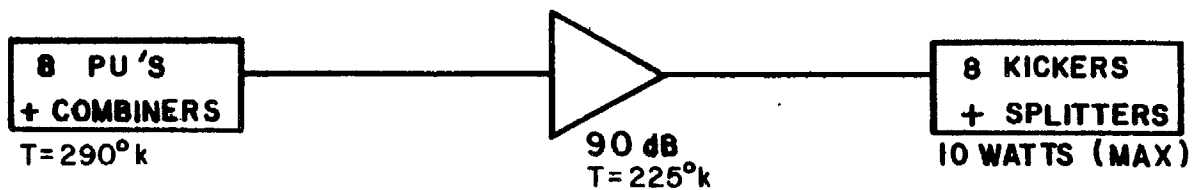
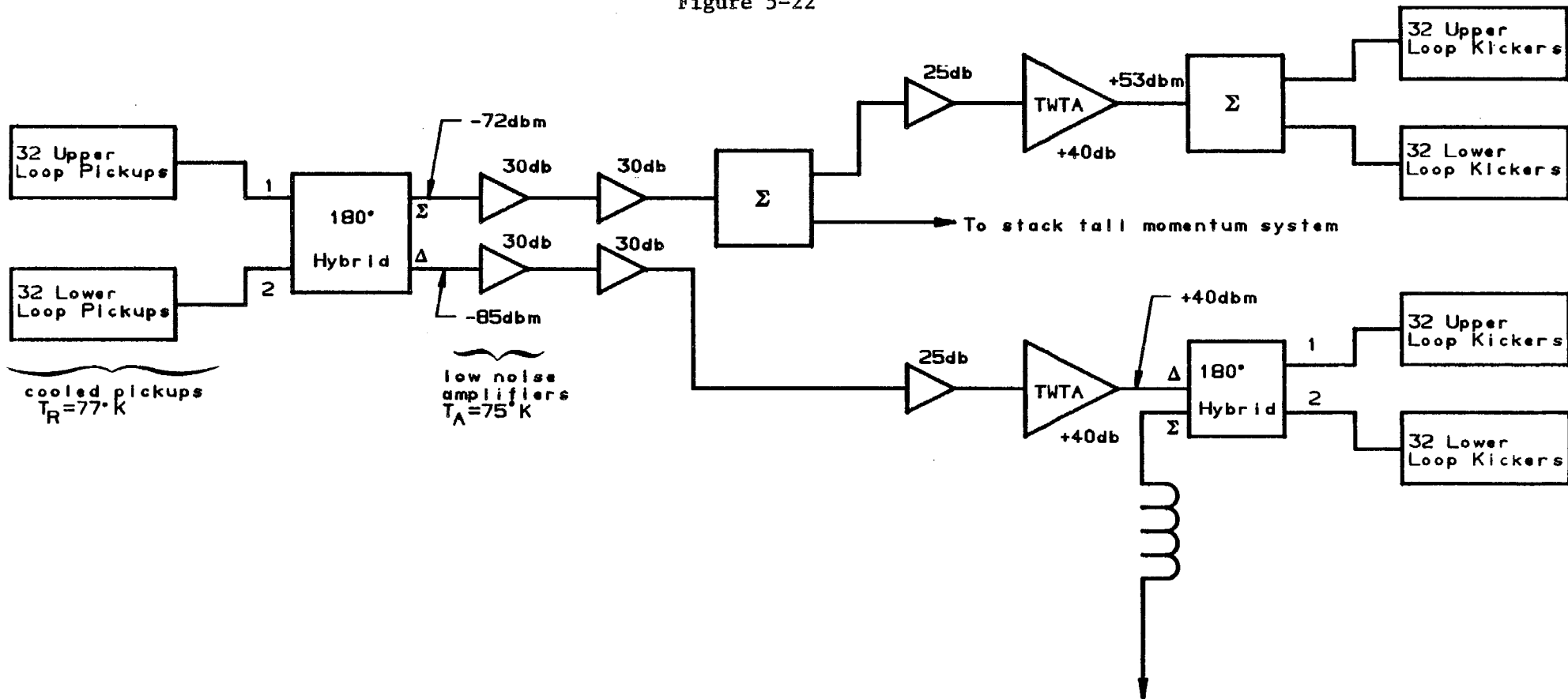


Figure 5-22



Stack Tail Betatron Cooling System

Figure 5-23

$$\frac{dE}{dt} = \frac{\phi}{\psi(E)},$$

where ϕ is the flux of particles and $\psi(E)$ is the density of particles. This approximation ignores fluctuations in energy gain in the stacking process. With this approximation, Eq. (5.13) is easily integrated numerically. Figure 5-24 shows the emittance reduction as a function of energy. The thermal power in each system is 10W and the Schottky betatron sideband power is 10W. The horizontal system has a large momentum Schottky signal as well-about 200W.

5.10.4 Operation of Betatron Cooling Systems. In the Accumulator we have available two betatron cooling systems, either of which is capable, or nearly capable, of cooling the beam emittance from 10 to 2π mm-mrad. The core system is clearly required so that a core of \bar{p} 's may be held for several hours without diffusion. The tail system serves two functions: 1) to cool the betatron amplitudes in a system with a low particle density (it is not necessary to wait one half to one hour for the core cooling system to do its work) and 2) to counteract possible betatron heating by the momentum-cooling system. The size of the latter effect is difficult to estimate; it depends on how well we are able to build the momentum kickers for the stack-tail system. If the effect is larger than expected, the gain of the stack-tail system can be raised to achieve better cooling, but, of course, the power requirements will be greater. Tentatively, however, we would plan to use the stack-tail system to reduce the beam emittance by about a factor of e and use the core system to reduce it below 2π mm-mrad.

5.11 Stochastic-Cooling Hardware

The purpose of this section is to outline the hardware and techniques we expect to use in order to meet the design requirements presented above. Although the design is not complete, it has been carried out in sufficient detail to make reliable cost estimates. In several instances alternative designs are possible. We present here the design that is most sound technically. Research and development are presently in progress to investigate alternatives that could lead to better system performance, reliability, or cost reduction.

Each stochastic cooling system is composed of 5 basic parts: beam pickup electrodes, low-level electronics (including preamplifiers), medium level electronics (including gain and phase correction circuits, filters etc.), high-level electronics (including traveling-wave tubes), and kicker electrodes. As several of the cooling systems share common elements in their design, and the performance of these elements effects for the proper functioning of the cooling system, they are discussed below.

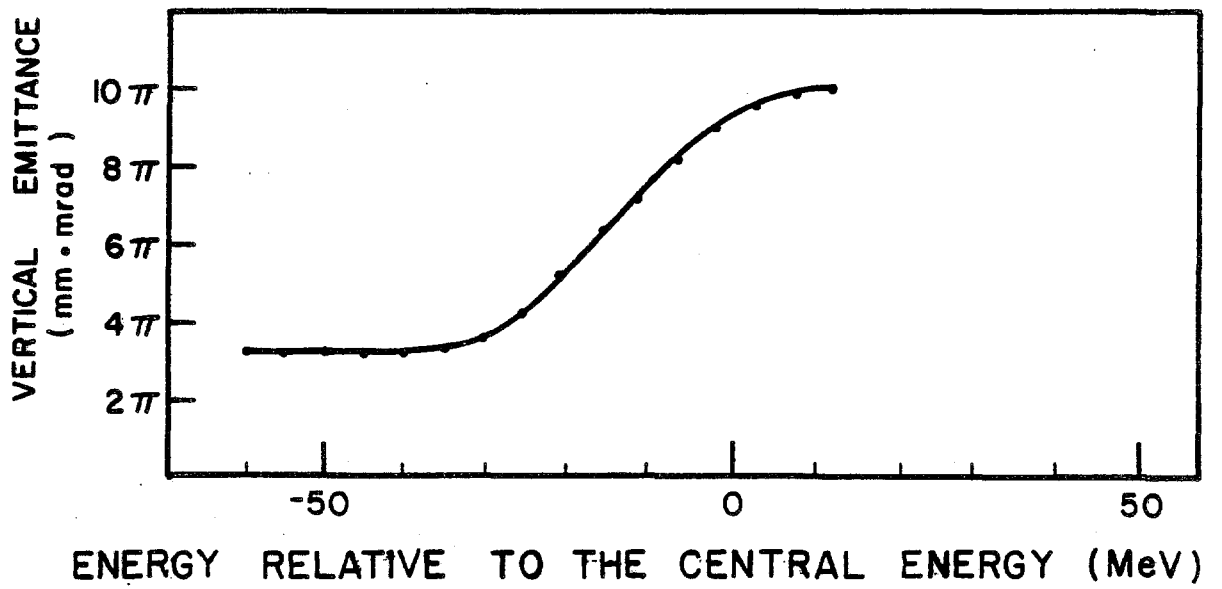
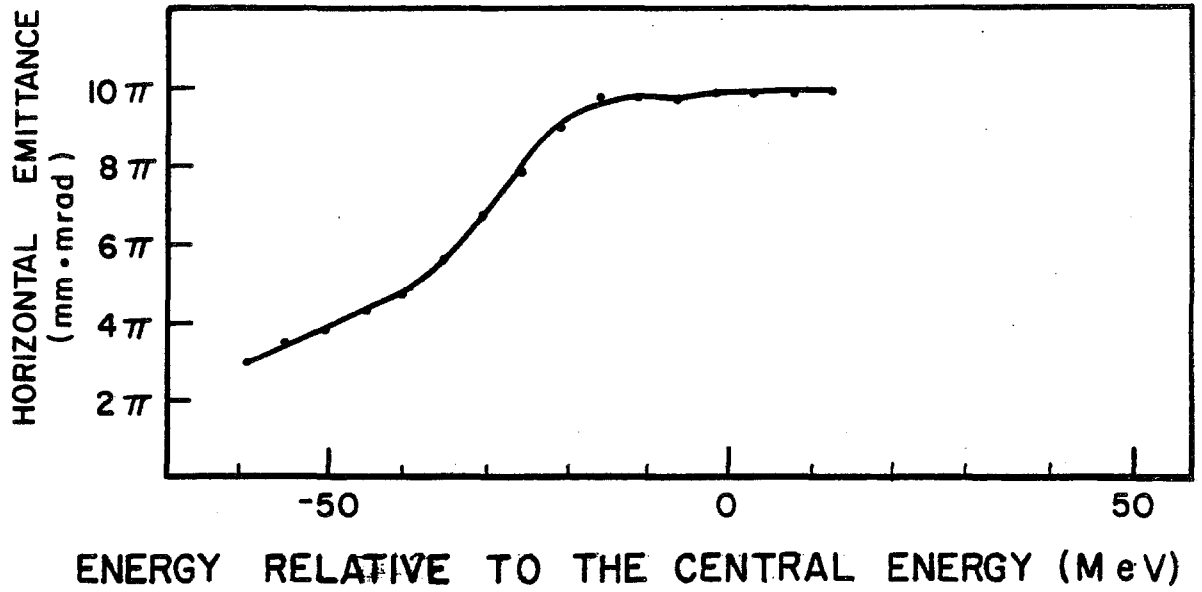


Figure 5-24

5.11.1 Pickup Electrodes. The design of the 1 to 2 GHz and the 2 to 4 GHz stochastic cooling systems is based on the known^{5,11} and measured¹² performance of quarter-wave loop (directional-coupler) pickups. The loop pickup is a segment of transmission line of well-defined characteristic impedance on which beam-wall (image) currents can be induced. The magnitude of the voltage induced on it depends on its characteristic impedance Z_{pu} , its effective length ℓ , its geometrical coupling $e(x,y)$ (which depends on the transverse beam location as well as the height of the vacuum chamber, and the amplitude of the beam current $i_b(\omega)$).

$$V_{pu}(\omega) = e(x,y) Z_{pu} \sin\left(\frac{\ell\omega}{c}\right) e^{i\pi/2} i_b(\omega), \quad (5.20)$$

where the 90° phase shift at the reference plane (the center of the loop) is due to the inductive nature of the coupling. The geometry of a typical pickup pair is shown in Fig. 5-25. Here h is the full height of the gap between the electrodes and w is their effective width. If the signals are added in a microwave power combiner circuit and the output signal is referenced to a transmission line of impedance Z_o , the output voltage is

$$V_{out}(\omega) = s(x,y) \sqrt{\frac{Z_{pu}Z_o}{2}} \sin\left(\frac{\ell\omega}{c}\right) e^{i\pi/2} i_b(\omega), \quad (5.21)$$

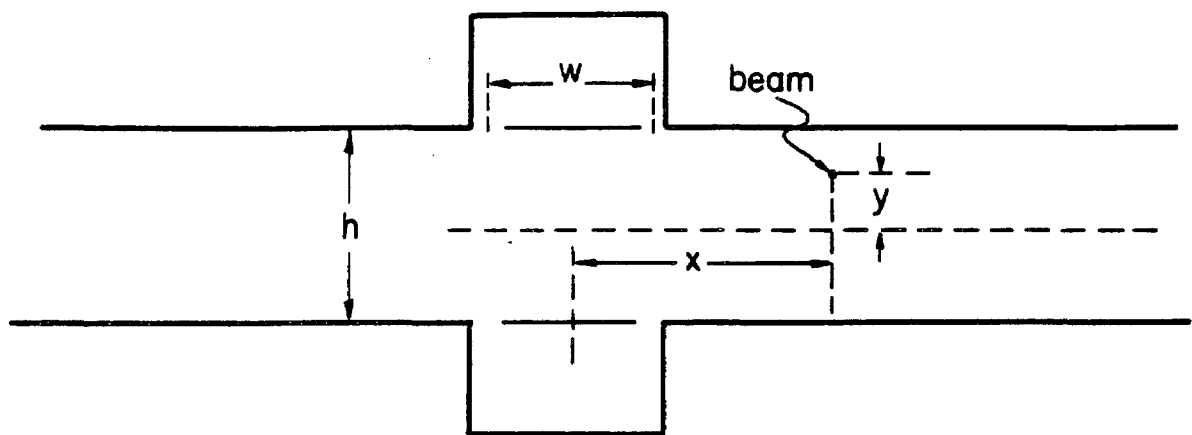
where $s(x,y) = e(x,y) + e(x,-y)$

$$= \frac{1}{\pi} \left[\tan^{-1} \left(\frac{\sinh \frac{\pi}{h}(x+w/2)}{\cos(\pi y/h)} \right) - \tan^{-1} \left(\frac{\sinh \frac{\pi}{h}(x-w/2)}{\cos(\pi y/h)} \right) \right] \quad (5.22)$$

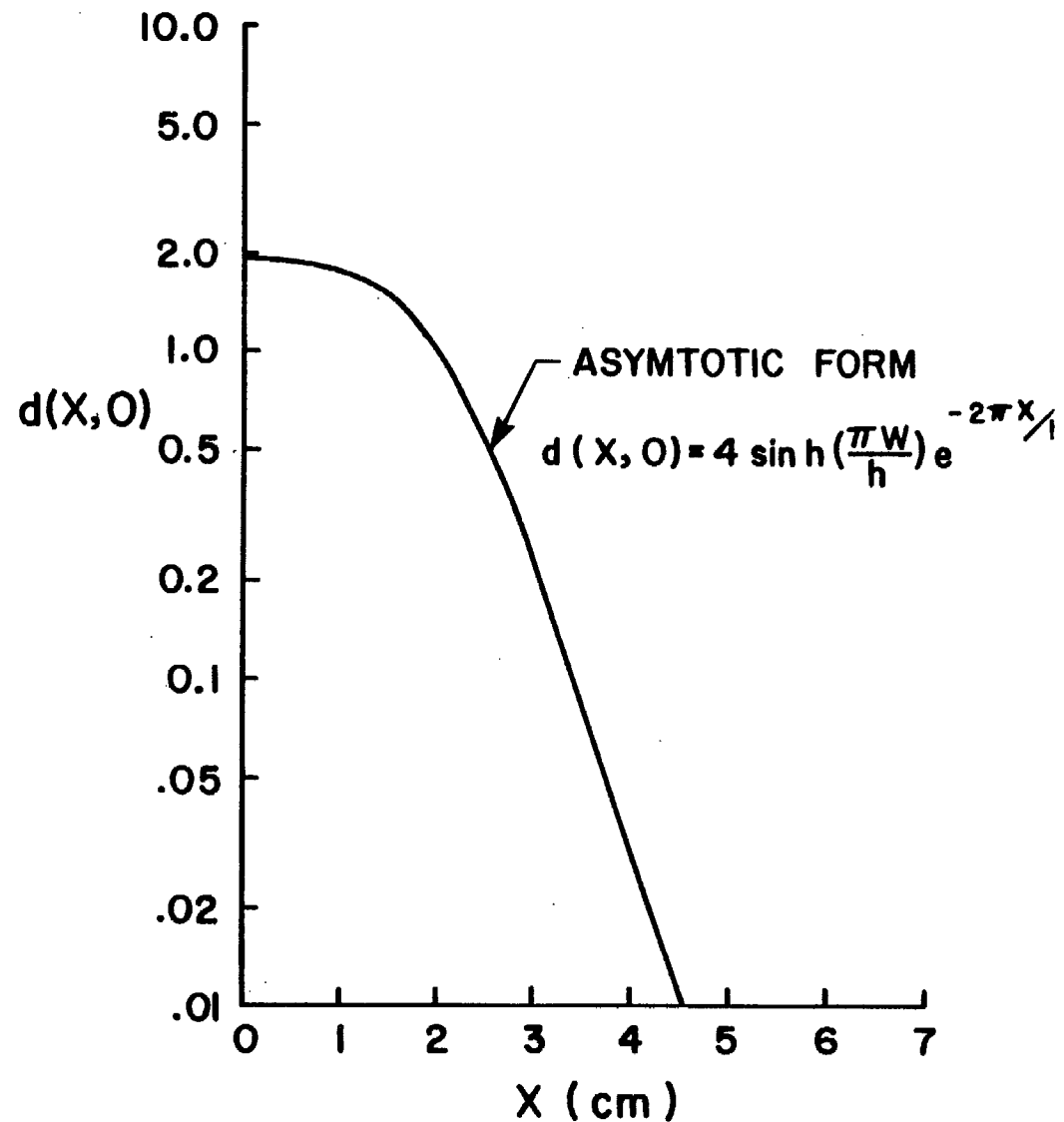
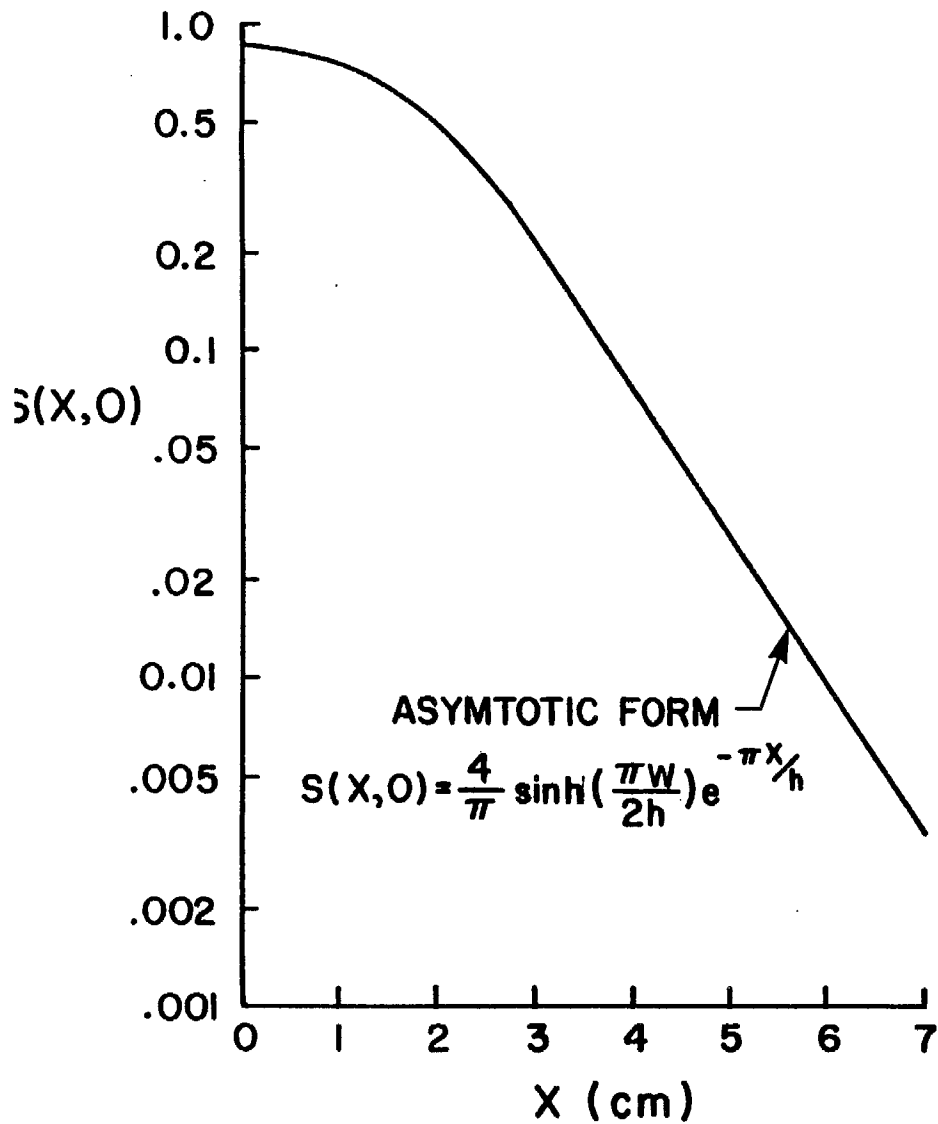
For $x = y = 0$,

$$s(0,0) = \frac{2}{\pi} \tan^{-1} \{ \sinh(\pi w/2h) \}. \quad (5.22a)$$

Transfer impedances of pickup pairs in sum mode are defined with a centered beam at center frequency ($\omega = \pi c/2\ell$) and in a $Z_o = 50$ ohm transmission line,



PICKUP - PAIR GEOMETRY



Plots of $S(X,0)$ and $d(X,0)$ us x for $h=3\text{cm}$ and $w=4\text{cm}$

$$Z_s = s(0,0) \sqrt{25 Z_{pu}} .$$

At large x , $s(x,0) \rightarrow \frac{4}{\pi} e^{-\pi x/h} \sinh(\pi w/2h)$

A plot $s(x,0)$ vs x is given in Fig. 5-26(a).

If the differences of the signals in the pickup electrode pair are combined into a transmission line of impedance Z_o , the output voltage is

$$V_{out}(\omega) = d(x,y) \frac{y}{h} \sqrt{\frac{Z_{pu} Z_o}{2}} \sin\left(\frac{\omega}{c}\right) e^{i\pi/2} i_b(\omega). \quad (5.23)$$

$$\text{where } d(x,y) = \{e(x,y) - e(x,-y)\} \frac{h}{y} ,$$

and the difference mode transfer impedance at $x = 0$ is

$$Z_d(0,y) = d(0,y) \frac{y}{h} \sqrt{25 Z_{pu}}, \quad (5.24)$$

where $d(0,y) = 2 \tanh(\pi w/2h) = \pi s(0,0)[1 - 1/3 s^3(0,0)]$

and at large x , $d(x,0) \rightarrow 4 \sinh(\pi w/h) e^{-2\pi x/h}$.

A plot of $d(x,0)$ vs x is presented in Fig. 5-26(b).

Microwave power combiners add power of coherent signals, and the coupling impedance of n loop-coupler pairs is \sqrt{n} times the impedance for a single pair, in both sum and difference modes. Figures 5-27 and 5-28 show a typical electrode assembly.

Based on calculations, as well as measurements with both wires and electron beams, the loop coupler characteristics shown in Table 5-VII are the values we use in this Design Report.

BEAM PICKUP ELECTRODE ASSEMBLY

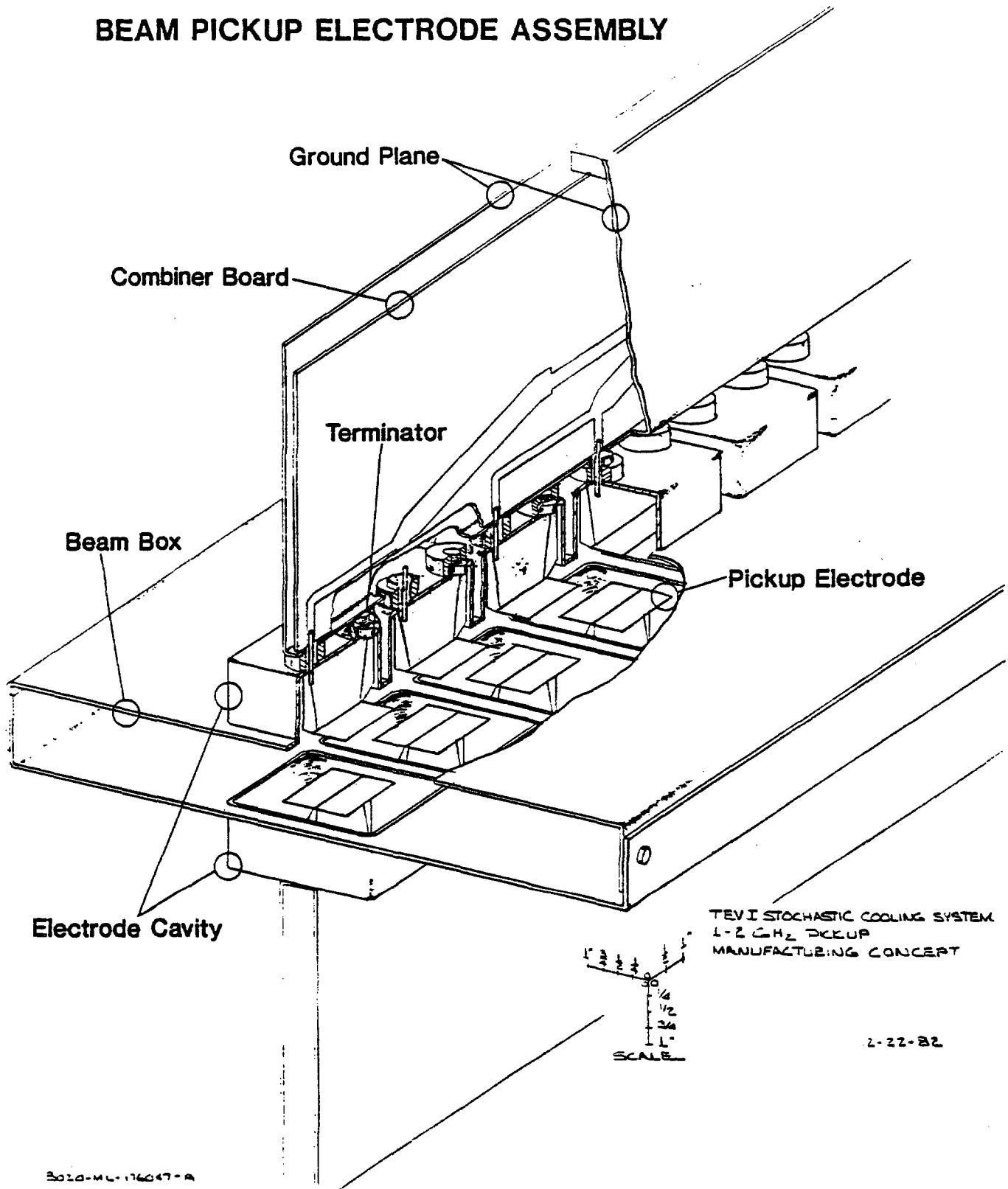
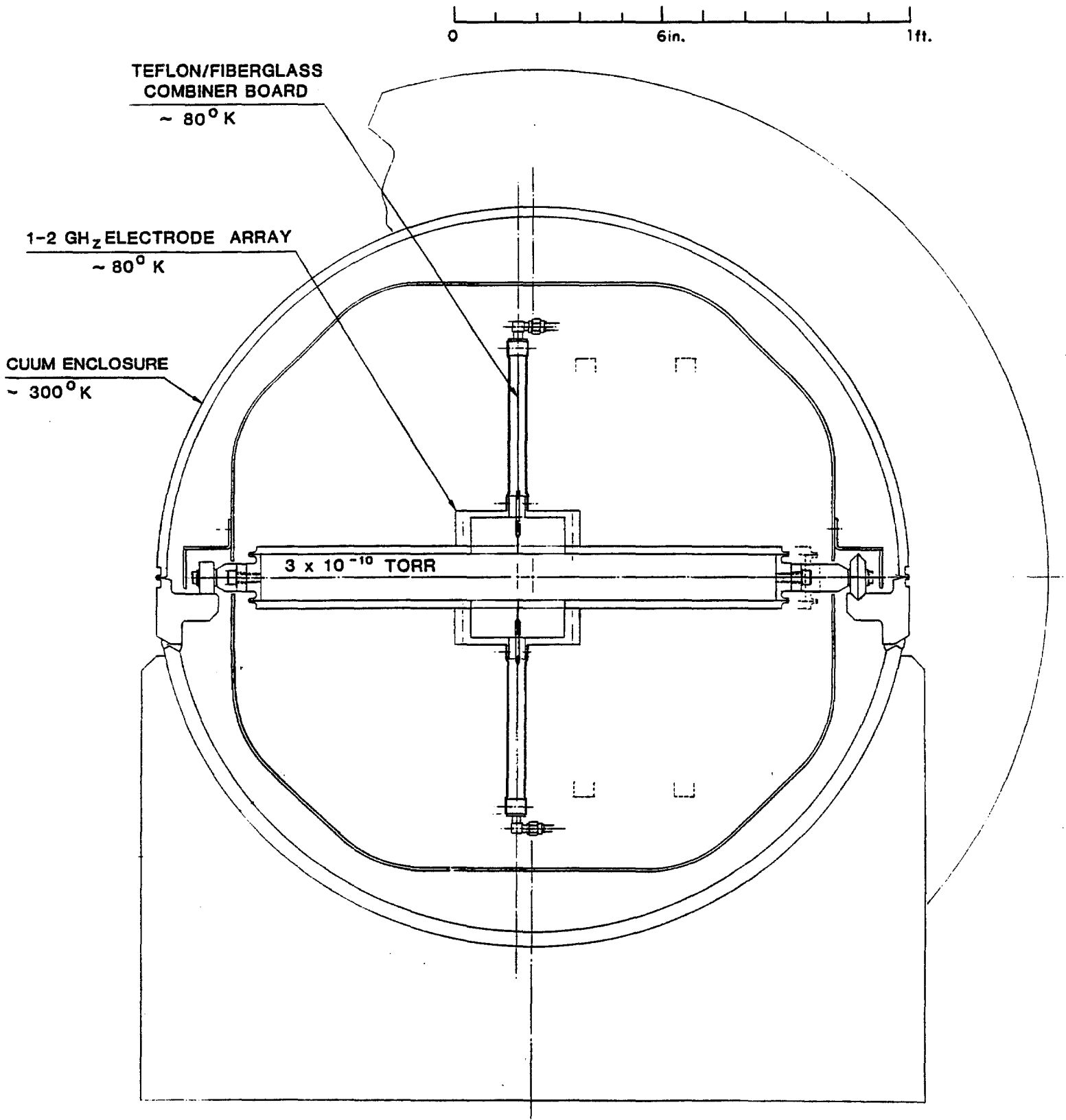


Figure 5-27



TYPICAL PICK-UP CROSS SECTION

Figure 5-28

TABLE 5-VII LOOP COUPLER CHARACTERISTICS

Characteristic		1-2 GHz band	2-4 GHz band
characteristic impedance	Z_{pu}	100	75 Ω
height (gap) typical	h^u	3.0	3.0 cm
effective width	w	4.0	2.5 cm
pairs per meter		15	25 per m
<u>Sum Mode</u>			
$s(0,0)$		0.843	0.664
transfer impedance	Z_s	42.2	28.8 Ω
<u>Difference Mode</u>			
$d(0,y)$		1.94	1.73
transfer impedance	Z_d	3230	2500 Ω/m

The electrode assemblies shown in Figs. 5-27 and 5-28 are approximately 1.2 meters long (for the 1-2 GHz band) and contain 16 pickup pairs. The signals are combined separately for top and bottom electrodes using a double-sided Teflon printed circuit board. The air-spaced ground plane yields a group velocity of about 0.98c. The electrodes are back-terminated in their characteristic impedance, and the whole assembly is cooled to liquid-nitrogen temperature to reduce the thermal noise power from the back termination, the skin effect losses in the circuit board, and teflon outgassing. In the 2-4 GHz band, it is quite possible that slot couplers will have a higher coupling impedance per unit length than loop couplers. A research and development program is underway in this area.

Tests on 16 pair 1-2 GHz electrode arrays connected in sum mode have been carried out at Argonne National Laboratory using a 20 MeV pulsed electron linear accelerator. Fast Fourier transforms of the electrode array output signal yield transfer-impedance measurements in the frequency domain. Transfer impedances at centerband of about 140 ohms have been measured in this manner (the calculated value is 168 ohms). The tests have also confirmed the $e^{-\pi x/h}$ spatial sensitivity, which is an important parameter in matching the electrode response to the expected antiproton spatial density in the Accumulator high-dispersion straight section. At large x , there is an indication that the beam excites resonances in the beam box which in turn are picked up by the electrodes. As the spatial sensitivity of the electrodes to these resonances is much flatter than the desired signal, they could dominate the electrode transfer impedance at large x . More beam tests are required to understand the magnitude of this effect, and to develop ways of attenuating these modes (e.g., use of ferrites in the beam box).

5.11.2 Preamplifiers. Commercial gallium-arsenide field-effect transistor (GaAsFet) amplifiers are available in the microwave frequency bands required for stochastic cooling. Although their thermal noise characteristics are relatively low (a 2.0 db noise figure amplifier,

available in the 1-2 GHz band¹³, has an equivalent noise temperature of 170 K) it would still contribute nearly 70% of the total thermal noise power. The design therefore includes preamplifiers cooled to liquid nitrogen temperatures. We expect equivalent noise temperatures of 75 K (NF = 1.0 db) and 120 K (NF = 1.5 db) for 1-2 GHz and 2-4 GHz amplifiers respectively. Minimization of thermal noise is not only important in relation to beam heating, but also in relation to the cost of extra traveling wave tube installed power required to amplify it.

Commercially available GaAsFet amplifiers designed to operate in the Mil spec temperature range (-55°C to 70°C) have been successfully operated as low as 77 K¹⁴. In this case a 1-2 GHz amplifier achieved an equivalent noise temperature of 120 K (NF = 1.5db). GaAsFet amplifiers have been specially designed for operation at liquid-helium temperatures, and equivalent noise temperatures of 20 K (NF = 0.2 db) have been achieved in narrow band operation¹⁵ (0.5 GHz bandwidth at 1.5 GHz).

We are presently pursuing parallel research and development efforts in this area. At Lawrence Berkeley Laboratory, a prototype GaAsFet amplifier has been built which has the following properties in the 1-2 GHz band:

Gain Average	33 db
Gain Flatness	±1.5 db
Phase Linearity	±15°
Noise Temperature Peak (NF=0.5)	40 K
Average (NF=0.35)	30 K
Input VSWR Peak	2.5:1
Average	1.75:1

Only slight improvements are seen when the amplifier is cooled to 14 K.

At Fermilab, measurements are being made on cooled commercially available amplifiers. This includes amplifiers with integrated bipolar biasing circuits which can only be cooled to -50°C, and amplifiers with separated biasing circuits, which can be cooled to 77°K. We have achieved average noise temperatures of 80 K and 110 K for amplifiers cooled to -50°C and 77 K respectively. Input VSWR has typically been better than 1.4:1.

Research and development is continuing in the 1-2 GHz band in both the above efforts. In addition, work is beginning in the 2-4 GHz band.

5.11.3 Notch Filters. Notch filters are needed in our design of the stochastic cooling system for several reasons. In one system, the stack tail momentum cooling system, notch filters are used both for reducing the microwave power at frequencies corresponding to particles in the core, and to assist in shaping the gain vs momentum (frequency) in the stack tail. In systems with poor signal to thermal noise ratio, notch filters are useful in reducing the extra traveling-wave tube installed power required to amplify it. If momentum cooling is implemented in the debuncher, a notch filter would be used to produce a phase inversion of the pickup sum

signal at the harmonics of the central revolution frequency. The tolerance on the frequency deviation of the notch centers at each harmonic of the revolution frequency ω_0 in the frequency bandwidth is of the order of (for the Accumulator)

$$\left| \frac{\omega_n - n\omega_0}{n\omega_0} \right| < \eta \frac{\delta p}{p} = 10^{-5},$$

Where $\eta = 0.02$, p is 8.9 GeV/c and δp is about 2 MeV/c.

Filter designs include both shorted stubs, which use reflections from the shorted end of a long transmission line (nominally half the circumference of the Accumulator), and correlator types, which use the constructive and destructive interference of the same signal transmitted over two transmission lines (whose lengths differ by about the circumference of the Accumulator).

In our application, the large circumference of the Accumulator, in combination with the very high frequencies used in the electronics, imposes severe restrictions on the selection of transmission lines. In room-temperature transmission lines, the skin effect conductor resistance causes dispersion as well as attenuation. This is reduced by using larger diameter transmission lines. However, the maximum size of the transmission line is limited, since higher order modes are excited and affect the dispersion. In particular, in a 7.5-cm diameter 50-ohm transmission line, the TE_{11} mode propagates at frequencies above 2.0 GHz. These effects are only marginally better at 76.6 ohms, the impedance at which skin effect losses are minimized.

Our present notch filter is based on a correlator circuit using a 1.6 mm diameter 50 ohm superconducting transmission line. In such a line the major attenuation (power loss) is due to the loss tangent in the dielectric, and results in an attenuation of about 1.0 db per km in the 1-2 GHz band. Early measurements showed that shorted-stub filters typically had much higher dispersion than the same cable when used as a correlator filter. This due to the fact that power reflected by a single discontinuity in a correlator filter is absorbed by the isolated port on the input hybrid splitter, and can only reach the output hybrid if it is re-reflected by another discontinuity. Recent measurements have been made on a 330 m line in a cryostat as shown in Fig. 5-29. Dispersion and notch depth measurements in the 1-2 GHz band are shown in Fig. 5-30. This performance is believed to be adequate for the stack tail system. Shorted-stub filters do offer some advantages over correlator filters, however, as they allow greater flexibility in gain and phase shaping within each Schottky band. Present measurements indicate that the present superconducting line does indeed provide adequate performance in terms of dispersion and notch depth when used as a shorted stub. Research is still

CRYOSTAT FOR SUPERCONDUCTING FILTER

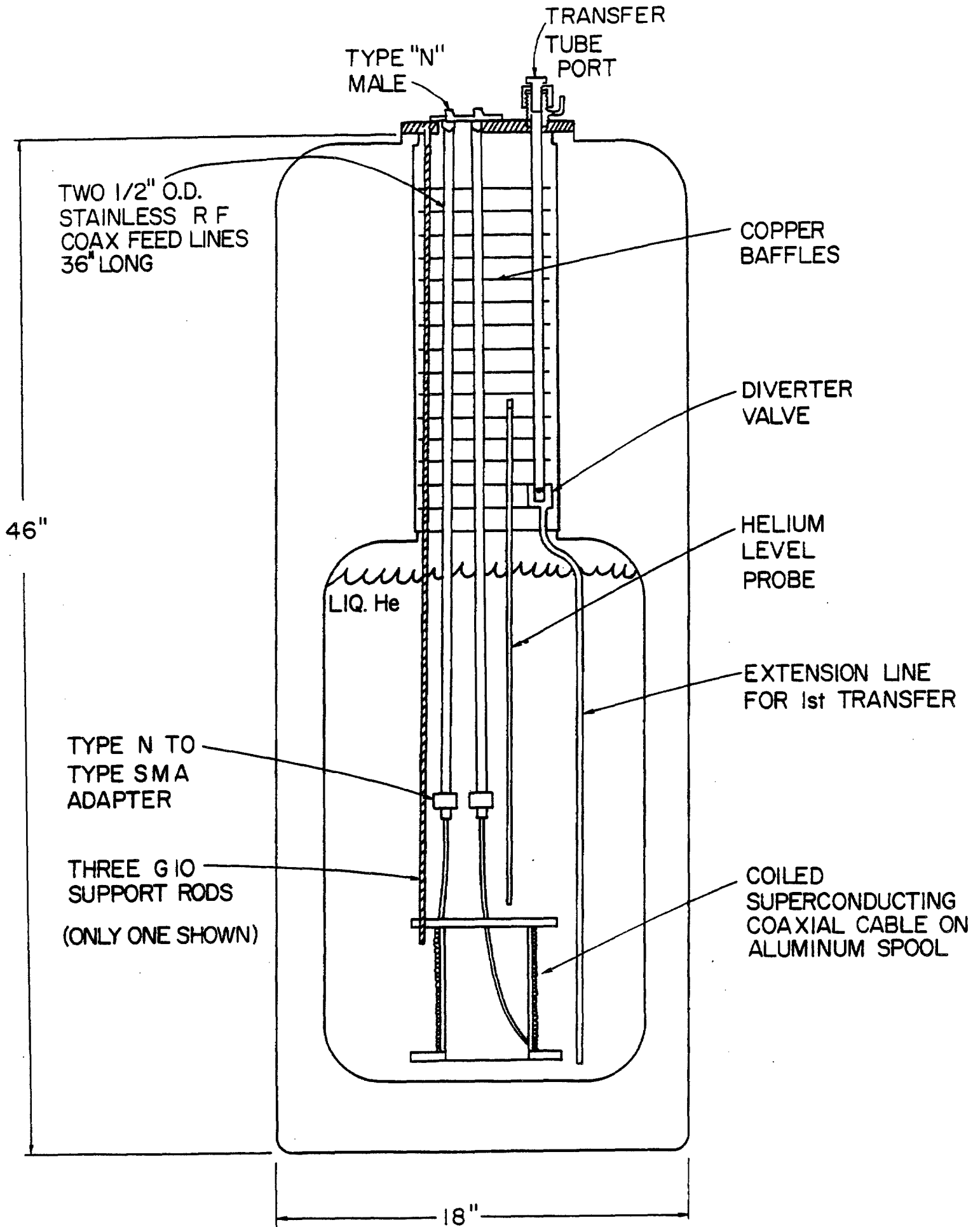


Figure 5-29

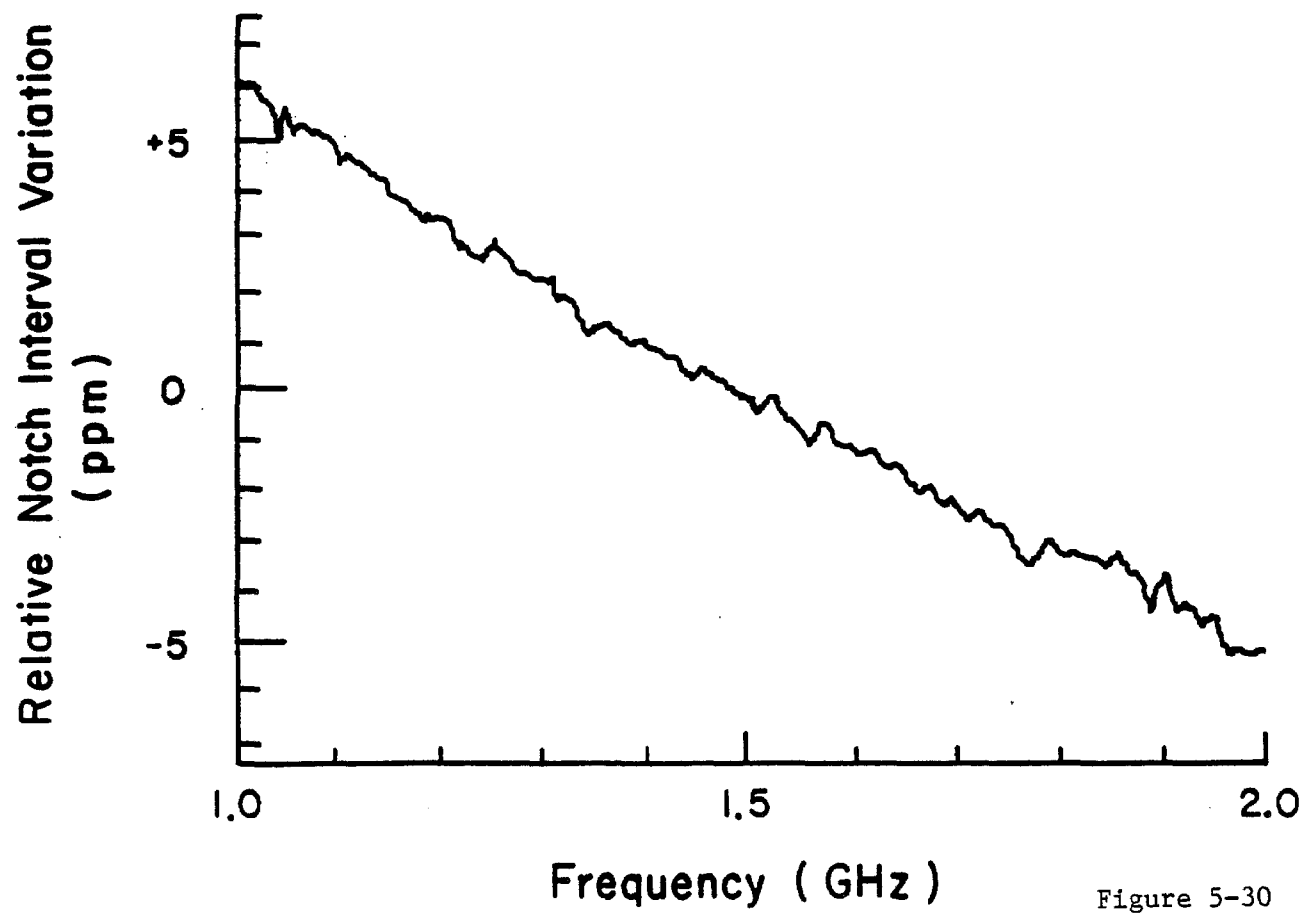
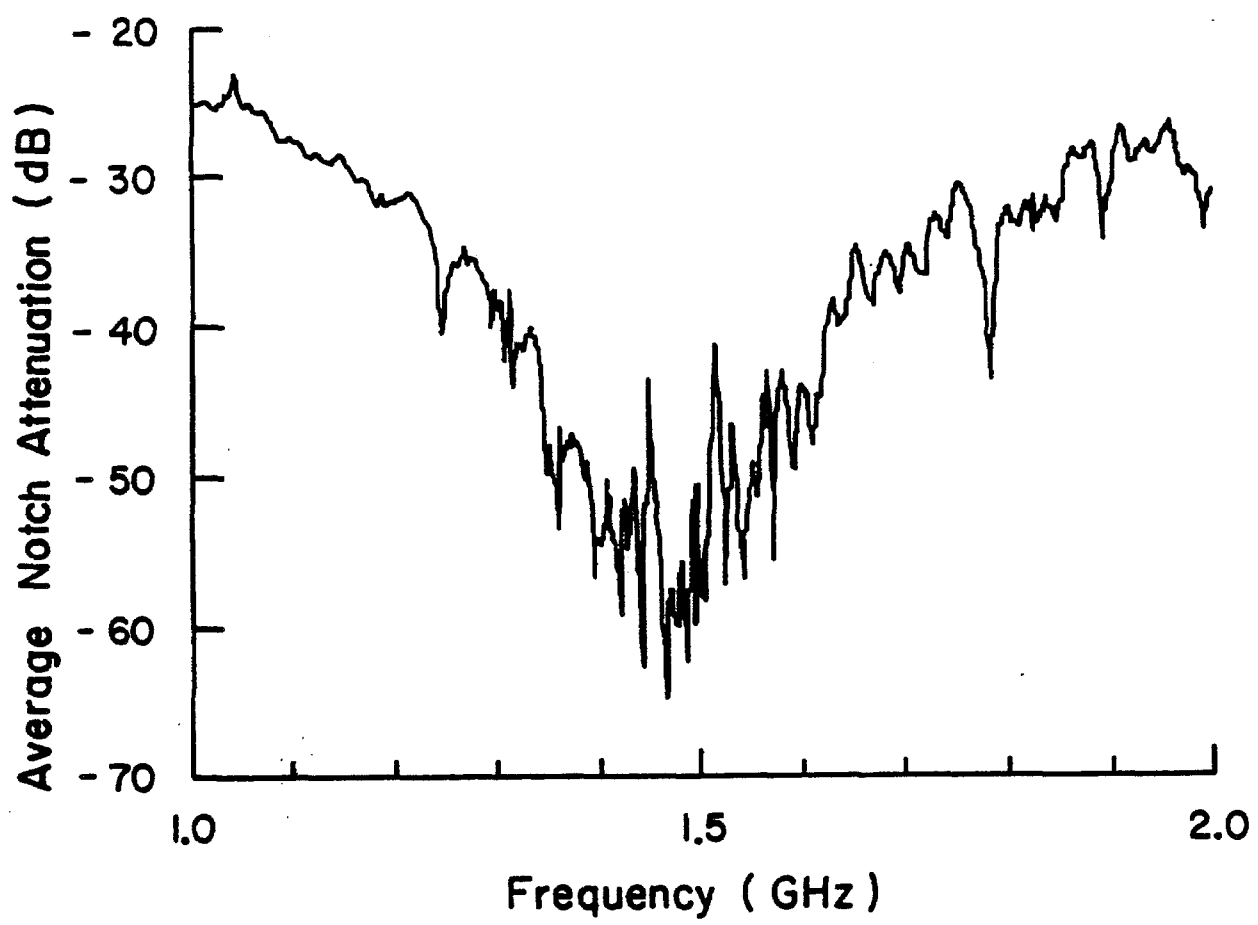


Figure 5-30

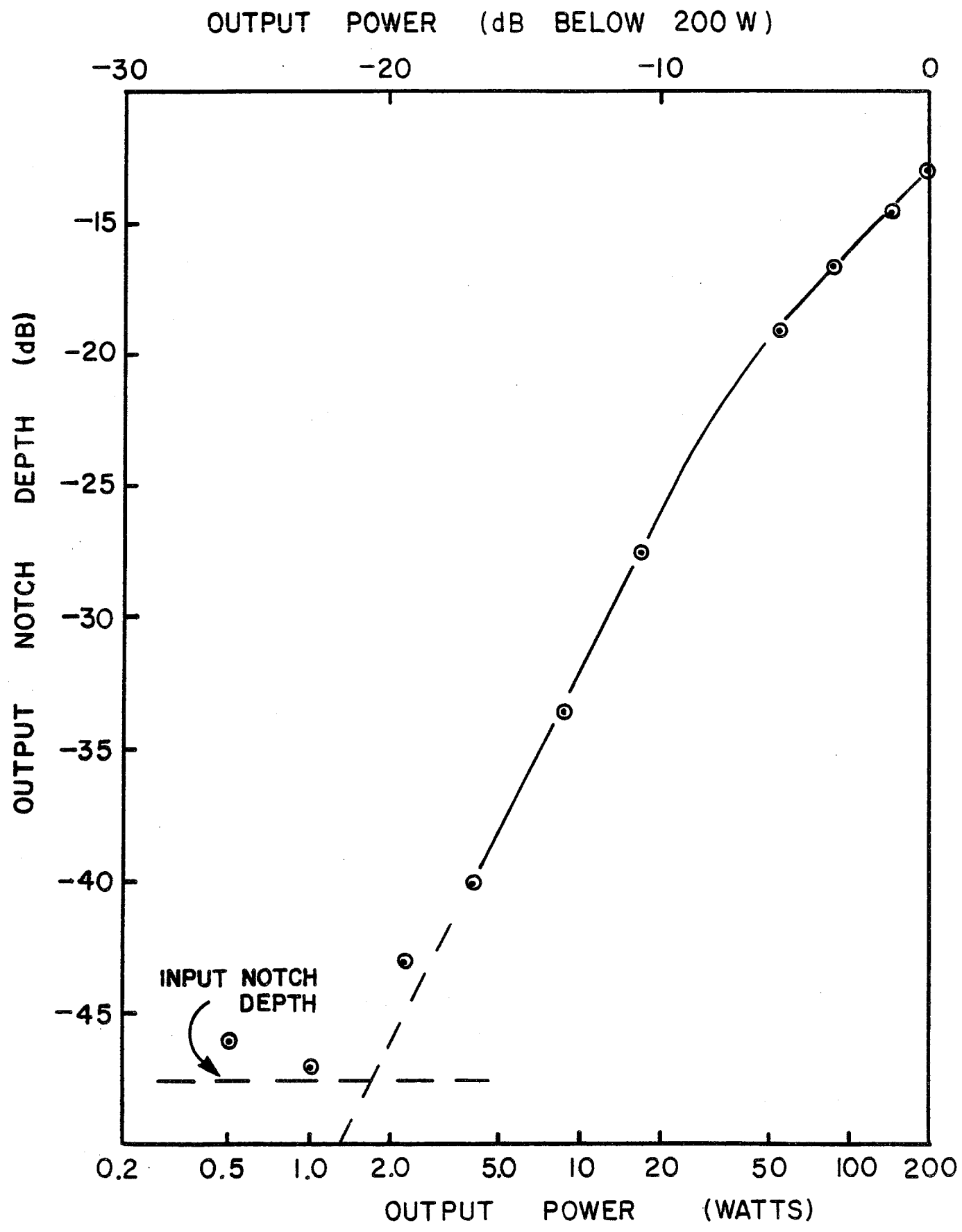


Figure 5-31

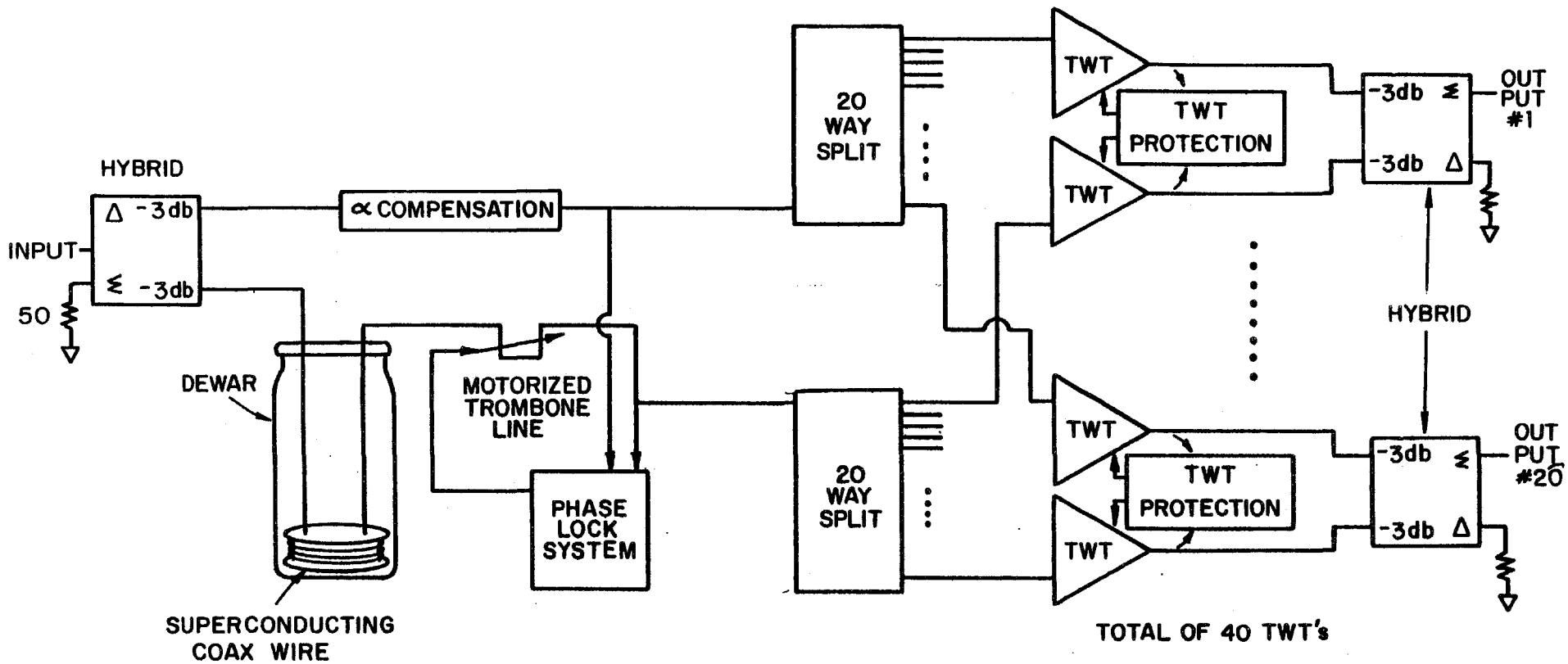
proceeding in this area. Research is also going on in the area of TWT correlator filters, to help control the TWT intermodulation (IM) distortion. This is discussed in the next section.

5.11.4 Traveling Wave Tubes (TWT's). The power amplifier stages in all our cooling systems are traveling wave tube amplifiers. Several commercial units are available in the 1-2 and 2-4 GHz bands with saturated output power ratings up to 200 watts. Traveling wave tubes are also available with power ratings above 1 kW:

Numerical studies show that in the stack tail momentum cooling system, the depth of the notches between the Schottky bands must be at least 40 db deep in order not to excessively heat the core. Even though notches of this depth can be obtained with the filters discussed above, the intermodulation distortion that occurs at higher power levels in TWT's can rapidly fill these in. Second-order intermodulation distortion can occur at the edges of the operating band of octave-bandwidth TWT's. Operation of the TWT's in a push-pull mode can reduce the second order IM products effectively, but, third-order IM distortion can occur at midband frequencies and is not reduced by operating the TWT's in push-pull mode. Measurements using a single TWT and a notched white-noise source show that the remaining notch depth at the TWT is only 13 dbc at full power (200 watts), but improves to about -30 dbc at 10 watts per TWT. This result is shown in Fig. 5-31. Since this measurement was made, tests on another design TWT with a higher bandwidth indicated a somewhat lower level of IM distortion at the same power levels. Specifically, the IM distortion improved to about -23 dbc from -20 dbc at 40 watts output power. The highly peaked Schottky spectrum produces a third-order intermodulation distortion which is naturally peaked in, rather than between, the Schottky bands, providing another 12 db of notch depth at core frequencies. To obtain 1600 watts of output power and notch depths of 40 db would require roughly 160 TWTs, each operating at about 10 watts.

The potential cost saving of being able to run the TWT's at 40 W rather than 10 has stimulated interest in using superconducting correlator filters on the output of the TWT's. In principle, the filter need only provide a notch depth of the order of 20 db, the remainder being provided by the TWT IM distortion of -20 dbc, and the IM form factor of the Schottky bands of 12 db. As a correlator filter using a superconducting transmission line is nearly lossless, we are investigating the possibility that such a filter could be used on the TWT outputs. Calculations show that the superconducting line could dissipate about 0.7 W/meter without quenching. In principle a superconducting correlator filter could carry several hundred watts of microwave power if the attenuation were 1 db per km. Such a power-correlator filter could be used on the output of a push-pull TWT pair to reduce the output power between the Schottky bands caused by IM distortion.

A research and development program has been directed toward building a power correlator filter capable of handling 80 watts of microwave power in



POWER CORRELATOR FILTER FOR STACKTAIL MOMENTUM COOLING

Figure 5-32

the 1-2 GHz band (this corresponds to 40 watts per TWT, and 40 watts in the superconducting line). Tests thus far have only achieved 50% of this power level, and the present belief is that the thermal coupling between the Teflon and the outer conductor is less than optimal, causing an additional temperature rise. Pulsed-power tests with more than 100 watts being transmitted through the superconducting cable indicate that the attenuation is about as expected (around 1 db per km) even at these high power levels, hence the present limit is not due to anomalous attenuation at high power levels.

If further research in this area is unsuccessful in achieving reliable operation at 40 watts in the superconducting line, then an alternative circuit in which the superconducting line and the TWTs are combined in the same correlator type loop circuit will be used. It is shown in Fig. 5-32. Such a circuit is more demanding on the TWT performance in the areas of gain and phase matching, phase linearity and IM distortion. It is believed that such a circuit could yield IM distortion reduction of the order of 6 db more than the same circuit without the filter. Hence present calculations show that IM distortion levels are marginal at 40 watts per TWT.

5.11.5 Kicker Electrode Assemblies. The kicker electrode assemblies are conceptually similar to the pickup electrode assemblies by virtue of the reciprocity theorem, which states that transfer impedances between pairs of terminals are unchanged when inputs and outputs are exchanged. The major differences are of a hardware nature: the combiner board is now a power splitter and some power dissipation and heating should be anticipated. The terminating resistor now must absorb microwave power, and means must be provided for heat removal. There is no thermal-noise problem as there was in the pickup case, so cryogenic cooling is only needed if adequate vacuum cannot be obtained otherwise, or if the terminating resistors cannot operate at 7 watts/resistor at room temperature. Tests on outgassing of materials are continuing in order to better understand their compatibility with the kicker electrode array design.

There is some concern that kicker electrodes will generate evanescent and propagating modes in the beam pipe. This is especially true of betatron cooling kickers, but can also be a problem in the momentum-cooling systems. Evanescent modes, even though highly damped, have phase velocities considerably different than the beam, and could lead to stochastic heating effects. The propagating modes, besides being able to heat the beam, can also propagate through the beam pipe back to pickup arrays and interfere with the pickup operation. The $TE_{1,1}$ cutoff in a 35 mm diameter beam pipe is about 5 GHz, so such insertions would have to be placed in low-dispersion areas of the ring.

5.11.6 Other Considerations. Most of the components in the stochastic-cooling electronics have a limited bandwidth of about an octave, and this normally causes the frequency derivative of the phase delay to be frequency dependent. This leads to two parameters that need to be known

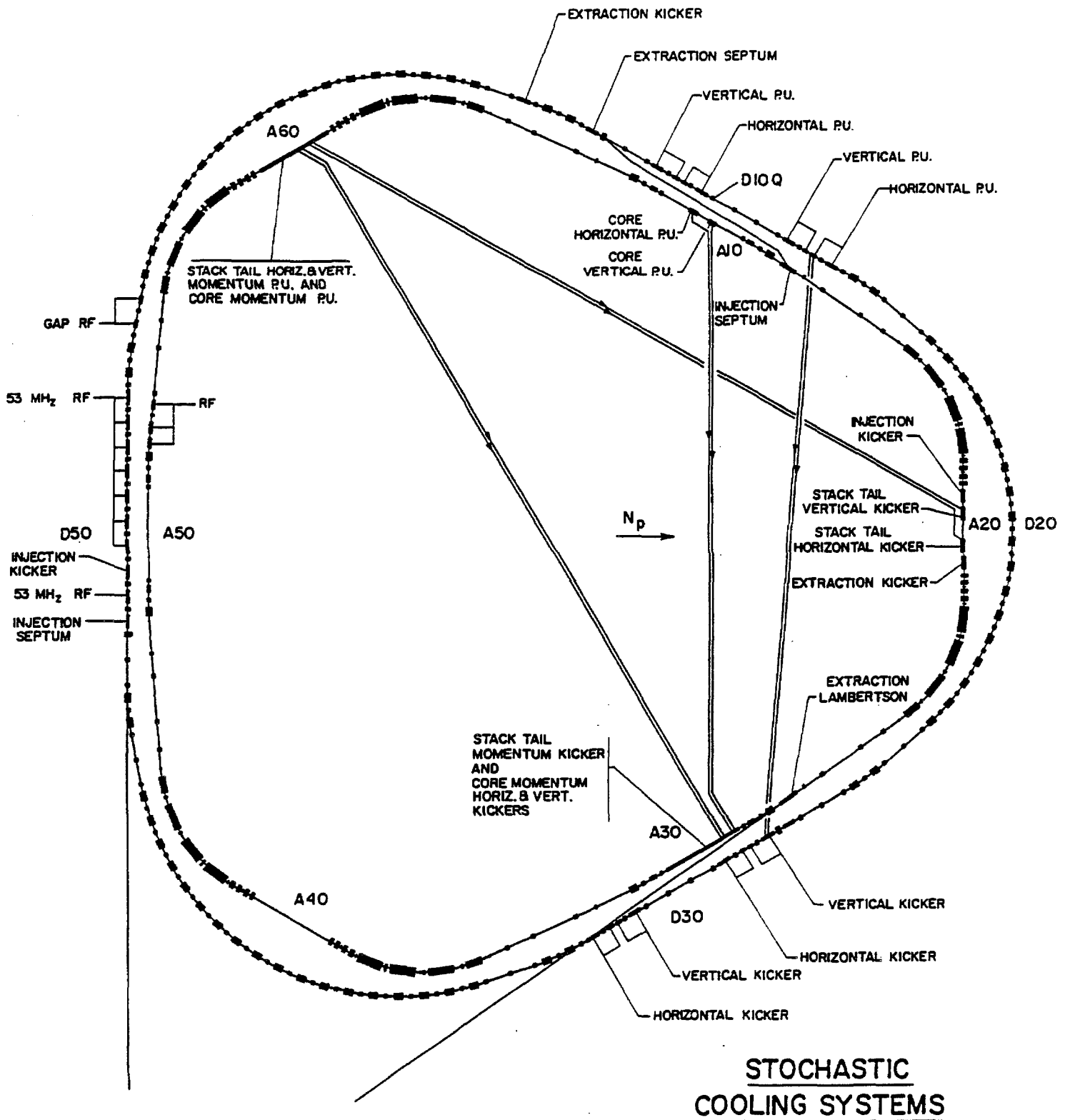


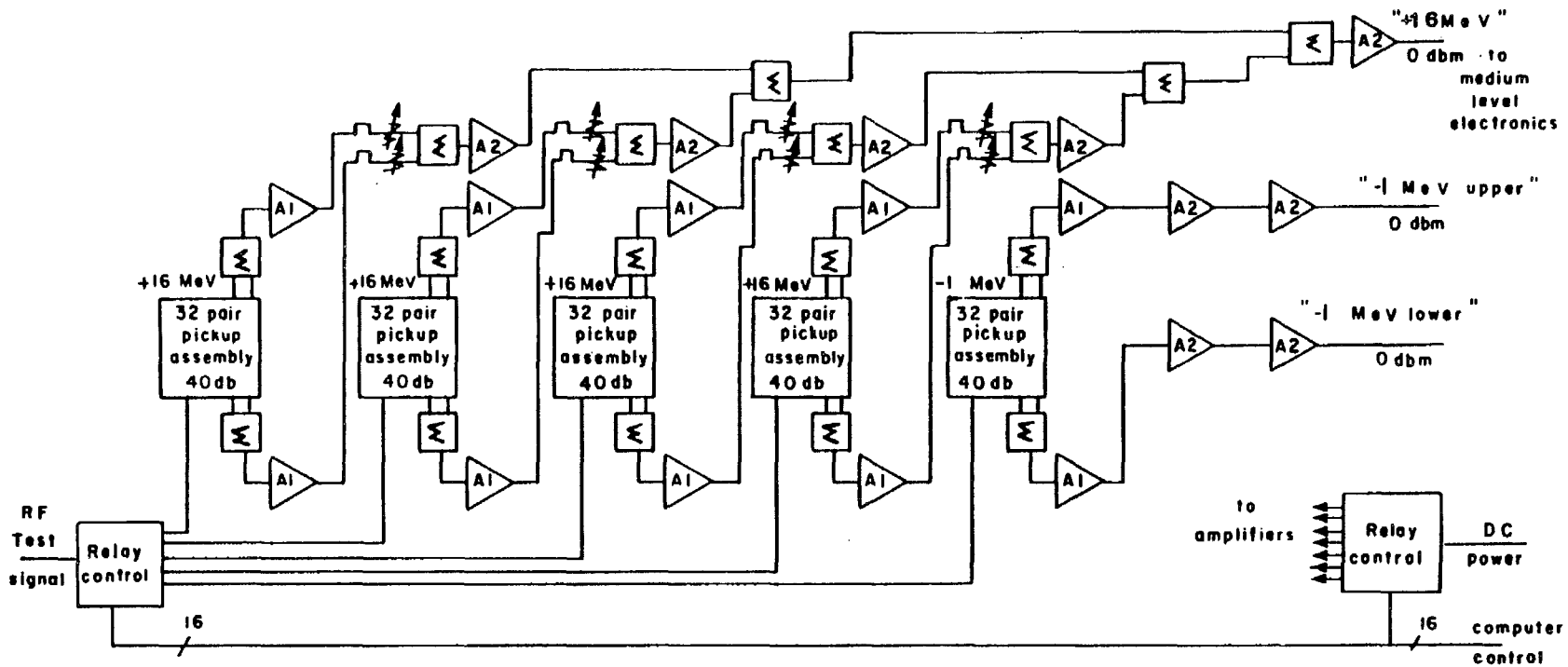
Figure 5-33

for each element. The group delay (the slope of a straight-line fit to the phase delay vs frequency data in the operating band) and the phase intercept (the zero frequency intercept of the above straight line) need to be measured for each component and accounted for the final system. Deviations from the average group delay at particular frequencies, as well as gain nonuniformity may have to be corrected. Special circuits to cause gain shaping and constant phase offset will need to be designed and built. In brief, the group delay is adjusted using cables so that the information signal arrives at the kicker at the correct time. The phase intercept correction assures that it arrives with the correct phase angle. The gain correction assures that the signal power is properly apportioned to each Schottky band.

The dispersion in the transmission lines carrying the signals across the ring also needs to be considered. In the 1-2 GHz stack tail systems, the largest diameter coaxial line which we can use is 1-5/8-in. diameter rigid line (air dielectric) as the TE_{11} mode propagates above 3.5 GHz. Calculations show that the expected dispersion is about 8 over the 1-2 GHz band for 150 m of line, based on the known skin effect losses. Preliminary measurements indicate that it may actually be somewhat larger, possibly due to excitation of evanescent modes at 2 GHz. In the 2-4 GHz range, the transmission line diameter would have to be limited to about 7/8", and the calculated dispersion would be about 18. This line will probably be of the foam dielectric type, because the time-delay requirements are not overly restrictive.

5.11.7 Accumulator Stochastic Cooling System Layout. There are 6 specific cooling systems in the Accumulator. Their location is shown in Fig. 5-33. Their basic operating parameters are outlined in Table 5-VIII. All 3 stack tail systems operate in the 1-2 GHz band, while the 3 core systems operate in the 2-4 GHz band. All kicker assemblies have been located remotely from the pickup electrodes to minimize coupling and feedback.

The largest system is the stack-tail momentum-cooling system, requiring about 1600 W of microwave power. The pickup electrodes are located in the 9 m dispersion short straight section A60, and the kickers in the zero dispersion long straight section A30. A block diagram of the low-level electronics is shown in Fig. 5-34a and b. Groups of 16 pickup electrodes are summed on an internal edge-supported teflon printed circuit board into low noise preamps. Signals are separately amplified for the upper and lower electrodes to allow for gain and phase correction, as well as for forming both sum and difference signals. Signal processing is done in the medium level of electronics as shown in Fig. 5-35. This includes 3 notch filters (superconducting correlators) with notch minima set at +4, -2, and -3 MeV relative to the core. After gain and phase corrections, the signals are amplified to about +20 dbm and transmitted across the ring to the high level electronics (TWT's). At present we estimate that 40 TWT's are needed if we can operate them at 40 W each and maintain a 40 db notch



32 pair pickup assembly = 2.4m long module containing 32 pair of 1-2 GHz loop couplers cooled to 77°K. Upper and lower electrode signals are separately brought to cooled GaAsFet amplifiers through vacuum chamber wall. A 40 db coupler built into assembly allows insertion of test signal.

Σ = 2:1 power/inphase power combiner/splitter.

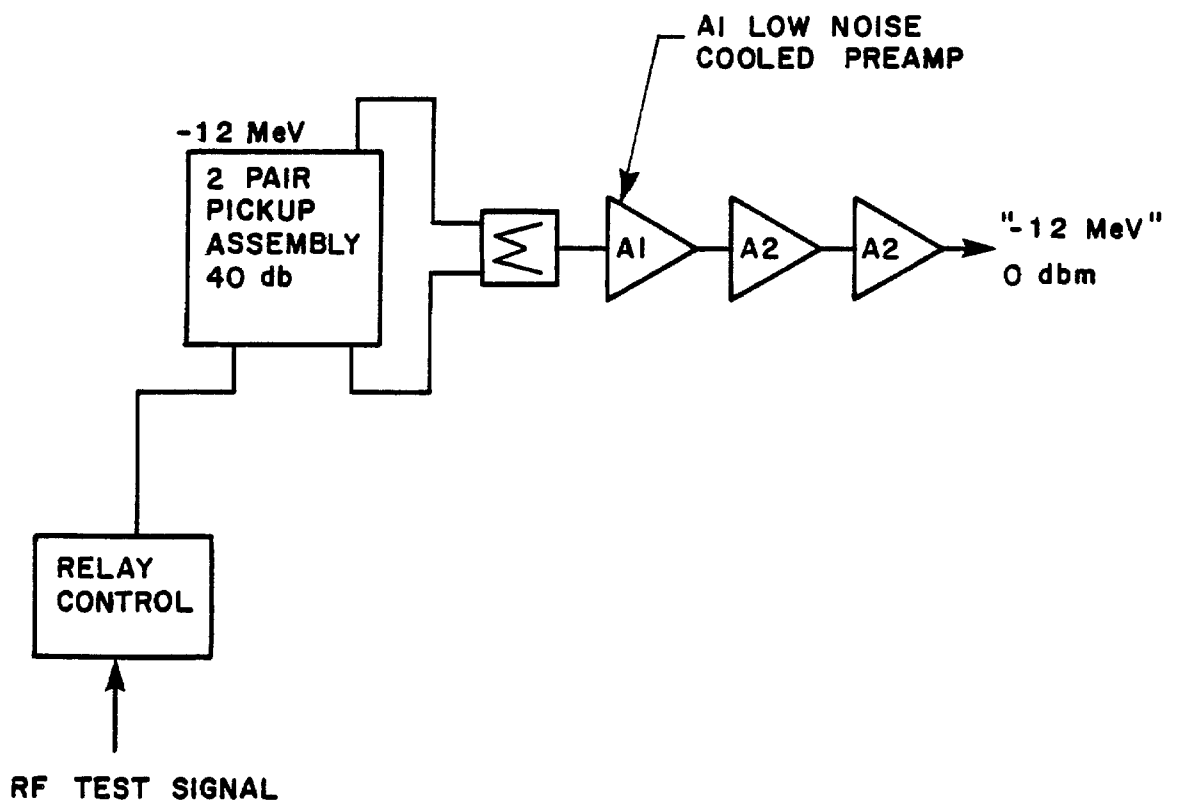
A1 Low noise GaAsFet amplifier cooled to 77°K. Gain about 30 db. Equivalent noise temperature about 75°K.

A2 Commercial bipolar 1-2 GHz amplifier, Avantek #UTC-20-104 or equivalent (gain = 23 db; equiv. noise temp. = 500°K).

Manually adjusted liner delay pad.

Manually adjusted attenuator pad.

Figure 5-34a



Stack Tail Momentum Low Level Electronics

Figure 5-34b

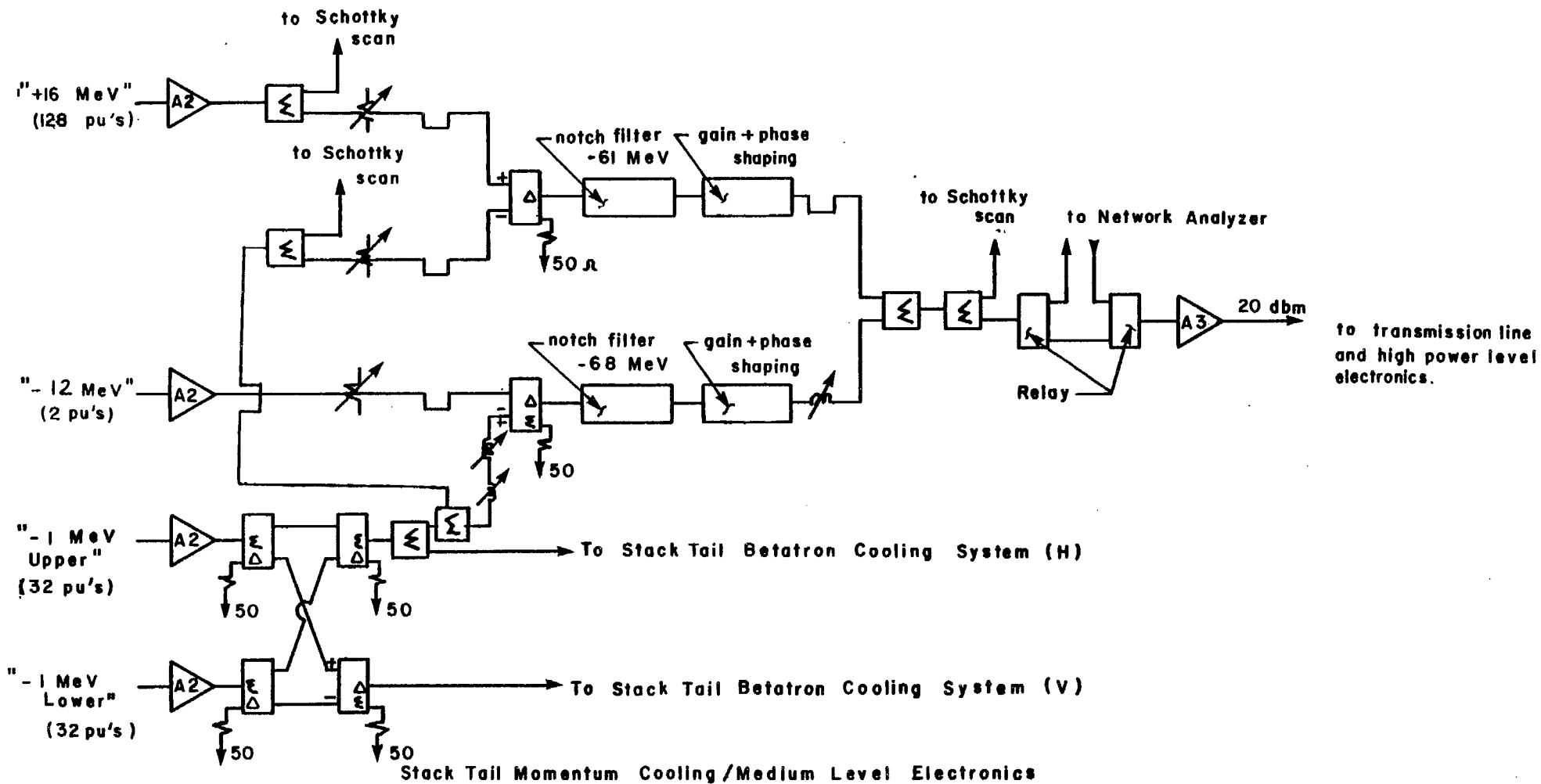
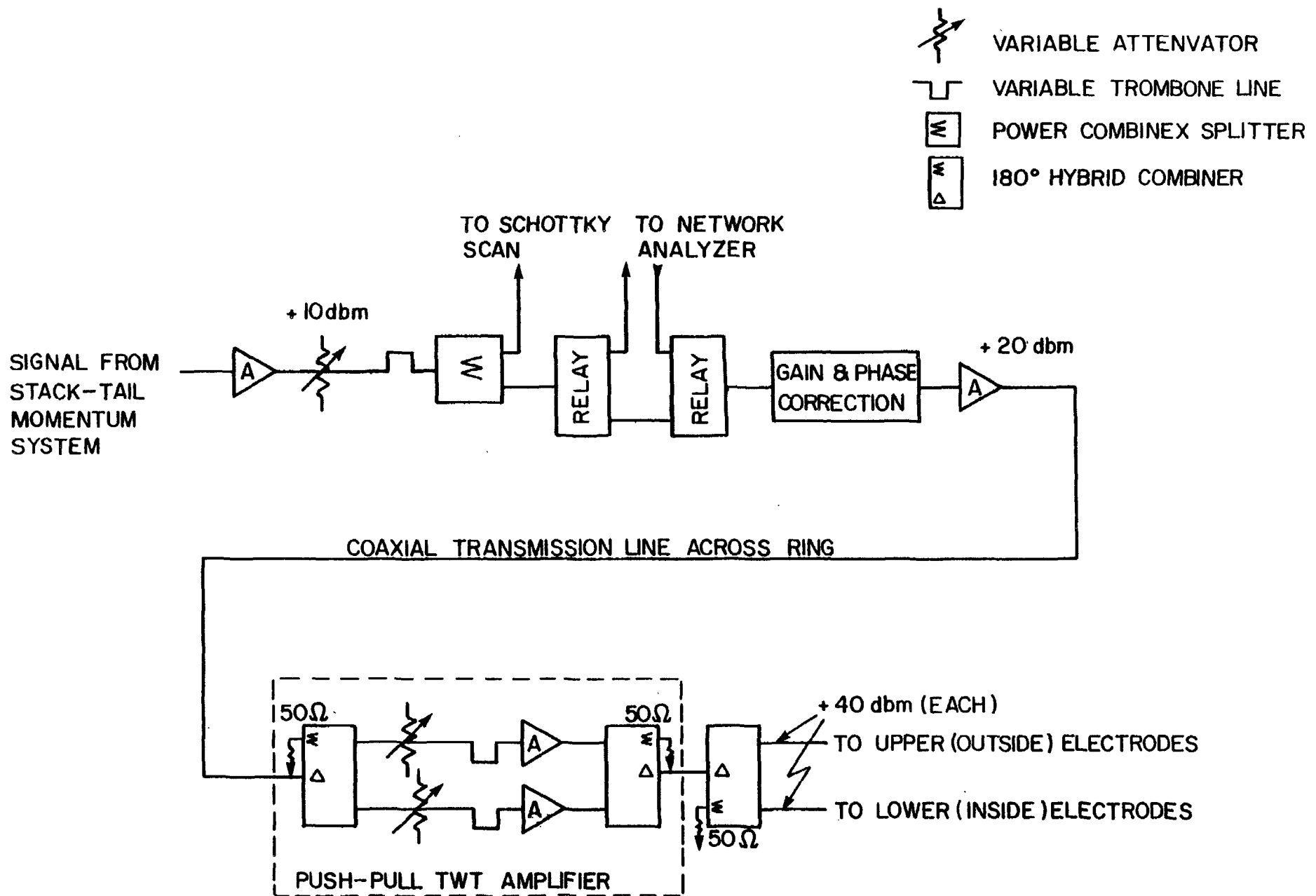


Figure 5-35



STACK-TAIL BETATRON COOLING SYSTEM (2 REQUIRED)

Figure 5-36

depth at the core frequency (this number includes the Schottky form factor of about 12 db).

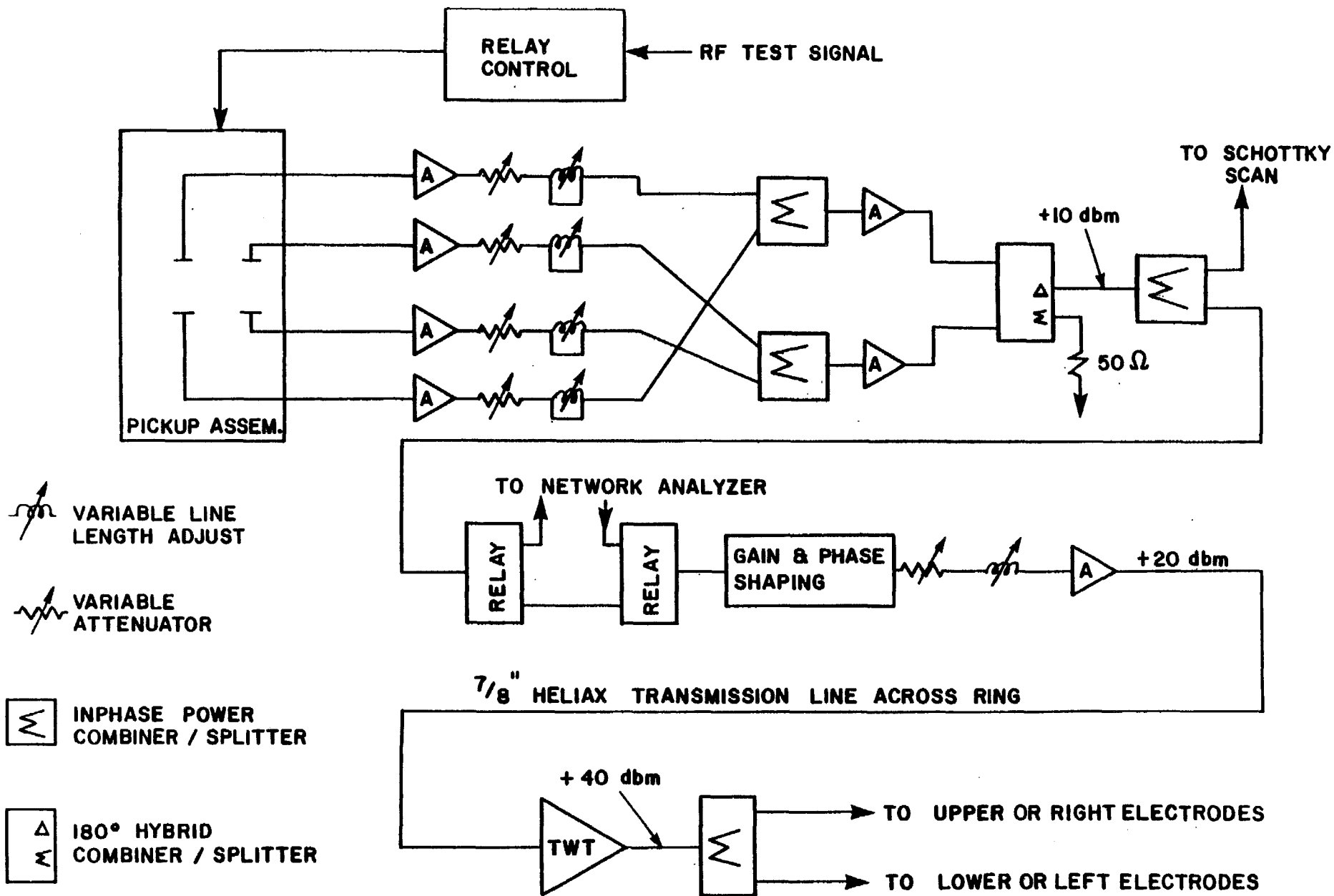
The stack-tail betatron cooling systems derive their pickup signals from the stack-tail momentum system as shown in Fig. 5-36. The kickers, however, are in straight Section A20, where the dispersion is about 9 m. The vertical and horizontal betatron systems require about 20 and 200 watts of output power respectively. As was pointed out earlier, the horizontal betatron signal is derived from beam in the asymptotic region of sum-mode pickups where the response is $e^{-\pi x/h}$, and hence there is a momentum Schottky signal as well as the normal betatron sidebands. It is expected that 1 TWT will be sufficient for the vertical and 2 for the horizontal system. It is possible that a notch filter could be used to reduce the momentum Schottky signal.

The core momentum system pickups are located in the high-dispersion straight Section A60 along with the stack-tail pickups. As indicated in Section 5.9.5 and Fig. 5-37, the core momentum pickups are double rows of pairs, each pair in sum mode. The difference signal of the two rows is then formed. These signals are processed as shown in Fig. 5-38 and also sent to kickers in the zero-dispersion straight section shared with the stack tail momentum kickers. This system requires about 30 W.

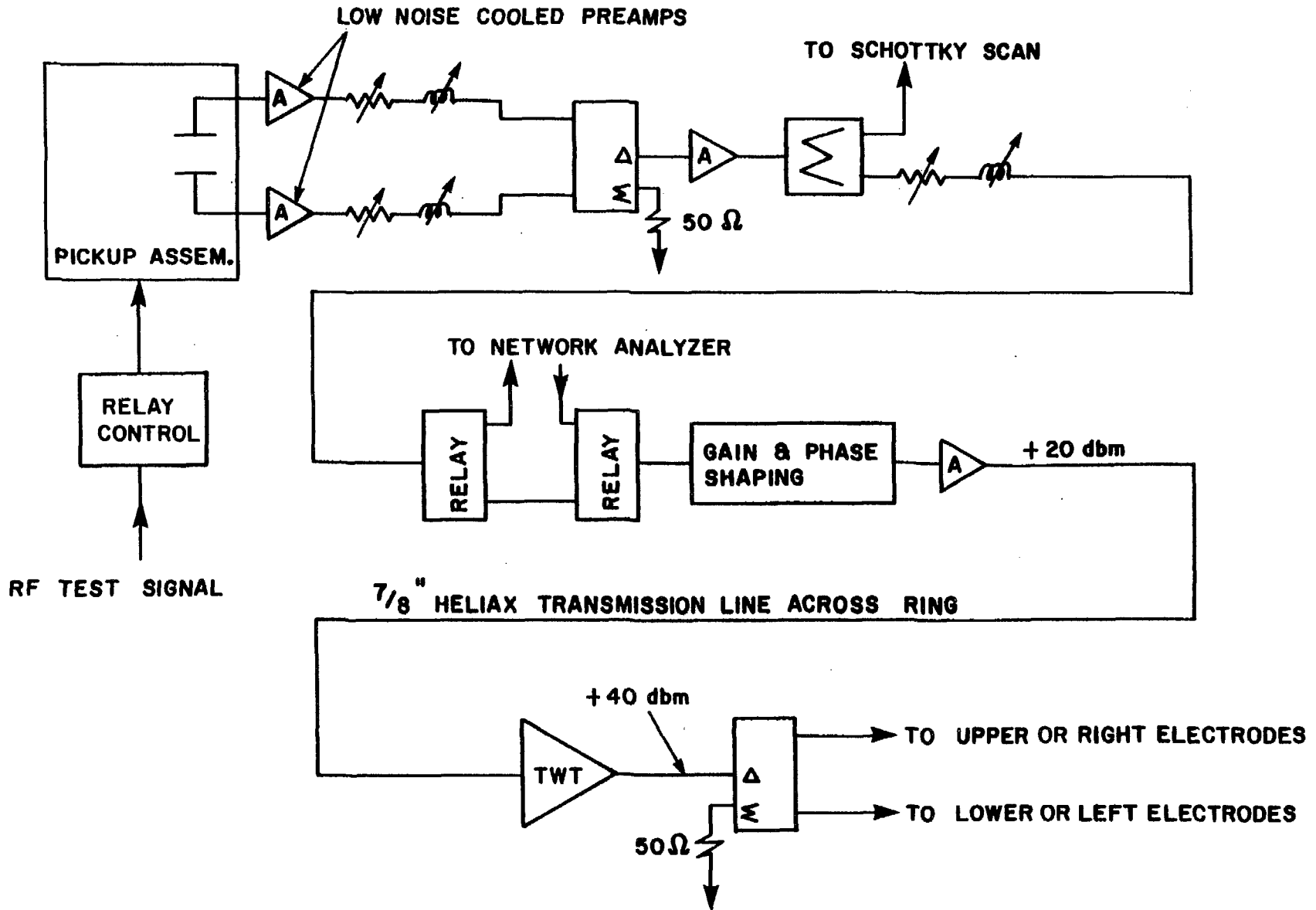
The core betatron system pickups are located in the zero-dispersion straight section A10. The signals are processed as per Fig. 5-38 and also sent to kickers in zero-dispersion straight section A30. Each system requires about 2 W.

TABLE 5-VIII ACCUMULATOR STOCHASTIC COOLING SYSTEMS

	<u>Stack tail Momentum</u>	<u>Stack tail Betatron</u>	<u>Core Momentum</u>	<u>Core Betatron</u>
Frequency band	1-2GHz	1-2GHz	2-4GHz	2-4GHz
Number of pickup pairs (loops)	128+32+8+2	(32)	32 + 32	8(x2)
Pickup characteristic impedance	100 Ω	100 Ω	75 Ω	75 Ω
Pickup sensitivity s(0,0) or d(0,0)	0.84(s)	1.94(d)	0.66(ds)	1.73(d)
Back termination thermal noise temperature	80 K	80 K	80 K	293 K
Amplifier equivalent thermal noise temperature	75 K	75 K	120 K	293 K
Amplifier gain (net)	150db	125db	110db	106db
Number of filters (superconducting correlators)	3	0	0	0
Output power		V+H		
-Schottky	1400W	10W+200W	30W	10W(x2)
-thermal	200W	10W+10W	0	0



2-4 GHz Core Momentum Cooling System



2-4 GHz Core Betatron Cooling System (2 Systems Required)

-total	1600W	20W+210W	30W	10W(x2)
Number of TWT's (200 watt saturated power)	40	1+2	1	1(x2)
Number of kicker pairs (loops)	160	32(x2)	32	8(x2)
Kicker characteristic impedance	100 Ω	100 Ω	75 Ω	75 Ω
Kicker sensitivity s(0,0) or d(0,0)	0.84(s)	1.94(d)	0.66(s)	1.73(d)
Spare time delay with air dielectric line ($\beta=.998$)	205 nsec	23 nsec	230 nsec	110 nsec
Spare time delay with heliax ($\beta=0.819$)	197 nsec	-34 nsec	166 nsec	63 nsec

References

1. A.G. Ruggiero, "Vacuum Considerations for the Accumulator Ring," Fermilab \bar{p} Note 194 (1982), unpublished.
2. D. Möhl, G. Petrucci, L. Thorndahl, and S. van der Meer, Physics Reports C, 58 (1980) 73-119.
3. S. van der Meer, "Stochastic Stacking in the Antiproton Accumulator," CERN/PS/AA/78-22 (1978); unpublished.
4. A.G. Ruggiero, "Stochastic Cooling - A Comparison with Bandwidth and Lattice Functions," Fermilab \bar{p} note 171 (1981), unpublished.
5. A.G. Ruggiero, "Pickup Loop Analysis" \bar{p} note 148 (1981), unpublished.
6. S. van der Meer, "A Different Formulation of the Longitudinal and Transverse Beam Response," CERN/PS/AA/80-4 (1980), unpublished.
7. A.G. Ruggiero, "Theory of Signal Suppression for Stochastic Cooling with Multiple Systems," Fermilab \bar{p} note 193 (1982), unpublished.
8. F. Sacherer, "Stochastic Cooling Theory," CERN/ISR/TH/78-11 (1978), unpublished.
9. A.G. Ruggiero, "Revised Intrabeam Scattering Calculation," Fermilab \bar{p} note 192 (1982), unpublished.
10. This discussion follows the discussion of C. Kim, "Design Options for the Fast Betatron Precooling Systems in the Debuncher or in the Injection Orbit," LBL Note BECON-25, unpublished.
11. Unslatter (CERN) unpublished; D. Neuffer, \bar{p} note 199; A. Ruggiero, \bar{p} Note 201.
12. F. Voelker (LBL) unpublished; J. Simpson (ANL) unpublished.
13. Avantek model ABG-2015 for example.
14. J. Shanley, Honeywell Inc., private communication (1982).
15. W. Weinreb et al; IEEE Trans. on Microwave Theory and Techniques 30, pg. 849 (1982).

CHAPTER 6

EXTRACTION OF ANTIPROTONS FROM THE ACCUMULATOR
AND TRANSFER TO THE MAIN RING

6.1 Accumulator Beam Manipulation and Extraction

Prior to extraction of the first \bar{p} bunch, a nearly Gaussian distribution of \bar{p} 's will exist in the core. The density can be characterized by two numbers, the total number of \bar{p} 's in the core, N_0 , and the rms energy spread, σ . If ϵ represents the energy difference between the particle energy and the most probable energy of the particles in the core, then the density function $\psi(\epsilon)$ can be written as

$$\psi(\epsilon) = \frac{N_0}{(2\pi)^{1/2} \sigma} \exp\left(-\frac{\epsilon^2}{2\sigma^2}\right) \quad (6.1)$$

The example presented here uses the following values for these parameters: $\sigma = 2.0$ MeV, $N_0 = 4.5 \times 10^{11}$ and $\psi(0) = 10^5 \text{eV}^{-1}$. Because we want to extract an assembly with the smallest longitudinal emittance, we begin the adiabatic capture with a bucket centered at the peak of the distribution. We plan to extract a single bunch containing 8×10^{10} \bar{p} 's. These \bar{p} 's exist within a range of ± 452.5 keV. The revolution period of the ring is 1.59 μsec , so the longitudinal emittance of the core region selected is 1.44 eV-sec. The Accumulator parameters which are used in this calculation are $R = 75.4716$ m, $\eta = 0.02$, $E_s = 8.938$ GeV, and $\Delta p/p = 1.6\%$ ($\Delta p = 142$ MeV/c) from core to extraction orbit. Because η (i.e. $\gamma_t^{-2} - \gamma^{-2}$) varies over the aperture, the rf parameters determining bucket areas must be varied accordingly.

The rf voltage required to develop a single bucket of area 1.44 eV-sec at harmonic h is $V = 2.44 h^3$. At $h = 1$, only 2.44 V is required and it may be difficult to establish such a low voltage with sufficient precision to control accurately the number of \bar{p} 's extracted. We propose to extract using a single $h = 2$ bucket with the remaining bucket suppressed. The required rf voltage is 19.5 V. Following adiabatic capture, a moving bucket will be established for deceleration to the extraction orbit.

The time required for this unstacking process depends upon the choice of rf voltage and synchronous phase angle. In order to minimize both the disturbance of the stacked \bar{p} 's and the particle loss from the moving bucket, the bucket will be moved very slowly, with a small phase angle. After the first \bar{p} bunch has been extracted and placed in the Tevatron at 150 GeV, the duration that this bunch is required to reside in the Tevatron at low field depends upon the time required to extract the remaining

bunches from the core. If the lifetime at 150 GeV is not long enough, it may be necessary to accelerate the process. Optimization of this time can only be accomplished after the Energy Saver and the Antiproton Source are operational. The rf voltage required to maintain the specified bucket area, the deceleration rate, and the time required for deceleration to the extraction orbit are shown in Table 6-I for several synchronous phase angles.

TABLE 6-I RF PARAMETERS FOR DECELERATION TO THE EXTRACTION ORBIT
(CONSTANT BUCKET AREA 1.44 EV-SEC.)

ϕ_s (deg)	$\Gamma = \sin \phi_s$	$\alpha(\Gamma)$	V_{rf} (volts)	Decel.Rate (MeV/sec)	Decel.Time (sec)
10	0.1736	0.696	36.2	3.33	43
20	0.3420	0.4918	72	12.93	11
30	0.500	0.3334	157	41.1	3.5

Frequency and phase control of the rf system during unstacking may be improved by a phase-lock system that partially locks the system to the coherent component of beam current. Since this component of current is of order 10 mA, detection and phase locking should not be technically difficult. The bunch length during the unstacking process will be about 500 nsec.

When the bunch reaches the extraction orbit, the rf voltage is raised to 100 V, resulting in a total bunch length of 200 nsec or about 60 meters. Since the momentum spread $\Delta p/p$ of this bunch is 5.2×10^{-4} , it can easily be injected into the Main Ring. The $h=2$ suppressed-bucket unstacking system is capable of producing a gap voltage of only 100 V, so the remaining 900 V is to be generated by a fixed-frequency $h=2$ system at 1.26 MHz. This system will, of course, create two buckets but only one will be populated with antiprotons because of the prebunching by the suppressed-bucket system. The total 1000-V bucket height will be about 12 MeV or $\pm 0.13\%$, so these buckets will not adversely affect antiprotons remaining in the cooled core.

After the 200-nsec bunch is established at the extraction orbit, the extraction-kicker shutter is closed, isolating the bunch from the remaining accumulated beam, and the single bunch is extracted and injected into the Main Ring.

Movement of the extraction bucket through part of the stack is a form of displacement acceleration resulting in partial replacement of some of the \bar{p} density in the core. Moreover, the cooling system will very quickly fill the depleted region left by the extracted bunch. During subsequent acceleration of the extracted bunch to 150 GeV and prior to the next

extraction, core cooling systems will re-establish a \bar{p} density in the core that is adequate for extraction.

The single bucket rf wave consists of one complete sinusoidal wave with a period of one half the rotation period. Because the fundamental frequency is 0.632 MHz, such a wave can easily be generated with Fourier components below 100 MHz. The accelerating structure may consist of an insulating gap in the beam pipe in parallel with a 50Ω resistance of sufficient power-dissipating capability. This structure will be contained within a shielded enclosure with sufficiently high shunt inductance (introduced by high-permeability ferrite) so that the load presented to a broad-band amplifier will be essentially real over the operating range. The power requirements will be less than 100 W. The 50Ω real impedance presented to the beam by this structure is well within the longitudinal-stability impedance limit.

The additional 900 V at $h=2$ is required only at a single frequency at the extraction momentum. It will be developed by a single ferrite-loaded resonant accelerating cavity with a shunt impedance of $1 \text{ k}\Omega$. This shunt impedance meets the beam-stability requirement and the required voltage can be developed with an excitation power of 400 W.

Extraction from the Accumulator occurs using a 2.1336 m long shuttered kicker and a 2.921 m long Lambertson magnet. The extraction orbit is rf displaced radially outward by 0.825% in $\Delta p/p$. At station A20 in the high dispersion straight section (See Fig. 5-1), the extraction closed orbit is displaced 71.5 mm outward. The orbit parameters are $\beta_x=7.06 \text{ m}$, $\beta_y=6.63 \text{ m}$, and $\alpha_x=\alpha_y=0$. A shuttered kicker centered 6.32 m downstream of station A20 gives the extracted beam an inward kick of 2.5 mrad and moves the extraction orbit to a position of $x=37.19 \text{ mm}$, $x_0=-0.002 \text{ mrad}$ at the entrance to the Lambertson magnet. Figure 6-1 shows the extraction orbit. The Lambertson then bends the beam up by 100 mrad.

6.2 Main Ring RF Capture and Acceleration

6.2.1 Introduction. We describe here the management of a single 1.5 eV-sec \bar{p} bunch in the Main Ring. The Main Ring is not capable of accelerating such a large emittance in a single bunch without excessive particle loss. For this reason, the bunch is broken up into several (12 or 13) adjacent bunches, accelerated to 150 GeV, and reconstituted into a single bunch at 150 GeV.

6.2.2 Injection and Rebunching. The \bar{p} bunch, about 200 nsec in length, is injected into a matched bucket in the Main Ring at $h=53$. The frequency is 2.5148 MHz and the bucket length, or period, is 397.6 nsec. By locking the phase of the Main Ring rf to that of the Accumulator, the \bar{p} bunch can be injected accurately into the Main Ring bucket. The required bucket height is 6.5 MeV, requiring 3300 volts.

KICKED EXTRACTION ORBIT IN ACCUMULATOR

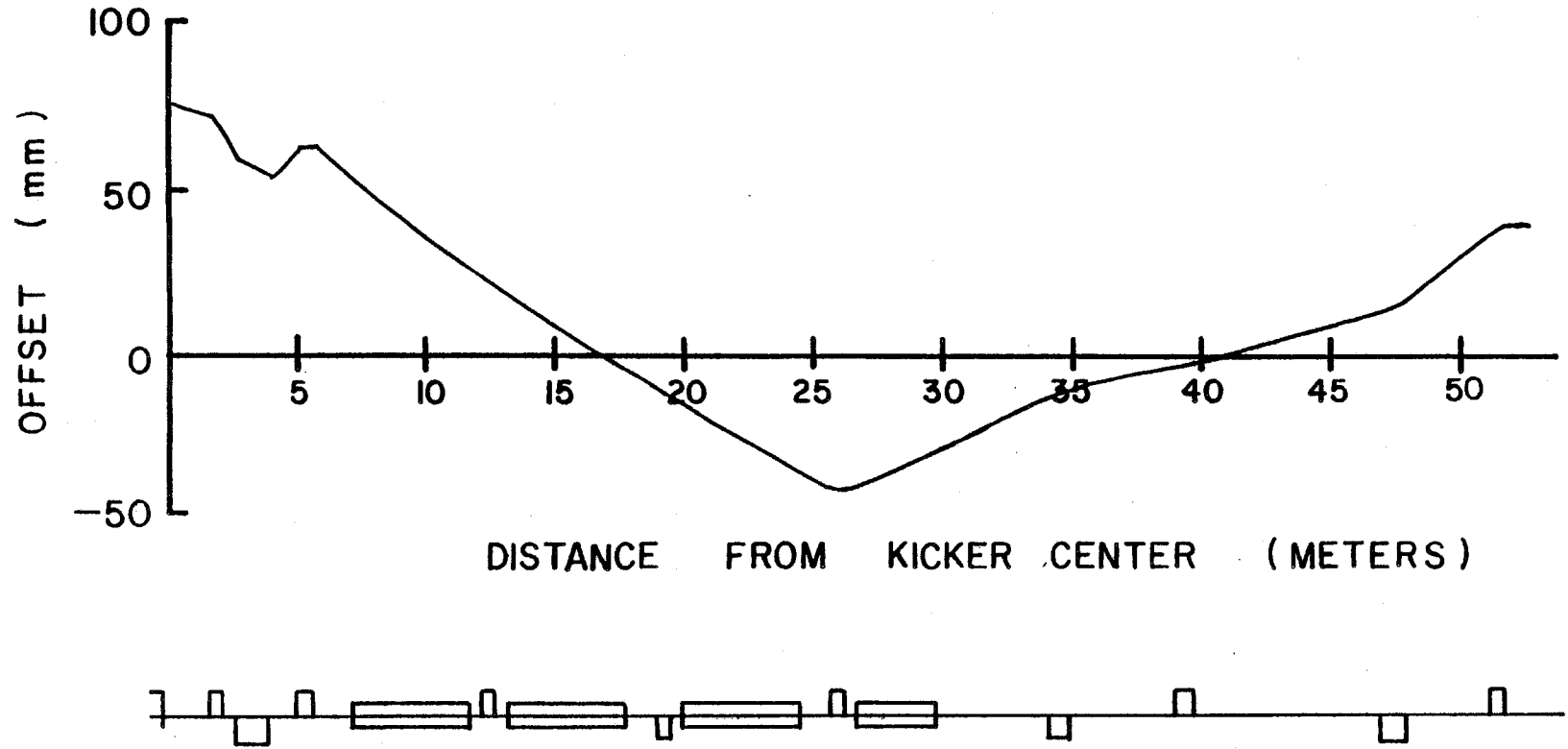


Figure 5-1

After injection, the $h = 53$ rf voltage is lowered adiabatically to 2.4 kV so that the bunch length increases to 244 nsec, which spans 13 "normal" $h = 1113$ rf periods in the Main Ring. With the bunch held at this length by the $h = 53$ rf voltage, the $h = 1113$, 52.813 MHz voltage is raised adiabatically so that the bunch is rebunched into 13 bunches. The bunch with the largest area, located at the center of the ensemble of bunches, has a longitudinal emittance of about 0.15 eV-sec. This can be accelerated easily in the Main Ring. This rebunching process is shown in Figs. 6-2 through 6-4 for a uniform initial distribution in the $h = 53$ bucket. After capture in $h = 1113$ buckets, the assembly of 13 adjacent bunches is accelerated to 150 GeV.

The longitudinal phase-space area is expected to increase by a factor 1.5 during acceleration. Recent studies in the Main Ring and careful simulation of transition crossing indicate that bunches with initial longitudinal emittance in the range of 0.2 to 0.3 eV-sec are diluted by a factor of about 1.25 between injection and $\gamma=21$, above transition. This dilution is accompanied by a slight bunch-to-bucket mismatch so that further dilution resulting from coherent bunch motion within the bucket results in total dilution during acceleration of about a factor of 1.5.

6.2.3 Bunch Recombination at 150 GeV. At 150 GeV, the Main Ring field is held on flat top while the 13 adjacent bunches are coalesced into a single bunch. The $h=1113$ rf voltage is reduced slowly over a period of 0.1 seconds to about 12 kV by counterphasing equal numbers of rf cavities. At this voltage, the bucket containing the center bunch is nearly full. Adjacent buckets are not quite full and the total longitudinal emittance of all the bunches is about 2.2 eV-sec. At this time, the $h=53$ rf system is turned on at a voltage level (700 V) such that the $h=53$ bucket is matched to a 2.2 eV-sec distribution extending over the filled $h=1113$ buckets, 245 nsec. At the same time the counterphased Main Ring rf voltage is turned off and replaced by a single small $h=1113$ rf cavity at 12 kV. The voltage of this cavity is then lowered slowly to (nominally) zero so that the adjacent bunches are adiabatically debunched into matched orbits in the $h=53$ bucket. A simulation of this process, starting with bunch distributions derived from previously simulated acceleration is shown in Figs. 6-5 and 6-6. The result is a uniform bunch of about 2.4 eV-sec matched to the $h=53$ bucket and spanning a range $\pm 2\pi/3$ radians.

The next step in the bunch-coalescence procedure is to rotate the extended low momentum spread distribution into a vertical strip with sufficiently short time duration so that it can be contained within a single 53-Mhz ($h = 1113$) bucket. Because the bunch initially spans a range of $\pm 2\pi/3$ radians in the $h = 53$ bucket, rotation within a $h = 53$ bucket created by a sinusoidal rf voltage at 2.53 MHz would not be satisfactory because of the spread in phase-oscillation period. Antiprotons on the outer edges of the distribution would lag behind those nearer the center and the vertical strip would be decidedly S-shaped. In order to "linearize" the synchrotron motion, the rf cavity wave-shape has been augmented with appropriate amounts of second, third, and fourth harmonics

H=53 BUNCH OF 1.5 EV_S AT 8 GEV IN M R TURN # 0
 HBCKT 5.56E+00 [MEV]. SBCKT 2.81E+00 [EV-S]. ES 8.938E+03 [MV]. NUS 1.36E-04
 OPDT 0. [MEV/S]. THS 0. [RAD]. THFP 5.927533E-02 [RAD]
 EV1 2.380E-03 [MV]. EV2 5.000E-03 [MV]. H1 53.. H2 1113.. ETA -8.17492E-03

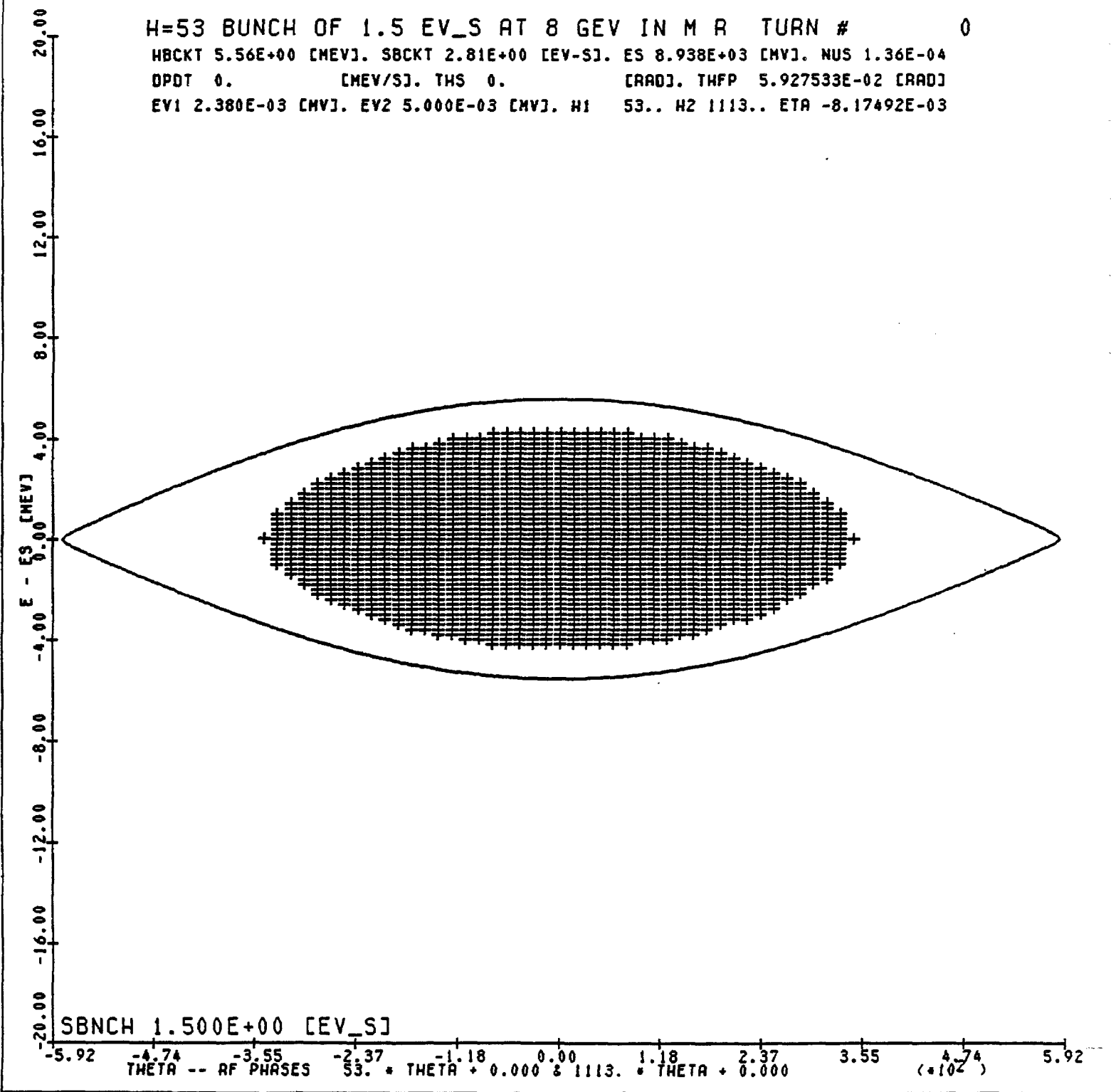


Figure 6-2 Uniform distribution of antiprotons with longitudinal emittance 1.5 eV-sec matched to h=53 bucket in Main Ring. The bunch covers a time span of about 245 nsec, or thirteen h-1113 stationary bucket lengths.

ADIABATIC CAPTURE AT H=1113 FROM H=53 TURN # 1500
 HBCKT 3.82E+00 [MEV]. SBCKT 9.19E-02 [EV-S]. ES 8.938E+03 [MV]. NUS 1.97E-03
 OPDT 0. [MEV/S]. THS 0. [RAD]. THFP 2.822635E-03 [RAD]
 EV1 2.380E-03 [MV]. EV2 2.363E-02 [MV]. H1 53.. H2 1113.. ETA -8.17492E-03

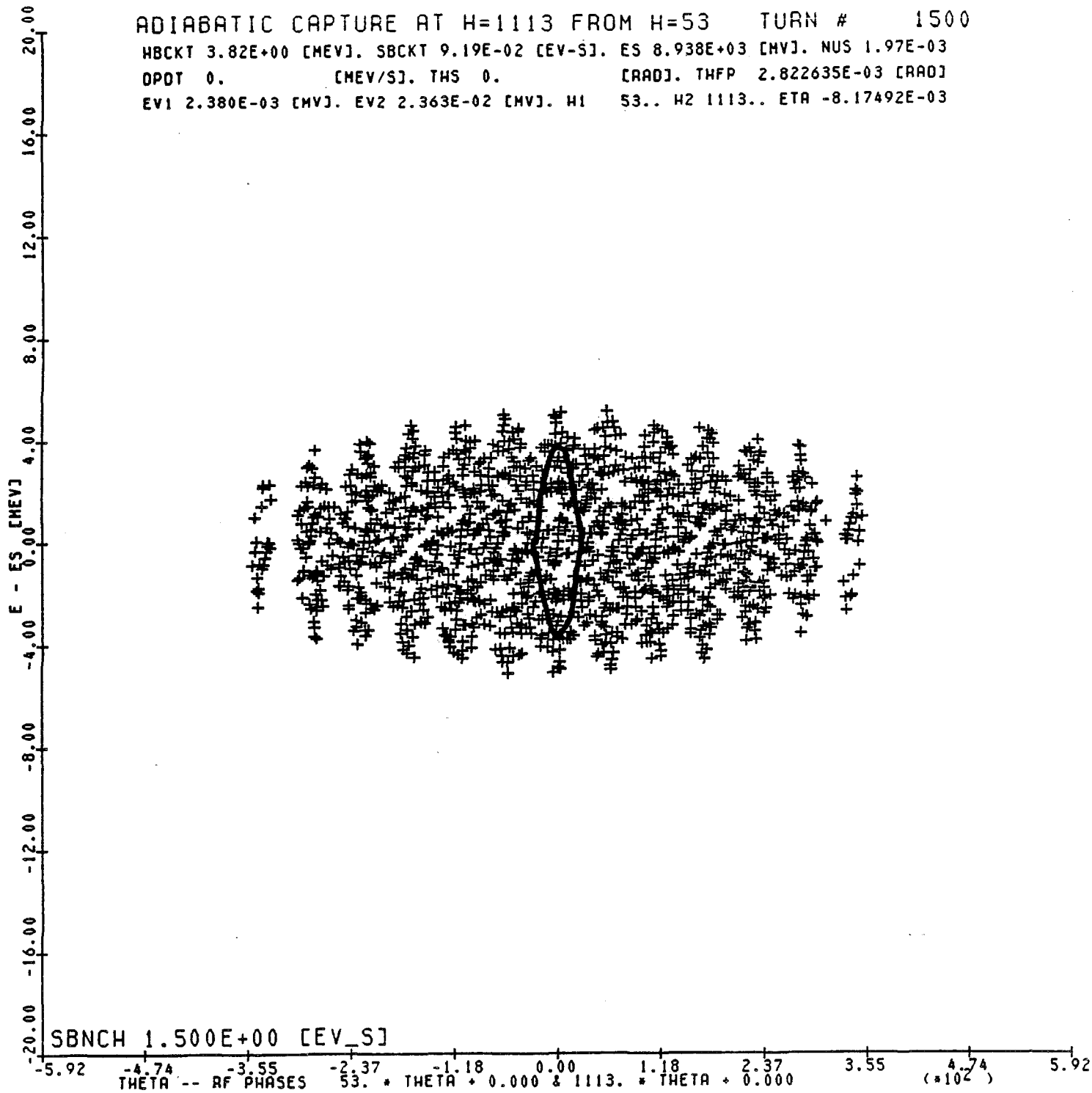


Figure 6-3 Antiproton distribution within an h=53 bucket partially bunched at h=1113 after 1509 turns. The h=1113 bucket size is shown for the center bucket.

FINAL H=1113 BUNCHES

TURN # 2500

HBCKT 1.76E+01 [MEV]. SBCKT 4.23E-01 [EV-S]. ES 8.938E+03 [MV]. NUS 9.05E-03
DPOT 0. [MEV/S]. THS 0. [RAD]. THFP 2.822635E-03 [RAD]
EV1 2.380E-03 [MV]. EV2 5.000E-01 [MV]. H1 53.. H2 1113.. ETA -8.17492E-03

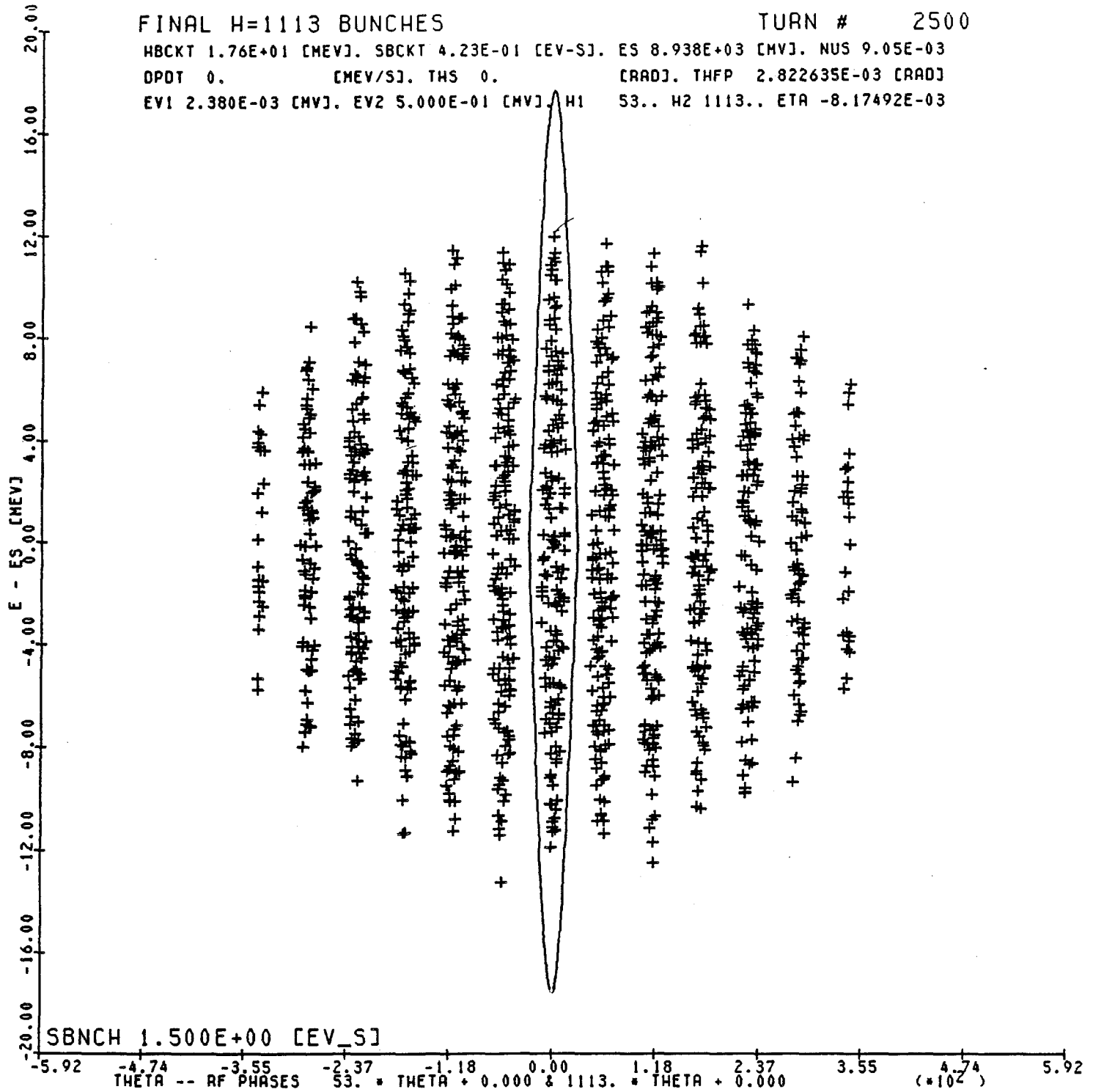


Figure 6-4 Completed bunching of antiprotons into 13 adjacent h=1113 buckets. The five center bunches each have an emittance of about .15 eV-sec and the sum of all the emittances is 1.6 eV-sec.

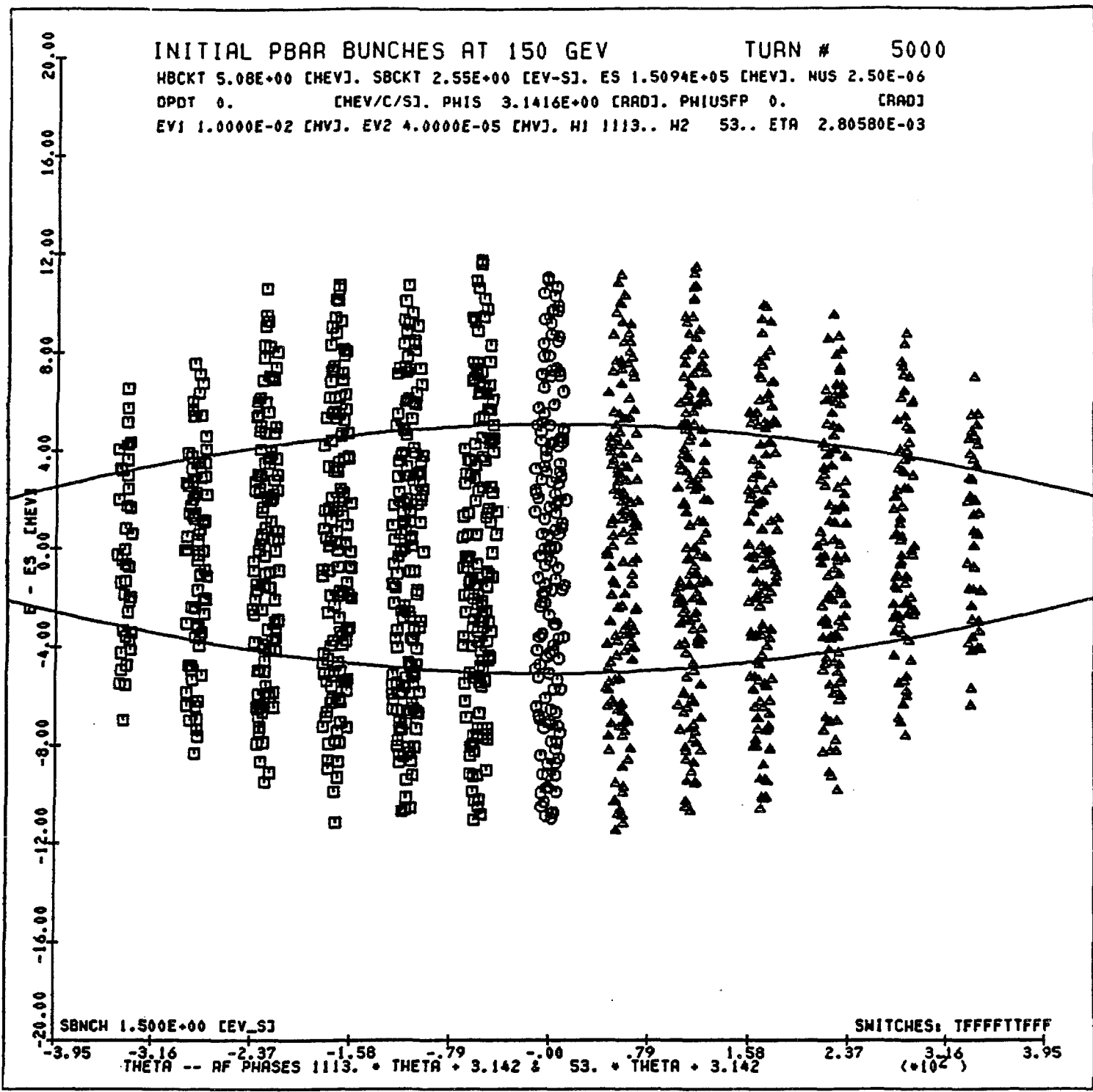


Figure 6-5 Adjacent antiproton bunches prior to final h=1113 debunching. The bucket outline shown is an h=53 bucket which will match the distribution of the coalesced bunches. The particles in the lefthand bunches have been indicated by squares, those in the center bunch by octagons, and those in the righthand bunches by triangles to aid in interpretation of the coalesced distribution shown in the following figure

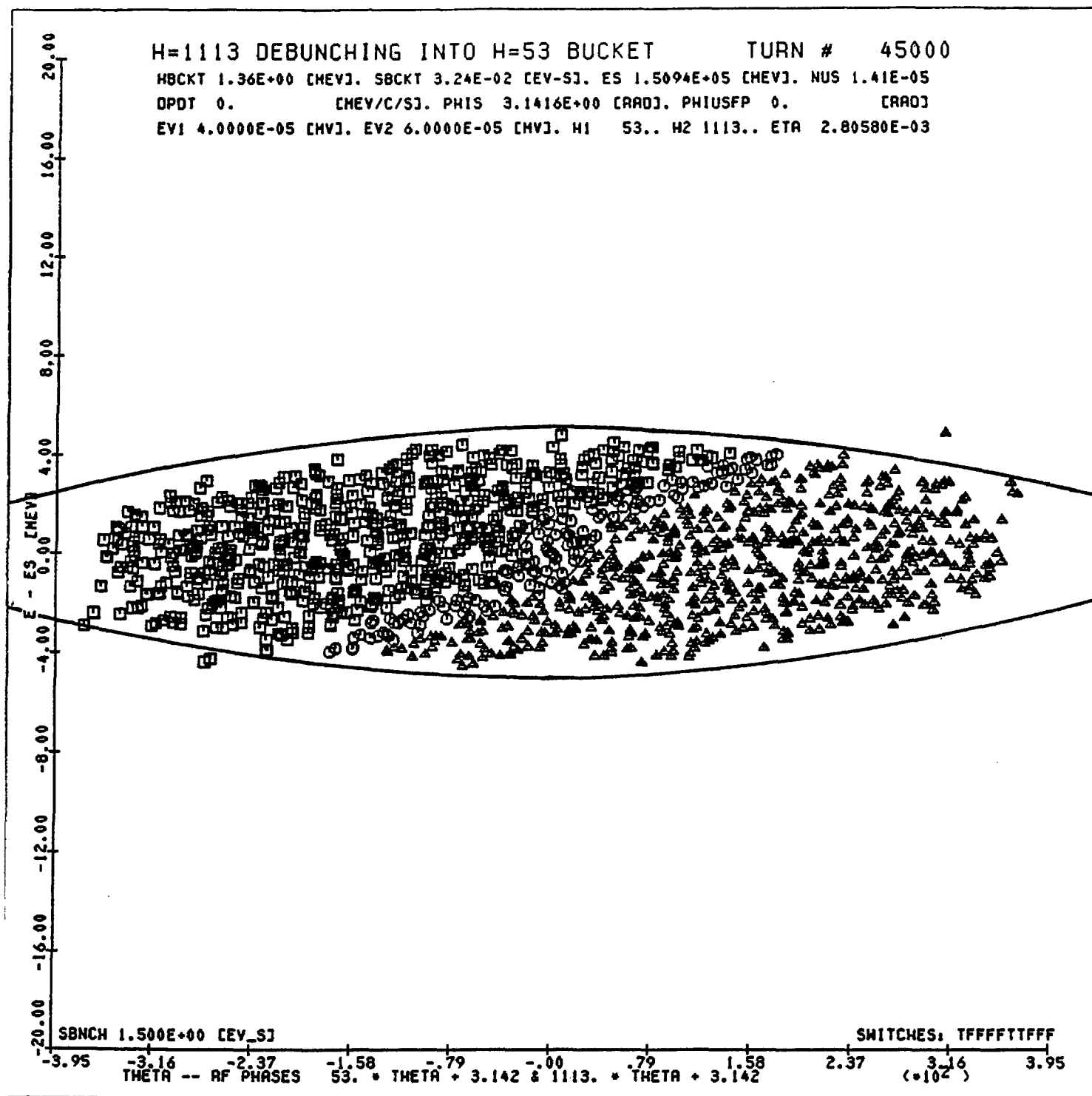


Figure 6-6 The antiproton distribution within the h=53 bucket following slow removal of the h=1113 rf voltage. The bunch extends over $\pm 13/21 \pi$ radians within within the bucket and the longitudinal emittance (95%) is about 2 eV-sec. Particles originating from h-1113 bunch left of the central bunch are indicated by squares, those from the central bunch by octagons, and those from the right-hand bunches by triangles.

so that the rf gap voltage is linear to within about 10 percent between $\pm 0.63\pi$ radians. In this circumstance, particles within the linear portion of the wave move with harmonic motion of nearly constant period so that the entire distribution reaches maximum momentum spread and minimum time spread at approximately the same time.

In Fig. 6-7, a simulated result of such a rotation is shown. The rf voltage used for this simulation was composed of a fundamental $h = 53$ voltage of 22.8 kV and a second-harmonic component of 4.9 kV at the correct phase angle for optimum linearization.

In Fig. 6-8, we show the results of a preliminary experiment in bunch coalescing. The experiment is done at $h = 159$ using four adjacent proton bunches. The successive oscilloscope traces starting at the bottom of the pictures show two or four proton bunches merging into a single bunch of larger intensity and emittance, as expected. Since the bucket covered only seven $h = 1113$ bucket lengths, the four bunches extended farther into the bucket than is proposed. This results in a more nonlinear process than will occur in the proposed scheme.

Following recapture, the rf voltage is raised to 1 MV. As a result, the bunch length shrinks to 12 nsec full width, and the bunch height grows to ± 166 MeV, corresponding to a momentum spread $\Delta p/p$ of $\pm 1.1 \times 10^{-3}$. The bunch parameters are ideal for injection into pre-established matching buckets in the Tevatron.

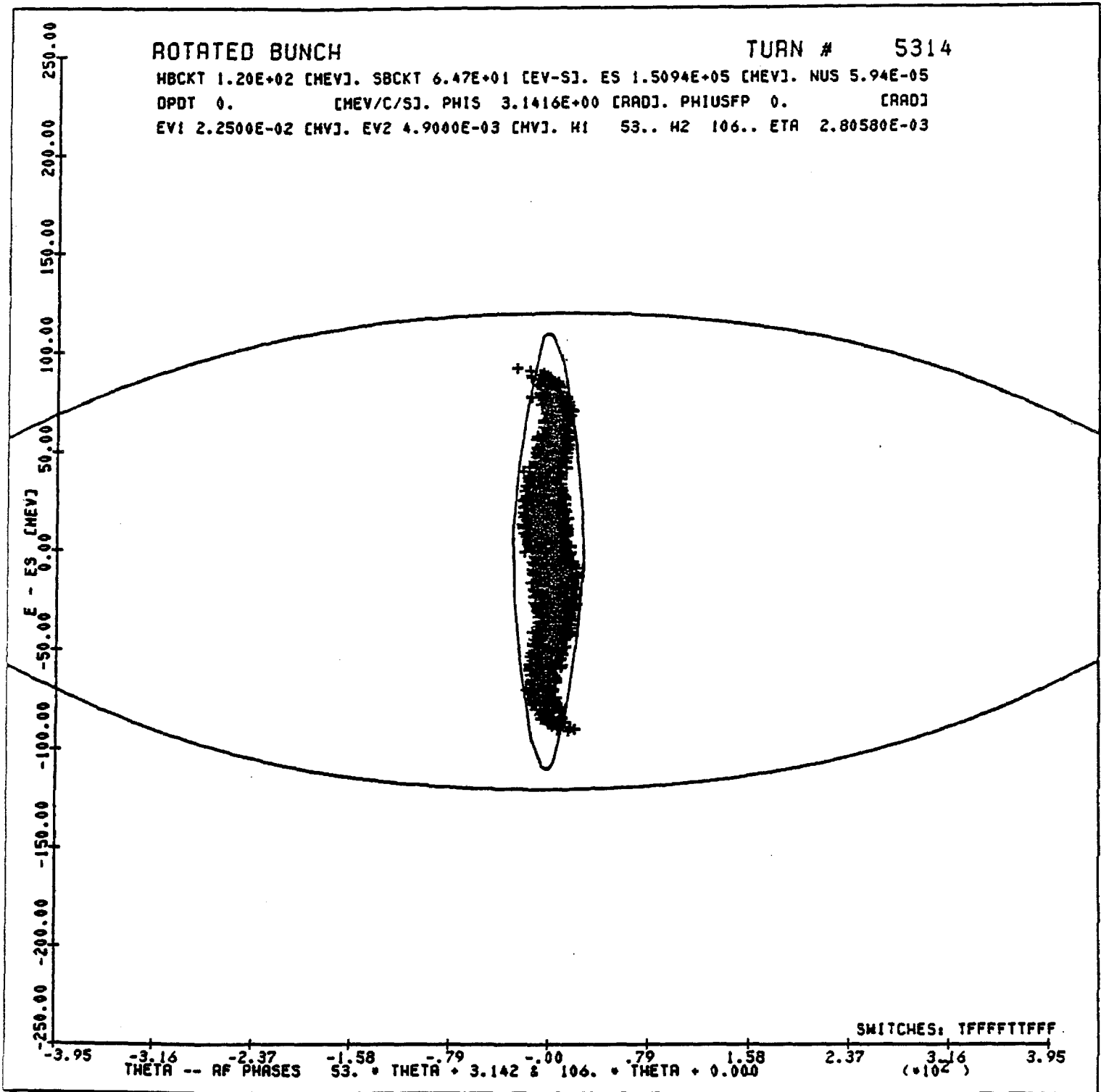


Figure 6-7 Antiproton distribution following bunch rotation in h=53 bucket. The rotated distribution has a full length of about 16 nsec and spans an energy range of ± 100 MeV.

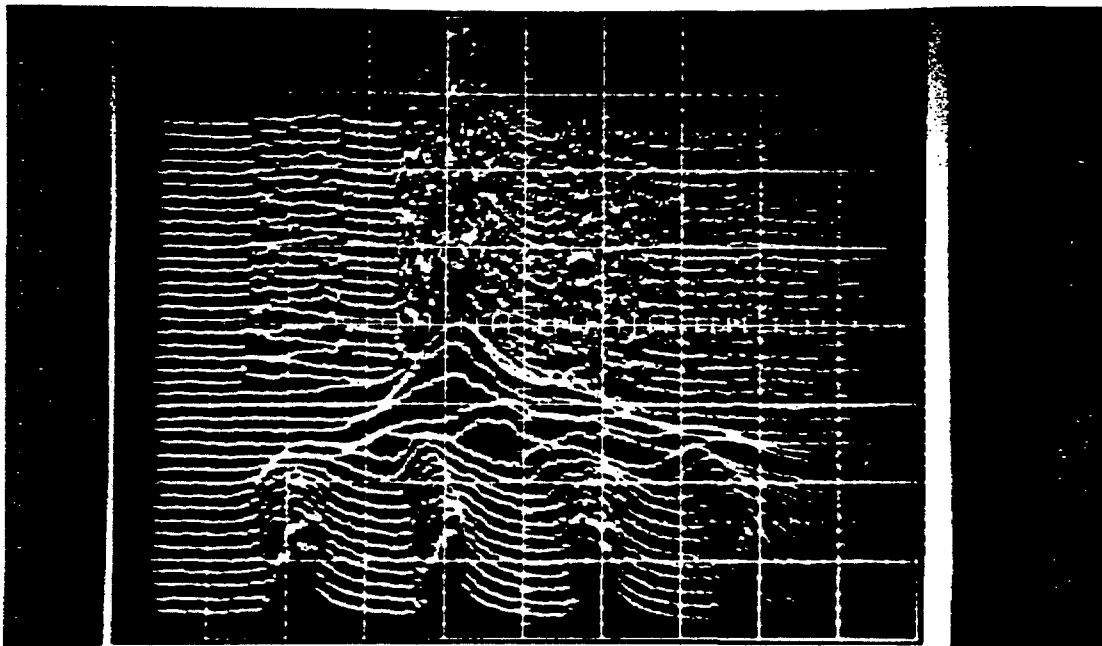


Figure 6-8a

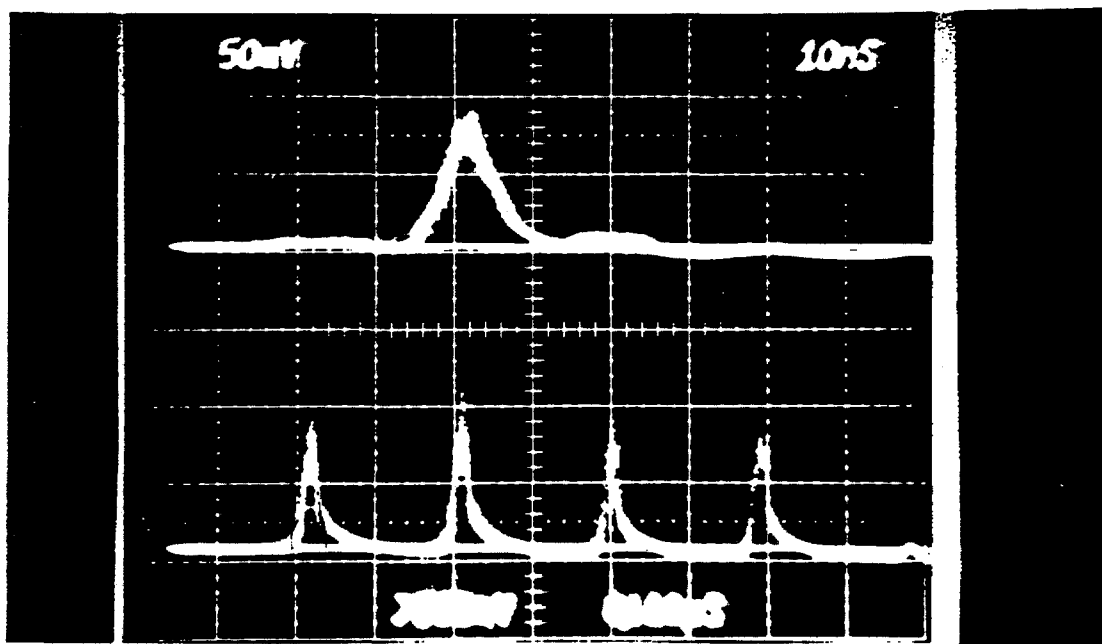


Figure 6-8b

Figure 6-8 Results of an early experiment in coalescing adjacent 53 MHz bunches in a lower harmonic bucket. The experiment was done at $h=159$ (7.5 MHz) where the lower harmonic bucket spans seven 53 MHz buckets. (a) The evolution of the coalescing process, time progressing upwards in 5ms steps. (b) The four bunches .1s before and .1s after coalescing. The coalescing efficiency (ratio of areas under the peaks) is about 90%. The time base is 10ns per major division in both pictures.

CHAPTER 7

THE MAIN RING IN TEVATRON I7.1 Functions of the Main Ring in Tevatron I

The Main Ring is required to perform five separate functions in the Tevatron I mode:

1. Acceleration of protons for antiproton production. During antiproton production and accumulation, the Main Ring will be required to accelerate single batches of protons (approx. 82 bunches) of intensity greater than 2×10^{12} protons per batch to 120 GeV. This will be done routinely on a 2-sec. cycle. Each of these acceleration cycles must include the bunch-narrowing technique and extraction at F17 described in Chapter 2.

During this mode of operation, a special low-level rf system must be used. This system will contain provision for transient beam-loading compensation and rf-cavity counterphasing. In addition, the technique for phase-locking the Main Ring to the Booster will be slightly different from that used during fixed-target operation.

2. Injection of \bar{p} 's from the Accumulator into the Main Ring. Bunches of antiprotons containing 10^{11} \bar{p} 's must be transported to the Main Ring and injected.

3. Acceleration of antiprotons to 150 GeV. After a sufficient number and density of antiprotons have been established in the Accumulator, the Main Ring must be used to accelerate groups of antiproton bunches to 150 GeV. This acceleration cycle must include the bunch manipulations at 8 GeV and at 150 GeV described in Sections 6.1 and 6.2. Special additions to the rf systems will be required to accomplish these manipulations. Following these acceleration cycles, the single antiproton bunches must be extracted at E0 for injection into the Tevatron.

4. Acceleration of protons to 150 GeV. The Main Ring will be required to accelerate groups of protons to 150 GeV, where they will be combined to form single proton bunches containing 10^{11} protons. This operation will be similar in many respects to the antiproton acceleration described above and the same special additions to the rf systems will be utilized.

5. Transfer of particles from the Main Ring into the Energy Saver. Transfers of 150 GeV protons and antiprotons are both described in Chapter 8.

7.2 Antiproton Injection

The antiproton bunches from the Accumulator are matched into the proton extraction line at EB5. They are then transported back down the 120-GeV extraction line and injected into the Main Ring at the F17 Lambertson. Special low-current power supplies are used to power the 120-GeV extraction line to ease regulation problems caused by running large power supplies at 5% levels.

The C48 kicker is also too strong for the reverse injection of the antiprotons at 8 GeV, so that an additional small kicker located at F14 needs to be added. The kicker is a 25 inch long ferrite (tape-wound steel) 380 G magnet with a rise and fall time of 20 μ sec. The gap is 5x3 inches (HXV) and the required current is 2280 A. When fed by 400 ft of 5 parallel RG213's as a simple L-C discharge circuit, the required capacitance is 23 μ F and the required discharge voltage is 1165 V.

7.3 Main Ring Acceleration and Rebunching Hardware

The processes of accelerating small groups of protons and cooled antiprotons to 150 GeV has been described previously in Chapter 6. In those descriptions reference was made to an rf system in the Main Ring operating at $h=53$ (2.515-2.529 MHz) and providing about 65 kV. This requirement will be met by installing two heavily ferrite-loaded rf cavities, each operating at the 20-kW level. These cavities will be refurbished and slightly modified cavities from the Princeton Pennsylvania Accelerator (PPA). Operation of these cavities in the Main Ring will require installation of an anode power supply of about 8 kV, 15 A (120 kW). Small additions to the low-level rf system will also be required to provide appropriate rf driving signals phase-locked to the integrally related $h=1113$ 53 MHz rf.

Small additions to the control system will also be required for remote operation of these systems.

7.4 Main Ring Overpass*

The performance of both the Antiproton Source and the Collider Detector can be significantly improved by bypassing the Main Ring beam around the Collider Detector at B0. This bypassing - called here the "Overpass" - has at least two advantages:

*The B0 overpass described here elevates the Main Ring beam by 21 feet. A 16-foot elevation overpass is also being considered at this time. In addition, a 6-foot overpass for the second colliding beam experimental area at D0 is presently being designed.

- (i) It allows elimination of the asymmetric hole for the Main Ring through the Collider Detector;
- (ii) It allows accumulation of antiprotons to proceed simultaneously with colliding-beam operation. This will increase the average luminosity of the entire system by eliminating the pause of several hours while the antiproton beam is being refreshed.

The design of an overpass for the Main Ring has been worked out in detail by T.L. Collins and is presented here. There are a number of constraints that such a design must satisfy:

- (a) Space must be generated for additional bending elements;
- (b) The new path must close smoothly on to the old path to high precision in both horizontal and vertical dimensions and at all energies with a minimum of programmed external control.
- (c) The path lengths must be the same in old and new paths, or differ by an integral number of rf wavelengths;
- (d) the betatron functions must match, as in any insertion; and
- (e) Any residual dispersion introduced outside the bypass must be negligibly small.

The overpass design limits Main Ring operation to 200 GeV or less. Some magnets are operated at twice the normal field. Consider a set of four bending magnets. The outer two magnets will be unchanged to provide the normal horizontal bend. The inner magnets will be rolled about the beam axis to produce a vertical bend of 32.471 mrad. Such four-magnet sets placed symmetrically around the long straight section (for example, at A41 and B12) will produce a 19 ft vertical separation, enough to miss the entire detector. The new orbit connects smoothly on both ends. A total of four sets (16 magnets) is in the additional circuit. The additional excitation of this circuit will be provided by a separate power supply.

The overpass has approximately 8 in. of extra orbit length. This undesired length is cancelled by combining the vertical bends with a slight inward bend to "cut across" the arc. The inward bend can be accomplished easily by a small inward roll of the vertical-bend magnets.

The betatron functions are easily matched across the insertion. The vertical dispersion introduced in the remainder of the ring must be balanced with some care. It has been reduced by this balancing to approximately 0.5 m, which is noticeable, but tolerable. Coordinates of the bypass insertion magnets are given in Table 7-I and the effect on the dispersion is shown in Table 7-II.

TABLE 7-I OVERPASS COORDINATES

Numbers in parentheses are for the original main ring ($Z=\theta_v=0$).

Station	x(Feet)	y(Feet)	θ_h (rad)	Z(inches)	θ_v (rad)
A39	962.531 (962.531)	2,285.083 (2,285.083)	.8175454 (.8175454)	0.000	0.00000
A42	1,034.911 (1,034.808)	2,350.493 (2,350.639)	.8535781 (.850017)	19.286	.0322656
A43	1,109.464 (1,109.175)	2,413.368 (2,413.813)	.8860663 (.882488)	57.063	.0322656
A44	1,186.021 (1,185.554)	2,473.789 (2,474.539)	.9185544 (.914959)	94.840	.0322656
A45	1,264.500 (1,263.864)	2,531.691 (2,532.754)	.9510426 (.947430)	132.617	.0322656
A46	1,344.818 (1,344.023)	2,587.013 (2,588.396)	.9835307 (.979902)	170.393	.0322656
A47	1,426.890 (1,425.946)	2,639.697 (2,641.406)	1.0160189 (1.012373)	208.180	.0322656
A48	1,510.566 (1,509.547)	2,689.860 (2,691.728)	1.00448499 (1.044844)	226.656	.0000000
B0	1,686.376 (1,685.357)	2,787.887 (2,789.756)	1.0692033 (1.069198)	226.656	.0000000
B11	1,772.743 (1,771.723)	2,835.248 (2,837.117)	1.0692033 (1.069198)	226.656	.0000000
B12	1,870.616 (1,869.596)	2,887.172 (2,889.042)	1.1016746 (1.101669)	226.656	.0000000
B13	1,958.274 (1,957.352)	2,929.994 (2,931.709)	1.1304914 (1.134140)	207.364	-.0322641
B14	2,047.177 (2,046.446)	2,970.092 (2,971.504)	1.1629795 (1.166611)	169.589	-.0322641
B15	2,137.335 (2,136.786)	3,007.281 (3,008.386)	1.1954677 (1.199083)	131.815	-.0322641
B16	2,228.654 (2,228.275)	3,041.523 (3,042.315)	1.2279558 (1.231554)	94.040	-.0322641

B17	2,321.037 (2,320.818)	3,072.779 (3,073.256)	1.2604440 (1.264025)	56.625	-.0322641
B18	2,414.047 (2,413.981)	3,102.116 (3,102.275)	1.2766880 (1.280261)	18.491	-.0322641
B19	2,507.920 (2,507.920)	3,128.673 (3,128.673)	1.3127319 (1.312732)	.000	.0000000

TABLE 7-II. MOMENTUM DISPERSION IN THE BEND PLANE WITH AND WITHOUT BYPASS

	With bypass	Without bypass		With bypass	Without bypass
A39 =	2.86m	2.84m	A42 =	5.77m	5.67m
A43 =	3.45	3.32	A44 =	5.63	5.36
A45 =	2.63	2.50	A46 =	3.36	3.26
A47 =	1.36	1.40	A48 =	1.74	2.00
B12 =	1.07	1.26	B13 =	2.02	2.13
B14 =	1.71	1.68	B15 =	4.04	3.84
B16 =	3.00	2.84	B17 =	5.91	5.65
B18 =	3.02	2.94	B19 =	4.17	4.13

7.5 Main Ring Diagnostics

7.5.1 Main Ring Position Detectors. The electronics used to read out the position of the Main Ring beam will be improved to have capabilities similar to the Energy Saver position detectors described in Sec. 8.6.1. This improvement is needed for commissioning the p system. Orbit information is necessary at both h=53 and h=1113 for both protons and antiprotons in the Main Ring.

7.6 D0 Overpass

A second Main Ring overpass will be built at D0 for the same purpose as the B0 overpass, to bypass the Main Ring beam around the detector or detectors. The D0 overpass is planned to minimize tunnel modifications. The beam is raised by 43.59" above the normal Main Ring centerline, giving a clearance of 43.59 + 25.50 = 69.09" over the Tevatron centerline. Eight new dipoles will be needed. A sketch of the overpass configuration is shown in Fig. 7-1 and the coordinates are given in Table 7-III.

No attempt has been made to localize the vertical dispersion. As a consequence, the vertical dispersion outside the overpass is rather large (~ 1.5 m at $\beta_y = 100$ m) in spite of the small up and down angle of 11.88 mrad. The overpass starts at C46 and ends at D14. It should be noted that the C48 kicker is inside the overpass. The clearance at D0 along the beamline for the D0 detector is ± 35 ft.

The the table below, each dipole is represented by the so-called dipole slot which is 251" long, 6"+239"+6". Regular stations are 96" from the end of the upstream dipole slot and 71.002" from the beginning of the downstream dipole slot. Station #11 and #49 are exactly 1,182" from station 0. Station #12 is 63.95" from the end of dipole #11-5 slot; 71.002" from the start of dipole slot #12-2. Station #48 is 96" from the end of dipole slot #47-5; , 322.002" from the beginning of dipole slot #48-3 (dipole #48-2 does not exist).

UE = upstream end of each dipole slot,

DE = downstream end of each dipole slot.

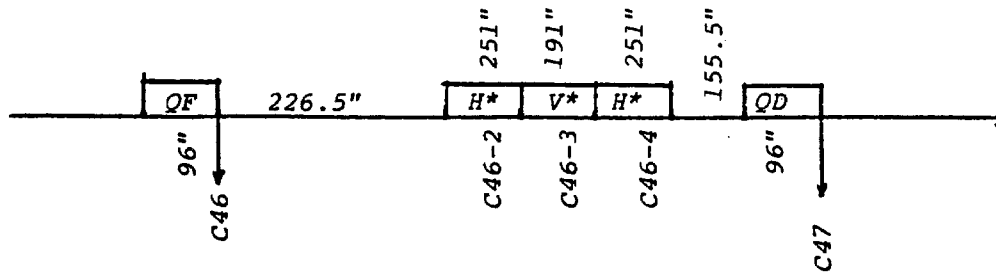
If the reference point is not specified, it is understood to have the same name as the overpass point in question. For example, the reference point for the overpass C46-2UE is the main ring C46-2UE.

All numbers are in inches. The height from the doubler beam line is (25.5" + H). The specified roll of V* is always "wall-side up, aisle-side down". The going-up and -down angle is 11.881 mrad.

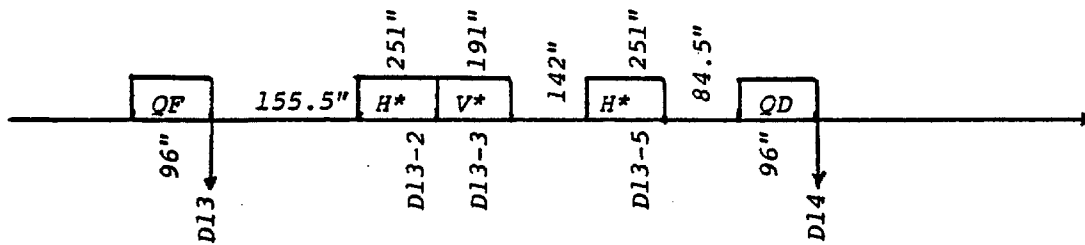
TABLE 7-III

Station or Dipole Slot	Refer. Pt. Main Ring	Longitud. Dist.	Radial Dist.	Height	Roll (mrad)
C46		0	0	0	
C46-2UE		155.500	0	0	
C46-2DE	H*	155.495	.243	0	
C46-3UE					
C46-3DE	V*	95.486	.240	1.135	214.0
C46-4UE					
C46-4DE	H*	95.462	-.653	4.117	
C46-5 is missing					
C47		-.052	-1.545	7.106	
C47-2UE		-.057	-1.729	7.949	
C47-2DE		-.059	-2.378	10.931	
C47-3UE					
C47-3DE		-.055	-3.027	13.913	
C47-4UE					

C47-4DE			-.047	-3.677	16.879	
C47-5UE						
C47-5DE			-.033	-4.325	19.877	
C48			-.040	-4.574	21.018	
C48-3UE			-.064	-5.407	24.844	
C48-3DE			-.036	-6.056	27.826	
C48-4UE						
C48-4DE			-.002	-6.705	30.808	
C48-5UE						
C48-5DE			.036	-7.354	33.790	
C49			.036	-7.354	35.674	
V* UE	DO		-611.018	-9.242	42.458	214.0
V* DE	DO		-420.023	-9.490	43.593	



The last vertical bend is at dipole D13-3:



Note that dipoles C46-5 and D13-4 are missing in the overpass. Special dipoles are as designed by Stan Snowden ("Overpass Dipoles-II", a memo from Stan to Tim Toohig, 6/23/83):

H* slot 251" = 6" + 239" + 6", aperture 2" x 4", bend angle = $4\pi/774$.

V* slot 191" = 6" + 179" + 6", aperture 3" x 3", $(4\pi/774) \times (179/239)$

Two vertical dipoles for bend-down are located in the long straight:

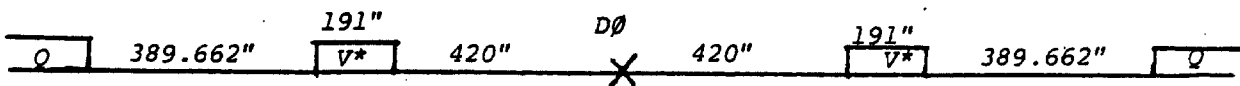


Figure 7-1

CHAPTER 8

THE ENERGY SAVER IN TEVATRON I8.1 Functions of the Energy Saver in Tevatron I

The Tevatron I project uses the Energy Saver Ring as a 1 TeV storage ring for bunched-beam collisions. The construction of this ring was a separate project undertaken for the purpose of operating the Fermilab fixed-target program at 500-GeV. It was recognized that the Energy Saver could be used as a 1-TeV storage ring if proper attention was given to a number of details such as position monitors and beam transfer systems.¹ Since the field quality for slow extraction was at least as stringent as the requirement for colliding beams, the Energy Saver was inherently a useful storage ring. For that reason, the Energy Saver was designed so that it could be modified in the future to operate as a 1 TeV collider. These modifications are part of the Tevatron I project.

The Energy Saver, after modification, will perform the following functions in the Tevatron I project:

1. Injection. It will sequentially accept bunches of 150-GeV protons and antiprotons from the Main Ring, one bunch at a time.
2. Acceleration. After the appropriate number of bunches has been stored, it will simultaneously accelerate the proton and antiproton bunches to the collision energy.
3. Collision. After acceleration, the beams will be stored and the low-beta sections described in Chapter 9 will be turned on to increase the luminosity.

The material presented in Sections 8.2 and 8.3 is based on the Superconducting Accelerator Design Report, May, 1979. Since 1979, there have been a number of changes in the design. The changes that are important to the use of the Energy Saver as a collider are described in this chapter. The most notable of these are: the correction coils are separate from the quadrupole windings, the rf system has been expanded to handle the larger longitudinal emittance of the antiprotons, and the beam transfer at E0 has been simplified substantially after it was decided to make the circumference of the Energy Saver exactly the same as the Main Ring.

8.2 Energy Saver Lattice

8.2.1 Ring Location and Normal Lattice. The lattice of the Energy Saver ring is constrained by the requirement that it fit beneath the Main Ring magnets. Therefore, it has the same basic configuration as the Main Ring,

which has 6 superperiods with 6 long straight sections and normal cells with 8 dipoles and 2 quadrupoles. Because the Energy Saver dipole ends could not be placed directly under the Main Ring ends, the Energy Saver dipoles are displaced 15.5 in. upstream of their Main Ring counterparts.² Figures 8-1 and 8-2 sketch the position of the quadrupole in the lattice and the position of a normal cell relative to the Main Ring lattice. The beam center line is 25.5 inches below Main Ring center line. The circumference of the two rings is identical. At the time the Superconducting Accelerator Design Report was prepared, it was proposed to make the two rings differ in circumference by 4.4 cm, as a way of providing for pp collisions with the Main Ring and Saver. That option has been dropped because it compromised the beam transfer between the Main Ring and the Saver.³

Like the Main Ring, the present lattice has a medium straight section at location 17 formed by omitting two dipoles. Its layout is shown in Fig. 8-3. There are long straight sections of "normal" configuration, ones with high beta for extraction, and ones with low beta for colliding-beam interactions. These are discussed separately in subsequent sections. Table 8-I summarizes the warm straight-section lengths available in the lattice. It gives the drift lengths between "effective" magnetic ends of the elements, the available warm length and the space allotted for the cryogenic bypasses of cold-to-warm transitions and vacuum isolation.

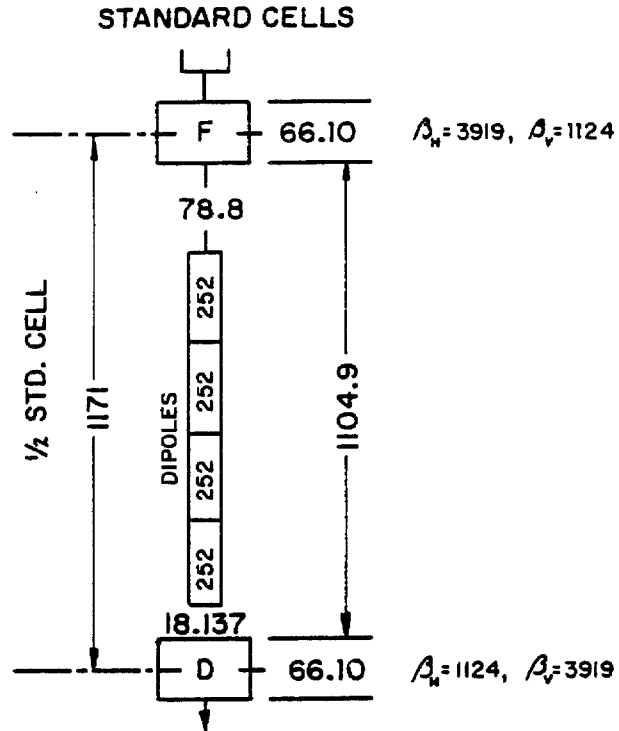
TABLE 8-I WARM STRAIGHT-SECTION LENGTHS

(In.) Location of Warm Regions	Drift Length ^a (In.)	Available Warm Length (In.)	Hot-Cold Transition	
			Upstream	Downstream
Median location 17 (standard quadrupole with corrections)	566.2	493.2	39	34
Normal- β median location 48	310.9	238.9	36	36
High- β median location 48	308.7	236.7	36	36
Normal- β doublet space 49,11	150.36	78.36	36	36
High- β doublet space 49,11	151.65	79.65	36	36
Long straight section	2094.2	2022.2	36	36
Low- β long straight section	600.24	528.24	36	36

^aMagnetic lengths used throughout to define drift lengths.

All medium straight sections at 17 and 48 locations, and all long straight sections are warm. The space between the long straight-section doublets is warm only where necessary.

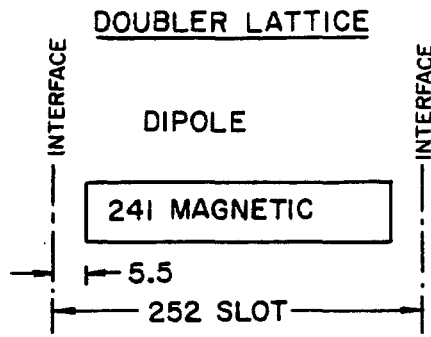
8.2.2 Normal and High-Beta Long Straight Sections. Figure 8-4 shows the geometry of the normal long straight section together with amplitude



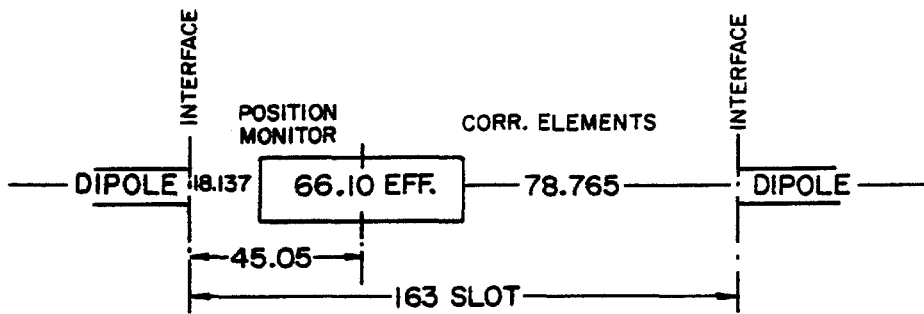
All dimensions in inches, slot length for dipoles, effective magnetic length for quads except for focussing, D-F 1/2-cell is similar.

Phase advance 1/2-cell = 33.903°

Figure 8-1 Locations of elements in standard cell.



Dipoles are 252" flange to flange. Assume effective magnetic length $\ell = \frac{1}{B_0} \int B d\ell = 241''$. Each Dipole bends $\theta = 2\pi/774$ Rad. Quads are in series with bends. At a current (nom. 4527A) when dipole $B_0\ell = 245 \text{ kG} \times 241''$, I assume a quad grad. $G_0 = 19.627 \text{ kG/in}$ or $k = (G_0\theta/B_0\ell)^{1/2} = .003833/\text{in}$.



Standard quad. Showing effective length $\frac{1}{G_0} \int G d\ell$ and its position in cryostat. There are many non standard quads.

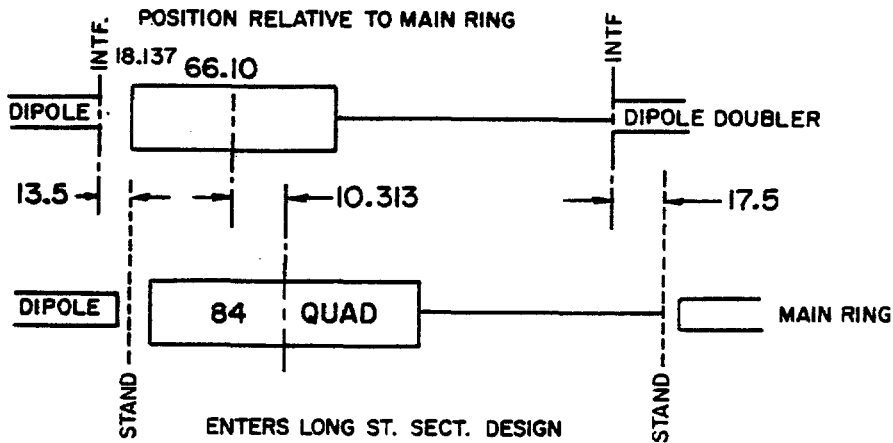


Figure 8-2 Locations of superconducting magnets relative to Main Ring.

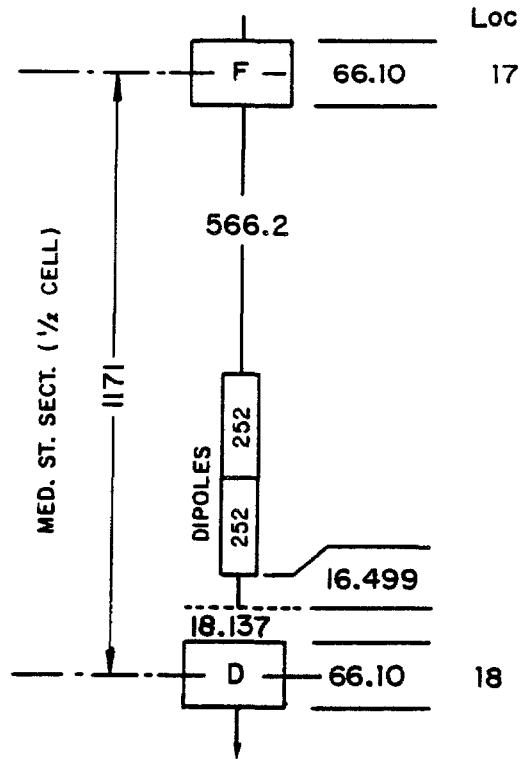
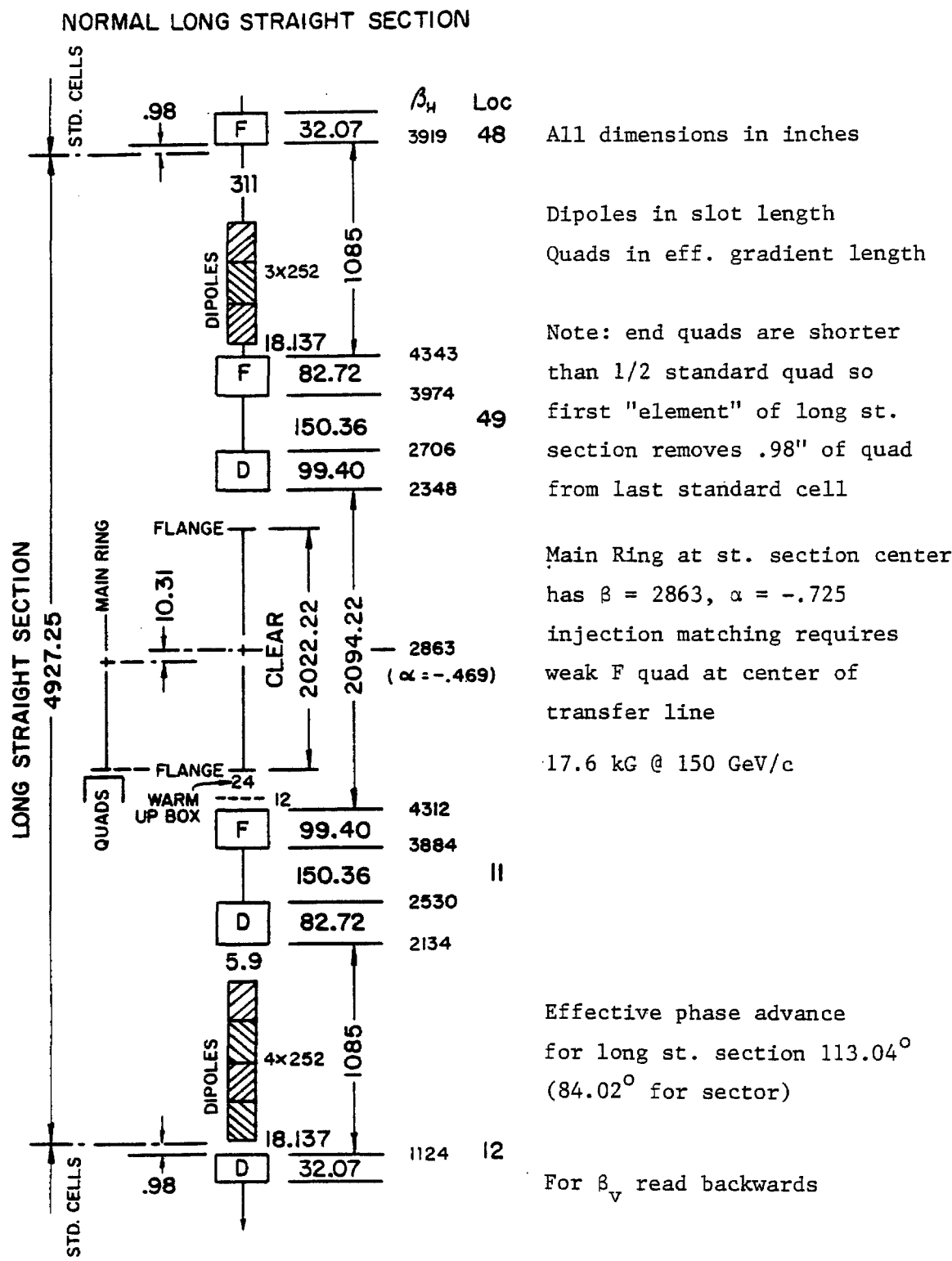


Figure 8-3 Medium straight section. A standard 1/2-cell with two dipoles omitted. A space of 16-1/2 inches must be inserted at downstream end to close the geometric orbit in the shifted Doubler.



All dimensions in inches

Dipoles in slot length
Quads in eff. gradient length

Note: end quads are shorter than 1/2 standard quad so first "element" of long st. section removes .98" of quad from last standard cell

Main Ring at st. section center has $\beta = 2863$, $\alpha = -.725$
injection matching requires weak F quad at center of transfer line

17.6 kG @ 150 GeV/c

Effective phase advance for long st. section 113.04°
(84.02° for sector)

For β_v read backwards

Figure 8-4 Normal long straight section.

functions. The design is very similar to normal Main Ring straight sections with the exception that two, rather than four, quadrupoles are used at either end of the straight section. CO, EO, FO are normal long straight sections. With this choice for EO, the lattice functions of the Main Ring and Energy Saver are matched nicely for the purpose of beam transfer.

The high-beta long straight section is illustrated in Fig. 8-5. Here the order of focusing in the doublets is reversed and lengths of all six quadrupoles are slightly changed. A large horizontal beta is produced at the upstream end of the straight section. High-beta straight sections were chosen for AO and DO because they facilitated resonant extraction, which places the most severe demands on the size of the good-field aperture. Since the good-field aperture of the superconducting magnets is not large, the use of high-beta at this location of the extraction electrostatic and magnetic septa reduces the aperture required for extraction in the rest of the magnet ring. This choice, which was made for fixed-target operation, will not affect the collider performance.

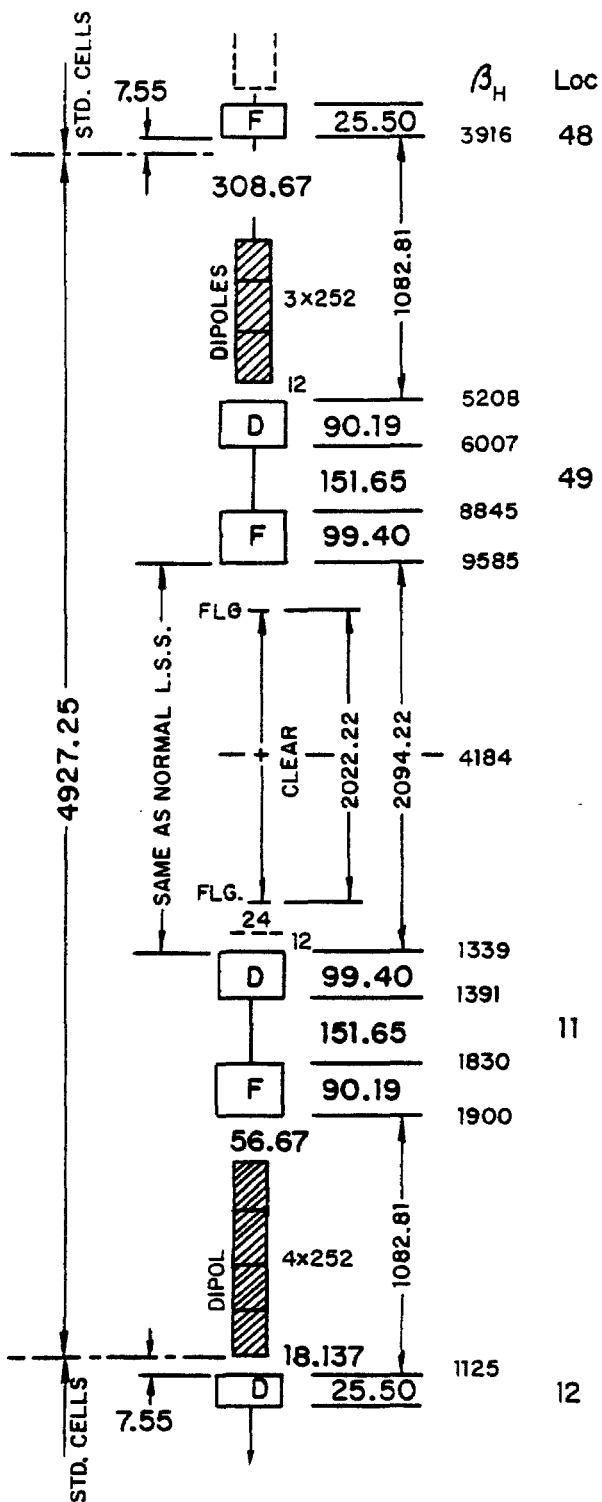
8.2.3 Lattice Elements. Table 8-II lists the various elements required for a ring incorporating two high-beta long straight sections and four normal long straight sections. The lengths shown are magnetic lengths in inches.

TABLE 8-II LATTICE ELEMENTS

<u>Element</u>	<u>Magnetic Length (In.)</u>	<u>Number</u>
Dipole	241.0	774
Standard quadrupole	66.1	180
Long straight inner quadrupole	99.4	12
Normal long straight short quadrupole (48,12 location)	32.07	8
Outer quadrupole	82.72	8
High beta long straight short quadrupole (48,12 location)	25.5	4
Outer quadrupole	90.19	4

8.2.4 Low-Beta Long Straight Section. The low-beta straight section at BO is made by replacing the 32.07 in. quadrupoles at each end of the normal straight section with stronger, separately powered 66.10 in. quadrupoles and adding eight additional quadrupoles within the 2054 in. clear space around BO. During injection these eight quadrupoles are turned off and the two 66.10 in. quadrupoles are excited to a lower current than those in the rest of the ring. After injection and acceleration, the inner eight quadrupoles are turned on, and all ten quadrupoles are slowly adjusted until the final beta-value of 1 m is reached. This process is described in detail in Chapter 9. It is noted that these eight quadrupoles will be turned off during fixed-target operation. The additional elements required

HI - BETA LONG STRAIGHT SECTION



All dimensions in inches

Dipoles in slot length

Quads in eff. gradient length

Note: D-F order is not normal

Effective phase advance for hi-beta section is 112.12°

Hi-beta sector = long st. + 31 half cells $\phi = 83.11^\circ$

Ring = 2 hi-beta sectors + 4 normal sectors

$\nu = 19.4$

Figure 8-5 High-beta long straight section.

for the low-beta are listed in Table 8-III. A layout of the magnet elements of the low-beta straight section is shown in Fig. 9-1.

TABLE 8-III LOW-BETA QUADRUPOLES

<u>Element</u>	<u>Magnetic Length (In.)</u>	<u>Number</u>
Outer quadrupole(48,12 location)	66.1	2
	144.0	6
Inner quadrupole	180.0	2

8.3 Correction Systems

8.3.1 Types of Correction Elements. The correction magnets are built as a cluster of three functionally different superconducting coils concentric with one another and with beam-tube center line.* Since it was chosen to mount the coils on the cold cold beam pipe, or spool piece, between the quadrupole and the adjacent dipole in each cell, the correction magnet package is now called a spool piece. There are two basic types of spool pieces, the regular spool piece associated with each regular cell quadrupole, and the others. The distinction arises from the fact that each regular spool piece has two clusters of magnets, while the others have only one cluster of magnets. The upstream cluster of regular spool pieces contains dipole, sextupole, and quadrupole windings and the downstream cluster contains octupole, sextupole, and quadrupole windings. The orientations of the dipole winding and the downstream sextupole and quadrupole windings provide further differentiation of the types spool piece. The shorter spool pieces also contain three coils. Altogether there are seven types of spool pieces. The types of coils on each spool piece are given in Table 8-IV. The designations for the type of coils are as follows; horizontal dipole (H), vertical dipole (V), sextupole (S), quadrupole (Q), skew quadrupole (SQ), skew sextupole (SS), and octupole (E). Table 8-IV lists the types of spool pieces and Tables 8-IVa and 8-IVb give coil dimensions and parameters.

lp

TABLE 8-IV ENERGY SAVER SPOOL PIECES

Spool piece Type (Code)	Upstream (DSQ coils)	Downstream (OSQ coils)	Length (in.)
"A"	H, S, Q,	None	43
"B"	V, S, Q	None	43
"C"	H, S, Q	E, SS, SQ	72
"D"	V, S, Q	E, SS, SQ	72
"E"	H, S, Q	E, S, Q	72
"F"	V, S, Q	E, S, Q	72
"G"	H, S, Q	E, S, SQ	72

TABLE 8-IVa DC MAGNETIC PARAMETERS OF CORRECTION ELEMENT COIL ASSEMBLIES

Package	Coil	T(bare) (G) (a)	Iron Factor	T(iron) (G) (a)	Effective Length (in.)(b)	$\int Bdl$ at 50A and 1" (kG-in.)	Inductance (mH)		
							warm----- bare(c)	-----cold----- iron(d)	iron(e)
DSQ	Dipole	89.20	1.466	130.80	27.69	181.10	475	696	686
	Sext	32.25	1.259	40.60	28.31	57.46	462	582	556
	Quad	31.67	1.662	52.63	28.56	75.16	293	487	479
OSQ	Octu	21.76	1.054	22.94	28.88	33.12	198	209	198
	Sext	24.51	1.281	31.39	28.32	44.45	300	384	370
	Octu	31.76	1.662	52.63	28.56	75.16	293	487	479

(a) Gauss at 1"/amp.

(b) Average of outer and inner coil lengths.

(c) Based on inductance-bridge measurements before installation of Al pipe.

(d) Base value x iron factor.

(e) Allowance for screening effect of superconductor.

TABLE 8-IVb PHYSICAL PARAMETERS OF CORRECTION ELEMENT COIL ASSEMBLIES

Package (a)	Coil	Coil inner radius (in.)	Coil outer radius (in.)	Iron inner radius (in.)	θ_{\min} (b)	θ_{\max} (b)	Coil inner length (in.)	Coil outer length (in.)	Iron length (in.)	Total turns	Coil-end geometry N=end
DSQ	Dipole	1.602	1.814	2.504	0°	60°	25-3/8	30	30	1170 (2x585)	0
	Sext	1.854	2.142	2.504	0°	20°	26-5/8	30	30	1965 (3x655)	2
	Quad	2.182	2.335	2.504	0°	30°	27-1/8	30	30	1240 (4x310)	0
OSQ	Octu	1.602	1.870	2.504	0°	15°	27-3/4	30	30	1500 (4x375)	2
	Sext	1.910	2.142	2.504	0°	20°	26-5/8	30	30	1560 (3x520)	2
	Quad	2.182	2.335	2.504	0°	30°	27-1/8	30	30	1240 (4x310)	0

(a) Packages include either normal or skew coils depending on subclass spec.

(b) Half angles given for normal coil-angles chosen to cancel 3rd harmonic.

(c) Using coil-end geometry ω per Snowdon's definition (memo dated 10/24/80).

"H" H, V, SQ None 50

8.3.2 Correction Magnet Circuits. The current leads of each coil are separately brought out of the spool piece cryostat, thereby making it possible to excite each coil independently. As will be discussed later, the dipoles are individually excited in order to correct orbit dislocations locally. The sextupoles, quadrupoles, and octupoles are series connected in functional groups in order to adjust global properties such as the tune and chromaticity.

Tables 8-V, 8-VI, and 8-VII show the type of spool piece at each quadrupole location, by pairs of sectors. Superscripts designate the arrangement of the coils into global circuits, which will be used when the Energy Saver is commissioned. Coil windings that are not noted in those tables are not connected to power supplies, although this could be done if a need arose.

TABLE 8-V COIL CIRCUITS IN SPOOL PIECES IN SECTORS A AND D

Quad Loc.	Spool Type	Upstream Coils	Downstream Coils	Quad Loc.	Spool Type	Upstream Coils	Downstream Coils
11	"H"	H, V, SQ ⁴	-----	12	"D"	V	SS ³
13	"G"	H, S ^f , Q	SQ ⁰	14	"D"	V, S ^d , Q	SS ³
15	"A"	H, S ^f , Q	-----	16	"D"	V, S ^d , Q	SS ³
17	"C"	H, S ^f , Q	SQ ⁰	18	"D"	V, S ^d , Q	SS ³
19	"C"	H, S ^f , Q	SQ ¹	21	"B"	V, S ^d , Q	-----
22	"C"	H, S ^f , Q	SS ² , SQ ⁰	23	"D"	V, S ^d , Q	E ⁴ , SS ⁴
24	"C"	H, S ^f , Q	SS ² , SQ ²	25	"B"	V, S ^d , Q	-----
26	"C"	H, S ^f , Q	SS ² , SQ ⁰	27	"D"	V, S ^d , Q	E ⁴ , SS ⁴
28	"C"	H, S ^f , Q	SS ² , SQ ¹	29	"B"	V, S ^d , Q	-----
32	"C"	H, S ^f , Q	SS ¹ , SQ ⁰	33	"D"	V, S ^d , Q	E ⁴
34	"C"	H, S ^f , Q	SS ¹ , SQ ²	35	"B"	V, S ^d , Q	-----
36	"C"	H, S ^f , Q	E ³ , SS ¹ , SQ ⁰	37	"D"	V, S ^d , Q	E ⁴ , SS ⁴
38	"C"	H, S ^f , Q	SS ¹	39	"B"	V, S ^d , Q	-----
42	"C"	H, S ^f , Q	E ³ , SQ ⁰	43	"D"	V, S ^d , Q	SS ⁴
44	"C"	H, S ^f , Q	-----	45	"B"	V, S ^d , Q	-----
46	"C"	H, S ^f , Q	SQ ⁰	47	"D"	V, S ^d , Q	-----
48	"A"	H	-----	49	"H"	H, S ^d , V, SQ ⁴	-----

TABLE 8-VI COIL CIRCUITS IN SPOOL PIECES IN SECTORS B AND E

Quad Loc.	Spool Type	Upstream Coils	Downstream Coils	Quad Loc.	Spool Type	Upstream Coils	Downstream Coils
11	"H"	H, V, SQ ⁴	-----	12	"D"	V	
13	"C"	H, S ^f , Q	SQ ⁰	14	"D"	V, S ^d , Q	
15	"A"	H, S ^f , Q	-----	16	"D"	V, S ^d , Q	

17	"C"	H, S ^f , Q	E ¹ , SQ ⁰	18	"D"	V, S ^d , Q	
19	"E"	H, S ^f , Q	E ¹ , Q ¹	21	"B"	V, S ^d , Q	-----
22	"C"	H, S ^f , Q	E ² , SQ ⁰	23	"F"	V, S ^d , Q	E ⁴ , Q ²
24	"E"	H, S ^f , Q	E ² , Q ³	25	"B"	V, S ^d , Q	-----
26	"C"	H, S ^f , Q	E ¹ , SQ ⁰	27	"F"	V, S ^d , Q,	E ⁴ , Q ⁴
28	"E"	H, S ^f , Q	E ¹ , Q ¹	29	"B"	V, S ^d , Q	-----
32	"C"	H, S ^f , Q	E ² , SQ ⁰	33	"F"	V, S ^d , Q	E ⁴ , Q ²
34	"E"	H, S ^f , Q	E ² , Q ³	35	"B"	V, S ^d , Q	-----
36	"C"	H, S ^f , Q	E ³ , SQ ⁰	37	"F"	V, S ^d , Q	E ⁴ , Q ⁴
38	"C"	H, S ^f , Q		39	"B"	V, S ^d , Q	-----
42	"C"	H, S ^f , Q	E ³ , SQ ⁰	43	(D)	V, S ^d , Q	
44	"C"	H, S ^f , Q		45	"B"	V, S ^d , Q	-----
46	"C"	H, S ^f , Q	SQ ⁰	47	(D)	V, S ^d , Q	
48	"A"	H	-----	49	"H"	H, V, SQ ⁴	

TABLE 8-VII COIL CIRCUITS IN SPOOL PIECES IN SECTORS C AND F

Quad Loc.	Spool Type	Upstream Coils	Downstream Coils	Quad Loc.	Spool Type	Upstream Coils	Downstream Coils
11	"H"	H, V, SQ ⁴		12	F	V	S ³
13	"C"	H, S, Q	SQ ⁰	14	"F"	V, S, Q	S ³
15	"A"	H, S, Q	-----	16	"F"	V, S, Q	S ³
17	"C"	H, S, Q	E ¹ , SQ ⁰	18	"F"	V, S, Q	S ³
19	"E"	H, S, Q	E ¹ , Q ¹	21	"B"	V, S, Q	-----
22	"C"	H, S, Q	E ² , S ² , SQ ⁰	23	"F"	V, S, Q	E ⁴ , S ⁴ , Q ⁴
24	"E"	H, S, Q	E ² , S ² , Q ³	25	"B"	V, S, Q	-----
26	"G"	H, S, Q	E ¹ , S ² , Q ¹ 0	27	"F"	V, S, Q	E ⁴ , S ⁴ , Q ⁴
28	"E"	H, S, Q	E ¹ , S ² , Q ¹	29	"B"	V, S, Q	-----
32	"G"	H, S, Q	E ² , S ¹ , SQ ⁰	33	"F"	V, S, Q	E ⁴ , Q ²
34	"E"	H, S, Q	E ² , S ¹ , Q ³	35	"B"	V, S, Q	-----
36	"G"	H, S, Q	E ³ , S ¹ , SQ ⁰	37	"F"	V, S, Q	E ⁴ , S ⁴ , Q ⁴
38	"E"	H, S, Q	S ¹	39	"B"	V, S, Q	-----
42	"C"	H, S, Q	E ³ , SQ ⁰	43	"F"	V, S, Q	S ⁴
44	"C"	H, S, Q		45	"B"	V, S, Q	-----
46	"C"	SQ ⁰		47	"D"	V, S, Q	
48	"A"	H	-----	49	"H"	H, V, SQ ⁴	

8.3.3 Coil Strength Requirements. The Q^f and Q^d quadrupoles are used to adjust the machine tune. There is a Q^f quadrupole adjacent to every regular horizontally focusing main quadrupole and a Q^d quadrupole next to every vertically focusing main quadrupole. The Q^f quadrupoles are connected in one series circuit, and the Q^d quadrupoles are connected in another. The S^f and S^d sextupoles are also designated in the same way by the adjacent main quadrupole. The S^f and S^d circuits are used to adjust the chromaticity.

The remaining correction magnets will be used initially for half-integer resonant extraction. The Q^1 and Q^3 circuits will be used for half-integer extraction. The Q^2 and Q^4 circuits, which will not be powered initially, can be used in conjunction with the Q^1 and Q^3 circuits to correct the $2\nu_x = 39$ and $2\nu_y = 39$ resonances. The 48 skew quadrupoles located in standard cells, SQ^0 , are connected in series. These will be used to compensate the difference resonance, $\nu_x - \nu_y = 0$. If needed, skew quadrupoles at the ends of the long straight sectors, SQ^3 , can also be excited to provide additional compensation of the $\nu_x - \nu_y = 0$ resonance.

The circuits SQ^1 and SQ^2 , when powered, can be used to manipulate the half-integer sum resonance $\nu_x + \nu_y = 39$. The circuits S^1 , S^2 , S^3 , and S^4 , when powered, can affect the driving terms of the $3\nu_x$ and $\nu_x + \nu_y$ resonance should the need arise. Similarly, the skew sextupoles SS^1 , SS^2 , SS^3 , and SS^4 are installed at the locations given in the tables for driving the $2\nu_x + \nu_y$ and $3\nu_y$ resonances.

Octupoles are arranged in four circuits. Circuits E^1 and E^2 provide the two phases of the 39th harmonic for resonant extraction. Circuits E^3 and E^4 produce the zero-harmonic nonlinearity for control of tune versus betatron-oscillation amplitude. The strengths of the coils appropriate for 1 TeV are expressed as field integrals at 1 in. radius.

Steering Dipoles. The primary function of the steering dipoles is the correction of the closed orbit at all energies. The rigidity of the superconducting-magnet system and the tight tolerance on orbit centering imposed by extraction rules out the movement of magnets for orbit correction. In order to make efficient use of the available magnet aperture, it was specified that the closed-orbit excursions be limited to ± 0.1 in. during extraction. This requirement is met by using the steering dipoles. The steering-dipole strength was determined to be 170 kG-in. on the basis of the following analysis:

It is likely that orbit distortions will be large during the initial operation. At points in the normal cells where the amplitude function is a maximum, the rms orbit distortion due to dipole field errors and quadrupole misalignments can be written as

$$\langle x^2 \rangle^{1/2} = \frac{1}{4}(a^2 + \frac{5}{9}b^2)^{1/2} > 1/2 \text{ in.}, \quad (8.1)$$

Here a denotes the rms dipole field error in units of 0.1%, and b the rms quadrupole misalignment in units of 0.01 in. In the horizontal plane, a arises from the fluctuation in the field-length product from dipole to dipole. In the vertical plane, a receives contributions from both rotational alignment error and any uncertainty or instability in the dipole field direction. It was assumed that the typical misalignment error introduced into the orientation of the dipole vertical plane during

installation was 1 mrad and the stability of that of the vertical plane also had an error of 1 mrad. It was assumed that the quad placement accuracy was 0.02 in. This leads to an rms closed-orbit distortion of 0.5 in. The dipole strength required to compensate the deflection generated locally by the quadrupole misalignment and by the 8 neighboring main dipoles, is, for uncorrelated dipole errors

$$(\int Bd\ell)_{\text{rms}} = 23(a^2 + 0.31b^2)^{1/2} \text{ kG/in.}, \quad (8.2)$$

where a and b have the same significance as in the previous expression. The assumptions made for alignment in the previous paragraph require a 41 kG/in. field integral to correct the rms error. For Gaussian errors, a steering strength of about 130 kG/in. is needed to have 90% probability of successful correction at 100 locations. The steering dipole was designed for a strength of 170 kG/in. This was considered adequate to meet the concerns of the preceding paragraphs.

Trim quadrupoles. Since the main dipoles and quadrupoles are connected in series, trim quadrupoles assume the burden of tune correction and adjustment. Appropriate quadrupole harmonic terms are needed for half-integer extraction.

One of the main functions of the trim quadrupoles will be compensate for the large incremental increase in tune caused by the low-beta interaction regions used in colliding beams. A typical interaction-region will introduce an added betatron phase advance of close to 180° in both planes of oscillation. The trim quadrupoles must, in effect, lower both tunes by approximately 0.5 to restore the operating point. The B0 design described in Chapter 9 produces a shift in tune of 200°. The required trim-quadrupole strength at 1000-GeV may be inferred from

$$\begin{aligned} \Delta\nu_H &= 0.0214(B'\ell)_F - 0.0062(B'\ell)_D \\ \Delta\nu_V &= -0.0062(B'\ell)_F + 0.0214(B'\ell)_D \end{aligned} \quad (8.3)$$

The subscripts indicate the focusing character in the horizontal plane of the adjacent quadrupole. A reduction of both tunes by 0.5 requires a contribution to trim quadrupole strength of 33 kG/in.

Tune corrections that must be made to compensate for magnet errors require considerably smaller strengths. A systematic quadrupole term b_1 in the dipoles would produce tune shifts $\pm 1.1 \times 10^3 b_1$ in the two planes of motion. On the basis of the production of 764 dipoles, the average value of b_1 is less than 10^{-5} /inch. This b_1 makes an inconsequential demand on the trim-quad strengths.

The trim-quadrupole strength was specified at 60 kG/in., safely above the requirement imposed by a single interaction region after allowance for

tune correction. In order to operate two interaction regions, somewhat greater strength is required. The quad can be excited to higher currents if necessary, although a special supply will be required. Alternatively, the operating point of the collider can be shifted from 19.4 to 19.6 to allow a greater tuning range.

Sextupoles. The principal role of the sextupoles is control of the chromaticity. At the time of the Superconducting Acceleration Design Report, May 1979, high-field sextupole moments were cause for concern because b_2 was large. On the basis of the production of 764 magnets, the average value of b_2 is measured to be $10^{-4}/\text{in}^2$. As the following analysis shows b_2 is no longer a cause for concern.

The contributions to the chromaticity from systematic sextupole terms in the dipoles and from chromatic aberration in the quadrupoles can be written as

$$\begin{aligned} \xi_H &= 2.64 \times 10^5 \langle b_2 \rangle - 22 & b_2 \text{ in } (\text{in.})^{-2} & \quad (8.4) \\ \xi_V &= -2.45 \times 10^5 \langle b_2 \rangle - 22, \end{aligned}$$

The constant value of -22 is due to the natural chromaticity of the basic lattice exclusive of enhancements from colliding-beam interaction regions. The magnet-selection criteria impose a bound of $6.0 \times 10^{-4} \text{ in.}^{-2}$ on the magnitude of b_2 . The measured average value of b_2 leads to a chromaticity in one plane or the other of about 50. Compensation of this effect requires sextupole strengths of 4.5 and 1.5 kG/in. at horizontally focussing and defocussing quadrupoles respectively.

A colliding-beam interaction region can be expected to increase the natural chromaticity. For example: the design presented in Chapter 9 increases the magnitude of the chromaticity by 9 units, to -31. The sextupole associated with the standard-cell quadrupole was designed to have a strength of 50 kG/in., a value which is conservatively beyond the minimum requirements.

Octupoles. The major purpose of the octupoles is to facilitate resonant extraction. They provide the nonlinearity that divides the phase plane into stable and unstable regions for the case of half-integer extraction. On the basis of the requirements for resonant extraction, the individual octupole strength has been specified as 30 kG/in.

Skew quadrupoles. At an early stage of the operation of the Main Accelerator at high energy, it was observed that a large horizontal oscillation would couple over into the vertical in a single turn. On the basis of magnet measurements, the same thing will occur in the Energy Saver. For that reason, skew quadrupoles were incorporated into the spool pieces as noted in Tables 8-V, 8-VI, and 8-VII. The skew quadrupole is similar in all respects to the trim quadrupole except that it is rotated by 45° . It has the same strength of 60 kG/in.

8.3.4 Excitation. In this section, the tolerances on the currents delivered to the correction and adjustment magnets and their arrangement in circuits are discussed. The coils were specified to achieve their nominal design strengths at a current of 50 A. The coils can be separately powered at much higher currents. As noted earlier the circuits for exciting the coils are given in Tables 8-V, 8-VI, and 8-VII.

Current Tolerances. Because of their role in orbit correction, the steering dipoles inherently require independent bipolar power supplies. Stability and ripple suppression at 0.1% of full scale are sufficient to satisfy the demands of injection and extraction. Each of the global circuits, defined in 8.3.2, is powered by a precision supply which provides a current stability in the range of 0.1% to .005%. The most severe requirement these supplies must satisfy is to provide a relatively unmodulated resonant extraction over 10 seconds.

8.3.5 Power Supplies. Two distinct types of power supplies have been built, one with an accuracy of 0.1% in regulation for the steering dipoles, and a high precision supply for the other elements. There are 180 steering dipoles in the standard cells of the lattice, and at least 4 dipoles will be installed at each long straight section. There will therefore be a need for over 200 supplies of the first variety.

The design value is $\pm 50A$. The supplies will be designed with load compensation and a conventional roll-off characteristic of 20 db/decade.

Steering-Dipole Supplies. The current stability and ripple limit for these supplies is $\pm 0.1\%$ of full scale. To complete the specifications, the bandwidth and voltage must be determined. It is reasonable to have a bandwidth that allows the power supply output to follow a constant ramp input within $\pm 0.1\%$ of full scale. The error between programmed input and supply output for a constant ramp is

$$\epsilon = \frac{AB}{2\pi f_0} \quad , \quad (8.5)$$

where ϵ is the lag error (amps), A is the power supply DC gain (amps/volt), B is the input voltage ramp rate (volts/s), and f_0 is the power supply bandwidth or corner frequency (Hz)

For an error of 0.1% (0.05A) and a ramp from 0 to 50 A in 10 s, a power supply bandwidth of 20 Hz is adequate. With this 20 Hz bandwidth, the equation above then yields a maximum output ramp rate for 0.1% accuracy of 6.3 A/s.

The supplies will be installed in the existing Main-Ring service buildings. The longest lead from the supply to dipole and back will be 1200 ft. At 50A and 35°C, the voltage drop in that length of No. 1 wire is

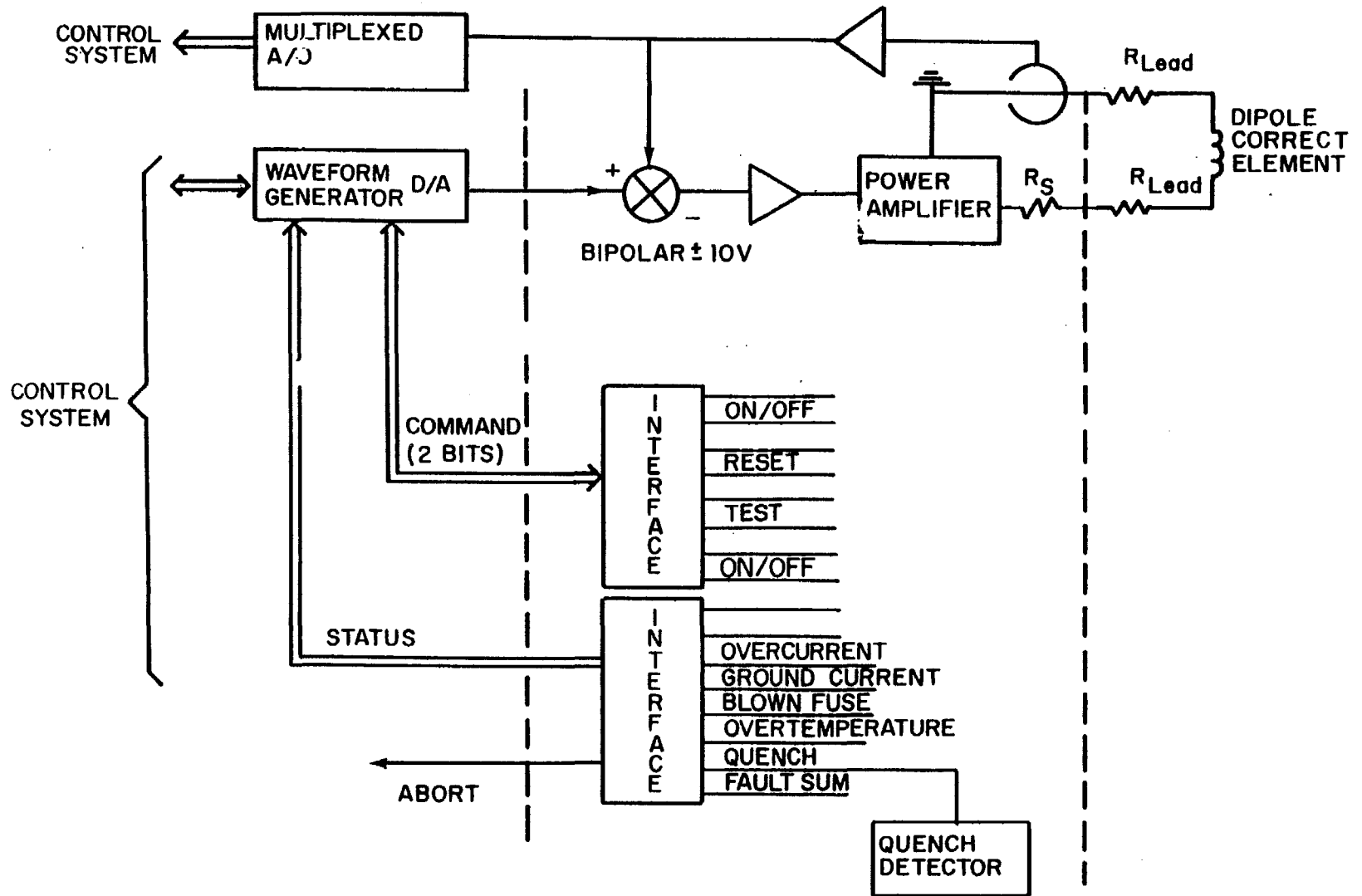


Figure 8-6

8.1 V. The load inductance will be approximately 0.7 H; at the maximum ramp rate, for 0.1% accuracy, the drop across the magnet would be 4.4 V. A maximum power-supply output of 15 V satisfies these requirements and provides a higher slewing capability for current changes under conditions where the accuracy specification can be relaxed.

A block diagram of such a supply is shown in Fig. 8-6. The control system provides a bipolar analog reference waveform from a generator with 12 bit resolution and 2 bits for commands to operate. The current reading is returned to the control system via a multiplexed A/D along with 8 status and fault bits. Isolation is provided between the control system and the power supply for command, status, and faults by means of optical couplers. Isolation of the analog signals is accomplished through differential drivers and receivers.

High-Precision Supplies. These supplies are to have a stability and ripple limit in the range 0.005% to 0.01% of full scale current. They are rated at $\pm 50A$, $\pm 600V$. The low ripple current is achieved with a bipolar transistorized output regulator.

It is noted that certain of these supplies have a relatively high output voltage. To reduce transistor-bank dissipation, these supplies use a bipolar SCR preregulator to provide variable voltage to the output transistor regulator. The preregulators are adjusted to keep a nearly constant voltage across the output transistor banks and thus reduce the transistor-bank requirements. The transistor-bank regulators for the various high-precision supplies are essentially the same. The same is true of the preregulator.

The reference voltage is provided by a high precision 16 bit D/A and the current sensor is a high-quality current transducer with a stability of 1 ppm/ $^{\circ}C$. The waveform generator is located within the supply to minimize noise pickup. Quench detection is also provided by comparing the voltage across one half the series regulators to the other half.

8.4 Main Ring Extraction and Energy Saver Injection and Abort

The design of the antiproton beam transfer was simplified considerably once the circumference of the Energy Saver was made equal to the Main Ring. Fig. 8-7 is a schematic representation of the E0 straight section, which shows both the proton and antiproton transfer lines.

The proton injection for colliding beams will proceed with the transfer of a single bunch from the Main Ring to the Tevatron. The bunch will be kicked horizontally across a magnetic septum (Lambertson magnets) in the Main Ring at the upstream end of E0 using the existing extraction kicker magnet at C48. This initiates a downward bend (16.6 mrad) towards the superconducting string at E11, 25.5 in. below the Main Ring. The vertical dog-leg is completed by two more Lambertson magnets at the downstream end of the long straight section which brings the beam back on

INJECTION LINE SCHEMATIC (VERTICAL)

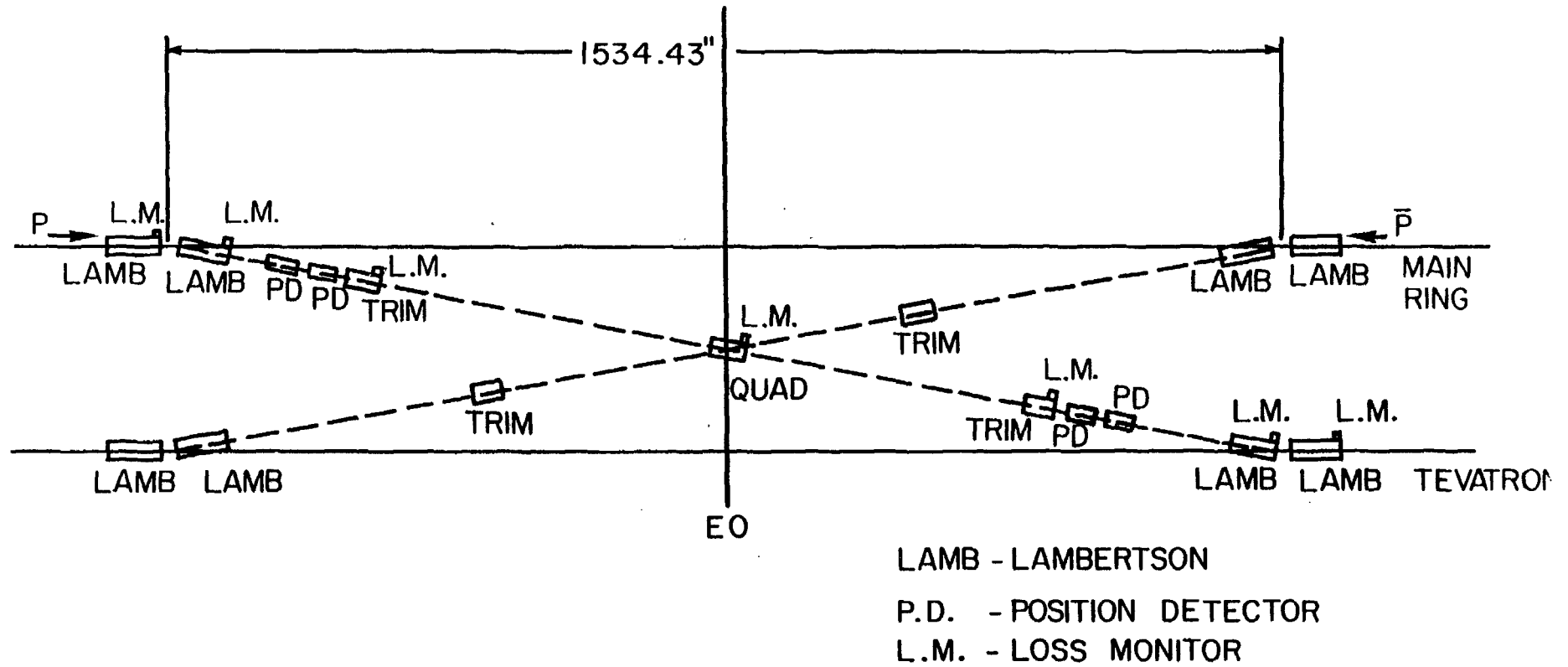


Figure 8-7

to the horizontal plane. The beam is then placed on the closed orbit by another fast rise-time kicker magnet located at the warm E17 medium straight in the Tevatron. Although the basic lattice structures of the Main Ring and the Tevatron are similar, a transverse-emittance dilution of approximately 30% would occur if no attempt were made to match the beam shape. A quadrupole in the injection line will be used to provide both horizontal and vertical matching. Horizontal beam steering is accomplished in the Main Ring and the injection line by a series of bump magnets; the correction dipoles accomplish the corresponding function in the Tevatron.

The antiproton injection uses four additional Lambertsons and two trims, as shown in Fig. 8-7. The matching quad is common to both lines. The \bar{p} transfer is accomplished in the same manner as for protons with the Main Ring extraction kicker located at E17 and the saver injection kicker located at D48.

Table 8-VIII lists the kicker requirements for six bunches of protons and six bunches of antiprotons, all equally spaced. This establishes the maximum number of bunches that can be injected. Nevertheless, it is not planned to exceed 3 bunches of protons and 3 bunches of antiprotons at this time. This table is based on injecting the antiprotons first, one bunch at a time, and then interspersing the proton bunches among the antiproton bunches one bunch at a time. The specifications for the proton transfer kickers were set by the requirements for fixed target operations.

Table 8-IX lists the requirements of the proton and antiproton abort kickers. Again the requirements for the proton abort kicker are met in the existing design for fixed-target application, and two additional identical units will suffice for the \bar{p} abort kicker.

The abort dump for the protons has been designed for the much more intense proton beam that occurs during fixed-target operation. The \bar{p} dump will be a 10 ft long steel block located in the CO straight section, since the \bar{p} beam intensity is two orders of magnitude smaller. The use of the C48 kicker to inject protons at E0 creates the possibility of introducing uncomfortably large amplitude oscillations through D sector of the Main Ring. In order to reduce the size of these oscillations where possible, three bump magnets have been installed in the Main Ring at C22, C32 and D38. These three magnets can be excited to produce a closed orbit 180° out of phase with the kicked beam and thus reduce the effective orbit excursions by a factor of 2 throughout most of the sector. Precise control of the beam position in the Main Ring across the long straight section, essential to ensure loss free injection, is provided by another set of bump magnets at D46 and E17. Powered in series these magnets generate an orbit bump similar to that currently used in the Main Ring for extraction. A hypothetical closed orbit suitable for injection is shown in Fig. 8-8. The orbit excursions between C22 and D38, D46 and E17 are apparent. Figure 8-9 shows the same closed orbit modified by firing the kicker that produces the orbit cusp at C48. The orbit amplitude remains approximately constant up to D38, after which the amplitude increases to a maximum offset of 48 mms

MAIN RING CLOSED ORBIT
PRIOR TO INJECTION

HORIZONTAL PROJECTION
TUNE: 19.420
MAX. OFFSET: 2.34 cm

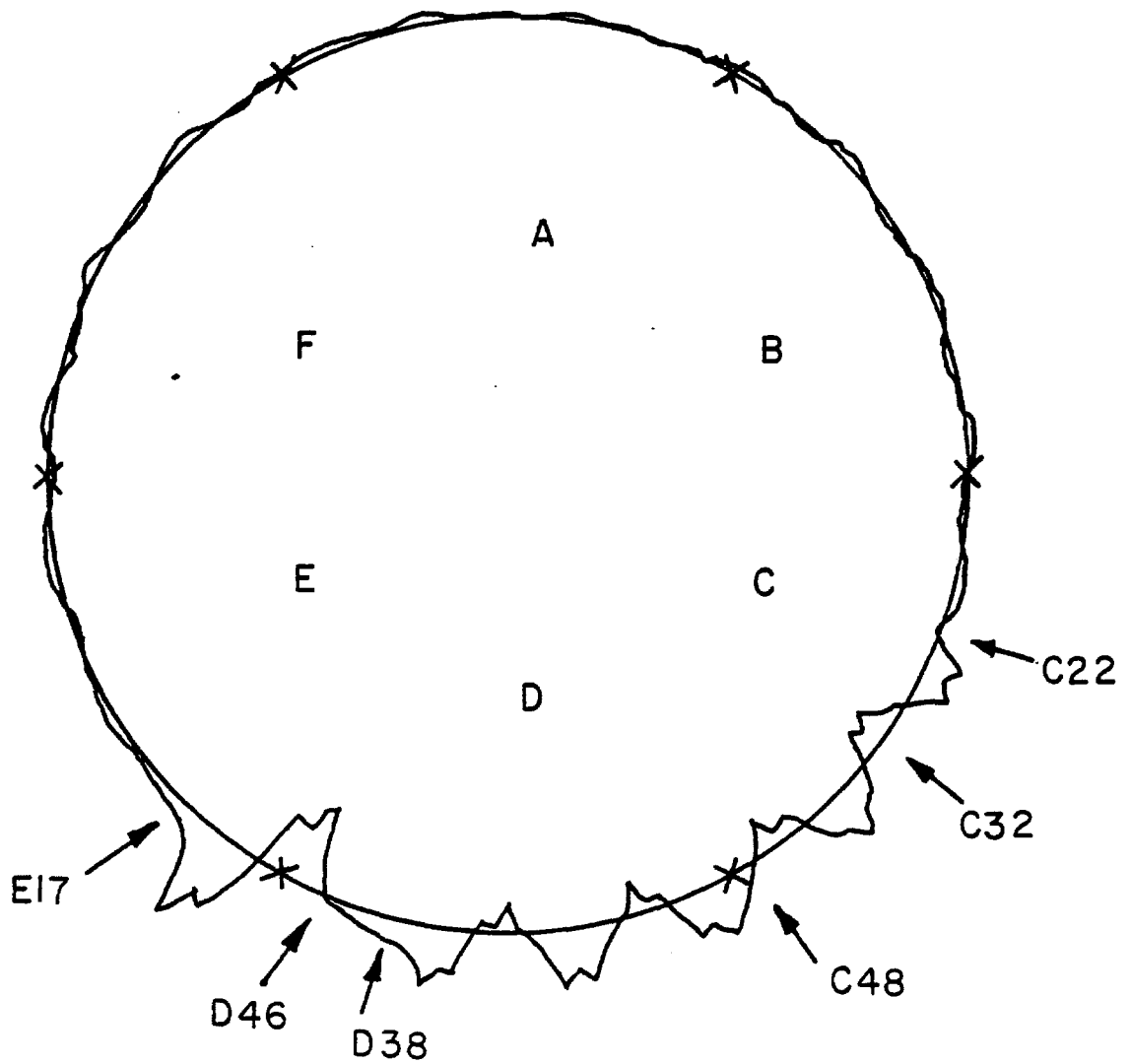


Figure 8-8

at D48. The horizontal orbits across the long straight section are shown in more detail in Fig. 8-10a, where the error bars on the Main Ring orbits give the expected beam size (± 4 mm) at the Lambertson septum. With these injection parameters, one can see an intrabeam separation of 7 mm with the septum offset at 25 mm. The corresponding Tevatron orbits are shown in Fig. 8-10b. The closed orbit bump between E11 and E17 is generated by the correction coil dipoles at E11, E13, E15, and E17 and serves to reduce orbit excursions within the restricted aperture of the Tevatron as well as decrease the integrated field strength required from the kicker magnet at E17.

The same bump magnets used for the proton extraction in the Main Ring are used to reduce the required kick for the antiproton extraction kicker and an appropriate 3-bump using the D46, D48, and D49 Saver correction dipoles will be used to reduce the maximum orbit distortions at injection and reduce requirements on the \bar{p} injection kicker, in a way analogous to the proton injection 4-bump.

The injection Lambertson magnets are similar in design to the present Main Ring extraction devices. The magnets have 12 turns of water-cooled 0.46"-square copper giving a useful dipole field aperture of 3.5" x 0.9". The nominal operation current of 1575 A produces a 9 kG field. The maximum useable field is defined by the saturation of the steel (Republic Steel LoCore 'B') and is 12 kG. The septum is 2 in. thick and is formed with a half angle of 45° .

TABLE 8-VIII EXTRACTION AND INJECTION MAGNET PARAMETERS

	p Extraction	p Injection	\bar{p} Extraction	\bar{p} Injection
B-l	1.97 kG-m	1.33 kG-m	2.5 kG-m	2.5 kG-m
Rise time	20 μ sec	1.39 μ sec	20 μ sec	3.4 μ sec
Fall time	--	2.0 μ sec	--	3.4 μ sec
Magnets	6	4	1	4
Magnet impedance	25 Ω	12.5 Ω	5.5 Ω	10 Ω
Magnet length (m)	1	1	1	1
No. of pulse-forming networks	1	1	1	1
PFN impedance	12.5 Ω	6.25 Ω	1 Ω	10 Ω
Gap (inches)				
HxV	6x2	2x2	6x2	2x2
Voltage	56 kV	43 kV	15 kV	50 kV

TABLE 8-IX ABORT MAGNET PARAMETERS

P Abort	\bar{p} Abort

MAIN RING INJECTION ORBIT

HORIZONTAL PROJECTION

TUNE: 19.420

MAX. OFFSET: -4.82 cm

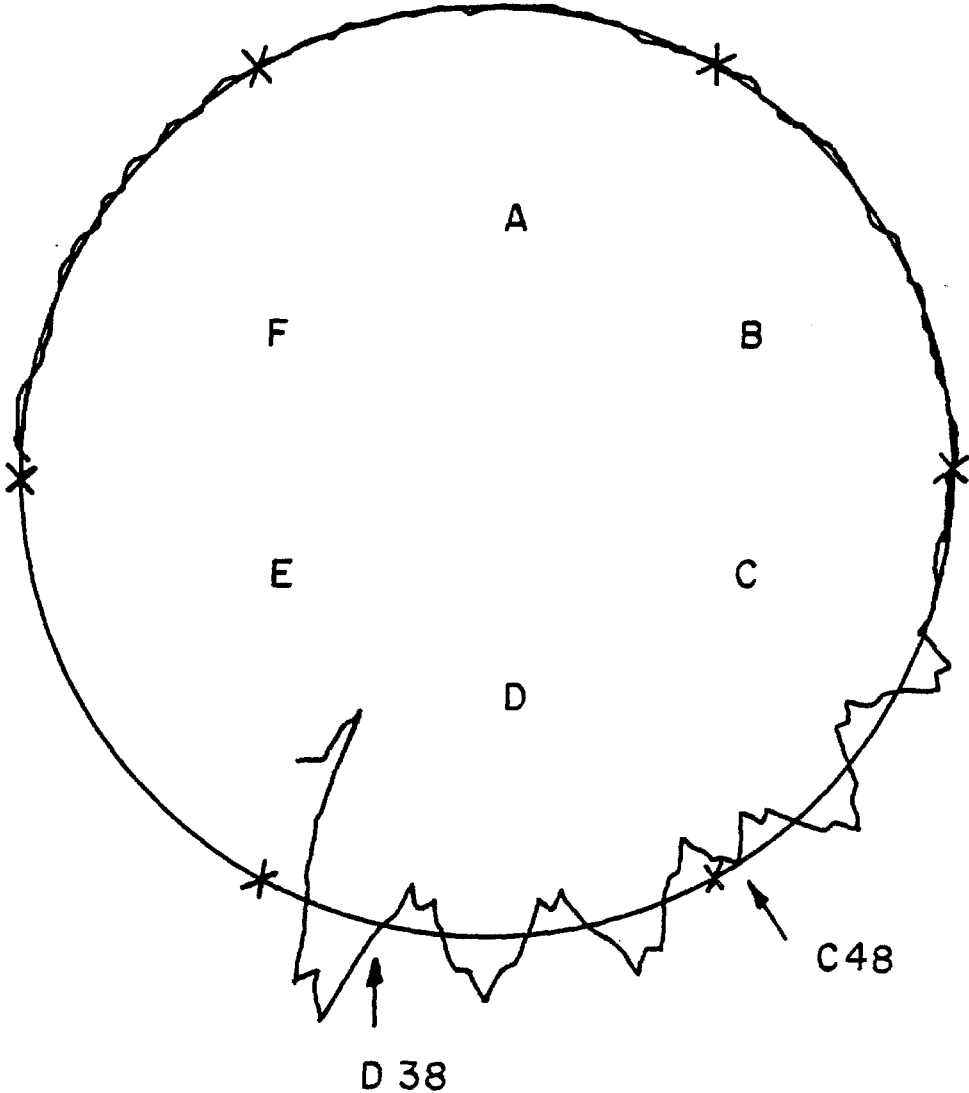


Figure 8-9

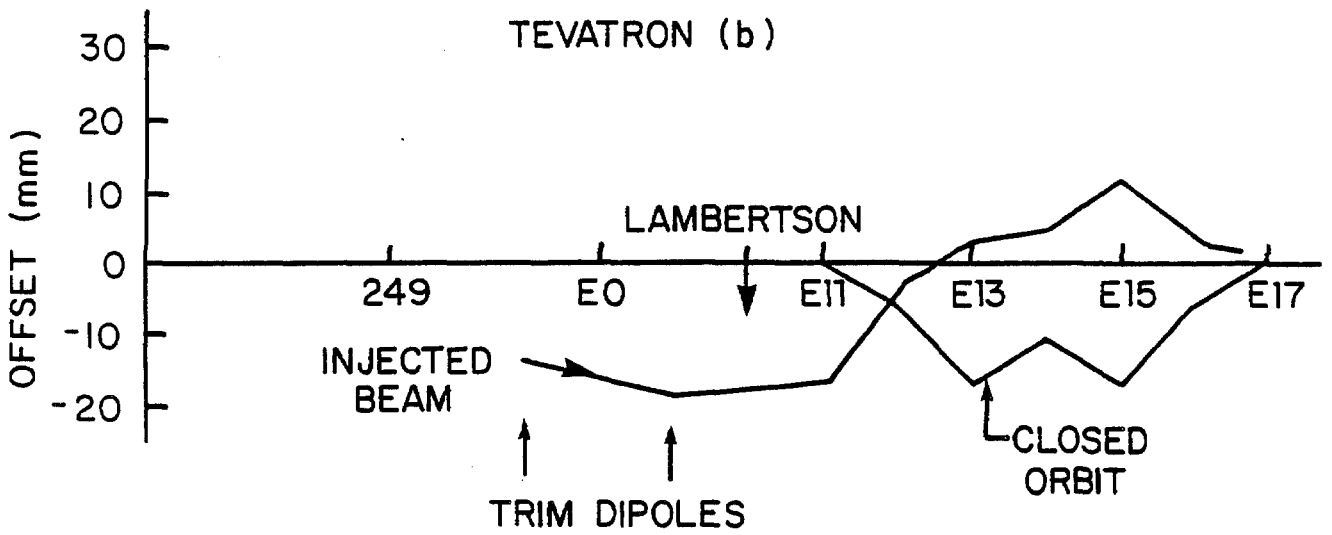
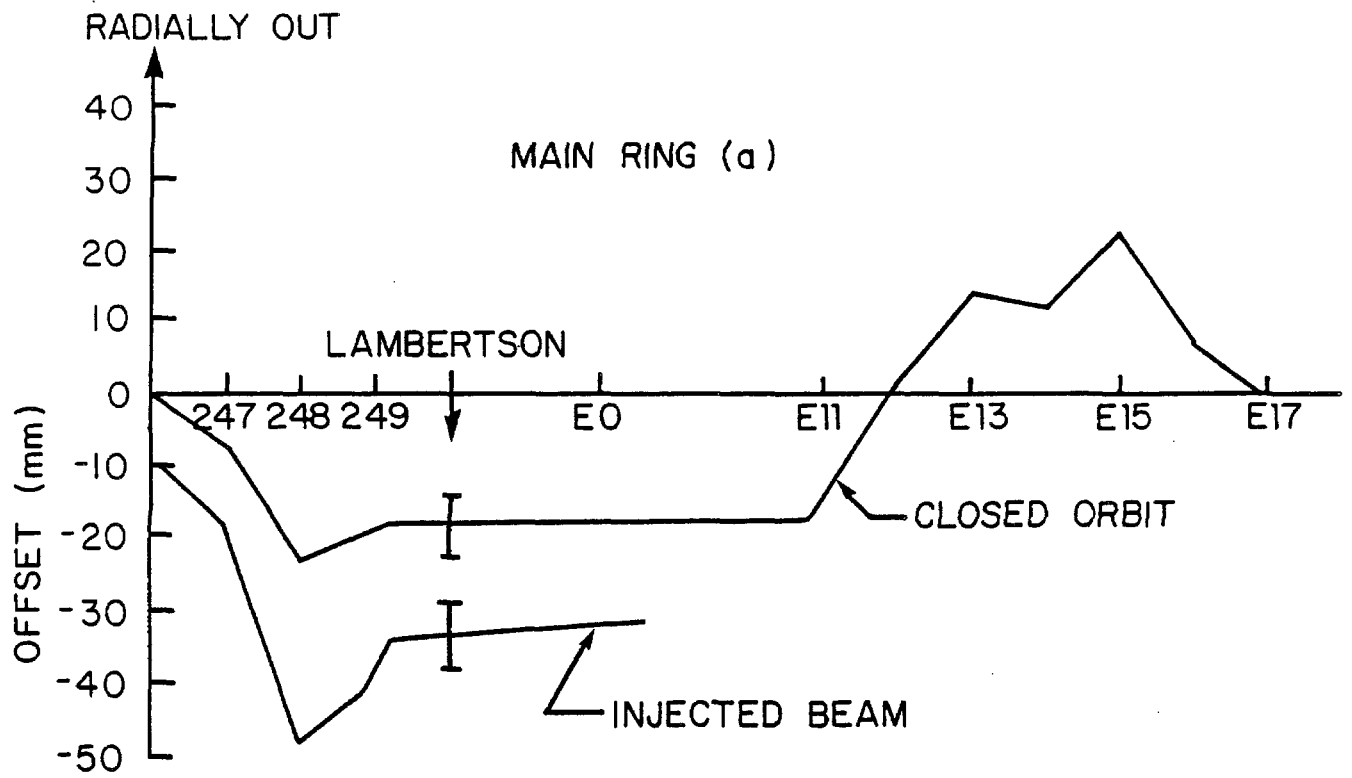


Figure 8-10

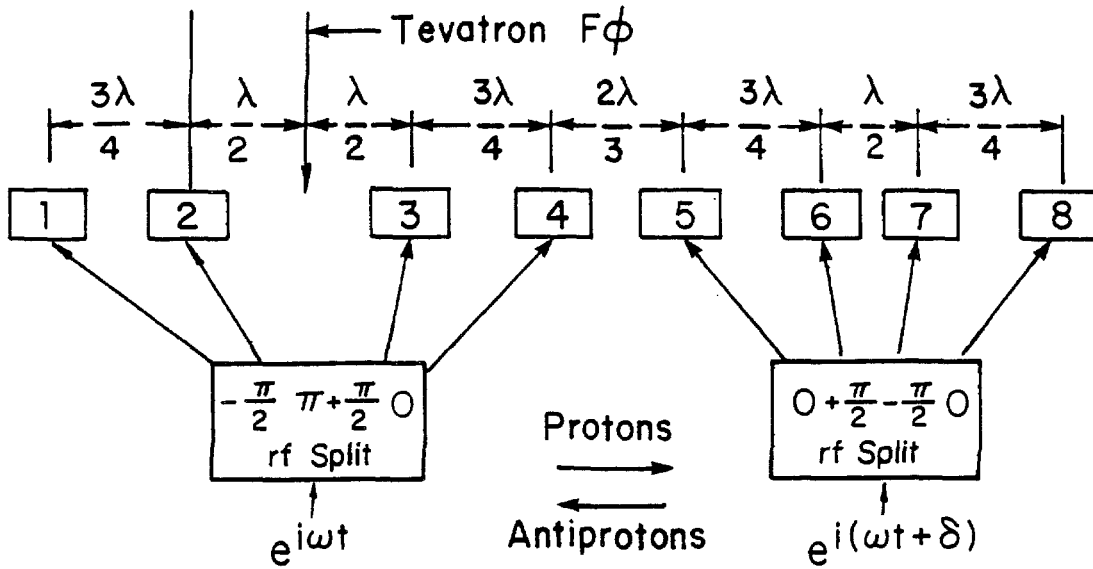
B- λ	24 kG-m	15 kG-m
Rise time	3.2 μ sec	2.0 μ sec.
Location	B-48	C-17
No. module	4	2
Length	2 m	2 m
I_{\max}	19 kA	15 kA

8.5 Acceleration of Protons and Antiprotons

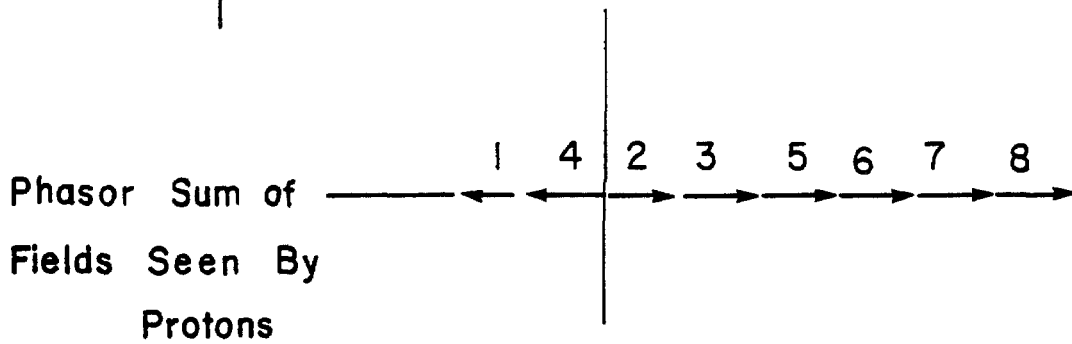
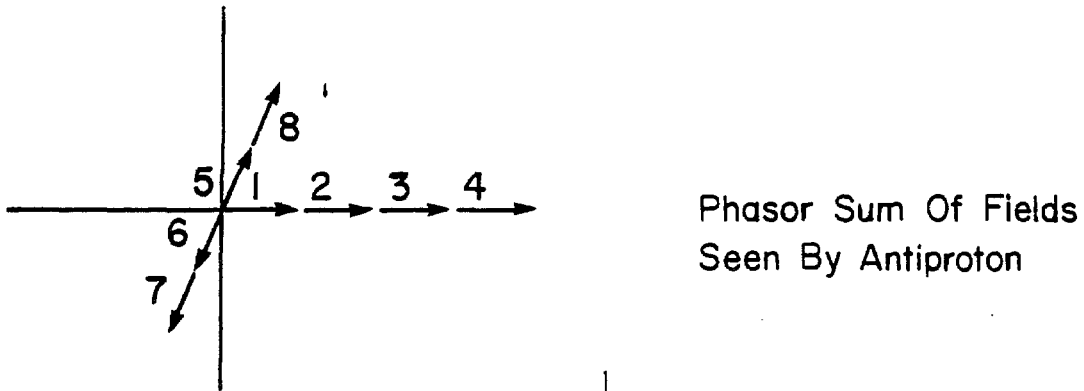
8.5.1 Energy Saver RF Requirements for Colliding Beams. When the Energy Saver is used for colliding beams, the rf system must be able to accelerate protons and antiprotons simultaneously from 150 to 1000-GeV. Because the longitudinal emittances of proton and antiproton bunches may be slightly different, it may be necessary to provide different bucket areas for each in order to minimize dilution during acceleration and storage. Dynamic phase adjustment of proton and antiproton buckets will be necessary in order to damp coherent dipole oscillations of the separate bunches. The rf system should also have the capability of moving the azimuthal location of the $\bar{p}p$ collision point. These functions can be satisfied if the rf system allows independent control of the amplitude and phase of the proton and antiproton buckets.

Independent control can be achieved by arranging the cavities in pairs with appropriate spacing and phasing. Consider a pair of cavities separated in space by $3/4\lambda$ ($\lambda=2\pi R/h$, the rf wavelength at $\beta=1$). If the phase of the rf voltage on the downstream cavity is advanced by $\pi/2$ radians the rf fields encountered by a particle moving downstream through the two cavities will be exactly in phase. These same fields are exactly out of phase for a particle moving from the downstream cavity to the upstream cavity.

There will be eight Energy Saver rf accelerating cavities, each of which is capable of sustaining 35-GeV/sec accelerating voltage for colliding beam operations. Five of these cavities will be built as part of Tevatron I. Four cavities will be arranged in two pairs with a spacing of $3/4\lambda$ to accelerate protons and the remaining four will be arranged in two pairs with the same spacing to accelerate antiprotons as shown in Fig. 8-11a. Cavities 1, 2, 3, 4 are phased so that they couple to antiprotons, which move to the left. Cavities 5, 6, 7, 8 couple to protons, which move to the right. The center of cavity number 2 is located at the Tevatron FO location. Since this location is symmetrically located with respect to the design collision points at D0 and B0, bunches that collide at those points must arrive at the FO point at the same time (i.e., they collide there also, in the case where there are three bunches each of protons and antiprotons in the Collider). The arbitrary angle δ is adjusted to establish the correct collision point. For the spacing shown the required value of δ is $\pi/6$ radians.



(a)



(b)

Figure 8-11

These cavities will be adequate for an acceleration rate of 34-GeV/sec at a synchronous phase of 30°. The acceleration time to 1000-GeV will then be 25 sec. The bucket size is ample. The relative phase between the two sets of cavities is adjustable, so that the \bar{p} and p bunches can be rotated relative to each other to move the collision point to any desired azimuth.

8.5.2 Failure Modes. The requirement of orthogonal control of the two sets of cavities establishes uniquely the spacing between pairs of cavities. However, the precise location of the cavities and the selection of which set to assign to protons or antiprotons is arbitrary. The collision point can be adjusted by selection of arbitrary phase angles δ , as illustrated. The effect of the failure of a single cavity on beam size, luminosity and stability of the collision point is determined by cavity location and deployment. Failure of any rf cavity will always result in some beam deterioration, but the damage can be minimized by optimum cavity placement and selection.

The placement of cavities will be partially limited by the location of penetrations and equipment in the RF Building and the FO Straight Section. The cost of rearranging equipment may not justify the gains that the optimum arrangement provides. The distribution described here is a partial optimization consistent with existing constraints.

In Fig. 8-11b the instantaneous fields seen by protons and antiprotons are shown. A failure of any one of the proton cavities, 5-8, would result in a sudden change in the phase and amplitude of the rf field seen by antiprotons. The antiproton bunches would immediately start a coherent dipole oscillation about the new phase angle, together with higher-order oscillations resulting from a change in bucket size. This would appear as an oscillation of the collision point and ultimately a dilution of the antiproton bunch length to cover the entire oscillation range. This dipole motion can be prevented by automatically turning off a second proton cavity so that the balance is restored. Removal of two proton cavities results in a reduction in bucket height by a factor of 0.707. This will cause a bunch quadrupole oscillation with attendant dilution and bunch lengthening, but no dipole motion of the bunch or collision point.

On the other hand, failure of one of the antiproton cavities, 1-4, does not cause a phase displacement of the proton field, so no additional cavity need be removed from the system. Such a failure results in a decrease in the antiproton bucket height by a factor of 0.866 with a small attendant quadrupole oscillation and bunch lengthening. The effect on the proton bucket height and bunch length is to increase or decrease it by an even smaller factor. In summary, the cavity locations and assignments are such as to minimize the effect of failure of any cavity on the quality of the antiproton bunches at the expense in some cases, of proton bunch quality.

It is conceivable that if many faults occur, resulting in unacceptable dilution of proton bunches, both beams could be decelerated to 150-GeV and the proton bunches replaced with fresh ones while keeping the old antiproton bunches.

8.6 Energy Saver Diagnostics

At the time the Energy Saver components were fabricated, it was recognized that it would be used as a collider. For that reason the beam position detectors were designed so that the proton and antiproton beam could be detected simultaneously. Since the decision to build this type of monitor was made after the preparation of the Superconducting Accelerator Design Report, a description of them is given in Section 8.6.1. The beam-loss monitors of the Energy Saver are described in 8.6.2. Following the first year of operation of the SPS collider the requirements for diagnostics in the Energy Saver were reviewed. The additional diagnostic equipment that should be added to the Energy Saver for colliding beams is given in Section 8.6.3.

8.6.1 Energy Saver Position Detectors. The position detectors in the Tevatron are of the directional-coupler type⁵. There are 216 detectors in all, 108 each for vertical-position measurement (in vertical focusing quadrupoles) and for horizontal-position measurement (in the horizontally focusing quadrupoles). The pickups have about 24 db of directivity (i.e. rejection of signals from beam traveling in the unwanted direction) so that the pickups can be used to detect \bar{p} 's in the presence of p's and vice versa.

The fast electronics for extracting the position signal from the pickup signal uses amplitude to phase (AM to PM) conversion to provide a large dynamic range of beam intensity⁶. The electronics was specifically designed to detect single isolated bunches with p's or \bar{p} 's (collider mode) as well as contiguous filled buckets (batch mode) for fixed-target operation. The lower limit of sensitivity for operation in these modes is about 3×10^9 p's per bucket (collider mode) or 1×10^8 p's per bucket (batch mode). The position-signal rise time is about 70 nsec due to the presence of a half-wavelength resonant filter which rings when hit by a signal from isolated p or \bar{p} buckets. The estimated precision of position measurement is about ± 0.5 mm at the lowest intensities. Precision of ± 30 microns has been obtained with high intensities in a detector installed in the Main Ring.

The microprocessor-controlled digitizing electronics allows simultaneously digitizing the position signal from all 216 detectors with about 100 nsec (least significant bit) resolution on the timing for each detector. This "FLASH" picture of a single turn of beam can be used to examine the beam orbit for any complete revolution including injection. Other operating modes include measurements of beam position averaged over many turns to average out the contributions of betatron oscillations.

These latter measurements have large RAM memories associated with them to store many measurements without requiring readout by the Host control computer. These data are used to determine closed orbits for correction-coil programming and for orbit reconstruction in case of a beam-induced quench. The microprocessor circuits can initiate beam aborts if the beam exceeds preset position limits.

The electronics has been designed and built to detect beams in either direction. In order to fully implement these features, coaxial relays are installed in the tunnel to select the proper pair of ports from the directional coupler pickups. A signal to control them is provided in the Service Buildings. In addition, a Saver Clock signal (a signal with diphase encoded timing signals on a 10 MHz carrier) is installed in the \bar{p} direction around the ring. The electronics is equipped to receive this at the same time it controls the coaxial relays. A control cable for the coaxial relays will also be installed.

8.6.2 Beam Loss Monitors. The Tevatron beam-loss monitor system, like the beam-position system has detectors at every quadrupole (a total of 216 around the ring). They are argon filled chambers designed to have a very large dynamic range and fast response. Their signals are amplified in a fast risetime integrating 4-decade logarithmic readout. Real-time analog output signals are also available for fast time plots. The 60 msec integration time of the electronics corresponds to the response time of the Doubler magnets to beam-induced heating, and therefore is a good monitor of the likelihood of inducing quenches. The beam-loss monitor system, like the beam-position system, can initiate a beam abort if the radiation level exceeds preset limits.

8.6.3 Diagnostics for the Energy Saver Collider Operation. Initial experience from the CERN SPS collider has shown the importance of adequate beam diagnostics. In the Fermilab Collider, much of the tuning of the transfers, acceleration, and storage parameters will necessarily be done with antiprotons, which are relatively rare even if the \bar{p} accumulation works well. Thus, diagnostic devices should work at low beam intensities. Furthermore, since the time to improve transfer and storage efficiency of the Collider will be in competition with other uses of the Tevatron, there must be a complete set of diagnostic devices with well developed software at the onset of Collider commissioning.

The obvious requirement is to be able to measure the beam intensity, position and emittance as a function of time as the particles make their way to a successful store at 1 TeV.

Beam transfer lines will be equipped with sensitive intensity and profile monitors. The Main Ring and Tevatron will have position and intensity measuring devices that will be well developed by the time collider commissioning begins.

In order to measure the profile of circulating p's and \bar{p} 's in the Tevatron, we are planning to construct several flying wire scanners⁷. These devices flip a thin-wire filament through the circulating beam at about 5 m/sec, and the resultant scattered flux is monitored by several scintillator telescopes placed both upstream and downstream of the flying wire. Such a device would be placed near (and in) the BO Colliding Detector Facility to measure beam position as well as profile. Each flying wire can measure only one coordinate, so several are needed. Such a device has been implemented at the CERN SPS and is recognized as an important diagnostic tool⁸.

Motion of the wire through the beam is about 0.1 mm per turn, which results in about 10 points across a beam 1 mm in diameter. The scattered flux from p's and \bar{p} 's are quite directional, and hence the p and \bar{p} beam profiles are recorded simultaneously in the two sets of scintillators. The emittance blowup per scan is about 6×10^{-6} mm-mrad, hence for the SPS about 200 scans per hour is equivalent to multiple scattering by the residual gas. The heating of the wire (a low-Z material such as beryllium or carbon) is not excessive. The particle flux lost is less than 0.02% per scan.

Longitudinal emittances will be monitored by the devices associated with the Main Ring and Tevatron low level rf systems.

Schottky scans should be adequate for tune measurements. An active tune measurement is also under consideration.

The intensity and position devices in the Tevatron can give information on individual bunches of protons or antiprotons. In addition, the flying-wire scanner gives bunch-by-bunch information.

References

1. Superconducting Accelerator Design Report, May 1979, Fermilab, Chapter 14.
Fermilab Report UPC 73, F.E. Mills and D.E. Young, November 11, 1978.
Fermilab Report UPC 129, F.T. Cole, April 24, 1980
Fermilab Report UPC 132, S. Ohnuma, June 26, 1980
2. Fermilab Report UPC 96, T.L. Collins, April 1979.
3. Fermilab Report UPC 17, L.C. Teng, December 1, 1978
4. D. Ciazynski and P. Mantsch, "Correction Magnet Packages for the Energy Saver" IEEE Trans. on Nuclear Science, Vol. NS-28 , No. 3, 3275 (1981).
D. Ciazynski and P. Mantsch, "Typical Problems of Correction Magnets for Fermilab", IEEE Trans. on Magnets, Mag-17, 165 (1980).
5. R. Shafer et al., IEEE Trans. Nucl. Sci. 28 , No. 3, page 2290 (1981).
6. Ibid, page 2323.
7. L.R. Evans and R.E. Shafer, Proc. Workshop on Intensity Limitations in Storage Rings, BNL 57236, page 68 (1979).
8. A. Barisy et al., IEEE Trans. on Nucl. Sci. 28 , page 2180 (1981).

CHAPTER 9

INTERACTION REGIONS AND EXPERIMENTAL FACILITIES9.1 EXPERIMENTAL AREAS

9.1.1 BO Experimental Area. A general-purpose detector is being designed and constructed by the Colliding Detector Facility Department, CDF. The desire to measure antiproton-proton collisions and available technology both demand a large, massive and complicated apparatus. The BO Colliding Beam Experimental Area has been designed to handle the assembly, installation, operation and maintenance of such a detector.

The project includes the following:

BO Collision Hall an underground structure that will replace approximately 100 ft of the Main Accelerator enclosure, and will contain the experimental physics detectors and both the accelerator and Energy Saver beam components. On the outside wall (away from the accelerator center) will be a large door and movable shield wall that will provide access to the Assembly Hall.

BO Transition and Equipment Bypass Enclosure an underground structure that connects the Collision Hall to the existing Main Accelerator enclosures, and provides a passage for personnel, utilities, and magnet-moving vehicles around the BO Collision Hall.

BO Assembly Hall a large pit at the elevation of the Collision Hall and adjoining to the shield door passage, with a service floor at grade level, all covered by a highbay building with an overhead crane. The various experimental physics detectors will be assembled, tested and serviced in this hall prior to placement in the BO Collision Hall.

BO Site Development hardstands, access roads, drainage facilities, relocation of utilities, extension of services and temporary earth retaining structures for construction sequencing and adjacent road and building protection.

BO Primary Power 13.8 kV feeders, substations and switchgear for extending primary power to the BO Experimental Area and into the BO Assembly Hall.

The BO Collision Hall connects with and becomes a part of the Main Accelerator and Energy Saver enclosures. All systems, services and utilities are designed for compatibility with these systems. Access to the BO Assembly Hall will be from the adjacent Road D near the Industrial Buildings.

At the time of writing, construction of the B0 area is almost complete.

9.1.2 D0 Experimental Area. This experimental area is still in the process of definition and conceptual design.

9.2 B0 Low Beta Design¹

9.2.1 Lattice Design. As discussed in Chapter 6, the \bar{p} and p bunches are placed at equal spacings around the circumference of the Tevatron, arranged so that one of their crossings occurs in the B0 long straight section, the location of the Collider Detector Facility. There will also be crossings in the D0 long straight section, the second colliding-beam experimental area, at present in a primordial state of design.

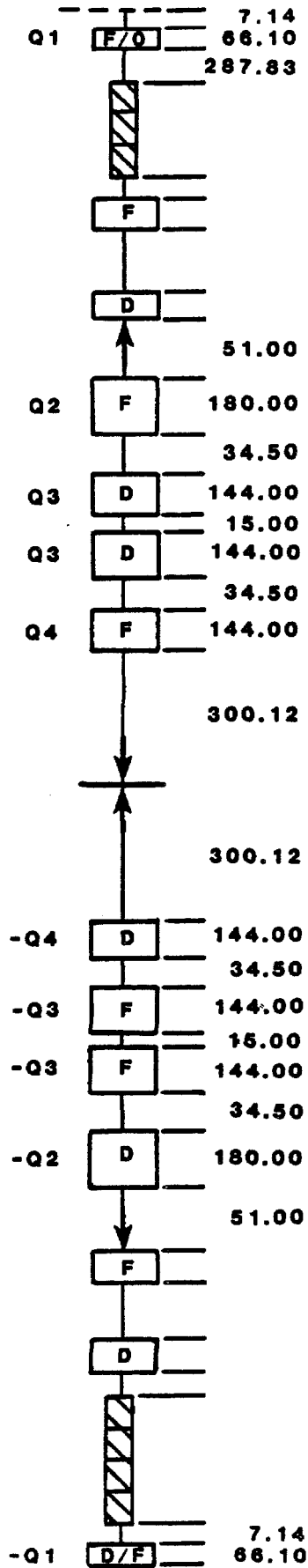
The luminosity can be enhanced for given beam currents by focusing the beams down to narrow waists at the collision point, using extra quadrupoles on either side of the collision point. These quadrupoles give a decrease in the amplitude function β and the low β gives the narrow waist.

It is desirable for our purposes to achieve a minimum β value of 1 meter. Given the Tevatron lattice and dimensions, it is possible to achieve this minimum with a design that utilizes quadrupoles having gradients of 25 kG/in. and requires replacement of a single normal-cell quadrupole on either side of B0, at A48 and B12, by longer quadrupoles. The design uses four separately powered quadrupole buses and either can be adiabatically varied from the normal $\beta^* = 72$ m configuration to $\beta^* = 1$ m, while causing very little betatron mismatch or manipulation outside the interaction region except for correction-quadrupole changes to preserve the overall tunes and sextupole changes to maintain the desired chromaticity.

A layout of the 25 kG/in. low-beta insertion is shown in Fig. 9-1. It requires the replacement of the 32 in. quadrupoles at A48 and B12 with separately powered 66 in. quadrupoles and the addition of two 180 in. quadrupoles and 6 144 in. quadrupoles within the long straight section. These ten quadrupoles are powered anti-symmetrically on four separate circuits and must reach a maximum gradient of 25.5 kG/in. at 1 TeV. In order to keep maximum luminosity point close to the Tevatron B0 location, the quadrupoles at A48 and B12 must be pushed as far upstream as possible. To do this, the normal dipole interface-to-quadrupole magnetic length has been reduced from 18.137 in. to 7.137 in. by changing the upstream bellows and moving the beam detector to the downstream end of the quadrupoles. This motion puts the maximum luminosity point 0.9 in. downstream of the Tevatron B0 for the final low beta of 1 m.

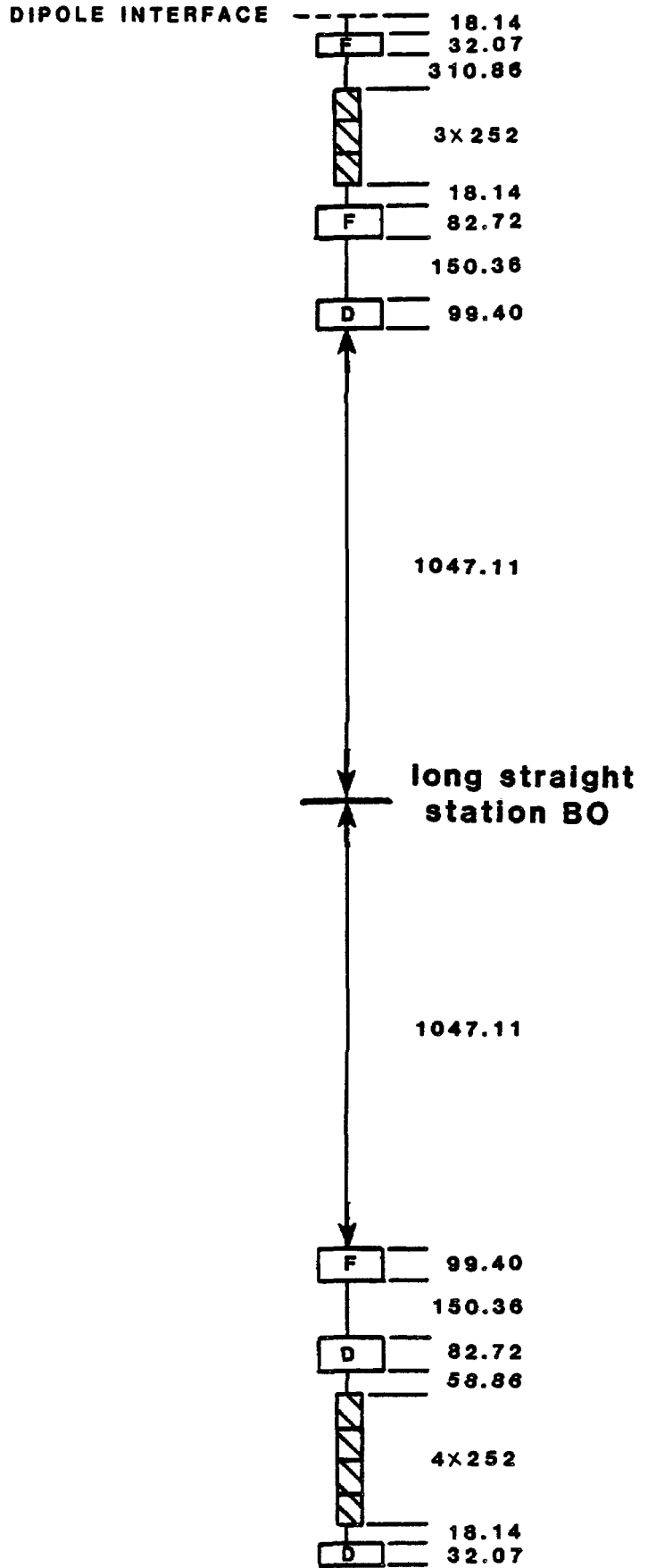
9.2.2 Transition to Low Beta. For normal fixed-target operation, Q1 must run at approximately 10 kG/in. and Q2, Q3, and Q4 must all be off. By contrast, in the low-beta configuration, all the quadrupoles must be on and running quite hard. The problem is to find a method of connecting these

low beta straight section



(a)

normal long straight section



(b)

Figure 9-1

two solutions in a stepwise continuous manner while maintaining the overall tune of the Tevatron. This is by no means a simple straightforward process. The two solutions are in fact quite different and probably cannot be connected without disturbing the normal lattice functions outside the insertion region. A method has been found, however, that does not greatly disturb the rest of the ring. This sequence takes the lattice from a retuned fixed mode to a low beta of 1 m.

In all this sequence, the Tevatron has been retuned to 19.585 in each plane. For particle-antiparticle collisions it is desirable to be above the half integer and the value of 0.585 centers the tune in a region free of all resonances of order lower than 11th. The correction quadrupoles consist of two families, QFC and QDC, located next to the corresponding quadrupoles, QF or QD, at all stations 13 through 47. These corrections have a range of approximately ± 2 kG/in. at 50 amps. QFC has ranges from +0.4 kG/in. to -0.9 kG/in. QDC is given by

$$QDC = 0.0457 - QFC \text{ (kG/in.)}$$

In this turn-on sequence, there is some disturbance to the lattice functions outside the insertion region, for three distinct reasons:

1. The "off" solution and the "low-beta" solution are, in fact, quite different. It is doubtful that they can be connected without allowing some mismatch.
2. The initial sequence, in steps of less than 1/3 kG/in., was not a very smooth curve. Some amount of mismatch was allowed in order to produce smoother curves.
3. It was found that a higher luminosity can be achieved in the "1 meter low-beta" by introducing some mismatch. This is because the long straight sections are not exactly antisymmetric; one side has more dipole edge focusing than the other, while the low beta quads of necessity are symmetric.

The amount of disturbance to the normal lattice, however, is quite small and should cause no problem since this turn-on will not start until high energy where the beam is very small.

9.3 Hardware Modifications

9.3.1 Magnets. Special quadrupoles have been designed and are being built for the B0 interaction region. These magnets use special cable with 20 micron filaments and a copper-to-superconductor ratio of 1.3 (as opposed to 8 microns and a ratio of 1.8). This cable has a short sample limit of 5250A at 6.5T. The new quadrupole has added turns to reach higher fields.

There are many new features of the new design. The strength of the coil collars has been carefully considered, as has quench protection. A

smaller cross section is being considered to give less interference with the Collider Detector. Because the special quads are powered separately from the regular Superconducting Ring magnets, the regular excitation currents are bypassed through the quads in a notch at the outside of the coil collar.

The beam monitor and correction magnet at B12 have been redesigned in a special package and relocated downstream of the special quad. Dipole fields will arise from quad misalignment. Even though shimming will be done, misalignments in the high- β regions adjacent to the low- β interaction region can give large orbit distortions and trim dipoles are being designed for correction.

9.3.2 Power Supplies and Bus. Four separate power supplies and associated circuits will be needed for the 1-m β^* design. The supplies will be modified Tevatron holding supplies capable of providing up to 6000 A. The supplies will be located in an annex to the B0 service building and the power will be transported to the magnets via water-cooled copper bus (total length of 4 circuits is 2700 ft). For a current of 6000 A, the power consumed by the bus is 770 kW. Power will enter the magnets through lead boxes constructed especially to fit the 15 in. space provided for them.

9.3.3 Refrigeration. Liquid-He refrigeration needs are as follows: quadrupoles (50 W), four pairs of 5-kA leads at 10 W each (40 W + 56 l/hr), two turnaround boxes at 10 W each (20 W), two feed boxes (45 W) and U tubes (5 W), for a total of 160 W plus 60 liters per hour. This refrigeration need can be met initially by the A4(C4) and B1(D1) satellite refrigeration systems. Later, it may be desirable to provide stand-alone refrigeration, and it would certainly be needed if operation at 1.8 K is desired. The 60 liters per hour of liquid He will come from the Central Helium Liquifier through the A4 and B1 refrigerator and magnet systems. The estimated LN₂ requirement is 250 W. Refrigeration estimates for the interaction-region detector magnets are not included here, because it is expected that those needs will be satisfied by separate refrigeration.

9.3.4 Vacuum. Pressure in the interaction region straight section should not exceed 10^{-9} Torr. This means the warm vacuum pipe through the detector plus a transition piece on either side will require special preparation (possible bakeout). The transition pieces will contain isolation valves and ion pumps, as well as the connections to turbomolecular and roughing pumps.

9.4 D0 Low-Beta Design

At this time, the D0 low-beta region is still being designed.

References

1. D.E. Johnson, Tevatron B0 Low Beta Tuning Report, Fermilab Report TM-1106, May 1982 (unpublished).

CHAPTER 10

PERFORMANCE AND LUMINOSITY

In this chapter we describe colliding-beam performance at 1000 GeV in the Energy Saver. For this purpose, we assume that beams of protons and antiprotons have been accelerated and are circulating in opposite directions so they collide in the center of the low-beta insertions at B0 and D0.

We assume the populations for a two beams are those required for a luminosity of $10^{30} \text{ cm}^{-2}\text{s}^{-1}$. Larger luminosity figures are also possible.

10.1 Beam Geometry

As an example, it is possible to create three bunches of antiprotons, each with 6×10^{10} particles and each with a longitudinal phase area of 3 eV-sec, which we define as the area including 95% of the population with a biGaussian distribution. To prepare the necessary number of antiprotons in the Accumulator will take a little more than 2 hours.

Similarly, we can assume that three proton bunches, each with 6×10^{10} particles and a longitudinal area of 3 eV-sec coexist with the antiproton beam. Both beams have equally spaced bunches since the harmonic number 1113 can be divided by 3. In principle, there are therefore 6 equally spaced collision regions. We assume here that beams are not kept separated by electrostatic deflectors. We also assume that two sets of four rf cavities exist, giving orthogonal control of the two beams, as discussed in Sec. 8.5. In this mode of operation, there will be a total of 1.4 MV/turn for each beam.

Using the equations of Chapter 2, which apply to the Tevatron as well as to the Main Ring, we obtain the rms bunch length $\sigma_e = 40 \text{ cm}$ and the rms momentum spread $\sigma_p/p = 1.2 \times 10^{-4}$. The area of the stationary bucket is 12.7 eV-sec, four times larger than the bunch area. Finally, the phase-oscillation period is $T_s = 27 \text{ msec}$.

10.2 Beam Cross Section at the Collision Point

As a result of the transverse stochastic cooling in the Debuncher and Accumulator Rings, and because the two beams have roughly the same number of particles, the two beams have the same emittance in both horizontal and vertical planes. The normalized emittance is assumed to be $24 \pi \text{ mm-mrad}$. That is, $\epsilon_v = \epsilon_H = 0.023 \pi \text{ mm-mrad}$ at 1000-GeV (this includes 95% of the beam) distributions.

A low-beta figure of 1 m is expected in both planes and therefore the rms beam radius is

$$\sigma = 0.06 \text{ mm}$$

or

$$\sigma^2 = 3.5 \times 10^{-5} \text{ cm}^2$$

Since the low-beta insertion has very small dispersion, there will be negligible contribution to the beam size from momentum spread. In Fig. 10-1 we show the variation of the beta and dispersion in the interaction region. Observe that the beta minima are about 10 cm apart. The dispersion is approximately 18 cm. For comparison in Fig. 10-1, we also show the longitudinal distribution of a bunch.

10.3 Luminosity

Because the low-beta value of 1 m is larger than the rms bunch length (0.4 m), a formula for luminosity valid for constant beam sizes is a good approximation.¹⁴ Thus

$$L = \frac{N_p N_{\bar{p}} B f_0}{4\pi\sigma^2},$$

where $N_p = 6 \times 10^{10}$ is the number of protons per bunch, $N_{\bar{p}} = 6 \times 10^{10}$ is the number of antiprotons per bunch, $B = 3$, the number of bunches per beam, and $f_0 = 4.77 \times 10^4$ Hz is the revolution frequency. This gives

$$L = 1.0 \times 10^{30} \text{ cm}^{-2} \text{ sec}^{-1}.$$

The distribution of the luminosity in the interaction region is shown in Fig. 10-2. It is approximately Gaussian with an rms value of 26 cm. This figure has already been adjusted by a factor 0.92 because of the variation of beta with bunch length. This luminosity figure is clearly within reach with the methods and the techniques described in this report. Several alternative luminosity scenarios can be invented. For instance, it is possible to replenish the Collider every hour with only one single bunch of protons and antiprotons with 10^{11} particles each, for the same luminosity of $10^{30} \text{ cm}^{-2} \text{ sec}^{-1}$.

Higher luminosity figures can also be expected, as high as $6 \times 10^{30} \text{ cm}^{-2} \text{ sec}^{-1}$, by improving either the stochastic cooling (a factor of two), or

BETA AND DISPERSION FUNCTION IN THE INTERACTION REGION

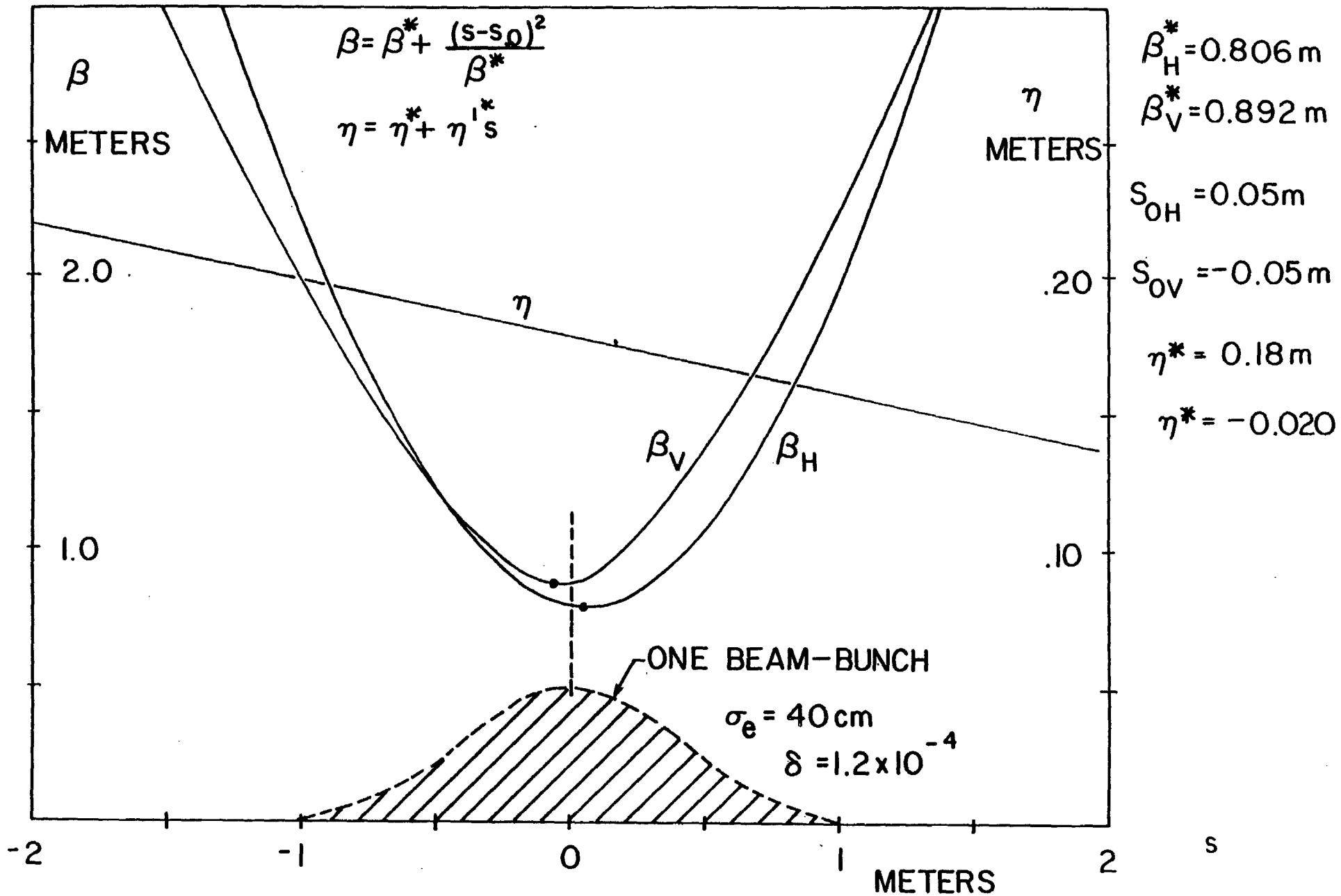


Figure 10-1

DISTRIBUTION OF THE LUMINOSITY

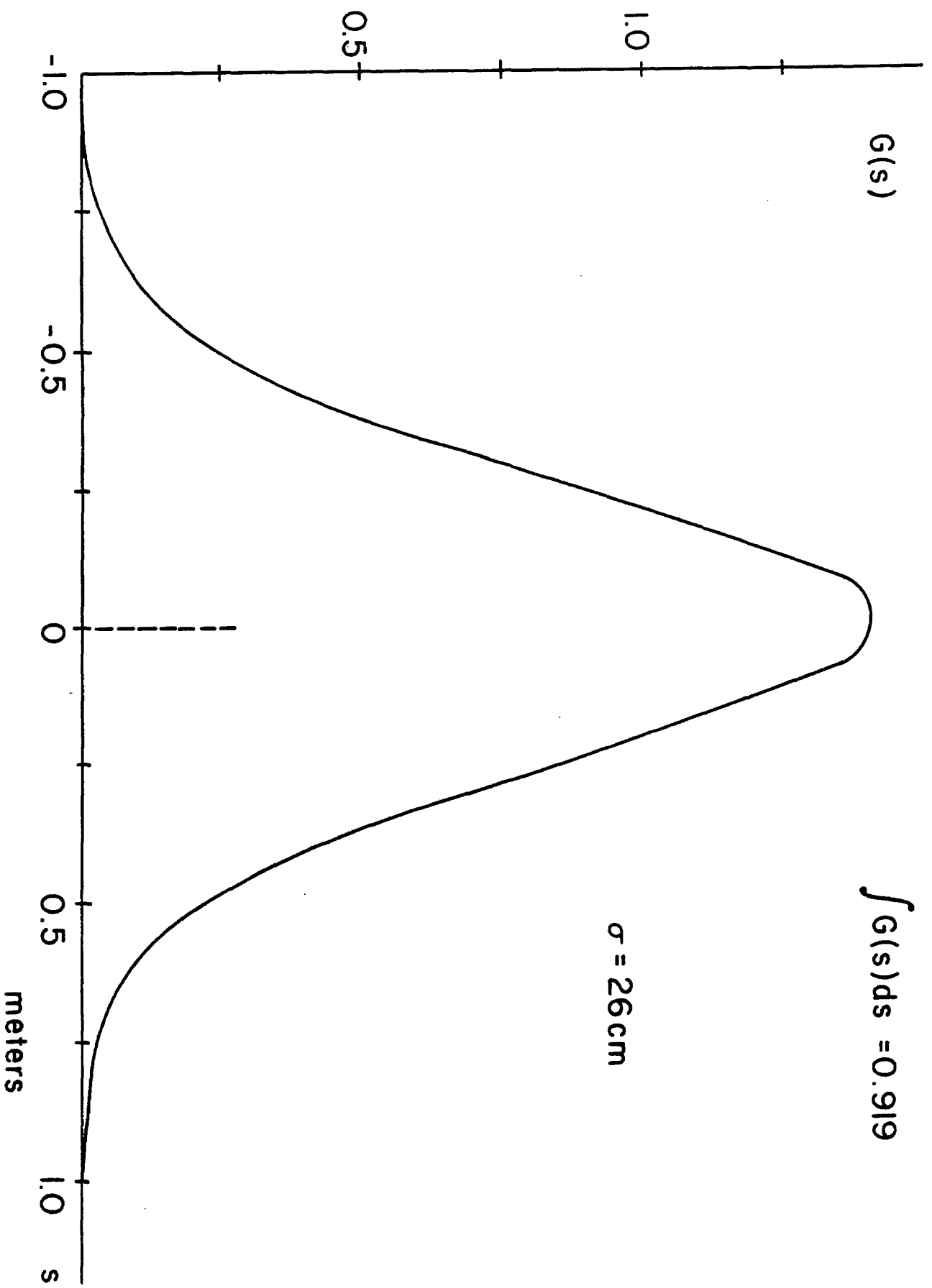


Figure 10-2

the beam intensity in the Main Ring and Tevatron (also possibly by a factor of two) or with 6 bunches per beam instead of the 3 assumed here.

10.4 Beam-Beam Tune Shift

Collisions are head on, the emittances of both beams in both planes are all equal, and the lattice functions are approximately the same in both planes. The beam-beam tune shift is therefore the same for both beams, is independent of the beam energy, and does not depend on the lattice functions. The linear beam-beam tune shift is given by

$$\xi = \frac{3 N r_0}{2 \epsilon_N},$$

where $N = 6 \times 10^{10}$ is the number of particles per bunch, $\epsilon_N = 24\pi$ mm-mrad is the normalized emittance and $r_0 = 1.535 \times 10^{-18}$ m is the classical proton radius. We have

$$\xi = 0.0017/\text{crossing}$$

Even with a low-beta insertion, the beam cross-section in the other five collision regions with normal β values is round and the contribution to the beam size from the momentum spread is negligible. The tune shift per crossing is therefore the same at each crossing so long as the collision is head-on, or at least at an angle $\theta \ll \sigma/\sigma_e$. If there is a total of 6 crossings, the total tune-shift per turn

$$\xi_{\text{tot}} = 6 \xi = 6 \times 0.0017 = 0.01.$$

10.5 Single-Beam and Luminosity Lifetime

We have investigated four possible sources of lifetime deterioration in the Tevatron: scattering by the residual gas, intrabeam scattering, beam-beam effects and beam-beam cross sections. An analysis of periodic or random crossings of nonlinear resonances has also been carried out. This will help to determine not only possible limits on the nonlinearities in the Energy Saver superconducting magnets, but also on the amount of coherent and incoherent noise amplitude allowable.

10.5.1 Effects of Residual Gas¹. The following effects have been investigated:

- (i) Multiple Coulomb Scattering
- (ii) Single Coulomb Scattering
- (iii) Nuclear Scattering

The first effect causes a beam-emittance growth, which leads both to a luminosity decay and a single-beam lifetime in a finite aperture. The single-beam lifetime due to multiple Coulomb scattering is very long and this effect is quite negligible. The second and third effects cause an intensity decay, but the third effect is more important than the second.

The average vacuum pressure expected in the Tevatron is 10^{-8} Torr in the warm regions and 5×10^{-11} Torr in the cold regions with the gas composition:

warm region: 60% H₂ and 40% CO
 cold region: 75% H₂ and 25% He

The intensity decay per beam due to single Coulomb and nuclear scattering is

$$\frac{1}{I} \frac{dI}{dt} = -1.07 \times 10^{-6}/\text{sec} . \quad (10.1)$$

The emittance growth due to multiple Coulomb scattering is

$$\frac{1}{\epsilon} \frac{d\epsilon}{dt} = 1.3 \times 10^{-6}/\text{sec} . \quad (10.2)$$

These effects combined lead to a luminosity decay of

$$\frac{1}{L} \frac{dL}{dt} = -3.44 \times 10^{-6}/\text{sec} ,$$

giving a loss of 23% of the luminosity in 20 hours.

10.5.2 Intrabeam Scattering² To estimate intrabeam scattering diffusion rates for the colliding-beam mode, we have used the same computer code we used to estimate intrabeam scattering for the Accumulator. For our estimate, we have used the actual Tevatron lattice with the low-beta

10.5.3 Beam - Beam Effects. Beam-beam effects have been extensively simulated on the computer. Several issues have been discussed, studied, and, we hope, resolved.

A systematic search for Arnold's diffusion for the Tevatron parameters has given negative results.^{3,4} We have been able to simulate in some cases up to 20 minutes real time of collisions. From our data, we can extrapolate beam-beam lifetimes of several days. We believe the stability of the system arises from the "roundness" of the beam geometry and of the lattice functions.⁵

We found that the addition of the nonlinear beam-beam interaction to a system already affected by external random noise (such as gas scattering) causes an enhancement of the diffusion rates.⁶ The largest enhancement encountered was a factor 6 for a beam-beam tune shift of 0.06 in proximity to the fourth-order resonance.

We have investigated beam-beam interactions with the beam centers offset or oscillating around each other.⁷ This could be caused by either a dipole oscillation or a finite dispersion in the collision region coupled to the momentum oscillation. We have not noticed any effect of significance.

Of more serious concern are the effects created by betatron tune oscillations. If proper care is not taken, it is possible to cause an emittance growth of a factor two in a few minutes.⁸ Fortunately, we have found a threshold and the growth can be tuned out by either adjusting the betatron tunes or by improving the power-supply regulation to better than 10^{-4} and flattening the lattice chromaticity.

At present, we are investigating multiple crossings per revolution, 2 or 6 instead of 1. The emittance growth due to the beam-beam effect has been modeled by the equation

$$\frac{1}{\epsilon_0} \frac{d\epsilon}{dt} = \frac{\sqrt{n_c}}{\tau_{BB}} \frac{N/N_0}{\epsilon/\epsilon_0} \quad (10.5)$$

with n_c the number of crossings and $\tau_{BB} = 100$ hours, which fits observations in the CERN SPS.

10.5.4 Total Cross Section. As the two bunched beams interact with each other, there is a continuous loss of luminosity due to particles being removed by single events or as the beam size grows under the effect of multiple scattering. The total cross-section is built from four pieces,¹⁵ diagrammatically shown in Fig. 10-3. If σ is the cross-section in mb and p the momentum in GeV, the following equations apply

10.5.3 Beam - Beam Effects. Beam-beam effects have been extensively simulated on the computer. Several issues have been discussed, studied, and, we hope, resolved.

A systematic search for Arnold's diffusion for the Tevatron parameters has given negative results.^{3,4} We have been able to simulate in some cases up to 20 minutes real time of collisions. From our data, we can extrapolate beam-beam lifetimes of several days. We believe the stability of the system arises from the "roundness" of the beam geometry and of the lattice functions.⁵

We found that the addition of the nonlinear beam-beam interaction to a system already affected by external random noise (such as gas scattering) causes an enhancement of the diffusion rates.⁶ The largest enhancement encountered was a factor 6 for a beam-beam tune shift of 0.06 in proximity to the fourth-order resonance.

We have investigated beam-beam interactions with the beam centers offset or oscillating around each other.⁷ This could be caused by either a dipole oscillation or a finite dispersion in the collision region coupled to the momentum oscillation. We have not noticed any effect of significance.

Of more serious concern are the effects created by betatron tune oscillations. If proper care is not taken, it is possible to cause an emittance growth of a factor two in a few minutes.⁸ Fortunately, we have found a threshold and the growth can be tuned out by either adjusting the betatron tunes or by improving the power-supply regulation to better than 10^{-4} and flattening the lattice chromaticity.

At present, we are investigating multiple crossings per revolution, 2 or 6 instead of 1. The emittance growth due to the beam-beam effect has been modeled by the equation

$$\frac{1}{\epsilon_0} \frac{d\epsilon}{dt} = \frac{\sqrt{n_c}}{\tau_{BB}} \frac{N/N_0}{\epsilon/\epsilon_0} \quad (10.5)$$

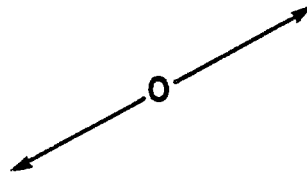
with n_c the number of crossings and $\tau_{BB} = 100$ hours, which fits observations in the CERN SPS.

10.5.4 Total Cross Section. As the two bunched beams interact with each other, there is a continuous loss of luminosity due to particles being removed by single events or as the beam size grows under the effect of multiple scattering. The total cross-section is built from four pieces,¹⁵ diagrammatically shown in Fig. 10-3. If σ is the cross-section in mb and p the momentum in-GeV, the following equations apply

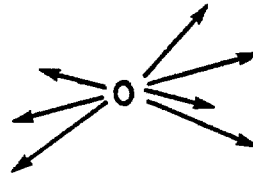
CROSS SECTIONS

THE TOTAL CROSS-SECTION IS BUILT FROM FOUR PIECES:

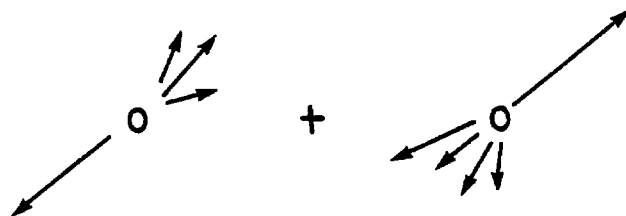
ELASTIC



CORE



SINGLE DIFFRACTIVE



DOUBLE DIFFRACTIVE

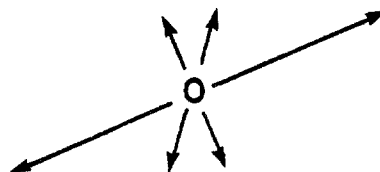


Figure 10-3

for elastic:

$$\frac{d\sigma}{dx'^2} = 18p^2\sigma e^{-18p^2x'^2} \quad (10.6)$$

for single-diffraction and a given beam particle:

$$\frac{d\sigma_{SD}}{d\delta dx'^2} = \frac{6.1p^2}{\delta} e^{-9p^2x'^2} \quad (10.7)$$

for double-diffraction

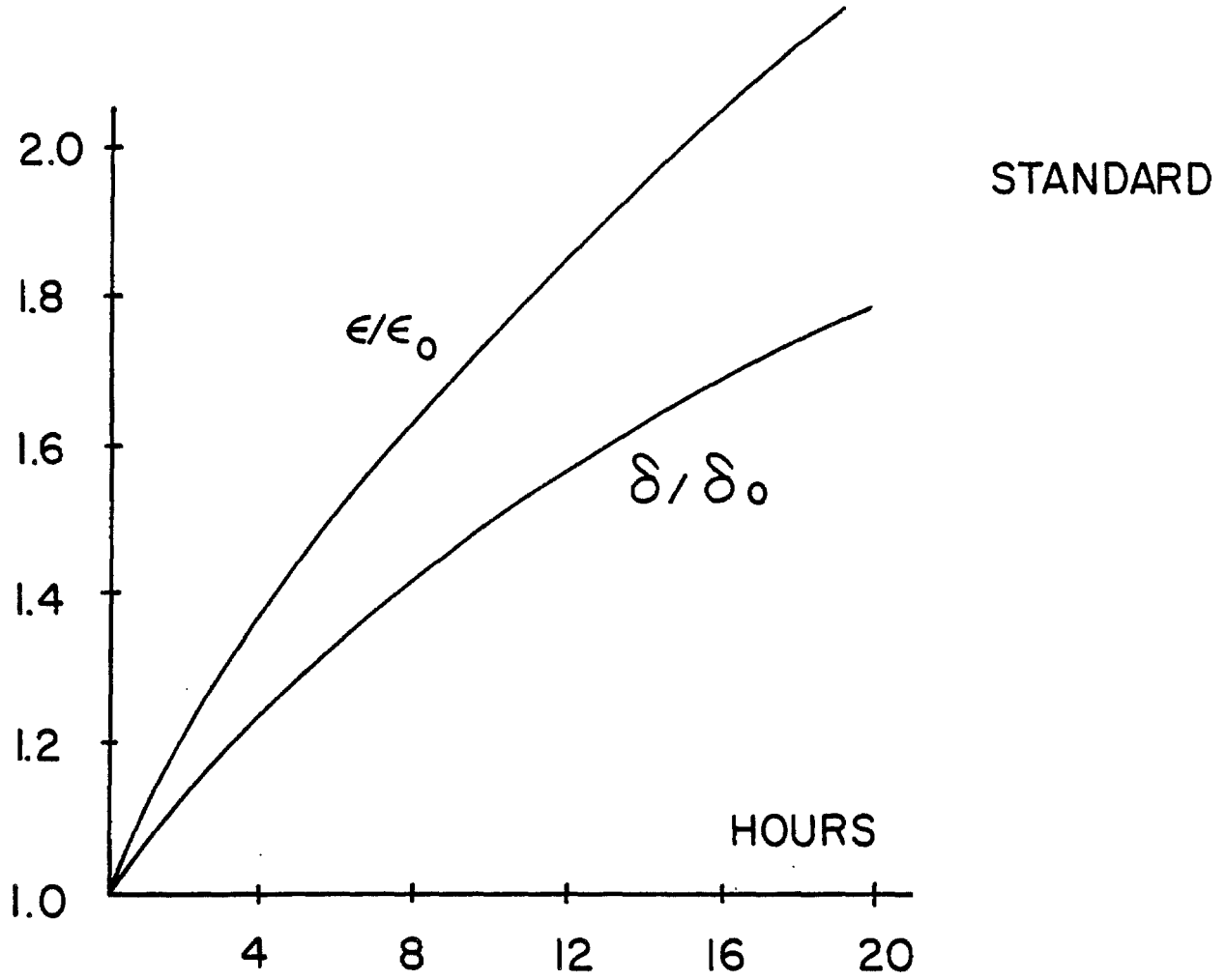
$$\frac{d\sigma_{DD}}{d\delta dx'^2} = \frac{5.3p^2}{\delta} e^{-9p^2x'^2} \quad (10.8)$$

and for the core:

$$\sigma_{CORE} = 26.3 \text{ mb} . \quad (10.9)$$

10.5.5 Luminosity Lifetime. All the effects discussed before have been taken into account to estimate the luminosity lifetime. In Fig. 10-4 we show the variation of the emittance and the momentum spread with time. The luminosity variation with time is shown in Fig.10-5 for an initial value of $10^3 \text{ cm}^{-2} \text{ sec}^{-1}$, which corresponds to the case discussed in the previous sections. The luminosity lifetime is about 20 hours. As we have seen, each beam is made of three bunches, each with 10^{11} particles and a longitudinal area of 3 eV-sec. The beam intensities, both average and peak, are very modest. A considerable effort has been made in the recent past to estimate the longitudinal stability of each beam for both individual bunch and bunch-to-bunch modes.^{9,10} The beam-wall impedance expected in the Tevatron was estimated¹¹ to be $|Z_n|/n \sim 1 \text{ ohm}$. In Fig. 10-7 we give an estimate of the longitudinal-coupling impedance verses the harmonic number. Every contribution from the vacuum-chamber equipment has been included except for the major rf system. Because of the small longitudinal beam density, we believe the beams are quite stable. Moreover, a longitudinal damper operating on each individual bunch is planned.

Fewer calculations have been done for the case of transverse instabilities. But again we do not foresee major problems. In addition, a transverse active damper has been proposed¹² that will be fast enough to operate on individual bunches in both radial and vertical modes of oscillation.

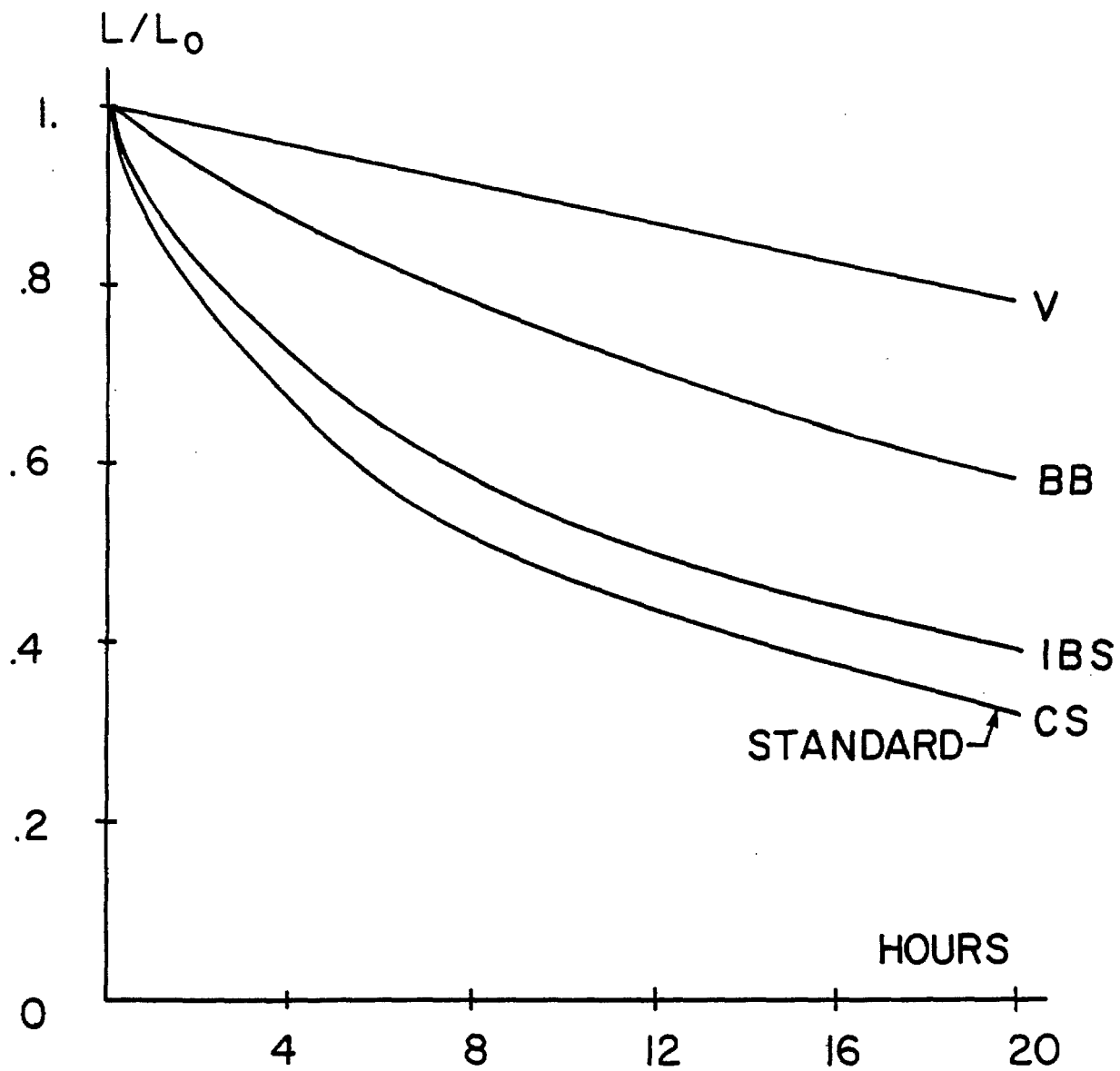


$$\frac{1}{\epsilon_0} \frac{d\epsilon}{dt} \sim \frac{1}{9.2h}$$

FROM INITIAL SLOPES

$$\frac{1}{\delta_0} \frac{d\delta}{dt} \sim \frac{1}{13.6h}$$

Figure 10-4



- V VACUUM EFFECTS ONLY.
- BB BEAM-BEAM EFFECTS ADDED TO ABOVE.
- IBS INTRA BEAM SCATTERING ADDED TO ABOVE.
- CS CROSS-SECTIONS ADDED TO ABOVE.

Figure 10-5

10.6 Collider Filling Strategy.^{13,14}

Because of the luminosity deterioration as a function of time, the refilling of the Tevatron I Collider with fresh beams of protons and antiprotons can be thought of as follows.

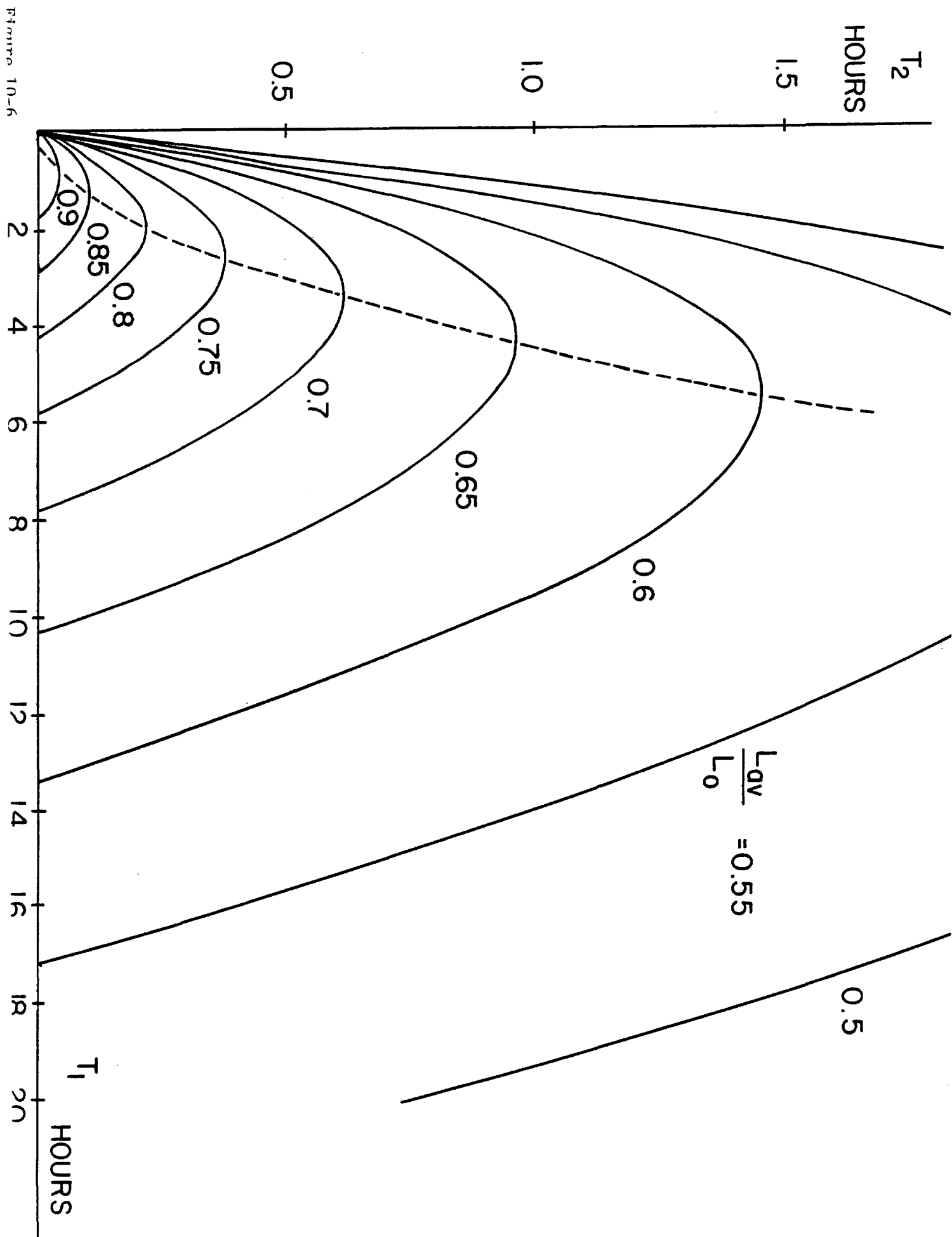
Let T_1 be the running time, that is, the period when colliding beam experiments are usefully done, and let T_2 be the period of pause, that is without beams in the storage ring. One can also include in T_2 the average failure time. The useful average luminosity L_{av} normalized to the initial luminosity L_0 is

$$\frac{L_{av}}{L_0} = \frac{1}{T_1 + T_2} \int_0^{T_1} \frac{L(t)}{L_0} dt \quad (10.10)$$

where $L(t)$ is the actual luminosity as a function of time as given in Fig. 10-5.

For a given ratio L_{av}/L_0 one can derive from Eq. (10.10) the pause T_2 as a function of the running period T_1 . This is shown in Fig. 10-6. For instance, with the present accumulation scheme, except at the first filling, one can produce enough antiprotons for the goal luminosity of $10^{30} \text{cm}^{-2} \text{sec}^{-1}$ in less than 2 hours, it is therefore conceivable to run for a period of 2 hours and rest, for refilling and other inconveniences, for 6 minutes. This would correspond to an average luminosity of 80% of the initial value. To do better than this would require larger production of antiprotons.

FIGURE 10-6



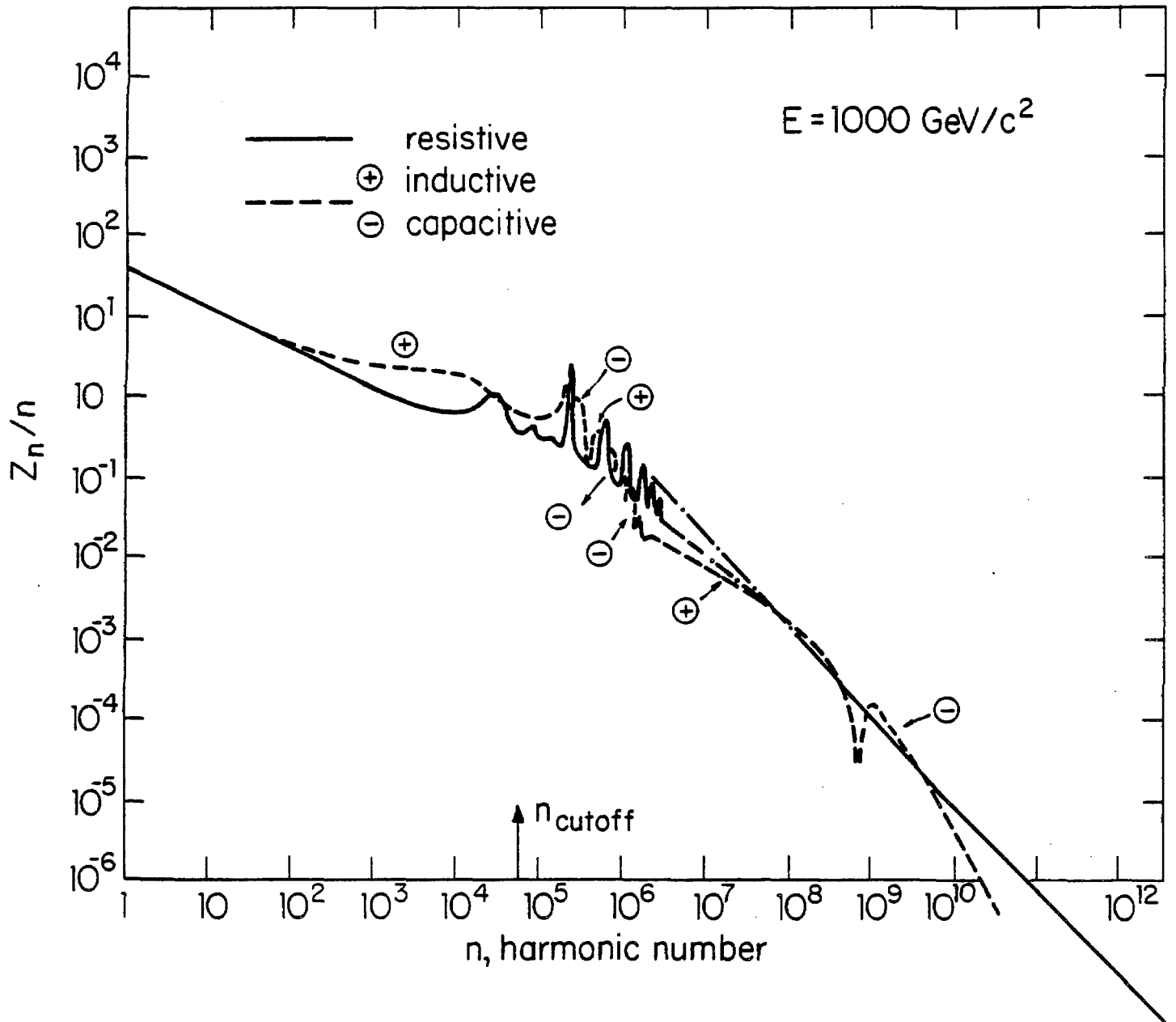


Figure 10-7

References

1. H. Mizuno, S. Ohnuma, A. G. Ruggiero, "Vacuum and Beam Lifetime in the Doubler," UPC No. 119, Fermilab 21, 1979.
2. A.G. Ruggiero, "Revised Intrabeam Scattering Calculations," Fermilab \bar{p} -note 192 (1982), unpublished.
3. D. Neuffer, A. Riddiford, A. Ruggiero, "Searches for Arnold's Diffusion and Chaotic Motion in the Beam-Beam Interaction," 1983 Particle Accelerator Conference IEEE Trans. NS-30, p. 2427 (1983).
4. D. Neuffer, A. Riddiford, A. Ruggiero, "Long Time Simulation of the Beam-Beam Interaction," FN-343, Fermilab, July 1981.
5. A.G. Ruggiero, Particle Accelerators, 12, 45 (1982).
6. D. Neuffer, A. Riddiford, A. Ruggiero, "A Theoretical Model and Computer Simulations to Describe Diffusion Enhancement by the Beam-Beam Interaction," 1983 Particle Accelerator Conference IEEE Trans. NS-30, p. 2430 (1983).
7. D. Neuffer, A. Riddiford, A. Ruggiero, "Effects of Transient and Modulation of Beam Displacement on Long-time Stability with the Beam-Beam Interaction," FN-358, Fermilab, March 1982.
8. D. Neuffer, A. Riddiford, A. Ruggiero, "Study of Periodic Tune Modulation with the Beam-Beam Effect," 1983 Particle Accelerator Conference IEEE Trans. NS-30, p. 2433 (1983).
9. A.G. Ruggiero, "Individual Bunch Longitudinal Instabilities," Fermilab, UPC-72, Jan. 1979.
10. A.G. Ruggiero, "Bunch-to-Bunch Longitudinal Instabilities," Fermilab, UPC-81, Jan. 1979.
11. King-Yuen Ng, "An Estimate of the Longitudinal Coupling Impedance of the Energy Doubler," Fermilab, UPC-150, May 1981.
12. H.W. Miller, "Transverse Active Dampers for the Tevatron," Fermilab, UPC-36, Jan. 1979.
13. A.G. Ruggiero, "Average Luminosity Performance for Tevatron I , Fermilab, \bar{p} note 224, September 1982.
14. A.G. Ruggiero, "Tevatron I Collider Performance", Fermilab, \bar{p} note 240, October 1982.

CHAPTER 11

BEAM - TRANSPORT LINES11.1 120-GeV Proton Transport From F17 to Target (Line AP-1)

The extraction energy for the protons to be used for antiproton production was 80-GeV in an earlier design. It was decided to raise this energy to 120-GeV in order to increase antiproton production. The earliest choice for a 120-GeV extracted beam was to upgrade the then-existing 80-GeV line, which extended 1000 ft from F17 to F25 within the Main Ring tunnel. Although this design satisfied most of the project requirements, it possessed a number of undesirable features. Its estimated power consumption of 2 MW would place a heavy burden on the operating cost of the Antiproton Source. The elements of the 80-GeV line were placed immediately above the Main Ring magnets, below which the Energy Saver magnets have now been installed. As a consequence, difficult operational problems would be encountered wherever work had to be performed on the Main Ring or the Energy Saver. It was necessary to dismantle the 80-GeV beam in many locations in order to install the Energy Saver. The location of the original \bar{p} hall, which is very close to F25, limited the ability to vary the proton targeting. The 80-GeV line had been put in the Main Ring tunnel because the 400-GeV operating schedule in 1977 and 1978 did not allow the several-month interruption that was believed to be needed to modify the Main Ring tunnel at F18 in order to build a more flexible beam. This constraint is no longer relevant. For these reasons, a more efficient and flexible beam design was developed.

The design of the 120-GeV proton transport line was based on the following requirements:

- (i) It must leave the Main Ring tunnel as close as possible to location F18.
- (ii) The target elevation is to be 7.0 ft above Main Ring beam height.
- (iii) It must transport a 120-GeV proton beam with a momentum spread of $\pm 0.2\%$.
- (iv) It must be possible to bypass the target and collection system in the reverse direction.
- (v) It must transport the 8.9-GeV/c cooled antiproton beam with an emittance of 2.0π mm-mrad.
- (vi) It must produce a round proton beam spot at the target which can be varied from 0.2 mm to 0.8 mm rms.
- (vii) It must have zero dispersion at the target.

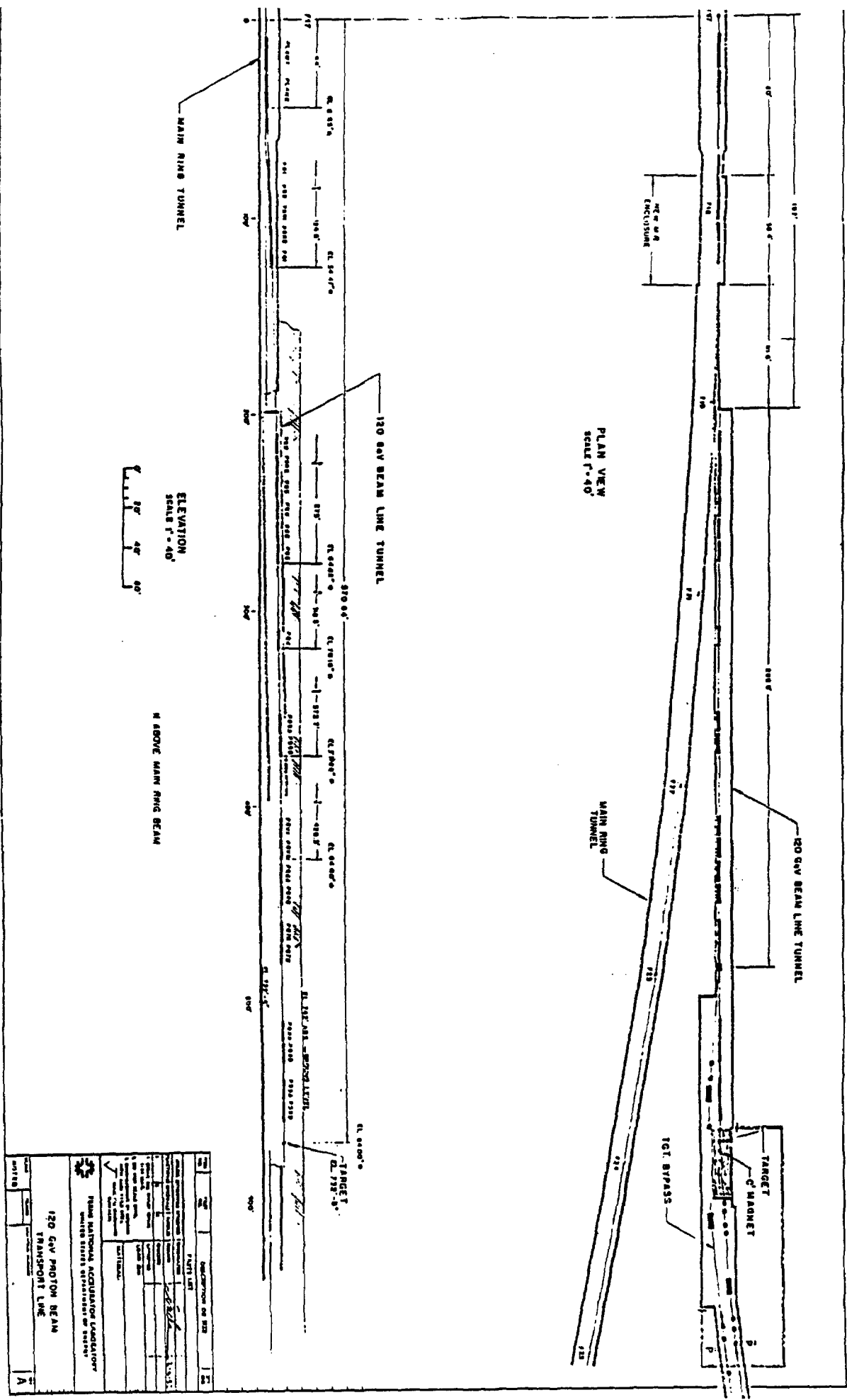
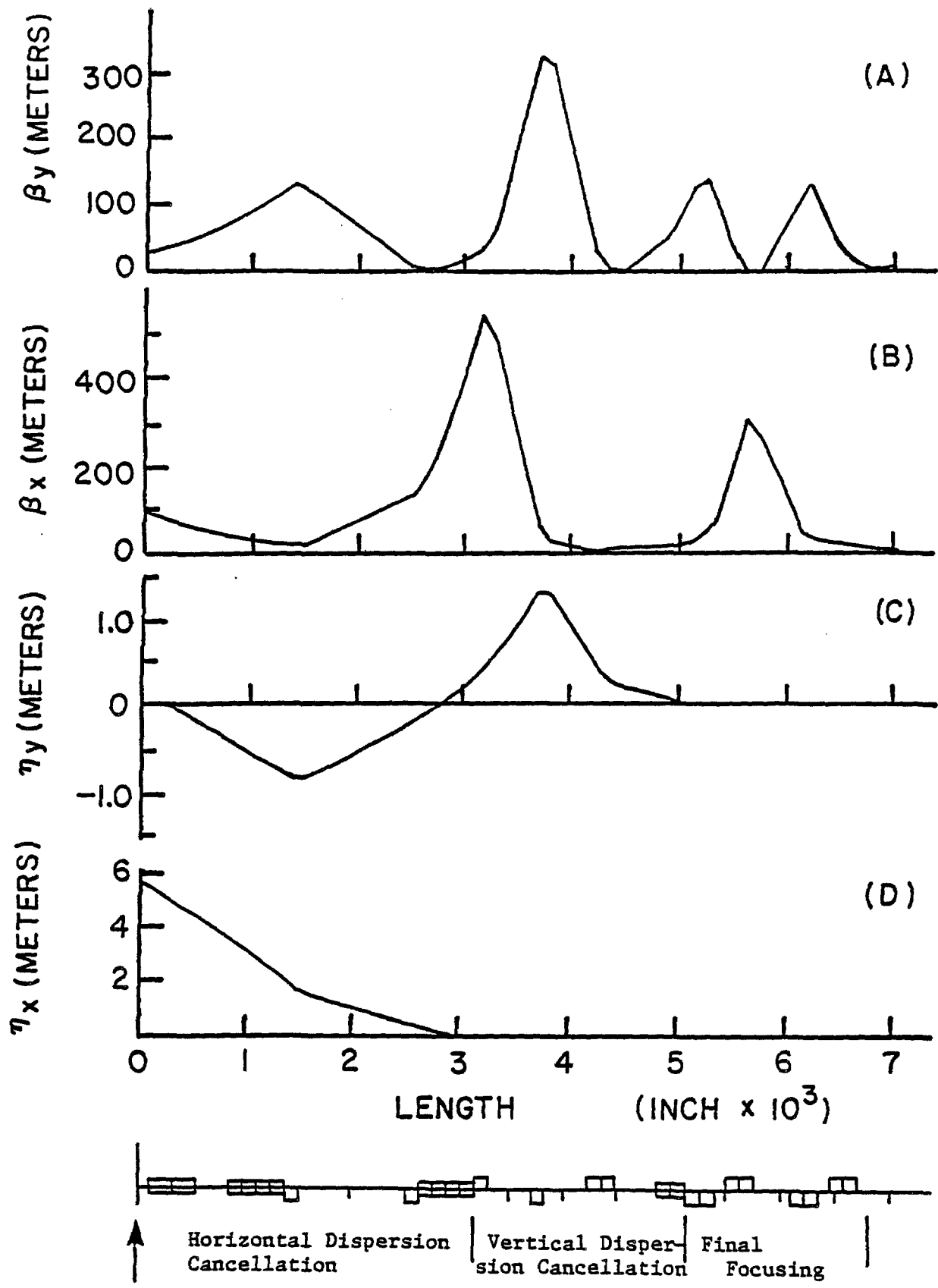


Figure 11-1

 FERMI NATIONAL ACCELERATOR LABORATORY UNITED STATES DEPARTMENT OF ENERGY	
120 GeV PROTON BEAM TRANSPORT LINE	
TITLE: 120 GeV PROTON BEAM TRANSPORT LINE DATE: 11/11/80 DRAWN BY: [Signature] CHECKED BY: [Signature]	REVISIONS: NO. 1: [Signature] NO. 2: [Signature]
PROJECT NO.: 80-11 DRAWING NO.: 11-1	SCALE: AS SHOWN SHEET NO.: A



F17

Figure 11-2 Twiss parameters β_y , β_x and dispersion functions η_y , η_x through the 120^{GeV} beam transport system.

(viii) The power consumption must remain below 500 kW.

A layout of the beam is shown in Fig. 11-1 and its parameters are tabulated in Table 11-I. In Fig. 11-2 we show the behavior of the monoenergetic β_y , β_x , η_y , and η_x through the system from extraction to the target. The beam consists of 10 EPB dipoles excited to a field of 13 kG or less and 14-3Q120 quadrupoles excited to a field gradient of 4.75 kG/in. or less. Three of the dipoles, indicated by (R), are rotated by 45° to achieve the necessary vertical and horizontal bends with the minimum number of magnets. The Main Ring tunnel must be widened over a distance of roughly 18 m in order to accommodate the four EPB dipoles and one 3Q120. The length of the beam is 174 m, of which 41 m is located in the Main Ring tunnel. The remainder of the beam elements are located in a new 115-m long enclosure. The new enclosure and the Main Ring tunnel are connected by an 18-m long pipe.

A 4.5° bending magnet, which bends the reverse antiproton beam to the left, is placed within the final focus section between PQ7B and PQ8A in order to allow the target and antiproton collection lens to be bypassed whenever cooled antiprotons are transported back to F17. The total power consumption of the beam is estimated to be less than 390 kW. In Table 11-II the gradients of the four final focusing quadrupoles, which obtain the required range of beam sizes, are listed.

TABLE 11-I 120-GEV TRANSPORT ELEMENTS

NAME	DIST. FROM F17(m)	TYPE	FIELD (T)	GRADIENT (T/m)	FUNCTION
P-LAM1	2.74	Lamberston	1.25		Bend up
P-LAM2	8.38	Lambertson	1.25		Bend up
PB1	21.7	EPB	1.271		Bend Left
PB2	25.0	EPB	1.271		Bend Left
PBR1	28.4	EPB (R)	1.271		Bend Left/Down
PBR2	31.7	EPB (R)	1.271		Bend Left/Down
PQ1	35.1	3Q120		6.59	Vertical Focusing
PQ2	64.2	3Q120		4.85	Vertical Focusing
PBR3	67.5	EPB (R)	1.271		Bend Right/Down
PB3	70.9	EPB	1.271		Bend Right
PB4	74.2	EPB	1.271		Bend Right
PB5	77.6	EPB	1.271		Bend Right
PQ3	80.9	3Q120		12.09	Horiz. Focusing
PQ4	94.1	3Q120		15.96	Vertical Focusing
PQ5A	107.3	3Q120		18.30	Horiz. Focusing
PQ5B	110.7	3Q120		18.30	Horiz. Focusing
PBV1	123.7	EPB	0.782		Bend Down
PBV2	127.0	EPB	0.782		Bend Down
PQ6A	130.7	3Q120		11.43	Vertical Focusing

PQ6B	134.1	3Q120	11.43	Vertical Focusing
PQ7A	139.6	3Q120	10.27	Horiz. Focusing
PQ7B	143.0	3Q120	10.27	Horiz. Focusing
PQ8A	154.9	3Q120	12.38	Vertical Focusing
PQ8B	158.3	3Q120	12.38	Vertical Focusing
PQ9A	163.9	3Q120	9.27	Horiz. Focusing
PQ9B	167.2	3Q120	9.27	Horiz. Focusing
TARGET	174.1			

TABLE 11-II GRADIENT OF FINAL FOCUSING QUADRUPOLES
AS A FUNCTION OF BEAM SIZE AT THE TARGET, IN T/m.
(MAXIMUM GRADIENT 18T/m)
QUADRUPOLES

$\beta^*(m)$	$\sigma(mm)$	PQ6A/B	PQ7A/B	PQ8A/B	PQ9A/B
1.17	0.20	-13.2	+10.3	-12.1	+13.2
4.69	0.40	-11.4	+10.3	-12.4	+ 9.3
18.75	0.79	-10.3	+ 9.7	- 9.8	+ 2.0

11.2 8-GeV Antiproton Transport to Debuncher (Line AP-2)

The antiproton transport line is shown symbolically in Fig. 11-3. This beam line can transport an 8-GeV beam with 20π mm-mrad transverse emittance and $|\Delta p/p| > 4.0\%$. The match to the Debuncher is accomplished with an integrated efficiency of 80% over the 4.0% passband in $\Delta p/p$. Independent controls for emittance definition in both x and y planes and $\Delta p/p$ selection are possible using collimators. The detailed design can be found in Reference 9.

The "source" for the beam line is the center of the 5.0 cm \bar{p} production target. For the purpose of the transport calculations we have assumed a circular spot and a β^* of 2.25 cm. The lithium lens collector then performs point to parallel optics for negatives with a momentum of 8.9-GeV/c (8-GeV \bar{p}). The beam line consists of five basic sections: (i) cleanup, (ii) long transport, (iii) left bend, (iv) long transport, and (v) injector. Section (i) uses a pulsed C magnet to bend the 8-GeV \bar{p} 3° left, and two quadrupole doublets and another 3° bend left in order to complete the achromatic transformation. Charge, central momentum and vertical emittance ϵ_y are selected within this section using collimators. The long transport sections (ii) and (iv) consist of 90° FODO quadrupole cells and matching quadrupole lenses. The periodic structure has a cell length of 88.81 ft. with $\beta_{max}/\beta_{min}=45.93m/7.98m$. The left bend (iii) which deflects the antiproton by 36.53° , consists using of six dipoles. Horizontal emittance (ϵ_x) selection is performed at the entrance and exit of this section where β_x is nearly 80 m. The fine $\Delta p/p$ selection is performed in the center of the left bend section where $\beta_x = 5.0$ m and a maximum in the dispersion $\eta_x^* = 2.62$ m is obtained. The first-order momentum resolving

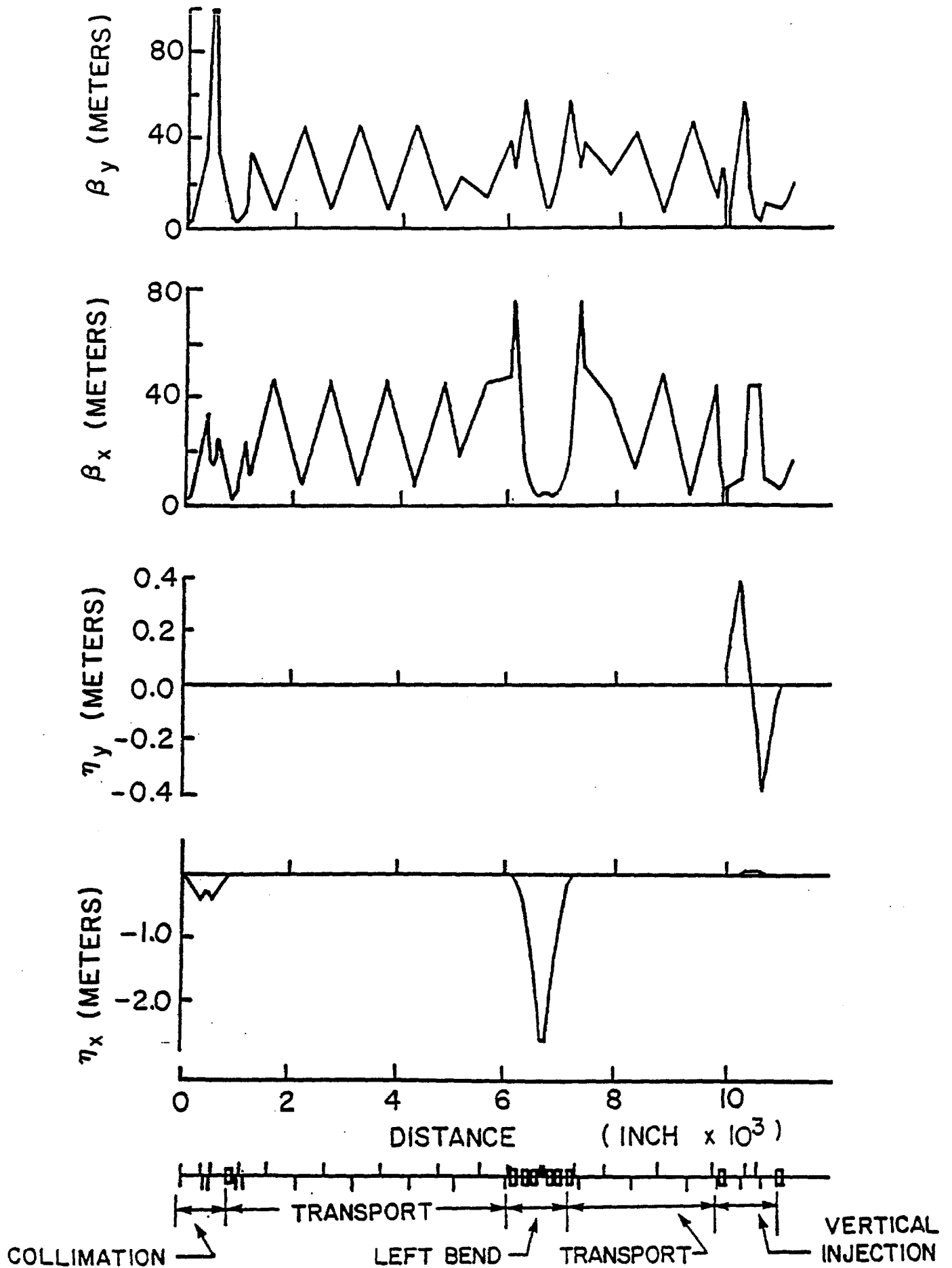


Figure 11-3 The antiproton transport line to the Debuncher monoenergetic envelope functions β_y , β_x and dispersion functions η , η_x .

power is 1.31 for $\epsilon_x = 20\pi$ mm-mrad and $\Delta p/p = 1.0\%$ and 2.62 for $\epsilon_x = 5\pi$ mm-mrad. The injector (v) is an achromatic vertical translation ending at the downstream end of the 2.1 m long current septum. The beam is deflected downward by 48 inches using 3.62° bends.

The components for the beam line are listed in Table 11-V.

TABLE 11-III BEAM TRANSPORT TARGET TO DEBUNCHER

COORDINATES GIVEN AT DOWNSTREAM END OF ELEMENT
(TOWARD DEBUNCHER)
MAIN RING STATION A0/ AT X=0.0, Y=0.0

NAME	LENGTH (IN)	FIELD (KG-KG/M)	X (FT)	Y (FT)	Z (FT)
TARGET			585.940	-2064.263	732.500
LITHIUM LENS	5.9055	9754.00	585.215	-2063.598	
C-MAGNET	11.811	51.75	581.934	-2060.622	
IQ1	27.60	154.70	561.184	-2043.495	
IQ2	27.60	-130.45	557.880	-2040.768	
IQ3	27.60	-130.45	552.250	-2036.121	
IQ4	27.60	154.70	548.947	-2033.394	
IB1	65.37	9.35	527.402	-2015.795	
IQ5	27.60	155.43	515.067	-2006.655	
IQ6	27.60	-155.43	510.641	-2003.376	
IQ7	27.60	44.98	481.358	-1981.679	
IQ8	27.60	-44.98	446.211	-1955.636	
IQ9	27.60	44.98	411.064	-1929.593	
IQ10	27.60	-44.98	375.917	-1903.551	
IQ11	27.60	44.98	340.770	-1877.508	
IQ12	27.60	-44.98	305.623	-1851.466	
IQ13	27.60	44.98	270.476	-1825.423	
IQ14	27.60	-44.98	250.490	-1810.614	
IQ15	18.00	37.91	199.266	-1772.659	
IQ16	25.20	-99.99	186.012	-1762.838	
IQ17	32.60	99.99	182.906	-1760.537	
IB2	98.43	12.61	174.482	-1754.837	
IQ18	25.20	-64.33	169.374	-1751.835	
IB3	98.43	12.61	158.798	-1746.123	
IB4	98.43	12.61	147.517	-1741.493	
IQ19	25.20	64.33	141.882	-1739.633	
IQ20	25.20	64.33	135.488	-1737.523	
IB5	98.43	12.61	123.937	-1734.168	
IB6	98.43	12.61	111.933	-1732.023	
IQ21	25.20	-64.33	106.041	-1731.394	
IB7	98.43	12.61	94.051	-1730.553	
IQ22	32.60	100.25	89.359	-1730.553	
IQ23	25.20	-103.81	83.468	-1730.553	
IQ24	18.00	63.26	39.522	-1730.553	

SCALES, MIN. HOR -100.00 MM
MAX. 100.00

HORIZONTAL BEAM SIZE
TARGET TO DEBUNCHER

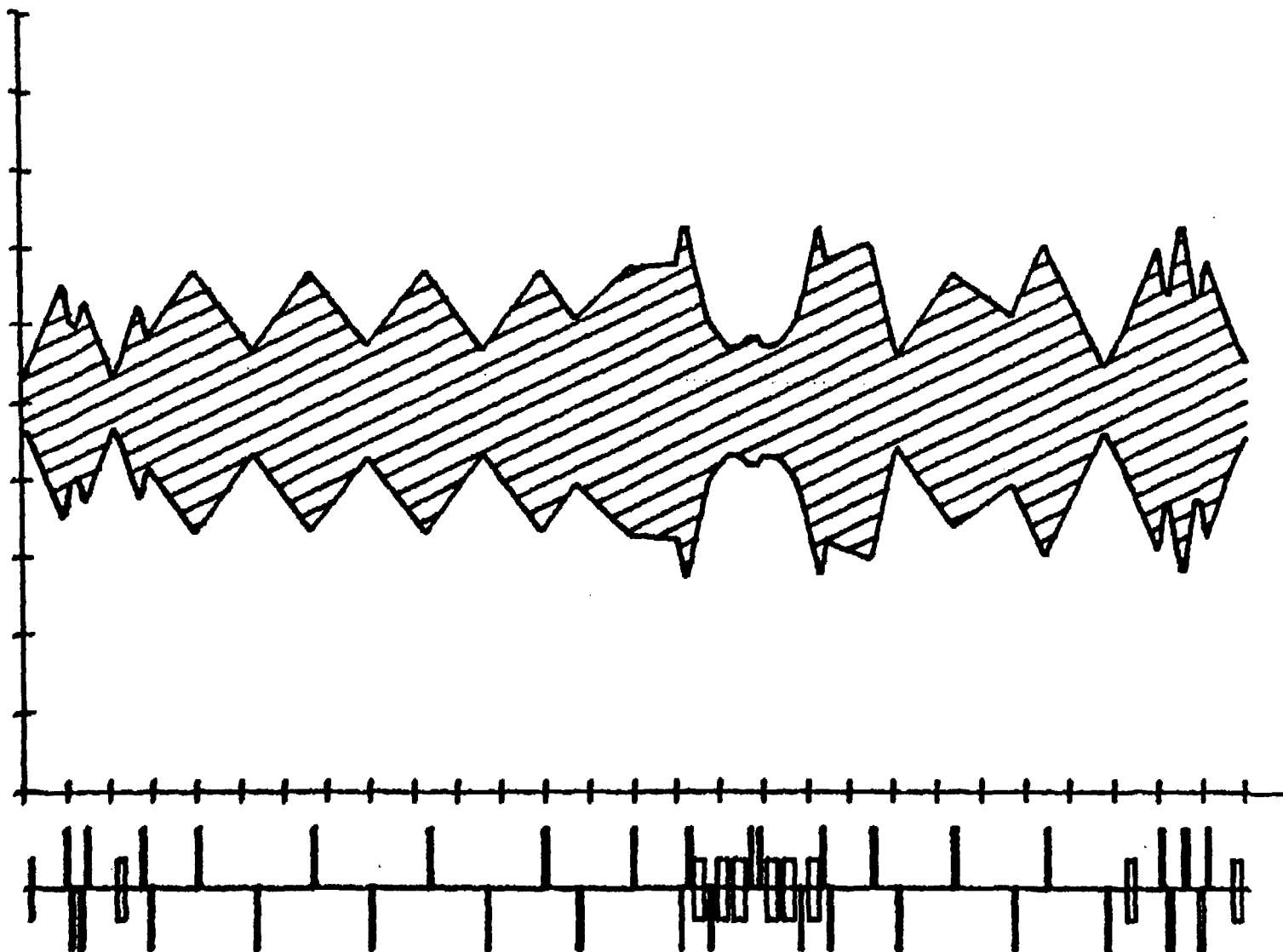


Figure 11-4a

SCALES, MIN. VER -100.00 MM
MAX. 100.00

VERTICAL BEAM SIZE
TARGET TO DEBUNCHER

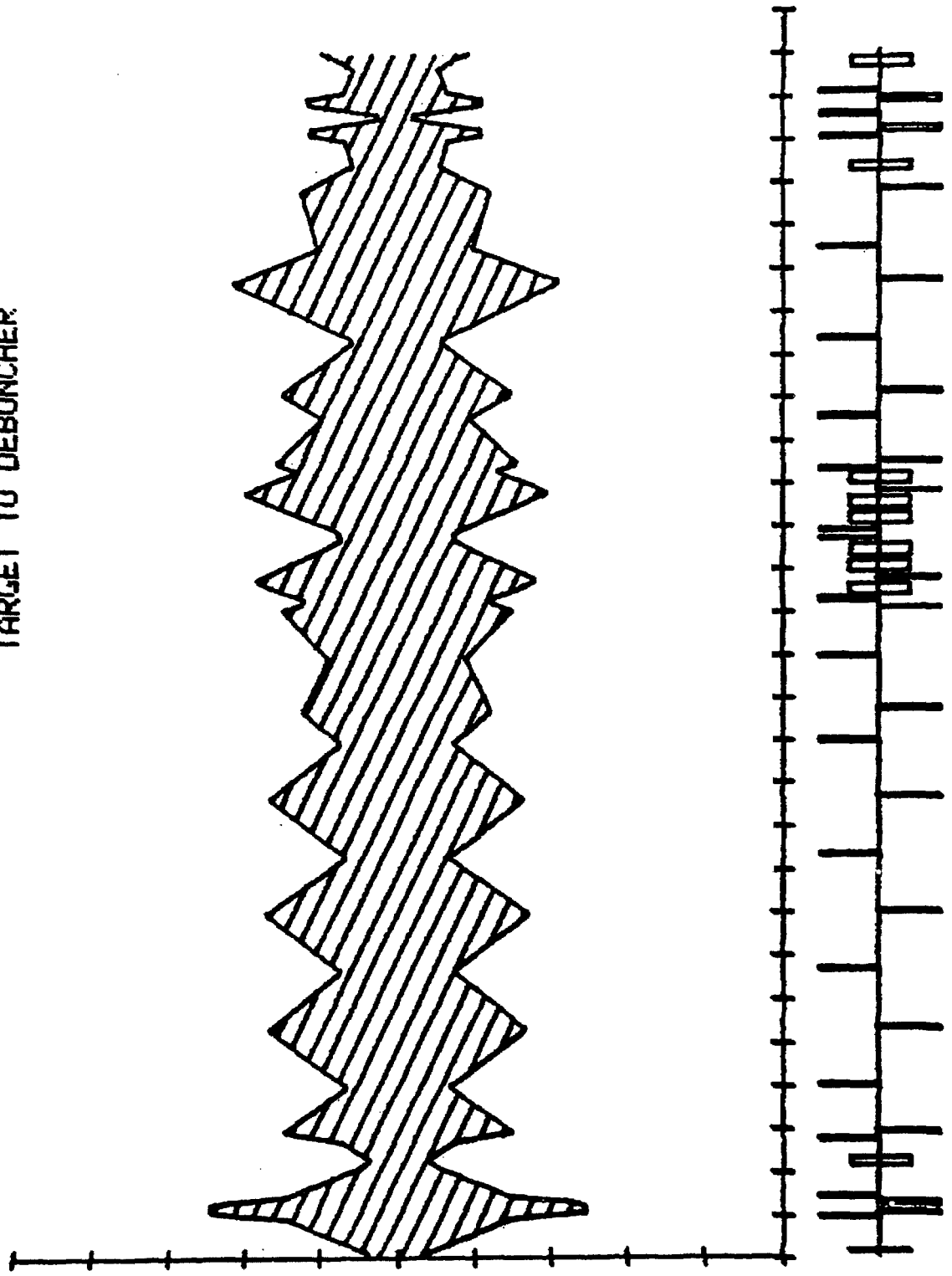


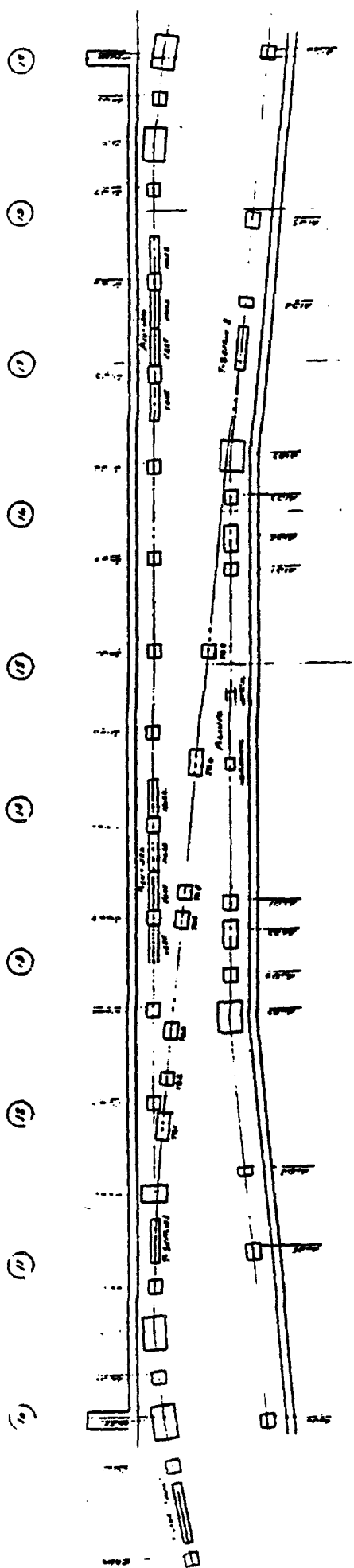
Figure 11-4b

IQ25	32.60	-63.47	22.513	-1730.553	
IQ26	18.00	58.27	-18.141	-1730.552	
IQ27	18.00	-58.27	-61.545	-1730.552	
IQ28	18.00	58.27	-101.668	-1730.552	
IQ29	32.60	-167.99	-146.819	-1730.552	732.500
IQ30	32.60	161.10	-150.536	-1730.552	732.500
IBV1	120.00	6.15	-161.529	-1730.552	732.184
IQ31	50.16	-148.46	-180.319	-1730.551	730.994
IQ32	50.16	148.46	-189.092	-1730.551	730.438
IQ33	50.16	-148.46	-195.137	-1730.551	730.055
NOW IN DEBUNCHER RING					
D4Q5	34.40	83.73	-215.554	-1730.551	728.500
I-SEPTUM	84.00	5.63	-223.545	-1730.551	728.500

Fig. 11-3 shows the evolution of the monoenergetic β_y and β_x envelope functions and the beam dispersions η_y and η_x through the transport line from the target to the downstream end of the injection kicker. Figure 11-4 shows beam envelopes through the line.

11.3 Debuncher to Accumulator Transfer (Line D to A)

The beam transfer between the Debuncher and the Accumulator is a horizontal transfer taking place in the 10 straight section. Extraction from the Debuncher is accomplished with a kicker and a septum magnet, as shown in Fig. 11-5. The quadrupole after the septum magnet, QD3, has a large aperture to accommodate both the circulating and the extracted beam. This quad kicks the beam further to the inside of the ring toward the Accumulator. The horizontal displacement of the extracted beam from the magnet axis is 5 in. After extraction, the beam is transported to the Accumulator with no further bending through a string of 6 quadrupoles. At the Accumulator, the beam is injected onto a path displaced from the central momentum by $\Delta p/p = +0.775\%$ with a 12-kG 7 ft long pulsed septum placed between A1B3 and A1S3. Finally the beam is kicked onto the proper orbit in the Accumulator with a 500-G, 7 ft long shutter kicker placed in the A20 straight section. A plot of the lattice functions of the transfer line is shown in Fig. 11-6 and the elements are listed in Table 11-IV. Figure 11-7 shows beam envelopes through the line.



Plan - Drawing 11/6

Beam Transfer From Debuncher To Accumulator

Figure 11-5

SCALES, MIN. BETA 0.00 ETA -10.00 LATTICE FUNCTIONS
 MAX. 200.00 10.00 DEBUNCHER TO ACCUMULATOR

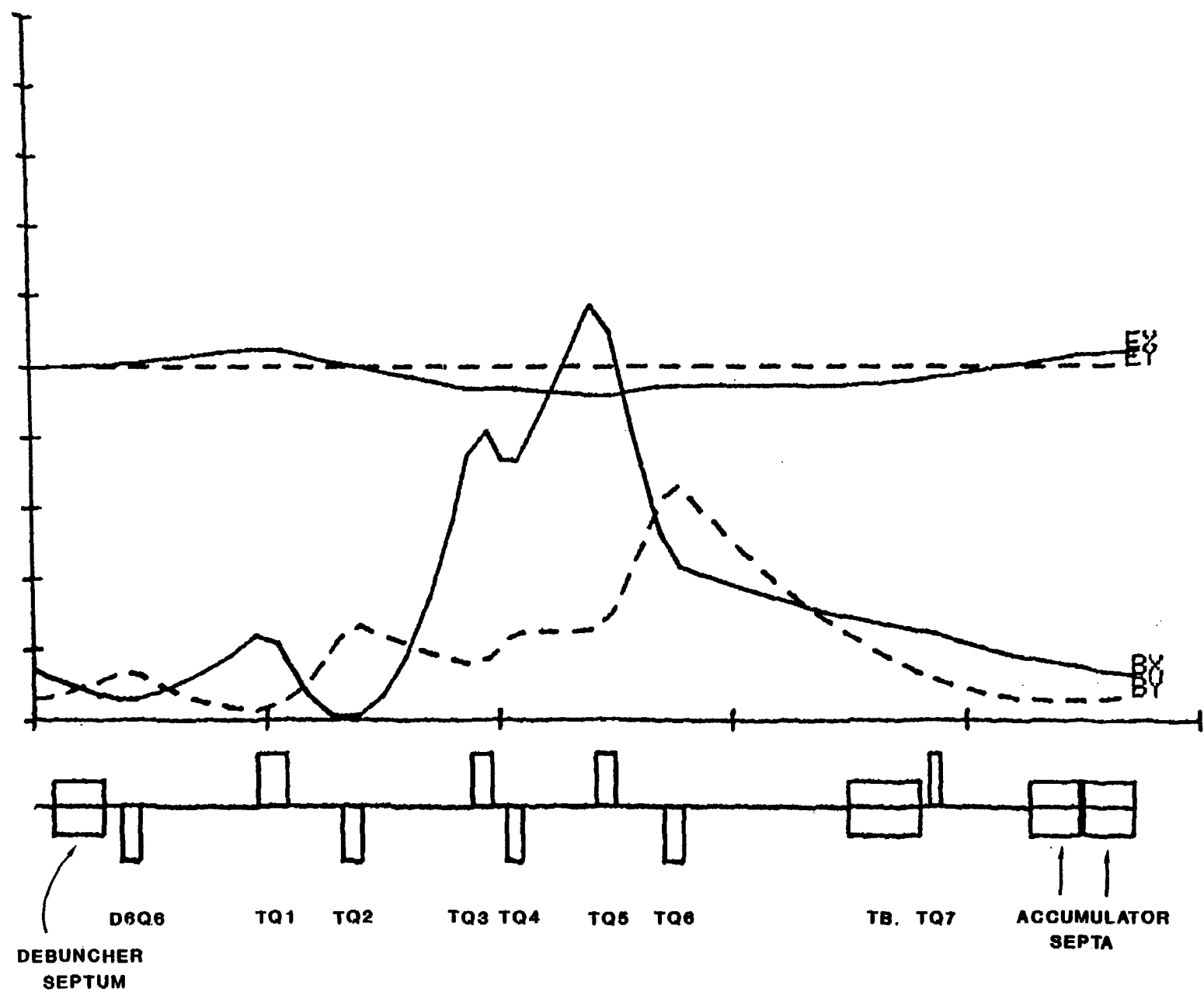


Figure 11-6

SCALES. MIN. HOR -100.00 MM HORIZONTAL BEAM SIZE
 MAX. 100.00 DEBUNCHER TO ACCUMULATOR

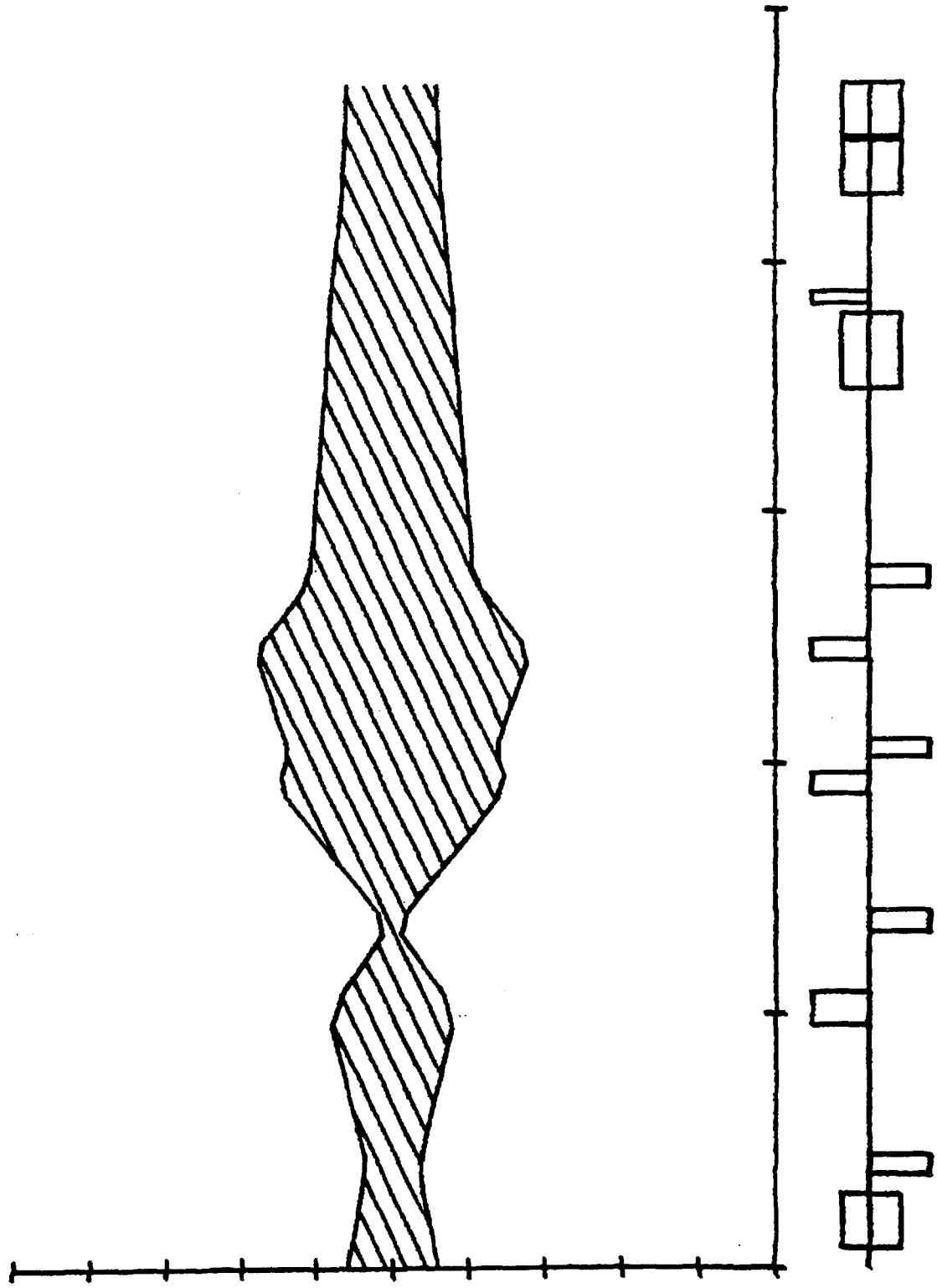


Figure 11-7a

SCALES, MIN. USER -100.00 MM
MAX. 100.00

VERTICAL BEAM SIZE
DEBUNCHER TO ACCUMULATOR

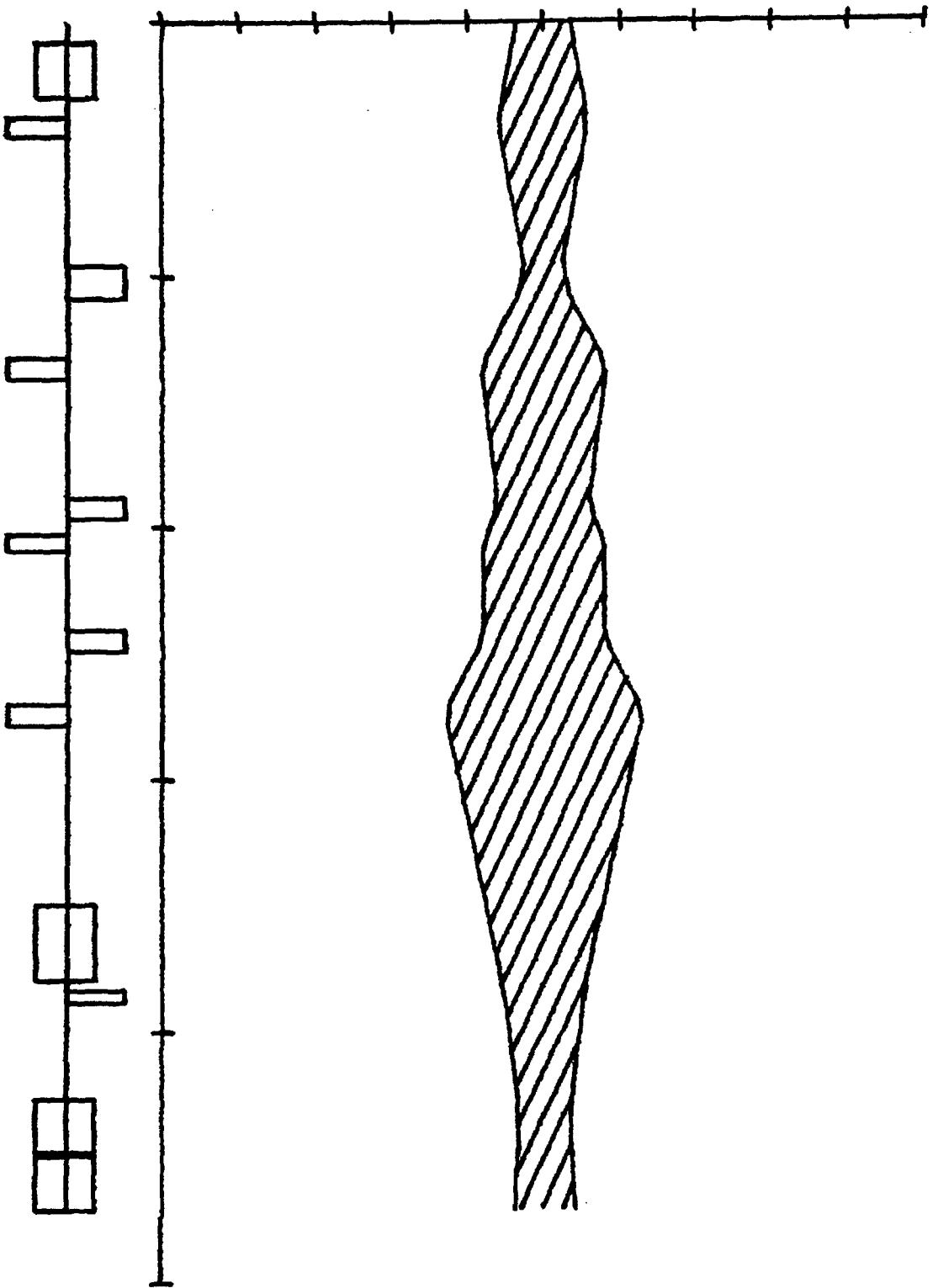


Figure 11-7b

TABLE 11-IX BEAM TRANSFER, DEBUNCHER TO ACCUMULATOR

Element	Name	Length (m)	Field
Debuncher kicker		3.0480	459.32 G
Septum	TS1	2.1336	7.03 kG
Drift		0.3099	
Debuncher Quad	D6Q6	0.4140	-96.24 kG/m
Drift		5.1272	
Quad	TQ1	1.3120	70.12 kG/m
Drift		2.1527	
Quad	TQ2	0.8280	-90.68 kG/m
Drift		4.4904	
Quad	TQ3	0.8280	90.68 kG/m
Drift		0.5818	
Quad	TQ4	0.7010	-90.68 kG/m
Drift		5.2097	
Quad	TQ5	1.3120	70.12 kG/m
Drift		3.5860	
Quad	TQ6	0.8280	-90.68 kG/m
Drift		4.8706	
Quad	TQ7	0.7010	94.22 kG/m
Drift		5.8240	
Septum	TS2	2.1336	11.72 kG
Accumulator Kicker		2.1336	515.56 G

11.4 Accumulator to Main Ring Transport (Line AP-3)

Two separate downward bends of 50 mrad each eventually restores the extracted beam to target height ($\Delta z=48.0$ in.). Then the beam is taken through four modules consisting of: (i) long transport, (ii) left bend, (iii) long transport, and (iv) target bypass. Following this, the beam rejoins the 120-GeV proton line just downstream of quadrupole PQ7B and is reverse-injected into the Main Ring at F17. The orbit parameters are identical for 120-GeV protons and 8-GeV antiprotons at this point.

The long transport (iii) parallels the long transport carrying the hot \bar{p} to the Debuncher. The target bypass is an achromatic transport using three dipoles and three quadrupoles. Figure 11-8 shows the behavior of the monoenergetic β_y , β_x , η_y , and η_x functions through the extraction system, starting at the Lambertson and ending at the downstream end of EB6. Figure 11-9 shows beam envelopes through the line.

Table 11-V lists the antiproton transport line elements from the Accumulator to the match point in the proton extraction line (EB6).

TABLE 11-V BEAM TRANSPORT ACCUMULATOR TO TARGET BYPASS

X,Y,Z Site Coordinates

Coordinates given at end of element (toward target)

Main Ring Station A0 at X=0.0, Y=0.0

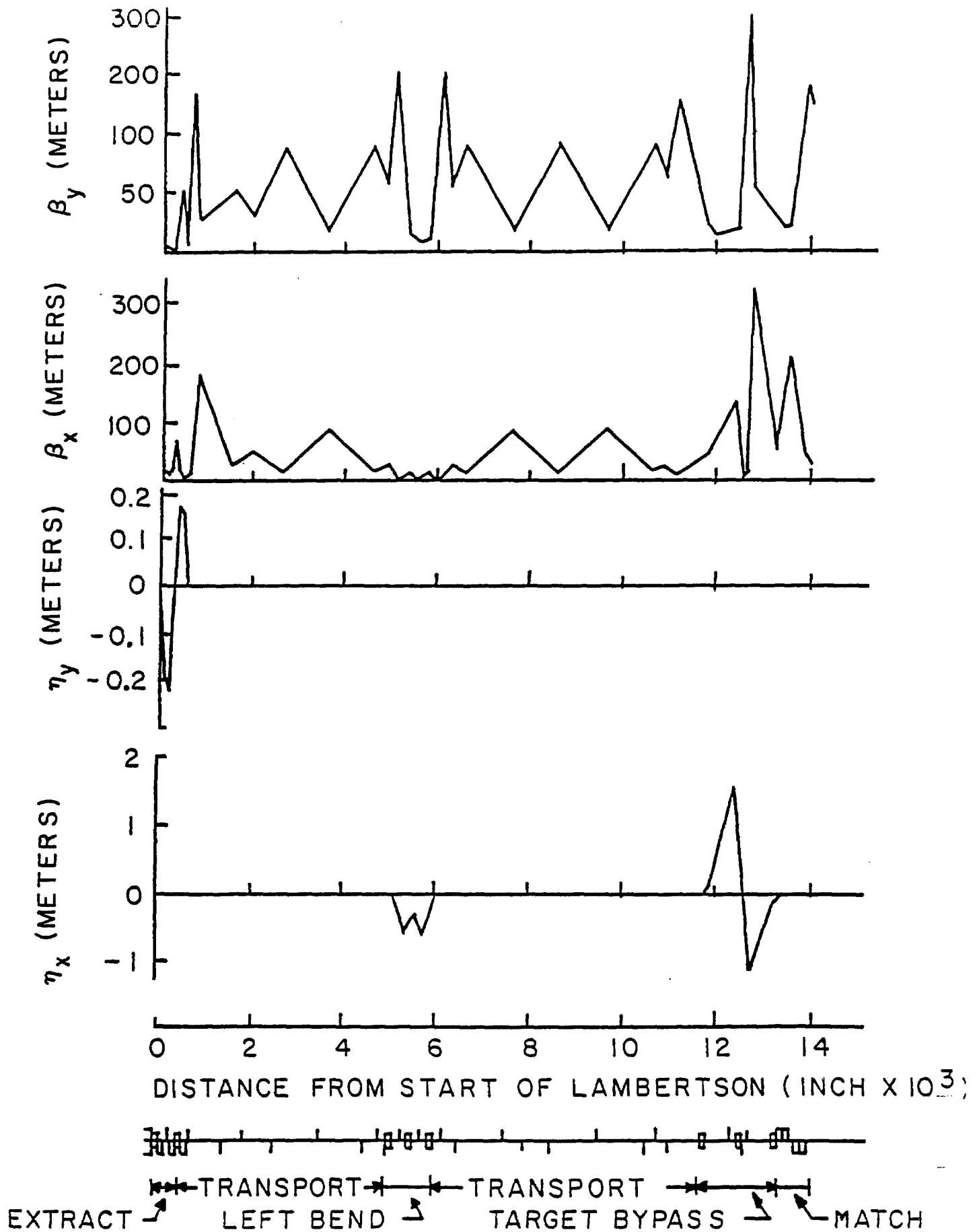


Figure 11-8 Beam functions β_y , β_x and dispersion functions η_y , η_x for the antiproton beam transport from the Accumulator to the 120 GeV proton transport line.

NAME	LENGTH (IN)	FIELD (KG-KG/M)	X (FT)	Y (FT)	Z (FT)
ACCUMULATOR RING					728.500
E-LAMBERTSON	115.00	10.15	-117.287	-1350.965	728.979
EQ1	27.60	-149.90	-108.199	-1363.943	730.570
EBV1	75.00	7.79	-103.892	-1370.094	731.167
EQ2	32.60	149.90	-100.775	-1374.545	731.439
EQ3A	32.60	-186.99	-96.224	-1381.013	731.834
EQ3B	32.60	-186.99	-94.118	-1384.053	732.020
EQ4	25.20	149.90	-91.452	-1387.860	732.253
EBV2	75.00	7.79	-86.827	-1394.466	732.500
EQ5	27.60	149.90	-84.934	-1397.169	
EQ6	32.60	-149.90	-82.420	-1400.760	
EQ7	18.00	-10.83	-74.605	-1411.921	
EQ8	51.64	33.35	-56.994	-1437.072	
EQ9	18.00	-33.33	-33.701	-1470.338	
EQ10	18.00	66.10	-0.222	-1518.150	
EQ11	18.00	-68.49	17.277	-1543.142	
EQ12	18.00	68.49	55.185	-1597.281	
EQ13	18.00	-68.49	101.488	-1663.409	
EQ14	18.00	18.47	111.220	-1677.308	
EQ15	18.00	99.34	122.940	-1694.045	
EB1	98.43	12.74	128.952	-1701.864	
EQ16	27.60	-13.94	136.041	-1709.975	
EB2	98.43	12.74	152.636	-1728.293	
EQ17	27.60	109.27	163.734	-1738.531	
EB3	98.43	12.74	176.839	-1750.022	
EQ18	18.00	-103.08	179.651	-1752.105	
EQ19	18.00	114.32	200.074	-1767.238	
EQ20	25.20	-36.29	214.676	-1778.058	
EQ21	18.00	36.29	280.264	-1826.656	
EQ22	18.00	-36.29	347.246	-1876.288	
EQ23	18.00	36.29	414.228	-1925.920	
EQ24	18.00	-36.29	481.210	-1975.552	
EQ25	18.00	66.85	501.346	-1990.472	
EQ26	18.00	-61.33	510.619	-1997.342	
EB4	98.43	12.43	563.486	-2037.050	
EQ27	25.20	129.29	597.944	-2068.671	
EB5	65.37	14.03	609.774	-2079.818	
EQ28	27.60	-143.19	612.849	-2083.120	
EQ29	32.60	141.99	618.300	-2088.975	
EB6	65.37	14.03	652.144	-2125.010	732.500
PQ7B	120.00	11.03	661.100	-2133.229	

PQ7B IS IN LINE AP-1.

11.5 Booster Test Beam Line (Line AP-4)

SCALES, MIN. HDR -100.00 MM
MAX. 100.00

HORIZONTAL BEAM SIZE
ACCUMULATOR TO TARGET BYPASS

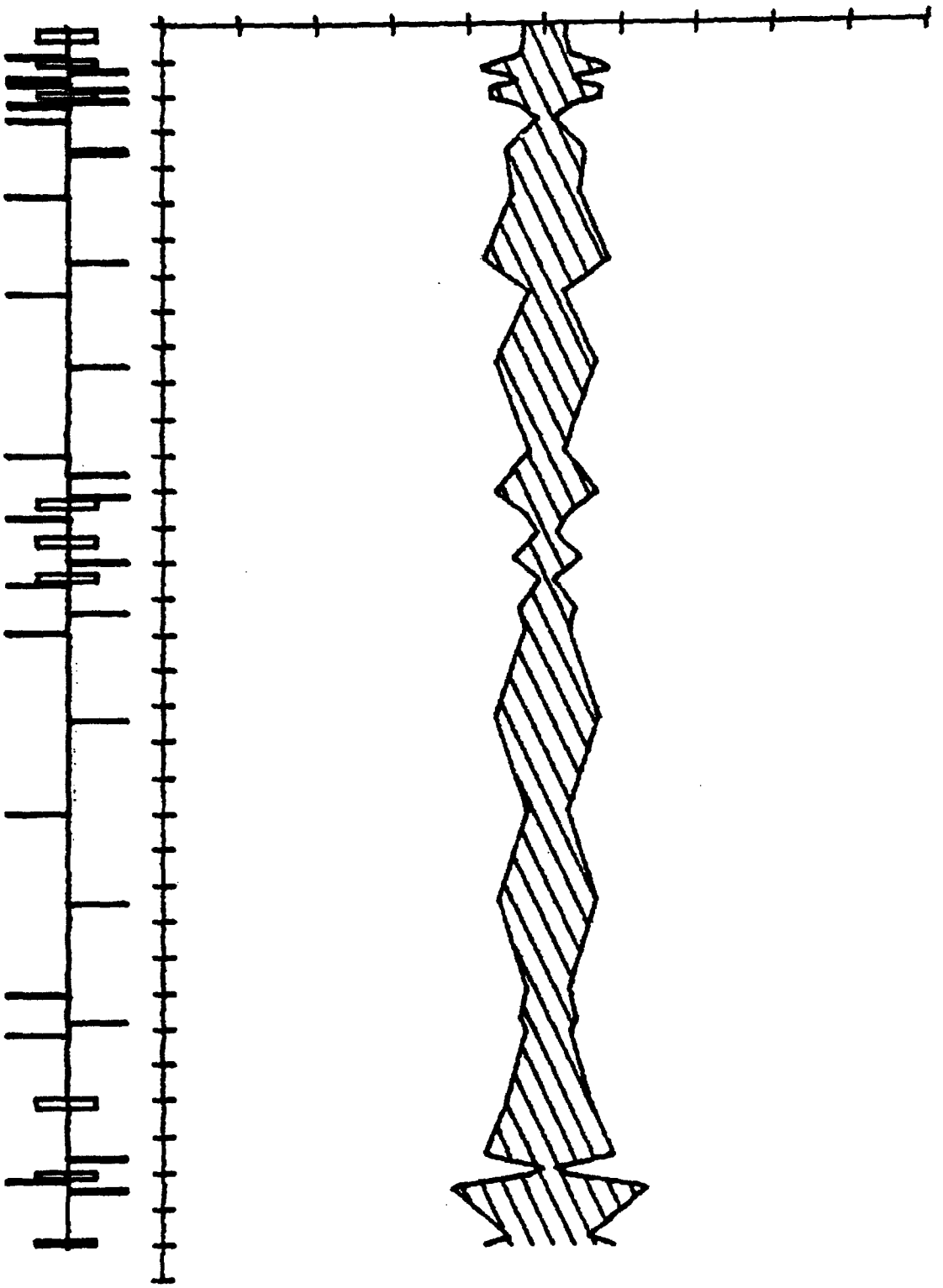


Figure 11-9a

SCALES, MIN. VER. -100.00 MM
 MAX. 100.00
 VERTICAL BEAM SIZE
 ACCUMULATOR TO TARGET BYPASS

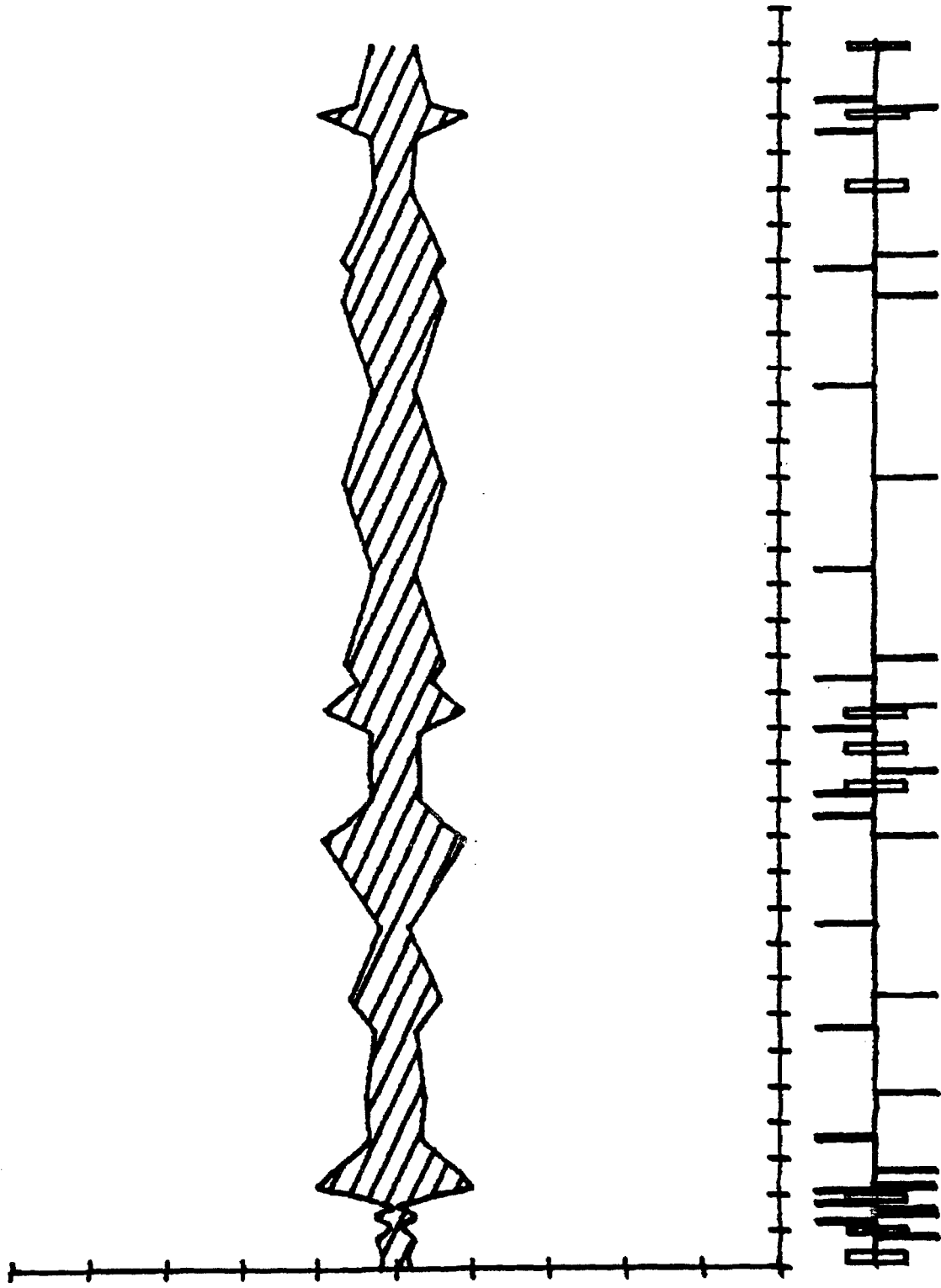


Figure 11-9b

This section describes the beam line connecting the Booster to the Debuncher Ring. The 8-GeV kinetic energy beam is extracted vertically from the Booster with a kicker and a pulsed septum at Booster long straight 3. At 1.5 ft above the Booster beam height, the extracted beam is bent down by 10 mrad to level, taken out of the Booster enclosure and focused down to a 6 mm spot on a Be target. With a set of vertical dipoles, the targeting angle is varied from 10 mrad to 50 mrad down. The target is followed by a dump and collimator set at a level that collects secondary 8-GeV protons. The variable targeting angle allows the intensity of the secondary to vary from 10^7 to 10^{11} per Booster batch. The beam is bent up and transported to the Debuncher at the same elevation as the other beam lines. Finally, the beam is bent down and injected vertically into the Debuncher with a Lambertson magnet at station D23 in a manner similar to the antiproton injection line.

Lattice functions for this line are shown in Figs. 11-9 and 11-10 and the line is described in Table 11-VI.

TABLE 11-VI XYZ COORDINATES OF BOOSTER TO DEBUNCHER LINE

(Coordinates given at end of element (toward Debuncher) Main Ring Station A0 at X=0.0, Y=0.0)

NAME	LENGTH (IN)	FIELD (KG-KG/M)	X (FT)	Y (FT)	Z (FT)
BOOSTER LONG STRAIGHT 3			-488.791	-689.897	726.500
B-SEPTUM	84.00	7.28	-485.293	-695.956	726.683
BQ1	32.60	-142.28	-474.283	-715.026	727.836
BB1	60.00	-12.14	-471.284	-720.220	728.000
BQ2	25.20	142.28	-462.365	-735.669	727.818
BQ3	25.20	-142.28	-458.148	-742.972	727.734
BB2	60.00	10.00	-437.700	-778.389	727.326
BB3	60.00	-10.00	-434.784	-783.440	727.267
TARGET			-433.534	-785.605	727.242
COLLIMATOR					
BEND UP .573 DEG; BEND LEFT .363 DEG.					
DUMP					
BB4	120.00	10.49	-411.872	-822.582	727.781
BQ4	18.00	25.84	-405.669	-833.169	729.110
BQ5	18.00	-20.53	-392.859	-855.035	731.854
BB5	120.00	-10.49	-387.312	-864.504	732.500
BQ6	18.00	-152.02	-386.048	-866.661	732.500
BQ7	18.00	154.12	-384.279	-869.681	732.500
BEAM PIPE					
BQ8	27.60	118.61	-146.351	-1275.813	732.500
BQ9	27.60	-129.92	-144.683	-1278.660	732.500
BQ10	18.00	24.91	-139.302	-1287.844	732.500
BB6	120.00	-6.31	-133.075	-1298.473	732.176
MID D2Q5		90.60	-107.183	-1342.670	728.847

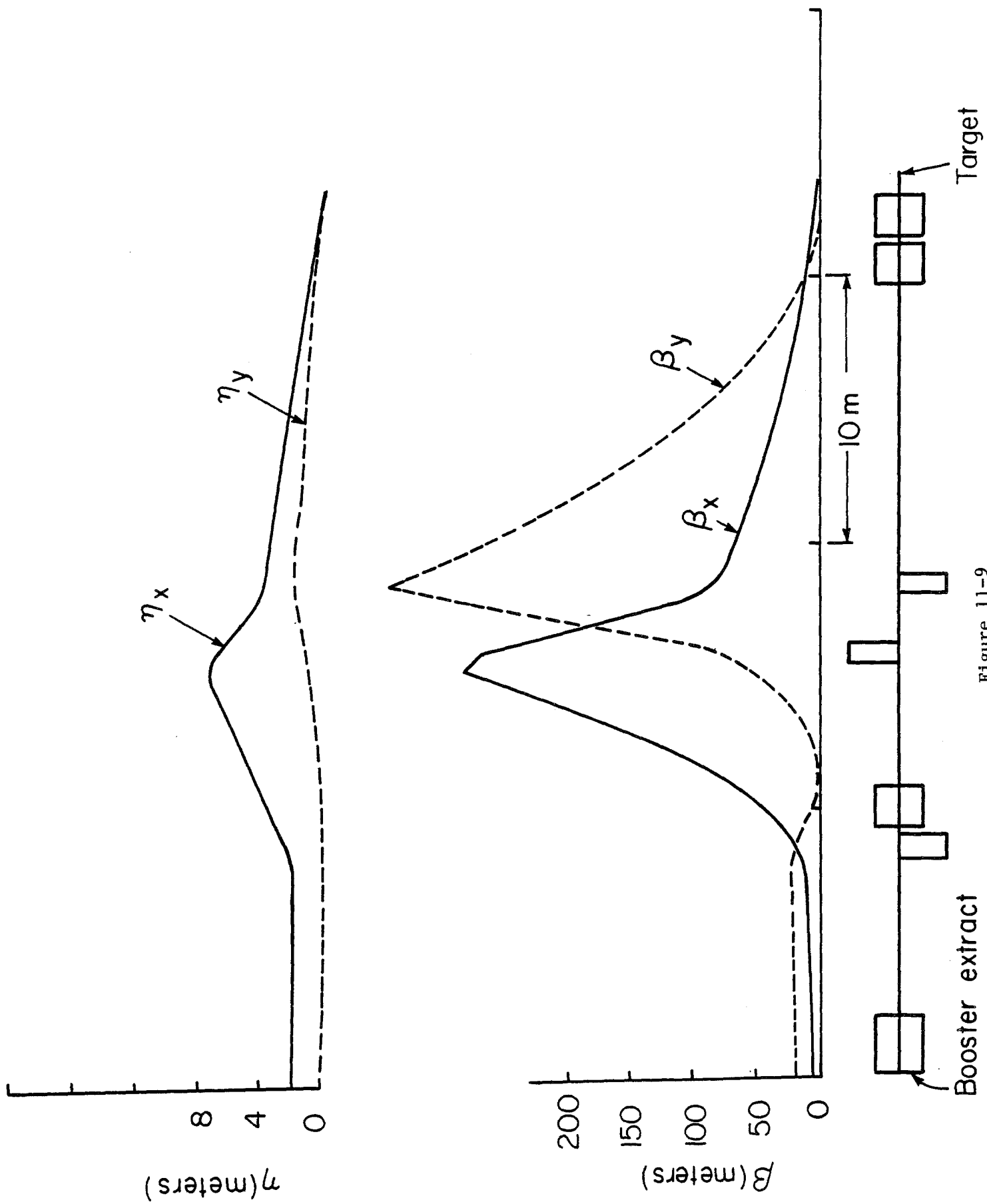


Figure 11-9

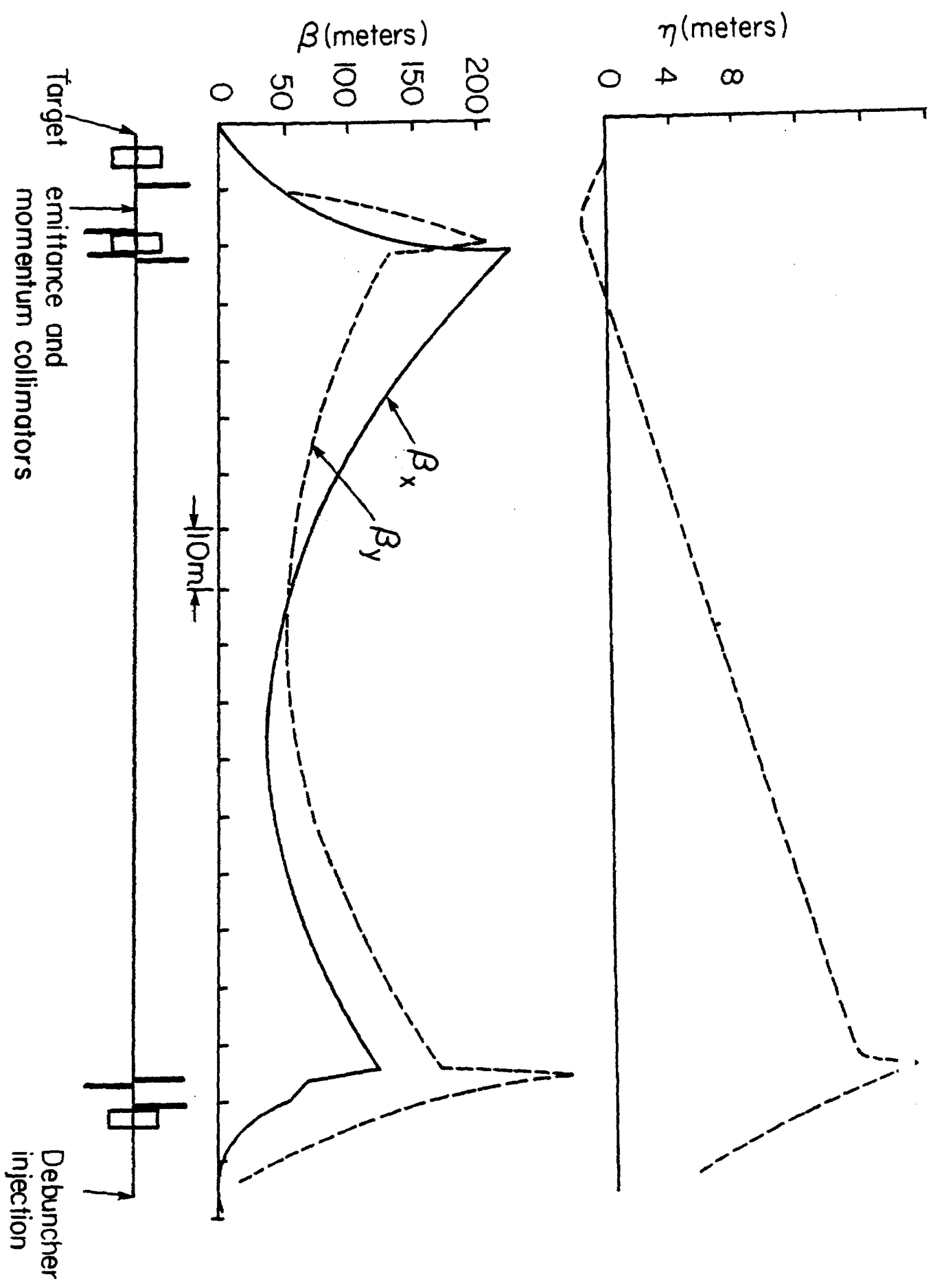


Figure 11-10

DEBUNCHER RING

728.500

11.6 Beam-Line Vacuum Systems

The vacuum in the 5 beam lines is required to be comparable in quality to that of the Debuncher (1×10^{-8}). It is planned to use SEM grid profile monitors in the beam lines. There are 3 lines that connect directly with the Accumulator ring: AP-4, D to A, and AP-3. The first two lines have thin windows to isolate their vacuum system from the Accumulator vacuum system. The AP-3 line uses differential pumping to isolate the Accumulator vacuum from the almost 1000 times worse vacuum in the Main Ring.

CHAPTER 12

MAGNETS12.1 Magnets

The main magnet systems of the Debuncher and Accumulator rings and all five beam lines will with few exceptions utilize four magnet cross-section types, a small and a large dipole and a small and large quadrupole. These magnets will each come in a number of different lengths, but will retain the advantages of common laminations and coil designs. In addition, many of the correction elements in the ring and beam lines will be of the same design. Table 12-I shows the magnet types and lengths to be used and their disposition around the project.

The parameters of the major dipole and quadrupole types are given in Tables 12-II and 12-III.

In these designs, higher multipole content has been minimized by empirical chamfering of the poles of the end packs. These end packs are made of standard laminations glued to make a rigid assembly.

These magnets are rich in copper in order to lower the excitation and therefore to decrease operating cost.

Figures 12-1 through 12-4 show the four types of magnet cross sections.

12.2 Magnet Power Supplies

12.2.1 Debuncher. The Debuncher ring has 111 small quadrupoles, 3 larger quadrupoles, and 66 small dipoles. The small dipoles and large quadrupoles are in series and fed by one ring bus using a 1200-A power supply. Three 300-A supplies run the SQ elements (QF, QD, and QSS buses). The total tunnel equipment consists of the 180 major magnetic elements, 33 shunts, and 186 correction magnets, dipoles and sextupoles. These elements are operated from 57 power supplies and 33 shunt controllers placed in the service buildings. The table below shows the relationship of tunnel and service building equipment.

TABLE 12-IV DEBUNCHER POWER SUPPLIES

<u>Magnetic Element</u>	<u>Type</u>	<u>Power Supply</u> (A)
B	66 SD	1200
D2Q5, D4Q5, D6Q6	3 LQ	
QF	42 SQ-27.6	300
D1Q5, D3Q5, D5Q5, D6Q5	4 SQ-32.6	

TABLE 12-I TEVATRON I MAGNETS

<u>Magnet</u>	<u>Length</u> (in.)	<u>Debuncher</u>	<u>Accum</u>	<u>AP1</u>	<u>AP2</u>	<u>DA</u>	<u>AP3</u>	<u>AP4</u>	<u>Refer</u>
Small Quadrupole									
SQA	18		18		5	1	16	5	1
SQB	25.2		6		6		3	2	1
SQC	27.6	102	18		14	1	5	2	2
SQD	32.6	9	6		5	4	5	1	1
SQE	51.6		6		3	1	1		1
Large Quadrupole									
LQA	17.2		6						1
LQB	25.3		6						1
LQC	30.4		12						1
LQD	32.6	3							1
LQE	34.4		6						1
Large Quadrupole									
LDA	180		12						1
Small Dipole									
SDA	180		6						1
SDB	120		6						1
SDC	60		4						1
SDD	65.2	66			1		2		1
SDE	98.4				6		4		1
Modified Main Ring Bl's									
MWGB1	60		2		1		2	1	1
MWGB2	120					1			1
Existing Dipoles									
EPB	120			10				3	
AVB	60							2	1
Existing Quadrupoles									
3Q120A	120			14					15
Lambertsons									
Lamb	204			2					1
Lamb	115						1		
Septum Magnets									
Sept	84					4		1	1
Booster Septum								1	
Correction Elements									
RSex	8	138	12						1
SSex	12		12						1
BL Trim Dipole		28	30	3	7	3	7	5	1

TABLE 12-II DIPOLE MAGNET PARAMETERS

MAGNET DATA LATEST REVISION 8/10/83

INPUT PARAMETERS AND COMPUTED FIELDS

DIPOLES * INPUT DATA

MAGNET TYPE		SDA	SDB	SDC	SDD	SDE	SDP	LDA	LDP
GAP *	IN	2.375	2.375	2.375	2.375	2.375	2.375	2.375	2.375
GOOD FIELD WIDTH *	IN	4	4	4	4	4	4	10	10
ARC LENGTH *	IN	180	120	60	65.3702	98.4252	48	180	48
RADIUS OF CURVATURE *	IN	687.549	687.549	687.549	687.549	926.083	687.549	687.549	687.549
BEND ANGLE	RAD	.2617995	.1745330	.0872665	.0950772	.1062812	.0698132	.2617995	.0698132
FE LENGTH	IN	176.9364	117.2977	57.43096	62.79558	95.82888	45.44025	176.9364	45.44025
FE SAGITTA	IN	5.715439	2.505982	.5999127	.7172840	1.240349	.3754970	5.715439	.3754970
FE WIDTH *	IN	45.25	45.25	45.25	45.25	45.25	45.25	57	57
FE HEIGHT *	IN	29	29	29	29	29	29	35	35
COIL PROTRUSION *	IN	11	11	11	11	11	11	11	11
PANCAKE TURNS *		56	56	56	56	56	56	56	56
SADDLE TURNS *		16	16	16	16	16	16	16	16
PANCAKE H2O PATHS *		4	4	4	4	4	4	4	4
SADDLE H2O PATHS *		1	1	1	1	1	1	1	1
WATER FLOW	GAL/MIN	6.517570	7.728468	10.04321	9.746194	8.364456	10.82087	6.428168	10.41549
FIELD	KG	16.98848	16.98848	16.98848	16.98848	12.61268	16.98848	17.01224	17.01224
CURRENT *	AMP	1178.61	1178.61	1178.61	1178.61	875.03	1178.61	1179.44	1179.44
AMPFAC *		1.04	1.04	1.04	1.04	1.04	1.04	1.04	1.04
MAGNET RESISTANCE	OHM	.0197479	.0141110	.0084727	.0089774	.0120845	.0073449	.0202802	.0078773
VOLTAGE	VOLT	23.27503	16.63136	9.986067	10.58091	10.57431	8.656817	23.91932	9.290813
POWER	WATT	27432.18	19601.88	11769.68	12470.76	9252.836	10203.01	28211.40	10957.96
H2O TEMP RISE	DEG C	15.99404	9.638024	4.453234	4.862299	4.203594	3.583025	16.67712	3.997914
STORED ENERGY	JOULE	113569.1	75833.05	37952.65	41347.08	34311.22	30365.59	163040.8	43593.12
INDUCTANCE	HENRY	.1635121	.1091813	.0546427	.0595298	.0896232	.0437191	.2344092	.0626753
L/R TIME	SEC	8.279991	7.737322	6.449224	6.631042	7.416368	5.952279	11.55851	7.956432
CAPACITANCE *	NF								
TOTAL MAGNET WT	LB	58372.03	39286.32	20150.44	21864.57	32418.56	16319.41	90766.62	16843.74

MAGNET DATA LATEST REVISION 8/10/83

INPUT PARAMETERS AND COMPUTED FIELDS

DIPOLES * INPUT DATA

MAGNET TYPE		SDA	SDB	SDC	SDD	SDE	SDP	LDA	LDP
LENGTH EXTENSION *	IN	2.55	2.55	2.55	2.55	2.55	2.55	2.55	2.55
THICKNESS LAMS **	IN	.0598	.0598	.0598	.0598	.0598	.0598	.0598	.0598
NUMBER LAMS		5918	3923	1921	2100	3205	1520	5918	1520
CHAMFER *	IN	2.5	2.5	2.5	2.5	2.5	2.5	2.5	2.5
REDUCED ANGLE	RAD	.2507277	.1635126	.0762763	.0840851	.0981179	.0588265	.2507277	.0588265
PANCAKE END *	IN	30.1	30.1	30.1	30.1	30.1	30.1	36.31	36.31
SADDLE END *	IN	64.25	64.25	64.25	64.25	64.25	64.25	68	68
TOTAL PANCAKE LENGTH	IN	22678.61	15962.57	9244.892	9846.212	13548.12	7901.161	23374.13	8596.681
TOTAL SADDLE LENGTH	IN	7572.403	5653.534	3734.198	3906.004	4963.690	3350.275	7692.403	3470.275
TOTAL CU LENGTH	IN	30251.01	21616.10	12979.09	13752.22	18511.81	11251.44	31066.53	12066.96
WT/IN CU *	LB/IN	.36632	.36632	.36632	.36632	.36632	.36632	.36632	.36632
TOTAL CU WT.	LB	11081.55	7918.411	4754.500	5037.712	6781.245	4121.626	11380.29	4420.367
WATER HOLE DIAM *	IN	.375	.375	.375	.375	.375	.375	.375	.375
H2O PRESSURE **	PSI	70	70	70	70	70	70	70	70
TURB FLOW PARM **	ENGLISH	19600	19600	19600	19600	19600	19600	19600	19600
LAM FLOW PARM **	ENGLISH	31900	31900	31900	31900	31900	31900	31900	31900
TURB PANCAKE FLOW	GAL/MIN	5.358423	6.386954	8.392557	8.132248	6.932753	9.078200	5.278098	8.703217
LAM PANCAKE FLOW	GAL/MIN	31.15425	44.26199	76.42438	71.75705	52.15006	89.42168	30.22723	82.18694
TURB SADDLE FLOW	GAL/MIN	1.159147	1.341514	1.650656	1.613946	1.431703	1.742669	1.150070	1.712274
LAM SADDLE FLOW	GAL/MIN	5.831497	7.810768	11.82542	11.30528	8.896294	13.18055	5.740527	12.72477
LAMINATION AREA *	SQ IN	447.51	447.51	447.51	447.51	447.51	447.51	759.44	447.51
IRON DENSITY **	LB/CU IN	.284	.284	.284	.284	.284	.284	.284	.284
LAM WT.	LB	7.600152	7.600152	7.600152	7.600152	7.600152	7.600152	12.89772	7.600152
TOTAL LAM WT.	LB	44974.70	29815.41	14598.13	15961.74	24358.33	11550.26	76323.62	11550.26
STRUCTURE AREA *	SQ IN	44	44	44	44	44	44	57.75	57.75
UNIT STRUCT VOL *	CU IN	279	279	279	279	279	279	448	448
STRUCTURE WT.	LB	2315.785	1552.497	797.8151	865.1251	1278.986	647.5254	3062.703	873.1118
RESIST/LENGTH *	OHM/IN	6.528E-7	6.528E-7	6.528E-7	6.528E-7	6.528E-7	6.528E-7	6.528E-7	6.528E-7
INDUCT/LENGTH *	HENRY/IN	.000911	.000911	.000911	.000911	.000911	.000911	.001306	.001306
H2O SP HT * GAL/MIN WATT OC		.0038	.0038	.0038	.0038	.0038	.0038	.0038	.0038
TRANSFER CONST *	KG/IN AMP	.014414	.014414	.014414	.014414	.014414	.014414	.014424	.014424

TABLE 12-III QUADRUPOLE MAGNET PARAMETERS

MAGNET DATA LATEST REVISION 8/10/83

INPUT PARAMETERS AND COMPUTED FIELDS

QUADS * INPUT DATA

MAGNET TYPE		SQA	SQB	SQC	SQD	SQE	SQP	LQA	LQB	LQC	LQE	LQD
POLE TIP DIAMETER*	IN	3.5	3.5	3.5	3.5	3.5	3.5	6.625	6.625	6.625	6.625	6.625
GOOD FIELD WIDTH *	IN	5	5	5	5	5	5	10	10	10	10	10
EFFECTIVE LENGTH *	IN	18	25.2	27.6	32.6	51.64	49.42	17.284	25.3	30.4	34.4	32.68
FE LENGTH	IN	16.58	23.78	26.18	31.18	50.22	48	14.604	22.62	27.72	31.72	30
COIL PROTRUSION *	IN	4	4	4	4	4	4	6	6	6	6	6
FE WIDTH *	IN	30.5	30.5	30.5	30.5	30.5	30.5	54.75	54.75	54.75	54.75	54.75
FE HEIGHT *	IN	29	29	29	29	29	29	51.75	51.75	51.75	51.75	51.75
NUMBER TURNS *		132	132	132	132	132	132	40	84	84	84	84
NUMBER H2O PATHS *		4	4	4	4	4	4	1	2	2	2	1
WATER FLOW	GAL/MIN	1.512802	1.373134	1.334519	1.263527	1.070031	1.088122	1.763305	3.147041	2.994803	2.889726	2.933536
GRADIENT *	KG/IN	2.499471	2.499471	2.499471	2.499471	2.499471	2.499471	2.250133	2.250133	2.250133	2.250133	2.250133
CURRENT *	AMP	234.45	234.45	234.45	234.45	234.45	234.45	1206.7	1206.7	1206.7	1206.7	1206.7
AMPFAC *		1	1	1	1	1	1	1.015	1.015	1.015	1.015	1.015
MAGNET RESISTANCE	OHM	.0323385	.0392517	.0415561	.0463569	.0646385	.0625069	.0029307	.0074107	.0081833	.0087892	.0085286
VOLTAGE	VOLT	7.581752	9.202554	9.742821	10.86838	15.15450	14.65475	3.560550	8.942462	9.874730	10.60592	10.29151
POWER	WATT	1777.542	2157.539	2284.204	2548.091	3552.972	3435.806	4296.516	10790.87	11915.84	12798.16	12418.76
120 TEMP RISE	DEG C	4.464997	5.970757	6.504200	7.663267	12.61767	11.99871	9.259184	13.02980	15.11958	16.82963	16.08685
STORED ENERGY	JOULE	1182.336	1655.270	1812.915	2141.342	3391.990	3246.169	12583.83	18419.98	22133.10	25045.35	23793.06
INDUCTANCE	HENRY	.04302	.060228	.065964	.077914	.1234196	.1181138	.017284	.0253	.0304	.0344	.03268
L/R TIME	SEC	1.330305	1.534406	1.587349	1.680742	1.909382	1.889611	5.857690	3.413994	3.714904	3.913897	3.831795
CAPACITANCE *	NF											
TOTAL MAGNET WT	LB	2927.012	4069.174	4449.895	5245.063	8263.446	7911.280	7703.009	12766.49	15380.70	17431.06	16549.40

MAGNET DATA LATEST REVISION 8/10/83

INPUT PARAMETERS AND COMPUTED FIELDS

QUADS * INPUT DATA

MAGNET TYPE		SQA	SQB	SQC	SQD	SQE	SQP	LQA	LQB	LQC	LQE	LQD
LENGTH EXTENSION *	IN	1.42	1.42	1.42	1.42	1.42	1.42	2.68	2.68	2.68	2.68	2.68
THICKNESS LAMS **	IN	.0598	.0598	.0598	.0598	.0598	.0598	.0598	.0598	.0598	.0598	.0598
NUMBER LAMS		555	795	876	1043	1680	1605	488	757	927	1061	1003
NO LENGTH *	IN	17.1	17.1	17.1	17.1	17.1	17.1	26.3	26.3	26.3	26.3	26.3
TOTAL CU LENGTH	IN	8891.52	10792.32	11425.92	12745.92	17772.48	17186.4	3272.32	8218.56	9075.36	9747.36	9458.4
W/IN CU *	LB/IN	.06576	.06576	.06576	.06576	.06576	.06576	.26519	.26519	.26519	.26519	.26519
WATER HOLE DIAM *	IN	.1875	.1875	.1875	.1875	.1875	.1875	.375	.375	.375	.375	.375
WATER PRESSURE **	PSI	70	70	70	70	70	70	70	70	70	70	70
WATER FLOW PARM **	ENGLISH	19600	19600	19600	19600	19600	19600	19600	19600	19600	19600	19600
AM FLOW PARM **	ENGLISH	31900	31900	31900	31900	31900	31900	31900	31900	31900	31900	31900
WATER FLOW	GAL/MIN	1.512802	1.373134	1.334519	1.263527	1.070031	1.088122	1.763305	3.147041	2.994803	2.889726	2.933536
AM WATER FLOW	GAL/MIN	4.966355	4.091655	3.864761	3.464516	2.484653	2.569383	13.49454	21.49206	19.46301	18.12119	18.67481
MINIATION AREA *	SQ IN	239.72	239.72	239.72	239.72	239.72	239.72	801.01	801.01	801.01	801.01	801.01
ION DENSITY **	LB/CU IN	.284	.284	.284	.284	.284	.284	.284	.284	.284	.284	.284
AM WT.	LB	4.071213	4.071213	4.071213	4.071213	4.071213	4.071213	13.60371	13.60371	13.60371	13.60371	13.60371
TOTAL LAM WT.	LB	2257.549	3237.908	3564.694	4245.499	6838.003	6535.726	6644.436	10291.50	12611.87	14431.77	13649.21
STRUCTURE AREA *	SQ IN	18	18	18	18	18	18	46	46	46	46	46
BIT STRUCT VOL *	CU IN	0	0	0	0	0	0	0	0	0	0	0
STRUCTURE WT.	LB	84.75696	121.5634	133.8322	159.3922	256.7246	245.376	190.7867	295.5077	362.1341	414.3901	391.92
TOTAL CU WT.	LB	384.7064	709.7030	751.3685	838.1717	1168.718	1130.178	867.7865	2179.480	2406.695	2584.902	2508.273
RESIST/LENGTH *	OHM/IN	3.637E-6	3.637E-6	3.637E-6	3.637E-6	3.637E-6	3.637E-6	9.017E-7	9.017E-7	9.017E-7	9.017E-7	9.017E-7
DUCT/LENGTH *	HENRY/IN	.00239	.00239	.00239	.00239	.00239	.00239	.001	.001	.001	.001	.001
W/SP HT * GAL/MIN WATT	OC	.0038	.0038	.0038	.0038	.0038	.0038	.0038	.0038	.0038	.0038	.0038
TRANSFER CONST *	KG/IN AMP	.010661	.010661	.010661	.010661	.010661	.010661	.0018647	.0018647	.0018647	.0018647	.0018647

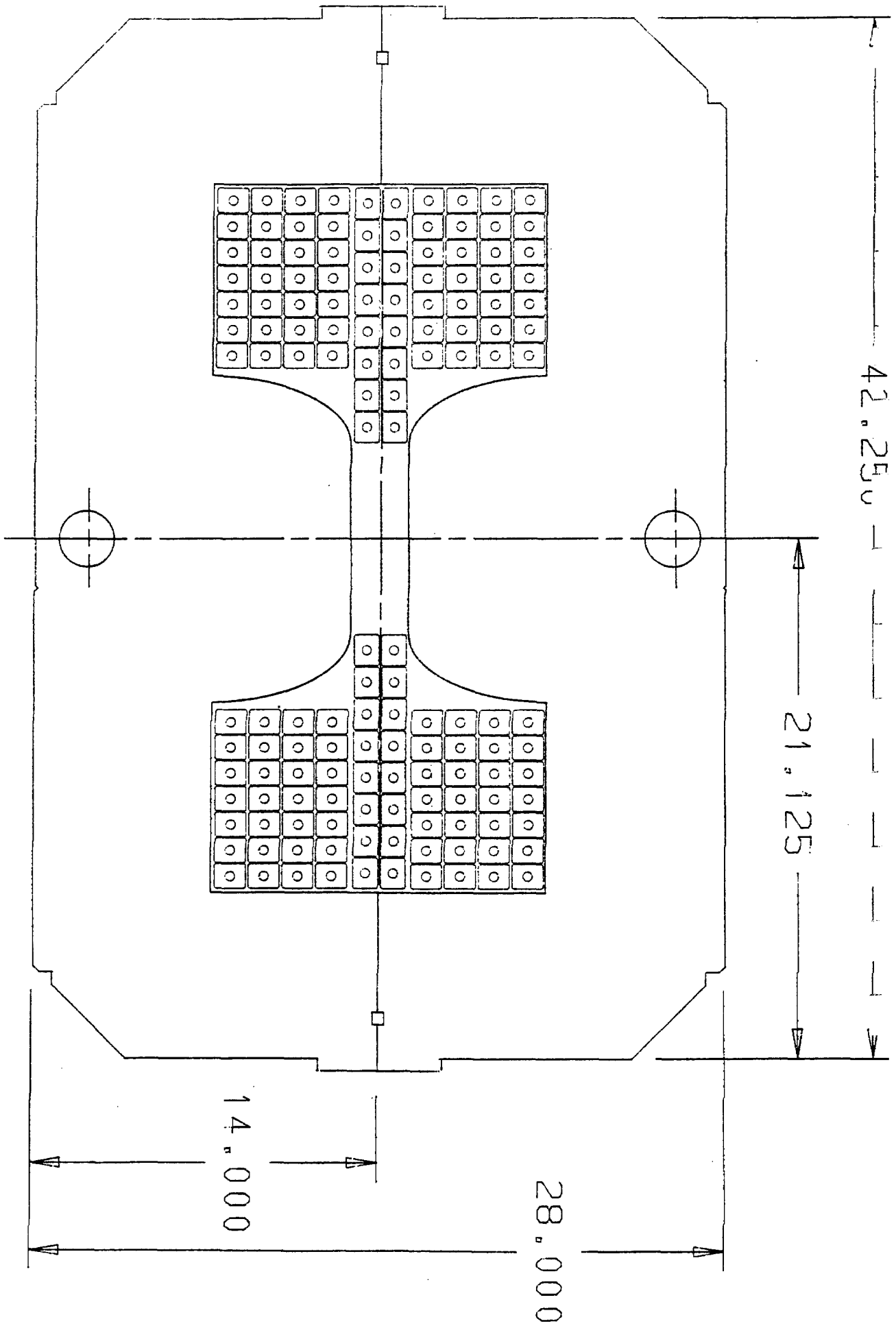


Figure 12-1

SMALL DIPOLE

units are in inches

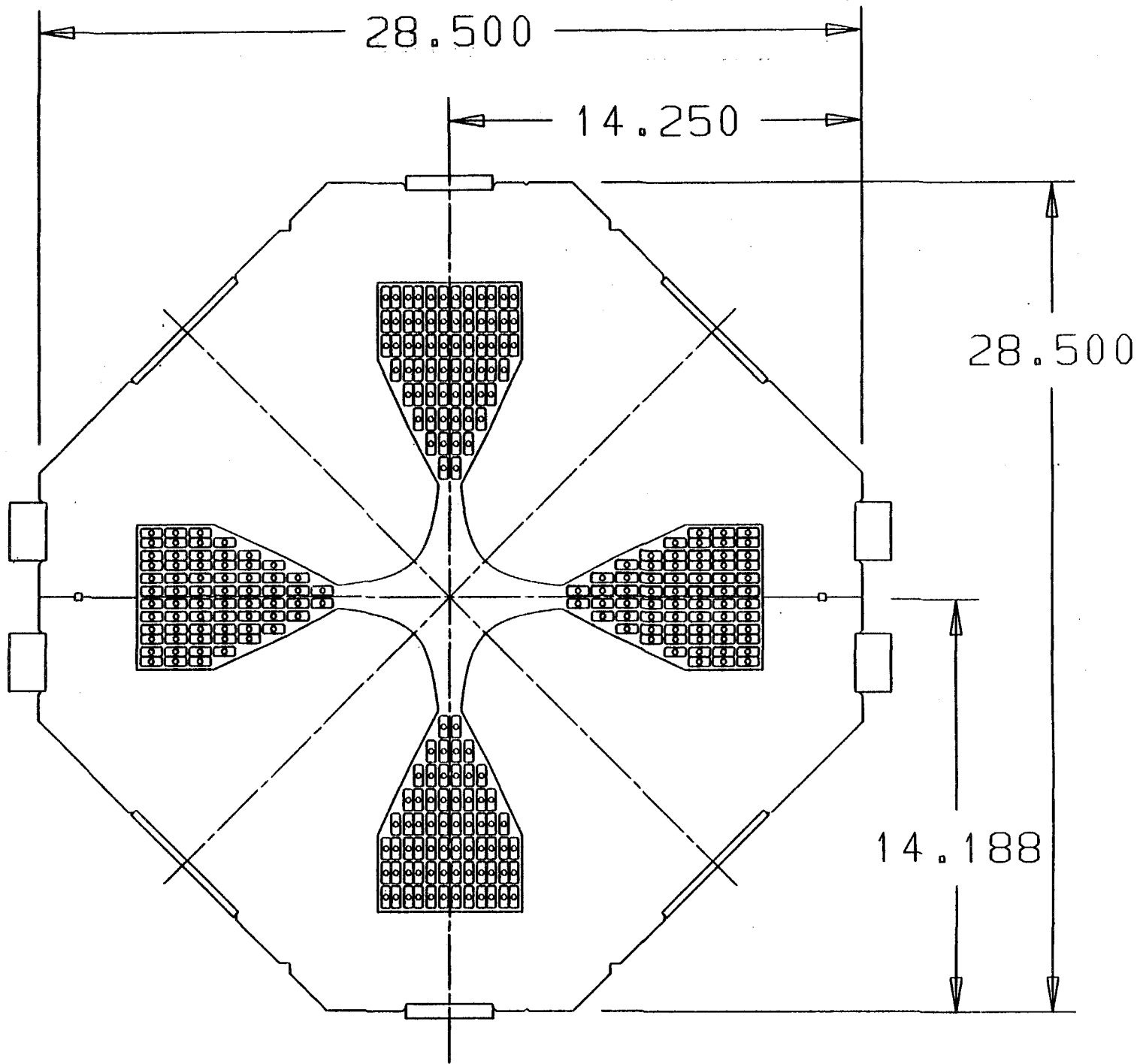
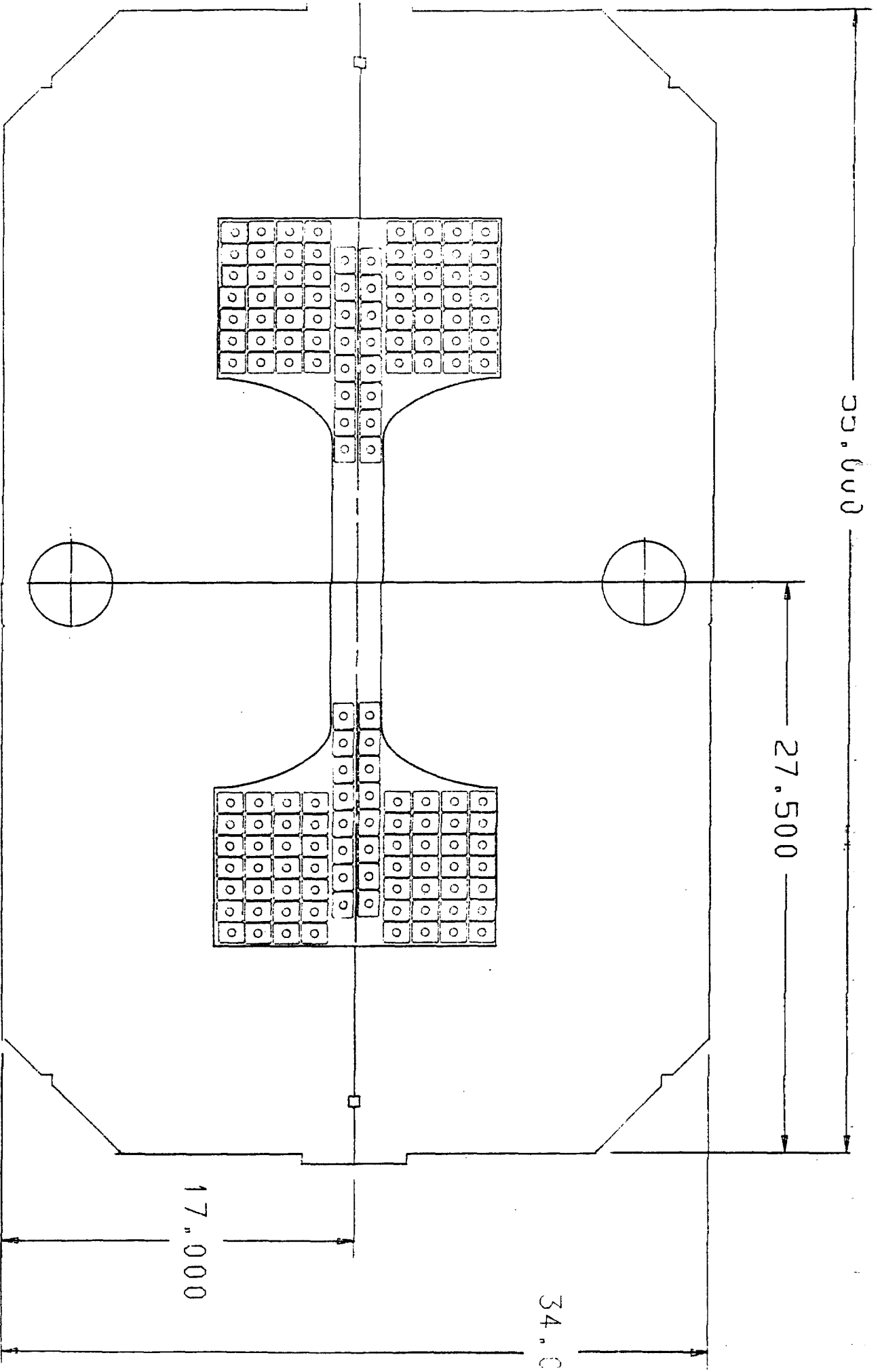


Figure 12-2

SMALL APERTURE QUAD (SQ)

units are in inches



LARGE DIPOLE (LD)

Figure 12-3

units are in inches

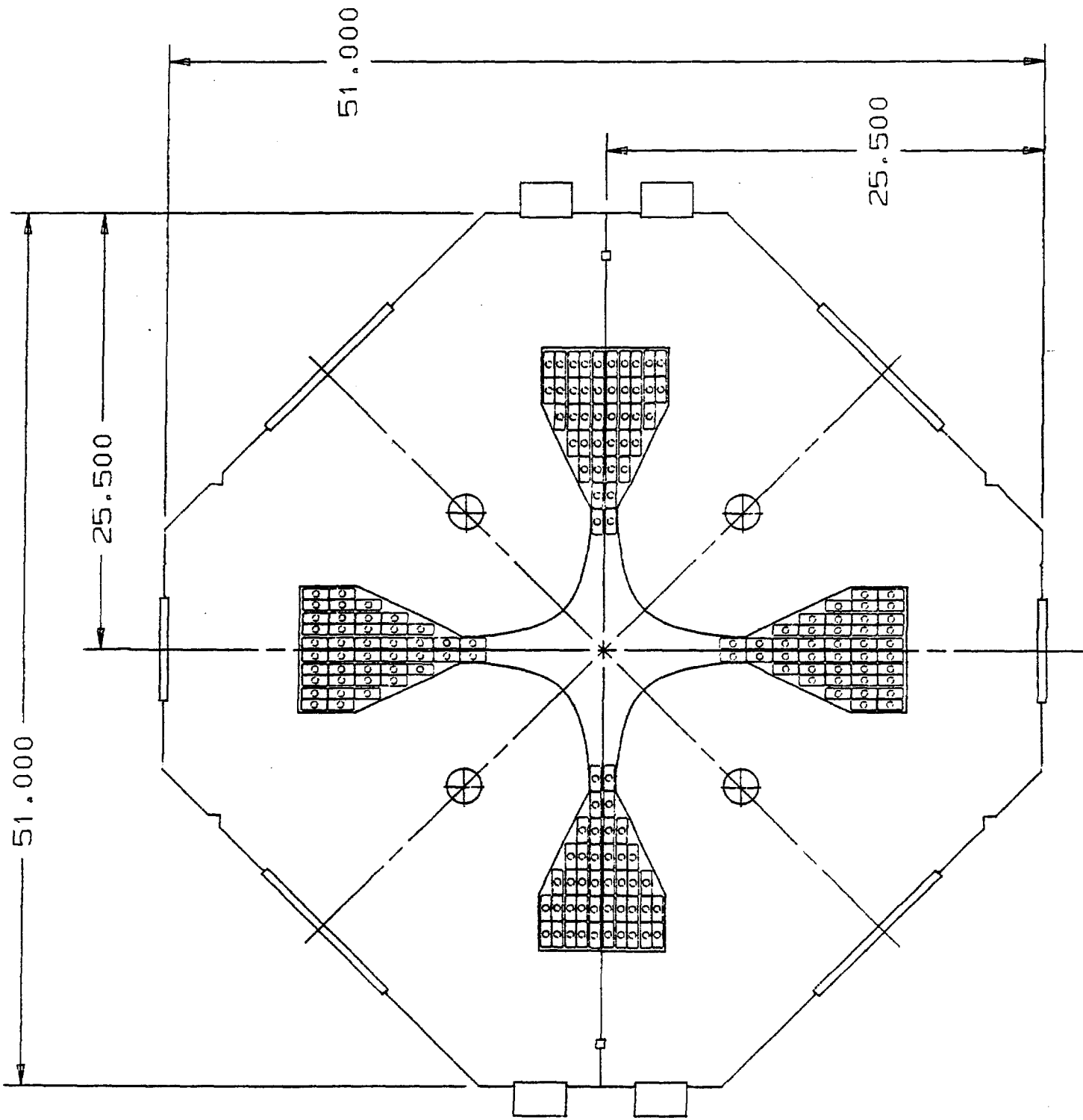


Figure 12-4 LARGE QUAD (LQ)

units are in inches

QD	39 SQ-27.6	300
DnQ6, (n=1,5)	5 SQ-32.6	
DnQ0, (n=1,3,5)	21 SQ-27.6	300
DnQ2, Q3, Q4, (n=1,6)		
D2Q5, D4Q5, D6Q6	3 LQ-32.6	3-50 (shunt)
D2Q5, D4Q5, D6Q6	3 LQ-32.6	3-200 (trim)
D1Q5, D3Q5, D5Q5, D6Q5	9 SQ-32.6	30-40 (shunt)
DnQ6, (n=1,5)		
DnQ0, (n=1,3,5)	21 SQ-27.6	
DnQ2, Q3, Q4, (n=1,6)		
Hor Corr Dipoles	24	24-10 (bipolar)
Ver Corr Dipoles	24	24-10 (bipolar)
SF Sextupoles	72 - S	200
SD Sextupoles	66 - S	200

12.2.2 Accumulator. The Accumulator has 54 small quadrupoles, 30 large quadrupoles, 12 large dipoles, and 18 small dipoles. There are two 1200-A supplies, one feeding all the dipoles, and the other feeding the LQ. There are two 300-A supplies feeding the SQ. Each of the 30 dipoles in the Accumulator has a shunt. These supply horizontal corrections.

In addition, there are 24 standard vertical-correction magnets. Besides the dipole shunts there are shunts on the quadrupoles. In the Accumulator there are also 4 kinds of sextupoles. There are 2 families of "regular" sextupoles, 6 of each and two systems of combination sextupole-octupole correction magnets. In the tunnel are 114 major magnetic elements, 114 shunts, and 48 correction elements. These connect to 34 power supplies and 114 shunt controllers. The table below summarizes these requirements.

TABLE 12-V ACCUMULATOR POWER SUPPLIES

<u>Magnetic Element</u>	<u>Type</u>	<u>Power Supply</u>
B	2 MOD-B1-60	1200
	4 SD-60	
	6 SD-120	
	6 SD-180	
	12 LD	
Q10 F	6 LQ-18	1200
Q14 F	6 LQ-25.3	
Q12, Q13 D	12 LQ-30.4	

PB1,2	2 EPB-120	500 KW Blue Tr
PBR1, 2	2 EPB-120	
PQ1,2	2 3Q120A	2 200
PBR3, PB3-5		4 EPB-120 500 KW Blue Tr
PQ3,4	2 3Q120A	2 500
PQnA,B (n=5,9)		10 3Q120A 5 500
PBV1,2	2 EPB-120	1200
F17 Kicker		
PLAM1, PLAM2 rev		2 LAM-204 100
PB1,2 rev		2 EPB-120 100
PBR1, 2 rev		2 EPB-120
PQ1,2 rev		2 3Q120A 2 30
PB3, PB3-5 rev		4 EPB-120 100
PQ3,4 rev		2 3Q120A 2 30
PQnA,B (n=5,9) rev		10 3Q120A 5 30
PBV1,2 rev		2 EPB-120 100
3 Trim Dipoles		3 New Trim 3 100 (Bipolar)

AP-2 transports antiprotons from the target to the Debuncher. The first two elements in this line are the Li-lens and the C-magnet. The transport consists of 33 standard Tevatron I quadrupoles, IQ1 - IQ33, and 8 bending magnets, IB1 - IB7, and IBV1. The first 7 bending magnets in the line are standard Tevatron I SD's. The vertical bend, IBV1 is a rotated 5 ft modified B1.

Tentatively, 7 correction elements have been placed in this line. Finally, there are 12 shunts.

From an operational point of view the I-line also includes D4Q5. The lithium lens is discussed in Section 3.2.2.

TABLE 12-VII AP-2, 8-GEV TARGET TO DEBUNCHER

<u>Magnetic Element</u>	<u>Type</u>	<u>Power</u>	<u>Supply</u>
	(A)		
Li-Lens			
C - Magnet			
IQ1, 4-6	5 SQ-27.6	500	
IQ2, 3	2 SQ-27.6	500	
IB1	SD-65.37	1200	

IQ7 - 14	7 SQ-27.6	200
IQ15	SQ-18	
IQ16, 23	2 SQ-25.2	500
IQ17, 22	2 SQ-32.6	
IQ18 -21	4 SQ-25.2	200
IQ24, 26	- 28	4 SQ-18
IQ25	SQ-32.6	
IB 2 - 7	6 SD-98.4	1200
IQ 29 - 30		2 SQ-32.6 500
IQ 31 - 33		3 SQ-51.64 500
IBV1	MOD-B1-60	1200
IQ1, 4	2 SQ	2 10 (shunt)
IQ15	SQ	20 (shunt)
IQ16, 17, 22		3 SQ 3 20 (shunt)
IQ24, 25	2 SQ	2 20 (shunt)
IQ26, 27, 28, 30		4 SQ 4 20 (shunt)
ISEPT	SEPT-84	
IKICK	3 Kickers	1-PS
7 Trims	7 New Trim	7 50 (bipolar)

The line transferring antiprotons from the Debuncher to the Accumulator is relatively simple. It consists of 2 kickers and 2 septa, one of each in each ring, a series of 7 quadrupoles requiring 3 supplies and 1 shunt, a modified B1 and 5 trim magnets.

TABLE 12-VIII DA 8-GEV D TO A

<u>Magnetic Element</u>	<u>Type Power Supply</u>	<u>(A)</u>
DKICK	3 500 g-3 m	1-PS
TDSEP	SEPT-84	
TB1	MOD-B1-120	1200
TQ1	SQ-51.64	500
TQ2, 3	2 SQ-32.6	
TQ4	SQ-27.6	200
TQ5	SQ-51.64	
TQ6	SQ-32.6	
TQ7	SQ-27.6	100

TQ2, 3, 4, 6	4 SQ 4 20 (shunt)
TASEP SEPT-84	
AKICK 3 Kickers	1-PS
5 Trim Magnets	5 New Trim 5 50 (bipolar)

AP-3 has 30 quads, EQ1-EQ29 (EQ3A and EQ3B are run as a pair), 1 Lambertson, and 8 dipoles, EBV1 - EBV2, and EB1 - EB6. The E-line shares PQ7B with the P-line. There are 15 large power supplies, 7 trim magnet supplies, and 8 shunts.

TABLE 12-IX AP-3, IX-GV A TO MR

<u>Magnetic Element</u>	<u>Type Power Supply</u> (A)
EKICK 1 Kicker	1-PS
E-LAM LAM-115	1200
EQ1, 5 2 SQ-27.6	500
EQ2, 6 2 SQ-22.6	
EQ4 SQ-25.2	
EQ3A, B 2 SQ-32.6	500
EQ7 SQ-18	30
EQ8 SQ-51.64	100
EQ9 SQ-18	
EQ10-13 4 SQ-18	200
EQ14 SQ-18	200
EQ16 SQ-27.6	200
EQ15 SQ-18	500
EQ17 SQ-27.6	
EQ18, 19 2 SQ-18	
EQ20 SQ-25.2	200
EQ21 - 24 4 SQ-18	
EQ25, 26 2 SQ-18	200
EQ27 SQ-25.2	500
EQ28 SQ-27.6	
EQ29 SQ-32.6	
EBV1, 2 2 MOD-B1-60	1200

CHAPTER 13

CONTROLS13.1 General Requirements and Architecture

The requirements of the Tevatron I control system go beyond those customary in many accelerators because of the long cycle time for antiproton collection. The system must monitor and control the repetitive sequence of antiproton production, transport, injection, debunching, cooling, and extracting over this entire cycle without significant loss of antiprotons. This will require extensive automatic control and feedback.

In addition, the Tevatron I control system must interface with the existing Energy Saver control system at several stages of the process. Their functions are so intertwined that it is efficient to build the Tevatron I control system as an extension of the Energy Saver control architecture and the description given in this chapter will follow that architecture.

In this note unless otherwise stated, a cycle means a standard Tevatron I 2 second cycle.

13.2 Computer Configuration

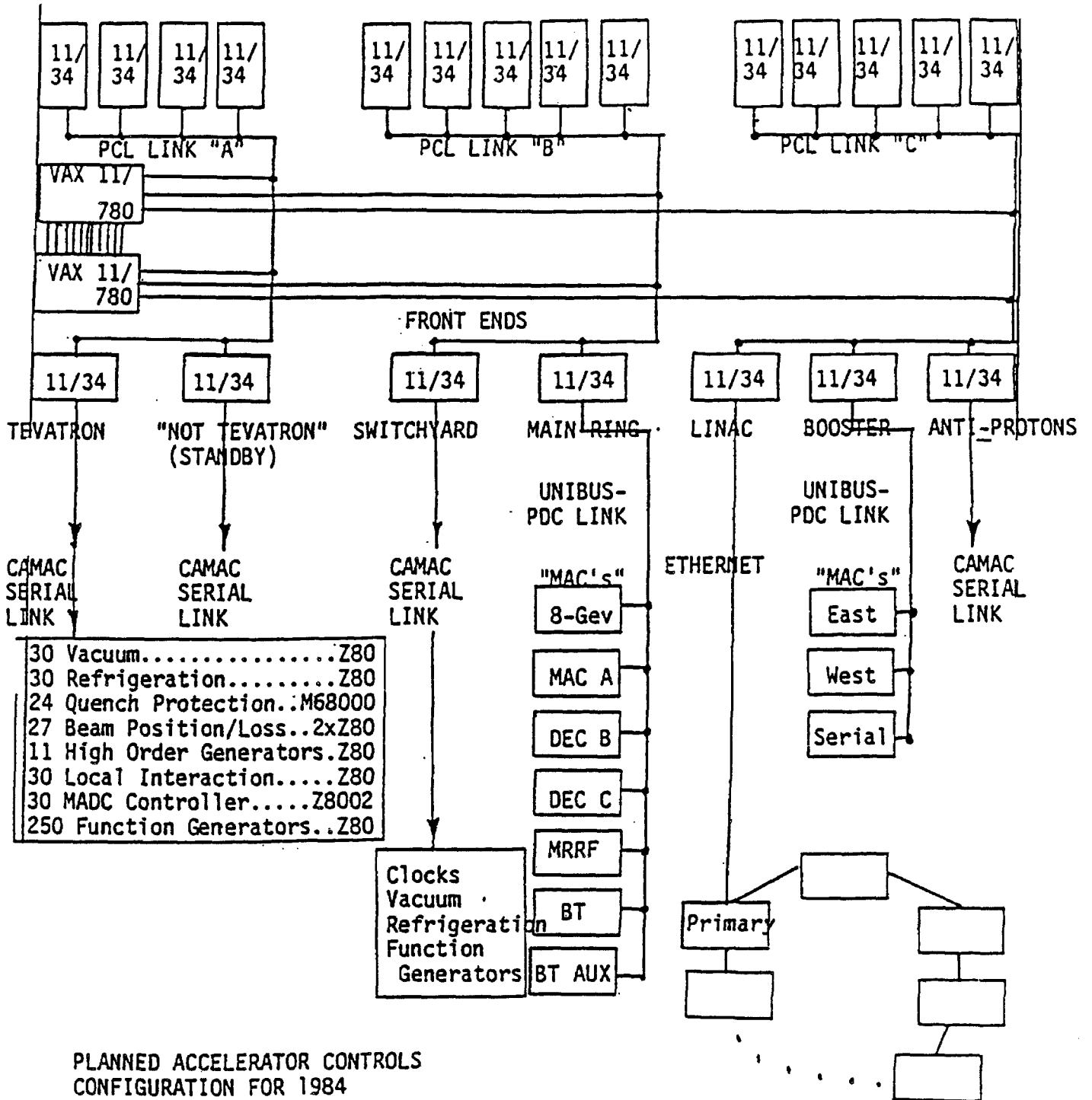
The complete Tevatron computer configuration is shown in Fig. 13-1. Four PDP-11's will be used for the Tevatron I control system. Three of these will run the three control consoles, and one will be the \bar{p} front end called "DEC-P", presently a PDP 11/34, to be upgraded to an 11/44. There are 3 PCL links in the full system. As indicated, 5 console PDP-11/34's communicate directly with the Linac, Booster and DEC-P front ends through a PCL. The number of consoles available for Tev I operation is not fixed since, in principle, any console in the system can communicate with Tev I devices.

A CAMAC System similar to the Energy Saver system will be used. This system adheres to the IEEE 583 standard. Most modules will be those types developed by the controls group, but commercially available CAMAC modules can also be used.

15-Hz data rates are supported in the standard way, i.e. using the console front end combination. Success with the Energy Saver is proof that this approach will work. CAMAC-190 modules, or other modules containing local buffer memories mandate the need for block-transfer facilities.

Each console supports the following devices: a color monitor, a storage scope, a color-graphics monitor, an alarm-message display monitor, a keyboard, and a touch panel.

CONSOLES



PLANNED ACCELERATOR CONTROLS
CONFIGURATION FOR 1984

As of May 19, 1983 the Booster,
Anti-Protons, and Main Ring Systems
are not installed/complete.

"SDLC" Link-
15 Stations --
All are M68000's with
Local Interaction

Figure 13-1

Devices in the Main Ring will be controlled from the "old" system. This includes F17 extraction.

By October 1984, the Main Ring (MR) system will be accessible from a standard console. One will therefore be able to combine parameter pages and displays for MR parameters and Tevatron I devices. No problems are expected from having MR and Tevatron I devices related to extraction on two different PCL links.

13.3 Software

Local intelligence will be incorporated where necessary. In the Energy Saver the RLI system has limited application and has only been implemented for the refrigerator and vacuum multibus crates. The RLI requires microprocessor programming for each system it is to control. It is necessary to identify specific cases where the RLI will be useful before investing in its implementation in Tevatron I.

The required Tev I software effort falls into several categories:

1. modification of existing microprocessor programs: 170 (vacuum), 190's (12, 14 bit ADC systems), REF (refrigerator for stochastic cooling), slow loop controls for stochastic cooling and RF, etc. The effort required on each will depend on how much can be taken over from the ED.
2. new microprocessor programs: e.g. GPIB/RS-232 interface, BPM/BLM systems.
3. DEC-P. The software philosophy is that the front-end programs in DEC-T, DEC-S, and DEC-P are identical. In that case, changes required to drive special devices are incorporated into all the front-end programs.
4. RLI.
5. Applications programs.

13.4 Communications

The \bar{p} link system has been defined by R. Ducar and is shown schematically in Fig. 13-2.

12 - 1/2 in. Helix, 50 ohm cables run from the Main Control Room to Service Bldg 10. From there 6 - 3/8 in. Helix, 50 ohm cables branch to the Tevatron I locations Buildings 30, 50 (AP10, AP30, AP50), Target Building (APT), F23 and F27.

An additional location is the power-supply building next to the Booster, designated as BSE = Booster Stair Enclosure. Equipment in BSE

LINK SYSTEM - P BAR

RF LINKS: PIOX, PIOR, BTR, & TCLK (4)
TWO CONSOLES AT BLDG 10 (4)

MISC.: BEAM PERMIT LOOP (HIGH LEVEL D/C) SPARE

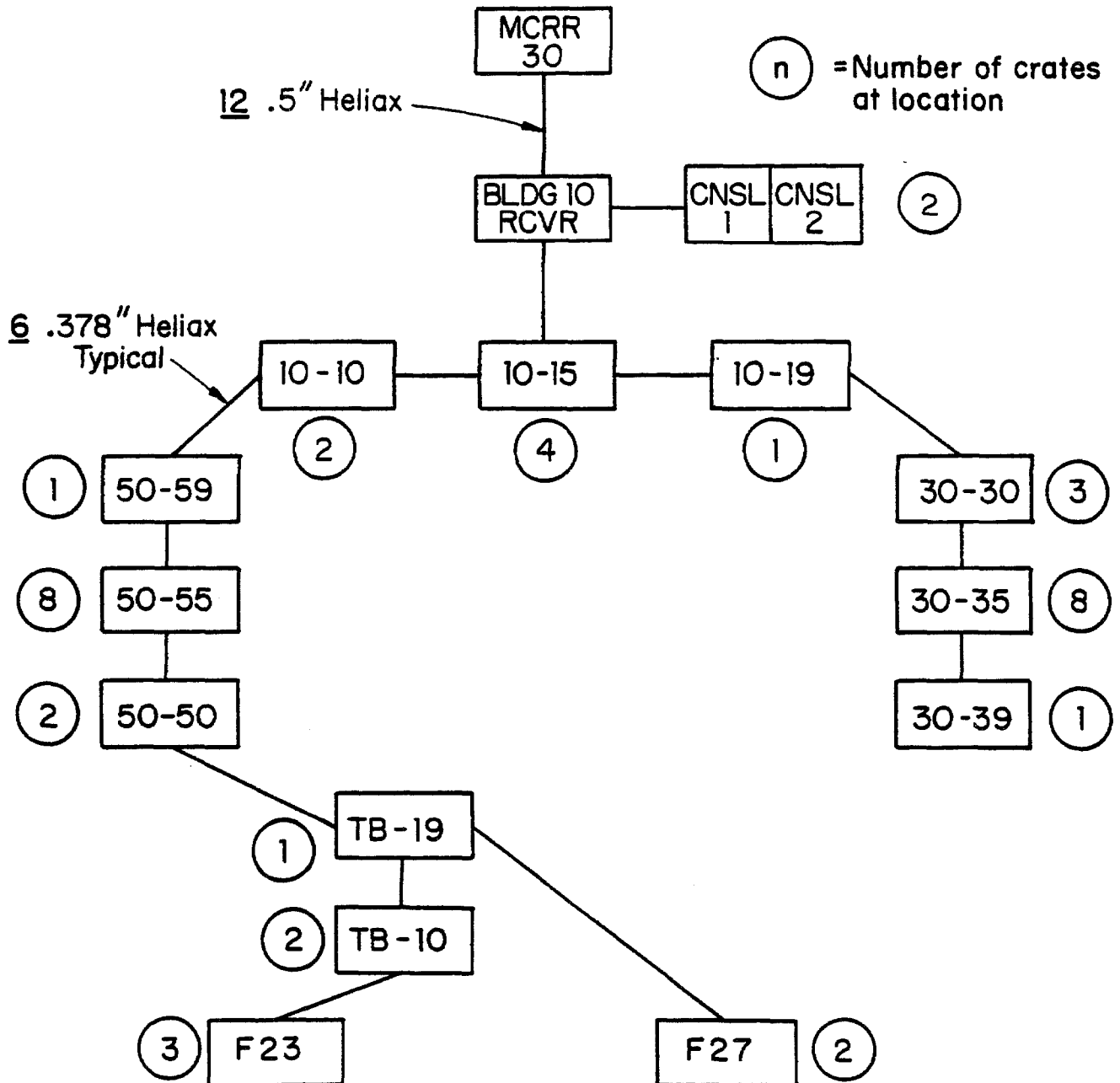


Figure 13-2

will tie in through the Booster front-end computer. It is assumed that Tevatron I devices in the B-line (AP-4) requiring equipment in the B West Gallery will be plugged into existing CAMAC crates.

AP10, AP30, and AP50 are each 216 ft long; there will be 3 control points in each of them. APTB is 144 ft long; two control nodes are planned there. In addition are F23, F27, and BSE, making a total of 14. The 13 repeaters that tie in through DEC-P are shown in fig. 2. An approximate number of crates controlled at each point are shown on Fig. 13-2. This is still being refined, as is the exact location within the buildings of the control clusters.

Additional repeater stations and CAMAC crates will be placed in 5 stub rooms. These will T-off from the main communications loop (not shown in Fig. 13-2).

13.5 Magnet Controls

None of the main magnet power supplies require microprocessor control or function generators. Magnet protection (thermal interlocks etc) are read out in status bits. For magnet elements in series, the protective devices will be hardwired to the power supply for those elements. This will require several hardwire loops around the rings. Reversing ring polarities will be done manually by reversing cables of all appropriate elements.

The five main ring buses will be driven by 5 main supplies, 3 delivering 1200 amps, 2 delivering 300 amps. Each will be regulated to 16 bit accuracy. Each supply will have an internal, commercially available 0-10 volt DAC (Analogic). 16 parallel lines will go from the CAMAC crate to opto-isolators at the power supply. Two CAMAC-017's are required for each power supply to provide the 16 drivers plus the necessary status and control bits.

Each of the 5 supplies will contain a commercial Racal-Dana DVM. Each of these will connect to the control system using a GPIB interface. In addition, measurement of the current ripple is needed. An internal comparator in each power supply will generate a difference signal which will be sent to a MADC/190 channel.

Of the 76 DC power supplies requiring 14 bit control, 73 will use CAMAC-119's. A 16-bit DAC is built into a CAMAC-119. A 190 reads an MADC having 14-bit capability. In the 3 300 A Debouncer quad supplies, the DAC will be in the power supply cabinet.

Correction elements are bipolar, 11 bits plus sign. They use a CAMAC-053 (quad unit) and standard MADC/190 channel.

Shunts use either 12 or 14-bit channels without the on/off or status bits. They will be controlled by a new DAC system, a CAMAC-054 designed

for this application. The 054 is a single-width CAMAC module having 6 channels.

Ramped supplies and kickers, also requiring 14-bit accuracy, will use a CAMAC-165, a new module which also has applications in the switchyard.

Timing of pulsed devices requires two programmable timers: (1) a programmable predet that counts MR revolutions, (2) a programmable 15-bit delay to set the time relative to the desired MR revolution to 1 ns resolution. The same system of programmable predet revolution counter plus proramable high resolution delay can also be used for D to A transfer and for extraction from the Accumulator. The "hole" in the beam is used to trigger the revolution counter. In both applications this has to be done very stably (to 1 ns). It is necessary to measure and readback these time delays. This can be done with a commercial TDC with 1 ns resolution. A TCLK event is needed to start the module.

13.6 Vacuum Controls

At each of 9 locations there is a 170 module and a CIA. A tenth unit will be purchased and can serve as a spare or can be hooked up to the control system and used in a vacuum development laboratory. Locations assumed are 2 each in AP10, AP30, AP50, (one for the D and one for the A), and one each in buildings F23, F27, APTB. Sector valve control is done by a hard wire system. The total number of devices controlled and monitored by these 9 CIA crates is 184: 128 ion pumps, 28 P-gauges, 12 I-gauges and 16 sector valves.

Additional vacuum control systems not yet completely defined are roughing, Accumulator bake-out, Accumulator residual gas analysis. These may or may not make use of spare slots in the CIA crate.

13.7 RF Control Systems

The location of equipment to be controlled or monitored is in buildings 10 and 50. There are 2 main systems in the Debuncher: (1) 53 MHz system which requires a counter-phasing system to reduce voltage to a low value, (2) gap preserving system. In the Accumulator are (1) a stacking system, h=10, 6.289 MHz, and (2) an unstacking system. These subdivide further, for controls purposes, into 9 separate systems.

1. Debuncher high gradient cavity, power amplifier, and drivers. Two cavities/module. Location: AP50.
2. Debuncher high level system. AP50.
3. Debuncher Gap and Diagnostic System. AP50.
4. Debuncher Low Level System. Location AP10.

5. Accumulator Stacking System. Location AP50.
6. Accumulator Unstacking System. Location AP50.
7. Accumulator Unstacking System, $h=2$ bunch narrowing or $h=83$ splitting. Location AP50.
8. Accumulator Low Level System.
9. Accumulator 53 MHz System.

The RF controls use standard modules. The estimate of modules needed was influenced by the number being used in the Tevatron RF system. Local microprocessors will be used for slow loop control. A precision frequency meter will require a GPIB interface.

There are additional rf controls needed for the MR \bar{p} production cycle:

1. Main Ring phase lock to Booster for single batch acceleration
2. Low level rf system for single batch acceleration and bunch rotation

There are additional controls needed for MR p and \bar{p} acceleration:

1. 53 MHz rf system and controls
2. 2.5 MHz rf system and controls
3. higher harmonics in the 2.5 MHz system
4. accelerate 1 to 14 bunches and their coalescence
5. instrumentation for \bar{p} and p coalescence and acceleration

Energy Saver rf controls:

1. Phase locking of the Main Ring to the Energy Saver
2. Colliding region position control.

13.8 Stochastic Cooling Controls and Monitoring

Stochastic Cooling Controls and Monitoring are centralized in building 30. For control and monitoring purposes the following classification may be useful: (1) beam pickup electrodes, (2) low level electronics (including preamplifiers), (3) medium level electronics (including gain and phase correction, circuits, filters, etc), (4) high level electronics (including TWT), (5) kicker electrodes.

1. Amplifier power supplies. There are a total of 120. 49 of them are in service building 30; the remaining 71 are in the tunnel or adjoining stub rooms distributed as follows: A60, 24; A10, 26; A20, 3; A30, 18. Each amplifier power supply requires a control bit (on/off), a status bit, and current and voltage monitoring.
2. TWT power supplies. There are 62 travelling wave tube power supplies distributed as follows: A20 tunnel or stub room, 3; A30 tunnel or stub room, 18; A30 service building, 41. Each supply requires the following monitoring and controls (taken from the TWT power supply specification).
 1. 5 status bits: timeout state off/on, standby state off/on, beam on/off, local/remote, fault.
 2. Analog helix voltage remote monitor output, 1 mV per volt. 1% accuracy implies 7 bits + sign is adequate.
 3. 3 control bits: AC power on/off, fault reset, beam voltage on/off.
 4. DAC to control the helix voltage.
 5. Turn on permit signal.
3. TWT protection monitor. n = 41 distributed as follows: A20 tunnel or stub room, 2; A30 tunnel or stub room, 18; A30 service building, 21. Each monitor measures forward and reverse TWT power as well as power delivered to the kickers. Each monitor will contain a microprocessor which protects TWT's from a disaster. The output from the microprocessor to the control system can be some digital numbers (powers) and bits (status).
4. PIN diode switch. n = 8 distributed as follows: A20 tunnel or stub room, 2; A30 tunnel or stub room, 4; A30 service building, 2. Requires a control bit and a status bit. (on/off).
5. PIN diode attenuators. n = 8 distributed the same as the switches. Each requires a DAC with a look up table to provide the proper current or voltage to change the attenuation level. Status is monitored. Should the table be in the host or reside in the module.
6. Trombones. n = 90. 29 of these are in the A30 service building. The remaining 61 are in the tunnel or stub rooms: A60, 13; A10, 10; A20, 8; A30, 30. These are delay lines whose length is changed by a stepping motor actuator. Readback of the position can be done either with a linear pot with a local voltage reference or by a shaft position encoder.

7. Coaxial relays. These will be used for a variety of functions. Test signals can be inserted into amplifiers. Multiplexed coaxial relays switch the spectrum analyzers and the network analyzer to different places.

Coaxial relays in trunk lines (medium level electronics) are used to inject and extract signals, and also used while beam is on. The total number is 100, but provision should probably be made in the control system to add more later. They are all in the tunnel or adjacent stub rooms distributed as follows: A60, 15; A10, 20; A20, 9; A30, 56. Each relay requires a control bit and a status bit. or CAMAC-181?

8. 3 spectrum analyzers, 2 in bldg 10 and 1 in bldg 30 require GPIB interfaces.
9. The network analyzer in building 10 requires a special interface to the HP-9826 computer. This may consist of two separate things: (1) an interface between an O80 module and one of the GPIB buses in the HP computer for block data transfer. Data rates expected are 100-200 Kbytes every 20 minutes or so during startup of the system. Data will be passed through DEC-P to the VAX without any work done on it by DEC-P. (2) an interface using either RS-232 or GPIB to another bus of the HP computer for chit-chat. This will be a short list of commands that load already written programs from the Winchester Disk into the HP computer and make inquiries as to whether or not the processing is done or how far along it is. A command will also allow termination of the program in the HP:

In addition there are cryogenics systems needed for stochastic cooling:

1. Refrigeration. Will be done in a way similiar to the Energy Saver and use a multibus REF crate connected to the CAMAC system by an O80 module.
2. Compressor. This a separate REF crate.
3. Extra refrigeration monitoring points. A10: 10, A20: 10, A30: 15, and A60: 30. These are thermocouples or some other type of temperature sensitive device and will probably go to ADC channels.
4. There will be a small number of devices to control valves, monitor flows, etc. on cryogenics. These are not yet defined but will be bits, ADC's etc.
5. 3 to 22 Dewars each have a He level controller. A status bit says that the level is high enough to cover the filter.

13.9 TeV I Beam Diagnostics Interface to the Controls System

13.9.1 Beam Position Monitors. In the Energy Saver the BPM/BLM system is run by a multibus crate containing 2 microprocessors. It would be useful to take over as much of this system, including software, as possible. There are, however, some major differences between the Accumulator and Debuncher BPM's and those in the Energy Saver and Main Ring. Besides larger apertures, the pickups have to be bidirectional and sensitive at various frequencies.

The number of beam position detectors in the Accumulator and Debuncher rings has been worked out by Mills, Ruggiero, and Holmes, and puts either a H or V detector at every quadrupole. Six additional pickups are added in the Debuncher. Six more V pickups have been added in the Accumulator.

Thus the total number are 48 H and 42 V in the Accumulator, and 60 H and 60 V in the Debuncher. The total number in the rings is 210. This is more than the canonical number of 4 to 5 per betatron wavelength but allows for some redundancy. Typically there are usually a small percent that are not working at one time. These detectors will be capacitive pickups with preamps located in the tunnel. Each pickup has two plates so position and intensity information can be derived either with hardware or software (choice not yet made).

Beam position monitors in the Accumulator will also be used as clearing electrodes.

13.9.2 Beam Loss Monitors. It is assumed that the number of loss monitor is roughly equal to the number of BPM's and that they are of the same type as the Energy Saver BLM's. Additional loss monitors are needed in the beam lines and around the target station.

13.9.3 Beam Current Monitors. There needs to be one in each ring and one in each beam line. In the D one needs to measure pulse to pulse variations to accuracy of about 1% for optimizing targeting. Sensitivity desired is 0.1 μA or 10^7 p's. The precision current monitors will need GPIB interfaces to the control system.

13.9.4 Beam Profile Measurements. There are several possibilities: flying wire scanners, SWIC's, segmented or grid SEM's, gas jets with collection of ions. SEM grids appear to be the best solution for the beam lines and gas jets for the Debuncher and Accumulator rings.

Each SEM grid will require an interface containing a microprocessor. The FNAL secondary beam line SWIC scanner produces a digitized profile, calculates the mean and sigma of the distribution, and has snapshot capability. This information can be interfaced into the control system. Once this is done, graphical displays, emittance measurements, etc. are possible using the VAX. The numbers needed are approximately AP-2, 7; AP-3, 7; T-line, 4; for a total of 20.

CHAPTER 14

CONVENTIONAL CONSTRUCTION

The Tevatron I project includes a considerable amount of conventional construction - site development, buildings, utilities, roads and parking. This construction is divided into two parts, the construction for the antiproton source and the construction for the experimental areas at B0 and D0 in the Main Ring. This chapter is a brief outline of these construction projects. More detailed descriptions and drawings can be found in the Design Reports and Title I Reports for these areas. At this time of writing, the D0 area is still being defined and is therefore not included here.

14.1 Antiproton Source Construction

The conventional construction related to the production and accumulation of antiprotons includes:

F18 Extraction Hall consists of an underground enclosure replacing 55 ft of the Main Ring enclosure and containing magnets used to extract the 120-GeV proton beam from the Main Ring Accelerator.

Pretarget Enclosure consists of an underground enclosure containing magnets used to transport the 120-GeV proton beam from the F18 Extraction Hall to the Target Hall.

Target Hall consists of an underground enclosure containing a proton targeting station and the magnets used for antiproton beam transport and return bypass. The Target Hall also consists of a high bay building at grade with an overhead crane.

Antiproton Transport Enclosure consists of an underground enclosure containing magnets used for both the beam injection into and for the beam extraction from the Debuncher-Accumulator Rings.

Debuncher-Accumulator Rings Enclosure consists of an underground enclosure containing the magnets for both accelerator rings. The Rings Enclosure also consists of the equipment access hatches and the personnel accesses to the Service Buildings.

Service Building 10 consists of a structure at grade containing power supplies, ventilation equipment and a control room to be used for initial commissioning.

Service Building 30 consists of a structure at grade containing power supplies, ventilation equipment and cryogenic compressors.

Service Building 50 consists of a structure at grade containing power supplied for both magnets and rf systems, and ventilation equipment.

Site Development consists of new and relocated roads, parking and hardstands, drainage systems and structures, utility extensions and landscaping.

Primary Power consists of duct banks, primary feeders, switchgear, substations and Master Substation work.

Process Water consists of extensions to and new equipment for Low Conductivity Water, Chilled Water and Heating Water systems. The locations of these structures are shown in Fig. 14-1.

These packages are described in more detail below.

14.1.1 F18 Extraction Hall. The F18 Extraction Hall is a widened portion of the Main Ring Enclosure approximately 55 ft long. A new rectangular cross section 11'-6" wide x 8'-0" high will replace the existing circular arch cross section 10'-0" wide x 8'-0" high. The additional area is required for the F18 extraction magnets as well as for cable trays, bus and piping displaced by these magnets. The F18 hall is shown in Fig. 14-2.

A short construction time with minimal interruption to the Main Ring has influenced the planned construction at F18 Extraction Hall. The existing Main Ring base slab at Elev. 722'-6" will be reused and widened. Five Main Ring arch precast sections will be removed and will be replaced with nine new rectangular precast sections. The two new precast end sections have partial end wall transitions to match the adjoining arch sections. Only a short concrete filler is poured for the walls and roof. The precasts are set in a grout bed and all joints are caulked and covered with a membrane.

The Main Ring and Energy Saver magnet strings will be left in place in the F18 area and will be carefully boxed around and protected. Much of the existing cable trays and piping will be temporarily supported on this boxing so that the precast arch sections may be removed. After the new precast sections are in place, the trays and piping will be reattached and additional services and lighting installed.

An operational requirement for maintaining the helium transfer piping on top of the Main Ring Berm severely constrains the earthwork at F18 Extraction Hall. The helium piping will be supported above the excavation by using paired lightweight trusses over two 90 ft spans. Excavation work will be done along and under these pipe trusses. The backfilling work will also be done around and under these trusses. The helium piping and F18 Extraction Hall geometry require that the pick point for the precast sections pass under the pipe trusses. A large "C" structural member will be used on the mobile cranes to lift up the existing sections and replace the new precast sections.

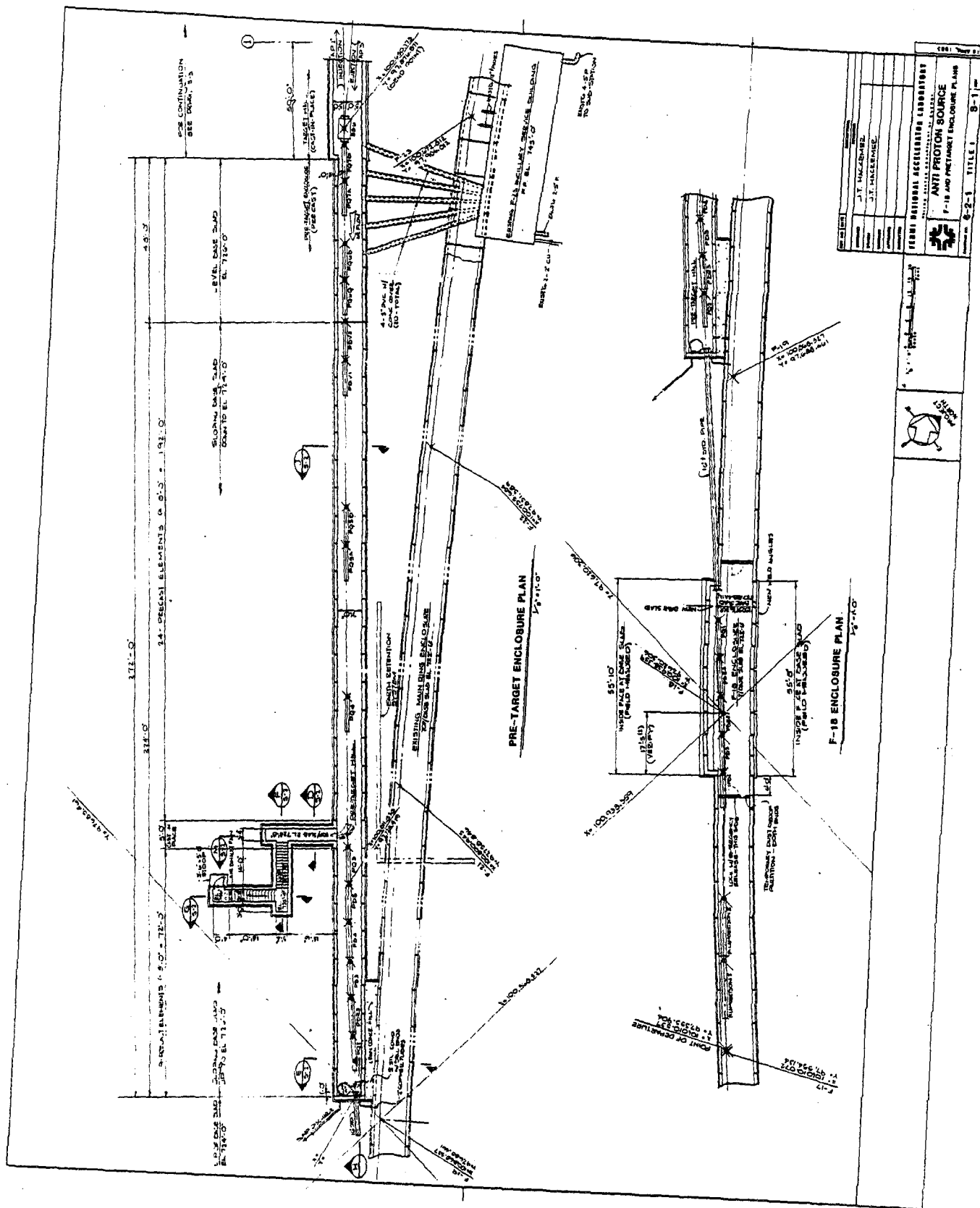


Figure 14-2

Lighting and power for the new F18 Extraction Hall will be extended from the adjoining Main Ring sections. Similarly, the ventilation for the new hall will be the same as for the present F18 enclosure.

14.1.2 Pretarget Enclosure.

The Pretarget Enclosure is an underground structure approximately 325 ft long and links the F18 Extraction Hall to the Target Hall. Throughout most of this length, a rectangular cross section 7'-0" wide and 8'-0" high is used and contains the beam transport magnets for the 120-GeV proton beam. It is also shown in Fig. 14-2.

The floor slab of the Pretarget Enclosure rises in elevation from 724'-0" to 726'-0", approximately paralleling the rise in beam line. Near the south end of the enclosure is a personnel exit stairway, and at the north end the enclosure joins into the Target Hall.

A 65 ft long steel beam pipe connects the F18 Extraction Hall and the Pretarget Enclosure. In the length of this beam pipe, the extraction line has moved away from the Main Ring sufficient distance that the new Pretarget Enclosure may be constructed without interference to the existing Main Ring sections.

A soldier beam, wood lagging and earth tieback system is planned to retain uniform earth pressures around the adjacent Main Ring arch sections, and to minimize the excavation size. These soldier beams also are part of the helium pipe truss abutments used for the F18 construction.

Lighting and power will be extended from the Target Hall. Ventilation through the Pretarget Enclosure is done with an exhaust fan at the south personnel exit and make-up air from the Target Hall. Power communication conduits will join the Pretarget Enclosure to the Main Ring at the south end, and to the F23 Ancillary Service Building at the north end.

An earth shielding berm is placed above the entire length of the Pretarget Enclosure merging into the Main Ring berm at the south end and abutting to the Target Hall at the north end.

14.1.3 Antiproton Target Hall and 120 GeV Target Station. The 120-GeV Target Station is housed in a 144 ft long underground structure that is contiguous with the Pretarget Enclosure and the Antiproton Transport Enclosure. This structure is 8'-6" high and varies in width from 11'-6" to 16'-0". A large shaft 11'-6" wide and 37'-0" long contains the target vault steel core and provides access from the Target Hall above. Figure 14-3 shows plan views of the Target Hall.

The Target Hall is a large, high crane-bay building 57'-6" wide, 144'-0" long and 27'-0" above grade. A 20 ton bridge crane provides 17'-0" clear lift above the Target Hall floor at Elevation 747 ft.

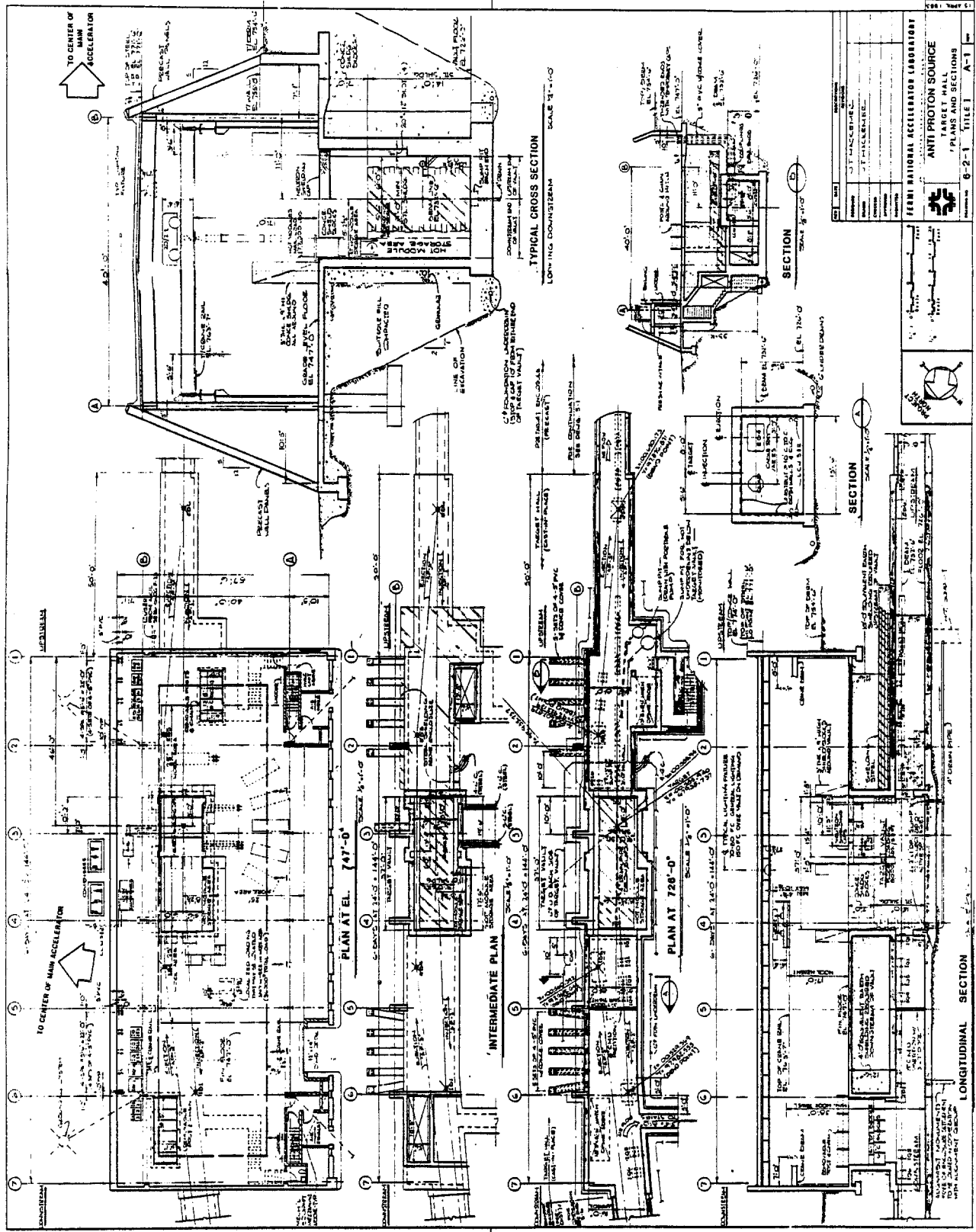


Figure 14-3

The exterior appearance of the Target Hall is akin to the Antiproton Service Buildings and reflects the construction of the Linac, Transfer Gallery and Cross Gallery. Sloping textured concrete walls along the long dimensions meet into massive end walls that retain the earth berm. Window, door and louver openings and contrasting wall panels interrupt the sloping walls in a symmetric pattern.

Access to the Target Hall is via existing and improved Kautz Road, which swings south of the Rings Enclosure and leads north to the Wilson Hall west parking areas. A large equipment door and two personnel doors open from the Target Hall to the parking area by Kautz Road.

A number of functions are served in the Target Hall. Access to the target vault and to the thirteen target modules is provided both for initial installation and subsequent maintenance and changeover. In addition, weather protection is afforded during the changeover times when target modules are being placed in shield caskets. The Target Hall also provides space for the power supplies and support equipment associated with the target-station and beam-transport magnets. Access to the Pretarget Enclosure and to the Antiproton Transport Enclosure is allowed through shielded vertical hatches. The Target Hall also provides physical security to the equipment within.

The Target Station is constructed within a concrete vault resting on undisturbed glacial till. This stratum is firm and dense with very low permeability. Along the sides of the target vault, underdrains will be placed and connected to a sump for ground water monitoring. Five ft of granular material adjacent to the concrete vault walls will assure drainage to the underdrains below.

Several closed-loop cooling water systems will be used for cooling target modules. Within the target vault, concrete floor curbs will limit spread of any accidental water leak in target modules. A separate sump will connect to this curbed area and the piping will be cast into the base slab. Similarly, at the floor above the vault opening, curbing will prevent water spills at grade from dropping into the vault.

Above the Target Vault, shield blocks will be placed and securely anchored to the floor. These shield walls will provide both physical and radiation protection during the time target modules are removed from the vault and placed in shielding caskets. At no time will repair work be done on radioactive modules components within the Target Hall.

Equipment access to the Pretarget Enclosure and Antiproton Transport Enclosure will be through two vertical hatches. At the upstream hatch, three ft of steel and nine ft of concrete will be used for the 120-GeV proton beam requirement. At the downstream hatch, 12 ft of concrete will provide the 8-GeV antiproton-beam requirement.

Personnel access is through two stairway/labyrinths. Interlocked doors will limit access during power-on and beam-on conditions.

Ventilation in the Target Hall will be maintained with positive pressure to assure no outflow of possible air contamination from the vault below. High efficiency particulate filters will be used at the upstream end of the target vault for the air system circulating through target modules.

Fire protection in the Target Hall will be served by a fire hydrant at the road, two hose cabinets within the building, portable Metal-X extinguishers throughout the area and ionization type smoke detectors. No sprinklers will be used in the Target Hall.

Secondary power enters the Target Hall from a substation along Kautz Road and serves the switchboard for the building. A small service of emergency power from the diesel generator at Service Building 50 will be extended to the Target Hall for crane and sump pump operation.

LCW cooling water will be extended from the F23 Main Ring Service Building. ICW water will be available for a primary heat exchange for the small closed loop water systems for the target modules.

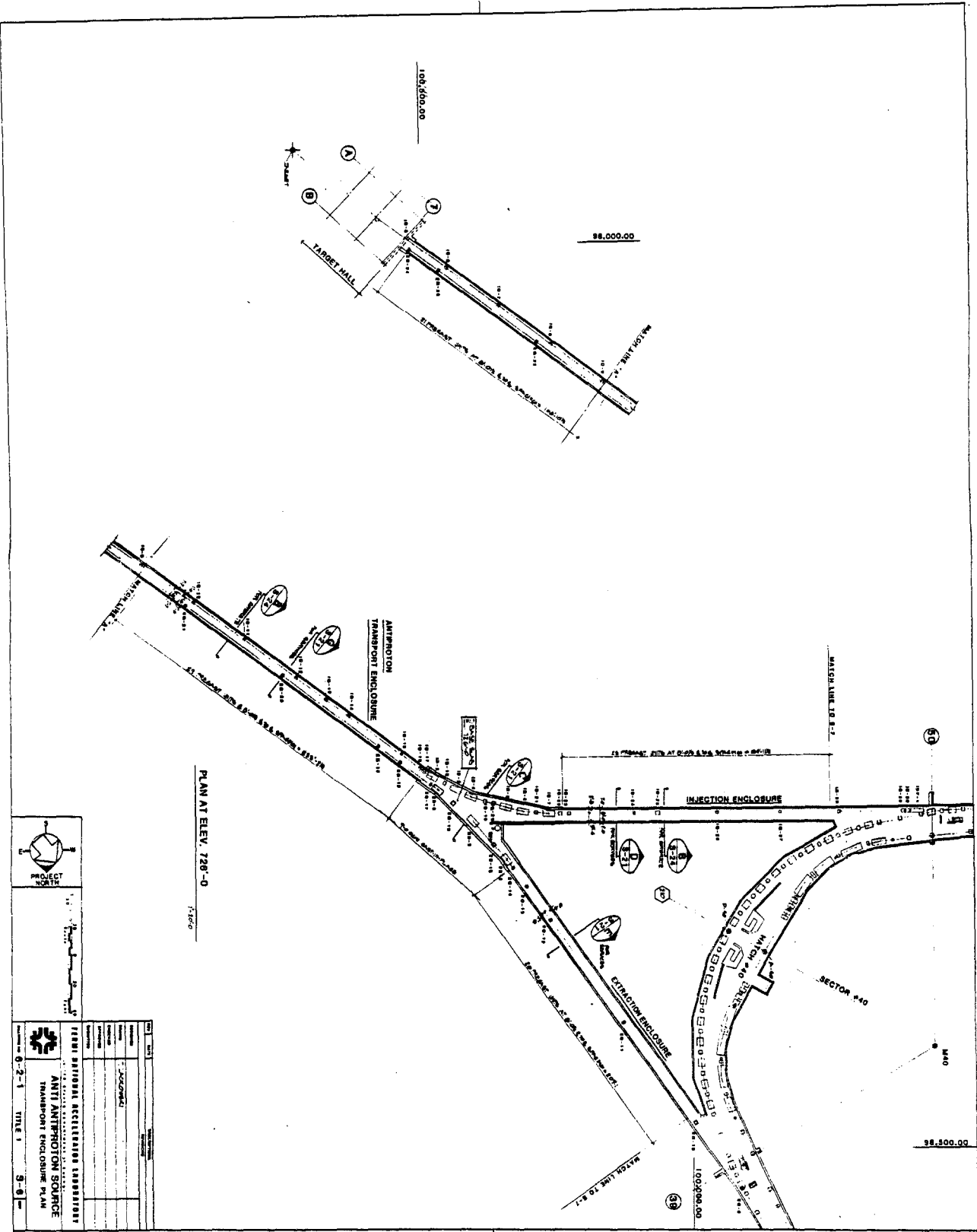
14.1.4 Antiproton Transport Enclosure. The Antiproton Transport Enclosure is an underground structure approximately 680 ft long and links the Target Hall to the Rings Enclosure. The first 400 ft of enclosure joins to a "Y" section 80 ft long, which divides into two enclosures, each 200 ft long, each connecting to Sector 50 and 30. It is shown in Fig. 14-4.

Through the long straight lengths of this enclosure, a rectangular cross section 8'-0" wide and 8'-0" high is used and contains the beam transport magnets for both the 8-GeV antiproton beam injected into the Debuncher Ring at Sector 50 and the antiproton beam extracted from the Accumulator Ring at Sector 30. A 9'-0" high enclosure and in width varying from 9'-0" to 30'-0" contains the larger dipole magnets that bend the beams through the legs of the "Y" section.

The magnets are suspended from the special inserts cast into the enclosure ceiling. Magnets and other equipment are rolled beneath the suspended magnets to install or replace such items without removing other magnets for access. Cable trays, piping and utilities are mounted on the ceiling or tightly against the walls.

In the section containing both the injected and extracted beam lines, only small quadrupoles are used and a reasonable personnel aisle is maintained. No hatches open directly into the Antiproton Transport Enclosure. Equipment access is made from both ends through the hatch in the Target Hall and Hatch 40 in the Rings Enclosure.

Figure 14-4



Precast inverted "U" sections placed on a poured slab are used for the straight sections and cast-in-place concrete is used at the "Y" section.

A low earth shielding berm above the entire length of the Antiproton Transport Enclosure defines the location of the enclosure. Design has shown that no additional steel shielding is required between the enclosure and the Indian Road crossing near Sector 40.

14.1.5 Debuncher-Accumulator Rings Enclosure. The Rings Enclosure is a doughnut-shaped underground structure approximately 1650 ft in perimeter. The doughnut is flattened in three places, and these straight sections are termed Sectors 10, 30 and 50. The intervening curved sections are Sectors 20, 40 and 60. There is basic three-fold symmetry throughout. This is shown in Fig. 14-5.

Antiprotons are injected into the Debuncher Ring at Sector 50; they are transferred from the Debuncher Ring to the Accumulator Ring at Sector 10 and are extracted from the Accumulator Ring at Sector 30. Tune-up protons from the Booster Enclosure are also injected into the Debuncher Ring at Sector 30.

The Rings Enclosure has a constant level floor throughout and at the same Elevation 726 ft. as the Target Hall and Antiproton Transport Enclosures. The Rings Enclosure is 8'-0" high and of width varying between 17'-8" to 35'-0". Most of the enclosure is clear span; only at Sectors 20, 40 and 60 are walls placed to reduce the very wide roof spans.

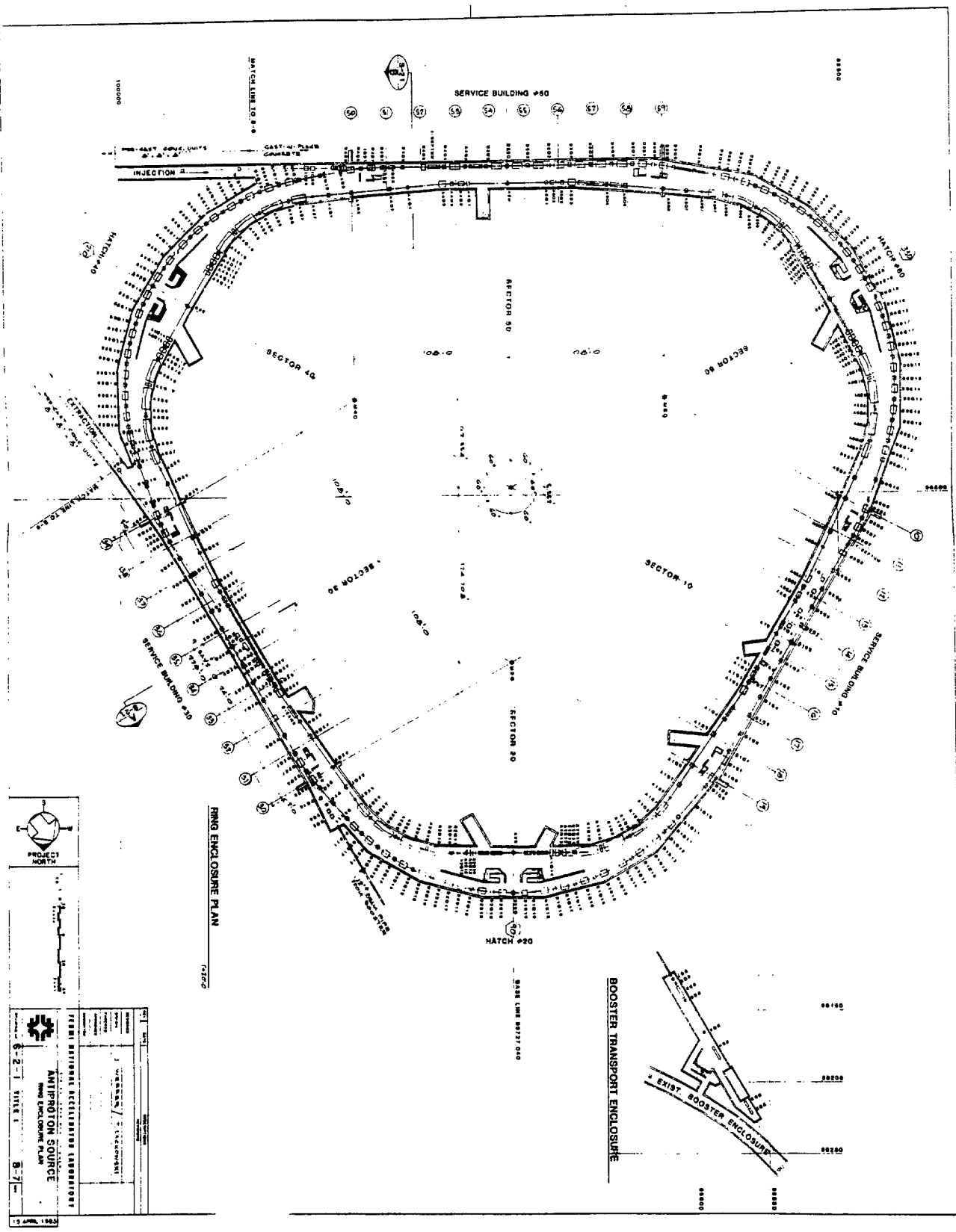
The Debuncher Ring is installed at Elevation 728'-6", or 30" above the floor along the outer wall of the enclosure. The Accumulator Ring is at the same height along the inside wall and the Sector 10 Beam Transfer is also at this height. Both Rings and Beam Transfer components are floor mounted. The Extracted Beam and both Injected Beams enter the Rings Enclosure at Elevation 732'-6", or 18" below the ceiling, and all these components are suspended from the ceiling.

Cable trays, power bus, piping and other utilities are ceiling-mounted or wall-mounted on both inner and outer walls. Numerous penetrations connect to the Service Buildings above Sector 10, 30 and 50.

Six stairway-labyrinths provide personnel access to and emergency egress from the Rings Enclosure. These stairways are located near the ends of the straight Sectors 10, 30 and 50 and connect to the Service Buildings above. There is also personnel access through the Antiproton Transport Enclosure that leads into and out of the Target Hall.

Three heavy equipment hatches are located at the curved Sectors 20, 40 and 60. These hatches are fitted for removable concrete shield blocks so that the shielding integrity of the entire Rings Enclosure is maintained. Equipment also may be rolled into the Rings Enclosure through the

Figure 14-5



Antiproton Transport Enclosures. Lightweight and compact equipment may be lowered into the Rings Enclosure via a 500 pound equipment lift that connects to the Service Buildings at Sector 10, 30 and 50. During construction and prior to final backfilling, an open wall panel and earth ramp will temporarily provide access into Sector 30 where the Booster beam pipe eventually will be installed.

Ventilation of the Rings Enclosure will be accomplished with three air intakes in the Sector 10, 30 and 50 and three exhaust fans at the Sectors 20, 40 and 60. A portion of this ventilation system will provide the air supply for the Antiproton Transport Enclosures.

Earth berm defines the location of the Rings Enclosure below. The berm is interrupted by the Service Buildings and by the Hatches. Berms from the beam transport lines join into the Rings berm.

14.1.6 Antiproton Service Buildings. The three Antiproton Service Buildings 10, 30 and 50 derive their numbers from the Rings Enclosure Sectors over which the buildings are sited. These service buildings interrupt the Rings Enclosure Berm and, with the berm, emphasize the shape and location of the Debuncher/Accumulator Rings below.

The three service buildings are identical in exterior appearance and nearly identical in interior construction and function. Each building is 35 ft wide and 220 ft long and approximately 14 ft high. Sloping textured concrete walls along the long dimension are interrupted with window, door and louver openings and contrasting texture panels. The end walls are vertical with a massive appearance abutting into the earth berm. The architecture reflects the construction of the Linac, Transfer Gallery and Cross Gallery.

Access to the three service buildings is from a loop road comprised of Kautz Road, Giese Road and Indian Road. A personnel door and an equipment door is near each end of a service building and opens out on the front parking area.

The principal function of each service building is to provide space for the power supplies, control equipment, detection electronics and cryogenic equipment that relate to the accelerator components in the Rings Enclosure below. Much of this equipment is audibly and electronically noisy and requires both water and air cooling systems.

Several special areas are partitioned off in the service buildings. In Service Building 10, a control room requires special air conditioning. In Service Building 30, a cryogenics room separates the machinery noise as well as special ventilation requirements from the balance of the building. Service Building 50 has no partitions, but rather wire cages around certain power supply systems.

Personnel access from the service buildings down to the Rings Enclosure below is through a stairway/labyrinth at each end of the building. Doors at the top of each stair provide radiation interlock, ventilation separation, entrance to the service building and emergency egress. Earth shielding is placed around the stair/labyrinths selectively to maintain the radiation shielding integrity.

The 500-pound equipment lifts are not personnel lifts, but are located, enclosed and shielded for both radiation and personnel safety requirements.

Ventilation equipment for both the Rings Enclosure and service building is contained in the service building. No external ventilation units are used. The air supply for the Rings Enclosure is brought into the left end of each building and fed down the stairway/labyrinth opening. Within each service building, approximately 5 to 7 air conditioning units will be installed under the sloping outside walls. Chilled water and heating water will connect to fan coils in these units.

Secondary power enters each service building at the left end. Process water systems enter each service building from headers in the Rings Enclosure below. Cryogenic piping from F3 enters Service Building 30 through a shielded below-floor trench. Conduits connect the Rings Enclosure to each service building.

14.1.7 Booster Beam Enclosure and 8 GeV Target Station. The Booster Beam Enclosure is an underground structure approximately 120 ft long and, together with beam pipe, links the Booster Accelerator to the Rings Enclosure at Sector 30. The first 25 ft of existing beam pipe connects the Beam Enclosure to the Booster Accelerator Enclosure. New beam pipe, 460 ft long, connects the Beam Enclosure to Sector 30.

The Booster Beam Enclosure is a rectangular cross section, 8'-0" wide by 8'-0" to 12'-0" high, and contains the Target Station equipment and beam transport magnets. The upstream group of magnets are floor mounted, and the downstream magnets are suspended from the ceiling as the beam pitches up and bends level to run to injection magnets in the Debuncher Ring at Sector 30.

Three types of access are provided into the Booster Beam Enclosure. For placing the Target Station steel plate and drawer modules, a removable roof slab is used above the Target Station. Steel is placed during the construction phase, and the roof slab replaced and backfilled over.

Magnets and other equipment are lowered into the enclosure through a new hatch that will be filled with concrete shield blocks during beam operations. Small items may be also rolled in from the adjacent Booster Accelerator enclosure at a common floor elevation.

Personnel access and emergency exit from both the Booster Accelerator Enclosure and the Beam Enclosure will be by a new stair structure which replaces the existing stairs that are demolished by the new construction.

Adjoining the stair structure and hatch opening at grade is a small power supply room, 13 ft x 20 ft. Conduits will run from this room down to the enclosure below and other conduits will connect the Booster Accelerator Enclosure to the Beam Enclosure. Ventilation fan and air supply equipment will also be contained in the power supply room.

A new parking area southwest of the Booster Berm will provide access to the equipment hatch. A low shielding berm will define the beam line and enclosure running from the Booster Berm to the Rings Enclosure Berm. Additional steel will be placed where required above the beam pipe that passes below the South Booster, Well Pond and Indian Roads.

14.1.8 Radiation Shielding. The Antiproton Source Enclosures will provide adequate personnel shielding. Consideration will be given to various operational conditions of the program and to the major components in the target halls, transport lines, and Debuncher/Accumulator Rings. Four conditions are of interest:

- a. Tune up with 8-GeV protons from Booster.
- b. Antiproton production and accumulation.
- c. Debuncher/Accumulator Enclosure access during tune up on the antiproton target.
- d. Work on the antiproton target station.

The sources of radiation considered are:

- a. During tune up with 8-GeV protons from the Booster:
 1. Targeting losses in the Booster area.
 2. Accidental loss of transferred beam in the 8-GeV line between Booster and the Debuncher Ring.
 3. Accidental loss of 8-GeV proton beam in the Debuncher/Accumulator Ring Enclosure.
 4. Residual activity of Booster target.
- b. During antiproton operation:
 1. Targeting losses in the antiproton target hall.

2. Accidental loss of beam in 120-GeV transport line between the Main Ring and the Debuncher Ring.
3. Accidental loss of stored 8-GeV beam in Accumulator Ring.
4. Residual activity of target.

Expected radiation levels under normal operations in all areas with the exception of the antiproton target station will be minimal in any accessible area. The area adjacent to the antiproton target station will be a designated radiation area with posting and authorized access only. Normal operation will be equivalent to the worst case for both the antiproton and Booster target stations. In other areas, accidental loss of the entire beam is the worst case. The following assumptions are being used in designing the shielding:

- a. Tune up of the Debuncher/Accumulator Rings:
 1. Targeting in the Booster area to reduce the 8-GeV intensity from $3E12$ protons per 2 sec to a maximum of $1E11$ protons per 2 sec transmitted to the Debuncher Ring.
 2. Injection of $1E11$ 8-GeV protons per 2 sec into the Debuncher and Accumulator Rings.
- b. Antiproton operation:
 1. Proton targeting for antiproton production with $3E12$ protons per 2 seconds at 120-GeV.
 2. Stored beam in Accumulator Ring of E12 at 8-GeV.

Antiproton production operation is the worst case for the 120-GeV transfer line and target station, and proton tune up is the worst case for the Accumulator Ring and the 8-GeV transfer line and Booster target station. Calculated dose rates assume these conditions.

Shielding materials to be used include compacted earth, regular density concrete and steel plate. Various combinations and thicknesses of these materials will be proportioned according to the limitations of economic design and space. Areas of special shielding design are described below:

Tune Up Booster Targeting: The Booster target area will be an exclusion area with no personnel access while the beam is on. All areas accessible to personnel while the beam is on will have adequate shielding to bring the radiation levels to 2.5 mrem/hr or less. Sufficient shielding of the target will be provided to allow beam off personnel access to the target area.

Outdoor Area Over 8 GeV Transfer Line: A combination of shielding and interlocked devices will be used to insure that the above ground loss rate under accident conditions will not exceed 10 mrem per hour.

Area Above Antiproton Target: This area will be an exclusion area. No personnel will be allowed to work in this area during normal operation. When not operating, personnel will be allowed access. Signs and concrete block walls with interlocked gates will be used to prevent access during beam on conditions.

Area Adjacent to Antiproton Target: Precast regular density 150 pcf concrete blocks will be placed on the floor to separate this from the area above the target and to provide shielding. This barrier will be 3 ft thick and 9 ft tall. Normally personnel will have access to the exterior side of this barrier. This indoor area will require access restricted to authorized personnel only.

Access Labyrinths: There will be several labyrinths throughout this project to permit access to areas of 8-GeV up to 120-GeV beam energy. They will provide a shielding effect equivalent to the adjacent shields. The labyrinths will be consistent with Fermilab experience.

Road Crossings: Access roads over beam enclosures and transfer lines will be shielded to conform with uncontrolled outdoor areas with minimal occupancy.

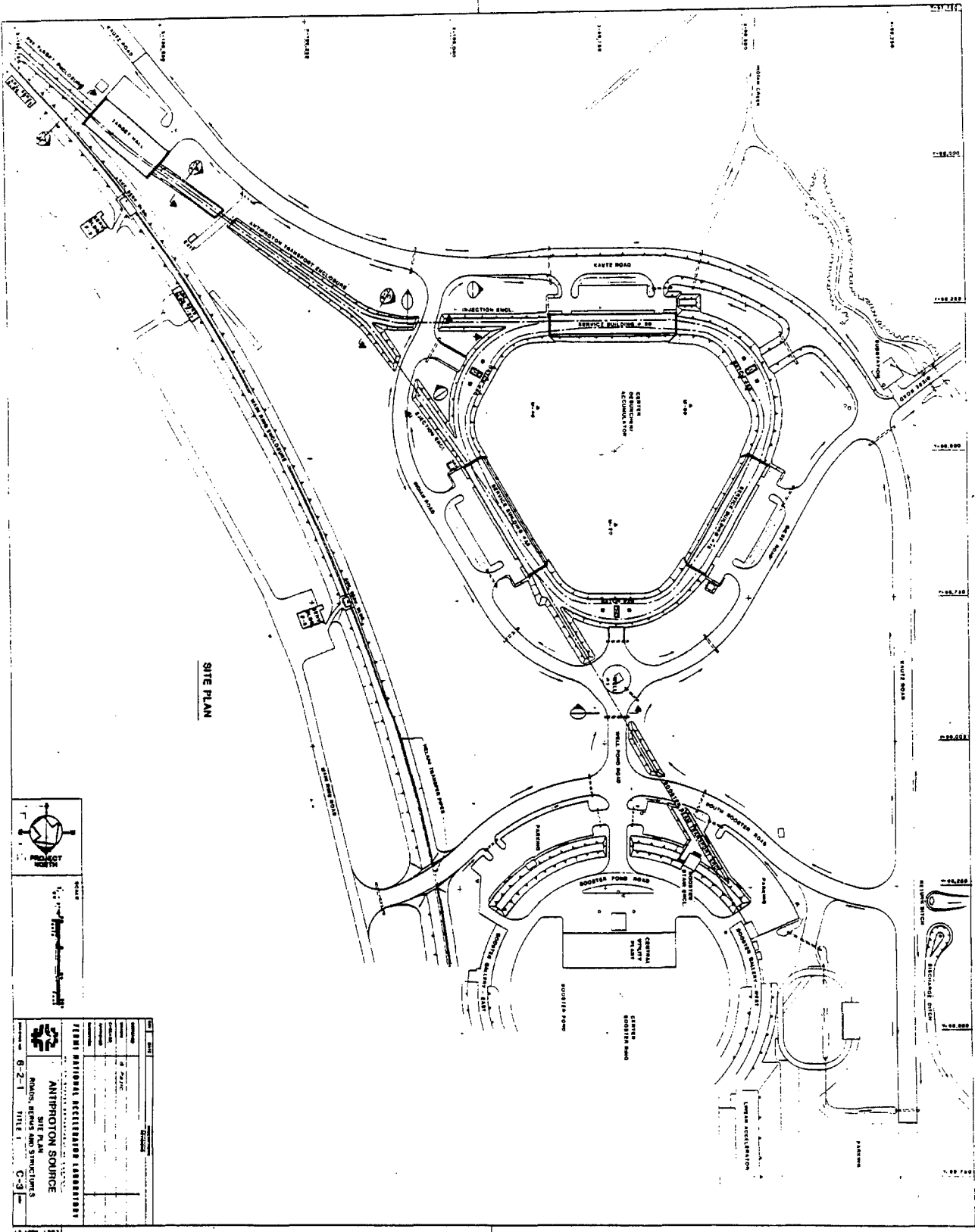
Air Activation: Air sampling equipment will be installed to monitor activation of air from targeting operations. Ventilation systems will be designed to protect occupied areas and to purge target areas prior to access.

Soil Activation: Sufficient shielding will be included around the targets to insure that calculated soil activation will be below release limits and Fermilab guidelines. Underdrain sumps for the target station will be available to monitor soil activation.

14.1.9 Survey and Alignment Control. A coordinated system of monuments, benchmarks and working points is planned for complete geometric control of the project construction from initial site work to final machine component alignment.

Two principal base lines, the Extraction Base and the Booster Base, relate the Main Ring, Booster and Antiproton geometries. Other monuments tie in the three-fold symmetry of the Antiproton Ring, the Target Hall and the Booster Beam Enclosure. Additional monuments are used for the road alignment and utility location

For component alignment, a series of offset lines and monuments will form a closed traverse through the Debuncher and Accumulator Rings



SITE PLAN

Figure 14-6

FERMI NATIONAL ACCELERATOR LABORATORY ANTIPROTON SOURCE SITES, ROADS AND STRUCTURES TITLE I C-3	
NO.	DATE
1	1/2/72
2	2/2/72
3	3/2/72
4	4/2/72
5	5/2/72
6	6/2/72
7	7/2/72
8	8/2/72
9	9/2/72
10	10/2/72
11	11/2/72
12	12/2/72
13	1/2/73
14	2/2/73
15	3/2/73
16	4/2/73
17	5/2/73
18	6/2/73
19	7/2/73
20	8/2/73
21	9/2/73
22	10/2/73
23	11/2/73
24	12/2/73
25	1/2/74
26	2/2/74
27	3/2/74
28	4/2/74
29	5/2/74
30	6/2/74
31	7/2/74
32	8/2/74
33	9/2/74
34	10/2/74
35	11/2/74
36	12/2/74
37	1/2/75
38	2/2/75
39	3/2/75
40	4/2/75
41	5/2/75
42	6/2/75
43	7/2/75
44	8/2/75
45	9/2/75
46	10/2/75
47	11/2/75
48	12/2/75
49	1/2/76
50	2/2/76
51	3/2/76
52	4/2/76
53	5/2/76
54	6/2/76
55	7/2/76
56	8/2/76
57	9/2/76
58	10/2/76
59	11/2/76
60	12/2/76
61	1/2/77
62	2/2/77
63	3/2/77
64	4/2/77
65	5/2/77
66	6/2/77
67	7/2/77
68	8/2/77
69	9/2/77
70	10/2/77
71	11/2/77
72	12/2/77
73	1/2/78
74	2/2/78
75	3/2/78
76	4/2/78
77	5/2/78
78	6/2/78
79	7/2/78
80	8/2/78
81	9/2/78
82	10/2/78
83	11/2/78
84	12/2/78
85	1/2/79
86	2/2/79
87	3/2/79
88	4/2/79
89	5/2/79
90	6/2/79
91	7/2/79
92	8/2/79
93	9/2/79
94	10/2/79
95	11/2/79
96	12/2/79
97	1/2/80
98	2/2/80
99	3/2/80
100	4/2/80

Enclosure. Reference to the internal offset traverse and the external monuments will be provided by sight lines through the equipment hatches and vertical sight tubes up through the berms. Other offset lines will extend the geometry through the Target Hall, Pretarget Enclosure, Antiproton Transport Enclosure and Booster Target Enclosure.

Elevation control benchmarks will be referenced to the Main Ring and Booster Systems. In strategic locations with the Target Hall and Debuncher Ring, concentrically sleeved deep concrete piers will be installed for long term stability of primary benches.

14.1.10 Roads, Hardstands and Parking. Access to the Antiproton Source site by Fermilab personnel is from relocated Kautz Road that runs along the west parking lot by Wilson Hall and the Booster Gallery Enclosures. The Subcontractor's construction traffic will be entering the site via the south Kautz Road entrance off Illinois Highway 56. The roads of the project are shown in Fig. 14-6.

Portions of three roads will surround the Antiproton Ring Enclosures. Relocated Kautz and Giese Roads provide access to Service Buildings 10 and 50 and to Hatch 60. The new Indian Road provides access to Service Building 30 and to Hatch 20 and 40. A short connector, Well Pond Road, joins Indian and Giese Roads to the present Booster area.

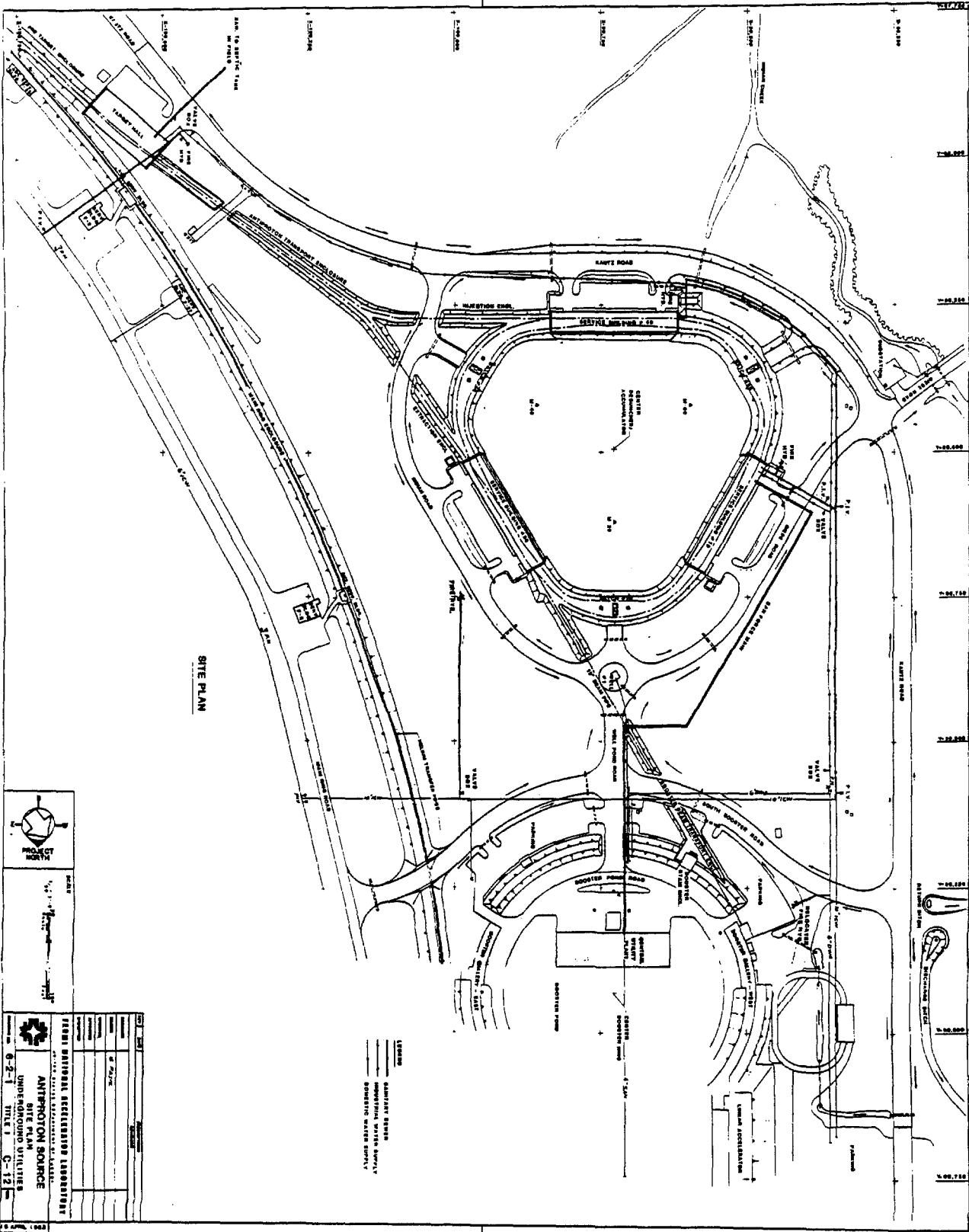
The new South Booster Road joins the relocated Kautz Road with the existing Main Ring Road. The existing berm crossing point is preserved to maintain the present Helium Transfer Line underpass. The South Booster Road intersects the new Well Pond Road and provides access to the new Booster Beam Enclosure as well as parking areas south of the Booster Berm. The present Kautz Road provides convenient access to the Target Hall and to the Pretarget Enclosure.

Parking areas are provided at each of the Antiproton Service Buildings, at the Target Hall and at the Booster Beam Enclosure. Additional parking is also provided between the South Booster Road and the existing Booster Berm.

Hardstand Areas adjacent to the Target Hall, Hatches and Service Buildings are provided. In addition, the adjacent road shoulders and designated parking areas may be used when an occasional large rigging job demands.

A portion of Kautz Road and Giese Road near Service Building 10, Hatch 60 and Service Building 50 will be constructed on a geotextile mat. Due to the considerable depth of unsuitable material at this location, it is not economic to remove such material and backfill with aggregate in the conventional manner. Instead, only the organically filled topsoil and clay layers will be removed, a heavy geotextile mat will be laid and a graded aggregate road subbase will be placed. The principal function of the

Figure 14-7



geotextile mat is to separate the road aggregate from the clayey-silt and fine sand lenses in the lower strata.

Concrete will be used for door aprons, sidewalks and ramps. Bituminous materials will be placed on all roads and parking areas. Coarse aggregate will surround substation pads and other mechanical equipment pads.

14.1.11 Underground Utilities. Power ducts, communication ducts, industrial cold water (ICW) piping, domestic water (DOM) piping and sanitary sewers (SAN) will be extended from existing utility corridors near the Central Utility Plant, south of the Booster Berm, and along the Main Ring Road. These are all shown in Fig. 14-7.

A new 13.8-kV power duct bank will be installed for the Antiproton Source and will run under the existing Main Ring Road. The duct bank will connect from Manhole P71 near the S & C Switches to new manholes along the Main Ring A-Sector and F-Sector Service Buildings and to the new substations at the Target Hall and the three Antiproton Service Buildings.

A new communication duct bank will also parallel the new power duct and connect Service Building 30 to the Main Ring. Other duct bank extensions will join the Pretarget Enclosure to the Service Building F23, the Antiproton Transport Enclosure to Service Building F27 and the Antiproton Ring Enclosures to the Central Utility Plant.

Another group of six communication duct banks connect various sectors of the Antiproton Ring Enclosures with minimum length, nearly straight line runs across the interior of the Ring. Sector 10 is joined with two duct banks to Sector 30; Sector 20 is joined to Sector 40, 50 and 60; and Sector 30 is joined to Sector 60.

Industrial cold water (ICW) piping will be extended from the utility corridor by the South Booster Road at two places. These lines will run along Giese Road, Indian Road and Kautz Road and will serve fire hydrants and hose cabinets at Service Buildings 10, 30 and 50. ICW piping will also be extended from the Main Ring Road corridor under the Main Ring Berm and to the Target Hall fire hydrants and hose cabinets.

Domestic water (DOM) piping will parallel portions of the new ICW piping and will connect to Service Building 10 and the Target Hall. Domestic water will not be available at Service Building 30 and 50.

Sanitary sewers (SAN) will be extended with a lift station from the Central Utility Plant along Well Pond Road and Giese Road to Service Building 10. Sanitary facilities will not be available at Service Building 30 and 50. Due to the remote location, the Target Hall sanitary lines will be connected to a septic field system south of Kautz Road.

14.1.12 Primary Power, Switchgear and Substations. The Antiproton Source will be powered from three primary feeders. Two of these feeders are existing feeders that will power the geographical extremities of the project that are near the Main Ring and the Booster Accelerators. One new dedicated feeder will power the bulk of the Antiproton Source loads.

The existing Main Ring Pulsed Feeder 21A4 will connect to the existing Service Building F23, in which are housed the power supplies for the Pretarget Enclosure.

The existing Booster Pulsed Feeder 41 will connect to the new power supplies for the Booster Beam Enclosure.

The new dedicated Feeder 49 will power the Target Hall and the existing Service Building F27 in which are power supplies for the Antiproton Transport Enclosure. However, the principal load for Feeder 49 will be the primary loop around the Antiproton Ring connecting the substations at the new Service Buildings 10, 30 and 50.

A three-way air switch will be installed to provide feeder backup at the Service Building F3 area. Both Feeder 49 and Feeder 48 will be connected to the Antiproton Source primary loop through this switchgear so that each feeder backs up the other. Local switchgear at the Service Buildings 10, 30 and 50 will not be used, but the primary feeder loop ends will be in the substation cubicle to allow manual cable disconnect for primary cable replacement in any part of the loop.

The existing Feeder 48 will be replaced by new feeder cable installed through the new duct bank from the S & C Switchgear to the Service Building F0 area. Direct buried cables will connect all present Feeder 48 loads to the nearest power manhole of the new installation.

The new dedicated Feeder 49 will be derived by freeing up one leg of Feeder 22B at the P71 manhole near the S & C Switchgear. New feeder cable will extend through the new duct bank to Manhole F23 as well as to the new three-way air switch at F3. From this switchgear, Feeder 49 extends through the duct bank that surrounds the Antiproton Rings Enclosure.

An existing 1.5-MVA substation will be used at Service Building F23, and will be connected to pulsed Feeder 21A4. At Service Building F27, a 1.5-MVA substation will be connected to the dedicated Antiproton Feeder 49. A 0.5-MVA substation will be installed at the Target Hall and will be connected to Feeder 49.

Three new 1.5-MVA substations will be installed at Service Buildings 10, 30 and 50. In addition, at Service Building 50, two 1.0-MVA special substations configured for 12-phase operation of power supplies will be installed.

14.1.13 Secondary Power and Distribution. 480-volt, 3-phase power will be brought into the three Service Buildings and the Target Hall and will be terminated into large switchboards. Branch feeders and smaller 480-volt panelboards will distribute the power through the Service Buildings, down through the Rings Enclosure, Pretarget Enclosure and Antiproton Transport Enclosure. Stepdown transformers and smaller panels will provide 120/208 volt, 1 and 3-phase power as required.

The 12-phase power from the special power-supply transformers will be brought in directly to the power-supply equipment at Service Building 50. Except for this case, all other technical power and all house power will be obtained from the same substations and switchboards.

Regulated power from static line conditioners or motor-generator equipment will not be furnished in the Service Buildings or Rings Enclosure. It may be that the dedicated Feeder 49 serving only the Antiproton Source loads, will provide sufficient isolation from other pulsed loads. An alternative that will be considered in Title II design is to reactivate the reserve 345 kV Master Substation Transformer 82 and use this equipment to supply the Feeder 49 loads.

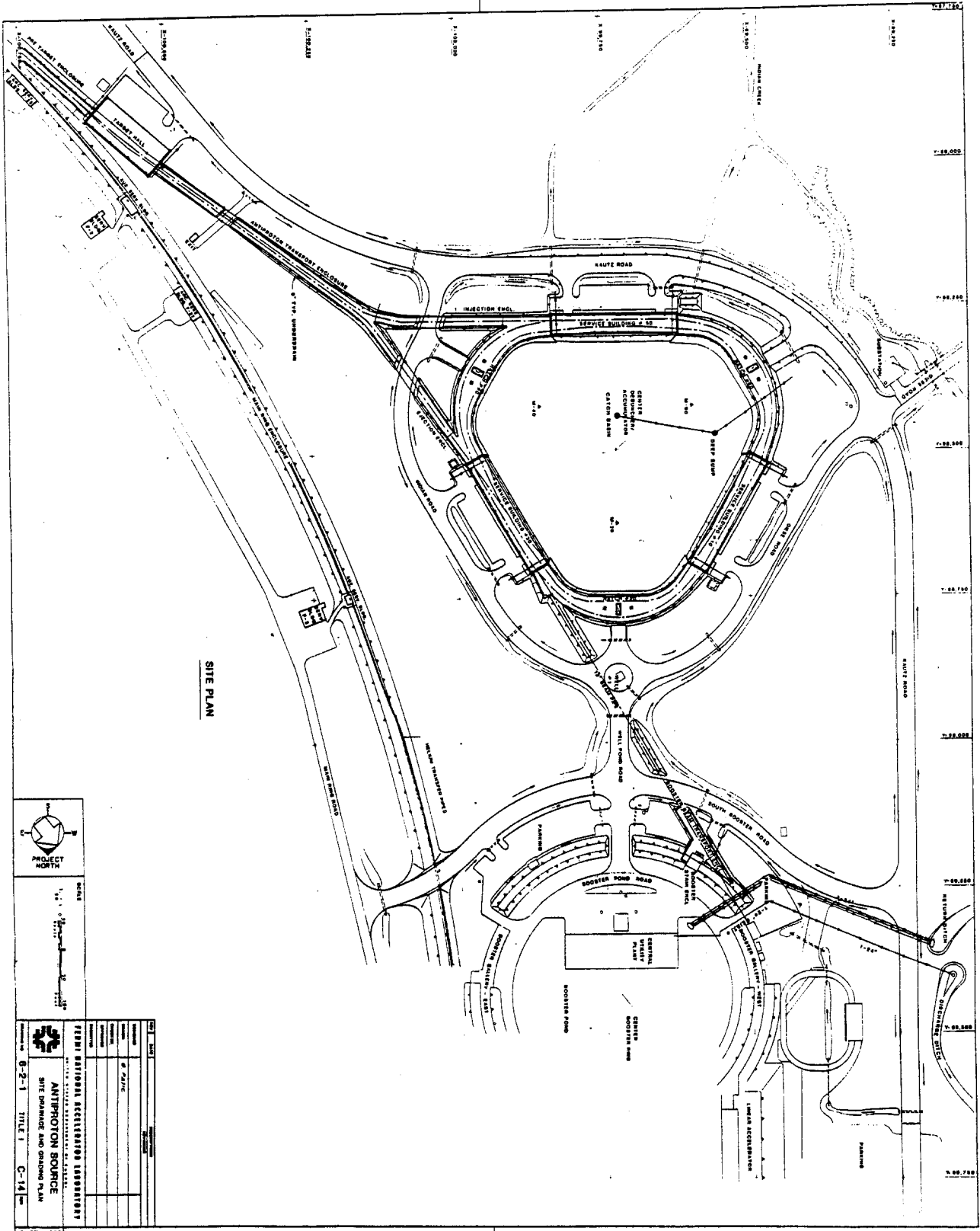
Emergency power will be provided in limited amounts for critical equipment by a 480-volt, 3-phase diesel driven generator mounted next to the substations at Service Building 50. Automatic switch-over and start-up equipment will be provided. Connected loads will be limited to deep sump pumps, instrument air compressors and critical cryogenic equipment such as LHe pumps or vacuum pumps.

14.1.14 Process-Water Systems. The four process water systems that will be used in the various areas of the Antiproton Source include Cooling Pond Water (CPW), Low Conductivity Water (LCW), Hot Water (HTW) and Chilled Water (CHW). In addition, two small closed loop subsystems will be used for the targeting and dump components in the Target Hall. Air cooling is planned in the Booster Target Station.

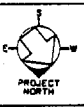
Existing CPW intake and discharge piping from the Booster Pond to the existing Swan Lake and Kidney Pond ditches will be rerouted for the Kautz Road/South Booster Road construction. The intake pipe will be replaced with larger capacity pipe and the intake structure in the Booster Pond will be rebuilt. The discharge piping will be rerouted to a new bubbler on the west side of Kautz Road. Ditches will be realigned to suit.

The LCW cooling system for the Antiproton Target Hall and Pretarget Enclosure will be extended from the Main Ring LCW system at Service Building F23. Similarly, the LCW cooling systems for the Booster Enclosure will be extended from the Booster LCW system at Booster Station 3.

The LCW cooling system for the Rings Enclosure will be derived from new equipment in the Central Utility Plant and new piping that extends



SITE PLAN



SCALE
 1" = 100' (Horizontal)
 1" = 20' (Vertical)

FERMI NATIONAL ACCELERATOR LABORATORY
ANTIPROTON SOURCE
 SITE PLAN AND GRADING PLAN
 DRAWING NO. B-2-1 TITLE 1 C-14

Figure 14-8

along Well Pond Road into the Hatch 20 area. Primary heat exchange for this LCW system will be to the Booster Pond, Kidney Pond and Swan Lake air-water surfaces. Except for the shared primary heat exchange, the new LCW system will be completely independent of the existing Linac, Booster and RF systems in the Central Utility Plant. New CPW/LCW heat exchanger, duplex pumps, expansion tanks, piping and controls will be installed on the upper platform in the east end of the Central Utility Plant. New LCW headers will extend out the south utility tunnel and continue as direct buried piping into the Hatch 20 area.

Hot water will be used for the fan coil units of the Service Buildings and Rings Enclosure. However, due to remote location, hot water is not economic to use in the Target Hall, Pretarget Enclosure and Booster Beam Enclosures. Electric fan coils will be used for these areas instead. There is sufficient capacity in the Central Utility Plant boilers and the HTW piping will be extended down the south utility tunnel and continue as direct buried piping into the Hatch 20 area.

The chilled water required for the fan coil units and other electronic equipment in the Service Buildings and Rings Enclosure will also be obtained from the existing chiller systems in the Central Utility Plant. Chilled water for the Booster Beam Enclosures will be obtained from the nearby existing Booster Gallery. For the Target Hall and Pretarget Enclosure, raw chilled water will be obtained from the systems in the RF Building near Ring Service Building F2.

Piping for the LCW, CHW and HTW systems will be direct buried from the Central Utility Plant into the Rings Enclosure. Within the enclosure, the piping will be wall or ceiling mounted. Headers will be extended from the enclosure up to the Service Buildings.

14.1.15 Finished Site Drainage. Site drainage after all construction is complete will be accomplished with surface grading to open ditches that will drain south and west into Indian Creek. Only the area enclosed by the Rings Enclosure Berm will be drained through catch basins and a pumped deep sump. The drainage plan is shown in Fig. 14-8.

Roof drainage will be collected within the buildings and will be routed out the buildings, under the roads and parking areas and into the adjacent road ditches. Discharge piping from the underdrains deep sumps will also be run to these road ditches. Roads and parking areas are crowned and sloped toward ditches as well. Swales and slopes along the Main Ring Berm and the new Antiproton Source Berms will divert surface drainage away from the buildings and to the road ditches. A small dike along the eastern bank of the Indian Creek contains a high water overflow.

14.1.16 Landscaping. Special precautions will be observed during construction work to protect and preserve the large specimen oak trees within the meadow area bounded by the Antiproton Ring Berm. Trees will be fenced at the drip line where possible; temporary sheeting will be used where deep conduit trenches run near the trees and regrading around these trees will be avoided.

The meadow area within the ring will be graded only where needed for drainage to the catch basins. Topsoil will be replaced and the natural field grasses will be allowed to reappear. The meadow will not be mowed in the future.

Topsoil will be replaced on all other new or disturbed earthwork. Grass seed will be planted on flat areas, a limited amount of sod will be placed at ditch bottoms, and crown vetch cover will be sown on berm slopes and crests.

14.2 BO COLLIDING BEAM AREA

The construction includes:

BO Collision Hall consisting of an underground structure that will replace approximately 100 ft of the Main-Accelerator enclosure, and will contain the experimental physics detectors and both the accelerator and Energy Saver beam components. On the outside wall (away from the accelerator center) will be a large door and moveable shield wall that will provide access to the Assembly Hall.

BO Transition and Equipment By-pass Enclosure consisting of an underground structure that connects the Collision Hall to the existing main accelerator enclosures, and provides a passage for personnel, utilities and magnet moving vehicle around the BO Collision Hall.

BO Assembly Hall consisting of a large pit at the elevation of the Collision Hall and adjoining to the shield-door passage, with a service floor at grade level, all covered by a high-bay building with an overhead crane. The various experimental physics detectors will be assembled, tested, and serviced in this hall prior to placement in the BO Collision Hall.

BO Site Development consisting of hardstands, access roads, drainage facilities, relocation of utilities, extension of services, and temporary earth retaining structures for construction sequencing and adjacent road and building protection.

BO Primary Power consisting of 13.8-kV feeders, substations and switchgear for extending primary power to the BO Experimental Area and into the BO Assembly Hall.

More detailed descriptions of these individual packages follows below. A general plan of the building is shown in Fig. 14-9.

14.2.1 B0 Colliding Beam Experimental Area. The B0 Experimental Area has two completely underground structures, the Collision Hall and the Transition and Equipment Bypass Enclosure, and has a third above-ground structure, the Assembly Hall. All these structures connect with each other and to the main ring enclosure at the B0 straight section.

The Collision Hall is a large cast-in-place concrete structure which will replace approximately 100 ft of the main ring enclosure. The central region portion of the Collision Hall, 50 ft long, 50 ft wide and 35 ft high with a pit 4 ft deep, will contain the 2400-ton Central Detector. The backward and forward regions, which adjoin the central region, are 25 ft long, 36 ft wide and 30 ft high. Various toroidal magnets and detectors, ranging in weight from 400 to 600 tons will occupy the backward/forward regions.

The Transition and Equipment Bypass Enclosure is at both ends of and along the south wall of the Collision Hall. The transition portion, 15 ft wide, 10 ft high, and 40-50 ft long abuts up to the precast arch elements of the main ring enclosure. The Equipment Bypass, 7 ft wide, 9 ft high and approximately 160 ft long, joins into the transition portion. A stair shaft connect the forward region to the forward end of the bypass. All structures are cast-in-place concrete.

The Major Access Passage, approximately 34 ft wide, 37 ft high and 37 ft long connects the Collision Hall to the Assembly Hall. To the west end of the Major Access is a personnel labyrinth and the Minor Access Passage, 5 ft wide and 9 ft high. Moveable concrete shield doors block the Major and Minor Access Passages during accelerator operations. All structures are cast-in-place concrete.

The Assembly Hall is a steel structure at grade level, approximately 98 ft wide, 175 ft long and 31 ft high. The floor level inside the Hall is depressed 4 ft below the outside grade and reached by the ramp at the west end. A lower floor level, approximately 72 ft wide and 100 ft long, matches the floor and pit of the Collision Hall central region and Major Access passage. All below grade portions of the Assembly Hall are cast-in-place concrete.

Within the Assembly Hall is a crane bay, 75 ft wide and 175 ft long. A top-riding bridge crane with a 50-ton main hook and 10-ton auxiliary hook, traverses this area and serves both the grade level floor as well as the lower level. At the east end of the Assembly Hall, a portion of the foundation extends beyond the wall to form a drop hatch, 16 ft wide and 20 ft long.

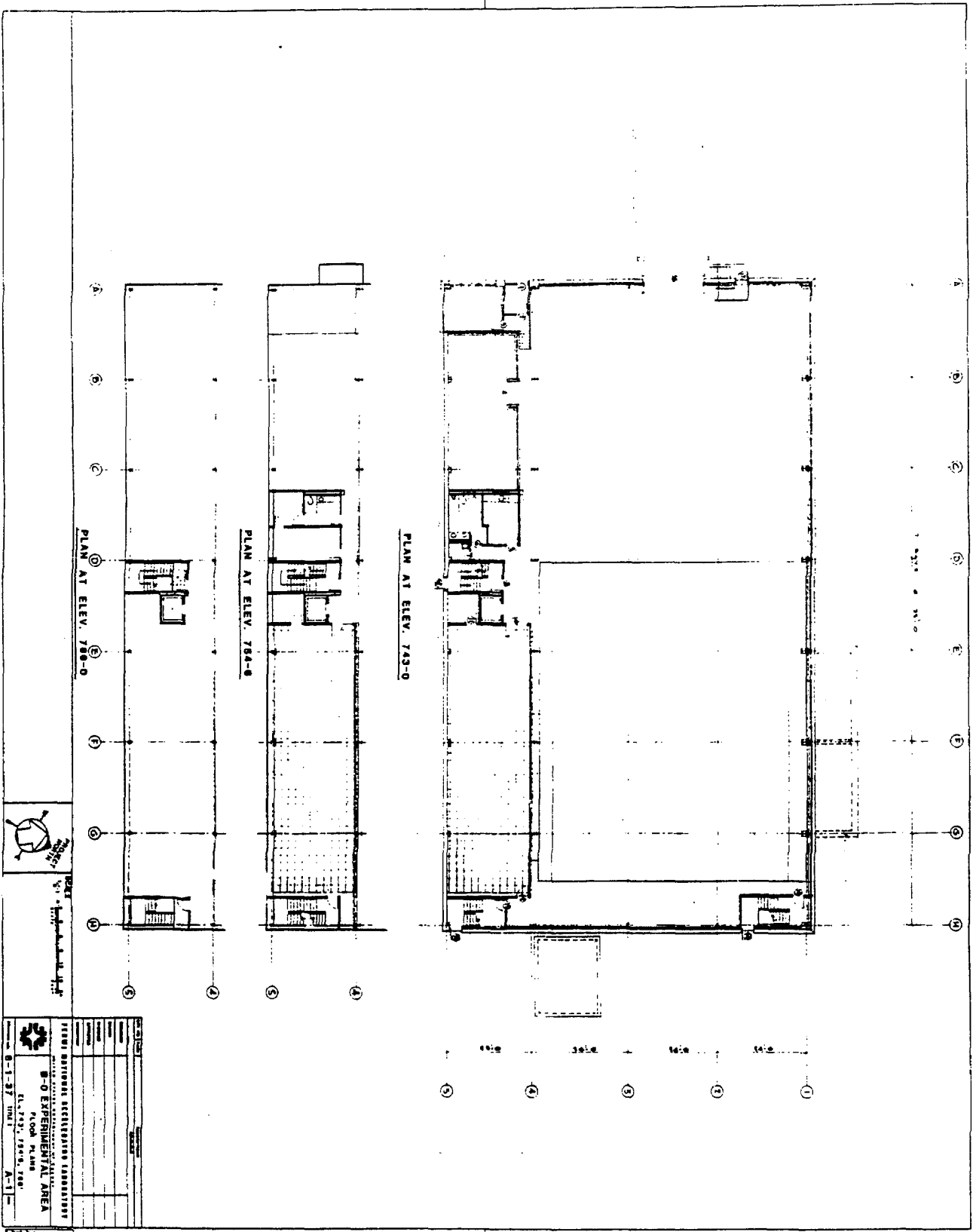


Figure 14-9

The south bays of the Assembly Hall contain three floors. At the grade level is a Counting Room directly above the Major Access Passage, an Equipment Room, a Reception Office, a Kitchenette and a Men's Toilet. On the middle level is another Counting Room, a Women's Toilet, an Electronics Shop Area and an Electrical Equipment Area. The upper level will be used for mechanical equipment, storage and a Shop Area.

Three stairways and an elevator facilitate personnel access to the various floor levels in the Assembly Hall. Near the center of the south wall is a 2000 lb. elevator and stairway that serves all four levels in the Assembly Hall. In the northeast corner is another stairway serving the lower level and the grade level, while in the southeast corner is the third stairway that serves the grade, middle and upper levels. All stairways exist to the outside at grade level.

The main entrance to the Assembly Hall is on the west wall near the south corner. A small canopy is above a double door which leads into the Hall past a small reception office. Two other doors are on the east wall, another door is on the south wall, and no doors are on the north wall which is along side of Road D. An equipment door, 16 ft wide and 16 ft high, is on the west wall at the ramp.

The exterior of the Assembly Hall resembles that of the four industrial buildings to the north of Road D. A precast concrete wall 5 ft high capped with a ribbon of windows surround the Assembly Hall on the east, north and west elevations. Solid concrete walls that match the abutting earth shield berms are used on the south elevation. Vertical steel siding in a colored enamel finish is used above the concrete and window ribbon. The roof has the same slight slope as the industrial building roofs.

Embedded floor tracks and steel floor plates facilitate the movement of the large detector and shield-door loads on the lower operating floor levels in the Collision Hall and the Assembly Hall. The track system under the central detector will have indexing holes for the hydraulic lateral-moving systems. Other pull anchors will be provided for moving the shield doors and equipment transporters. Within the Collision Hall over the backward/forward regions, the roof will be designed for a future 5 ton underhung bridge crane.

The heating, ventilating, and air-conditioning systems in the Collision Hall will provide a variable rate of air exchange dependent on the operating mode and the season. To accommodate the wide spread of equipment head load, the air changes will vary between 1 to 12 per hour. The temperature will range between 60° and 80°F and the relative humidity will not exceed 60%.

A large air-handling unit, with chilled-water cooling coils, electric heating coils and filters will be mounted at grade between the Assembly Hall and the berm at the west end of the Collision Hall. Intake air will

be distributed through underground ducts to four louvers on the west end wall of the Backward Region of the Collision Hall. A purge fan mounted at grade at the east end of the Collision Hall will exhaust air through underground ducts and four louvers on the east end wall of the Forward Region of the Collision Hall. Bypass and mixing dampers on both the air intake and exhaust systems will allow the maximum use of outside air for economic temperature control in the Collision Hall.

During short periods after beam shutdown in the Collision Hall, or in the event of accidental helium or other gas release, the air systems will operate on 100% outside air to rapidly purge the area. The intake and exhaust ducts are located on both sides of the beam lines as well as at floor level and ceiling level.

The Transition and Equipment Bypass enclosures will be ventilated by the systems in the main ring enclosure. Shielding walls may be used at either end of the Collision Hall during collider operations and partitions will isolate the air systems of the Collision Hall and main ring enclosure.

In the Assembly Hall, high-bay and other open areas, the seasonal temperature range will be 60° to 95°F, with no humidity control. Roof exhaust fans will ventilate at the rate of 1 to 2 air changes per hour. An air handling unit located on the upper level, with electric heating coils and intake and bypass dampers will provide make-up air. Additional heating along the outside walls, at doors and in the lower level pit will be provided by electric wall-hung heaters.

The Counting Rooms on the grade and middle levels will be air conditioned the year round. Temperature will range from 70° to 80°F, relative humidity will vary between 40% to 50% and ventilation will be between 4 to 8 changes per hour.

Two air-conditioning systems will be used in each of the Counting Rooms. For the electronic racks, a pair of air-conditioning units will distribute air into the underfloor cable space plenum, up through floor cut-outs and out the top of the racks. The second system will include an air-handling unit with both heating and cooling coils, ceiling diffusers and ductwork above the suspended ceiling. Heating will be provided by electric coils and chilled water coils will be used for cooling.

The reception office, toilets and kitchenette will be air conditioned from the same air-conditioning unit that serves the Counting Room ceilings.

The plumbing systems for the Assembly Hall include toilet facilities for the specified occupancy, electric water coolers, hot and cold domestic-water supply and connection to the site sewer system. Floor drains at the ramp, equipment door, the hatch and in the pits will connect to adjacent underdrain piping.

Underdrains at a level below the structural concrete mats will connect to two deep sumps. Granular backfill material will be placed around all outside walls to insure complete drainage and avoid buildup of hydrostatic pressure on the walls.

Fire protection systems will vary according to the occupancy, location and size of the area. In the Assembly Hall high bay and other open areas, wet sprinklers sized for "ordinary hazard" are provided. Dry pipe sprinklers with pre-action valving in combination with Halon systems are used for the Counting Rooms and the associated ceiling and floor spaces. Hose cabinets are placed at strategic locations about the Assembly Floors and the various levels. A wet standpipe with valving, alarms, siamese connection is located in the northwest corner of the Assembly Hall.

In the Collision Hall and Transition and Equipment Bypass Enclosure, the scientific equipment will serve as fire detectors similar to the operation of the main accelerator and other high radiation areas at Fermilab. Gas detectors will be installed and interlocked with the purge system where the possibility of flammable gas leaks may exist.

Electrical power will be distributed to local power panels from switchboards in the Assembly Hall. High intensity vapor lighting will be used in the high bays and fluorescent lighting will be used in rooms with normal height. Lighting levels will vary between 50 to 150 ft candles depending on the location. Exit lights and exterior lighting will be provided.

14.2.2 200-GeV Vertical Beam Bypass. See Sec. 7.3.

14.2.3 Experimental Equipment Foundations. The physical size and weight of the experimental detectors require massive and relatively stable foundations at approximately 18 ft below the colliding beams. A program of soil exploration down to bedrock has been run to better delineate the subsoil conditions and define foundation alternates.

Three foundation types have been studied; driven H-piling, drilled cast-in-place concrete caissons, and cast-in-place concrete mats. The H-piling technique has proved impractical due to extreme driving resistance indicated by the tough clays and scattered boulders at the depths required. Similarly, the drilled concrete caisson technique has installation difficulties and high cost disadvantages as well.

The massive concrete mat that serves as both an equipment foundation and a base for the underground structures has been investigated in considerable detail. Long term settlement has been computed to be on the order of 1/2". Of this amount, only 3/16" to 1/4" change is expected with the moving detector and shield door loads. The time for this settlement is short (several hours) since the design soil bearing pressure (6000 psf) is less than the creep pressure, indicating soil behavior as a linearly elastic material. No progressive long term settlement is expected since

the design soil bearing pressure is lower than the original in-situ earth pressure and preconsolidation stress.

14.2.4 Radiation Shielding. The B0 Colliding Beam Experimental Area will be designed to provide adequate personnel shielding. Consideration will be given to various operational conditions of the experimental program and to the location of the major detectors in the Collision Hall. Three conditions are of interest:

1. Detectors in place with Colliding Beams.
2. Detectors in place with Fixed-Target Operations.
3. Detectors removed with Fixed Target Operations.

The sources of radiation that are considered are:

1. Accidental loss of beam on magnets in the vicinity of the B0 Collision Hall during acceleration
2. Accidental loss of beam during antiproton production
3. Accidental loss of stored beam
4. Higher intensities of these losses during fixed-target operations

Expected radiation levels under normal operations in all these cases are minimal in any accessible area. Accidental loss of the entire beam is the worst case for all three operating conditions and shielding has been designed for this worst case under the following assumptions:

1. Fixed-target operation has beam of 1×10^{14} at 1000-GeV with a 50 second cycle.
2. Colliding-beam operation has two beams each of 2×10^{12} @ 1000 GeV going in opposite directions. Antiproton production takes place using a proton beam of 2.5×10^{13} protons at 100-GeV with a 2 second cycle.

With these assumptions for accelerator operations, fixed target operations is the worst case and all calculated dose rates assume fixed target operations.

Shielding materials to be used include compacted earth, regular density concrete, high density concrete and steel plate. Various combinations and thicknesses of these materials will be proportioned according to the limitations of economic design and space. Areas of special shielding design are described below.

Berm above Collision Hall: Compacted earth at 130 pcf will be placed above the poured concrete roof slab for a total thickness combination of 11 ft. No personnel are normally required to work in or near this berm area. Calculated dose rate for an accidental loss at this location is 100 mrem/10¹⁴ 1000-GeV protons. This

outdoor area will require a radiation detector set to trip the beam after one such loss. In addition, signs and fences with interlocked gates that permit no access during beam on conditions will be used.

Shield Door at Collision Hall: Precast regular-density 150 pcf concrete blocks will be placed on a concrete-filled structural base frame. The door will be 12 ft thick with 1/4" staggered cracks in the block stack. Top and bottom clearances on the door will be 3" nominal, and a lapped side joint will provide 3" overlap for 6 ft thickness. Normally personnel will be working on the Assembly Hall side of the door. Calculated dose rate for an accidental loss at this location is 50 mrem/10¹⁴ 1000-GeV protons. This indoor area will require restricted to authorized personnel only.

Counting Room at Grade Level: Shielding for this area is provided by the aforementioned shielding door and the 12 ft of structural concrete and earth backfill of the Collision Hall major access passageway. Similar dose rates and access restrictions will apply.

Labyrinth between Collision Hall and Assembly Hall: This labyrinth will be sized with three legs and two cul-de-sacs, on the basis of Fermilab experience in previous construction. Calculated dose rate at this labyrinth for an accidental loss is 40 mrem/10¹⁴ 1000 GeV protons. This labyrinth is located in the same physical area as the Shield Door and will be subject to the same access restrictions.

CHAPTER 15

OPTIONS FOR FUTURE IMPROVEMENTS

The Antiproton Source design must include not only the best system for antiproton production utilizing presently known techniques, but also provisions for improvements either from new inventions or from operational experience. In this chapter, we discuss a number of possible improvements that could increase the peak luminosity or decrease the accumulation time, thus increasing the average luminosity. It is to be emphasized that these improvements are not part of the construction project.

15.1 Momentum Cooling in the Debuncher

As was pointed out in Chapter 4, there is time during the 2-sec Debuncher cycle for cooling after the initial debunching. It is planned to do transverse cooling as part of the initial design. But it is also possible to cool in momentum by a factor 2 during the same time. This will reduce the cooling power needed in the Accumulator or increase the initial cooling speed for the same power.

The momentum cooling will utilize a notch filter (Thorndahl method). The gain shaping is obtained with a long shorted cable that resonates at harmonics of the revolution frequency. This method is preferred to the Palmer method, where the gain variation is obtained with two pairs of pickups in difference mode in a large dispersion region. Because of the large electronic gain needed to obtain the desired cooling rate, thermal noise is a potential problem. Cooling would actually be impossible for our case with the Palmer method, since in it noise is not effectively filtered and would cause the equilibrium beam width to be larger than the initial beam spread. With the filter method, the thermal noise still predominates, but its effect is greatly reduced. The method is very similar to the one used for the precooling step in the CERN AA Ring.

At the start, the beam has a very small energy spread, between 25 and 30 MeV. To get a significant signal, large bandwidth and a large value of η are required. We assume a bandwidth from 2 GHz to 4 GHz and $\eta = -0.004$. An even larger value of η would be desirable, but then extremely high rf voltages would be needed for debunching.

To sharpen the depth of the notches and to cut down thermal noise in the frequency region where there is no beam, the filter will use a cable whose delay matches the revolution period and whose far end is shorted. This filter creates notches not only at harmonics of the revolution frequency, but also at frequencies halfway between. The overlap factor, the ratio of the beam Schottky band width to the separation of neighboring notches, ranges from 0.1 at the lower end to 0.2 at the upper end of the bandwidth.

The signal loss caused by beam dispersion and the cable delay between pickups and kickers is not a problem. If the distance between pickups and kickers is 0.35 times the circumference length, the fraction of signal lost is only 0.5% at the lower end of the bandwidth and 2% at the upper end.

The signal cable is approximately 125 m long. There is a time difference of about 150 nsec between the beam path length and the cable delay. Power amplifiers have electronic delays around 60 nsec.

The room-temperature performance of a copper cable seems to be adequate for the signal cable, where with a 4.45 in. outer diameter, we expect fractional losses between 18% at 2 GHz to 25% at 4 GHz. These losses can be compensated by raising the electronic gain. The phase variation is also reasonably small; from 3% at 2 GHz to 4% at 4 GHz.

To make cooling possible, differentiation of the signal in the network is required. This is accomplished with a short cable, one or two inches long, shorted at the far end.

Pickups and kickers will be made of strip-lines. They will be used for both momentum and betatron cooling. Pickups and kickers have the same configuration. They are grouped in four tanks. Each tank is 4.5 m long and accommodates 4 x 128 plates. The plates are shorted to ground at the upstream ends and their downstream ends are combined together. The combination is done under vacuum, and there are only two leads coming out at the downstream end of each tank.

15.2 Target Development

In order to achieve targets that would survive smaller beam spots (larger energy density deposited) the following approaches to target design are under study:

- (i) Laminated targets with the plane of the laminations perpendicular to the proton beam would decrease the amount of material flow within the plastic zone.
- (ii) Filamented targets would allow the introduction of slip planes across large temperature gradients, resulting in a lowering of the stresses.
- (iii) Powder targets produced by embedding high-density particles in graphite by powder metallurgy would incorporate the excellent shock and high-temperature properties of graphite, allowing enough energy deposition to melt the metal particles. The lower antiproton yield resulting from the lower average target density could be overcome by a much smaller beam spot.

A research and development program to test these ideas will be underway before the \bar{p} source becomes operational.

15.3 Improvements in Stochastic Cooling

The pace of electronic development is strikingly rapid and we expect that high-power, large-bandwidth systems will be significantly improved in the next decade. In particular, we expect that bandwidth will increase by raising the high-frequency end of amplifier systems and that electronic noise will be lowered. Either of these developments could aid the cooling in the Accumulator. If we could predict what these advances might be, we could design them into the system. Failing that, we can make the design as flexible as possible, leaving aperture and straight-section space for testing and installation of these systems. We plan to utilize the shorter 4 ft and 10 ft straight sections for development tests of new cooling systems.

15.4 Electron Cooling of the Core

It would be possible at some later time to add an electron core-cooling system to the Accumulator. This system could be used in several different ways:

- (i) to counteract intrabeam scattering of a stochastically cooled antiproton beam and to increase its density beyond what stochastic cooling can achieve;
- (ii) to use the electron beam directly as the accumulating cooling system. This would require that the transverse emittance of the antiproton beam be reduced stochastically to approximately 0.5π mm-mrad before electron cooling. This stochastic cooling could be done with large momentum spread to get good mixing. Use of electron cooling would then give very high accumulation rates.

We can expect to do this core cooling at full energy, 8-GeV. Electron beams based on electrostatic generators are now being developed for free-electron laser studies with electron energies of 3 to 6 MeV and beam currents of 5 to 10A. The cooling region would be unmagnetized and could be installed in one long straight section of the Accumulator.

For this application, an electron beam of good emittance, good reliability, and very good collection efficiency would be required. We are now engaged in a program in collaboration with National Electrostatics Corporation to measure emittance and collection efficiency and to investigate long-pulse operation.

APPENDIX A

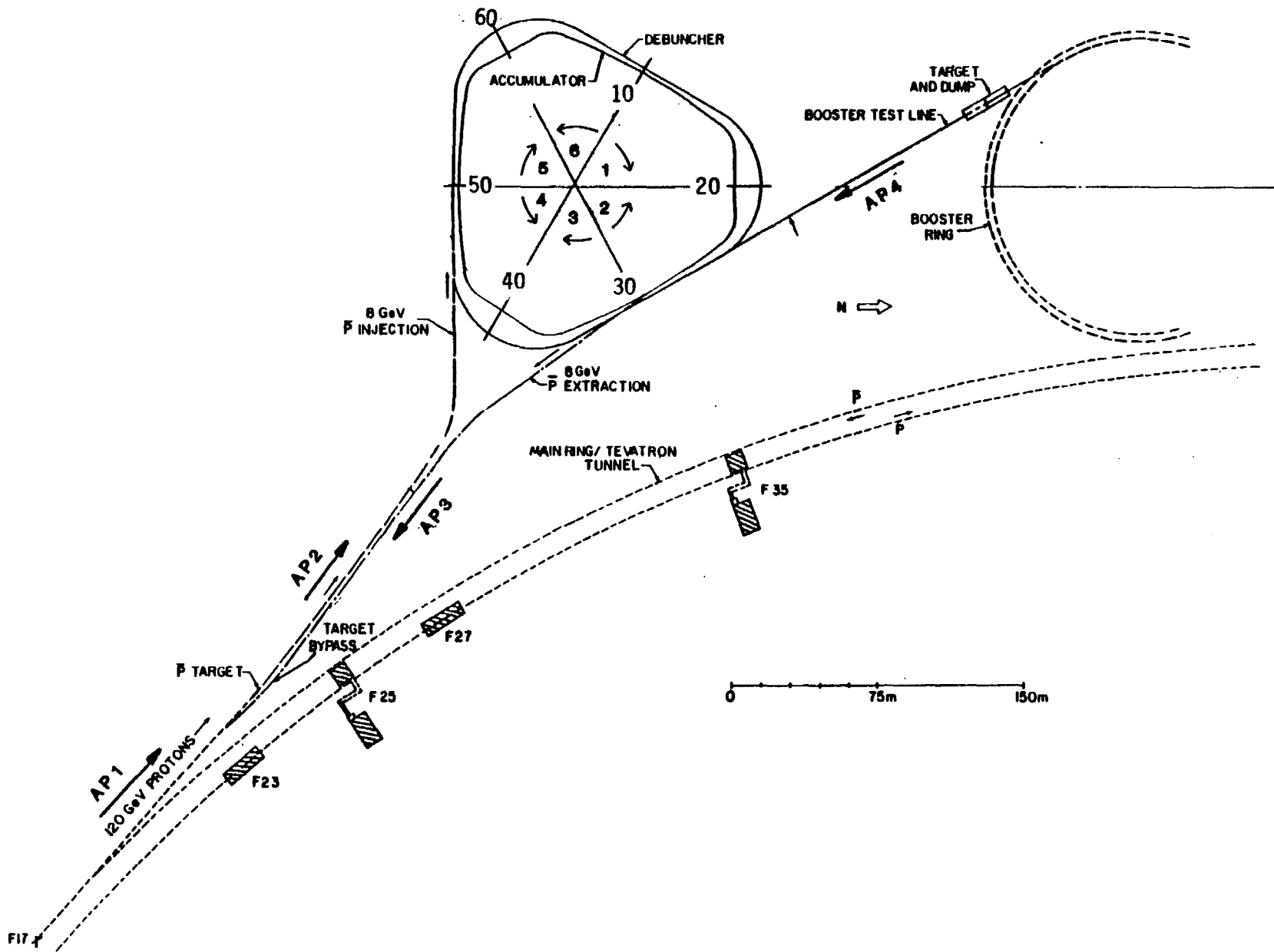


Figure A-1

APPENDIX A. BEAM LINE, ACCUMULATOR, AND DEBUNCHER MAGNET NOTATION

The Tevatron I Antiproton Source consists, in part, of five beam transfer lines and the two rings. Lists of element names for each of these are given below.

1. BEAM TRANSFER LINES

Each transfer line is numbered along the beam direction. (See Fig. A-1) Each element is designated by a three to five character label consisting of a line label, magnet label, and magnet number. The following magnet codes are used:

B	horizontal	dipole
BV	vertical	dipole
BR	rotated	dipole (45°)
Q	quadrupole	
S	sextupole,	when used.

- A. 120-GeV proton line, MR to Target Line AP-1 (Antiproton 1, similar to N1, M1, M2, etc.)

All elements in this line start with "P" for proton. The elements in this line, in sequential order are:

<u>NAME</u>	<u>DESCRIPTION</u>
Main Ring F17	Extraction Location
PLAM1	Extraction Lamberts
PLAM2	
PB1	Horizontal Dipoles
PB2	
PBR1	Rotated Dipoles
PBR2	
PQ1	Quadrupoles
PQ2	
PBR3	
PB3	
PB4	
PB5	
PQ3	
PQ4	
PQ5A	Pair of quadrupoles run as one
PQ5B	
PBV1	Vertical Dipoles
PBV2	
PQ6A	
PQ6B	
PQ7A	
PQ7B	
PQ8A	

ELamb	Extraction lambertson
EQ1	
EBV1	Vertical dipole
EQ2	
EQ3A, EQ3B	Pair of quadrupoles run as one
EQ4	
EBV2	Second vertical dipole
EQ5-EQ15	String of quadrupoles
EB1	
EQ16	
EB2	
EQ17	
EB3	
EQ18-EQ26	
EB4	Horizontal dipole to bypass target
EQ27	
EB5	
EQ28, EQ29	
EB6	Last element in this line
PQ7B	Quadrupole in line AP-1 into which this line merges

D. 8-GeV proton test line, Booster to Debuncher. Line AP-4

All elements in this line begin with "B" for Booster. The elements in this line, in order, are:

<u>NAME</u>	<u>DESCRIPTION</u>
Booster LS3	Extraction station, beginning of line
BSEPT	Extraction septum
BQ1	Dipoles
BBV1	All dipoles in this line are vertical
BQ2, BQ3	
BBV2, BBV3	Angle varying dipoles
Target	Target to produce secondary protons
BBV4	
BQ4, BQ5	
BBV5	
BQ6, BQ7	
BQ8-BQ10	
BBV6	
D2Q5	Large aperture quadrupole in Debuncher lattice
BDSEP	Injection septum in Debuncher
Debuncher	End of line

E. Transfer line from Debuncher to Accumulator. Line D-to-A.

All elements in this line begin with "T" for transfer. The elements in this line, in order, are:

<u>NAME</u>	<u>DESCRIPTION</u>
Debuncher	Beginning of line
TDSEP	Extraction septum in Debuncher
D6Q6	Large aperture quadrupole in Debuncher lattice
TQ1-TQ7	
TASEP	Injection septum in Accumulator

2. ACCUMULATOR AND DEBUNCHER RINGS

The Accumulator and Debuncher ring elements are designated by a four to five character name, determined by ring stations. There are six primary stations in each machine, defined by the symmetry points. These sectors are:

Accumulator: A10, A20, A30, A40, A50, A60
 Debuncher: D10, D20, D30, D40, D50, D60

The meaning of A10, for example is

Accumulator, sector 1, station zero, etc.

See Fig. A-1 for the primary stations and sector numbers.

In the Accumulator, all elements begin with "A" and similarly "D" in the Debuncher. In both machines, a station goes from the station marker to the leading edge of a quadrupole, and from the leading edge of a quadrupole to the leading edge of the next quadrupole. All elements downstream of the quadrupole are labeled by the station designation of that quadrupole. Thus a typical position in the Accumulator might be "A1Q4", meaning Accumulator, sector one, quadrupole at station 4. Everything between A1Q4 and the next station, A1Q5 is in station A1Q4.

The elements and stations in the Accumulator start at A10 and go toward A20. They are:

<u>NAME</u>	<u>DESCRIPTION</u>
A10	Station marker for sector 1
A1Q1	Quadrupole beginning station 1
A1Q2	Quadrupole beginning station 2
A1Q3	Quadrupole beginning station 3
A1B3	Dipole after station 3
A1Q4	Quadrupole beginning station 4
A1Q5	
A1Q6	
A1Q7	
A1S7	Sextupole after station 7
A1B7	Dipole after station 7
A1Q8	
A1B8	
A1Q9	Beginning of station 9
A1S9	

A1Q10	End of station 9, beginning of station 10
A1B10	
A1S10	
A1Q11	
A1Q12	
A1S12	
A1Q13	
A1Q14	
A20	Station marker for sector 2

Both the Accumulator and Debuncher have mirror symmetry about all zero station markers. In order to relate the magnets in one sector to their counterparts in the other sector, the magnets can not be numbered in order while moving about the rings in a clockwise manner. Rather, at each zero station the numbers reverse. Thus, the stations and elements from A20 to A30 are:

<u>NAME</u>	<u>DESCRIPTION</u>
A20	Station marker for sector 2
A2Q14	
A2Q13	
A2S12	
A2Q12	
A2Q11	
A2S10	
A2B10	
A2Q10	End of station 9, beginning of station 10
A2B9	
A2S9	
A2Q9	
A2B8	
A2Q8	
A2B7	Dipole after station 7
A2S7	Sextupole after station 7
A2Q7	
A2Q6	
A2Q5	
A2Q4	
A2B3	Dipole after station 3
A2Q3	Quadrupole beginning station 3
A2Q2	
A2Q1	
A30	Station marker for sector 3

To find all the rest of the stations, simply take the above and put in the appropriate sector numbers. (See arrows and station markers in Fig. A-1)

The magnet numbers increase in a clockwise manner in sectors 1, 3, 5, and increase in a counter-clockwise manner in sectors 2, 4, and 6.

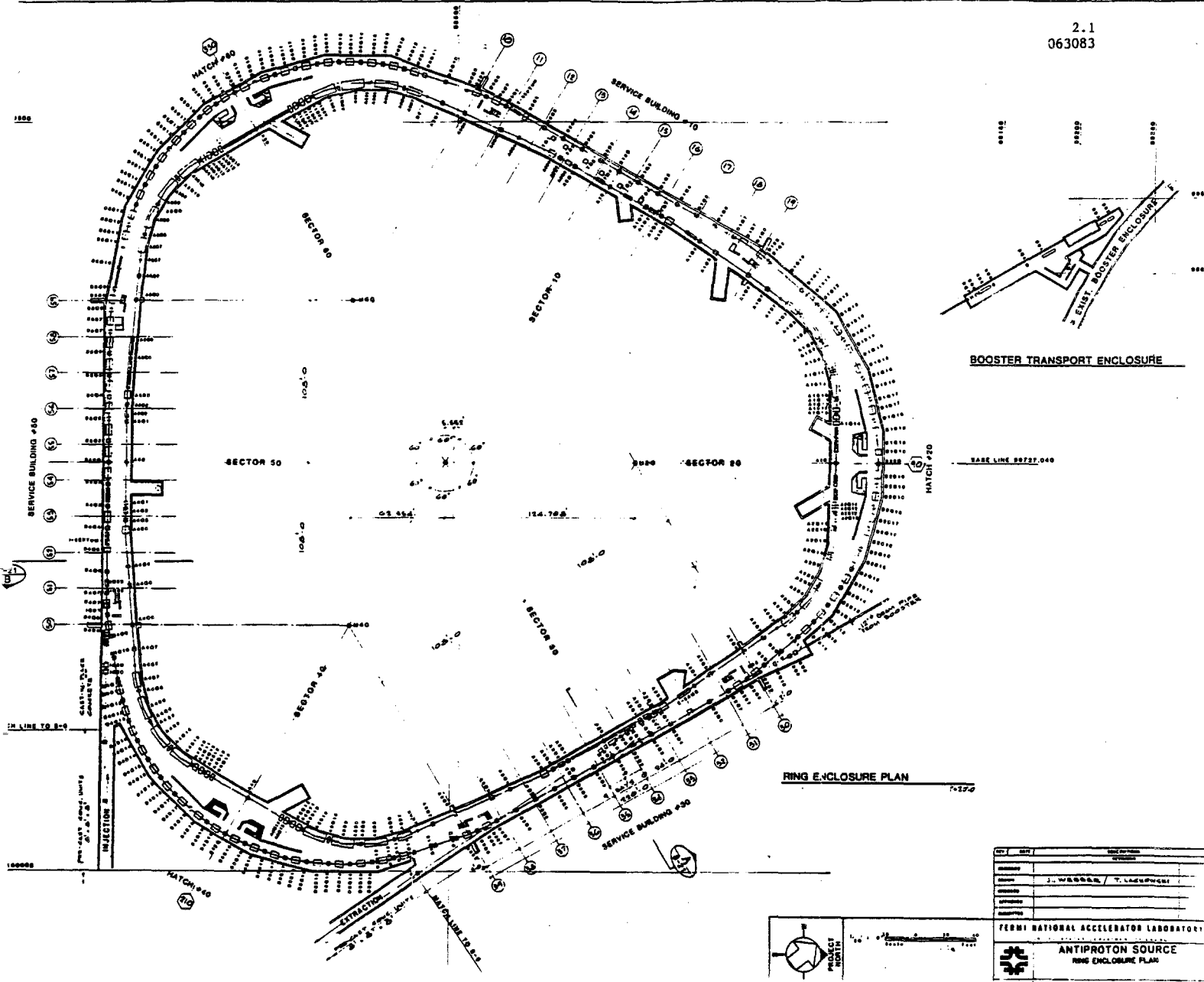
The Debuncher is numbered in exactly the same manner, except that there is a quadrupole at the symmetry points. That is D10, D20, etc. is in the middle of a quadrupole. This special quadrupole is called D10Q, D20Q, etc. The list of stations and elements in sector 1 is:

<u>NAME</u>	<u>DESCRIPTION</u>
D10Q	Zero station marker quadrupole.
D1Q2	This quadrupole ends station 1 and begins station 2. Note that there is no Q1.
D1Q3	
D1Q4	
D1Q5	
D1Q6	
D1Q7	
D1B7	
D1Q8	
D1B8	
D1Q9	
D1Q10	
D1Q11	
D1B11	
D1Q12	
D1B12	
D1Q13	
D1B13	
D1Q14	
D1B14	
D1Q15	
D1B15	
D1Q16	
D1B16	
D1Q17	
D1B17	
D1Q18	
D1B18	
D1Q19	
D1B19	
D20Q	Zero station marker quadrupole. This ends station 19.

Again, from D20Q to D30Q is the reverse of the above, substituting sector 2 for sector 1.

In the Debuncher, the sextupoles are not explicitly listed, but said to be downstream of a particular magnet, for example, there is a focussing sextupole downstream of D1B8, just as well be vacuum valves, monitors, etc.

See Fig. A-2 for an almost readable diagram of all magnets.



BOOSTER TRANSPORT ENCLOSURE

RING ENCLOSURE PLAN

REV.	DATE	DESCRIPTION

J. W. WOODS / T. LACROIX
 FERMIL NATIONAL ACCELERATOR LABORATORY
ANTIPROTON SOURCE
 RING ENCLOSURE PLAN

Figure A-2

APPENDIX B

APPENDIX B.
TEVATRON I
PARAMETER BANK

(AR2)

(FERMILAB, JUNE 1983)

- A. MAIN RING
- B. TARGETRY
- C. TRANSPORT LINES
- D. DEBUNCHER RING
- E. ACCUMULATOR RING
- F. SUPERCONDUCTING RING
- G. COLLIDER AT B0
- H. COLLIDER AT D0
- I. SYNCH FILES

TABLES OF TEVATRON I PARAMETERS

A. MAIN RING

AA. GENERAL MAIN RING PARAMETERS

AA.1 GENERAL MAIN RING PARAMETERS

AB. OPERATION MODE WITH PROTONS FOR TARGETRY

AB.1 INJECTION FROM THE BOOSTER

AB.2 PROTON ACCELERATION TO 120 GEV

AB.3 RF MANIPULATION FOR PROTON TARGETRY

AB.4 PROTON EXTRACTION AT 120 GEV

AC. OPERATION MODE WITH PROTONS FOR COLLIDER

AC.1 INJECTION FROM THE BOOSTER

AC.2 ACCELERATION TO 150 GEV

AC.3 BUNCH RECOMBINATION FOR COLLIDER

AC.4 EXTRACTION AT 150 GEV

AD. OPERATION MODE WITH ANTIPROTONS FOR COLLIDER

AD.1 ANTIPROTON INJECTION TO THE MAIN RING

AD.2 BUNCH SPLITTING AT 8 GEV

AD.3 ACCELERATION TO 150 GEV

AD.4 BUNCH RECOMBINATION FOR COLLIDER

AD.5 EXTRACTION AT 150 GEV (ANTIPROTONS)

AE. MAIN RING WITH OVERPASS

AE.1 GENERAL PARAMETERS

AE.2 MAGNETS AND DRIFTS

AE.3 LATTICE STRUCTURE

AE.4 LATTICE FUNCTIONS

AE.5 APERTURE REQUIREMENTS

B. TARGETRY

BA. PROTON TRANSPORT TO TARGET (SEE CA)

BB. TARGET

BB.1 TARGETRY

BB.2 TARGET ENERGY DEPOSITION

BC. LITHIUM LENS

BC.1 LITHIUM LENS

BC.2 LI LENS ELECTRICAL PARAMETERS

BC.3 LI LENS OPERATING PARAMETERS

BD. ANTIPROTON TRANSPORT TO DEBUNCHER (SEE CB)

BE. DUMP

C. TRANSPORT LINES

CA. PROTONS, MAIN RING TO TARGET

CA.1 MAGNETS

CA.2 LATTICE STRUCTURE

CA.3 LATTICE FUNCTIONS

CA.4 APERTURE REQUIREMENTS

CA.5 X,Y,Z SITE COORDINATES

CB. ANTIPROTONS, TARGET TO DEBUNCHER

CB.1 MAGNETS

CB.2 LATTICE STRUCTURE

CB.3 LATTICE FUNCTIONS

CB.4 APERTURE REQUIREMENTS

CB.5 X,Y,Z SITE COORDINATES

CC. ANTIPROTONS, DEBUNCHER TO ACCUMULATOR RING

CC.1 MAGNETS

CC.2 LATTICE STRUCTURE

CC.3 LATTICE FUNCTIONS

CC.4 APERTURE REQUIREMENTS

CC.5 X,Y,Z SITE COORDINATES

- CD. ANTIPROTONS, ACCUMULATOR RING TO MAIN RING
 - CD.1 MAGNETS
 - CD.2 LATTICE STRUCTURE
 - CD.3 LATTICE FUNCTIONS
 - CD.4 APERTURE REQUIREMENTS
 - CD.5 X,Y,Z SITE COORDINATES
- CE. PROTONS, BOOSTER TO DEBUNCHER RING
 - CE.1 MAGNETS
 - CE.2 LATTICE STRUCTURE
 - CE.3 LATTICE FUNCTIONS
 - CE.4 APERTURE REQUIREMENTS
 - CE.5 X,Y,Z SITE COORDINATES
- CF. PROTONS, MAIN RING TO SUPERCONDUCTING RING
 - CF.1 MAGNETS
 - CF.2 LATTICE STRUCTURE
 - CF.3 LATTICE FUNCTIONS
 - CF.4 APERTURE REQUIREMENTS
 - CF.5 X,Y,Z SITE COORDINATES
- CG. ANTIPROTONS, MAIN RING TO SUPERCONDUCTING RING
 - CG.1 MAGNETS
 - CG.2 LATTICE STRUCTURE
 - CG.3 LATTICE FUNCTIONS
 - CG.4 APERTURE REQUIREMENTS
 - CG.5 X,Y,Z SITE COORDINATES

D. DEBUNCHER

DA. INJECTION TO DEBUNCHER RING

DA.1 LATTICE AND PARAMETERS

DA.2 MAGNETS AND DRIFTS

DA.3 LAMBERTSON MAGNET

DA.4 KICKER MAGNET

DB. LATTICE

DB.1 GENERAL

DB.2 MAGNETS

DB.3 DRIFTS (EFFECTIVE)

DB.4 LATTICE STRUCTURE

DB.5 LATTICE FUNCTIONS

DB.6 APERTURE REQUIREMENTS

DC. MAGNETS

DC.1 DIPOLES

DC.2 QUADRUPOLES

DC.3 SEXTUPOLES

DD. VACUUM

DE. RF

DF. STOCHASTIC COOLING

DG. EXTRACTION

DH. TRANSFER FROM DEBUNCHER RING TO ACCUMULATOR RING

E. ACCUMULATOR

EA. TRANSFER FROM DEBUNCHER RING TO ACCUMULATOR RING

EB. INJECTION TO ACCUMULATOR RING

EC. LATTICE

EC.1 GENERAL

EC.2 MAGNETS

EC.3 DRIFTS (EFFECTIVE)

EC.4 LATTICE STRUCTURE

EC.5 LATTICE FUNCTIONS

EC.6 APERTURE REQUIREMENTS

ED. MAGNETS

ED.1 DIPOLES

ED.2 QUADRUPOLES

ED.3 SEXTUPOLES

ED.4 OCTUPOLES

EE. VACUUM

EF. RF

EG. STOCHASTIC COOLING

EG.1 MOMENTUM TAIL COOLING SYSTEM

EG.2 MOMENTUM CORE COOLING SYSTEM

EG.3 BETATRON TAIL COOLING SYSTEMS

EG.4 BETATRON CORE COOLING SYSTEMS

EH. EXTRACTION

F. SUPERCONDUCTING RING

FA. TRANSFER FROM MAIN RING

FB. INJECTION TO SUPERCONDUCTING RING

FC. LATTICE

FD. MAGNETS

FE. VACUUM

FF. RF

FG. ABORT

G. BO COLLIDER

GA. LOW BETA INSERTION

GB. PERFORMANCE PARAMETERS

GC. EXPERIMENTAL AREAS

H. DO COLLIDER

HA. LOW BETA INSERTION

HB. PERFORMANCE PARAMETERS

HC. EXPERIMENTAL AREAS

I. SYNCH FILES

THE TABLES

TO SEE IF THE TABLES HAVE BEEN UPDATED SINCE THIS PRINTING:

1. LOG-ON THE CYBER ON YOUR OWN DISK AREA AT ANY TERMINAL.
2. TYPE: G,PARAM/UN=94669
PARAM
3. FOLLOW INSTRUCTIONS APPEARING ON THE SCREEN.

AA.1 GENERAL MAIN RING PARAMETERS

10.55.34.

CHANGED 5/24/83
PRINTED 5/24/83

ASSUME OVERPASS (SEE AE)

	<u>INJECTION</u>	<u>MAXIMUM</u>
KINETIC ENERGY, GEV	8.0	200
BETA	0.994475	0.999989
GAMMA	9.5262	214.16
MOMENTUM, GEV/C	8.8889	200.94
MAGNETIC RIGIDITY, TM	29.65	670.3
DIPOLE FIELD STRENGTH, T	0.0397	0.896
QUADRUPOLE FIELD GRADIENT, T/M	0.534	12.07
BETATRON TUNES (H & V)	19.4	
TRANSITION ENERGY (GAMMA/T)	18.75	
AVERAGE RADIUS, M	1000.0	
DIPOLE BENDING RADIUS, M	747.8	
HORIZONTAL BETATRON ACCEPTANCE	3.0 PI.MM.MRAD	
VERTICAL BETATRON ACCEPTANCE	2.5 PI.MM.MRAD	
MOMENTUM APERTURE, DP/P	+- 0.3 %	+- .35 %
REVOLUTION PERIOD, MICROSEC	21.075	20.959
MAX. DISPERSION, HOR. (M)	6.	
VERT. (M)	0.5	
MAX. BETA VALUE, M	120.	
PERIODICITY	NONE	
PHASE ADVANCE/REGULAR CELL	70 DEG	
STANDARD RF FREQUENCY, MHZ	52.8117	53.1045
HARMONIC NUMBER (H)	1113	
MAX. RF VOLTAGE, MV	4.0	

AB.1 INJECTION FROM THE BOOSTER

10.55.34. CHANGED 5/24/83
PRINTED 5/24/83

INJECTION KINETIC ENERGY	8.0 GEV
BETA	0.994475
GAMMA	9.5262
MOMENTUM	8.8889 GEV/C
MAGNETIC RIGIDITY	29.65 TM
NO. OF BOOSTER BATCHES INJECTED	ONE
MODE OF TRANSFER	SINGLE-TURN EXTRACTION FROM BOOSTER AND INJECTION TO MAIN RING, BUCKET-TO-BUCKET
BETATRON EMITTANCE (H & V, 95 % OF BEAM)	2.5 PI.MM.MRAD
NO. OF BUNCHES	80
NO. OF PROTONS/BUNCH	2.5E+10
NO. OF PROTONS/PULSE	2.0E+12
INDIVIDUAL BUNCH AREA (95 % OF BEAM)	0.1 - .15 EV.SEC
RF FREQUENCY	52.8117 MHZ
RF VOLTAGE	1.2 MV
BUCKET AREA, STATIONARY	0.66 EV.SEC
BUCKET HEIGHT, DP/P	+ - .31 %

AB.2

PROTON ACCELERATION TO 120 GEV

10.55.34.

CHANGED 5/24/83

PRINTED 5/24/83

KINETIC ENERGY, GEV	8.0	120.
TRANSITION KINETIC ENERGY, GEV	16.65	
REVOLUTION FREQUENCY, KHZ	47.451	47.712
HARMONIC NUMBER	1113	
RF FREQUENCY, MHZ	52.812	53.1035
RF VOLTAGE, MV	1.2	.75
ACCELERATION RATE, MAX, GEV/S	125	
SYNCHROTRON PHASE ANGLE	0 - 50 DEG	130 - 135 DEG
BUCKET AREA, EV.SEC	0.66	3.3
INDIVIDUAL BUNCH AREA AT 120 GEV (95 % OF BEAM) EV.SEC	0.2	
MAIN RING CYCLE PERIOD:	2.0 SEC	
FRONT PORCH	0.1 SEC	
ACCELERATION TO 120 GEV	1.2 SEC	
FLAT TOP	0.2 SEC	
FALL OFF PERIOD	0.5 SEC	

EXTRACTION KINETIC ENERGY 120 GEV
MAGNETIC RIGIDITY (B-RHO) 403.27 T.M
BEAM PULSE LENGTH TO BE EXTRACTED 21 MICROSEC
REVOLUTION PERIOD 20 MICROSEC
BEAM EMITTANCE AT EXTRACTION
(H & V, 95% OF BEAM) 0.2 PI.MM-MRAD
BEAM FULL MOMENTUM SPREAD
AT EXTRACTION, 95% OF BEAM 0.4%
EXTRACTION MODE: (A) 4-MAGNET LOCAL HORIZ. BUMP CENTERED AT F17
(B) HORIZONTAL KICK OUTWARD
(C) LAMBERTSON MAGNETS FOR VERTICAL EXTRACTION
HORIZONTAL DISPLACEMENT AT F17
WITH 4-MAGNET BUMP +- 37 MM
KICKER LOCATION C48
HORIZONTAL DISPLACEMENT BY KICKER AT F17 +43 MM
ANGULAR DISPLACEMENT BY KICKER AT F17 +0.847 MRAD
LOCATION OF LAMBERTSON F17
NUMBER OF LAMBERTSON MAGNETS 2
LAMBERTSON MAGNET LENGTH / EACH 204 INCHES
LAMBERTSON MAGNET FIELD STRENGTH 13 KG

CONTINUED

AB.4 (CONTINUED)

HORIZONTAL PLANE LATTICE FUNCTIONS:

LOCATION	BETA (M)	ALPHA	PHASE RELATIVE TO F17 (MODULO 360 DEG)	SPACE AVAILABLE (IN.)
C48 KICKER	102.414	0.46696	-90.11 DEG	(EXISTING)
F12	29.601	-0.5731	-168.30 DEG	0.0
F13	95.356	1.8584	-135.74 DEG	0.0
F14	28.383	-0.5893	-99.29 DEG	34.0
F15 (BUMP 1)	97.247	1.8396	-66.32 DEG	42.5
F16	30.093	-0.6239	-31.47 DEG	42.0
F17 (BUMP 2) (EXTRACTION)	99.648	1.9388	0.00 DEG	32.0
F18 (BUMP 3)	28.865	-0.5582	35.20 DEG	52.0
F19	94.322	1.8156	68.42 DEG	0.0
F21	28.912	-0.6177	104.71 DEG	28.0
F22 (BUMP 4)	99.541	1.8926	136.92 DEG	27.5
F23	30.073	-0.5983	171.32 DEG	35.0
F24	97.400	1.9056	203.21 DEG	0.0
F25	28.365	-0.5666	239.23 DEG	35.0
F26	95.244	1.8100	272.60 DEG	43.5

INJECTION KINETIC ENERGY	8.0 GEV
REVOLUTION FREQUENCY	47.451 KHZ
HARMONIC NUMBER	1113
RF FREQUENCY	52.813 MHZ
RF VOLTAGE	1.2 MV
RF BUCKET AREA	0.66 EV.SEC
RF BUCKET HEIGHT, DP/P	+ - .31 %
NO. OF BOOSTER BATCHES INJECTED	3, EQUALLY SPACED
MODE OF TRANSFER	SINGLE-TURN EXTRACTION FROM BOOSTER AND INJECTION TO MAIN RING OF A SINGLE BATCH, BUNCH-TO-BUCKET
NO. OF BUNCHES/BATCH	7, SELECTED NEXT TO EACH OTHER, AFTER REMOVING UNWANTED BUNCHES WITH SUPERDAMPER
NO. OF PROTONS/BUNCH	1.2E+10
NO. OF PROTONS/BATCH	8E+10
INDIVIDUAL BUNCH AREA (95 % OF BEAM)	0.1 EV.SEC
BETATRON EMITTANCE (H & V, 95 % OF BEAM)	2.5 PI.MM.MRAD
MAIN RING FRONT PORCH PERIOD	0.3 SEC

AC.2 ACCELERATION TO 150 GEV

09.53.05. CHANGED 5/24/83
PRINTED 6/10/83

KINETIC ENERGY	8.0	150.	GEV
TRANSITION KINETIC ENERGY		16.65	GEV
REVOLUTION FREQUENCY	47.451	47.71	KHZ
HARMONIC NUMBER		1113	
RF FREQUENCY	52.813	53.105	MHZ
RF VOLTAGE	1.2	.68	MV
SYNCHRONOUS PHASE ANGLE	0 - 50	130 - 135	DEG
ACCELERATION RATE, MAX		125	GEV/SEC
ACCELERATION TIME		2.0	SEC
BETATRON EMITTANCE (H & V 95 % OF BEAM)	2.5	0.15	PI.MM.MRAD
INDIVIDUAL BUNCH AREA (95 % OF BEAM)	0.15	0.2	EV.SEC
STATIONARY BUCKET AREA	0.66	3.5	EV.SEC
BUCKET HEIGHT, DP/P	+ - .31 %	+ - .1 %	
PHASE OSCILLATION PERIOD	1.65	14	MSEC

AC.3 PROTON BUNCH RECOMBINATION FOR COLLIDER CHANGED 6/10/83

----- 09.53.05. PRINTED 6/10/83

KINETIC ENERGY 150 GEV

RF VOLTAGE	INITIAL	FINAL
H=53	3.93E+2	3.93E+2
H=1113	6.8E+5	1.0E+2

RF FREQUENCY

H=53	2.53 MHZ
H=1113	53.105 MHZ

NUMBER OF BUNCHES

H=53	1
H=1113	7

RECOMBINATION TIME .8 SEC

BUNCH EMITTANCE APPROX. 1 EVS

BUNCH LENGTH 39.5 M

MOMENTUM SPREAD (APPROX. 95%) 6.7E-5

AC.4

EXTRACTION AT 150 GEV (PROTONS)

CHANGED 5/31/83

----- 09.53.05.

PRINTED 6/10/83

KINETIC ENERGY 150 GEV

RF VOLTAGE

H=53 45 KV

H=106 -9.8 KV

BUNCH ROTATION TIME

79 MS

FINAL EMITTANCE (EQUIVALENT 95% ELLIPSE)

(LESS THAN 1.5 EVS)

RF VOLTAGE AT EXTRACTION (H=1113)

1.0 MV

BUNCH WIDTH (95%)

2.3 M

BUNCH HEIGHT DP/P (95%)

1.6E-3

AD.1 ANTIPROTON INJECTION TO THE MAIN RING CHANGED 6/10/83
----- 09.53.05. PRINTED 6/10/83

KINETIC ENERGY 8.0 GEV

RF VOLTAGE

H=53 2 KV

H=1113 3 KV

RF FREQUENCY

H=53 2.5148 MHZ

H=1113 52.8117 MHZ

MODE OF TRANSFER - SINGLE TURN EXTRACTION FROM ACCUMULATOR

- SYNCHRONOUS INJECTION INTO MAIN RING H=53 BUCKETS

NUMBER OF BUNCHES	1
BUNCH EMITTANCE	1.5 EVS (OR 1.5 - 2 EVS)
BUNCH INTENSITY	8E+10 (OR 8E+10 - E+11)
BUNCH LENGTH	73.4 M
BUNCH HEIGHT DP/P (95%)	8.710E-4
TRANSVERSE EMITTANCE (H & V)	2.5 PI MM MRAD

KINETIC ENERGY 8 GEV

RF VOLTAGE	INITIAL	FINAL
H=53	2 KV	2 KV
H=1113	3 KV	500 KV

RF FREQUENCY

H=53	2.5148 MHZ
H=1113	52.8117 MHZ

NUMBER OF BUNCHES	1	13
ANTIPROTONS/BUNCH	8E+10	8E+9
BUNCH LONG EMITTANCE	1.5	.15 MAX EVS
BUNCH LENGTH	73.4 M	2.54 M
BUNCH HEIGHT		
DP/P (95%)	8.7E-4	2.6E-3

AD.3

ACCELERATION TO 150 GEV
-----09.53.05. CHANGED 5/31/83
PRINTED 6/10/83

	INITIAL	FINAL
KINECTIC ENERGY	8.0	150.00
TRANSITION ENERGY		16.65 GEV
REVOLUTION FREQUENCY	47.451	47.71
HARMONIC NUMBER		1113
RF FREQUENCY	52.813	53.1035
RF VOLTAGE	1.2 MV	.68 MV
SYNCHRONOUS PHASE	0-50 DEGREES	130-180 DEGREES
ACCELERATION RATE (MAX)		125 GEV
ACCELERATION TIME		2.0 SEC
TRANSVERSE EMITTANCE (95%)	2.5	.15 PI MM MRAD
INDIVIDUAL BUNCH AREA (MAX)	.15	.2 EVS
BUCKET HEIGHT DP/P (95%)	+ .31%	+ .1%
PHASE OSCILLATION PERIOD	1.5 M SEC	14 M SEC

KINETIC ENERGY		150 GEV
ROTATION FREQUENCY		47.71 KHZ
RF FREQUENCY		
H=53		2.53 MHZ
H=1113		53.105 MHZ
RF VOLTAGE	INITIAL	FINAL
H=53	98 V	98 V
H=1113	6.8E+5 V	APPROX. 100 V
NUMBER OF BUNCHES		
H=53		1
H=1113	13	
RECOMBINATION TIME		.8 S
BUNCH EMITTANCE		APPROX. 2 EVS
BUNCH LENGTH		73.4 M
MOMENTUM SPREAD		
(95% DP/P)		6.9E-5

AD.5

EXTRACTION AT 150 GEV (ANTIPROTONS)
----- 09.53.05.

CHANGED 6/10/83
PRINTED 6/10/83

KINETIC ENERGY 150 GEV

RF FREQUENCY

 H=53 2.529 MHZ

 H=106 5.058 MHZ

RF VOLTAGE

 H=53 20 KV

 H=106 -4.4 KV

BUNCH ROTATION TIME 115 MS

FINAL EMITTANCE

 (95% EQUIVALENT ELLIPSE) LESS THAN APPROX. 3 EVS

RF VOLTAGE AT EXTRACTION 1.0 MV

 H=1113

BUNCH WIDTH 95% 3.93 M

BUNCH HEIGHT

 (95% DP/P) 2.2E-3

BB.1 TARGETRY

12.17.52. CHANGED 5/25/83
 PRINTED 6/ 9/83

TARGET MATERIAL	TUNGSTEN-RHENIUM
LENGTH OF TARGET	6 CM
TARGET DISK	8 CM
PROTON BEAM:	
BETA.STAR, PROTON (H & V)	4.6 M
ALPHA.STAR, PROTON (H & V)	0.
ETA.STAR, PROTON (DISPERSION)	0. M
ETA.PRIME.STAR, PROTON	0.
PROTON RMS SPOT SIZE (H & V)	0.39 MM
NO. OF BOOSTER BATCHES / M R CYCLE	ONE
TIME INTERVAL BETWEEN BATCHES	2.0 SEC
MAIN RING CYCLE TIME	2.0 SEC
NUMBER OF PROTONS / BATCH	1.8E+12
NUMBER OF PROTON BUNCHES / BATCH	80
ANTIPROTON BEAM:	
ANTIPROTON PRODUCTION MOMENTUM	8.889 GEV/C
KINETIC ENERGY	8.0 GEV
BETA	0.99448 M
GAMMA	9.5264 1/M
MAGNETIC RIGIDITY (B-RHO)	29.65 T.M
MOMENTUM SPREAD ACCEPTED, FULL DELTA P/P,	3%

CONTINUED

BB.1 (CONTINUED)

EMITTANCE ACCEPTED (H & V)	20 PI.MM-MRAD
AVERAGE ANTIPROTON ANGLE	23.8MRAD
BETA.STAR, ANTIPROTON (H & V)	0.11 M
ANTIPROTON SPOT SIZE (H & V)	1.5 MM
PBAR PRODUCTION CROSS-SECTION, D3N/DPDOMEGA=0.252 PBARS/(GEV/C) STER.INT.P	
ANTIPROTON ABSORPTION LENGTH	9.29 CM
PROTON ABSORPTION LENGTH	9.86 CM
CALCULATED ANTIPROTONS/PROTONS	3.7E-5
TOTAL NUMBER OF ANTIPROTONS / M R CYCLE	6.7E+7
NUMBER OF ANTIPROTON BUNCHES / M R CYCLE	80
NUMBER OF ANTIPROTONS / BUNCH	8.4E+5
ANTIPROTON BUNCH LENGTH (AT TARGET, RMS)	5 CM
ANTIPROTON BUNCH AREA (95% OF BEAM)	0.24 EV.SEC
PROTON BUNCH TIMING	18.83115 NSEC
ANTIPROTON BUNCH TIMING	SAME
PROTON BUNCH SPACING (CENTER-TO-CENTER)	5.64527 M
ANTIPROTON BUNCH SPACING	5.61427 M
ANTIPROTON BUNCHING FREQUENCY	53.1035 MHZ

TARGET MATERIAL	TUNGSTEN/TUNGSTEN ALLOYS
LENGTH	6 CM
120 GEV PROTONS/PULSE	1.8+12
TOTAL BEAM ENERGY	3.46E+4 JOULES
REPETITION RATE	0.5 HZ
BEAM PULSE DURATION	1.6E-6 SEC
ENERGY DEPOSITED/PROTON GEV	1.26 GEV (1.82E-10 JOULES)
ENERGY DEPOSITED/PULSE	346 JOULES
AVERAGE ENERGY DEPOSITED	173 WATTS
AVERAGE TEMPERATURE	LESS THAN 100 DEG C
PROTON RMS BEAM SIZE (H & V)	0.39 MM
PEAK ENERGY DENSITY/PROTON	13.4 GEV/CM3
PEAK ENERGY DENSITY/PULSE	200 JOULES/GM
PEAK TEMPERATURE RISE	LESS THAN 1500 DEG C

BC.1 LITHIUM LENS

09.53.05. CHANGED 5/25/83
 PRINTED 6/10/83

TRANSFORMER:

OVERALL DIAMETER	42 CM
OVERALL LENGTH	24 CM
I.D. OF PRIMARY	16 CM
CORE AREA	154 SQ CM

LITHIUM LENS:

OVERALL DIAMETER	9 CM
OVERALL LENGTH	24 CM
LITHIUM CONDUCTOR DIAMETER	2 CM
LENGTH	15 CM
BERYLLIUM WINDOW THICKNESS	0.5 CM
TITANIUM COOLING JACKET THICKNESS	0.1 CM

TRANSFORMER (PRIMARY):

RESISTANCE	.49 MILLIOHM
STRAY INDUCTANCE	.44 MICRO. H
NO. OF TURNS	8

LI LENS & TRANSFORMER (SECONDARY):

RESISTANCE	.126 MILLIOHM
INDUCTANCE	31 NANO. H

REFLECTED PRIMARY CIRCUIT PARAMETERS:

RESISTANCE	8.6 MILLIOHM
INDUCTANCE	2.4 MICRO. H
DAMPING FACTOR ALPHA = $R/2L$	1780 HZ

PULSED POWER SUPPLY:

PULSE LENGTH	0.33 MSEC
VOLTAGE	2.5 KV
CAPACITANCE	4600 MICRO F
INITIAL STORED ENERGY	14.4 KJ
REPITION RATE	0.5 HZ

TRANSFORMER (PRIMARY):

PEAK CURRENT	83 KA
DISSIPATED ENERGY/PULSE	570 J
DISSIPATED POWER	290W
NET MAGNETIC FORCE ON PRIMARY TURNS	7700 LBS
CORE BIAS	10 A

LITHIUM LENS & TRANSFORMER (SECONDARY):

PEAK CURRENT	670 KA
DISSIPATED ENERGY/PULSE	9800 J
DISSIPATED POWER	4.9 KW
NET AXIAL MAGNETIC FORCE ON LENS	33000 LBS
TEMP RISE/PULSE	120 DEG C (MAX)
	35 DEG C (MIN)

MAGNETIC FIELD (LITHIUM):

AC SKIN DEPTH	.45 CM
PEAK SURFACE FIELD	13.5 T
PHASE AT BEAM TIME	117 DEG
AVE. FIELD GRADIENT AT BEAM TIME	1100 T/M
PEAK MAGNETIC PRESSURE	16000 PSI
AVE. NON-LINEARITY	2.8 %

KINETIC ENERGY AT INJECTION 8.0 GEV
MOMENTUM 8.8889 GEV/C
MAGNETIC RIGIDITY 296.501 KG-M
EMITTANCE INJECTED (H & V) 20 PI.MM.MRAD
MOMENTUM SPREAD INJECTED,
FULL DP/P, MAX, 4 %

METHOD: VERTICAL INJECTION ON A HORIZONTALLY
CENTERED ORBIT, FOLLOWED
BY KICKING ON REFERENCE PLANE

STRING OF ELEMENTS:

FROM THE UPSTREAM END OF COMMON QUAD QF3
TO THE DOWNSTREAM END OF THE KICKER (KICK)

QF3 OS SM S1 QD2 LA QF2 O1 KICK

LOCATION OF THE LAMBERTSON (SM) STATION D4-4

LOCATION OF THE KICKER (KICK) STATION D4-2

DRIFT ELEMENTS	LENGTH
S1	1.2929 M
O1	0.4636 M
LA	3.731264 M
OS	0.3048 M

SEE ALSO TABLES DB.3 AND DB.4

QUADRUPOLES:	EFFECTIVE LENGTH	B'/(B.RHO)	BORE RADIUS
QF3	0.8280 M	0.32494 1/M**2	8.41 CM
QD2	0.7010 M	-0.38679 1/M**2	4.45 CM
QF2	0.7010 M	0.35881 1/M**2	4.45 CM

SEE ALSO TABLES DB.2 AND DC.2

LOCATION	STATION D4-4		
EFFECTIVE LENGTH	2.1336 M		
BENDING FIELD	5.6335 KG		
BENDING ANGLE	40.5384 MRAD		
BENDING RADIUS	52.6316 M		
BEAM HORIZONTAL DISPLACEMENT FROM REFERENCE ORBIT	CENTERED WITH REFERENCE ORBIT		
BEAM VERTICAL DISPLACEMENT FROM REFERENCE ORBIT:	BEAM VERTICAL ANGLE FROM REFERENCE ORBIT:		
UPSTREAM QF3	13.4 CM		64.4 MRAD
DOWNSTREAM QF3	9.1 CM		35.4 MRAD
UPSTREAM SM	8.0 CM		35.4 MRAD
DOWNSTREAM SM	4.8 CM		-5.2 MRAD
UPSTREAM QD2	5.5 CM		-5.2 MRAD
DOWNSTREAM QD2	5.3 CM		9.7 MRAD
MAX. FULL BEAM SIZE (H X V) IN THE SEPTUM MAGNET	35 X 26 MM**2		
MIN. SEPARATION BETWEEN INJECTED AND CIRCULATING BEAMS EDGE TO EDGE	22 MM		
APERTURE	5.0 CM (H) X 10.0 CM (V)		

DA.4 KICKER MAGNET

13.15.19. CHANGED 5/18/83
 PRINTED 5/31/83

LOCATION	STATION D4-2
EFFECTIVE LENGTH	3.048 M
BENDING ANGLE (HORIZONTAL)	6.17 MRAD
BENDING FIELD	600 G
FALL-OFF TIME	200 NSEC
BEAM VERTICAL DISPLACEMENT:	
UPSTREAM	9.4 MM
DOWNSTREAM	0.0 MM
APERTURE, FULL	4.0 CM (H) X 5.4 CM (V)

KINETIC ENERGY	8.0 GEV
BETA	0.99448
GAMMA	9.5264
MOMENTUM (P)	8.8889 GEV/C
MAGNETIC RIGIDITY (B-RHO)	296.5 KG.M
BENDING FIELD (B)	17.0 KG
BENDING RADIUS (RHO)	17.44 M
AVERAGE RADIUS (R)	80.4182 M
REVOLUTION PERIOD	1.6948 MICROSEC
PACKING FACTOR (RHO/R)	21.7%
SUPERPERIODICITY	3
RF HARMONIC NUMBER (H)	90
FOCUSSING STRUCTURE	SEPARATED FUNCTIONS
NORMAL CELL STRUCTURE	FODO
HORIZONTAL BETATRON TUNE	9.73
VERTICAL BETATRON TUNE	9.77
TRANSITION ENERGY (GAMMA/T)	7.648
$\text{ETA} = 1/(\text{GAMMA}/\text{T})^{**2} - 1/\text{GAMMA}^{**2}$	0.0061
NATURAL CHROMATICITY: HORIZONTAL	-10.8
VERTICAL	-11.0

DIPOLES	EFFECTIVE LENGTH	STRENGTH	NUMBER
B	1.6604 M	17.0 KG	66
QUADRUPOLES	EFFECTIVE LENGTH	B'/(B-RHO)	NUMBER
QF	0.701 M	0.33652	42
QD	0.701	-0.32928	39
QF1	0.701	0.37747	3
QD1	0.701	-0.34714	6
QF2	0.701	0.35881	6
QD2	0.701	-0.38679	6
QF3	0.828	0.32494	6
QD3	0.828	-0.32459	6
SEXTUPOLES	EFFECTIVE LENGTH	B''/(B-RHO)(*)	NUMBER
SF	0.2 M	0.70365 1/M**2	36
SD	0.2	-1.0671	33

(*) STRENGTHS REQUIRED FOR CHROMATICITY CANCELLATION IN BOTH PLANES

DB.3

LATTICE DRIFTS (EFFECTIVE)

13.15.19.

CHANGED 5/18/83

PRINTED 5/31/83

O	0.735431 M
OO	1.035431
OS	0.300000
LA	3.731264
LB	3.667764
LC	3.131264
LZ	3.604264

REGULAR CELL (*)

(.C)	QF/2	.OF1	B	.OD2	QD
		.OD1	B	.OF2	QF/2

WHERE

.OF1 =	OS	SF	O
.OD1 =	OS	SD	O
.OF2 =	O	SF	OS
.OD2 =	O	SD	OS

HALF REGULAR CELL (*)

(.CH)	QF/2	.OF1	B	.OD2	QD/2
-------	------	------	---	------	------

SPECIAL CELLS FOR DISPERSION KILLER (*)

(.C1)	QF/2	OO	B	OO	QD
		OO	B	.OF2	QF/2

(.CS)	QF/2	.OF1	LC	.OD2	QD
		.OD1	LC	.OF2	QF/2

SPECIAL CELLS FOR LONG STRAIGHT SECTIONS (*)

(.CS1)	QF1/2	LA	QD1	LA	QF2/2
(.CS2)	QF2/2	LA	QD2	LB	QF3/2
(.CS3)	QF3/2	LZ	QD3	LB	QF/2

HALF OF A SUPERPERIOD STRUCTURE:

.CS1	.CS2	.CS3	.C1	.CS
.C	.C	.C	.C	.CH

SUPERPERIOD STRUCTURE:

.CS + MIRROR REFLECTION OF .CS

(*) QX/2 DENOTES HALF OF A REGULAR QX QUAD

	BETA/H	BETA/V	ETA
MAXIMA	17.83 M	16.94 M	2.09 M
REGULAR CELL(*):			
MAX	14.97	14.88	2.09
MIN	5.24	5.23	1.28 (**)
QF1 (MAX)	17.83	5.73	-0.0009
QD1	4.79	16.94	-0.0004
QF2	11.81	5.32	-0.0003
QD2	4.44	13.64	0.0001
QF3	17.60	3.52	0.0007
QD3	5.74	13.82	0.0005

(*) INCLUDES DISPERSION KILLER

(**) EXCLUDES DISPERSION KILLER WHERE $ETA/MIN = 0.0$ M

BETATRON ACCEPTANCE: HORIZONTAL 20.PI MM-MRAD
VERTICAL 20.PI MM-MRAD

MOMENTUM APERTURE: +- 2%

MAXIMUM BEAM DIMENSIONS (FULL):

	HORIZ. (MM)	VERTICAL (MM)
B	101.54	32.66
QF	118.14	20.43
QD	73.36	34.50
QF1	36.88	21.96
QD1	20.23	36.82
QF2	30.73	20.64
QD2	18.86	33.04
QF3	37.54	16.78
QD3	21.44	33.24

EFFECTIVE ARC LENGTH	1.660402 M
BENDING RADIUS	17.4412353 M
IRON LENGTH	62.8 INCHES
BENDING ANGLE	95.20 MRAD
FULL GAP	60 MM
GOOD FIELD WIDTH	100 MM
SAGITTA	2.0 CM
CONDUCTOR: 1" X 1.25" CROSS SECTION	0.375" CROSS SECTION HOLE DIAMETER
1/16" CORNER RADIUS	1.1362 SQ. IN. AREA
URNS: PANCAKE COILS	56
SADDLE COILS	16
CONDUCTOR LENGTHS: PANCAKE COILS	9740.3"/MAGNET
SADDLE COILS	3680.45"/MAGNET
TOTAL CONDUCTOR LENGTH	13420.75"/MAGNET
COIL PROTRUSION/END	11"
CU WEIGHT/MAGNET	4906.625 LBS
TOTAL CU WEIGHT	161.92 TONS
RESISTANCE/MAGNET (43 DEG C)	8.73 MILLI-OHM
CURRENT AT 1.7T	1175.6 A
VOLTAGE AT 1.7T	10.3 V
POWER/MAGNET	12.065 KW
TOTAL POWER/DIPOLES	0.7963 MW
FULL CROSS SECTION (W X H)	45.25" X 29"
LAMINATION THICKNESS	0.0598"
IRON WEIGHT/MAGNET	16826.865 LBS
TOTAL IRON WEIGHT	555.3 TONS
COOLING WATER PRESSURE	42 PSI
WATER FLOW	2.4 GALLONS/MIN.

TYPE	REGULAR	LONG-SMALL APERTURE	LONG-LARGE APERTURE
EFFECTIVE LENGTH	27.6"	32.6"	32.6"
IRON LENGTH	26.18"	31.18"	30"
POLETIP RADIUS	44.5 MM	44.5 MM	84.1 MM
CONDUCTOR:	0.312"X 0.75" 0.1875" HOLE DIA 1/16" CORNER RADIUS AREA=0.20309 SQ IN		0.625"X 1.5" 0.375" HOLE DIA 1/16" CORNER RADIUS AREA=0.8237 SQ IN
TOTAL CONDUCTOR LENGTH/MAGNET	11069.52"	12389.52"	8804.88"
COIL PROTRUSION	4"	4"	6"
CU WEIGHT/MAGNET	722.84 PD	809.04 PD	22332.41 PD
TOTAL CU/WEIGHT	36.9 TONS	36.4 TONS	3.5 TONS
RESISTANCE/MAGNET (43 DEG C)	40.3 M OHM	45.1 M OHM	7.9 M OHM
CURRENT AT 10 T/M	250 A	230 A	1310 A
VOLTAGE AT 10 T/M	10.1 V	10.4 V	10.35 V
POWER/MAGNET	2.5 KW	2.4 KW	13.6 KW
TOTAL POWER/QUADS	0.258 MW	0.022 MW	0.041 MW
FULL CROSS SECTION (W X H)	30.5X29 SQ IN	30.5X29 SQ IN	54.75X51.75 SQ IN
LAMINATION THICKNESS	0.0598"	0.0598"	0.0598"
IRON WEIGHT	1.85 TONS	2.20 TONS	7.02 TONS
TOTAL IRON WEIGHT	188.6 TONS	19.8 TONS	21.1 TONS
COOLING WATER PRESSURE	19 PSI	26 PSI	3.1 PSI
WATER FLOW	0.8 GAL/MIN	1 GAL/MIN	2.2 GAL/MIN
NO. OF TURNS, TOTAL	4X33	4X33	4X21

MAXIMUM STRENGTH, B"L/B-RHO	0.22 M-2
BORE RADIUS	50 MM
EFFECTIVE LENGTH	0.2 M
MAXIMUM FIELD, B"	33 T/M2
AMPERE-TURNS	600 AT/POLE
CURRENT	119 A
URNS	5 TURNS/POLE
CONDUCTOR SIZE	.3294" RECT/ 0.18" HOLE DIA/ AREA .07723 SQ IN
CURRENT DENSITY	1.55 KA/SQ IN
RESISTANCE	5 MICRO OHM/MAGNET
VOLTAGE DROP	0.65 V/MAGNET
THERMAL LOSS	77 W/MAGNET

DIPOLES	EFFECTIVE LENGTH	STRENGTH
B3	1.5240 M	16.839 KG
B7	3.0480 M	16.839 KG
B8, B9, B10	4.5720 M	16.839 KG
QUADRUPOLES	EFFECTIVE LENGTH	STRENGTH
Q1	0.64008 M	103.8087 KG/M
Q2	1.31166	-103.8087
Q3	0.70104	103.8087
Q4	0.45720	96.6333
Q5	0.82804	- 97.4126
Q6	0.70104	96.6333
Q7	0.70104	- 97.4126
Q8	0.45720	96.6333
Q9	0.45720	- 97.4126
Q10	0.45720	40.8765
Q11	0.87376	89.3989
Q12	0.77220	- 89.3989
Q13	0.77220	- 89.3989
Q14	0.64262	89.3989
SEXTUPOLES	EFFECTIVE LENGTH	STRENGTH
S7	0.3048 M	35.7175 KG/M2
S9	0.3048	-219.5244
S10	0.3048	134.7943
S12	0.3048	-170.5021
OCTUPOLES	EFFECTIVE LENGTH	STRENGTH
OC10	0.3048	-325.1426 KG/M3
OC12	0.3048	778.6057

EC.3

LATTICE DRIFTS (EFFECTIVE)

13.15.19.

CHANGED 5/26/83
PRINTED 5/31/83

LS	7.94650
LS*	7.84488
01	0.51241
02	0.96060
03	0.90420
OB3	6.42366
04	3.26100
05	7.33776
06	4.18716
07	0.30480
OS7	3.83584
OB7	0.50800
08	1.21920
OB8	0.50800
09	0.30480
OS9	0.60960
OB9	0.50800
010	0.50800
OB10	0.29190
OS10	0.29190
011	0.52102
012	0.21780
OS12	0.21780
013	0.49722

STRUCTURE OF HALF A SUPERPERIOD

STRING OF ELEMENTS FROM CENTER OF ZERO-DISPERSION STRAIGHT

SECTION TO CENTER OF LARGE-DISPERSION STRAIGHT SECTION

```
.CS =      LS  Q1  A1  O1  Q2  Q2  O2  Q3  Q3  O3  B3
          OB3 Q4  Q4  O4  Q5  Q5  O5  Q6  Q6  O6  Q7  Q7
          O7  S7  OS7 B7  OB7 Q8  Q8  O8  B8  OB8 Q9  Q9
          O9  S9  OS9 B9  OB9 Q10 Q10 O10 B10 OB10 S10 OS10
          Q11 Q11 O11 Q12 Q12 O12 S12 OS12 Q13 Q12 O13 Q14
          Q14 LS*
```

SUPERPERIOD STRUCTURE:

```
.CS + MIRROR REFLECTION OF .CS
```

	BETA-H	BETA-V	ETA-H
MAXIMA	33.23 M	31.04 M	8.949 M
B3	24.59	9.40	0.067
B7	17.82	16.01	-0.088
B8	15.96	18.80	0.891
B9	23.05	15.73	4.669
B10	31.97	9.12	8.065
Q1	16.01	19.98	0.001
Q2	14.59	30.32	0.001
Q3	26.32	12.60	0.001
Q4	14.31	8.13	0.645
Q5	2.95	28.90	0.680
Q6	29.99	2.98	1.915
Q7	6.60	31.04	0.634
Q8	14.57	8.35	-0.050
Q9	7.60	20.23	1.239
Q10	26.22	4.91	5.325
Q11	31.96	15.86	8.726
Q12	16.72	27.14	6.978
Q13	13.22	27.39	7.542
Q14	15.88	16.90	8.949
	BETA-H	BETA-V	ETA-H
(*) CENTER OF ZERO- DISPERSION LONG STRAIGHT SECTION	7.764 M	7.267 M	0.002 M
(**) CENTER OF LARGE DISPERSION LONG STRAIGHT SECTION	7.580	7.514	8.949

(*) TOTAL LENGTH = 15.8930 M (**) TOTAL LENGTH = 15.6898 M

(ALPHA*-H = ALPHA*-V = ETA' = 0)

EC.6

APERTURE REQUIREMENTS

11.43.15.

CHANGED 5/31/83
PRINTED 6/ 9/83

BETATRON ACCEPTANCE: HORIZONTAL 10 PI MM-MRAD

VERTICAL 10 PI MM-MRAD

MOMENTUM APERTURE: $\pm 1.25\%$

ED.1

LATTICE MAGNETS; DIPOLES

14.13.48.

CHANGED 5/31/83
PRINTED 6/28/83

TYPE	B3	B7	B8	B9 & B10
NUMBER OF MAGNETS	6	6	6	12
EFFECTIVE LENGTH (M)	1.5240	3.0480	4.5720	4.5720
BENDING FIELD (KG)	16.839	16.839	16.839	16.839
SAGITTA (CM)	1.66	6.65	14.96	14.96
DIPOLE GEOMETRY	CURVED WITH PARALLEL EDGES			
BENDING ANGLE (MRAD)	87.266	174.533	261.799	261.799
BENDING RADIUS (M)	17.464	17.464	17.464	17.464
IRON LENGTH (IN)	57.43	117.30	176.94	176.94
GAP HEIGHT (IN)	2.36	2.36	2.36	2.36
GAP WIDTH (IN)	7.68	7.68	7.68	11.22
COIL END EXTENSION (IN)	2.55	2.55	2.55	2.55
NO. OF TURNS	72	72	72	72
CURRENT EXCITATION (AMPS)	1150	1150	1150	1150
POWER / MAGNET (KW)	10.879	18.309	25.737	26.471

TYPE	NUMBER	EFFECTIVE LENGTH	STRENGTH
Q1	6	0.64008 M	103.8087 KG/M
Q2	6	1.31166	-103.8087
Q3	6	0.7104	103.8087
Q4	6	0.45720	96.6333
Q5	6	0.82804	-97.4126
Q6	6	0.70104	96.6333
Q7	6	0.70104	-97.4126
Q8	6	0.45720	96.6333
Q9	6	0.45720	-97.4126
Q10	6	0.45720	40.8765
Q11	6	0.87376	89.3989
Q12	6	0.77220	-89.3989
Q13	6	0.77220	-89.3989
Q14	6	0.64262	89.3989

OTHER PARAMETERS:

TYPE	Q1 - Q9	Q10	Q11 - Q14
POLE TIP RADIUS	44.5 MM	85 MM	85 MM
NO. OF TURNS	132	40	84
POLE TIP FIELD (MAX)	4.5 KG	2.7 KG	7.7 KG
CURRENT EXCITATION (AMPS)	266	1150	1150
POWER / MAGNET (KW)	2.20-4.48	3.51	8.98-10.79

TYPE	NUMBER	EFFECTIVE LENGTH	STRENGTH
S7	6	0.3048	35.7175 KKG/M2
S9	6	0.3048	-219.5244
S10	6	0.3048	134.7943
S12	6	0.3048	-170.5021

OTHER PARAMETERS:

TYPE	S7,S9	S10,S12
POLE TIP RADIUS	?	?
NO OF TURNS	?	?
POLE TIP FIELD	?	?
CURRENT EXCITATION (AMPS)	?	?
POWER / MAGNET (KW)	?	?

ED.4

LATTICE MAGNETS; OCTUPOLES

11.43.15. CHANGED 5/31/83
 PRINTED 6/ 9/83

TYPE	NUMBER	EFFECTIVE LENGTH	STRENGTH
OC10	6	0.3048	-325.1426 KG/M3
OC12	6	0.3048	778.6057

OTHER PARAMETERS:

POLE TIP RADIUS	?
NO OF TURNS	?
POLE TIP FIELD	?
CURRENT EXCITATION (AMPS)	?
POWER / MAGNET (KW)	?

TYPE	NUMBER	EFFECTIVE LENGTH	STRENGTH
S7	6	8.0 "	53.57 KG/M2
S9	6	8.0	-330.1
S10	6	8.0	202.7
S12	6	8.0	-256.3

OTHER PARAMETERS:

TYPE	S7,S9
POLE TIP RADIUS	2.8125 "
NO OF TURNS	6 PER POLE
POLE TIP FIELD (KG)	0.14, 0.84
CURRENT EXCITATION (AMPS)	42.5, 262
POWER / MAGNET (KW)	.061, 0.375

ED.4

LATTICE MAGNETS; OCTUPOLES

16.01.37. CHANGED 6/10/83
 PRINTED 6/10/83

TYPE	NUMBER	EFFECTIVE LENGTH	STRENGTH
OC10	6	8.0	-487.9 KG/M3
OC12	6	8.0	406.4

APPENDIX C

APPENDIX C.

FINAL SITE COORDINATES FOR ACCUMULATOR RING.
 COORDINATES ARE GIVEN AT BEND CENTER
 AND DOWNSTREAM END OF EACH MAGNET.
 COORDINATES ARE LISTED IN CLOCKWISE MANNER.

MAIN RING STATION A0 IS X=0.0, Y=0.0

3 OCT 1983. DE JOHNSON

NAME	LENGTH(IN)	X(FEET)	Y(FEET)	THETA(RAD)	S(METERS)
A10		-457.627	-1398.934	.523599	
A10	0.00	-457.627	-1398.934	.523599	0.0000
A1Q1		-444.066	-1375.446	.523599	
A1Q1	25.20	-443.541	-1374.537	.523599	8.5866
A1Q2		-441.625	-1371.218	.523599	
A1Q2	51.64	-440.549	-1369.354	.523599	10.4106
A1Q3		-438.398	-1365.629	.523599	
A1Q3	27.60	-437.823	-1364.633	.523599	12.0722
A1B3		-435.089	-1359.898	.523599	
A1B3	60.00	-433.655	-1357.849	.610865	14.5004
A1Q4		-421.136	-1339.971	.610865	
A1Q4	18.00	-420.706	-1339.356	.610865	21.3813
A1Q5		-413.790	-1329.480	.610865	
A1Q5	32.60	-413.011	-1328.367	.610865	25.4703
A1Q6		-398.525	-1307.678	.610865	
A1Q6	27.60	-397.865	-1306.736	.610865	33.5191
A1Q7		-389.326	-1294.541	.610865	
A1Q7	27.60	-388.666	-1293.599	.610865	38.4073
A1S7		-383.021	-1285.536	.610865	
A1S7	12.00	-382.734	-1285.127	.610865	41.5597
A1B7		-377.426	-1277.545	.610865	
A1B7	120.00	-373.881	-1274.001	.785398	45.9007
A1Q8		-372.172	-1272.292	.785398	
A1Q8	18.00	-371.642	-1271.762	.785398	46.8659
A1B8		-363.480	-1263.599	.785398	
A1B8	180.00	-356.947	-1259.828	1.047198	52.6571
A1Q9		-354.854	-1258.620	1.047198	
A1Q9	18.00	-354.205	-1258.245	1.047198	53.6223
A1S9		-352.906	-1257.495	1.047198	
A1S9	12.00	-352.473	-1257.245	1.047198	54.2319
A1B9		-344.208	-1252.473	1.047198	
A1B9	180.00	-336.922	-1250.521	1.308997	59.4135
A1Q10		-334.588	-1249.895	1.308997	
A1Q10	18.00	-333.863	-1249.701	1.308997	60.3787
A1B10		-324.967	-1247.317	1.308997	
A1B10	180.00	-317.424	-1247.317	1.570796	65.4587
A1S10		-315.966	-1247.317	1.570796	
A1S10	12.00	-315.466	-1247.317	1.570796	66.0554
A1Q11		-313.075	-1247.317	1.570796	
A1Q11	34.40	-311.642	-1247.317	1.570796	67.2211
A1Q12		-308.666	-1247.317	1.570796	
A1Q12	30.40	-307.399	-1247.317	1.570796	68.5143
A1S12		-306.185	-1247.317	1.570796	
A1S12	12.00	-305.685	-1247.317	1.570796	69.0369
A1Q13		-303.704	-1247.317	1.570796	
A1Q13	30.40	-302.437	-1247.317	1.570796	70.0268
A1Q14		-299.752	-1247.317	1.570796	
A1Q14	25.30	-298.697	-1247.317	1.570796	71.1666
A20		-272.960	-1247.317	1.570796	

NAME	LENGTH (IN)	X (FEET)	Y (FEET)	THETA (RAD)	S (METERS)
A20	0.00	-272.960	-1247.317	1.570796	79.0115
A2Q14		-246.168	-1247.317	1.570796	
A2Q14	25.30	-245.113	-1247.317	1.570796	87.4991
A2Q13		-242.215	-1247.317	1.570796	
A2Q13	30.40	-240.949	-1247.317	1.570796	88.7684
A2S12		-239.734	-1247.317	1.570796	
A2S12	12.00	-239.234	-1247.317	1.570796	89.2910
A2Q12		-237.253	-1247.317	1.570796	
A2Q12	30.40	-235.986	-1247.317	1.570796	90.2810
A2Q11		-232.844	-1247.317	1.570796	
A2Q11	34.40	-231.410	-1247.317	1.570796	91.6757
A2S10		-229.953	-1247.317	1.570796	
A2S10	12.00	-229.453	-1247.317	1.570796	92.2724
A2B10		-220.952	-1247.317	1.570796	
A2B10	180.00	-213.666	-1249.270	1.832596	97.1363
A2Q10		-211.331	-1249.895	1.832596	
A2Q10	18.00	-210.607	-1250.089	1.832596	98.1015
A2B9		-201.711	-1252.473	1.832596	
A2B9	180.00	-195.178	-1256.245	2.094395	103.1815
A2S9		-193.013	-1257.495	2.094395	
A2S9	12.00	-192.580	-1257.745	2.094395	104.0959
A2Q9		-191.065	-1258.620	2.094395	
A2Q9	18.00	-190.415	-1258.995	2.094395	104.8579
A2B8		-182.439	-1263.599	2.094395	
A2B8	180.00	-177.106	-1268.933	2.356195	109.9379
A2Q8		-173.747	-1272.292	2.356195	
A2Q8	18.00	-173.217	-1272.822	2.356195	111.6143
A2B7		-168.493	-1277.545	2.356195	
A2B7	120.00	-165.618	-1281.652	2.530727	115.1703
A2S7		-162.898	-1285.536	2.530727	
A2S7	12.00	-162.612	-1285.946	2.530727	116.7681
A2Q7		-156.593	-1294.541	2.530727	
A2Q7	27.60	-155.934	-1295.483	2.530727	120.3167
A2Q6		-147.395	-1307.678	2.530727	
A2Q6	27.60	-146.735	-1308.620	2.530727	125.2049
A2Q5		-132.129	-1329.479	2.530727	
A2Q5	32.60	-131.350	-1330.592	2.530727	133.3807
A2Q4		-124.783	-1339.970	2.530727	
A2Q4	18.00	-124.353	-1340.585	2.530727	137.0989
A2B3		-110.830	-1359.898	2.530727	
A2B3	60.00	-109.579	-1362.064	2.617994	145.0466
A2Q3		-107.521	-1365.629	2.617994	
A2Q3	27.60	-106.946	-1366.625	2.617994	146.6518
A2Q2		-104.294	-1371.218	2.617994	
A2Q2	51.64	-103.218	-1373.081	2.617994	148.9241
A2Q1		-101.853	-1375.446	2.617994	
A2Q1	25.20	-101.328	-1376.356	2.617994	150.0765
A30		-88.292	-1398.934	2.617994	

NAME	LENGTH (IN)	X (FEET)	Y (FEET)	THETA (RAD)	S (METERS)
A30	0.00	-88.292	-1398.934	2.617994	158.0230
A3Q1		-74.732	-1422.422	2.617994	
A3Q1	25.20	-74.207	-1423.331	2.617994	166.6096
A3Q2		-72.290	-1426.650	2.617994	
A3Q2	51.64	-71.214	-1428.514	2.617994	168.4337
A3Q3		-69.064	-1432.239	2.617994	
A3Q3	27.60	-68.489	-1433.235	2.617994	170.0953
A3B3		-65.755	-1437.970	2.617994	
A3B3	60.00	-64.697	-1440.237	2.705260	172.5235
A3Q4		-55.474	-1460.018	2.705260	
A3Q4	18.00	-55.157	-1460.697	2.705260	179.4043
A3Q5		-50.061	-1471.625	2.705260	
A3Q5	32.60	-49.487	-1472.856	2.705260	183.4933
A3Q6		-38.813	-1495.746	2.705260	
A3Q6	27.60	-38.327	-1496.788	2.705260	191.5421
A3Q7		-32.035	-1510.281	2.705260	
A3Q7	27.60	-31.549	-1511.323	2.705260	196.4303
A3S7		-27.390	-1520.244	2.705260	
A3S7	12.00	-27.179	-1520.697	2.705260	199.5827
A3B7		-23.267	-1529.085	2.705260	
A3B7	120.00	-21.970	-1533.927	2.879793	203.9238
A3Q8		-21.344	-1536.261	2.879793	
A3Q8	18.00	-21.150	-1536.985	2.879793	204.8890
A3B8		-18.163	-1548.135	2.879793	
A3B8	180.00	-18.163	-1555.678	3.141593	210.6802
A3Q9		-18.163	-1558.095	3.141593	
A3Q9	18.00	-18.163	-1558.845	3.141593	211.6454
A3S9		-18.163	-1560.345	3.141593	
A3S9	12.00	-18.163	-1560.845	3.141593	212.2550
A3B9		-18.163	-1570.388	3.141593	
A3B9	180.00	-20.115	-1577.674	3.403392	217.4366
A3Q10		-20.740	-1580.008	3.403392	
A3Q10	18.00	-20.935	-1580.733	3.403392	218.4018
A3B10		-23.318	-1589.629	3.403392	
A3B10	180.00	-27.090	-1596.161	3.665192	223.4818
A3S10		-27.819	-1597.424	3.665192	
A3S10	12.00	-28.069	-1597.857	3.665192	224.0785
A3Q11		-29.264	-1599.928	3.665192	
A3Q11	34.40	-29.981	-1601.169	3.665192	225.2441
A3Q12		-31.469	-1603.746	3.665192	
A3Q12	30.40	-32.102	-1604.843	3.665192	226.5373
A3S12		-32.709	-1605.895	3.665192	
A3S12	12.00	-32.959	-1606.328	3.665192	227.0599
A3Q13		-33.950	-1608.044	3.665192	
A3Q13	30.40	-34.583	-1609.141	3.665192	228.0499
A3Q14		-35.926	-1611.466	3.665192	
A3Q14	25.30	-36.453	-1612.379	3.665192	229.1897
A40		-49.322	-1634.669	3.665192	

NAME	LENGTH(IN)	X(FEET)	Y(FEET)	THETA(RAD)	S(METERS)
A40	0.00	-49.322	-1634.669	3.665192	237.0346
A4Q14		-62.718	-1657.871	3.665192	
A4Q14	25.30	-63.245	-1658.784	3.665192	245.5221
A4Q13		-64.694	-1661.294	3.665192	
A4Q13	30.40	-65.327	-1662.391	3.665192	246.7915
A4S12		-65.935	-1663.443	3.665192	
A4S12	12.00	-66.185	-1663.876	3.665192	247.3141
A4Q12		-67.175	-1665.592	3.665192	
A4Q12	30.40	-67.809	-1666.689	3.665192	248.3040
A4Q11		-69.380	-1669.410	3.665192	
A4Q11	34.40	-70.097	-1670.652	3.665192	249.6988
A4S10		-70.826	-1671.914	3.665192	
A4S10	12.00	-71.076	-1672.347	3.665192	250.2955
A4B10		-75.326	-1679.709	3.665192	
A4B10	180.00	-80.660	-1685.043	3.926991	255.1594
A4Q10		-82.369	-1686.752	3.926991	
A4Q10	18.00	-82.899	-1687.282	3.926991	256.1246
A4B9		-89.411	-1693.794	3.926991	
A4B9	180.00	-95.944	-1697.566	4.188790	261.2046
A4S9		-98.109	-1698.816	4.188790	
A4S9	12.00	-98.542	-1699.066	4.188790	262.1190
A4Q9		-100.057	-1699.941	4.188790	
A4Q9	18.00	-100.707	-1700.316	4.188790	262.8810
A4B8		-108.683	-1704.921	4.188790	
A4B8	180.00	-115.969	-1706.873	4.450590	267.9610
A4Q8		-120.557	-1708.102	4.450590	
A4Q8	18.00	-121.282	-1708.296	4.450590	269.6374
A4B7		-127.733	-1710.025	4.450590	
A4B7	120.00	-132.727	-1710.462	4.625123	273.1934
A4S7		-137.451	-1710.875	4.625123	
A4S7	12.00	-137.949	-1710.919	4.625123	274.7912
A4Q7		-148.402	-1711.833	4.625123	
A4Q7	27.60	-149.547	-1711.934	4.625123	278.3398
A4Q6		-164.378	-1713.231	4.625123	
A4Q6	27.60	-165.524	-1713.331	4.625123	283.2280
A4Q5		-190.892	-1715.551	4.625123	
A4Q5	32.60	-192.245	-1715.669	4.625123	291.4038
A4Q4		-203.650	-1716.667	4.625123	
A4Q4	18.00	-204.397	-1716.732	4.625123	295.1220
A4B3		-227.884	-1718.787	4.625123	
A4B3	60.00	-230.386	-1718.787	4.712389	303.0696
A4Q3		-234.502	-1718.787	4.712389	
A4Q3	27.60	-235.652	-1718.787	4.712389	304.6748
A4Q2		-240.956	-1718.787	4.712389	
A4Q2	51.64	-243.107	-1718.787	4.712389	306.9471
A4Q1		-245.838	-1718.787	4.712389	
A4Q1	25.20	-246.888	-1718.787	4.712389	308.0996
A50		-272.960	-1718.787	4.712389	

NAME	LENGTH (IN)	X (FEET)	Y (FEET)	THETA (RAD)	S (METERS)
A50	0.00	-272.960	-1718.787	4.712389	316.0461
A5Q1		-300.081	-1718.787	4.712389	
A5Q1	25.20	-301.131	-1718.787	4.712389	324.6327
A5Q2		-304.964	-1718.787	4.712389	
A5Q2	51.64	-307.115	-1718.787	4.712389	326.4567
A5Q3		-311.417	-1718.787	4.712389	
A5Q3	27.60	-312.567	-1718.787	4.712389	328.1183
A5B3		-318.035	-1718.787	4.712389	
A5B3	60.00	-320.527	-1718.569	4.799656	330.5465
A5Q4		-342.269	-1716.667	4.799656	
A5Q4	18.00	-343.016	-1716.602	4.799656	337.4274
A5Q5		-355.027	-1715.551	4.799656	
A5Q5	32.60	-356.380	-1715.432	4.799656	341.5164
A5Q6		-381.541	-1713.231	4.799656	
A5Q6	27.60	-382.687	-1713.131	4.799656	349.5652
A5Q7		-397.517	-1711.833	4.799656	
A5Q7	27.60	-398.663	-1711.733	4.799656	354.4534
A5S7		-408.468	-1710.875	4.799656	
A5S7	12.00	-408.966	-1710.832	4.799656	357.6058
A5B7		-418.186	-1710.025	4.799656	
A5B7	120.00	-423.028	-1708.728	4.974188	361.9468
A5Q8		-425.362	-1708.102	4.974188	
A5Q8	18.00	-426.087	-1707.908	4.974188	362.9120
A5B8		-437.236	-1704.921	4.974188	
A5B8	180.00	-443.769	-1701.149	5.235988	368.7032
A5Q9		-445.862	-1699.941	5.235988	
A5Q9	18.00	-446.511	-1699.566	5.235988	369.6684
A5S9		-447.810	-1698.816	5.235988	
A5S9	12.00	-448.243	-1698.566	5.235988	370.2780
A5B9		-456.508	-1693.794	5.235988	
A5B9	180.00	-461.842	-1688.460	5.497787	375.4596
A5Q10		-463.551	-1686.751	5.497787	
A5Q10	18.00	-464.081	-1686.221	5.497787	376.4248
A5B10		-470.593	-1679.709	5.497787	
A5B10	180.00	-474.365	-1673.176	5.759587	381.5048
A5S10		-475.094	-1671.914	5.759587	
A5S10	12.00	-475.344	-1671.481	5.759587	382.1015
A5Q11		-476.539	-1669.410	5.759587	
A5Q11	34.40	-477.256	-1668.169	5.759587	383.2672
A5Q12		-478.744	-1665.592	5.759587	
A5Q12	30.40	-479.377	-1664.495	5.759587	384.5603
A5S12		-479.984	-1663.443	5.759587	
A5S12	12.00	-480.234	-1663.010	5.759587	385.0829
A5Q13		-481.225	-1661.294	5.759587	
A5Q13	30.40	-481.858	-1660.197	5.759587	386.0729
A5Q14		-483.201	-1657.871	5.759587	
A5Q14	25.30	-483.728	-1656.958	5.759587	387.2127
A60		-496.597	-1634.669	5.759587	

NAME	LENGTH (IN)	X (FEET)	Y (FEET)	THETA (RAD)	S (METERS)
A60	0.00	-496.597	-1634.669	5.759587	395.0576
A6Q14		-509.993	-1611.466	5.759587	
A6Q14	25.30	-510.520	-1610.553	5.759587	403.5451
A6Q13		-511.969	-1608.044	5.759587	
A6Q13	30.40	-512.602	-1606.947	5.759587	404.8145
A6S12		-513.210	-1605.895	5.759587	
A6S12	12.00	-513.460	-1605.462	5.759587	405.3371
A6Q12		-514.450	-1603.746	5.759587	
A6Q12	30.40	-515.084	-1602.649	5.759587	406.3271
A6Q11		-516.655	-1599.927	5.759587	
A6Q11	34.40	-517.372	-1598.686	5.759587	407.7218
A6S10		-518.101	-1597.424	5.759587	
A6S10	12.00	-518.351	-1596.991	5.759587	408.3185
A6B10		-522.601	-1589.629	5.759587	
A6B10	180.00	-524.553	-1582.343	6.021386	413.1824
A6Q10		-523.179	-1580.008	6.021386	
A6Q10	18.00	-525.373	-1579.284	6.021386	414.1476
A6B9		-527.756	-1570.388	6.021386	
A6B9	180.00	-527.756	-1562.845	6.283185	419.2276
A6S9		-527.756	-1560.343	.000000	
A6S9	12.00	-527.756	-1559.845	.000000	420.1420
A6Q9		-527.756	-1558.095	.000000	
A6Q9	18.00	-527.756	-1557.345	.000000	420.9040
A6B8		-527.756	-1548.135	.000000	
A6B8	180.00	-525.804	-1540.849	.261800	425.9840
A6Q8		-524.575	-1536.261	.261800	
A6Q8	18.00	-524.381	-1535.536	.261800	427.6604
A6B7		-522.652	-1529.089	.261800	
A6B7	120.00	-520.533	-1524.541	.436332	431.2164
A6S7		-518.529	-1520.244	.436332	
A6S7	12.00	-518.318	-1519.791	.436332	432.8142
A6Q7		-513.884	-1510.281	.436332	
A6Q7	27.60	-513.398	-1509.239	.436332	436.3628
A6Q6		-507.106	-1495.746	.436332	
A6Q6	27.60	-506.620	-1494.704	.436332	441.2510
A6Q5		-495.858	-1471.625	.436332	
A6Q5	32.60	-495.284	-1470.394	.436332	449.4268
A6Q4		-490.445	-1460.018	.436332	
A6Q4	18.00	-490.128	-1459.338	.436332	453.1450
A6B3		-480.165	-1437.970	.436332	
A6B3	60.00	-478.914	-1435.804	.523599	461.0927
A6Q3		-476.856	-1432.239	.523599	
A6Q3	27.60	-476.281	-1431.243	.523599	462.6979
A6Q2		-473.629	-1426.650	.523599	
A6Q2	51.64	-472.553	-1424.787	.523599	464.9701
A6Q1		-471.188	-1422.422	.523599	
A6Q1	25.20	-470.663	-1421.512	.523599	466.1226
A10		-457.627	-1398.934	.523599	
A10	0.00	-457.627	-1398.934	.523599	474.0691

** END OF LISTING **

APPENDIX D

DP

V CHR PVEC
AGR SUB FXPT 2 -3 V .SP 1
INCR 1 DP .005
END CALL CHR
FIN
STBP

SYNCH RUN DRSM

```

.....
DEBUNCHER RING LATTICE A. G. RUGGIERO
THERE ARE THREE LONG STRAIGHT SECTIONS WITH ZERO DISPERSION
EACH LONG STRAIGHT SECTION HAS BEEN BRIDGED WITH REGULAR CELL QUADS
HARMONIC NUMBER IS 90
TWO QUADRUPOLE LENGTHS ARE 27.6 AND 32.6 INCHES
APRIL 9, 1983 A. G. RUGGIERO
.....

*** BRHO * // 29.6501
*** BO * // 1.7
*** RHOI * // 0.0 BRHO
*** LB * // 1.660402

*** LQ * // 0.35052
*** LOS * // 0.41402

*** KF * // 0.336518
*** KD * // -0.329283

*** DD DRF // 1.0354310
*** OS DRF // 0.3
*** LC DRF // 0.7354310
*** SC DRF // 1.660402
*** SR DRF // 0.3731264
*** SZ DRF // 0.3667764
*** Z DRF // 0.3604264

*** B MAG // LB. 0. 1. RHOI S
*** QF MAG // LQ KF 1.
*** QD MAG // LQ KD 1.

*** SF SXTP // 0.0 0.14073 1.
*** SD SXTP // 0.0 -0.21342 1.
*** .DF1 BNL // OS 0.0 0.0 0.0 0.0
*** .DD1 BNL // 0.0 0.0 0.0 0.0
*** .DF2 BNL // 0.0 0.0 0.0 0.0
*** .DD2 BNL // 0.0 0.0 0.0 0.0
*** .C BNL // QF 0.0 0.0 0.0 0.0
*** .LA BNL // SR 0.0 0.0 0.0 0.0
*** .LB BNL // SR 0.0 0.0 0.0 0.0
*** .LZ BNL // Z 0.0 0.0 0.0 0.0
*** .CH BNL // QF1 0.0 0.0 0.0 0.0
*** .CS1 BNL // .LA 0.0 0.0 0.0 0.0
*** .CS2 BNL // .LA 0.0 0.0 0.0 0.0
*** .CS3 BNL // .LA 0.0 0.0 0.0 0.0
*** .C1 BNL // .C1 0.0 0.0 0.0 0.0
*** .C2 BNL // .C2 0.0 0.0 0.0 0.0
*** .C3 BNL // .C3 0.0 0.0 0.0 0.0
*** KQ1 * // 0.377469
*** KQ2 * // 0.347140
*** KQ3 * // 0.358812
*** KP1 * // 0.386791
*** KP2 * // 0.324942
*** KP3 * // 0.324886

*** QF1 MAG // LQ KF1 1.
*** QF2 MAG // LQ KF2 1.
*** QF3 MAG // LQ KF3 1.
*** QD1 MAG // LQ -KD1 1.
*** QD2 MAG // LQ -KD2 1.
*** QD3 MAG // LQ -KD3 1.
*** .SP BNL // .CT .C .C .C .C .C .CH

```

POS	S(M)	NUX	NUY	BETAX(M)	BETAY(M)	ETAX(M)	ETAY(M)	ETAS(M)	ALPHAX	ALPHAY	DETAX	DEYAY	
0	0.0000	0.000000	0.000000	17.83321	5.73406	-.00091	0.00000	0.00000	0.00000	0.00000	-.00000	0.00000	
0	3505	.00318	.00957	17.02364	6.02589	-.00089	0.00000	0.00000	0.00000	2.26819	-.84539	.00012	0.00000
0	3526	.00482	.01892	15.38155	6.69638	-.00085	0.00000	0.00000	0.00000	2.13352	-.95156	.00012	0.00000
0	1.0768	.01092	.02734	15.86135	7.44610	-.00080	0.00000	0.00000	0.00000	1.99886	-1.05774	.00012	0.00000
0	1.3699	.01345	.03491	12.39994	8.27506	-.00076	0.00000	0.00000	0.00000	1.86420	-1.16391	.00012	0.00000
1	1.8430	.02052	.04172	11.05902	9.18324	-.00071	0.00000	0.00000	0.00000	1.72953	-1.27008	.00012	0.00000
1	2.2162	.02622	.04787	9.81860	10.17066	-.00067	0.00000	0.00000	0.00000	1.59487	-1.37626	.00012	0.00000
1	2.5893	.03266	.05342	8.67867	11.23732	-.00062	0.00000	0.00000	0.00000	1.46020	-1.48243	.00012	0.00000
1	2.9624	.03995	.05846	7.63924	12.38320	-.00058	0.00000	0.00000	0.00000	1.32554	-1.58861	.00012	0.00000
1	3.3355	.04824	.06303	6.70030	13.60832	-.00054	0.00000	0.00000	0.00000	1.19088	-1.69578	.00012	0.00000
10	3.7087	.05774	.06720	5.86183	14.91267	-.00049	0.00000	0.00000	0.00000	1.05621	-1.80096	.00012	0.00000
10	4.0818	.06858	.07101	5.12390	16.29626	-.00045	0.00000	0.00000	0.00000	.92155	-1.90713	.00012	0.00000
10	4.4523	.08001	.07435	4.47257	16.94478	-.00041	0.00000	0.00000	0.00000	-.22980	-.08334	.00007	0.00000
10	4.7828	.09183	.07769	4.79246	16.18270	-.00040	0.00000	0.00000	0.00000	-.42219	2.05979	.00002	0.00000
10	5.1360	.10380	.08154	5.14175	14.69068	-.00039	0.00000	0.00000	0.00000	-.51393	1.93891	.00002	0.00000
10	5.5201	.11492	.08579	5.55950	13.28886	-.00038	0.00000	0.00000	0.00000	-.60546	1.81803	.00002	0.00000
10	5.9022	.12517	.09050	6.04570	11.97726	-.00038	0.00000	0.00000	0.00000	-.69739	1.69715	.00002	0.00000
10	6.2763	.13457	.09573	6.60037	10.75586	-.00037	0.00000	0.00000	0.00000	-.78913	1.57626	.00002	0.00000
10	6.6485	.14318	.10157	7.22348	9.62468	-.00036	0.00000	0.00000	0.00000	-.88086	1.45538	.00002	0.00000
10	7.0216	.15104	.10811	7.91506	8.58370	-.00035	0.00000	0.00000	0.00000	-.97260	1.33450	.00002	0.00000
20	7.3947	.15820	.11545	8.67509	7.63293	-.00035	0.00000	0.00000	0.00000	-1.06433	1.21361	.00002	0.00000
20	7.7678	.16475	.12371	9.50358	6.77237	-.00034	0.00000	0.00000	0.00000	-1.15607	1.09273	.00002	0.00000
20	8.1410	.17072	.13303	10.40053	6.00202	-.00033	0.00000	0.00000	0.00000	-1.24780	.97185	.00002	0.00000
20	8.5141	.17618	.14354	11.36593	5.32488	-.00033	0.00000	0.00000	0.00000	-1.33954	.85097	.00002	0.00000
20	8.8866	.18096	.15446	11.81366	4.96611	-.00031	0.00000	0.00000	0.00000	-.08104	.72100	.00006	0.00000
20	9.2151	.18577	.16596	11.25962	5.14721	-.00029	0.00000	0.00000	0.00000	1.48753	-.58732	.00010	0.00000
20	9.5883	.19131	.17661	10.18529	5.62188	-.00025	0.00000	0.00000	0.00000	1.38103	-.68482	.00010	0.00000
20	9.9614	.19745	.18670	9.19443	6.16930	-.00021	0.00000	0.00000	0.00000	1.27452	-.78232	.00010	0.00000
20	10.3345	.20426	.19589	8.28305	6.78949	-.00018	0.00000	0.00000	0.00000	1.16802	-.87981	.00010	0.00000
20	10.7076	.21182	.20422	7.45116	7.48243	-.00014	0.00000	0.00000	0.00000	1.06152	-.97731	.00010	0.00000
30	11.0808	.22023	.21178	6.69873	8.24812	-.00010	0.00000	0.00000	0.00000	.95561	-1.07481	.00010	0.00000
30	11.4539	.22958	.21854	6.02579	9.08658	-.00007	0.00000	0.00000	0.00000	.84831	-1.17230	.00010	0.00000
30	11.8270	.23907	.22483	5.43233	9.99779	-.00003	0.00000	0.00000	0.00000	.74201	-1.26980	.00010	0.00000
30	12.2001	.24847	.23054	4.91834	10.98176	0.00000	0.00000	0.00000	0.00000	.63550	-1.36729	.00010	0.00000
30	12.5733	.25771	.23571	4.48383	12.03849	.00004	0.00000	0.00000	0.00000	.52900	-1.46479	.00010	0.00000
35	12.9464	.26795	.24043	4.12881	13.16757	.00008	0.00000	0.00000	0.00000	.42250	-1.56229	.00010	0.00000
36	13.3296	.27910	.24456	4.05811	13.64450	.00011	0.00000	0.00000	0.00000	-.21764	-.22441	.00011	0.00000
37	13.6474	.30496	.24873	4.44371	12.86320	.00015	0.00000	0.00000	0.00000	1.96912	-.89980	.00013	0.00000
38	14.0142	.31716	.25354	5.15854	11.46976	.00020	0.00000	0.00000	0.00000	-1.04916	1.83005	.00013	0.00000
38	14.3810	.32768	.25895	5.98294	10.17834	.00025	0.00000	0.00000	0.00000	-1.19853	1.69097	.00013	0.00000
40	14.7478	.33676	.26505	6.91691	8.98853	.00030	0.00000	0.00000	0.00000	-1.34789	1.55190	.00013	0.00000
41	15.1145	.34463	.27198	7.96044	7.90154	.00034	0.00000	0.00000	0.00000	-1.49726	1.41283	.00013	0.00000
42	15.4813	.35148	.27988	9.11354	6.91616	.00039	0.00000	0.00000	0.00000	-1.64662	1.27375	.00013	0.00000
43	15.8481	.35749	.28892	10.37621	6.03280	.00044	0.00000	0.00000	0.00000	-1.79599	1.13468	.00013	0.00000
44	16.2149	.36277	.29930	11.74844	5.25147	.00048	0.00000	0.00000	0.00000	-.99561	-.94535	.00013	0.00000
45	16.5816	.36746	.31122	13.23024	4.57214	.00053	0.00000	0.00000	0.00000	-2.09471	-.85653	.00013	0.00000
46	16.9484	.37163	.32490	14.82161	3.99484	.00058	0.00000	0.00000	0.00000	-2.24408	-.71746	.00013	0.00000
47	17.3152	.37536	.34049	16.52254	3.51955	.00062	0.00000	0.00000	0.00000	-2.39344	-.57839	.00013	0.00000
48	17.7292	.37919	.36009	17.59682	3.28856	.00066	0.00000	0.00000	0.00000	-.15255	-.01013	.00004	0.00000
49	18.1432	.38299	.37964	16.76654	3.53696	.00066	0.00000	0.00000	0.00000	2.12099	-.60095	-.00005	0.00000

POS	SUM	NUX	NUY	BETAX(M)	BETAY(M)	ETA(X(M))	ETA(Y(M))	ETA(S(M))	ALPHAX	ALPHAY	DETA(X)	DETA(Y)
50 Z	18.5037	38657	37487	15.28022	4.02015	0.0064	0.0000	0.0000	2.00279	-7.3945	0.0005	0.0000
51 Z	18.6641	39051	40822	15.87918	4.60332	0.0064	0.0000	0.0000	1.88459	-6.7836	0.0005	0.0000
52 Z	19.2245	39486	41086	16.56310	5.28648	0.0064	0.0000	0.0000	1.76639	-0.0106	0.0005	0.0000
53 Z	19.3849	39966	41300	17.33220	6.06962	0.0064	0.0000	0.0000	1.65288	1.2947	0.0005	0.0000
54 Z	19.5454	40500	41383	18.18701	6.95275	0.0057	0.0000	0.0000	1.54216	1.2947	0.0005	0.0000
55 Z	20.3058	41095	41656	9.12672	7.93586	0.0055	0.0000	0.0000	1.43117	1.43117	0.0005	0.0000
56 Z	20.6662	41761	41761	7.25164	9.01896	0.0052	0.0000	0.0000	1.31958	1.31958	0.0005	0.0000
57 Z	21.0266	42507	41932	8.02020	10.20204	0.0052	0.0000	0.0000	1.17537	1.17537	0.0005	0.0000
58 Z	21.3871	43345	42462	11.48511	11.48511	0.0050	0.0000	0.0000	1.04928	1.04928	0.0005	0.0000
59 Z	21.7475	44288	42834	8.73793	12.86816	0.0049	0.0000	0.0000	0.93857	0.93857	0.0005	0.0000
60 QD3	22.1079	45343	43493	5.33373	13.91588	0.0048	0.0000	0.0000	0.8475	0.8475	0.0002	0.0000
61 R	22.4683	46518	44318	6.11223	12.19246	0.0050	0.0000	0.0000	0.7661	0.7661	0.0008	0.0000
62 R	22.8287	47720	45265	6.91223	10.47226	0.0052	0.0000	0.0000	0.69593	0.69593	0.0008	0.0000
63 R	23.1891	49031	46865	7.73804	8.75226	0.0056	0.0000	0.0000	0.63534	0.63534	0.0008	0.0000
64 R	23.5495	50455	49411	8.61309	7.09177	0.0059	0.0000	0.0000	0.58475	0.58475	0.0008	0.0000
65 R	24.9126	52003	50009	9.54255	5.33872	0.0062	0.0000	0.0000	0.54416	0.54416	0.0008	0.0000
66 R	25.2730	53680	50661	10.52125	3.72298	0.0065	0.0000	0.0000	0.51357	0.51357	0.0008	0.0000
67 R	25.6334	55494	51381	11.55000	2.09171	0.0071	0.0000	0.0000	0.49292	0.49292	0.0008	0.0000
68 R	25.9938	57451	52229	12.62873	0.46044	0.0077	0.0000	0.0000	0.48233	0.48233	0.0008	0.0000
70 R	25.3745	59226	53071	13.76746	5.93046	0.0077	0.0000	0.0000	0.48174	0.48174	0.0008	0.0000
71 QF	25.7349	61100	53923	14.96619	5.27177	0.0080	0.0000	0.0000	0.48115	0.48115	0.0008	0.0000
72 QF	26.0953	63073	54775	16.22502	4.61308	0.0084	0.0000	0.0000	0.48056	0.48056	0.0008	0.0000
73 QF	26.4557	65146	55627	17.54385	3.95439	0.0089	0.0000	0.0000	0.47997	0.47997	0.0008	0.0000
74 QF	26.8161	67319	56480	18.92268	3.29570	0.0094	0.0000	0.0000	0.47938	0.47938	0.0008	0.0000
75 QF	27.1765	69592	57332	20.36151	2.63701	0.0099	0.0000	0.0000	0.47879	0.47879	0.0008	0.0000
76 QF	27.5369	72065	58185	21.86034	1.97832	0.0104	0.0000	0.0000	0.47820	0.47820	0.0008	0.0000
77 QF	27.8973	74638	59038	23.41917	1.31963	0.0109	0.0000	0.0000	0.47761	0.47761	0.0008	0.0000
78 QF	28.2577	77311	59891	25.03800	0.66094	0.0114	0.0000	0.0000	0.47702	0.47702	0.0008	0.0000
80 B	34.0725	68765	68900	14.15222	7.92070	0.0112	0.0000	0.0000	1.41414	1.41414	0.0000	0.0000
81 SF	34.4329	69718	69765	15.38093	6.64700	0.0116	0.0000	0.0000	1.26143	1.26143	0.0000	0.0000
82 SF	34.7933	70671	70620	16.60964	5.37330	0.0120	0.0000	0.0000	1.10872	1.10872	0.0000	0.0000
83 SF	35.1537	71624	71573	17.83835	4.10060	0.0124	0.0000	0.0000	0.95602	0.95602	0.0000	0.0000
84 SF	35.5141	72577	72522	19.06706	2.82791	0.0128	0.0000	0.0000	0.80331	0.80331	0.0000	0.0000
85 QF	35.8745	73530	73479	20.29577	1.55522	0.0132	0.0000	0.0000	0.65060	0.65060	0.0000	0.0000
86 QF	36.2349	74483	74432	21.52448	0.28253	0.0136	0.0000	0.0000	0.49789	0.49789	0.0000	0.0000
87 SF	36.5953	75436	75385	22.75319	0.00984	0.0140	0.0000	0.0000	0.34518	0.34518	0.0000	0.0000
88 QF	36.9557	76389	76338	24.01190	0.00000	0.0144	0.0000	0.0000	0.19247	0.19247	0.0000	0.0000
89 LC	37.3161	77342	77291	25.27061	0.00000	0.0148	0.0000	0.0000	0.03976	0.03976	0.0000	0.0000
90 D	39.2402	76936	78819	5.91070	13.61977	1.05019	0.0000	0.0000	0.77056	0.77056	0.0006	0.0000
91 SD	39.6006	77889	78919	5.91070	13.61977	1.05019	0.0000	0.0000	0.77056	0.77056	0.0006	0.0000
92 SD	39.9610	78842	79958	5.91070	13.61977	1.05019	0.0000	0.0000	0.77056	0.77056	0.0006	0.0000
93 QD	40.3214	79795	80968	5.91070	13.61977	1.05019	0.0000	0.0000	0.77056	0.77056	0.0006	0.0000
94 QD	40.6818	80748	81931	5.91070	13.61977	1.05019	0.0000	0.0000	0.77056	0.77056	0.0006	0.0000
95 SD	40.5413	80716	82446	5.90981	13.50643	1.04938	0.0000	0.0000	0.76983	0.76983	0.0006	0.0000
96 SD	40.9017	81669	82961	5.90892	13.39309	1.04857	0.0000	0.0000	0.76910	0.76910	0.0006	0.0000
97 D	41.2621	82622	83476	5.90803	13.27975	1.04776	0.0000	0.0000	0.76837	0.76837	0.0006	0.0000
98 LC	42.0225	83575	84491	5.90714	13.16641	1.04695	0.0000	0.0000	0.76764	0.76764	0.0006	0.0000
99 Q	43.6725	86445	86952	5.90625	13.05307	1.04614	0.0000	0.0000	0.76691	0.76691	0.0006	0.0000

POS	S(M)	NUX	NUY	BETAX(M)	BETAY(M)	ETAX(M)	ETAY(M)	ETAS(M)	ALPHAX	ALPHAY	DETAX	DETAY
100 SF	43.6725	.86445	.85942	13.37317	5.91571	1.97048	0.00000	.05574	-1.61367	.78450	.24434	0.00000
101 OS	43.9725	.86789	.86702	14.36562	5.46959	2.04378	0.00000	.05574	-1.69452	.70258	.24434	0.00000
102 QF	44.3230	.87167	.87833	14.96791	5.22666	2.08673	0.00000	.05574	-1.00000	-.00000	-.00011	0.00000
103 QF	44.6736	.87545	.88884	14.36562	5.46959	2.04371	0.00000	.05574	-1.69452	.70258	.24456	0.00000
104 OS	44.9736	.87889	.89724	13.37317	5.91571	1.97034	0.00000	.05574	-1.61367	-.78450	-.24456	0.00000
105 SF	44.9736	.87889	.89724	13.37317	5.91571	1.97034	0.00000	.05574	-1.61367	-.78450	-.24456	0.00000
106 O	45.7090	.88849	.91519	11.14544	7.21730	1.79048	0.00000	.05574	-1.41547	-.98533	-.24434	0.00000
107 B	47.3694	.91813	.94481	7.19273	11.16210	1.46400	0.00000	.20951	-.96869	-1.37970	-.14929	0.00000
108 O	48.1048	.93611	.95441	5.91368	13.33215	1.35421	0.00000	.20951	-.77050	-1.57101	-.14929	0.00000
109 SD	48.1048	.93611	.95441	5.91368	13.33215	1.35421	0.00000	.20951	-.77050	-1.57101	-.14929	0.00000
110 OS	48.4048	.94451	.95786	5.47563	14.29817	1.30942	0.00000	.20951	-.68965	-1.64905	-.00016	0.00000
111 OS	48.7553	.95200	.96166	5.23710	14.88411	1.28332	0.00000	.20951	-.68965	-1.64905	-.00016	0.00000
112 OS	49.1058	.96558	.96546	5.47563	14.29817	1.30930	0.00000	.20951	-.68965	-1.64905	-.00016	0.00000
113 OS	49.4059	.97389	.96892	5.91367	13.33215	1.35399	0.00000	.20951	-.77050	-1.57101	-.14895	0.00000
114 SD	49.4059	.97389	.96892	5.91367	13.33215	1.35399	0.00000	.20951	-.77050	-1.57101	-.14895	0.00000
115 O	50.1413	.99188	.97852	7.19272	11.16211	1.46356	0.00000	.20951	-.96869	-1.37970	.14895	0.00000
116 B	51.8017	1.02152	1.00813	11.14544	7.21732	1.78946	0.00000	.36321	-1.41547	-.98533	.24423	0.00000
117 O	52.5371	1.03111	1.02609	13.37313	5.91573	1.96907	0.00000	.36321	-1.61366	.78450	.24423	0.00000
118 SF	52.8876	1.03111	1.02609	13.37313	5.91573	1.96907	0.00000	.36321	-1.61366	.78450	.24423	0.00000
119 OS	53.2381	1.03456	1.03448	14.36558	5.46960	2.04234	0.00000	.36321	-1.69451	.70258	.24423	0.00000
120 QF	53.1876	1.03834	1.04500	14.96786	5.22668	2.08528	0.00000	.36321	-.00000	-.00000	-.00006	0.00000
121 QF	53.5382	1.04212	1.05551	14.36557	5.46961	2.04230	0.00000	.36321	-1.69451	-.70258	-.24434	0.00000
122 OS	53.8887	1.04556	1.06391	13.37312	5.91573	1.96900	0.00000	.36321	-1.61367	-.78451	-.24434	0.00000
123 SF	54.2392	1.04956	1.06391	13.37312	5.91573	1.96900	0.00000	.36321	-1.61367	-.78451	-.24434	0.00000
124 O	54.5897	1.05513	1.08186	11.14540	7.21733	1.78931	0.00000	.36321	-1.41547	-.98534	-.24434	0.00000
125 B	56.2940	1.08480	1.11147	7.19271	11.16215	1.46320	0.00000	.51690	-.96869	-1.37971	-.14906	0.00000
126 O	56.9694	1.10278	1.12107	5.91365	13.33220	1.35357	0.00000	.51690	-.77050	-1.57102	-.14906	0.00000
127 SD	56.9694	1.10278	1.12107	5.91365	13.33220	1.35357	0.00000	.51690	-.77050	-1.57102	-.14906	0.00000
128 OS	57.2694	1.11117	1.12453	5.47561	14.29822	1.30886	0.00000	.51690	-.68965	-1.64905	-.14906	0.00000
129 OS	57.6200	1.12167	1.12833	5.23708	14.88417	1.28282	0.00000	.51690	-.00000	-.00000	-.00000	0.00000
130 QO	57.9705	1.13217	1.13213	5.47561	14.29822	1.30886	0.00000	.51690	-.68965	-1.64905	-.14906	0.00000
131 OS	58.2705	1.14056	1.13559	5.91365	13.33220	1.35357	0.00000	.51690	-.77050	-1.57102	-.14906	0.00000
132 SD	58.2705	1.14056	1.13559	5.91365	13.33220	1.35357	0.00000	.51690	-.77050	-1.57102	-.14906	0.00000
133 O	59.0059	1.15855	1.14519	7.19271	11.16215	1.46320	0.00000	.51690	-.96869	-1.37971	-.14906	0.00000
134 B	60.6663	1.18819	1.17480	11.14540	7.21733	1.78931	0.00000	.67058	-1.41547	-.98534	.24434	0.00000
135 O	61.4017	1.19778	1.19275	13.37312	5.91573	1.96900	0.00000	.67058	-1.61367	.78451	.24434	0.00000
136 SF	61.4017	1.19778	1.19275	13.37312	5.91573	1.96900	0.00000	.67058	-1.61367	.78451	.24434	0.00000
137 OS	61.7017	1.20123	1.20115	14.36557	5.46961	2.04230	0.00000	.67058	-1.69451	.70258	.24434	0.00000
138 QF	62.0523	1.20500	1.21166	14.96786	5.22668	2.08528	0.00000	.67058	-.00000	-.00000	.00006	0.00000
139 QF	62.4028	1.20878	1.22218	14.36558	5.46960	2.04234	0.00000	.67058	-1.69451	-.70258	-.24423	0.00000
140 OS	62.7028	1.21223	1.23057	13.37313	5.91573	1.96907	0.00000	.67058	-1.61366	-.78450	-.24423	0.00000
141 SF	62.7028	1.21223	1.23057	13.37313	5.91573	1.96907	0.00000	.67058	-1.61366	-.78450	-.24423	0.00000
142 O	63.4382	1.22182	1.24852	11.14541	7.21732	1.78946	0.00000	.67058	-1.41547	-.98533	-.24423	0.00000
143 B	65.0986	1.25146	1.27814	7.19272	11.16211	1.46356	0.00000	.82428	-.96869	-1.37970	-.14895	0.00000
144 O	65.8340	1.26945	1.28774	5.91367	13.33215	1.35399	0.00000	.82428	-.77050	-1.57101	-.14895	0.00000
145 SD	65.8340	1.26945	1.28774	5.91367	13.33215	1.35399	0.00000	.82428	-.77050	-1.57101	-.14895	0.00000
146 OS	66.1340	1.27784	1.29120	5.47563	14.29817	1.30930	0.00000	.82428	-.68965	-1.64905	-.00016	0.00000
147 QO	66.4846	1.28834	1.29500	5.23710	14.88411	1.28332	0.00000	.82428	-.00000	-.00000	-.00016	0.00000
148 QO	66.8351	1.29883	1.29879	5.47563	14.29817	1.30942	0.00000	.82428	-.68965	-1.64905	-.00016	0.00000
149 OS	67.1351	1.30723	1.30225	5.91368	13.33215	1.35421	0.00000	.82428	-.77050	-1.57101	-.14929	0.00000

POS	S(M)	NUX	NUY	BETAX(M)	BETAY(M)	ETAX(M)	ETAY(M)	ETAS(M)	ALPHAX	ALPHAY	DETAX	DEYAY	
150	SD	67.1351	1.30723	1.30225	5.91368	13.33215	1.35421	0.00000	.82428	-.77050	1.57101	-.14929	0.00000
151	D	67.8705	1.32521	1.31185	7.19273	11.16210	1.46400	0.00000	.82428	-.96869	1.37970	-.14929	0.00000
152	B	69.5309	1.35485	1.34147	11.14544	7.21730	1.79058	0.00000	.97806	-.69452	-.98533	-.24456	0.00000
153	O	70.2663	1.36445	1.35942	13.37317	5.91571	1.97034	0.00000	.97806	-.61367	-.78450	-.24456	0.00000
154	SF	70.2663	1.36445	1.35942	13.37317	5.91571	1.97034	0.00000	.97806	-.61367	-.78450	-.24456	0.00000
155	OS	70.5663	1.36789	1.36782	14.36562	5.46959	2.04371	0.00000	-.97806	1.69452	-.70258	-.24456	0.00000
156	OF	70.9169	1.37167	1.37833	14.36791	5.22666	2.08673	0.00000	.97806	.00000	-.00000	-.00011	0.00000
157	OF	71.2674	1.37545	1.38884	14.36562	5.46959	2.04378	0.00000	-.97806	1.69452	-.70258	-.24456	0.00000
158	OS	71.5674	1.37889	1.39724	13.37317	5.91571	1.97048	0.00000	.97806	1.61367	-.78450	-.24456	0.00000
159	SF	71.5674	1.37889	1.39724	13.37317	5.91571	1.97048	0.00000	.97806	1.61367	-.78450	-.24456	0.00000
160	D	72.3028	1.38849	1.41519	11.14544	7.21730	1.79079	0.00000	.97806	1.41548	-.98533	-.24456	0.00000
161	B	73.9632	1.41813	1.44480	7.19273	11.16210	1.46467	0.00000	1.13188	-.96869	-.137970	-.14907	0.00000
162	O	74.6986	1.43611	1.45440	5.91368	13.33215	1.35504	0.00000	1.13188	.77050	-.137101	-.14907	0.00000
163	SD	74.6986	1.43611	1.45440	5.91368	13.33215	1.35504	0.00000	1.13188	.77050	-.137101	-.14907	0.00000
164	OS	74.9986	1.44451	1.45786	5.47563	14.29817	1.31032	0.00000	1.13188	.68966	-.136905	-.14907	0.00000
165	OD	75.3492	1.45500	1.46166	5.23710	14.08411	1.28431	0.00000	1.13188	.00000	-.00000	-.00016	0.00000
166	OD	75.6997	1.46550	1.46846	5.47563	14.29817	1.31043	0.00000	1.13188	-.68966	1.54905	-.14940	0.00000
167	OS	75.9997	1.47389	1.46892	5.91367	13.33215	1.35526	0.00000	1.13188	-.77050	1.57101	-.14940	0.00000
168	SD	75.9997	1.47389	1.46892	5.91367	13.33215	1.35526	0.00000	1.13188	-.77050	1.57101	-.14940	0.00000
169	D	76.7351	1.49188	1.47882	7.19272	11.16211	1.46513	0.00000	1.13188	-.96869	1.37970	-.14940	0.00000
170	B	78.3955	1.52152	1.50813	11.14544	7.21732	1.79180	0.00000	1.28577	-1.41547	-.98533	-.24468	0.00000
171	O	79.1310	1.53111	1.52608	13.37313	5.91573	1.97175	0.00000	1.28577	-1.61366	-.78450	-.24468	0.00000
172	SF	79.1310	1.53111	1.52608	13.37313	5.91573	1.97175	0.00000	1.28577	-1.61366	-.78450	-.24468	0.00000
173	OS	79.4310	1.53956	1.53448	14.36558	5.46960	2.04515	0.00000	1.28577	-1.69451	-.70258	-.24468	0.00000
174	OF	79.7815	1.53834	1.54500	14.36786	5.22668	2.08819	0.00000	1.28577	.00000	-.00000	-.00006	0.00000
175	OF	80.1320	1.54212	1.53581	14.36567	5.46961	2.04519	0.00000	1.28577	1.69451	-.70258	-.24457	0.00000
176	OS	80.4320	1.54556	1.56391	13.37312	5.91573	1.97182	0.00000	1.28577	1.61367	-.78451	-.24457	0.00000
177	SF	80.4320	1.54556	1.56391	13.37312	5.91573	1.97182	0.00000	1.28577	1.61367	-.78451	-.24457	0.00000
178	D	81.1674	1.55915	1.58786	11.14540	7.21733	1.79196	0.00000	1.28577	1.41547	-.98534	-.24457	0.00000
179	B	82.8278	1.58479	1.61167	7.19271	11.16215	1.46547	0.00000	1.43968	-.96869	1.37971	-.14929	0.00000
180	D	83.5633	1.60278	1.62107	5.91365	13.33220	1.35567	0.00000	1.43968	.77050	-1.57102	-.14929	0.00000
181	SD	83.5633	1.60278	1.62107	5.91365	13.33220	1.35567	0.00000	1.43968	.77050	-1.57102	-.14929	0.00000
182	OS	83.8633	1.61117	1.62483	5.47563	14.29822	1.31088	0.00000	1.43968	.68965	-1.66905	-.14929	0.00000
183	OD	84.2138	1.62167	1.62833	5.23708	14.08417	1.28481	0.00000	1.43968	.00000	-.00000	-.00000	0.00000
184	REFL	168.4276	3.24334	3.25666	17.83321	5.73406	-.000091	0.00000	2.87937	.00000	-.00000	-.00000	0.00000
CIRCUMFERENCE = 505.2827CM													
(DS/S)/RMBZB = .0870881M													
THETX = 6.28318638 RAD													
THETY(183) = 0.00000000 RAD													
TCAN = (7.64818, 0.00000)													
NUX = 9.73002													
NUY = 9.76997													
DNUX7(DP/P) = .39620													
DNUY7(DP/P) = .39105													
MAXIMA --- BETX(1) = 17.83321													
MINIMA --- BETX(36) = 4.05811													
BETY(12) = 16.94478													
BETY(48) = 3.28656													
ETAX(174) = 2.08819													
ETAX(33) = .CCCC													
ETAY(184) = 0.00000													
ETAY(184) = 0.00000													
*** DP --- // -0.02													
*** V PVEC // DP													
*** CHR SUB 0 0 //													
*** AGP FXPT 2 -3 // V .SP I													
*** INCR 1 // DP .003													
*** END 0 0 //													

CALCULATION OF THE EQUILIBRIUM ORBIT AND BETATRON FUNCTIONS OF AGR

INITIAL REFERENCE RAY DEFINED BY V

X = 0.00000000 DX = 0.00000000 Y = 0.00000000 DY = 0.00000000 DS = 0.00000000 DP/P = -0.02000000 1.00000000

7X7 MATRIX FOR AGR

.06055299	17.87971570	0.00000000	0.00000000	0.00000000	.03138991	.00026699
-.05572423	.06055299	0.00000000	0.00000000	0.00000000	.00186192	.00001584
0.00000000	0.00000000	-.02881698	5.10131547	0.00000000	0.00000000	0.00000000
0.00000000	0.00000000	-.19586508	-.02881698	0.00000000	0.00000000	0.00000000
-.00185192	-.03138991	0.00000000	0.00000000	1.00000000	-2.83177215	.06130947
0.00000000	0.00000000	0.00000000	0.00000000	0.00000000	1.00000000	0.00000000
0.00000000	0.00000000	0.00000000	0.00000000	0.00000000	0.00000000	1.00000000

EIGENVALUES OF THE 4X4 SUBMATRIX

X... LMD1 = (.06055299 .99816498), C(1) = 1.00000000, MU(1) = 1.51020627 RAD, Q(1) = .72107038
 1/LMD1 = (.06055299 -.99816498), C(2) = 1.00000000, MU(2) = -1.51020627 RAD, Q(2) = .27892962
 Y... LMD3 = (-.02881698 .99958470), C(3) = 1.00000000, MU(3) = -1.59961729 RAD, Q(3) = -.76376100
 1/LMD3 = (-.02881698 -.99958470), C(4) = 1.00000000, MU(4) = -1.59961729 RAD, Q(4) = .23623900

EIGENVALUE = (.06055299, .99816498), EIGENVECTOR = (4.23232626, 0.00000000)
 (0.00000000, -.23627668)
 (0.00000000, 0.00000000)
 (0.00000000, 0.00000000)

EIGENVALUE = (.06055299, -.99816498), EIGENVECTOR = (4.23232626, 0.00000000)
 (0.00000000, -.23627668)
 (0.00000000, 0.00000000)
 (0.00000000, 0.00000000)

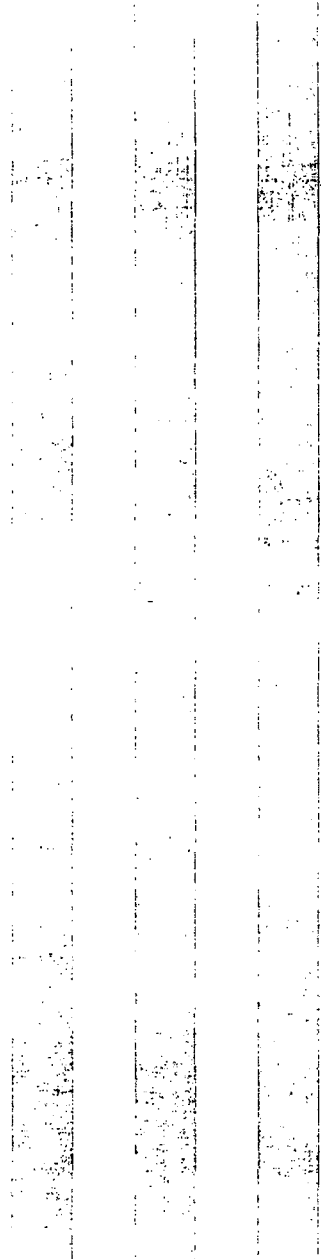
EIGENVALUE = (-.02881698, .99958470), EIGENVECTOR = (0.00000000, 0.00000000)
 (0.00000000, 0.00000000)
 (2.25907833, 0.00000000)
 (0.00000000, -.44265840)

EIGENVALUE = (-.02881698, -.99958470), EIGENVECTOR = (0.00000000, 0.00000000)
 (0.00000000, 0.00000000)
 (2.25907833, 0.00000000)
 (0.00000000, -.44265840)

	X	DX	Y	DY	DS	DP/P
EQ ORBIT	.00034772	0.00000000	0.00000000	0.00000000	0.00000000	-0.02000000 1.00000000
ETA ORBIT	.03341318	.00000000	0.00000000	0.00000000	0.00000000	1.00000000 0.00000000

EIGENVECTORS 1 AND 3 IN POLAR COORDINATES

	X1	X2	X3	DX1	DX2	DX3	Y1	Y2	Y3	DY1	DY2	DY3
1	0.232325	0.000000	0.236277	1.570796	0.000000	0.000000	0.000000	0.000000	0.000000	0.000000	0.000000	0.000000
3	0.000000	0.000000	0.000000	0.000000	2.259078	0.000000	0.000000	0.000000	0.000000	0.000000	0.000000	0.000000



POS	(M)	OK	QY	(M)	(M)	(M)	AX	AV	(M)	EXP	(M)	EYP	XCG	(M)	DRCD	(M)	YCD	(M)	DYCD
50	7	30	40	14.49	2.09	2.09	2.09	60	002223	0.000000	0.000000	0.000000	2571	0.00000	0.0215	0.00000	0.00000	0.00000	
51	7	40	47	12.66	1.84	1.84	1.84	93	002223	0.000000	0.000000	0.000000	2571	0.00000	0.0215	0.00000	0.00000	0.00000	
52	7	41	45	11.38	1.71	1.71	1.71	21	002223	0.000000	0.000000	0.000000	2353	0.00000	0.0215	0.00000	0.00000	0.00000	
53	7	41	45	10.19	1.59	1.59	1.59	21	002223	0.000000	0.000000	0.000000	2353	0.00000	0.0215	0.00000	0.00000	0.00000	
54	7	42	45	9.04	1.46	1.46	1.46	34	002223	0.000000	0.000000	0.000000	2161	0.00000	0.0215	0.00000	0.00000	0.00000	
55	7	43	47	7.16	1.21	1.21	1.21	61	002223	0.000000	0.000000	0.000000	2083	0.00000	0.0215	0.00000	0.00000	0.00000	
56	7	43	47	6.33	1.09	1.09	1.09	75	002223	0.000000	0.000000	0.000000	2026	0.00000	0.0215	0.00000	0.00000	0.00000	
57	7	44	48	5.53	0.97	0.97	0.97	88	002223	0.000000	0.000000	0.000000	1928	0.00000	0.0215	0.00000	0.00000	0.00000	
58	7	44	48	4.94	0.88	0.88	0.88	99	000012	0.000000	0.000000	0.000000	1814	0.00000	0.0215	0.00000	0.00000	0.00000	
59	7	45	49	4.40	0.80	0.80	0.80	110	002262	0.000000	0.000000	0.000000	1880	0.00000	0.0215	0.00000	0.00000	0.00000	
60	8	48	50	3.98	0.72	0.72	0.72	120	002262	0.000000	0.000000	0.000000	1986	0.00000	0.0215	0.00000	0.00000	0.00000	
61	8	49	50	3.66	0.66	0.66	0.66	129	002262	0.000000	0.000000	0.000000	2091	0.00000	0.0215	0.00000	0.00000	0.00000	
62	8	50	50	3.48	0.61	0.61	0.61	120	002262	0.000000	0.000000	0.000000	2196	0.00000	0.0215	0.00000	0.00000	0.00000	
63	8	50	50	3.36	0.58	0.58	0.58	111	002262	0.000000	0.000000	0.000000	2302	0.00000	0.0215	0.00000	0.00000	0.00000	
64	8	51	51	3.27	0.56	0.56	0.56	101	002262	0.000000	0.000000	0.000000	2407	0.00000	0.0215	0.00000	0.00000	0.00000	
65	8	51	51	3.20	0.54	0.54	0.54	96	002262	0.000000	0.000000	0.000000	2512	0.00000	0.0215	0.00000	0.00000	0.00000	
66	8	52	52	3.14	0.52	0.52	0.52	91	002262	0.000000	0.000000	0.000000	2617	0.00000	0.0215	0.00000	0.00000	0.00000	
67	8	52	52	3.09	0.51	0.51	0.51	86	002262	0.000000	0.000000	0.000000	2722	0.00000	0.0215	0.00000	0.00000	0.00000	
68	8	53	53	3.04	0.50	0.50	0.50	81	002262	0.000000	0.000000	0.000000	2827	0.00000	0.0215	0.00000	0.00000	0.00000	
69	8	53	53	3.00	0.49	0.49	0.49	76	002262	0.000000	0.000000	0.000000	2932	0.00000	0.0215	0.00000	0.00000	0.00000	
70	8	54	54	2.97	0.48	0.48	0.48	71	002262	0.000000	0.000000	0.000000	3037	0.00000	0.0215	0.00000	0.00000	0.00000	
71	8	54	54	2.94	0.47	0.47	0.47	66	002262	0.000000	0.000000	0.000000	3142	0.00000	0.0215	0.00000	0.00000	0.00000	
72	8	55	55	2.91	0.46	0.46	0.46	61	002262	0.000000	0.000000	0.000000	3247	0.00000	0.0215	0.00000	0.00000	0.00000	
73	8	55	55	2.88	0.45	0.45	0.45	56	002262	0.000000	0.000000	0.000000	3352	0.00000	0.0215	0.00000	0.00000	0.00000	
74	8	55	55	2.86	0.44	0.44	0.44	51	002262	0.000000	0.000000	0.000000	3457	0.00000	0.0215	0.00000	0.00000	0.00000	
75	8	56	56	2.84	0.43	0.43	0.43	46	00134	0.000000	0.000000	0.000000	3562	0.00000	0.0215	0.00000	0.00000	0.00000	
76	8	56	56	2.82	0.42	0.42	0.42	41	00134	0.000000	0.000000	0.000000	3667	0.00000	0.0215	0.00000	0.00000	0.00000	
77	8	56	56	2.80	0.41	0.41	0.41	36	00134	0.000000	0.000000	0.000000	3772	0.00000	0.0215	0.00000	0.00000	0.00000	
78	8	56	56	2.78	0.40	0.40	0.40	31	00134	0.000000	0.000000	0.000000	3877	0.00000	0.0215	0.00000	0.00000	0.00000	
79	8	57	57	2.76	0.39	0.39	0.39	26	00134	0.000000	0.000000	0.000000	3982	0.00000	0.0215	0.00000	0.00000	0.00000	
80	8	57	57	2.74	0.38	0.38	0.38	21	00134	0.000000	0.000000	0.000000	4087	0.00000	0.0215	0.00000	0.00000	0.00000	
81	8	57	57	2.72	0.37	0.37	0.37	16	00134	0.000000	0.000000	0.000000	4192	0.00000	0.0215	0.00000	0.00000	0.00000	
82	8	57	57	2.70	0.36	0.36	0.36	11	00134	0.000000	0.000000	0.000000	4297	0.00000	0.0215	0.00000	0.00000	0.00000	
83	8	57	57	2.68	0.35	0.35	0.35	6	00134	0.000000	0.000000	0.000000	4402	0.00000	0.0215	0.00000	0.00000	0.00000	
84	8	57	57	2.66	0.34	0.34	0.34	1	00134	0.000000	0.000000	0.000000	4507	0.00000	0.0215	0.00000	0.00000	0.00000	
85	8	58	58	2.64	0.33	0.33	0.33	0	00943	0.000000	0.000000	0.000000	4612	0.00000	0.0215	0.00000	0.00000	0.00000	
86	8	58	58	2.62	0.32	0.32	0.32	0	00943	0.000000	0.000000	0.000000	4717	0.00000	0.0215	0.00000	0.00000	0.00000	
87	8	58	58	2.60	0.31	0.31	0.31	0	00601	0.000000	0.000000	0.000000	4822	0.00000	0.0215	0.00000	0.00000	0.00000	
88	8	58	58	2.58	0.30	0.30	0.30	0	00601	0.000000	0.000000	0.000000	4927	0.00000	0.0215	0.00000	0.00000	0.00000	
89	8	58	58	2.56	0.29	0.29	0.29	0	00601	0.000000	0.000000	0.000000	5032	0.00000	0.0215	0.00000	0.00000	0.00000	
90	8	59	59	2.54	0.28	0.28	0.28	0	00601	0.000000	0.000000	0.000000	5137	0.00000	0.0215	0.00000	0.00000	0.00000	
91	8	59	59	2.52	0.27	0.27	0.27	0	00601	0.000000	0.000000	0.000000	5242	0.00000	0.0215	0.00000	0.00000	0.00000	
92	8	59	59	2.50	0.26	0.26	0.26	0	01104	0.000000	0.000000	0.000000	5347	0.00000	0.0215	0.00000	0.00000	0.00000	
93	8	59	59	2.48	0.25	0.25	0.25	0	01104	0.000000	0.000000	0.000000	5452	0.00000	0.0215	0.00000	0.00000	0.00000	
94	8	59	59	2.46	0.24	0.24	0.24	0	01774	0.000000	0.000000	0.000000	5557	0.00000	0.0215	0.00000	0.00000	0.00000	
95	8	59	59	2.44	0.23	0.23	0.23	0	01774	0.000000	0.000000	0.000000	5662	0.00000	0.0215	0.00000	0.00000	0.00000	
96	8	59	59	2.42	0.22	0.22	0.22	0	00943	0.000000	0.000000	0.000000	5767	0.00000	0.0215	0.00000	0.00000	0.00000	
97	8	59	59	2.40	0.21	0.21	0.21	0	00943	0.000000	0.000000	0.000000	5872	0.00000	0.0215	0.00000	0.00000	0.00000	
98	8	59	59	2.38	0.20	0.20	0.20	0	00601	0.000000	0.000000	0.000000	5977	0.00000	0.0215	0.00000	0.00000	0.00000	
99	8	59	59	2.36	0.19	0.19	0.19	0	00601	0.000000	0.000000	0.000000	6082	0.00000	0.0215	0.00000	0.00000	0.00000	

POS	S	QX	QY	BX	BY	AX	AY	EX	EXP	EY	EYP	XCC	DXCO	YCO	DYCO
	(M)			(M)	(M)			(M)		(M)		(MM)	(MM)	(MM)	(MM)
150	SD	67.12	1.31	1.31	6.22	-1.81	1.53	1.37197	.15040	0.000000	0.000000	-27.5352	-3.0255	0.0000	0.0000
151	SD	67.85	1.33	1.32	7.62	-1.01	1.53	1.48248	.15040	0.000000	0.000000	-29.7603	-3.0255	0.0000	0.0000
152	SD	69.91	1.33	1.33	8.77	-1.45	1.53	1.81118	.24770	0.000000	0.000000	-36.3757	-4.9706	0.0000	0.0000
153	SD	70.23	1.33	1.36	9.99	-1.64	1.53	1.99335	.24770	0.000000	0.000000	-40.0313	-4.9706	0.0000	0.0000
154	SD	70.23	1.33	1.36	9.99	-1.72	1.53	1.99335	.25927	0.000000	0.000000	-40.0313	-5.0657	0.0000	0.0000
155	OS	70.55	1.37	1.37	10.01	-1.81	1.74	2.07113	.25927	0.000000	0.000000	-41.5570	-5.0657	0.0000	0.0000
156	OS	70.90	1.37	1.38	10.55	-1.00	1.74	2.11697	.00124	0.000000	0.000000	-42.4535	-1.0119	0.0000	0.0000
157	OS	71.25	1.38	1.39	11.00	2.66	1.81	2.07199	-.25684	0.000000	0.000000	-41.5653	3.0623	0.0000	0.0000
158	OS	71.55	1.38	1.40	11.94	6.12	1.73	1.99494	-.25684	0.000000	0.000000	-40.0466	3.0623	0.0000	0.0000
159	OS	71.99	1.40	1.40	13.94	6.12	1.65	1.99494	-.24526	0.000000	0.000000	-40.0466	4.9472	0.0000	0.0000
160	D	72.28	1.39	1.42	11.67	7.42	1.45	1.81457	-.24526	0.000000	0.000000	-36.4083	4.9472	0.0000	0.0000
161	D	73.94	1.43	1.43	7.60	11.28	1.01	1.48990	-.14796	0.000000	0.000000	-29.8316	3.0020	0.0000	0.0000
162	D	74.68	1.44	1.46	8.26	13.40	1.81	1.38109	-.14796	0.000000	0.000000	-27.6238	3.0020	0.0000	0.0000
163	SD	74.68	1.44	1.46	8.26	13.40	1.81	1.38109	-.15635	0.000000	0.000000	-27.6238	3.0851	0.0000	0.0000
164	OS	74.68	1.44	1.46	8.26	14.39	1.77	1.33418	-.15635	0.000000	0.000000	-26.6983	3.0851	0.0000	0.0000
165	OS	75.32	1.45	1.46	5.50	14.92	1.04	1.30718	-.00175	0.000000	0.000000	-26.1624	-1.0171	0.0000	0.0000
166	OS	75.68	1.47	1.47	5.72	13.39	1.09	1.23342	-.15993	0.000000	0.000000	-26.7103	-3.1199	0.0000	0.0000
167	SD	75.68	1.47	1.47	5.72	13.39	1.09	1.38340	-.15993	0.000000	0.000000	-27.6463	-3.1199	0.0000	0.0000
168	SD	75.68	1.47	1.47	5.72	13.40	1.73	1.38340	-.15152	0.000000	0.000000	-27.6463	-3.0367	0.0000	0.0000
169	D	76.71	1.49	1.48	7.37	11.27	1.35	1.40483	-.15152	0.000000	0.000000	-29.8796	-3.0367	0.0000	0.0000
170	B	78.37	1.52	1.51	11.00	7.41	-1.33	1.82537	.24882	0.000000	0.000000	-36.5136	-4.9819	0.0000	0.0000
171	D	79.10	1.53	1.53	13.17	6.11	-1.51	2.00836	.24882	0.000000	0.000000	-40.1774	-4.9819	0.0000	0.0000
172	OS	79.10	1.53	1.53	13.17	6.11	-1.59	2.00836	.26052	0.000000	0.000000	-40.1774	-5.0978	0.0000	0.0000
173	OS	79.40	1.53	1.54	14.15	8.65	-1.67	2.00852	.26052	0.000000	0.000000	-41.7068	-5.0978	0.0000	0.0000
174	OS	79.76	1.54	1.55	14.73	8.39	1.03	2.13247	.00060	0.000000	0.000000	-42.6044	-4.0059	0.0000	0.0000
175	OS	80.11	1.54	1.56	14.10	8.45	1.73	2.08694	-.25934	0.000000	0.000000	-41.7109	5.0863	0.0000	0.0000
176	OS	80.41	1.54	1.56	13.09	6.11	1.65	2.00914	-.25934	0.000000	0.000000	-40.1850	5.0863	0.0000	0.0000
177	OS	80.41	1.54	1.56	13.09	6.11	1.57	2.00914	-.24763	0.000000	0.000000	-40.1850	4.9703	0.0000	0.0000
178	OS	81.14	1.55	1.58	10.92	7.40	1.38	1.82703	-.24763	0.000000	0.000000	-36.5256	4.9703	0.0000	0.0000
179	B	82.80	1.58	1.61	7.10	11.25	1.94	1.49845	-.15033	0.000000	0.000000	-29.9147	3.0252	0.0000	0.0000
180	D	83.53	1.60	1.62	5.86	13.37	1.74	1.38789	-.15033	0.000000	0.000000	-27.6698	3.0252	0.0000	0.0000
181	SD	83.53	1.60	1.62	5.86	13.37	1.78	1.38789	-.15878	0.000000	0.000000	-27.6698	3.1087	0.0000	0.0000
182	OS	83.53	1.61	1.62	5.43	14.36	1.70	1.34026	-.15878	0.000000	0.000000	-26.7572	3.1087	0.0000	0.0000
183	OS	84.18	1.62	1.63	5.18	14.96	1.00	1.31253	-.00000	0.000000	0.000000	-26.2143	0.0000	0.0000	0.0000
184	REFL	168.37	3.24	3.25	17.91	5.10	-1.00	0.03341	-.00000	0.000000	0.000000	-3.477	0.0000	0.0000	0.0000

CIRCUMFERENCE = 503.1081 M THETA = 6.28318638 RAD NUX = 9.72107 DNUX/(DP/P) = .32692
(DS/SI)/RADIUS = 99.8890 M THETA(183) = 0.00000000 RAD NUZ = 9.76376 DNUZ/(DP/P) = .43820
IGAM = (7.71077, 0.00000)

MAXIMA --- BETX(1) = 17.91259 BETY(77) = 16.29623 ETAX(174) = 2.13247 ETAY(184) = 0.00000
MINIMA --- BETX(36) = 3.95271 BETY(48) = 3.21594 ETAX(32) = .00008 ETAY(184) = 0.00000

*** INCA 1 // DP .005000 VALUE = -.015000

SUB. CHR ITER. 2

CALCULATION OF THE EQUILIBRIUM ORBIT AND BETATRON FUNCTIONS OF AGR

INITIAL REFERENCE ORBIT DEFINED BY V
 $\lambda = -0.0034772$ $DX = 0.0000000$ $Y = 0.0000000$ $DY = 0.0000000$ $DP/P = -0.0150000$ 1.90090000

7X7 MATRIX FOR AGR

0.0547951	17.88030476	0.0000000	0.0000000	0.0000000	0.0000000	0.0000000	-0.2442197	-0.0016680
-0.0575532	0.0547951	0.0000000	0.0000000	0.0000000	0.0000000	0.0000000	-0.0144164	0.00000985
0.0000000	0.0000000	-0.03127569	0.0000000	0.0000000	0.0000000	0.0000000	0.0000000	0.0000000
0.0000000	0.0000000	-0.19013207	-0.03127569	0.0000000	0.0000000	0.0000000	0.0000000	0.0000000
-0.0144164	-0.02442197	0.0000000	0.0000000	1.0000000	0.0000000	0.0000000	-2.84351346	-0.4525735
0.0000000	0.0000000	0.0000000	0.0000000	0.0000000	0.0000000	0.0000000	1.0000000	0.0000000
0.0000000	0.0000000	0.0000000	0.0000000	0.0000000	0.0000000	0.0000000	0.0000000	1.0000000

EIGENVALUES OF THE 4X4 SUBMATRIX

$X \dots \text{LMD1} = \{ 0.0547951, -0.03127569, -0.03127569, -0.03127569 \}$; $\xi(1) = 1.0000000$; $\text{MU}(1) = -1.51528832 \text{ RAD}$; $\xi(2) = 0(2) = -0.72349688$
 $Y \dots \text{LMD3} = \{ -0.03127569, -0.03127569, -0.03127569, -0.03127569 \}$; $\xi(3) = 1.0000000$; $\text{MU}(3) = -1.60207112 \text{ RAD}$; $\xi(4) = 0(4) = -0.25506452$
 EIGENVALUE = { 0.0547951, -0.03127569, -0.03127569, -0.03127569 }
 EIGENVECTOR = { 0.9994993, 0.0000000, 0.0000000, 0.0000000 }
 EIGENVALUE = { 0.0547951, -0.03127569, -0.03127569, -0.03127569 }
 EIGENVECTOR = { 0.0000000, 0.0000000, 0.0000000, 0.0000000 }

EIGENVALUE = { 0.0000000, 0.0000000, 0.0000000, 0.0000000 }
 EIGENVECTOR = { 0.0000000, 0.0000000, 0.0000000, 0.0000000 }
 EIGENVALUE = { 0.0000000, 0.0000000, 0.0000000, 0.0000000 }
 EIGENVECTOR = { 0.0000000, 0.0000000, 0.0000000, 0.0000000 }

EIGENVALUE = { 0.0000000, 0.0000000, 0.0000000, 0.0000000 }
 EIGENVECTOR = { 0.0000000, 0.0000000, 0.0000000, 0.0000000 }

	X	DX	Y	DY	DP/P
EO ORBIT	-0.0019630	0.0000000	0.0000000	0.0000000	-0.0150000
ETA ORBIT	0.2585647	0.0000000	0.0000000	0.0000000	1.0000000

POS		S	QX	QY	BX	BY	AX	AY	EX	EXP	EY	EYP	XCG	DXCD	YCD	DYCD
		(M)			(M)	(M)			(M)		(M)		(M)	(M)	(M)	(M)
100	SF	43.67	.87	.87	13.80	6.09	-1.69	.81	1.98658	.25347	0.000000	0.000000	-29.9030	3.7622	0.0000	0.0000
101	OS	43.97	.88	.88	14.84	5.63	-1.78	.73	2.06262	.25347	0.000000	0.000000	-31.0317	3.7622	0.0000	0.0000
102	OF	44.22	.88	.88	15.47	5.37	-.00	-.00	2.10706	-.00086	0.000000	0.000000	-31.6522	3.7622	0.0000	0.0000
103	OF	44.57	.88	.90	14.83	5.62	1.78	-.73	2.06202	-.25515	0.000000	0.000000	-31.0271	3.7752	0.0000	0.0000
104	OS	44.97	.89	.91	13.79	6.09	1.70	-.61	1.98548	-.25515	0.000000	0.000000	-29.8945	3.7752	0.0000	0.0000
105	SF	44.97	.89	.91	13.79	6.09	1.64	-.78	1.98548	-.24660	0.000000	0.000000	-29.8945	3.7114	0.0000	0.0000
106	O	45.71	.90	.93	11.52	7.38	1.44	-.98	1.80412	-.24660	0.000000	0.000000	-27.1650	3.7114	0.0000	0.0000
107	B	47.37	.93	.95	7.48	11.27	1.00	-1.36	1.67647	-.14982	0.000000	0.000000	-22.2222	3.2601	0.0000	0.0000
108	B	48.10	.94	.96	6.16	13.40	.80	-1.54	1.36628	-.14982	0.000000	0.000000	-20.5601	2.2601	0.0000	0.0000
109	SD	48.10	.94	.96	6.16	13.40	.82	-1.60	1.36628	-.15595	0.000000	0.000000	-20.5601	2.3059	0.0000	0.0000
110	OS	48.40	.94	.97	5.68	14.38	.75	-1.68	1.31950	-.15595	0.000000	0.000000	-19.8683	2.3059	0.0000	0.0000
111	OS	48.73	.95	.97	5.42	14.38	-.03	-.00	1.31950	-.00118	0.000000	0.000000	-19.4640	2.0093	0.0000	0.0000
112	OS	49.18	.95	.98	5.64	14.38	-.69	-.64	1.31867	-.15335	0.000000	0.000000	-19.8618	2.2869	0.0000	0.0000
113	OS	49.40	.98	.98	6.08	13.39	-.77	-1.61	1.36474	-.15335	0.000000	0.000000	-20.5478	2.2869	0.0000	0.0000
114	SD	49.40	.98	.98	6.08	13.39	-.74	-1.55	1.36474	-.14743	0.000000	0.000000	-20.5478	2.2412	0.0000	0.0000
115	O	50.16	1.00	.99	7.31	11.25	-.93	1.36	1.47316	-.16743	0.000000	0.000000	-22.1961	2.2412	0.0000	0.0000
116	B	51.07	1.03	1.02	11.07	7.35	-1.39	.98	1.79686	-.24421	0.000000	0.000000	-27.1076	3.6925	0.0000	0.0000
117	O	51.07	1.04	1.03	11.07	7.35	-1.54	.78	1.79646	-.24421	0.000000	0.000000	-29.8232	3.6925	0.0000	0.0000
118	SF	51.07	1.04	1.03	11.07	7.35	-1.59	.81	1.79646	-.25270	0.000000	0.000000	-29.8232	3.7560	0.0000	0.0000
119	OS	51.07	1.04	1.04	11.07	7.35	-1.67	.73	2.05227	-.25270	0.000000	0.000000	-30.9500	3.7560	0.0000	0.0000
120	OF	53.18	1.04	1.05	14.76	5.34	.02	.00	2.09667	-.00037	0.000000	0.000000	-31.6100	3.0030	0.0000	0.0000
121	OF	53.53	1.05	1.06	14.14	5.59	1.72	-.72	2.05201	-.25343	0.000000	0.000000	-30.9479	3.7619	0.0000	0.0000
122	OS	53.83	1.05	1.07	13.13	6.04	1.63	-.80	1.97599	-.25343	0.000000	0.000000	-29.8153	3.7619	0.0000	0.0000
123	SF	53.83	1.05	1.07	13.13	6.04	1.58	-.78	1.97599	-.24494	0.000000	0.000000	-29.8193	3.6984	0.0000	0.0000
124	O	54.58	1.06	1.09	10.96	7.33	1.38	-.97	1.79585	-.24494	0.000000	0.000000	-27.0994	3.6984	0.0000	0.0000
125	B	56.23	1.09	1.12	7.11	11.20	.94	-1.35	1.47094	-.14816	0.000000	0.000000	-22.1780	2.2471	0.0000	0.0000
126	O	56.96	1.11	1.13	5.87	13.32	.75	-1.54	1.36198	-.14816	0.000000	0.000000	-20.5254	2.2471	0.0000	0.0000
127	SD	56.96	1.11	1.13	5.87	13.32	.77	-1.60	1.36198	-.15426	0.000000	0.000000	-20.5254	2.2927	0.0000	0.0000
128	OS	57.26	1.12	1.13	5.43	14.30	.69	-1.68	1.31570	-.15426	0.000000	0.000000	-19.8336	2.2927	0.0000	0.0000
129	OO	57.61	1.13	1.14	5.19	14.90	-.00	-.00	1.28877	-.00010	0.000000	0.000000	-19.4372	2.0005	0.0000	0.0000
130	OO	57.96	1.14	1.14	5.43	14.30	-.70	1.68	1.31577	-.15446	0.000000	0.000000	-19.8380	2.2937	0.0000	0.0000
131	OS	58.26	1.14	1.14	5.88	13.32	-.78	1.60	1.36210	-.15446	0.000000	0.000000	-20.5261	2.2937	0.0000	0.0000
132	SD	58.26	1.14	1.14	5.88	13.32	-.75	1.54	1.36210	-.14836	0.000000	0.000000	-20.5261	2.2481	0.0000	0.0000
133	O	59.00	1.15	1.15	7.13	11.20	-.95	1.35	1.47121	-.14836	0.000000	0.000000	-22.1794	2.2481	0.0000	0.0000
134	B	60.66	1.19	1.18	11.00	7.33	-1.39	.97	1.79644	-.24514	0.000000	0.000000	-27.1024	3.6994	0.0000	0.0000
135	O	61.39	1.20	1.20	13.10	6.05	-1.59	.78	1.97672	-.24514	0.000000	0.000000	-29.8231	3.6994	0.0000	0.0000
136	SF	61.39	1.20	1.20	13.10	6.05	-1.64	.80	1.97672	-.25362	0.000000	0.000000	-29.8231	3.7622	0.0000	0.0000
137	OS	61.39	1.21	1.21	14.82	5.34	-1.73	.72	2.09281	-.25362	0.000000	0.000000	-30.9519	3.7622	0.0000	0.0000
138	OF	61.39	1.21	1.22	14.82	5.34	-.03	-.00	2.09752	-.00047	0.000000	0.000000	-31.6144	3.0035	0.0000	0.0000
139	OF	62.13	1.22	1.23	14.24	5.60	1.68	-.73	2.09314	-.25270	0.000000	0.000000	-30.9544	3.7560	0.0000	0.0000
140	OS	62.69	1.22	1.24	13.25	6.06	1.60	-.81	1.97733	-.25270	0.000000	0.000000	-29.8276	3.7560	0.0000	0.0000
141	SF	62.69	1.22	1.24	13.25	6.06	1.54	-.79	1.97733	-.24421	0.000000	0.000000	-29.8276	3.6925	0.0000	0.0000
142	OS	62.69	1.22	1.25	11.13	7.36	1.35	-.98	1.79773	-.24421	0.000000	0.000000	-27.1120	3.6925	0.0000	0.0000
143	B	63.09	1.26	1.28	7.39	11.26	.93	-1.36	1.47403	-.14743	0.000000	0.000000	-22.2005	2.2412	0.0000	0.0000
144	O	63.82	1.28	1.29	6.11	13.40	.75	-1.55	1.36561	-.14743	0.000000	0.000000	-20.5523	2.2412	0.0000	0.0000
145	SD	64.02	1.28	1.29	6.11	13.40	.77	-1.61	1.36561	-.15356	0.000000	0.000000	-20.5523	2.2869	0.0000	0.0000
146	OS	66.15	1.28	1.30	5.67	14.39	-.69	-1.69	1.31954	-.15356	0.000000	0.000000	-19.8662	2.2869	0.0000	0.0000
147	OO	66.47	1.29	1.30	5.44	14.39	-.03	-.00	1.32295	-.00129	0.000000	0.000000	-19.4685	2.0098	0.0000	0.0000
148	OO	66.82	1.30	1.30	5.71	14.39	-.75	1.68	1.32044	-.15616	0.000000	0.000000	-19.8731	2.3069	0.0000	0.0000
149	OS	67.12	1.31	1.31	6.18	13.41	-.83	1.60	1.36729	-.15616	0.000000	0.000000	-20.5652	2.3069	0.0000	0.0000

POS	SD	(M)	OX	OY	AX	AY	EX	EXP	EY	EYP	XCU	DYCD	YCG	DYCD
150	0	67	1	1	80	1.54	1.37229	15002	0	0.00000	0.00000	0.00000	0.00000	0.00000
151	0	67	1	1	80	1.54	1.37229	15002	0	0.00000	0.00000	0.00000	0.00000	0.00000
152	0	67	1	1	80	1.54	1.37229	15002	0	0.00000	0.00000	0.00000	0.00000	0.00000
153	0	67	1	1	80	1.54	1.37229	15002	0	0.00000	0.00000	0.00000	0.00000	0.00000
154	0	67	1	1	80	1.54	1.37229	15002	0	0.00000	0.00000	0.00000	0.00000	0.00000
155	0	67	1	1	80	1.54	1.37229	15002	0	0.00000	0.00000	0.00000	0.00000	0.00000
156	0	67	1	1	80	1.54	1.37229	15002	0	0.00000	0.00000	0.00000	0.00000	0.00000
157	0	67	1	1	80	1.54	1.37229	15002	0	0.00000	0.00000	0.00000	0.00000	0.00000
158	0	67	1	1	80	1.54	1.37229	15002	0	0.00000	0.00000	0.00000	0.00000	0.00000
159	0	67	1	1	80	1.54	1.37229	15002	0	0.00000	0.00000	0.00000	0.00000	0.00000
160	0	67	1	1	80	1.54	1.37229	15002	0	0.00000	0.00000	0.00000	0.00000	0.00000
161	0	67	1	1	80	1.54	1.37229	15002	0	0.00000	0.00000	0.00000	0.00000	0.00000
162	0	67	1	1	80	1.54	1.37229	15002	0	0.00000	0.00000	0.00000	0.00000	0.00000
163	0	67	1	1	80	1.54	1.37229	15002	0	0.00000	0.00000	0.00000	0.00000	0.00000
164	0	67	1	1	80	1.54	1.37229	15002	0	0.00000	0.00000	0.00000	0.00000	0.00000
165	0	67	1	1	80	1.54	1.37229	15002	0	0.00000	0.00000	0.00000	0.00000	0.00000
166	0	67	1	1	80	1.54	1.37229	15002	0	0.00000	0.00000	0.00000	0.00000	0.00000
167	0	67	1	1	80	1.54	1.37229	15002	0	0.00000	0.00000	0.00000	0.00000	0.00000
168	0	67	1	1	80	1.54	1.37229	15002	0	0.00000	0.00000	0.00000	0.00000	0.00000
169	0	67	1	1	80	1.54	1.37229	15002	0	0.00000	0.00000	0.00000	0.00000	0.00000
170	0	67	1	1	80	1.54	1.37229	15002	0	0.00000	0.00000	0.00000	0.00000	0.00000
171	0	67	1	1	80	1.54	1.37229	15002	0	0.00000	0.00000	0.00000	0.00000	0.00000
172	0	67	1	1	80	1.54	1.37229	15002	0	0.00000	0.00000	0.00000	0.00000	0.00000
173	0	67	1	1	80	1.54	1.37229	15002	0	0.00000	0.00000	0.00000	0.00000	0.00000
174	0	67	1	1	80	1.54	1.37229	15002	0	0.00000	0.00000	0.00000	0.00000	0.00000
175	0	67	1	1	80	1.54	1.37229	15002	0	0.00000	0.00000	0.00000	0.00000	0.00000
176	0	67	1	1	80	1.54	1.37229	15002	0	0.00000	0.00000	0.00000	0.00000	0.00000
177	0	67	1	1	80	1.54	1.37229	15002	0	0.00000	0.00000	0.00000	0.00000	0.00000
178	0	67	1	1	80	1.54	1.37229	15002	0	0.00000	0.00000	0.00000	0.00000	0.00000
179	0	67	1	1	80	1.54	1.37229	15002	0	0.00000	0.00000	0.00000	0.00000	0.00000
180	0	67	1	1	80	1.54	1.37229	15002	0	0.00000	0.00000	0.00000	0.00000	0.00000
181	0	67	1	1	80	1.54	1.37229	15002	0	0.00000	0.00000	0.00000	0.00000	0.00000
182	0	67	1	1	80	1.54	1.37229	15002	0	0.00000	0.00000	0.00000	0.00000	0.00000
183	0	67	1	1	80	1.54	1.37229	15002	0	0.00000	0.00000	0.00000	0.00000	0.00000
184	0	67	1	1	80	1.54	1.37229	15002	0	0.00000	0.00000	0.00000	0.00000	0.00000
185	0	67	1	1	80	1.54	1.37229	15002	0	0.00000	0.00000	0.00000	0.00000	0.00000
186	0	67	1	1	80	1.54	1.37229	15002	0	0.00000	0.00000	0.00000	0.00000	0.00000

CIRCUMFERENCE = 505.1521 M THEY(1) = 6.28318538 RAD. NUY = 9.72350
 (COS/SIN) = 0.9801818181818181 MUY(1) = 1.7.89920, 0.000000
 MINIMA --- BEY(181) = 1.90799 BEY(182) = 15.26279 BEY(183) = 2.11966 BEY(184) = 0.00000
 SUP. CLK 118

CALCULATION OF THE EQUILIBRIUM ORBIT AND BETATRON FUNCTIONS OF AGR .

INITIAL REFERENCE RAY DEFINED BY V
 X = 0.0019630 DX = 0.0000000 Y = 0.0000000 DY = 0.0000000 DS = 0.0000000 DP/P = -0.0100000 1.0000000

7X7 MATRIX FOR AGR

.05067066	17.96777943	0.00000000	0.00000000	0.00000000	.01668046	.00008116
-.05581672	.05067066	0.00000000	0.00000000	0.00000000	.00098074	.00000477
0.00000000	0.00000000	-.03433320	5.41052687	0.00000000	0.00000000	0.00000000
0.00000000	0.00000000	-.18460702	-.03433320	0.00000000	0.00000000	0.00000000
-.00098074	-.01668046	0.00000000	0.00000000	1.00000000	-2.85536107	.02970060
0.00000000	0.00000000	0.00000000	0.00000000	0.00000000	1.00000000	0.00000000
0.00000000	0.00000000	0.00000000	0.00000000	0.00000000	0.00000000	1.00000000

EIGENVALUES OF THE 4X4 SUBMATRIX

X... LMD1 = { .05067066 .99871542 } ; C(1) = 1.00000000, MU(1) = 1.52010396 RAD, Q(1) = -.72579618
 LMD1 = { .05367066 -.99871542 } ; C(2) = 1.00000000, MU(2) = -1.52010396 RAD, Q(2) = .27420382
 Y... LMD3 = { -.03433320 .99941044 } ; C(3) = 1.00000000, MU(3) = 1.60513628 RAD, Q(3) = .76639612
 LMD3 = { -.03433320 -.99941044 } ; C(4) = 1.00000000, MU(4) = -1.60513628 RAD, Q(4) = -.23360388

EIGENVALUE = (.05067066, .99871542), EIGENVECTOR = { 4.22998394, 0.00000000 }
 { 0.00000000, .23646752 }
 { 0.00000000, 0.00000000 }
 { 0.00000000, 0.00000000 }

EIGENVALUE = (.05067066, -.99871542), EIGENVECTOR = { 4.22998394, 0.00000000 }
 { 0.00000000, -.23646752 }
 { 0.00000000, 0.00000000 }
 { 0.00000000, 0.00000000 }

EIGENVALUE = (-.03433320, .99941044), EIGENVECTOR = { 0.00000000, 0.00000000 }
 { 0.00000000, 0.00000000 }
 { 2.32673990, -.00000000 }
 { .00000000, .42978590 }

EIGENVALUE = (-.03433320, -.99941044), EIGENVECTOR = { 0.00000000, 0.00000000 }
 { 0.00000000, 0.00000000 }
 { 2.32673990, .00000000 }
 { .00000000, -.42978590 }

	X	DX	Y	DY	DS	DP/P
EQ ORBIT	-.00008590	0.00000000	0.00000000	0.00000000	0.00000000	-0.01000000
ETA ORBIT	.01757078	.00000000	0.00000000	0.00000000	0.00000000	1.00000000

PO5	BEATRON FUNCTIONS	OF AGR	QX	QY	QZ	AX	AY	EX	EXP	EY	EYP	XCO	DXCD	YCO	DYCO
			(M)	(M)	(M)			(M)		(M)		(MM)	(MM)	(MM)	(MM)
0			0.00	0.00	0.00	0.00	0.00	-0.1757	0.00000	0.000000	0.000000	-0.0859	0.0000	0.0000	0.0000
1	QF1		0.25	0.00	0.00	1.7.89	5.41	-0.1716	-0.00234	0.000000	0.000000	-0.0839	0.0000	0.0000	0.0000
2			0.72	0.01	0.02	1.7.07	5.69	-0.1629	-0.00234	0.000000	0.000000	-0.0796	0.0000	0.0000	0.0000
3			1.18	0.01	0.03	1.3.41	9.34	-0.1541	-0.00234	0.000000	0.000000	-0.0754	0.0000	0.0000	0.0000
4			1.47	0.02	0.04	1.2.39	7.88	-0.1454	-0.00234	0.000000	0.000000	-0.0711	0.0000	0.0000	0.0000
5			1.84	0.02	0.04	11.03	8.77	-0.1366	-0.00234	0.000000	0.000000	-0.0669	0.0000	0.0000	0.0000
6			2.22	0.03	0.05	9.78	9.74	-0.1279	-0.00234	0.000000	0.000000	-0.0626	0.0000	0.0000	0.0000
7			2.59	0.03	0.06	3.63	10.80	-0.1192	-0.00234	0.000000	0.000000	-0.0584	0.0000	0.0000	0.0000
8			2.96	0.04	0.06	7.98	11.93	-0.1104	-0.00234	0.000000	0.000000	-0.0541	0.0000	0.0000	0.0000
9			3.34	0.05	0.07	6.63	13.15	-0.1017	-0.00234	0.000000	0.000000	-0.0499	0.0000	0.0000	0.0000
10			3.71	0.06	0.07	5.79	14.45	-0.0930	-0.00234	0.000000	0.000000	-0.0456	0.0000	0.0000	0.0000
11			4.08	0.07	0.08	5.09	15.82	-0.0842	-0.00234	0.000000	0.000000	-0.0414	0.0000	0.0000	0.0000
12			4.43	0.08	0.08	4.64	16.48	-0.0778	-0.00134	0.000000	0.000000	-0.0383	0.0000	0.0000	0.0000
13			4.78	0.09	0.08	4.71	17.44	-0.0747	-0.00041	0.000000	0.000000	-0.0368	0.0000	0.0000	0.0000
14			5.16	0.10	0.09	5.03	18.31	-0.0732	-0.00041	0.000000	0.000000	-0.0361	0.0000	0.0000	0.0000
15			5.53	0.11	0.09	5.46	19.96	-0.0717	-0.00041	0.000000	0.000000	-0.0354	0.0000	0.0000	0.0000
16			5.90	0.12	0.10	5.94	21.69	-0.0702	-0.00041	0.000000	0.000000	-0.0347	0.0000	0.0000	0.0000
17			6.28	0.13	0.10	6.49	23.51	-0.0688	-0.00041	0.000000	0.000000	-0.0339	0.0000	0.0000	0.0000
18			6.65	0.14	0.11	7.11	25.42	-0.0672	-0.00041	0.000000	0.000000	-0.0332	0.0000	0.0000	0.0000
19			7.02	0.15	0.11	7.80	27.41	-0.0657	-0.00041	0.000000	0.000000	-0.0325	0.0000	0.0000	0.0000
20			7.39	0.16	0.12	8.56	29.50	-0.0641	-0.00041	0.000000	0.000000	-0.0318	0.0000	0.0000	0.0000
21			7.77	0.17	0.12	9.44	31.69	-0.0626	-0.00041	0.000000	0.000000	-0.0311	0.0000	0.0000	0.0000
22			8.14	0.18	0.13	10.44	33.99	-0.0611	-0.00041	0.000000	0.000000	-0.0304	0.0000	0.0000	0.0000
23			8.52	0.19	0.13	11.57	36.40	-0.0596	-0.00041	0.000000	0.000000	-0.0296	0.0000	0.0000	0.0000
24			8.90	0.20	0.14	12.84	38.94	-0.0580	-0.00041	0.000000	0.000000	-0.0288	0.0000	0.0000	0.0000
25	QF2		9.22	0.20	0.17	11.15	5.15	-0.0516	-0.00185	0.000000	0.000000	-0.0257	0.0000	0.0000	0.0000
26			9.55	0.20	0.18	10.08	5.66	-0.0447	-0.00185	0.000000	0.000000	-0.0224	0.0000	0.0000	0.0000
27			9.96	0.20	0.19	9.09	6.24	-0.0378	-0.00185	0.000000	0.000000	-0.0190	0.0000	0.0000	0.0000
28			10.33	0.21	0.20	8.18	6.90	-0.0309	-0.00185	0.000000	0.000000	-0.0156	0.0000	0.0000	0.0000
29			10.71	0.21	0.21	7.35	7.64	-0.0240	-0.00185	0.000000	0.000000	-0.0122	0.0000	0.0000	0.0000
30			11.08	0.22	0.22	6.60	8.45	-0.0171	-0.00185	0.000000	0.000000	-0.0088	0.0000	0.0000	0.0000
31			11.46	0.23	0.23	5.94	9.33	-0.0102	-0.00185	0.000000	0.000000	-0.0055	0.0000	0.0000	0.0000
32			11.83	0.24	0.23	5.35	10.29	-0.0033	-0.00185	0.000000	0.000000	-0.0021	0.0000	0.0000	0.0000
33			12.20	0.25	0.24	4.84	11.33	-0.0035	-0.00185	0.000000	0.000000	-0.0013	0.0000	0.0000	0.0000
34			12.57	0.27	0.24	4.41	12.44	-0.00104	-0.00185	0.000000	0.000000	-0.0047	0.0000	0.0000	0.0000
35			12.95	0.28	0.24	4.06	13.63	-0.00173	-0.00185	0.000000	0.000000	-0.0081	0.0000	0.0000	0.0000
36			13.30	0.30	0.25	3.80	14.91	-0.00243	-0.00213	0.000000	0.000000	-0.0115	0.0000	0.0000	0.0000
37			13.65	0.33	0.25	3.53	16.29	-0.00324	-0.00252	0.000000	0.000000	-0.0154	0.0000	0.0000	0.0000
38			14.01	0.37	0.26	3.26	17.75	-0.00416	-0.00252	0.000000	0.000000	-0.0199	0.0000	0.0000	0.0000
39			14.38	0.43	0.26	3.03	19.31	-0.00509	-0.00252	0.000000	0.000000	-0.0244	0.0000	0.0000	0.0000
40			14.75	0.51	0.27	2.80	20.97	-0.00601	-0.00252	0.000000	0.000000	-0.0289	0.0000	0.0000	0.0000
41			15.11	0.60	0.27	2.57	22.76	-0.00694	-0.00252	0.000000	0.000000	-0.0333	0.0000	0.0000	0.0000
42			15.48	0.70	0.28	2.34	24.66	-0.00786	-0.00252	0.000000	0.000000	-0.0378	0.0000	0.0000	0.0000
43			15.84	0.81	0.28	2.11	26.67	-0.00878	-0.00252	0.000000	0.000000	-0.0423	0.0000	0.0000	0.0000
44			16.21	0.93	0.30	1.88	28.80	-0.00971	-0.00252	0.000000	0.000000	-0.0468	0.0000	0.0000	0.0000
45			16.58	1.06	0.31	1.65	31.04	-0.01063	-0.00252	0.000000	0.000000	-0.0513	0.0000	0.0000	0.0000
46			16.95	1.20	0.33	1.42	33.39	-0.01156	-0.00252	0.000000	0.000000	-0.0558	0.0000	0.0000	0.0000
47			17.32	1.35	0.34	1.19	35.84	-0.01248	-0.00252	0.000000	0.000000	-0.0602	0.0000	0.0000	0.0000
48			17.73	1.51	0.36	0.96	38.39	-0.01340	-0.00252	0.000000	0.000000	-0.0646	0.0000	0.0000	0.0000
49			18.14	1.68	0.38	0.73	41.04	-0.01431	-0.00104	0.000000	0.000000	-0.0689	0.0000	0.0000	0.0000

POS	S	OX	OY	(MX)	(MY)	AX	AY	EX	EXP	(R)	EYP	(XG)	(RG)	(YAG)	(RAG)	(DYG)
50	18.00	.39	.40	15.35	3.9	2.04	70	-.01273	.00104	0.00000	0.00000	-.0516	-.0019	0.00000	0.00000	0.00000
51	18.00	.39	.40	15.35	3.9	1.80	94	-.01236	.00104	0.00000	0.00000	-.0580	-.0019	0.00000	0.00000	0.00000
52	19.00	.41	.42	16.36	4.0	1.56	113	-.01123	.00104	0.00000	0.00000	-.0563	-.0019	0.00000	0.00000	0.00000
53	20.00	.42	.43	17.37	4.1	1.32	132	-.00985	.00104	0.00000	0.00000	-.0528	-.0019	0.00000	0.00000	0.00000
54	21.00	.43	.44	18.38	4.2	1.07	156	-.00818	.00104	0.00000	0.00000	-.0475	-.0019	0.00000	0.00000	0.00000
55	21.00	.43	.44	18.38	4.2	0.93	173	-.00673	.00104	0.00000	0.00000	-.0451	-.0019	0.00000	0.00000	0.00000
56	22.00	.44	.45	19.39	4.3	0.69	201	-.00488	.00225	0.00000	0.00000	-.0429	-.0032	0.00000	0.00000	0.00000
57	23.00	.45	.46	20.40	4.4	0.45	230	-.00293	.00449	0.00000	0.00000	-.0427	-.0054	0.00000	0.00000	0.00000
58	23.00	.45	.46	20.40	4.4	0.31	253	-.00197	.00673	0.00000	0.00000	-.0425	-.0074	0.00000	0.00000	0.00000
59	24.00	.46	.47	21.41	4.5	0.07	281	-.00111	.00897	0.00000	0.00000	-.0422	-.0094	0.00000	0.00000	0.00000
60	24.00	.46	.47	21.41	4.5	0.00	304	-.00072	.01122	0.00000	0.00000	-.0420	-.0114	0.00000	0.00000	0.00000
61	25.00	.47	.48	22.42	4.6	0.00	328	-.00033	.01346	0.00000	0.00000	-.0417	-.0134	0.00000	0.00000	0.00000
62	25.00	.47	.48	22.42	4.6	0.00	352	-.00014	.01570	0.00000	0.00000	-.0415	-.0154	0.00000	0.00000	0.00000
63	26.00	.48	.49	23.43	4.7	0.00	376	-.00011	.01794	0.00000	0.00000	-.0413	-.0174	0.00000	0.00000	0.00000
64	26.00	.48	.49	23.43	4.7	0.00	400	-.00011	.02018	0.00000	0.00000	-.0411	-.0194	0.00000	0.00000	0.00000
65	27.00	.49	.50	24.44	4.8	0.00	424	-.00011	.02242	0.00000	0.00000	-.0409	-.0214	0.00000	0.00000	0.00000
66	27.00	.49	.50	24.44	4.8	0.00	448	-.00011	.02466	0.00000	0.00000	-.0407	-.0234	0.00000	0.00000	0.00000
67	28.00	.50	.51	25.45	4.9	0.00	472	-.00011	.02690	0.00000	0.00000	-.0405	-.0254	0.00000	0.00000	0.00000
68	28.00	.50	.51	25.45	4.9	0.00	496	-.00011	.02914	0.00000	0.00000	-.0403	-.0274	0.00000	0.00000	0.00000
69	29.00	.51	.52	26.46	5.0	0.00	520	-.00011	.03138	0.00000	0.00000	-.0401	-.0294	0.00000	0.00000	0.00000
70	29.00	.51	.52	26.46	5.0	0.00	544	-.00011	.03362	0.00000	0.00000	-.0399	-.0314	0.00000	0.00000	0.00000
71	30.00	.52	.53	27.47	5.1	0.00	568	-.00011	.03586	0.00000	0.00000	-.0397	-.0334	0.00000	0.00000	0.00000
72	30.00	.52	.53	27.47	5.1	0.00	592	-.00011	.03810	0.00000	0.00000	-.0395	-.0354	0.00000	0.00000	0.00000
73	31.00	.53	.54	28.48	5.2	0.00	616	-.00011	.04034	0.00000	0.00000	-.0393	-.0374	0.00000	0.00000	0.00000
74	31.00	.53	.54	28.48	5.2	0.00	640	-.00011	.04258	0.00000	0.00000	-.0391	-.0394	0.00000	0.00000	0.00000
75	32.00	.54	.55	29.49	5.3	0.00	664	-.00011	.04482	0.00000	0.00000	-.0389	-.0414	0.00000	0.00000	0.00000
76	32.00	.54	.55	29.49	5.3	0.00	688	-.00011	.04706	0.00000	0.00000	-.0387	-.0434	0.00000	0.00000	0.00000
77	33.00	.55	.56	30.50	5.4	0.00	712	-.00011	.04930	0.00000	0.00000	-.0385	-.0454	0.00000	0.00000	0.00000
78	33.00	.55	.56	30.50	5.4	0.00	736	-.00011	.05154	0.00000	0.00000	-.0383	-.0474	0.00000	0.00000	0.00000
79	34.00	.56	.57	31.51	5.5	0.00	760	-.00011	.05378	0.00000	0.00000	-.0381	-.0494	0.00000	0.00000	0.00000
80	34.00	.56	.57	31.51	5.5	0.00	784	-.00011	.05602	0.00000	0.00000	-.0379	-.0514	0.00000	0.00000	0.00000
81	35.00	.57	.58	32.52	5.6	0.00	808	-.00011	.05826	0.00000	0.00000	-.0377	-.0534	0.00000	0.00000	0.00000
82	35.00	.57	.58	32.52	5.6	0.00	832	-.00011	.06050	0.00000	0.00000	-.0375	-.0554	0.00000	0.00000	0.00000
83	36.00	.58	.59	33.53	5.7	0.00	856	-.00011	.06274	0.00000	0.00000	-.0373	-.0574	0.00000	0.00000	0.00000
84	36.00	.58	.59	33.53	5.7	0.00	880	-.00011	.06498	0.00000	0.00000	-.0371	-.0594	0.00000	0.00000	0.00000
85	37.00	.59	.60	34.54	5.8	0.00	904	-.00011	.06722	0.00000	0.00000	-.0369	-.0614	0.00000	0.00000	0.00000
86	37.00	.59	.60	34.54	5.8	0.00	928	-.00011	.06946	0.00000	0.00000	-.0367	-.0634	0.00000	0.00000	0.00000
87	38.00	.60	.61	35.55	5.9	0.00	952	-.00011	.07170	0.00000	0.00000	-.0365	-.0654	0.00000	0.00000	0.00000
88	38.00	.60	.61	35.55	5.9	0.00	976	-.00011	.07394	0.00000	0.00000	-.0363	-.0674	0.00000	0.00000	0.00000
89	39.00	.61	.62	36.56	6.0	0.00	1000	-.00011	.07618	0.00000	0.00000	-.0361	-.0694	0.00000	0.00000	0.00000
90	39.00	.61	.62	36.56	6.0	0.00	1024	-.00011	.07842	0.00000	0.00000	-.0359	-.0714	0.00000	0.00000	0.00000
91	40.00	.62	.63	37.57	6.1	0.00	1048	-.00011	.08066	0.00000	0.00000	-.0357	-.0734	0.00000	0.00000	0.00000
92	40.00	.62	.63	37.57	6.1	0.00	1072	-.00011	.08290	0.00000	0.00000	-.0355	-.0754	0.00000	0.00000	0.00000
93	41.00	.63	.64	38.58	6.2	0.00	1096	-.00011	.08514	0.00000	0.00000	-.0353	-.0774	0.00000	0.00000	0.00000
94	41.00	.63	.64	38.58	6.2	0.00	1120	-.00011	.08738	0.00000	0.00000	-.0351	-.0794	0.00000	0.00000	0.00000
95	42.00	.64	.65	39.59	6.3	0.00	1144	-.00011	.08962	0.00000	0.00000	-.0349	-.0814	0.00000	0.00000	0.00000
96	42.00	.64	.65	39.59	6.3	0.00	1168	-.00011	.09186	0.00000	0.00000	-.0347	-.0834	0.00000	0.00000	0.00000
97	43.00	.65	.66	40.60	6.4	0.00	1192	-.00011	.09410	0.00000	0.00000	-.0345	-.0854	0.00000	0.00000	0.00000
98	43.00	.65	.66	40.60	6.4	0.00	1216	-.00011	.09634	0.00000	0.00000	-.0343	-.0874	0.00000	0.00000	0.00000
99	44.00	.66	.67	41.61	6.5	0.00	1240	-.00011	.09858	0.00000	0.00000	-.0341	-.0894	0.00000	0.00000	0.00000
00	44.00	.66	.67	41.61	6.5	0.00	1264	-.00011	.10082	0.00000	0.00000	-.0339	-.0914	0.00000	0.00000	0.00000

POS	SD	AM	OK	QY	IX	MY	AX	AY	IX	EXP	EXY	EYP	XCY	DYCO	YCO	DYCO
100	0.00	67.13	1.31	1.31	0.00	1.25	-79	1.52	1.31	1.9371	0.000000	0.000000	1.9371	1.52	0.0000	1.52
101	0.00	67.13	1.31	1.31	0.00	1.25	-79	1.52	1.31	1.9371	0.000000	0.000000	1.9371	1.52	0.0000	1.52
102	0.00	67.13	1.31	1.31	0.00	1.25	-79	1.52	1.31	1.9371	0.000000	0.000000	1.9371	1.52	0.0000	1.52
103	0.00	67.13	1.31	1.31	0.00	1.25	-79	1.52	1.31	1.9371	0.000000	0.000000	1.9371	1.52	0.0000	1.52
104	0.00	67.13	1.31	1.31	0.00	1.25	-79	1.52	1.31	1.9371	0.000000	0.000000	1.9371	1.52	0.0000	1.52
105	0.00	67.13	1.31	1.31	0.00	1.25	-79	1.52	1.31	1.9371	0.000000	0.000000	1.9371	1.52	0.0000	1.52
106	0.00	67.13	1.31	1.31	0.00	1.25	-79	1.52	1.31	1.9371	0.000000	0.000000	1.9371	1.52	0.0000	1.52
107	0.00	67.13	1.31	1.31	0.00	1.25	-79	1.52	1.31	1.9371	0.000000	0.000000	1.9371	1.52	0.0000	1.52
108	0.00	67.13	1.31	1.31	0.00	1.25	-79	1.52	1.31	1.9371	0.000000	0.000000	1.9371	1.52	0.0000	1.52
109	0.00	67.13	1.31	1.31	0.00	1.25	-79	1.52	1.31	1.9371	0.000000	0.000000	1.9371	1.52	0.0000	1.52
110	0.00	67.13	1.31	1.31	0.00	1.25	-79	1.52	1.31	1.9371	0.000000	0.000000	1.9371	1.52	0.0000	1.52
111	0.00	67.13	1.31	1.31	0.00	1.25	-79	1.52	1.31	1.9371	0.000000	0.000000	1.9371	1.52	0.0000	1.52
112	0.00	67.13	1.31	1.31	0.00	1.25	-79	1.52	1.31	1.9371	0.000000	0.000000	1.9371	1.52	0.0000	1.52
113	0.00	67.13	1.31	1.31	0.00	1.25	-79	1.52	1.31	1.9371	0.000000	0.000000	1.9371	1.52	0.0000	1.52
114	0.00	67.13	1.31	1.31	0.00	1.25	-79	1.52	1.31	1.9371	0.000000	0.000000	1.9371	1.52	0.0000	1.52
115	0.00	67.13	1.31	1.31	0.00	1.25	-79	1.52	1.31	1.9371	0.000000	0.000000	1.9371	1.52	0.0000	1.52
116	0.00	67.13	1.31	1.31	0.00	1.25	-79	1.52	1.31	1.9371	0.000000	0.000000	1.9371	1.52	0.0000	1.52
117	0.00	67.13	1.31	1.31	0.00	1.25	-79	1.52	1.31	1.9371	0.000000	0.000000	1.9371	1.52	0.0000	1.52
118	0.00	67.13	1.31	1.31	0.00	1.25	-79	1.52	1.31	1.9371	0.000000	0.000000	1.9371	1.52	0.0000	1.52
119	0.00	67.13	1.31	1.31	0.00	1.25	-79	1.52	1.31	1.9371	0.000000	0.000000	1.9371	1.52	0.0000	1.52
120	0.00	67.13	1.31	1.31	0.00	1.25	-79	1.52	1.31	1.9371	0.000000	0.000000	1.9371	1.52	0.0000	1.52

CIRCUMFERENCE = 395.1958 M THEYX = 6.28318638 RAD NUX = 9.72580 DNUY/DP/PP = .3612
 105/SI/87978 0849064 THEYI 183) = (7.67958, NUY = 9.76640 DNUY/DP/PP = .42451
 MINIMA --- BETX(36) = 17.89276 BETY(48) = 16.48276 ETAX(174) = 2.10892 ETAY(184) = 0.00000
 MAX --- BETX(36) = 17.89276 BETY(48) = 16.48276 ETAX(174) = 2.10892 ETAY(184) = 0.00000
 SUB CHR YER

CALCULATION OF THE EQUILIBRIUM ORBIT AND BETATRON FUNCTIONS OF AGR .

INITIAL REFERENCE RAY DEFINED BY :

X = -.00008530 DX = 0.00000000 Y = 0.00000000 DY = 0.00000000 DS = 0.00000000 DP/P = -.00500000 1.00000000

7X7 MATRIX FOR AGR

.04612244	17.84369784	0.00000000	0.00000000	0.00000000	.00822691	.00002195
-.05590731	.04612244	0.00000000	0.00000000	0.00000000	.00048218	.00000129
0.00000000	0.00000000	-.03787803	5.56903798	0.00000000	0.00000000	0.00000000
0.00000000	0.00000000	-.17930660	-.03787803	0.00000000	0.00000000	0.00000000
-.00043218	-.00822691	0.00000000	0.00000000	1.00000000	-2.86731298	.01462072
0.00000000	0.00000000	0.00000000	0.00000000	0.00000000	1.00000000	0.00000000
0.00000000	0.00000000	0.00000000	0.00000000	0.00000000	0.00000000	1.00000000

EIGENVALUES OF THE 4X4 SUBMATRIX

X... LMD1 = (.04612244 .99893579), C(1) = 1.00000000, MU(1) = 1.52465752 RAD, Q(1) = .72797034
 1/LMD1 = (.04612244 -.99893579), C(2) = 1.00000000, MU(2) = -1.52465752 RAD, Q(2) = .27202966
 Y... LMD3 = (-.03787803 -.99928237), C(3) = 1.00000000, MU(3) = -1.60868342 RAD, Q(3) = .76808976
 1/LMD3 = (-.03787803 -.99928237), C(4) = 1.00000000, MU(4) = -1.60868342 RAD, Q(4) = .23191024

EIGENVALUE = (.04612244, .99893579), EIGENVECTOR = (4.22702174, -.00000000)
 (0.00000000, -.23657319)
 (0.00000000, 0.00000000)
 (0.00000000, 0.00000000)

EIGENVALUE = (.04612244, -.99893579), EIGENVECTOR = (4.22702174, .00000000)
 (0.00000000, -.23657319)
 (0.00000000, 0.00000000)
 (0.00000000, 0.00000000)

EIGENVALUE = (-.03787803, .99928237), EIGENVECTOR = (0.00000000, 0.00000000)
 (0.00000000, 0.00000000)
 (2.36072814, 0.00000000)
 (-.00000000, .42359812)

EIGENVALUE = (-.03787803, -.99928237), EIGENVECTOR = (0.00000000, 0.00000000)
 (0.00000000, 0.00000000)
 (2.36072814, 0.00000000)
 (-.00000000, -.42359812)

	X	DX	Y	DY	DS	DP/P
EQ ORBIT	-.00001959	0.00000000	0.00000000	0.00000000	0.00000000	-.00500000
ETA ORBIT	.00862470	0.00000000	0.00000000	0.00000000	0.00000000	1.00000000

EIGENVECTORS 1 AND 3 IN POLAR COORDINATES

	ρ	θ	X_1	X_2	X_3	DX_1	DX_2	DX_3	Y_1	Y_2	Y_3	DY_1	DY_2	DY_3
1	0	-6.227022	0.000000	0.000000	0.000000	1.570796	0.000000	0.000000	0.000000	0.000000	0.000000	0.000000	0.000000	0.000000
3	0	0.000000	0.000000	0.000000	0.000000	0.000000	2.360728	0.000000	0.000000	0.000000	0.000000	0.423398	0.000000	1.570796

POS	S	OX	OY	OX	OY	AX	AY	EX	EXP	EY	EYP	XCC	DXCO	YCC	DYCC	
	(M)			(M)	(M)			(M)		(M)		(MM)	(MM)	(MM)	(MM)	
100	SF	43.67	.87	.86	13.51	5.98	-1.64	.79	1.97581	.24740	0.000000	0.000000	-9.8905	-1.2324	0.0000	0.0000
101	DS	43.37	.97	.87	14.52	5.53	-1.72	.71	2.05003	.24740	0.000000	0.000000	-10.2602	-1.2324	0.0000	0.0000
102	QF	44.32	.87	.88	15.13	5.29	.00	.00	2.09349	-.00030	0.000000	0.000000	-10.4768	.0010	0.0000	0.0000
103	QF	44.67	.88	.89	14.52	5.53	1.72	-.71	2.04982	-.24798	0.000000	0.000000	-10.2555	1.2344	0.0000	0.0000
104	DS	44.97	.88	.90	13.51	5.98	1.64	-.79	1.97543	-.24798	0.000000	0.000000	-9.8852	1.2344	0.0000	0.0000
105	SF	44.97	.88	.90	13.51	5.98	1.62	-.79	1.97543	-.24521	0.000000	0.000000	-9.8852	1.2275	0.0000	0.0000
106	Q	45.71	.99	.92	11.27	7.28	1.42	-.98	1.79509	-.24521	0.000000	0.000000	-6.9664	1.2275	0.0000	0.0000
107	B	47.37	.92	.95	7.27	11.21	.98	-1.37	1.46826	-.14944	0.000000	0.000000	-7.3451	.7487	0.0000	0.0000
108	B	48.10	.94	.96	6.00	13.37	.78	-1.58	1.35835	-.14944	0.000000	0.000000	-6.7984	.7487	0.0000	0.0000
109	SD	48.10	.94	.96	6.00	13.37	.79	-1.58	1.35835	-.15143	0.000000	0.000000	-6.7984	.7536	0.0000	0.0000
110	DS	48.40	.95	.96	5.55	14.34	.71	-1.66	1.31292	-.15143	0.000000	0.000000	-6.5724	.7536	0.0000	0.0000
111	OD	48.75	.96	.96	5.30	14.33	.01	-1.00	1.28640	-.00043	0.000000	0.000000	-6.4405	.0015	0.0000	0.0000
112	OD	49.10	.97	.97	5.53	14.34	-.69	1.67	1.31262	-.15056	0.000000	0.000000	-6.5713	-.7507	0.0000	0.0000
113	OD	49.40	.98	.97	5.97	13.36	-.77	1.59	1.35779	-.15056	0.000000	0.000000	-6.7965	-.7507	0.0000	0.0000
114	SD	49.40	.98	.97	5.97	13.36	-.76	1.57	1.35779	-.14857	0.000000	0.000000	-6.7965	-.7457	0.0000	0.0000
115	B	50.14	.99	.98	7.23	11.20	-.96	1.38	1.46705	-.14857	0.000000	0.000000	-7.3450	-.7457	0.0000	0.0000
116	B	51.80	1.02	1.01	11.13	7.26	-1.39	.99	1.79244	-.24434	0.000000	0.000000	-8.9774	-1.2245	0.0000	0.0000
117	OD	52.54	1.03	1.03	13.32	5.96	-1.59	.79	1.97214	-.24434	0.000000	0.000000	-9.8780	-1.2245	0.0000	0.0000
118	OD	52.54	1.03	1.03	13.32	5.96	-1.61	.79	1.97214	-.24710	0.000000	0.000000	-9.8780	-1.2314	0.0000	0.0000
119	SF	52.84	1.04	1.04	14.31	5.51	-1.69	-.71	2.04627	-.24710	0.000000	0.000000	-10.2474	-1.2314	0.0000	0.0000
120	QF	53.19	1.04	1.05	14.91	5.26	.01	.00	2.08971	-.00014	0.000000	0.000000	-10.4629	.0005	0.0000	0.0000
121	QF	53.54	1.04	1.06	14.30	5.50	1.70	-.71	2.04617	-.24738	0.000000	0.000000	-10.2471	1.2324	0.0000	0.0000
122	OD	53.84	1.05	1.07	13.30	5.95	1.62	-.79	1.97196	-.24738	0.000000	0.000000	-9.8774	1.2324	0.0000	0.0000
123	SF	54.04	1.05	1.07	13.30	5.95	1.60	-.78	1.97196	-.24462	0.000000	0.000000	-9.8774	1.2255	0.0000	0.0000
124	Q	54.57	1.06	1.08	11.09	7.24	1.41	-.98	1.79206	-.24462	0.000000	0.000000	-8.9761	1.2255	0.0000	0.0000
125	B	56.23	1.09	1.11	7.17	11.15	.96	-1.37	1.46620	-.14885	0.000000	0.000000	-7.3421	.7467	0.0000	0.0000
126	B	56.97	1.10	1.12	5.90	13.31	.76	-1.56	1.35673	-.14885	0.000000	0.000000	-6.7929	.7467	0.0000	0.0000
127	SD	56.97	1.10	1.12	5.90	13.31	.77	-1.58	1.35673	-.15083	0.000000	0.000000	-6.7929	.7516	0.0000	0.0000
128	DS	57.27	1.11	1.13	5.46	14.27	-.69	-1.65	1.31148	-.15083	0.000000	0.000000	-6.5674	.0000	0.0000	0.0000
129	OD	57.62	1.12	1.13	5.22	14.86	-.00	-.00	1.28514	.00001	0.000000	0.000000	-6.4361	-.0000	0.0000	0.0000
130	OD	57.97	1.13	1.13	5.46	14.27	-.69	1.65	1.31149	-.15086	0.000000	0.000000	-6.5674	-.7517	0.0000	0.0000
131	OS	58.27	1.14	1.14	5.99	13.31	-.77	1.58	1.35675	-.15086	0.000000	0.000000	-6.7930	-.7517	0.0000	0.0000
132	SD	58.27	1.14	1.14	5.99	13.31	-.76	1.56	1.35675	-.14888	0.000000	0.000000	-6.7930	-.7467	0.0000	0.0000
133	Q	59.00	1.16	1.15	7.17	11.15	-.96	1.37	1.46624	-.14888	0.000000	0.000000	-7.3421	-.7467	0.0000	0.0000
134	B	60.66	1.19	1.18	11.09	7.24	-1.41	.98	1.79213	-.24465	0.000000	0.000000	-8.9763	-1.2255	0.0000	0.0000
135	Q	61.40	1.20	1.20	13.31	5.95	-1.60	.78	1.97205	-.24465	0.000000	0.000000	-9.8776	-1.2255	0.0000	0.0000
136	SF	61.40	1.20	1.20	13.31	5.95	-1.62	.79	1.97205	-.24741	0.000000	0.000000	-9.8776	-1.2324	0.0000	0.0000
137	OS	61.70	1.20	1.20	14.30	5.50	-1.70	.71	2.04627	-.24741	0.000000	0.000000	-10.2473	-1.2324	0.0000	0.0000
138	QF	62.05	1.21	1.21	14.91	5.26	-.01	-.00	2.08981	-.00015	0.000000	0.000000	-10.4641	-.0005	0.0000	0.0000
139	QF	62.40	1.21	1.22	14.32	5.51	1.69	-.71	2.04638	-.24711	0.000000	0.000000	-10.2477	1.2314	0.0000	0.0000
140	DS	62.70	1.21	1.23	13.33	5.96	1.61	-.79	1.97225	-.24711	0.000000	0.000000	-9.8782	1.2314	0.0000	0.0000
141	SF	62.70	1.21	1.23	13.33	5.96	1.59	-.79	1.97225	-.24434	0.000000	0.000000	-9.8782	1.2245	0.0000	0.0000
142	Q	63.43	1.22	1.25	11.13	7.26	1.39	-.99	1.79255	-.24434	0.000000	0.000000	-8.9777	1.2245	0.0000	0.0000
143	B	65.09	1.25	1.28	7.24	11.20	.96	-1.38	1.46716	-.14857	0.000000	0.000000	-7.3452	.7457	0.0000	0.0000
144	Q	65.83	1.27	1.29	5.97	13.36	.76	-1.57	1.35790	-.14857	0.000000	0.000000	-6.7968	.7457	0.0000	0.0000
145	SD	65.83	1.27	1.29	5.97	13.36	.77	-1.59	1.35790	-.15056	0.000000	0.000000	-6.7968	.7507	0.0000	0.0000
146	OS	66.13	1.28	1.29	5.54	14.34	.69	-1.67	1.31273	-.15056	0.000000	0.000000	-6.5715	-.7507	0.0000	0.0000
147	OD	66.48	1.29	1.30	5.30	14.33	-.01	-.00	1.28651	-.00044	0.000000	0.000000	-6.4407	-.0015	0.0000	0.0000
148	OD	66.83	1.30	1.30	5.55	14.34	-.71	1.66	1.31304	-.15146	0.000000	0.000000	-6.5726	-.7537	0.0000	0.0000
149	DS	67.13	1.31	1.30	6.00	13.37	-.79	1.58	1.35848	-.15146	0.000000	0.000000	-6.7987	-.7537	0.0000	0.0000

POS	S	OX	OY	OX	OY	AX	AY	EX	EXP	EY	EYP	XCC	DXCO	YCO	DYCC
	(M)			(M)	(M)			(M)		(M)		(MM)	(MM)	(MM)	(MM)
150 SD	67.13	1.31	1.30	6.00	13.37	-.78	1.50	1.35848	-.14947	0.000000	0.000000	-6.7987	-.7487	0.0000	0.0000
151 O	67.87	1.33	1.31	7.29	11.21	-.93	1.37	1.46840	-.14947	0.000000	0.000000	-7.3453	-.7487	0.0000	0.0000
152 B	69.53	1.36	1.34	11.27	7.28	-1.62	-.98	1.79528	-.24524	0.000000	0.000000	-8.9868	-1.2275	0.0000	0.0000
153 O	70.26	1.37	1.36	13.51	5.98	-1.62	-.79	1.97563	-.24524	0.000000	0.000000	-9.8969	-1.2275	0.0000	0.0000
154 SF	70.26	1.37	1.36	13.51	5.98	-1.64	-.79	1.97563	-.24801	0.000000	0.000000	-9.8696	-1.2343	0.0000	0.0000
155 OS	70.56	1.37	1.37	14.52	5.53	-1.72	-.71	2.05004	-.24801	0.000000	0.000000	-10.2599	-1.2345	0.0000	0.0000
156 QF	70.91	1.37	1.38	15.13	5.28	-.00	-.00	2.09371	-.00030	0.000000	0.000000	-10.4772	-.9010	0.0000	0.0000
157 QF	71.26	1.38	1.39	14.52	5.53	1.72	-.71	2.05025	-.24742	0.000000	0.000000	-10.2606	-1.2325	0.0000	0.0000
158 OS	71.56	1.38	1.40	13.51	5.98	1.64	-.79	1.97602	-.24742	0.000000	0.000000	-9.8969	-1.2325	0.0000	0.0000
159 SF	71.56	1.38	1.40	13.51	5.98	1.62	-.79	1.97602	-.24465	0.000000	0.000000	-9.8509	-1.2256	0.0000	0.0000
160 O	72.30	1.39	1.42	11.27	7.28	1.42	-.98	1.79609	-.24465	0.000000	0.000000	-8.9895	1.2256	0.0000	0.0000
161 B	73.96	1.42	1.45	7.29	11.21	-.98	1.37	1.47019	-.14888	0.000000	0.000000	-7.3554	-.7468	0.0000	0.0000
162 O	74.69	1.44	1.45	6.00	13.37	-.78	1.56	1.36070	-.14888	0.000000	0.000000	-6.8062	-.7468	0.0000	0.0000
163 SD	74.69	1.44	1.45	6.00	13.37	-.79	1.56	1.36070	-.15087	0.000000	0.000000	-6.8062	-.7517	0.0000	0.0000
164 OS	74.69	1.44	1.46	5.55	14.34	-.71	1.66	1.31543	-.15087	0.000000	0.000000	-6.5806	-.7517	0.0000	0.0000
165 QD	75.34	1.45	1.46	5.30	14.93	-.01	-.00	1.28916	-.00043	0.000000	0.000000	-6.4496	-.9015	0.0000	0.0000
166 QD	75.69	1.47	1.47	5.54	14.34	-.69	1.67	1.31574	-.15176	0.000000	0.000000	-6.5817	-.7547	0.0000	0.0000
167 OS	75.99	1.47	1.47	5.97	13.36	-.77	1.59	1.36127	-.15176	0.000000	0.000000	-6.8081	-.7547	0.0000	0.0000
168 OS	75.99	1.47	1.47	5.97	13.36	-.76	1.57	1.36127	-.14977	0.000000	0.000000	-6.8081	-.7498	0.0000	0.0000
169 O	76.73	1.49	1.48	7.24	11.20	-.96	1.38	1.47141	-.14977	0.000000	0.000000	-7.3555	-.7498	0.0000	0.0000
170 B	78.39	1.52	1.51	11.13	7.26	-1.39	-.99	1.79878	-.24554	0.000000	0.000000	-8.9986	-1.2286	0.0000	0.0000
171 O	79.12	1.53	1.53	13.32	5.96	-1.59	-.79	1.97935	-.24554	0.000000	0.000000	-9.9021	-1.2286	0.0000	0.0000
172 SF	79.12	1.53	1.53	13.32	5.96	-1.61	-.79	1.97935	-.24832	0.000000	0.000000	-9.9021	-1.2355	0.0000	0.0000
173 OS	79.42	1.53	1.53	14.31	5.51	-1.69	-.71	2.05385	-.24832	0.000000	0.000000	-10.2728	-1.2355	0.0000	0.0000
174 QF	79.78	1.54	1.54	14.91	5.26	-.01	-.00	2.09755	-.00015	0.000000	0.000000	-10.4901	-.9003	0.0000	0.0000
175 QF	80.13	1.54	1.56	14.30	5.50	-1.70	-.71	2.05395	-.24802	0.000000	0.000000	-10.2731	1.2345	0.0000	0.0000
176 OS	80.43	1.54	1.56	13.30	5.95	1.62	-.79	1.97955	-.24802	0.000000	0.000000	-9.9028	1.2345	0.0000	0.0000
177 SF	80.43	1.54	1.56	13.30	5.95	1.60	-.78	1.97955	-.24525	0.000000	0.000000	-9.9028	1.2276	0.0000	0.0000
178 O	81.16	1.55	1.58	11.09	7.24	1.41	-.98	1.79918	-.24525	0.000000	0.000000	-9.9060	1.2276	0.0000	0.0000
179 B	82.82	1.58	1.61	7.17	11.15	-.96	-1.37	1.47230	-.14947	0.000000	0.000000	-7.3625	-.7488	0.0000	0.0000
180 O	83.56	1.60	1.62	5.90	13.31	-.76	-1.56	1.36237	-.14947	0.000000	0.000000	-6.8118	-.7488	0.0000	0.0000
181 SD	83.56	1.60	1.62	5.90	13.31	-.77	-1.58	1.36237	-.15147	0.000000	0.000000	-6.8118	-.7538	0.0000	0.0000
182 OS	83.86	1.61	1.62	5.46	14.27	-.69	-1.65	1.31693	-.15147	0.000000	0.000000	-6.5857	-.7538	0.0000	0.0000
183 QD	84.21	1.52	1.63	5.22	14.86	-.00	-.00	1.29047	-.00000	0.000000	0.000000	-6.4540	-.9000	0.0000	0.0000
184 RFFL	168.41	3.24	3.26	17.87	5.57	-.00	-.00	1.00862	-.00000	0.000000	0.000000	-.0196	0.0000	0.0000	0.0000

CIRCUMFERENCE = 505.2394 M THETA(183) = 6.28318638 RAD NUX = 9.72797 DNUX/(DP/P) = .37870
(DS/S)/RBDIBS = 1.8870255 M GAM = (7.66390, 0.00000) NUZ = 9.76809 DNUZ/(DP/P) = .41000
MAXIMA --- BETX(184) = 17.86771 BETY(12) = 19.71017 ETAX(174) = 2.09755 ETAY(184) = 0.00000
MINIMA --- BETX(36) = 4.02794 BETY(48) = 3.27399 ETAX(33) = -.00011 ETAY(184) = 0.00000
*** INCR = 1 DR = .00500 VALUE = 0.00000
SUB: CHR , ITER: 5

CALCULATION OF THE EQUILIBRIUM ORBIT AND BETATRON FUNCTIONS OF AGR

INITIAL REFERENCE PAV DEFINED BY V
 $X = -0.0001959$ $DX = 0.00000000$ $Y = 0.00000000$ $DY = 0.00000000$ $DS = 0.00000000$ $DP/P = 0.00000000$ 1.00000000

7X7 MATRIX FOR AGR

.04182933	17.81760225	0.00000000	0.00000000	0.00000000	-0.00087646	-0.00000000
-.05602607	.04182933	0.00000000	0.00000000	0.00000000	-0.0005125	-0.00000000
0.00000000	0.00000000	-.04180826	5.72904571	0.00000000	0.00000000	0.00000000
0.00000000	0.00000000	-.17424404	-.04180826	0.00000000	0.00000000	0.00000000
.00005125	.00087646	0.00000000	0.00000000	1.00000000	-2.87936746	-0.00000000
0.00000000	0.00000000	0.00000000	0.00000000	0.00000000	1.00000000	0.00000000
0.00000000	0.00000000	0.00000000	0.00000000	0.00000000	0.00000000	1.00000000

EIGENVALUES OF THE 4X4 SUBMATRIX

X... $\frac{1}{LMD1} = \begin{pmatrix} .04182933 & .99912477 \\ .04182933 & -.99912477 \end{pmatrix}$, $C(1) = 1.00000000$, $\mu(1) = -1.52895479$ RAD, $Q(1) = .73002214$
 $Q(2) = .26997786$
Y... $\frac{1}{LMD3} = \begin{pmatrix} -.04180826 & .99912565 \\ -.04180826 & -.99912565 \end{pmatrix}$, $C(3) = 1.00000000$, $\mu(3) = -1.61261677$ RAD, $Q(3) = .76996779$
 $Q(4) = .23003221$

EIGENVALUE = (.04182933, .99912477), EIGENVECTOR = (4.22293860, 0.00000000, 0.00000000, 0.00000000)

EIGENVALUE = (.04182933, -.99912477), EIGENVECTOR = (4.22293860, 0.00000000, 0.00000000, 0.00000000)

EIGENVALUE = (-.04180826, .99912565), EIGENVECTOR = (0.00000000, 0.00000000, 2.39458958, .00000000)

EIGENVALUE = (-.04180826, -.99912565), EIGENVECTOR = (0.00000000, 0.00000000, 2.39458958, .00000000)

	X	DX	Y	DY	DS	DP/P	
EQ ORBIT	-0.00000000	0.00000000	0.00000000	0.00000000	0.00000000	0.00000000	1.00000000
ETA ORBIT	-0.00091473	-0.00000000	0.00000000	0.00000000	0.00000000	1.00000000	0.00000000

PDS	S	QY	DX	BY	AX	AY	EX	EXP	EY	EYP	YCU	DXCU	YCU	BYCU
50 Z	18.50	30	12.29	4.02	2.00	74	0.000000	-0.0005	0.000000	0.000000	0.0000	0.0000	0.0000	0.0000
51 Z	18.50	30	12.29	4.02	1.98	74	0.000000	-0.0005	0.000000	0.000000	0.0000	0.0000	0.0000	0.0000
52 Z	18.50	30	12.29	4.02	1.97	74	0.000000	-0.0005	0.000000	0.000000	0.0000	0.0000	0.0000	0.0000
53 Z	18.50	30	12.29	4.02	1.95	74	0.000000	-0.0005	0.000000	0.000000	0.0000	0.0000	0.0000	0.0000
54 Z	20.31	45	9.13	3.04	1.41	157	0.000000	-0.0005	0.000000	0.000000	0.0000	0.0000	0.0000	0.0000
55 Z	20.31	45	9.13	3.04	1.41	157	0.000000	-0.0005	0.000000	0.000000	0.0000	0.0000	0.0000	0.0000
56 Z	20.31	45	9.13	3.04	1.40	157	0.000000	-0.0005	0.000000	0.000000	0.0000	0.0000	0.0000	0.0000
57 Z	20.31	45	9.13	3.04	1.38	157	0.000000	-0.0005	0.000000	0.000000	0.0000	0.0000	0.0000	0.0000
58 Z	22.16	47	5.23	13.82	1.10	29	0.000000	-0.0002	0.000000	0.000000	0.0000	0.0000	0.0000	0.0000
59 Z	22.16	47	5.23	13.82	1.10	29	0.000000	-0.0002	0.000000	0.000000	0.0000	0.0000	0.0000	0.0000
60 QD3	22.94	47	5.23	13.82	1.10	29	0.000000	-0.0002	0.000000	0.000000	0.0000	0.0000	0.0000	0.0000
61 R	23.31	49	6.17	11.12	1.00	34	0.000000	-0.0008	0.000000	0.000000	0.0000	0.0000	0.0000	0.0000
62 R	23.31	49	6.17	11.12	1.00	34	0.000000	-0.0008	0.000000	0.000000	0.0000	0.0000	0.0000	0.0000
63 R	23.31	49	6.17	11.12	1.00	34	0.000000	-0.0008	0.000000	0.000000	0.0000	0.0000	0.0000	0.0000
64 R	23.31	49	6.17	11.12	1.00	34	0.000000	-0.0008	0.000000	0.000000	0.0000	0.0000	0.0000	0.0000
65 R	24.04	50	8.21	9.34	1.10	14	0.000000	-0.0008	0.000000	0.000000	0.0000	0.0000	0.0000	0.0000
66 R	24.04	50	8.21	9.34	1.10	14	0.000000	-0.0008	0.000000	0.000000	0.0000	0.0000	0.0000	0.0000
67 R	24.04	50	8.21	9.34	1.10	14	0.000000	-0.0008	0.000000	0.000000	0.0000	0.0000	0.0000	0.0000
68 R	24.04	50	8.21	9.34	1.10	14	0.000000	-0.0008	0.000000	0.000000	0.0000	0.0000	0.0000	0.0000
69 R	24.04	50	8.21	9.34	1.10	14	0.000000	-0.0008	0.000000	0.000000	0.0000	0.0000	0.0000	0.0000
70 R	25.88	53	13.16	5.93	1.60	70	0.000000	-0.0008	0.000000	0.000000	0.0000	0.0000	0.0000	0.0000
71 R	26.59	53	14.37	5.29	1.70	61	0.000000	-0.0001	0.000000	0.000000	0.0000	0.0000	0.0000	0.0000
72 R	26.59	53	14.37	5.29	1.70	61	0.000000	-0.0001	0.000000	0.000000	0.0000	0.0000	0.0000	0.0000
73 R	26.59	53	14.37	5.29	1.70	61	0.000000	-0.0001	0.000000	0.000000	0.0000	0.0000	0.0000	0.0000
74 R	27.98	60	11.15	7.58	1.42	81	0.000000	-0.0001	0.000000	0.000000	0.0000	0.0000	0.0000	0.0000
75 R	29.64	62	7.20	13.02	1.97	53	0.07940	-0.0951	0.000000	0.000000	0.0000	0.0000	0.0000	0.0000
76 R	30.68	64	5.59	13.19	1.69	51	0.17801	-0.1778	0.000000	0.000000	0.0000	0.0000	0.0000	0.0000
77 R	31.03	64	5.59	13.19	1.69	51	0.17801	-0.1778	0.000000	0.000000	0.0000	0.0000	0.0000	0.0000
78 R	31.38	64	5.59	13.19	1.69	51	0.17801	-0.1778	0.000000	0.000000	0.0000	0.0000	0.0000	0.0000
79 R	32.41	66	7.57	12.22	1.97	53	0.15318	-0.15318	0.000000	0.000000	0.0000	0.0000	0.0000	0.0000
80 R	34.07	68	13.15	7.92	1.62	69	0.24025	-0.24025	0.000000	0.000000	0.0000	0.0000	0.0000	0.0000
81 R	34.81	70	13.33	6.46	1.91	69	0.24025	-0.24025	0.000000	0.000000	0.0000	0.0000	0.0000	0.0000
82 R	34.81	70	13.33	6.46	1.91	69	0.24025	-0.24025	0.000000	0.000000	0.0000	0.0000	0.0000	0.0000
83 R	34.81	70	13.33	6.46	1.91	69	0.24025	-0.24025	0.000000	0.000000	0.0000	0.0000	0.0000	0.0000
84 R	34.81	70	13.33	6.46	1.91	69	0.24025	-0.24025	0.000000	0.000000	0.0000	0.0000	0.0000	0.0000
85 R	35.10	71	14.37	5.89	1.70	69	0.10643	-0.00406	0.000000	0.000000	0.0000	0.0000	0.0000	0.0000
86 R	35.10	71	14.37	5.89	1.70	69	0.10643	-0.00406	0.000000	0.000000	0.0000	0.0000	0.0000	0.0000
87 R	35.10	71	14.37	5.89	1.70	69	0.10643	-0.00406	0.000000	0.000000	0.0000	0.0000	0.0000	0.0000
88 R	35.10	71	14.37	5.89	1.70	69	0.10643	-0.00406	0.000000	0.000000	0.0000	0.0000	0.0000	0.0000
89 R	35.10	71	14.37	5.89	1.70	69	0.10643	-0.00406	0.000000	0.000000	0.0000	0.0000	0.0000	0.0000
90 R	38.24	79	5.91	13.62	1.77	56	0.00406	-0.00406	0.000000	0.000000	0.0000	0.0000	0.0000	0.0000
91 R	39.54	77	5.42	13.49	1.60	56	0.00406	-0.00406	0.000000	0.000000	0.0000	0.0000	0.0000	0.0000
92 R	39.54	77	5.42	13.49	1.60	56	0.00406	-0.00406	0.000000	0.000000	0.0000	0.0000	0.0000	0.0000
93 R	40.24	80	5.44	13.49	1.60	56	0.00406	-0.00406	0.000000	0.000000	0.0000	0.0000	0.0000	0.0000
94 R	40.24	80	5.44	13.49	1.60	56	0.00406	-0.00406	0.000000	0.000000	0.0000	0.0000	0.0000	0.0000
95 R	40.54	80	5.91	13.51	1.77	64	0.24434	-0.24434	0.000000	0.000000	0.0000	0.0000	0.0000	0.0000
96 R	41.28	81	5.91	13.51	1.77	64	0.24434	-0.24434	0.000000	0.000000	0.0000	0.0000	0.0000	0.0000
97 R	41.28	81	5.91	13.51	1.77	64	0.24434	-0.24434	0.000000	0.000000	0.0000	0.0000	0.0000	0.0000
98 R	42.07	84	11.15	7.22	1.61	78	0.24434	-0.24434	0.000000	0.000000	0.0000	0.0000	0.0000	0.0000
99 R	42.07	84	11.15	7.22	1.61	78	0.24434	-0.24434	0.000000	0.000000	0.0000	0.0000	0.0000	0.0000

POS	S (M)	OX	OY	BX (M)	BY (M)	AX	AY	EX (M)	EXP	EY (M)	EYP	XCC (MM)	DXCO (MM)	YCE (MM)	DYCO (MM)
150 SD	67.14	1.31	1.30	5.91	13.33	-.77	1.57	1.35421	.14929	0.000000	0.000000	.0000	-.0000	0.0000	0.0000
151 D	67.87	1.33	1.31	7.19	11.16	-.97	1.38	1.46400	-.14929	0.000000	0.000000	.0000	-.0000	0.0000	0.0000
152 R	69.53	1.35	1.34	11.15	7.22	-1.42	.99	1.79048	-.24456	0.000000	0.000000	.0000	-.0000	0.0000	0.0000
153 D	70.27	1.36	1.36	13.37	5.92	-1.61	.78	1.97034	-.24456	0.000000	0.000000	.0000	-.0000	0.0000	0.0000
154 SF	70.27	1.36	1.36	13.37	5.92	-1.61	.78	1.97034	-.24456	0.000000	0.000000	.0000	-.0000	0.0000	0.0000
155 DS	70.57	1.37	1.37	14.37	5.47	-1.69	-.70	2.04371	-.24456	0.000000	0.000000	.0000	-.0000	0.0000	0.0000
156 QF	70.92	1.37	1.38	14.97	5.23	.00	-.00	2.08673	-.00011	0.000000	0.000000	.0000	-.0000	0.0000	0.0000
157 QF	71.27	1.38	1.39	14.37	5.47	1.69	-.70	2.04378	-.24434	0.000000	0.000000	.0000	-.0000	0.0000	0.0000
158 DS	71.57	1.38	1.40	13.37	5.92	1.61	-.78	1.97048	-.24434	0.000000	0.000000	.0000	-.0000	0.0000	0.0000
159 SF	71.57	1.39	1.40	13.37	5.92	1.61	-.78	1.97048	-.24434	0.000000	0.000000	.0000	-.0000	0.0000	0.0000
160 D	72.30	1.39	1.42	11.15	7.22	1.42	-.99	1.79079	-.24434	0.000000	0.000000	.0000	-.0000	0.0000	0.0000
161 B	73.96	1.42	1.44	7.19	11.16	.97	-1.38	1.46467	-.14907	0.000000	0.000000	.0000	-.0000	0.0000	0.0000
162 D	74.70	1.44	1.45	5.91	13.33	.77	-1.57	1.35504	-.14907	0.000000	0.000000	.0000	-.0000	0.0000	0.0000
163 SD	74.70	1.44	1.45	5.91	13.33	.77	-1.57	1.35504	-.14907	0.000000	0.000000	.0000	-.0000	0.0000	0.0000
164 DS	75.00	1.44	1.46	5.48	14.30	.69	-1.65	1.31032	-.14907	0.000000	0.000000	.0000	-.0000	0.0000	0.0000
165 QD	75.35	1.46	1.46	5.24	14.88	.00	-.00	1.28431	-.00016	0.000000	0.000000	.0000	-.0000	0.0000	0.0000
166 QD	75.70	1.47	1.47	5.48	14.30	-.69	1.65	1.31043	-.14940	0.000000	0.000000	.0000	-.0000	0.0000	0.0000
167 DS	76.00	1.47	1.47	5.91	13.33	-.77	1.57	1.35526	-.14940	0.000000	0.000000	.0000	-.0000	0.0000	0.0000
168 SD	76.00	1.47	1.47	5.91	13.33	-.77	1.57	1.35526	-.14940	0.000000	0.000000	.0000	-.0000	0.0000	0.0000
169 D	76.74	1.49	1.48	7.19	11.16	-.97	1.38	1.46513	-.14940	0.000000	0.000000	.0000	-.0000	0.0000	0.0000
170 B	78.40	1.52	1.51	11.15	7.22	-1.42	.99	1.79180	-.24468	0.000000	0.000000	.0000	-.0000	0.0000	0.0000
171 D	79.13	1.53	1.53	13.37	5.92	-1.61	.78	1.97175	-.24468	0.000000	0.000000	.0000	-.0000	0.0000	0.0000
172 SF	79.13	1.53	1.53	13.37	5.92	-1.61	.78	1.97175	-.24468	0.000000	0.000000	.0000	-.0000	0.0000	0.0000
173 DS	79.43	1.53	1.53	14.37	5.47	-1.69	-.70	2.04515	-.24468	0.000000	0.000000	.0000	-.0000	0.0000	0.0000
174 QF	79.78	1.54	1.54	14.97	5.23	.00	-.00	2.08819	-.00006	0.000000	0.000000	.0000	-.0000	0.0000	0.0000
175 QF	80.13	1.54	1.56	14.37	5.47	1.69	-.70	2.04519	-.24457	0.000000	0.000000	.0000	-.0000	0.0000	0.0000
176 DS	80.43	1.55	1.56	13.37	5.92	1.61	-.78	1.97182	-.24457	0.000000	0.000000	.0000	-.0000	0.0000	0.0000
177 SF	80.43	1.55	1.56	13.37	5.92	1.61	-.78	1.97182	-.24457	0.000000	0.000000	.0000	-.0000	0.0000	0.0000
178 D	81.17	1.56	1.58	11.15	7.22	1.42	-.99	1.79196	-.24457	0.000000	0.000000	.0000	-.0000	0.0000	0.0000
179 B	82.83	1.58	1.61	7.19	11.16	.97	-1.38	1.46547	-.14929	0.000000	0.000000	.0000	-.0000	0.0000	0.0000
180 D	83.56	1.60	1.62	5.91	13.33	.77	-1.57	1.35567	-.14929	0.000000	0.000000	.0000	-.0000	0.0000	0.0000
181 SD	83.56	1.60	1.62	5.91	13.33	.77	-1.57	1.35567	-.14929	0.000000	0.000000	.0000	-.0000	0.0000	0.0000
182 DS	83.86	1.61	1.62	5.48	14.30	.69	-1.65	1.31088	-.14929	0.000000	0.000000	.0000	-.0000	0.0000	0.0000
183 QD	84.21	1.62	1.63	5.24	14.88	-.00	.00	1.28481	.00000	0.000000	0.000000	.0000	-.0000	0.0000	0.0000
184 REFL	168.43	3.24	3.26	17.83	5.73	-.00	.00	-.00091	.00000	0.000000	0.000000	-.0000	0.0000	0.0000	0.0000

CIRCUMFERENCE = 505.2827 M THETA = 6.28318638 RAD NUX = 9.73002 DNUX/IDP/P = .39620
(DS/S)/RNDZBS = .8978988 M THETA(183) = 0.0000000 RAD NUU = 9.76997 DNUU/IDP/P = .39105
TGAM = (7.64818, 0.00000)

MAXIMA --- BETX(184) = 17.83321 BETY(12) = 16.94478 ETAX(174) = 2.08819 ETAY(184) = 0.00000
MINIMA --- BETX(36) = 4.05811 BETY(48) = 3.28656 ETAX(33) = .00000 ETAY(184) = 0.00000

*** INCR 1 // DP .005000 VALUE = .005000

SUB: CHR , ITER. 6

CALCULATION OF THE EQUILIBRIUM ORBIT AND BETATRON FUNCTIONS OF AGR .
 INITIAL REFERENCE RAY DEFINED BY V

X = -.00000000 DX = 0.00000000 Y = 0.00000000 DY = 0.00000000 DS = 0.00000000 DP/P = .00500000 1.00000000

7X7 MATRIX FOR AGR

.03773456	17.77701740	0.00000000	0.00000000	0.00000000	-0.01056744	.00002498
-.05617210	.03778456	0.00000000	0.00000000	0.00000000	-.00001690	.00000146
0.00000000	0.00000000	-.04603245	5.88965712	0.00000000	0.00000000	0.00000000
0.00000000	0.00000000	-.16942939	-.04603245	0.00000000	0.00000000	0.00000000
.00061690	.01056744	0.00000000	0.00000000	1.00000000	-2.89152294	-.01417847
0.00000000	0.00000000	0.00000000	0.00000000	0.00000000	1.00000000	0.00000000
0.00000000	0.00000000	0.00000000	0.00000000	0.00000000	0.00000000	1.00000000

EIGENVALUES OF THE 4X4 SUBMATRIX

X... LMD1 = { .03778456, -.99928591 }, C(1) = 1.00000000, MU(1) = -1.53300277 RAD, Q(1) = -.73195490
 1/LMD1 = { .03778456, -.99928591 }, C(2) = 1.00000000, MU(2) = -1.53300277 RAD, Q(2) = .26804510
 Y... LMD3 = { -.04603245, .99893995 }, C(3) = 1.00000000, MU(3) = -1.61684505 RAD, Q(3) = -.77198664
 1/LMD3 = { -.04603245, .99893995 }, C(4) = 1.00000000, MU(4) = -1.61684505 RAD, Q(4) = .22801336

EIGENVALUE = (.03778456, .99928591), EIGENVECTOR = (4.21778626, 0.00000000)
 (0.00000000, -.23709120)
 (0.00000000, 0.00000000)
 (0.00000000, 0.00000000)

EIGENVALUE = (-.03778456, -.99928591), EIGENVECTOR = (4.21778626, 0.00000000)
 (0.00000000, -.23709120)
 (0.00000000, 0.00000000)
 (0.00000000, 0.00000000)

EIGENVALUE = (-.04603245, .99893995), EIGENVECTOR = (0.00000000, 0.00000000)
 (0.00000000, 0.00000000)
 (2.42814890, .00000000)
 (.00000000, -.41183636)

EIGENVALUE = (-.04603245, -.99893995), EIGENVECTOR = (0.00000000, 0.00000000)
 (0.00000000, 0.00000000)
 (2.42814890, .00000000)
 (.00000000, -.41183636)

	X	DX	Y	DY	DS	DP/P	
EQ ORBIT	-.00002944	0.00000000	0.00000000	0.00000000	0.00000000	.00500000	1.00000000
ETA ORBIT	-.01098241	-.00000000	0.00000000	0.00000000	0.00000000	1.00000000	0.00000000

BETAatron FUNCTIONS OF AGR

POS	S (M)	OX	AGR	QY	RX (M)	UY (M)	AX	AY	EX (M)	EXP	EY (M)	EYP	XCL (MM)	DXCO (MM)	YCG (MM)	DYCO (MM)
0	0.00	0.00	0.00	0.00	17.79	0.00	0.00	0.00	-0.0000	0.0000	0.0000	0.0000	0.0294	0.0000	0.0000	0.0000
1	0.35	0.01	0.01	0.01	16.33	2.25	0.89	0.00	-0.01098	0.0000	0.0000	0.0000	0.0288	0.0038	0.0000	0.0000
2	1.07	0.02	0.02	0.03	15.36	2.25	0.89	0.00	-0.01073	0.0000	0.0000	0.0000	0.0279	0.0038	0.0000	0.0000
3	1.47	0.02	0.02	0.03	13.40	1.88	1.05	0.00	-0.00966	0.0000	0.0000	0.0000	0.0245	0.0038	0.0000	0.0000
4	1.84	0.02	0.02	0.03	11.06	1.72	1.22	0.00	-0.00959	0.0000	0.0000	0.0000	0.0230	0.0038	0.0000	0.0000
5	2.22	0.03	0.03	0.04	8.70	1.45	1.45	0.00	-0.00906	0.0000	0.0000	0.0000	0.0216	0.0038	0.0000	0.0000
6	2.59	0.03	0.03	0.04	7.46	1.25	1.70	0.00	-0.00853	0.0000	0.0000	0.0000	0.0202	0.0038	0.0000	0.0000
7	3.04	0.04	0.04	0.06	6.73	1.19	1.81	0.00	-0.00846	0.0000	0.0000	0.0000	0.0187	0.0038	0.0000	0.0000
8	3.71	0.05	0.05	0.07	5.90	1.05	1.85	0.00	-0.00833	0.0000	0.0000	0.0000	0.0158	0.0038	0.0000	0.0000
9	4.43	0.06	0.06	0.09	5.06	0.85	1.85	0.00	-0.00822	0.0000	0.0000	0.0000	0.0139	0.0038	0.0000	0.0000
10	5.15	0.07	0.07	0.11	4.21	0.72	1.85	0.00	-0.00809	0.0000	0.0000	0.0000	0.0120	0.0038	0.0000	0.0000
11	5.87	0.08	0.08	0.14	3.36	0.55	1.85	0.00	-0.00797	0.0000	0.0000	0.0000	0.0102	0.0038	0.0000	0.0000
12	6.65	0.09	0.09	0.17	2.50	0.40	1.85	0.00	-0.00786	0.0000	0.0000	0.0000	0.0084	0.0038	0.0000	0.0000
13	7.48	0.10	0.10	0.20	1.64	0.25	1.85	0.00	-0.00776	0.0000	0.0000	0.0000	0.0066	0.0038	0.0000	0.0000
14	8.36	0.11	0.11	0.23	0.78	0.10	1.85	0.00	-0.00767	0.0000	0.0000	0.0000	0.0049	0.0038	0.0000	0.0000
15	9.29	0.12	0.12	0.26	0.00	0.00	1.85	0.00	-0.00759	0.0000	0.0000	0.0000	0.0031	0.0038	0.0000	0.0000
16	10.27	0.13	0.13	0.29	0.00	0.00	1.85	0.00	-0.00752	0.0000	0.0000	0.0000	0.0013	0.0038	0.0000	0.0000
17	11.30	0.14	0.14	0.32	0.00	0.00	1.85	0.00	-0.00746	0.0000	0.0000	0.0000	0.0000	0.0038	0.0000	0.0000
18	12.37	0.15	0.15	0.35	0.00	0.00	1.85	0.00	-0.00741	0.0000	0.0000	0.0000	0.0000	0.0038	0.0000	0.0000
19	13.49	0.16	0.16	0.38	0.00	0.00	1.85	0.00	-0.00737	0.0000	0.0000	0.0000	0.0000	0.0038	0.0000	0.0000
20	14.65	0.17	0.17	0.41	0.00	0.00	1.85	0.00	-0.00734	0.0000	0.0000	0.0000	0.0000	0.0038	0.0000	0.0000
21	15.85	0.18	0.18	0.44	0.00	0.00	1.85	0.00	-0.00732	0.0000	0.0000	0.0000	0.0000	0.0038	0.0000	0.0000
22	17.10	0.19	0.19	0.47	0.00	0.00	1.85	0.00	-0.00731	0.0000	0.0000	0.0000	0.0000	0.0038	0.0000	0.0000
23	18.39	0.20	0.20	0.50	0.00	0.00	1.85	0.00	-0.00731	0.0000	0.0000	0.0000	0.0000	0.0038	0.0000	0.0000
24	19.73	0.21	0.21	0.53	0.00	0.00	1.85	0.00	-0.00731	0.0000	0.0000	0.0000	0.0000	0.0038	0.0000	0.0000
25	21.12	0.22	0.22	0.56	0.00	0.00	1.85	0.00	-0.00732	0.0000	0.0000	0.0000	0.0000	0.0038	0.0000	0.0000
26	22.56	0.23	0.23	0.59	0.00	0.00	1.85	0.00	-0.00733	0.0000	0.0000	0.0000	0.0000	0.0038	0.0000	0.0000
27	24.05	0.24	0.24	0.62	0.00	0.00	1.85	0.00	-0.00734	0.0000	0.0000	0.0000	0.0000	0.0038	0.0000	0.0000
28	25.59	0.25	0.25	0.65	0.00	0.00	1.85	0.00	-0.00735	0.0000	0.0000	0.0000	0.0000	0.0038	0.0000	0.0000
29	27.18	0.26	0.26	0.68	0.00	0.00	1.85	0.00	-0.00736	0.0000	0.0000	0.0000	0.0000	0.0038	0.0000	0.0000
30	28.82	0.27	0.27	0.71	0.00	0.00	1.85	0.00	-0.00737	0.0000	0.0000	0.0000	0.0000	0.0038	0.0000	0.0000
31	30.51	0.28	0.28	0.74	0.00	0.00	1.85	0.00	-0.00738	0.0000	0.0000	0.0000	0.0000	0.0038	0.0000	0.0000
32	32.25	0.29	0.29	0.77	0.00	0.00	1.85	0.00	-0.00739	0.0000	0.0000	0.0000	0.0000	0.0038	0.0000	0.0000
33	34.04	0.30	0.30	0.80	0.00	0.00	1.85	0.00	-0.00740	0.0000	0.0000	0.0000	0.0000	0.0038	0.0000	0.0000
34	35.88	0.31	0.31	0.83	0.00	0.00	1.85	0.00	-0.00741	0.0000	0.0000	0.0000	0.0000	0.0038	0.0000	0.0000
35	37.77	0.32	0.32	0.86	0.00	0.00	1.85	0.00	-0.00742	0.0000	0.0000	0.0000	0.0000	0.0038	0.0000	0.0000
36	39.71	0.33	0.33	0.89	0.00	0.00	1.85	0.00	-0.00743	0.0000	0.0000	0.0000	0.0000	0.0038	0.0000	0.0000
37	41.70	0.34	0.34	0.92	0.00	0.00	1.85	0.00	-0.00744	0.0000	0.0000	0.0000	0.0000	0.0038	0.0000	0.0000
38	43.74	0.35	0.35	0.95	0.00	0.00	1.85	0.00	-0.00745	0.0000	0.0000	0.0000	0.0000	0.0038	0.0000	0.0000
39	45.83	0.36	0.36	0.98	0.00	0.00	1.85	0.00	-0.00746	0.0000	0.0000	0.0000	0.0000	0.0038	0.0000	0.0000
40	47.97	0.37	0.37	1.01	0.00	0.00	1.85	0.00	-0.00747	0.0000	0.0000	0.0000	0.0000	0.0038	0.0000	0.0000
41	50.16	0.38	0.38	1.04	0.00	0.00	1.85	0.00	-0.00748	0.0000	0.0000	0.0000	0.0000	0.0038	0.0000	0.0000
42	52.40	0.39	0.39	1.07	0.00	0.00	1.85	0.00	-0.00749	0.0000	0.0000	0.0000	0.0000	0.0038	0.0000	0.0000
43	54.69	0.40	0.40	1.10	0.00	0.00	1.85	0.00	-0.00750	0.0000	0.0000	0.0000	0.0000	0.0038	0.0000	0.0000
44	57.03	0.41	0.41	1.13	0.00	0.00	1.85	0.00	-0.00751	0.0000	0.0000	0.0000	0.0000	0.0038	0.0000	0.0000
45	59.42	0.42	0.42	1.16	0.00	0.00	1.85	0.00	-0.00752	0.0000	0.0000	0.0000	0.0000	0.0038	0.0000	0.0000
46	61.86	0.43	0.43	1.19	0.00	0.00	1.85	0.00	-0.00753	0.0000	0.0000	0.0000	0.0000	0.0038	0.0000	0.0000
47	64.35	0.44	0.44	1.22	0.00	0.00	1.85	0.00	-0.00754	0.0000	0.0000	0.0000	0.0000	0.0038	0.0000	0.0000
48	66.89	0.45	0.45	1.25	0.00	0.00	1.85	0.00	-0.00755	0.0000	0.0000	0.0000	0.0000	0.0038	0.0000	0.0000
49	69.48	0.46	0.46	1.28	0.00	0.00	1.85	0.00	-0.00756	0.0000	0.0000	0.0000	0.0000	0.0038	0.0000	0.0000
50	72.12	0.47	0.47	1.31	0.00	0.00	1.85	0.00	-0.00757	0.0000	0.0000	0.0000	0.0000	0.0038	0.0000	0.0000
51	74.81	0.48	0.48	1.34	0.00	0.00	1.85	0.00	-0.00758	0.0000	0.0000	0.0000	0.0000	0.0038	0.0000	0.0000
52	77.55	0.49	0.49	1.37	0.00	0.00	1.85	0.00	-0.00759	0.0000	0.0000	0.0000	0.0000	0.0038	0.0000	0.0000
53	80.34	0.50	0.50	1.40	0.00	0.00	1.85	0.00	-0.00760	0.0000	0.0000	0.0000	0.0000	0.0038	0.0000	0.0000
54	83.18	0.51	0.51	1.43	0.00	0.00	1.85	0.00	-0.00761	0.0000	0.0000	0.0000	0.0000	0.0038	0.0000	0.0000
55	86.07	0.52	0.52	1.46	0.00	0.00	1.85	0.00	-0.00762	0.0000	0.0000	0.0000	0.0000	0.0038	0.0000	0.0000
56	89.01	0.53	0.53	1.49	0.00	0.00	1.85	0.00	-0.00763	0.0000	0.0000	0.0000	0.0000	0.0038	0.0000	0.0000
57	92.00	0.54	0.54	1.52	0.00	0.00	1.85	0.00	-0.00764	0.0000	0.0000	0.0000	0.0000	0.0038	0.0000	0.0000
58	95.04	0.55	0.55	1.55	0.00	0.00	1.85	0.00	-0.00765	0.0000	0.0000	0.0000	0.0000	0.0038	0.0000	0.0000
59	98.13	0.56	0.56	1.58	0.00	0.00	1.85	0.00	-0.00766	0.0000	0.0000	0.0000	0.0000	0.0038	0.0000	0.0000
60	101.27	0.57	0.57	1.61	0.00	0.00	1.85	0.00	-0.00767	0.0000	0.0000	0.0000	0.0000	0.0038	0.0000	0.0000
61	104.46	0.58	0.58	1.64	0.00	0.00	1.85	0.00	-0.00768	0.0000	0.0000	0.0000	0.0000	0.0038	0.0000	0.0000
62	107.70	0.59	0.59	1.67	0.00	0.00	1.85	0.00	-0.00769	0.0000	0.0000	0.0000	0.0000	0.0038	0.0000	0.0000
63	111.00	0.60	0.60	1.70	0.00	0.00	1.85	0.00	-0.00770	0.0000	0.0000	0.0000	0.0000	0.0038	0.0000	0.0000
64	114.35	0.61	0.61	1.73	0.00	0.00	1.85	0.00	-0.00771	0.0000	0.0000	0.0000	0.0000	0.0038	0.0000	0.0000
65	117.75	0.62	0.62	1.76	0.00	0.00	1.85	0.00	-0.00772	0.0000	0.0000	0.0000	0.0000	0.0038	0.0000	0.0000
66	121.20	0.63	0.63	1.79	0.00	0.00	1.85	0.00	-0.00773	0.0000	0.0000	0.0000	0.0000	0.0038	0.0000	0.0000
67	124.70	0.64	0.64	1.82	0.00	0.00	1.85	0.00	-0.00774	0.0000	0.0000	0.0000	0.0000	0.0038	0.0000	0.0000
68	128.25	0.65	0.65	1.85	0.00	0.00	1.85	0.00	-0.00775	0.0000	0.0000	0.0000	0.0000	0.0038	0.0000	0.0000
69	131.85	0.66	0.66	1.88	0.00	0.00	1.85	0.00	-0.00776	0.0000	0.0000	0.0000	0.0000	0.0038	0	

POS	S (M)	QX	QY	BX (M)	BY (M)	AX	AY	EX (M)	EXP	EY (M)	EYP	XCC (MM)	DXCO (MM)	YCO (MM)	DYCO (MM)
150 SD	67.14	1.31	1.30	5.83	13.23	-.76	1.58	1.35001	.14917	0.000000	0.000000	6.7437	-.7443	0.0000	0.0000
151 O	67.87	1.32	1.31	7.10	11.10	-.96	1.39	1.45971	-.14917	0.000000	0.000000	7.2910	-.7443	0.0000	0.0000
152 B	69.54	1.35	1.34	11.03	7.14	-1.41	-.79	1.78589	-.24394	0.000000	0.000000	8.9186	1.2182	0.0000	0.0000
153 O	70.27	1.36	1.36	13.24	5.84	-1.61	-.78	1.96529	-.24394	0.000000	0.000000	9.8145	1.2182	0.0000	0.0000
154 SF	70.27	1.36	1.36	13.24	5.84	-1.59	.77	1.96529	-.24125	0.000000	0.000000	9.8145	1.2115	0.0000	0.0000
155 OS	70.57	1.37	1.37	14.22	5.40	-1.67	-.69	2.03767	-.24125	0.000000	0.000000	10.1779	1.2115	0.0000	0.0000
156 QF	70.92	1.37	1.38	14.81	5.16	-.00	-.00	2.08009	-.000002	0.000000	0.000000	10.3910	-.0002	0.0000	0.0000
157 QF	71.27	1.37	1.39	14.22	5.40	1.66	-.69	2.03765	-.24128	0.000000	0.000000	10.1781	-1.2110	0.0000	0.0000
158 NS	71.57	1.38	1.40	13.24	5.84	1.59	-.77	1.96527	-.24128	0.000000	0.000000	9.8147	-1.2110	0.0000	0.0000
159 SF	71.57	1.38	1.40	13.24	5.84	1.61	-.78	1.96527	-.24398	0.000000	0.000000	9.8147	-1.2178	0.0000	0.0000
160 O	72.31	1.39	1.41	11.02	7.14	1.41	-.99	1.78584	-.24398	0.000000	0.000000	8.9192	-1.2178	0.0000	0.0000
161 B	73.97	1.42	1.44	7.10	11.10	.96	-1.39	1.45961	-.14920	0.000000	0.000000	7.2923	-.7438	0.0000	0.0000
162 O	74.70	1.44	1.45	5.83	13.28	.76	-1.58	1.34986	-.14920	0.000000	0.000000	6.7453	-.7438	0.0000	0.0000
163 SD	74.70	1.44	1.45	5.83	13.28	.75	-1.56	1.34989	-.14727	0.000000	0.000000	6.7453	-.7390	0.0000	0.0000
164 OS	75.00	1.44	1.46	5.41	14.24	.67	-1.64	1.30571	-.14727	0.000000	0.000000	6.5236	-.7390	0.0000	0.0000
165 QD	75.35	1.46	1.46	5.18	14.82	-.01	-.00	1.27398	-.000002	0.000000	0.000000	6.3946	.0003	0.0000	0.0000
166 QD	75.71	1.47	1.47	5.42	14.25	-.69	1.63	1.30569	.14722	0.000000	0.000000	6.5238	.7397	0.0000	0.0000
167 OS	76.01	1.47	1.47	5.86	13.29	-.77	1.55	1.34986	.14722	0.000000	0.000000	6.7457	.7397	0.0000	0.0000
168 SD	76.01	1.47	1.47	5.86	13.29	-.78	1.57	1.34986	.14915	0.000000	0.000000	6.7457	.7445	0.0000	0.0000
169 B	76.74	1.49	1.48	7.15	11.12	-.98	1.38	1.45955	-.14915	0.000000	0.000000	7.2932	.7445	0.0000	0.0000
170 B	78.40	1.52	1.51	11.16	7.17	-1.44	.98	1.78570	.24393	0.000000	0.000000	8.9211	1.2184	0.0000	0.0000
171 O	79.14	1.53	1.53	13.42	5.88	-1.64	.78	1.96510	.24393	0.000000	0.000000	9.8172	1.2184	0.0000	0.0000
172 SF	79.14	1.53	1.53	13.42	5.88	-1.62	-.77	1.96510	.24123	0.000000	0.000000	9.8172	1.2117	0.0000	0.0000
173 OS	79.44	1.54	1.53	14.42	5.44	-1.70	-.69	2.03747	-.24123	0.000000	0.000000	10.1807	1.2117	0.0000	0.0000
174 QF	79.79	1.54	1.55	15.02	5.20	-.01	-.00	2.07989	-.000001	0.000000	0.000000	10.3938	.0001	0.0000	0.0000
175 QF	80.14	1.54	1.56	14.43	5.44	1.69	-.70	2.03746	-.24125	0.000000	0.000000	10.1808	-1.2115	0.0000	0.0000
176 OS	80.44	1.55	1.56	13.44	5.87	1.61	-.78	1.96509	-.24125	0.000000	0.000000	9.8174	-1.2115	0.0000	0.0000
177 SF	80.44	1.55	1.56	13.44	5.87	1.62	-.79	1.96509	-.24394	0.000000	0.000000	9.8174	-1.2182	0.0000	0.0000
178 O	81.17	1.56	1.58	11.20	7.20	1.42	-.99	1.78568	-.24394	0.000000	0.000000	8.9214	-1.2182	0.0000	0.0000
179 B	82.84	1.59	1.61	7.22	11.19	-.98	-1.39	1.45950	-.14917	0.000000	0.000000	7.2939	-.7443	0.0000	0.0000
180 O	83.57	1.60	1.62	5.93	13.38	.78	-1.59	1.34980	-.14917	0.000000	0.000000	6.7465	-.7443	0.0000	0.0000
181 SD	83.57	1.60	1.62	5.93	13.38	-.77	-1.57	1.34980	-.14724	0.000000	0.000000	6.7465	-.7394	0.0000	0.0000
182 OS	83.87	1.61	1.62	5.40	14.33	-.69	-1.65	1.30563	-.14724	0.000000	0.000000	6.5247	-.7394	0.0000	0.0000
183 QD	84.22	1.62	1.63	5.25	14.33	-.00	.00	1.27991	.000000	0.000000	0.000000	6.3955	-.0000	0.0000	0.0000
184 REFL	168.44	3.24	3.26	17.79	5.90	-.00	.00	-0.01098	.000000	0.000000	0.000000	-0.0244	0.0000	0.0000	0.0000

CIRCUMFERENCE = 505.3227 M THETX = 6.28318638 RAD NUX = 9.73195 DNUX/(DP/P) = .41404
(DS/S)/RAD789 = .8871863 M THETY(183) = 0.00000000 RAD NUY = 9.77196 DNUY/(DP/P) = .36832
TGAM = (7.63240, 0.00000)

MAXIMA --- BETX(134) = 17.78972 BETY(12) = 17.13421 ETAX(120) = 2.08030 ETAY(184) = 0.00000
MINIMA --- BETX(36) = 4.09089 BETY(48) = 3.30098 ETAX(33) = -.00003 ETAY(184) = 0.00000

*** INCR 1 77 DP 005000 VALUE = .010000

SUB. CHR , ITER. 7

CALCULATION OF THE EQUILIBRIUM ORBIT AND BETATRON FUNCTIONS OF AGR .

INITIAL REFERENCE RAY DEFINED BY V

X = -.0032944 DX = 0.00000000 Y = 0.00000000 DY = 0.00000000 DS = 0.00000000 DP/P = .01000000 1.00000000

7X7 MATRIX FOR AGR

.03399034	17.72745044	0.00000000	0.00000000	0.00000000	-.02078433	.00010538
-.05634456	.03398034	0.00000000	0.00000000	0.00000000	-.00121228	.00000615
0.00000000	0.00000000	-.05047040	6.04994201	0.00000000	0.00000000	0.00000000
0.00000000	0.00000000	-.16486980	-.05047040	0.00000000	0.00000000	0.00000000
.00121228	.02078433	0.00000000	0.00000000	1.00000000	-2.90377804	-.02793087
0.00000000	0.00000000	0.00000000	0.00000000	0.00000000	1.00000000	0.00000000
0.00000000	0.00000000	0.00000000	0.00000000	0.00000000	0.00000000	1.00000000

EIGENVALUES OF THE 4X4 SUBMATRIX

X... LMD1 = (.03398034 .99942250), C(1) = 1.00000000, MU(1) = 1.53680944 RAD, Q(1) = .73377246
 I/LMD1 = (.03398034 -.99942250), C(2) = 1.00000000, MU(2) = -1.53680944 RAD, Q(2) = .26622754
 Y... LMD3 = (-.05047040 .99872556), C(3) = 1.00000000, MU(3) = 1.62128818 RAD, Q(3) = .77410808
 I/LMD3 = (-.05047040 -.99872556), C(4) = 1.00000000, MU(4) = -1.62128818 RAD, Q(4) = .22589192

EIGENVALUE = (.03398034, -.99942250), EIGENVECTOR = (4.21161417, 0.00000000)
 (0.00000000, .23743845)
 (0.00000000, 0.00000000)
 (0.00000000, 0.00000000)

EIGENVALUE = (-.03398034, -.99942250), EIGENVECTOR = (4.21161417, 0.00000000)
 (0.00000000, -.23743845)
 (0.00000000, 0.00000000)
 (0.00000000, 0.00000000)

EIGENVALUE = (-.05047040, .99872556), EIGENVECTOR = (0.00000000, 0.00000000)
 (0.00000000, 0.00000000)
 (2.46123184, 0.00000000)
 (.00000000, .40630061)

EIGENVALUE = (-.05047040, -.99872556), EIGENVECTOR = (0.00000000, 0.00000000)
 (0.00000000, 0.00000000)
 (2.46123184, 0.00000000)
 (.00000000, -.40630061)

	X	DX	Y	DY	DS	DP/P	
EQ ORBIT	-.00010986	0.00000000	0.00000000	0.00000000	0.00000000	.01000000	1.00000000
ETA ORBIT	-.02151543	-.00000000	0.00000000	0.00000000	0.00000000	1.00000000	0.00000000

EIGENVECTORS 1 AND 3 IN POLAR COORDINATES

POS	X1	X2	X3	OX1	OX2	OX3	Y1	Y2	Y3
0	4.211614	0.000000	0.000000	1.570796	0.000000	0.000000	0.000000	0.000000	0.000000
	0.000000	0.000000	0.000000	0.000000	2.461232	0.000000	0.000000	0.000000	0.000000
								0.000000	1.570796

BETAatron FUNCTIONS OF AGE

POS	(M)	QY	AX	AY	EX	EXP	EM	EYP	XFC	RACD	YCD	BYCD
0	0.00	0.00	0.00	0.00	0.00	0.00000	0.000000	0.000000	0.00000	0.0000	0.0000	0.0000
1	0.35	0.01	2.23	0.88	0.2152	0.00278	0.000000	0.000000	0.00000	0.0000	0.0000	0.0000
2	0.72	0.02	4.46	1.76	0.4304	0.00556	0.000000	0.000000	0.00000	0.0000	0.0000	0.0000
3	1.07	0.03	6.69	2.64	0.6456	0.00834	0.000000	0.000000	0.00000	0.0000	0.0000	0.0000
4	1.42	0.04	8.92	3.52	0.8608	0.01112	0.000000	0.000000	0.00000	0.0000	0.0000	0.0000
5	1.77	0.05	11.15	4.40	1.0760	0.01390	0.000000	0.000000	0.00000	0.0000	0.0000	0.0000
6	2.12	0.06	13.38	5.28	1.2912	0.01668	0.000000	0.000000	0.00000	0.0000	0.0000	0.0000
7	2.47	0.07	15.61	6.16	1.5064	0.01946	0.000000	0.000000	0.00000	0.0000	0.0000	0.0000
8	2.82	0.08	17.84	7.04	1.7216	0.02224	0.000000	0.000000	0.00000	0.0000	0.0000	0.0000
9	3.17	0.09	20.07	7.92	1.9368	0.02502	0.000000	0.000000	0.00000	0.0000	0.0000	0.0000
10	3.52	0.10	22.30	8.80	2.1520	0.02780	0.000000	0.000000	0.00000	0.0000	0.0000	0.0000
11	3.87	0.11	24.53	9.68	2.3672	0.03058	0.000000	0.000000	0.00000	0.0000	0.0000	0.0000
12	4.22	0.12	26.76	10.56	2.5824	0.03336	0.000000	0.000000	0.00000	0.0000	0.0000	0.0000
13	4.57	0.13	28.99	11.44	2.7976	0.03614	0.000000	0.000000	0.00000	0.0000	0.0000	0.0000
14	4.92	0.14	31.22	12.32	3.0128	0.03892	0.000000	0.000000	0.00000	0.0000	0.0000	0.0000
15	5.27	0.15	33.45	13.20	3.2280	0.04170	0.000000	0.000000	0.00000	0.0000	0.0000	0.0000
16	5.62	0.16	35.68	14.08	3.4432	0.04448	0.000000	0.000000	0.00000	0.0000	0.0000	0.0000
17	5.97	0.17	37.91	14.96	3.6584	0.04726	0.000000	0.000000	0.00000	0.0000	0.0000	0.0000
18	6.32	0.18	40.14	15.84	3.8736	0.05004	0.000000	0.000000	0.00000	0.0000	0.0000	0.0000
19	6.67	0.19	42.37	16.72	4.0888	0.05282	0.000000	0.000000	0.00000	0.0000	0.0000	0.0000
20	7.02	0.20	44.60	17.60	4.3040	0.05560	0.000000	0.000000	0.00000	0.0000	0.0000	0.0000
21	7.37	0.21	46.83	18.48	4.5192	0.05838	0.000000	0.000000	0.00000	0.0000	0.0000	0.0000
22	7.72	0.22	49.06	19.36	4.7344	0.06116	0.000000	0.000000	0.00000	0.0000	0.0000	0.0000
23	8.07	0.23	51.29	20.24	4.9496	0.06394	0.000000	0.000000	0.00000	0.0000	0.0000	0.0000
24	8.42	0.24	53.52	21.12	5.1648	0.06672	0.000000	0.000000	0.00000	0.0000	0.0000	0.0000
25	8.77	0.25	55.75	22.00	5.3800	0.06950	0.000000	0.000000	0.00000	0.0000	0.0000	0.0000
26	9.12	0.26	57.98	22.88	5.5952	0.07228	0.000000	0.000000	0.00000	0.0000	0.0000	0.0000
27	9.47	0.27	60.21	23.76	5.8104	0.07506	0.000000	0.000000	0.00000	0.0000	0.0000	0.0000
28	9.82	0.28	62.44	24.64	6.0256	0.07784	0.000000	0.000000	0.00000	0.0000	0.0000	0.0000
29	10.17	0.29	64.67	25.52	6.2408	0.08062	0.000000	0.000000	0.00000	0.0000	0.0000	0.0000
30	10.52	0.30	66.90	26.40	6.4560	0.08340	0.000000	0.000000	0.00000	0.0000	0.0000	0.0000
31	10.87	0.31	69.13	27.28	6.6712	0.08618	0.000000	0.000000	0.00000	0.0000	0.0000	0.0000
32	11.22	0.32	71.36	28.16	6.8864	0.08896	0.000000	0.000000	0.00000	0.0000	0.0000	0.0000
33	11.57	0.33	73.59	29.04	7.1016	0.09174	0.000000	0.000000	0.00000	0.0000	0.0000	0.0000
34	11.92	0.34	75.82	29.92	7.3168	0.09452	0.000000	0.000000	0.00000	0.0000	0.0000	0.0000
35	12.27	0.35	78.05	30.80	7.5320	0.09730	0.000000	0.000000	0.00000	0.0000	0.0000	0.0000
36	12.62	0.36	80.28	31.68	7.7472	0.10008	0.000000	0.000000	0.00000	0.0000	0.0000	0.0000
37	12.97	0.37	82.51	32.56	7.9624	0.10286	0.000000	0.000000	0.00000	0.0000	0.0000	0.0000
38	13.32	0.38	84.74	33.44	8.1776	0.10564	0.000000	0.000000	0.00000	0.0000	0.0000	0.0000
39	13.67	0.39	86.97	34.32	8.3928	0.10842	0.000000	0.000000	0.00000	0.0000	0.0000	0.0000
40	14.02	0.40	89.20	35.20	8.6080	0.11120	0.000000	0.000000	0.00000	0.0000	0.0000	0.0000
41	14.37	0.41	91.43	36.08	8.8232	0.11398	0.000000	0.000000	0.00000	0.0000	0.0000	0.0000
42	14.72	0.42	93.66	36.96	9.0384	0.11676	0.000000	0.000000	0.00000	0.0000	0.0000	0.0000
43	15.07	0.43	95.89	37.84	9.2536	0.11954	0.000000	0.000000	0.00000	0.0000	0.0000	0.0000
44	15.42	0.44	98.12	38.72	9.4688	0.12232	0.000000	0.000000	0.00000	0.0000	0.0000	0.0000
45	15.77	0.45	100.35	39.60	9.6840	0.12510	0.000000	0.000000	0.00000	0.0000	0.0000	0.0000
46	16.12	0.46	102.58	40.48	9.8992	0.12788	0.000000	0.000000	0.00000	0.0000	0.0000	0.0000
47	16.47	0.47	104.81	41.36	10.1144	0.13066	0.000000	0.000000	0.00000	0.0000	0.0000	0.0000
48	16.82	0.48	107.04	42.24	10.3296	0.13344	0.000000	0.000000	0.00000	0.0000	0.0000	0.0000
49	17.17	0.49	109.27	43.12	10.5448	0.13622	0.000000	0.000000	0.00000	0.0000	0.0000	0.0000
50	17.52	0.50	111.50	44.00	10.7600	0.13900	0.000000	0.000000	0.00000	0.0000	0.0000	0.0000

POS		S	OX	OY	OX	OY	AX	AY	EX	EXP	EY	EYP	XCO	DXCO	YCO	DYCO
		(M)			(M)	(M)			(M)		(M)		(MM)	(MM)	(MM)	(MM)
100	SF	43.67	.86	.85	13.12	5.76	-1.56	.77	1.96028	.23823	0.000000	0.000000	19.5557	2.4009	0.0000	0.0000
101	OS	43.97	.85	.86	14.08	5.33	-1.64	.66	2.03175	.23823	0.000000	0.000000	20.2759	2.4009	0.0000	0.0000
102	QF	44.32	.87	.87	14.66	5.09	-.00	.00	2.07367	.00009	0.000000	0.000000	20.6982	.0001	0.0000	0.0000
103	QF	44.67	.87	.88	14.08	5.33	1.64	-.68	2.03181	-.23806	0.000000	0.000000	20.2760	-2.4008	0.0000	0.0000
104	OS	44.97	.87	.89	13.11	5.76	1.57	-.78	1.96039	-.23806	0.000000	0.000000	19.5557	-2.4008	0.0000	0.0000
105	SF	44.97	.87	.89	13.11	5.76	1.60	-.78	1.96039	-.24338	0.000000	0.000000	19.5557	-2.4274	0.0000	0.0000
106	O	45.71	.88	.91	10.91	7.05	1.40	-.98	1.78140	-.24338	0.000000	0.000000	17.7705	-1.4843	0.0000	0.0000
107	B	47.37	.71	.94	7.00	11.02	.92	-1.39	1.45546	-.14909	0.000000	0.000000	14.5248	-1.4843	0.0000	0.0000
108	O	48.11	.93	.95	5.75	13.21	.75	-1.59	1.34381	-.14909	0.000000	0.000000	13.4332	-1.4843	0.0000	0.0000
109	SD	48.11	.93	.95	5.75	13.21	.73	-1.55	1.34581	-.14529	0.000000	0.000000	13.4332	-1.4653	0.0000	0.0000
110	OS	48.61	.94	.95	5.33	14.16	-.65	-1.63	1.30223	-.14529	0.000000	0.000000	12.9936	-1.4653	0.0000	0.0000
111	QD	48.76	.95	.96	5.11	14.74	-.02	-.01	1.27687	.00013	0.000000	0.000000	12.7377	-.0001	0.0000	0.0000
112	QD	49.11	.96	.96	5.36	14.17	-.69	1.61	1.30232	-.14555	0.000000	0.000000	12.9937	1.4655	0.0000	0.0000
113	OS	49.41	.97	.96	5.79	13.23	-.77	1.53	1.34598	-.14555	0.000000	0.000000	13.4333	1.4655	0.0000	0.0000
114	SD	49.41	.97	.96	5.79	13.23	-.79	1.57	1.34598	-.14935	0.000000	0.000000	13.4333	1.4845	0.0000	0.0000
115	O	50.14	.99	.97	7.10	11.06	-.99	1.38	1.45582	-.14935	0.000000	0.000000	14.5251	1.4845	0.0000	0.0000
116	QD	51.81	1.02	1.00	11.16	7.83	-.46	-.98	1.78221	-.24364	0.000000	0.000000	17.7711	-2.4276	0.0000	0.0000
117	QD	52.54	1.03	1.02	13.46	5.84	-1.66	.78	1.96140	-.24364	0.000000	0.000000	19.5564	-2.4276	0.0000	0.0000
118	SF	52.84	1.03	1.02	13.46	5.84	-1.62	.76	1.96140	-.23833	0.000000	0.000000	19.5564	-2.4010	0.0000	0.0000
119	OS	52.84	1.03	1.03	14.45	5.40	-1.70	-.68	2.03290	-.23833	0.000000	0.000000	20.2767	2.4010	0.0000	0.0000
120	QF	53.19	1.04	1.04	15.07	5.17	-.02	-.01	2.07482	.00005	0.000000	0.000000	20.6950	-.0000	0.0000	0.0000
121	QF	53.56	1.04	1.05	14.48	5.42	1.67	-.70	2.03293	-.23824	0.000000	0.000000	20.2768	-2.4009	0.0000	0.0000
122	OS	53.84	1.04	1.06	13.50	5.86	1.59	-.78	1.96146	-.23824	0.000000	0.000000	19.5565	-2.4009	0.0000	0.0000
123	SF	53.84	1.04	1.06	13.50	5.86	1.63	-.80	1.96146	-.24355	0.000000	0.000000	19.5565	-2.4276	0.0000	0.0000
124	QF	54.58	1.05	1.08	11.24	7.19	1.43	-1.01	1.78234	-.24355	0.000000	0.000000	17.7712	-2.4276	0.0000	0.0000
125	O	56.24	1.98	1.11	7.23	11.23	.98	-1.41	1.45610	-.14926	0.000000	0.000000	14.5252	-1.4845	0.0000	0.0000
126	B	56.97	1.10	1.12	5.94	13.45	.78	-1.61	1.34632	-.14926	0.000000	0.000000	13.4335	-1.4845	0.0000	0.0000
127	SD	56.97	1.10	1.12	5.94	13.45	.77	-1.57	1.34632	-.14546	0.000000	0.000000	13.4335	-1.4654	0.0000	0.0000
128	OS	57.27	1.11	1.12	5.50	14.62	.69	-1.65	1.30269	-.14546	0.000000	0.000000	12.9939	-1.4654	0.0000	0.0000
129	QD	57.63	1.12	1.12	5.27	15.00	-.00	-.00	1.27728	.00000	0.000000	0.000000	12.7379	.0000	0.0000	0.0000
130	QD	57.98	1.13	1.13	5.50	14.42	-.69	1.65	1.30269	-.14847	0.000000	0.000000	12.9939	1.4654	0.0000	0.0000
131	OS	58.28	1.14	1.13	5.94	13.45	-.77	1.57	1.34633	-.14547	0.000000	0.000000	13.4335	1.4654	0.0000	0.0000
132	SD	58.28	1.14	1.13	5.94	13.45	-.78	1.61	1.34633	-.14927	0.000000	0.000000	13.4335	1.4845	0.0000	0.0000
133	O	59.01	1.15	1.14	7.24	11.23	-.98	1.41	1.45611	-.14927	0.000000	0.000000	14.5253	1.4845	0.0000	0.0000
134	B	60.67	1.18	1.17	11.26	7.20	-1.44	1.00	1.78237	-.24356	0.000000	0.000000	17.7712	-2.4276	0.0000	0.0000
135	O	61.41	1.19	1.19	13.52	5.87	-1.64	-.80	1.96149	-.24356	0.000000	0.000000	19.5565	-2.4276	0.0000	0.0000
136	SF	61.41	1.19	1.19	13.52	5.87	-1.60	-.78	1.96149	-.23824	0.000000	0.000000	19.5565	-2.4009	0.0000	0.0000
137	OS	61.71	1.20	1.20	14.50	5.42	1.68	-.70	2.03296	-.23824	0.000000	0.000000	20.2768	-2.4009	0.0000	0.0000
138	QF	62.06	1.20	1.21	15.09	5.18	.02	-.01	2.07486	-.00004	0.000000	0.000000	20.6950	-.0000	0.0000	0.0000
139	QF	62.41	1.20	1.22	14.48	5.41	1.71	-.68	2.03294	-.23833	0.000000	0.000000	20.2768	-2.4010	0.0000	0.0000
140	OS	62.71	1.21	1.23	13.48	5.84	1.63	-.76	1.96144	-.23833	0.000000	0.000000	19.5565	-2.4010	0.0000	0.0000
141	SF	62.71	1.21	1.23	13.48	5.84	1.66	-.78	1.96144	-.24364	0.000000	0.000000	19.5565	-2.4276	0.0000	0.0000
142	O	63.44	1.22	1.24	11.19	7.14	1.46	-.98	1.78225	-.24364	0.000000	0.000000	17.7711	-2.4276	0.0000	0.0000
143	B	65.11	1.25	1.27	7.12	11.08	.99	-1.38	1.45586	-.14935	0.000000	0.000000	14.5251	-1.4845	0.0000	0.0000
144	O	65.84	1.27	1.28	5.81	13.25	.79	-1.57	1.34602	-.14935	0.000000	0.000000	13.4333	-1.4845	0.0000	0.0000
145	SD	65.84	1.27	1.28	5.81	13.25	.77	-1.53	1.34602	-.14555	0.000000	0.000000	13.4333	-1.4655	0.0000	0.0000
146	OS	66.14	1.27	1.29	5.37	14.19	.69	-1.61	1.30236	-.14555	0.000000	0.000000	12.9937	-1.4655	0.0000	0.0000
147	QD	66.49	1.28	1.29	5.12	14.76	-.02	-.01	1.27691	-.00013	0.000000	0.000000	12.7377	-.0001	0.0000	0.0000
148	QD	66.84	1.30	1.30	5.34	14.18	-.65	1.63	1.30227	-.14529	0.000000	0.000000	12.9936	1.4653	0.0000	0.0000
149	OS	67.14	1.30	1.30	5.76	13.22	-.73	1.55	1.34586	-.14529	0.000000	0.000000	13.4332	1.4653	0.0000	0.0000

CALCULATION OF THE EQUILIBRIUM ORBIT AND BETATRON FUNCTIONS OF AGR

INITIAL REFERENCE RAY DEFINED BY V

X = .00010986 DX = 0.00000000 Y = 0.00000000 DY = 0.00000000 DS = 0.00000000 DP/P = .01500000 1.00000000

7X7 MATRIX FOR AGR

.03040808	17.66739186	0.00000000	0.00000000	0.00000000	-0.03146645	.00024846
-.05654271	.03040808	0.00000000	0.00000000	0.00000000	-.00183500	.00001449
0.00000000	0.00000000	-.05505360	6.20894356	0.00000000	0.00000000	0.00000000
0.00000000	0.00000000	-.16056984	-.05505360	0.00000000	0.00000000	0.00000000
.00183500	.03146645	0.00000000	0.00000000	1.00000000	-2.91613147	-.04127261
0.00000000	0.00000000	0.00000000	0.00000000	0.00000000	1.00000000	0.00000000
0.00000000	0.00000000	0.00000000	0.00000000	0.00000000	0.00000000	1.00000000

EIGENVALUES OF THE 4X4 SUBMATRIX

X... LMD1 = { .03040808, .99953757 }, C(1) = 1.00000000, MU(1) = -1.54038355 RAD, Q(1) = .73547897
 1/LMD1 = { .03040808, -.99953757 }, C(2) = 1.00000000, MU(2) = -1.54038355 RAD, Q(2) = .26452103
 Y... LMD3 = { -.05505360, .99848340 }, C(3) = 1.00000000, MU(3) = -1.62587778 RAD, Q(3) = .77629945
 1/LMD3 = { -.05505360, -.99848340 }, C(4) = 1.00000000, MU(4) = -1.62587778 RAD, Q(4) = .22370055

EIGENVALUE = (.03040808, .99953757), EIGENVECTOR = { 4.20446983, 0.00000000 }
 { 0.00000000, .23784212 }
 { 0.00000000, 0.00000000 }
 { 0.00000000, 0.00000000 }

EIGENVALUE = (.03040808, -.99953757), EIGENVECTOR = { 4.20446983, 0.00000000 }
 { 0.00000000, -.23784212 }
 { 0.00000000, 0.00000000 }
 { 0.00000000, 0.00000000 }

EIGENVALUE = (-.05505360, .99848340), EIGENVECTOR = { 0.00000000, 0.00000000 }
 { 0.00000000, 0.00000000 }
 { 2.49366685, .00000000 }
 { .00000000, .40101588 }

EIGENVALUE = (-.05505360, -.99848340), EIGENVECTOR = { 0.00000000, 0.00000000 }
 { 0.00000000, 0.00000000 }
 { 2.49366685, -.00000000 }
 { .00000000, -.40101588 }

	X	DX	Y	DY	DS	DP/P
EO ORBIT	-.00024288	0.00000000	0.00000000	0.00000000	0.00000000	.01500000
ETA ORBIT	-.03249329	-.00000000	0.00000000	0.00000000	0.00000000	1.00000000

EIGENVECTORS 1 AND 3 IN POLAR COORDINATES

POS	X1	X2	X3	DX1	DX2	DX3	Y1	Y2	Y3
0	4.204470	0.000000	0.000000	1.570796	0.000000	0.000000	0.000000	0.000000	0.000000
	0.000000	0.000000	0.000000	0.000000	2.4993667	0.000000	0.000000	0.000000	1.570796

POS	Z	S	CV	OY	BX	UY	AX	AV	FX	EXP	EY	EYP	XCD	DXCD	YCD	DYCD
50	Z	0	39	0	15	17	1.95	-.79	.0152	-.00136	0	0	1	-.0110	0	0
51	Z	18	39	0	17	14	1.84	-.97	-.0103	-.00136	0	0	1	-.0110	0	0
52	Z	19	39	0	17	14	1.72	-.97	-.0103	-.00136	0	0	1	-.0110	0	0
53	Z	19	39	0	17	14	1.72	-.97	-.0103	-.00136	0	0	1	-.0110	0	0
54	Z	19	39	0	17	14	1.49	-.83	-.00956	-.00136	0	0	1	-.0110	0	0
55	Z	20	44	0	9	14	1.38	-.69	-.01907	-.00136	0	0	1	-.0110	0	0
56	Z	21	44	0	9	14	1.26	-.68	-.01958	-.00136	0	0	1	-.0110	0	0
57	Z	21	44	0	9	14	1.15	-.68	-.01909	-.00136	0	0	1	-.0110	0	0
58	Z	21	44	0	9	14	1.04	-.68	-.01760	-.00136	0	0	1	-.0110	0	0
59	Z	21	44	0	9	14	1.04	-.68	-.01711	-.00136	0	0	1	-.0110	0	0
60	QD3	22	44	0	5	14	1.25	-.79	-.01701	-.00097	0	0	1	-.0110	0	0
61	QD3	22	44	0	5	14	1.25	-.79	-.01701	-.00097	0	0	1	-.0110	0	0
62	QD3	22	44	0	5	14	1.25	-.79	-.01701	-.00097	0	0	1	-.0110	0	0
63	QD3	22	44	0	5	14	1.25	-.79	-.01701	-.00097	0	0	1	-.0110	0	0
64	QD3	22	44	0	5	14	1.25	-.79	-.01701	-.00097	0	0	1	-.0110	0	0
65	QD3	22	44	0	5	14	1.25	-.79	-.01701	-.00097	0	0	1	-.0110	0	0
66	QD3	22	44	0	5	14	1.25	-.79	-.01701	-.00097	0	0	1	-.0110	0	0
67	QD3	22	44	0	5	14	1.25	-.79	-.01701	-.00097	0	0	1	-.0110	0	0
68	QD3	22	44	0	5	14	1.25	-.79	-.01701	-.00097	0	0	1	-.0110	0	0
69	QD3	22	44	0	5	14	1.25	-.79	-.01701	-.00097	0	0	1	-.0110	0	0
70	QD3	22	44	0	5	14	1.25	-.79	-.01701	-.00097	0	0	1	-.0110	0	0
71	QD3	22	44	0	5	14	1.25	-.79	-.01701	-.00097	0	0	1	-.0110	0	0
72	QD3	22	44	0	5	14	1.25	-.79	-.01701	-.00097	0	0	1	-.0110	0	0
73	QD3	22	44	0	5	14	1.25	-.79	-.01701	-.00097	0	0	1	-.0110	0	0
74	QD3	22	44	0	5	14	1.25	-.79	-.01701	-.00097	0	0	1	-.0110	0	0
75	QD3	22	44	0	5	14	1.25	-.79	-.01701	-.00097	0	0	1	-.0110	0	0
76	QD3	22	44	0	5	14	1.25	-.79	-.01701	-.00097	0	0	1	-.0110	0	0
77	QD3	22	44	0	5	14	1.25	-.79	-.01701	-.00097	0	0	1	-.0110	0	0
78	QD3	22	44	0	5	14	1.25	-.79	-.01701	-.00097	0	0	1	-.0110	0	0
79	QD3	22	44	0	5	14	1.25	-.79	-.01701	-.00097	0	0	1	-.0110	0	0
80	QD3	22	44	0	5	14	1.25	-.79	-.01701	-.00097	0	0	1	-.0110	0	0
81	QD3	22	44	0	5	14	1.25	-.79	-.01701	-.00097	0	0	1	-.0110	0	0
82	QD3	22	44	0	5	14	1.25	-.79	-.01701	-.00097	0	0	1	-.0110	0	0
83	QD3	22	44	0	5	14	1.25	-.79	-.01701	-.00097	0	0	1	-.0110	0	0
84	QD3	22	44	0	5	14	1.25	-.79	-.01701	-.00097	0	0	1	-.0110	0	0
85	QD3	22	44	0	5	14	1.25	-.79	-.01701	-.00097	0	0	1	-.0110	0	0
86	QD3	22	44	0	5	14	1.25	-.79	-.01701	-.00097	0	0	1	-.0110	0	0
87	QD3	22	44	0	5	14	1.25	-.79	-.01701	-.00097	0	0	1	-.0110	0	0
88	QD3	22	44	0	5	14	1.25	-.79	-.01701	-.00097	0	0	1	-.0110	0	0
89	QD3	22	44	0	5	14	1.25	-.79	-.01701	-.00097	0	0	1	-.0110	0	0
90	QD3	22	44	0	5	14	1.25	-.79	-.01701	-.00097	0	0	1	-.0110	0	0

POS	S	OX	OY	OX	OY	AX	AY	EX	EXP	EY	EYP	XCG	DXCG	YCG	DYCG	
	(M)			(M)	(M)			(M)		(M)		(MM)	(MR)	(MM)	(MR)	
100	SF	43.67	-.95	.85	13.00	5.64	-1.54	.76	1.95553	.23520	0.000000	0.000000	29.2243	3.5699	0.0000	0.0000
101	OS	43.97	-.96	.86	13.94	5.25	-1.61	-.67	2.02609	.23520	0.000000	0.000000	30.2953	3.5699	0.0000	0.0000
102	OF	44.32	-.86	-.87	14.52	5.01	-.00	-.00	2.06748	.00010	0.000000	0.000000	30.9232	-.0006	0.0000	0.0000
103	OF	44.67	-.87	-.88	13.94	5.24	1.62	-.67	2.02616	-.23499	0.000000	0.000000	30.2957	-3.5688	0.0000	0.0000
104	OS	44.97	-.87	-.89	12.99	5.67	1.54	-.75	1.95567	-.23499	0.000000	0.000000	29.2250	-3.5688	0.0000	0.0000
105	SF	44.97	-.87	-.89	12.99	5.67	1.60	-.77	1.95567	-.24286	0.000000	0.000000	29.2250	-3.6280	0.0000	0.0000
106	O	45.71	-.88	-.91	10.79	6.96	1.40	-.98	1.77706	-.24286	0.000000	0.000000	28.5569	-3.6280	0.0000	0.0000
107	O	47.37	-.91	-.94	6.91	10.92	.94	-1.39	1.45127	-.14905	0.000000	0.000000	21.7019	-2.2205	0.0000	0.0000
108	O	48.11	-.93	-.95	5.67	13.12	.74	-1.59	1.34165	-.14905	0.000000	0.000000	20.0650	-2.2205	0.0000	0.0000
109	SD	48.11	-.93	-.95	5.67	13.12	.72	-1.53	1.34165	-.14343	0.000000	0.000000	20.0690	-2.1781	0.0000	0.0000
110	OS	48.41	-.94	-.95	5.26	14.06	-.64	-1.61	1.29862	-.14343	0.000000	0.000000	19.4155	-2.1781	0.0000	0.0000
111	OD	48.76	-.95	-.95	5.05	14.64	-.02	-.02	1.27359	.00016	0.000000	0.000000	19.0332	-.0009	0.0000	0.0000
112	OD	49.11	-.96	-.96	5.29	14.09	-.69	1.58	1.29873	.14376	0.000000	0.000000	19.4161	2.1799	0.0000	0.0000
113	OS	49.41	-.97	-.96	5.73	13.15	-.77	1.31	1.34186	.14376	0.000000	0.000000	20.0701	2.1799	0.0000	0.0000
114	SD	49.41	-.97	-.96	5.73	13.15	-.79	1.56	1.34186	.14938	0.000000	0.000000	20.0701	2.2222	0.0000	0.0000
115	O	50.14	-.99	-.97	7.05	10.99	1.00	1.37	1.45172	.14938	0.000000	0.000000	21.7043	2.2222	0.0000	0.0000
116	O	51.84	1.00	1.00	11.16	7.08	1.47	-.97	1.77805	.24319	0.000000	0.000000	26.5622	3.6297	0.0000	0.0000
117	O	52.58	1.03	1.02	13.48	5.80	1.68	-.77	1.95690	.24319	0.000000	0.000000	26.5636	3.6297	0.0000	0.0000
118	SF	52.58	1.03	1.02	13.48	5.80	1.63	-.75	1.95690	.23532	0.000000	0.000000	26.5636	3.5705	0.0000	0.0000
119	OS	52.84	1.03	1.03	14.49	5.37	1.71	-.67	2.02750	.23532	0.000000	0.000000	30.3028	3.5705	0.0000	0.0000
120	OF	53.19	1.03	1.04	15.10	5.15	-.03	-.02	2.06890	.00006	0.000000	0.000000	30.9307	-.0003	0.0000	0.0000
121	OF	53.54	1.04	1.05	14.52	5.40	1.66	-.70	2.02754	-.23520	0.000000	0.000000	30.3030	-3.5699	0.0000	0.0000
122	OS	53.84	1.04	1.06	13.55	5.84	1.58	-.79	1.95698	-.23520	0.000000	0.000000	29.2320	-3.5699	0.0000	0.0000
123	SF	53.84	1.04	1.06	13.55	5.84	1.64	-.81	1.95698	-.24307	0.000000	0.000000	29.2320	-3.6291	0.0000	0.0000
124	OF	54.58	1.05	1.08	11.28	7.19	1.44	-1.02	1.77821	-.24307	0.000000	0.000000	26.5630	-3.6291	0.0000	0.0000
125	O	56.24	1.08	1.10	7.25	11.29	-.99	-1.43	1.45206	-.14927	0.000000	0.000000	21.7062	-2.2216	0.0000	0.0000
126	O	56.98	1.10	1.11	5.95	13.54	.79	-1.63	1.34229	-.14927	0.000000	0.000000	20.0723	-2.2216	0.0000	0.0000
127	SD	56.98	1.10	1.11	5.95	13.54	.76	-1.37	1.34229	-.14364	0.000000	0.000000	20.0723	-2.1793	0.0000	0.0000
128	OS	57.28	1.11	1.12	5.51	14.51	.68	-1.65	1.29919	-.14364	0.000000	0.000000	19.4185	-2.1793	0.0000	0.0000
129	OD	57.63	1.12	1.12	5.28	15.03	-.00	-.00	1.27411	.00001	0.000000	0.000000	19.0379	-.0000	0.0000	0.0000
130	OD	57.98	1.13	1.13	5.32	14.51	-.69	1.65	1.29920	.14367	0.000000	0.000000	19.4186	2.1793	0.0000	0.0000
131	OS	58.28	1.13	1.13	5.95	13.54	-.77	1.57	1.34230	.14367	0.000000	0.000000	20.0724	2.1793	0.0000	0.0000
132	SD	58.28	1.13	1.13	5.95	13.54	-.79	1.63	1.34230	.14929	0.000000	0.000000	20.0724	2.2217	0.0000	0.0000
133	O	59.01	1.15	1.14	7.27	11.30	-.99	1.43	1.45209	.14929	0.000000	0.000000	21.7063	2.2217	0.0000	0.0000
134	O	60.68	1.19	1.17	11.32	7.20	-1.45	1.02	1.77827	.24310	0.000000	0.000000	26.5633	3.6292	0.0000	0.0000
135	O	61.41	1.19	1.19	13.60	5.86	-1.65	.81	1.95705	.24310	0.000000	0.000000	26.5633	3.6292	0.0000	0.0000
136	SF	61.41	1.19	1.19	13.60	5.86	-1.59	.79	1.95705	.23522	0.000000	0.000000	26.5633	3.5700	0.0000	0.0000
137	OS	61.71	1.19	1.19	14.58	5.41	-1.67	.70	2.02762	.23522	0.000000	0.000000	30.3033	3.5700	0.0000	0.0000
138	OF	62.06	1.20	1.20	15.16	5.17	-.02	-.02	2.06899	-.00003	0.000000	0.000000	30.9311	-.0003	0.0000	0.0000
139	OF	62.41	1.20	1.22	14.55	5.39	1.71	-.67	2.02759	-.23532	0.000000	0.000000	30.3031	-3.5705	0.0000	0.0000
140	OS	62.71	1.21	1.22	13.54	5.82	1.63	-.75	1.95699	-.23532	0.000000	0.000000	29.2320	-3.5705	0.0000	0.0000
141	SF	62.71	1.21	1.22	13.54	5.82	1.69	-.75	1.95699	-.24319	0.000000	0.000000	29.2320	-3.6297	0.0000	0.0000
142	O	63.45	1.22	1.24	11.21	7.10	-1.48	-.98	1.77815	-.24319	0.000000	0.000000	26.5626	-3.6297	0.0000	0.0000
143	O	63.11	1.24	1.27	7.08	11.03	1.01	-1.38	1.45181	-.14938	0.000000	0.000000	21.7047	-2.2222	0.0000	0.0000
144	O	65.85	1.26	1.28	5.76	13.20	.80	-1.57	1.34195	-.14938	0.000000	0.000000	20.0704	-2.2222	0.0000	0.0000
145	SD	65.95	1.26	1.28	5.76	13.20	.77	-1.51	1.34195	-.14376	0.000000	0.000000	20.0704	-2.1799	0.0000	0.0000
146	OS	66.15	1.27	1.29	5.32	14.13	.69	-1.59	1.29882	-.14376	0.000000	0.000000	19.4165	-2.1799	0.0000	0.0000
147	OD	66.50	1.28	1.29	5.07	14.69	-.02	-.02	1.27369	.00015	0.000000	0.000000	19.0355	-.0008	0.0000	0.0000
148	OD	66.85	1.29	1.29	5.28	14.11	-.64	1.62	1.29871	.14345	0.000000	0.000000	19.4159	2.1782	0.0000	0.0000
149	OS	67.15	1.30	1.30	5.69	13.16	-.72	1.54	1.34175	.14345	0.000000	0.000000	20.0694	2.1782	0.0000	0.0000

POS	SD	QX	QY	QZ	AX	AY	EXP	EY	EYP	XCI	DMCO	YCY	RYCO
150	SD	130	130	130	74	1.60	1.907	0.000000	0.000000	30.000000	3.5689	0.0000	0.0000
151	SD	132	131	130	30	1.30	1.4588	0.000000	0.000000	26.700000	3.5689	0.0000	0.0000
152	SD	133	132	130	34	1.30	1.4588	0.000000	0.000000	26.700000	3.5689	0.0000	0.0000
153	SD	134	133	130	34	1.30	1.4588	0.000000	0.000000	26.700000	3.5689	0.0000	0.0000
154	SD	135	134	130	34	1.30	1.4588	0.000000	0.000000	26.700000	3.5689	0.0000	0.0000
155	SD	136	135	130	34	1.30	1.4588	0.000000	0.000000	26.700000	3.5689	0.0000	0.0000
156	SD	137	136	130	34	1.30	1.4588	0.000000	0.000000	26.700000	3.5689	0.0000	0.0000
157	SD	138	137	130	34	1.30	1.4588	0.000000	0.000000	26.700000	3.5689	0.0000	0.0000
158	SD	139	138	130	34	1.30	1.4588	0.000000	0.000000	26.700000	3.5689	0.0000	0.0000
159	SD	140	139	130	34	1.30	1.4588	0.000000	0.000000	26.700000	3.5689	0.0000	0.0000
160	SD	141	140	130	34	1.30	1.4588	0.000000	0.000000	26.700000	3.5689	0.0000	0.0000
161	SD	142	141	130	34	1.30	1.4588	0.000000	0.000000	26.700000	3.5689	0.0000	0.0000
162	SD	143	142	130	34	1.30	1.4588	0.000000	0.000000	26.700000	3.5689	0.0000	0.0000
163	SD	144	143	130	34	1.30	1.4588	0.000000	0.000000	26.700000	3.5689	0.0000	0.0000
164	SD	145	144	130	34	1.30	1.4588	0.000000	0.000000	26.700000	3.5689	0.0000	0.0000
165	SD	146	145	130	34	1.30	1.4588	0.000000	0.000000	26.700000	3.5689	0.0000	0.0000
166	SD	147	146	130	34	1.30	1.4588	0.000000	0.000000	26.700000	3.5689	0.0000	0.0000
167	SD	148	147	130	34	1.30	1.4588	0.000000	0.000000	26.700000	3.5689	0.0000	0.0000
168	SD	149	148	130	34	1.30	1.4588	0.000000	0.000000	26.700000	3.5689	0.0000	0.0000
169	SD	150	149	130	34	1.30	1.4588	0.000000	0.000000	26.700000	3.5689	0.0000	0.0000
170	SD	151	150	130	34	1.30	1.4588	0.000000	0.000000	26.700000	3.5689	0.0000	0.0000
171	SD	152	151	130	34	1.30	1.4588	0.000000	0.000000	26.700000	3.5689	0.0000	0.0000
172	SD	153	152	130	34	1.30	1.4588	0.000000	0.000000	26.700000	3.5689	0.0000	0.0000
173	SD	154	153	130	34	1.30	1.4588	0.000000	0.000000	26.700000	3.5689	0.0000	0.0000
174	SD	155	154	130	34	1.30	1.4588	0.000000	0.000000	26.700000	3.5689	0.0000	0.0000
175	SD	156	155	130	34	1.30	1.4588	0.000000	0.000000	26.700000	3.5689	0.0000	0.0000
176	SD	157	156	130	34	1.30	1.4588	0.000000	0.000000	26.700000	3.5689	0.0000	0.0000
177	SD	158	157	130	34	1.30	1.4588	0.000000	0.000000	26.700000	3.5689	0.0000	0.0000
178	SD	159	158	130	34	1.30	1.4588	0.000000	0.000000	26.700000	3.5689	0.0000	0.0000
179	SD	160	159	130	34	1.30	1.4588	0.000000	0.000000	26.700000	3.5689	0.0000	0.0000
180	SD	161	160	130	34	1.30	1.4588	0.000000	0.000000	26.700000	3.5689	0.0000	0.0000
181	SD	162	161	130	34	1.30	1.4588	0.000000	0.000000	26.700000	3.5689	0.0000	0.0000
182	SD	163	162	130	34	1.30	1.4588	0.000000	0.000000	26.700000	3.5689	0.0000	0.0000
183	SD	164	163	130	34	1.30	1.4588	0.000000	0.000000	26.700000	3.5689	0.0000	0.0000
184	REFL	165	164	130	34	1.30	1.4588	0.000000	0.000000	26.700000	3.5689	0.0000	0.0000

CIRCUMFERENCE = 505.413 M THEX = 6.2831858 RAD NUX = 9.72518 DMUX/10P/PI = .45114
 (DS 3)/100000 THETX = (7.80070, 0.00000) NUY = 9.72518 DMUY/10P/PI = .41418
 MAXIMA --- BETX(184) = 17.67732 BETY(184) = 3.52012 ETAX(184) = 2.06839 ETAY(184) = 0.00000
 MINIMA --- BETX(184) = 17.67732 BETY(184) = 3.52012 ETAX(184) = 2.06839 ETAY(184) = 0.00000
 SUB. FILE: 9

CALCULATION OF THE EQUILIBRIUM ORBIT AND BETATRON FUNCTIONS OF AGR

INITIAL REFERENCE RAY DEFINED BY V
 X = -.00024288 DX = 0.00000000 Y = 0.00000000 DY = 0.00000000 DS = 0.00000000 DP/P = .02000000 1.00000000

7X7 MATRIX FOR AGR

.02705862	17.60331730	0.00000000	0.00000000	0.00000000	-.04255458	.00046025
-.05675588	.02705862	0.00000000	0.00000000	0.00000000	-.00248283	.00002685
0.00000000	0.00000000	-.05972548	6.36568879	0.00000000	0.00000000	0.00000000
0.00000000	0.00000000	-.15653182	-.05972548	0.00000000	0.00000000	0.00000000
.00243283	.04255458	0.00000000	0.00000000	1.00000000	-2.92858206	-.05421840
0.00000000	0.00000000	0.00000000	0.00000000	0.00000000	1.00000000	0.00000000
0.00000000	0.00000000	0.00000000	0.00000000	0.00000000	0.00000000	1.00000000

EIGENVALUES OF THE 4X4 SUBMATRIX

X... LMD1 = (.02705862, .99963385), C(1) = 1.00000000, MU(1) = 1.54373440 RAD, Q(1) = .73707888
 I/LMD1 = (.02705862, -.99963385), C(2) = 1.00000000, MU(2) = -1.54373440 RAD, Q(2) = .26292112
 Y... LMD3 = (-.05972548, .99821484), C(3) = 1.00000000, MU(3) = 1.63055738 RAD, Q(3) = .77653380
 I/LMD3 = (-.05972548, -.99821484), C(4) = 1.00000000, MU(4) = -1.63055738 RAD, Q(4) = .22146620

EIGENVALUE = (.02705862, .99963385), EIGENVECTOR = (4.19639907, -.00000000)
 (0.00000000, .23829955)
 (0.00000000, 0.00000000)
 (0.00000000, 0.00000000)

EIGENVALUE = (.02705862, -.99963385), EIGENVECTOR = (4.19639907, .00000000)
 (0.00000000, -.23829955)
 (0.00000000, 0.00000000)
 (0.00000000, 0.00000000)

EIGENVALUE = (-.05972548, .99821484), EIGENVECTOR = (0.00000000, 0.00000000)
 (0.00000000, 0.00000000)
 (2.52528669, 0.00000000)
 (-.00000000, .39599464)

EIGENVALUE = (-.05972548, -.99821484), EIGENVECTOR = (0.00000000, 0.00000000)
 (0.00000000, 0.00000000)
 (2.52528669, 0.00000000)
 (-.00000000, -.39599464)

	X	DX	Y	DY	DS	DP/P
EO ORBIT	-.00042983	0.00000000	0.00000000	0.00000000	0.00000000	.02000000 1.00000000
ETA ORBIT	-.04373807	-.00000000	0.00000000	0.00000000	0.00000000	1.00000000 0.00000000

POS	S	TX	QY	BX	BY	AX	AY	EX	EXP	EY	EYP	XCO	DXCO	YCO	DYCO
	(M)			(M)	(M)			(M)		(M)		(MM)	(MM)	(MM)	(MM)
50 Z	18.50	.31	.39	15.10	4.15	1.94	-.80	.02347	-.00169	0.000000	0.000000	.2869	-.0185	0.0000	0.0000
51 Z	18.86	.39	.40	13.74	4.77	1.82	-.94	.02786	-.00169	0.000000	0.000000	.2802	-.0185	0.0000	0.0000
52 Z	19.22	.39	.41	12.47	5.50	1.71	-1.08	.02725	-.00169	0.000000	0.000000	.2736	-.0185	0.0000	0.0000
53 Z	19.58	.39	.42	11.28	6.36	1.60	-1.23	.02664	-.00169	0.000000	0.000000	.2669	-.0185	0.0000	0.0000
54 Z	19.95	.40	.43	10.17	7.27	1.48	-1.37	.02603	-.00169	0.000000	0.000000	.2602	-.0185	0.0000	0.0000
55 Z	20.31	.40	.44	9.14	8.31	1.37	-1.51	.02542	-.00169	0.000000	0.000000	.2535	-.0185	0.0000	0.0000
56 Z	20.67	.41	.45	8.19	9.45	1.26	-1.65	.02481	-.00169	0.000000	0.000000	.2468	-.0185	0.0000	0.0000
57 Z	21.03	.42	.45	7.33	10.70	1.14	-1.80	.02420	-.00169	0.000000	0.000000	.2401	-.0185	0.0000	0.0000
58 Z	21.39	.42	.46	6.54	12.04	1.03	-1.94	.02359	-.00169	0.000000	0.000000	.2335	-.0185	0.0000	0.0000
59 Z	21.75	.43	.46	5.84	13.43	.92	-2.08	.02298	-.00169	0.000000	0.000000	.2268	-.0185	0.0000	0.0000
60 QD3	22.16	.45	.47	5.44	14.50	.08	-.30	.02289	.00128	0.000000	0.000000	.2253	.0111	0.0000	0.0000
61 QD3	22.58	.46	.47	5.70	13.98	-.73	1.54	.02405	.00433	0.000000	0.000000	.2361	.0414	0.0000	0.0000
62 R	22.94	.47	.48	6.27	12.88	-.83	1.45	.02564	.00433	0.000000	0.000000	.2512	.0414	0.0000	0.0000
63 R	23.31	.48	.48	6.91	11.85	-.93	1.36	.02723	.00433	0.000000	0.000000	.2664	.0414	0.0000	0.0000
64 R	23.69	.48	.49	7.63	10.88	-1.02	1.28	.02882	.00433	0.000000	0.000000	.2816	.0414	0.0000	0.0000
65 R	24.04	.49	.49	8.41	9.98	-1.12	1.19	.03041	.00433	0.000000	0.000000	.2967	.0414	0.0000	0.0000
66 R	24.41	.50	.50	9.27	9.14	-1.22	1.10	.03200	.00433	0.000000	0.000000	.3119	.0414	0.0000	0.0000
67 R	24.78	.50	.50	10.21	8.36	-1.32	1.01	.03359	.00433	0.000000	0.000000	.3271	.0414	0.0000	0.0000
68 R	25.14	.51	.51	11.21	7.66	-1.42	.92	.03518	.00433	0.000000	0.000000	.3422	.0414	0.0000	0.0000
69 R	25.51	.52	.52	12.29	7.01	-1.52	.83	.03677	.00433	0.000000	0.000000	.3572	.0414	0.0000	0.0000
70 R	25.88	.52	.53	13.43	6.43	-1.62	.74	.03836	.00433	0.000000	0.000000	.3726	.0414	0.0000	0.0000
71 R	26.24	.52	.54	14.66	5.92	-1.71	.66	.03995	.00433	0.000000	0.000000	.3878	.0414	0.0000	0.0000
72 QF	26.59	.53	.55	15.27	5.52	-.02	-.08	.04066	-.00030	0.000000	0.000000	.3943	-.0040	0.0000	0.0000
73 QF	26.94	.53	.56	14.68	6.04	1.68	-.83	.03974	-.00492	0.000000	0.000000	.3810	-.0492	0.0000	0.0000
74 QF	27.98	.54	.58	11.48	8.06	1.41	-1.12	.03465	-.00492	0.000000	0.000000	.3340	-.0492	0.0000	0.0000
75 R	29.64	.57	.61	7.52	12.47	-.98	-1.52	.10393	.08848	0.000000	0.000000	1.8010	1.8188	0.0000	0.0000
76 QD	30.63	.60	.62	5.78	15.90	.71	-1.80	.19555	.08848	0.000000	0.000000	3.6842	1.8188	0.0000	0.0000
77 QD	31.03	.61	.62	5.53	16.54	.00	-.00	.23098	.11206	0.000000	0.000000	4.3992	2.2746	0.0000	0.0000
78 QD	31.39	.62	.63	5.78	15.90	-.71	1.81	.27461	.14000	0.000000	0.000000	5.2854	2.8210	0.0000	0.0000
79 QD	32.41	.64	.64	7.52	12.44	-.98	1.53	.41957	.14000	0.000000	0.000000	8.2103	2.8210	0.0000	0.0000
80 R	34.07	.67	.66	11.47	8.01	-1.41	1.12	.72947	.23333	0.000000	0.000000	14.4395	4.6883	0.0000	0.0000
81 R	34.81	.68	.68	13.68	6.51	-1.60	.92	.90108	.23333	0.000000	0.000000	17.8874	4.6883	0.0000	0.0000
82 SF	34.81	.68	.68	13.68	6.51	-1.56	.90	.90108	.23113	0.000000	0.000000	17.8874	4.6663	0.0000	0.0000
83 SF	35.11	.68	.69	14.64	6.00	-1.64	.82	.97042	.23113	0.000000	0.000000	19.2813	4.6663	0.0000	0.0000
84 QF	35.46	.69	.70	15.20	5.69	-.05	.07	1.03170	.11729	0.000000	0.000000	20.5223	2.3566	0.0000	0.0000
85 QF	35.81	.69	.71	14.57	5.90	1.74	-.66	1.05212	-.00119	0.000000	0.000000	20.9282	-.0483	0.0000	0.0000
86 OS	36.11	.69	.71	13.55	6.32	1.66	-.74	1.05176	-.00119	0.000000	0.000000	20.9138	-.0483	0.0000	0.0000
87 SF	36.41	.69	.71	13.55	6.32	1.70	-.75	1.05176	-.00420	0.000000	0.000000	20.9138	-.0784	0.0000	0.0000
88 D	36.85	.70	.73	11.21	7.56	1.48	-.94	1.04867	-.00420	0.000000	0.000000	20.8521	-.0784	0.0000	0.0000
89 LC	38.51	.73	.76	7.07	11.36	1.01	-1.35	1.04170	-.00420	0.000000	0.000000	20.7258	-.0784	0.0000	0.0000
90 D	39.24	.75	.77	5.73	13.48	.80	-1.53	1.03861	-.00420	0.000000	0.000000	20.6682	-.0784	0.0000	0.0000
91 SD	39.24	.75	.77	5.73	13.48	.78	-1.47	1.03861	.00025	0.000000	0.000000	20.6682	-.0337	0.0000	0.0000
92 OS	39.54	.76	.77	5.29	14.38	.69	-1.54	1.03868	.00025	0.000000	0.000000	20.6580	-.0337	0.0000	0.0000
93 QD	39.89	.77	.78	5.04	14.90	.03	.08	1.05302	.11620	0.000000	0.000000	21.0572	.3187	0.0000	0.0000
94 QD	40.24	.78	.78	5.25	14.27	-.62	1.65	1.12065	.23668	0.000000	0.000000	22.2943	4.7634	0.0000	0.0000
95 OS	40.54	.79	.78	5.65	13.28	-.70	1.61	1.19169	.23668	0.000000	0.000000	23.7233	4.7634	0.0000	0.0000
96 SO	40.54	.79	.78	5.65	13.28	-.73	1.68	1.19165	.24253	0.000000	0.000000	23.7233	4.8222	0.0000	0.0000
97 D	41.28	.81	.79	6.87	10.97	-.93	1.47	1.37002	.24253	0.000000	0.000000	27.2657	4.8222	0.0000	0.0000
98 LC	42.94	.84	.82	10.71	6.89	-1.38	.99	1.77273	.24253	0.000000	0.000000	35.2766	4.8222	0.0000	0.0000
99 D	43.67	.85	.84	12.89	5.59	-1.58	.78	1.95110	.24253	0.000000	0.000000	38.8230	4.8222	0.0000	0.0000

POS	S	JX	QY	HX	BY	AX	AY	EX	EXP	EY	EYP	XCD	DXCD	YCD	BYCD
	(M)			(M)	(M)			(M)		(M)		(MM)	(MM)	(MM)	(MM)
100 SF	43.67	.95	.94	12.87	5.57	-1.51	.75	1.95110	.23219	0.000000	0.000000	38.8230	4.7183	0.0000	0.0000
101 OS	43.97	.36	.85	12.87	5.16	-1.59	.66	2.02075	.23219	0.000000	0.000000	40.2385	4.7183	0.0000	0.0000
102 QF	44.32	.36	.86	14.38	4.93	0.01	.81	2.06262	.00007	0.000000	0.000000	41.0384	-0.0010	0.0000	0.0000
103 QF	44.67	.86	.87	13.81	5.13	1.60	-.65	2.02080	-.09205	0.000000	0.000000	40.2382	-4.7163	0.0000	0.0000
104 OS	44.97	.87	.88	12.87	5.57	1.52	-.74	1.95118	-.23205	0.000000	0.000000	38.8243	-4.7163	0.0000	0.0000
105 SF	44.97	.87	.88	12.87	5.57	1.59	-.77	1.95118	-.24240	0.000000	0.000000	38.8243	-4.8203	0.0000	0.0000
106 O	45.71	.88	.90	10.60	6.45	1.39	-.97	1.77292	-.24240	0.000000	0.000000	35.2793	-4.8203	0.0000	0.0000
107 R	47.37	.91	.93	6.81	10.81	.93	-1.39	1.44719	-.14907	0.000000	0.000000	26.6526	-2.9529	0.0000	0.0000
108 O	48.11	.93	.94	5.59	13.01	.73	-1.59	1.33756	-.14907	0.000000	0.000000	26.6519	-2.9529	0.0000	0.0000
109 SD	48.11	.93	.94	5.59	13.01	.70	-1.52	1.33756	-.14169	0.000000	0.000000	26.6519	-2.8786	0.0000	0.0000
110 OS	48.41	.94	.95	5.19	13.94	.62	-1.60	1.29505	-.14169	0.000000	0.000000	25.7883	-2.8786	0.0000	0.0000
111 QD	48.76	.95	.95	4.99	14.52	-.03	-.02	1.27033	.00011	0.000000	0.000000	25.2857	-.0016	0.0000	0.0000
112 QF	49.11	.96	.95	5.23	13.97	-.68	1.56	1.29513	-.14191	0.000000	0.000000	25.7894	2.8818	0.0000	0.0000
113 OS	49.41	.97	.96	5.67	13.06	-.77	1.48	1.33771	-.14191	0.000000	0.000000	26.6540	2.8818	0.0000	0.0000
114 SD	49.41	.97	.96	5.67	13.06	-.80	1.56	1.33771	-.14930	0.000000	0.000000	26.6540	2.9561	0.0000	0.0000
115 O	50.15	.99	.97	7.00	10.91	-1.01	1.36	1.44750	.14930	0.000000	0.000000	28.8280	2.9561	0.0000	0.0000
116 O	51.81	1.02	1.00	11.16	7.02	-1.49	.96	1.77361	.24263	0.000000	0.000000	35.2891	4.8233	0.0000	0.0000
117 SF	52.54	1.02	1.02	13.51	5.75	-1.70	.76	1.95204	.24263	0.000000	0.000000	38.8364	4.8233	0.0000	0.0000
118 SF	52.94	1.02	1.02	13.51	5.75	-1.63	.73	1.95204	.23227	0.000000	0.000000	38.8364	4.7194	0.0000	0.0000
119 OS	52.94	1.03	1.03	14.51	5.34	-1.71	.65	2.02172	.23227	0.000000	0.000000	40.2522	4.7194	0.0000	0.0000
120 QF	53.19	1.03	1.04	15.13	5.12	-.03	-.03	2.06260	-.00004	0.000000	0.000000	41.0823	-.0006	0.0000	0.0000
121 QF	53.55	1.04	1.05	14.56	5.38	1.65	-.71	2.02175	-.23219	0.000000	0.000000	40.2526	-4.7183	0.0000	0.0000
122 SF	53.89	1.04	1.06	13.59	5.83	1.57	-.79	1.95209	-.23219	0.000000	0.000000	38.8371	-4.7183	0.0000	0.0000
123 SF	53.89	1.04	1.06	13.59	5.83	1.65	-.82	1.95209	-.24263	0.000000	0.000000	38.8371	-4.8224	0.0000	0.0000
124 O	54.58	1.05	1.07	11.32	7.19	1.44	-1.03	1.77372	-.24255	0.000000	0.000000	35.2906	-4.8224	0.0000	0.0000
125 R	56.24	1.08	1.10	7.26	11.36	.00	-1.45	1.44775	-.14922	0.000000	0.000000	28.8314	-2.9550	0.0000	0.0000
126 O	56.98	1.10	1.11	5.95	13.65	.79	-1.86	1.33801	-.14922	0.000000	0.000000	26.6581	-2.9550	0.0000	0.0000
127 SD	57.28	1.10	1.11	5.95	13.65	.76	-1.88	1.33801	-.14183	0.000000	0.000000	26.6581	-2.8807	0.0000	0.0000
128 OS	57.28	1.10	1.12	5.52	14.62	.68	-1.86	1.33801	-.14183	0.000000	0.000000	26.7939	-2.8807	0.0000	0.0000
129 QD	57.63	1.11	1.12	5.29	15.21	.60	-.00	1.27069	.00001	0.000000	0.000000	25.2907	-.0001	0.0000	0.0000
130 QD	57.98	1.12	1.12	5.53	14.62	-.69	1.65	1.29547	.14185	0.000000	0.000000	25.7940	2.8809	0.0000	0.0000
131 OS	58.28	1.13	1.13	5.97	13.66	-.77	1.57	1.33803	.14185	0.000000	0.000000	26.6583	2.8809	0.0000	0.0000
132 SD	58.28	1.13	1.13	5.07	13.66	-.80	1.65	1.33803	.14924	0.000000	0.000000	26.6583	2.9552	0.0000	0.0000
133 O	59.02	1.15	1.14	7.29	11.33	-1.00	1.45	1.44778	.14924	0.000000	0.000000	28.8316	2.9552	0.0000	0.0000
134 R	60.68	1.18	1.17	11.37	7.22	-1.46	1.03	1.77379	.24257	0.000000	0.000000	35.2912	4.8226	0.0000	0.0000
135 O	61.42	1.19	1.18	13.68	5.86	-1.66	-.82	1.95218	.24257	0.000000	0.000000	38.8379	4.8226	0.0000	0.0000
136 SF	61.42	1.19	1.18	13.68	5.86	-1.59	-.79	1.95218	.23221	0.000000	0.000000	38.8379	4.7185	0.0000	0.0000
137 OS	61.72	1.19	1.19	14.66	5.41	-1.66	.71	2.02185	.23221	0.000000	0.000000	40.2534	4.7185	0.0000	0.0000
138 QF	62.07	1.20	1.20	15.24	5.16	.03	.02	2.06270	-.00003	0.000000	0.000000	41.0831	-.0005	0.0000	0.0000
139 QF	62.42	1.20	1.21	14.62	5.38	1.72	-.66	2.02183	-.23227	0.000000	0.000000	40.2531	-4.7194	0.0000	0.0000
140 OS	62.72	1.20	1.22	13.61	5.80	1.64	-.74	1.95214	-.23227	0.000000	0.000000	38.8373	-4.7194	0.0000	0.0000
141 SF	62.72	1.20	1.22	13.61	5.80	1.71	-.77	1.95214	-.24263	0.000000	0.000000	38.8373	-4.8235	0.0000	0.0000
142 QD	63.45	1.21	1.24	11.25	7.08	1.50	-.97	1.77371	-.24263	0.000000	0.000000	35.2899	-4.8235	0.0000	0.0000
143 R	65.11	1.24	1.27	7.06	10.99	1.02	-1.37	1.44761	-.14930	0.000000	0.000000	28.8289	-2.9561	0.0000	0.0000
144 O	65.85	1.26	1.28	5.71	13.15	.81	-1.56	1.33781	-.14930	0.000000	0.000000	26.6548	-2.9561	0.0000	0.0000
145 SD	65.95	1.26	1.28	5.71	13.15	.77	-1.49	1.33781	-.14191	0.000000	0.000000	26.6548	-2.8818	0.0000	0.0000
146 OS	66.15	1.27	1.28	5.27	14.07	.69	-1.56	1.29523	-.14191	0.000000	0.000000	25.7903	-2.8818	0.0000	0.0000
147 QD	66.50	1.28	1.29	5.02	14.61	.03	.03	1.27043	.00010	0.000000	0.000000	25.2866	-.0013	0.0000	0.0000
148 QD	66.85	1.29	1.29	5.23	14.01	-.62	1.61	1.29516	.14171	0.000000	0.000000	25.7892	2.8788	0.0000	0.0000
149 OS	67.15	1.30	1.29	5.62	13.09	-.70	1.53	1.33767	.14171	0.000000	0.000000	26.6529	2.8788	0.0000	0.0000

POS	S	OX	OY	BX	OY	AX	AY	EX	EXP	EY	EYP	XCO	DXCO	YCO	DYCO
(H)	(H)	(H)	(H)	(H)	(H)	(H)	(H)	(H)	(H)	(H)	(H)	(H)	(H)	(H)	(H)
150 SD	67.15	1.10	1.29	5.67	13.07	- .73	1.61	1.33767	-14910	0.000000	0.000000	26.6529	2.9531	0.0000	0.0000
151 D	67.89	1.12	1.30	6.84	10.87	- .93	1.41	1.44732	-14910	0.000000	0.000000	26.8247	2.9531	0.0000	0.0000
152 D	69.55	1.15	1.34	10.69	6.47	-1.38	.98	1.77309	-24242	0.000000	0.000000	35.2808	4.8203	0.0000	0.0000
153 D	70.29	1.16	1.35	12.88	5.98	-1.58	.77	1.95137	-24242	0.000000	0.000000	38.8259	4.8203	0.0000	0.0000
154 SF	70.29	1.16	1.35	12.88	5.58	-1.52	.74	1.95137	-23208	0.000000	0.000000	36.8259	4.7165	0.0000	0.0000
155 OS	70.59	1.16	1.36	13.81	5.16	-1.59	-.66	2.02100	-23208	0.000000	0.000000	40.2408	4.7165	0.0000	0.0000
156 QF	70.94	1.17	1.37	14.37	4.93	-1.00	-.00	2.06182	-20007	0.000000	0.000000	41.0701	-4.0010	0.0000	0.0000
157 QF	71.29	1.17	1.39	13.81	3.16	1.60	-.66	2.02075	-23221	0.000000	0.000000	40.2401	-4.7185	0.0000	0.0000
158 OS	71.59	1.18	1.39	12.87	3.37	1.52	-.74	1.95128	-23221	0.000000	0.000000	38.8246	-4.7185	0.0000	0.0000
159 SF	71.59	1.18	1.39	12.87	3.57	1.59	-.77	1.95128	-24256	0.000000	0.000000	38.8246	-4.8224	0.0000	0.0000
160 D	72.32	1.19	1.41	10.60	6.86	1.39	-.98	1.77290	-24256	0.000000	0.000000	35.2780	-4.8224	0.0000	0.0000
161 D	73.96	1.22	1.44	6.83	10.84	.93	-1.40	1.44691	-14923	0.000000	0.000000	28.8186	-2.9551	0.0000	0.0000
162 D	74.72	1.24	1.44	8.69	13.05	.73	-1.60	1.33716	-14923	0.000000	0.000000	26.6433	-2.9551	0.0000	0.0000
163 SD	74.72	1.24	1.44	8.69	13.05	.70	-1.53	1.33716	-14185	0.000000	0.000000	26.6433	-2.8808	0.0000	0.0000
164 OS	75.02	1.24	1.46	5.21	13.99	.62	-1.60	1.29461	-14185	0.000000	0.000000	25.7811	-2.8808	0.0000	0.0000
165 OD	75.37	1.26	1.46	5.00	14.56	-.03	-.02	1.26982	-00011	0.000000	0.000000	25.2776	-4.0015	0.0000	0.0000
166 OD	75.72	1.27	1.47	5.25	14.02	-.69	1.56	1.29453	-14163	0.000000	0.000000	25.7800	-2.8777	0.0000	0.0000
167 OS	76.02	1.28	1.47	5.69	13.11	-.77	1.49	1.33702	-14163	0.000000	0.000000	26.6433	-2.8777	0.0000	0.0000
168 SD	76.02	1.28	1.47	5.69	13.11	-.80	1.56	1.33702	-14901	0.000000	0.000000	26.6433	-2.9520	0.0000	0.0000
169 D	76.76	1.29	1.48	7.03	10.95	-1.02	1.37	1.44661	-14901	0.000000	0.000000	28.8143	-2.9520	0.0000	0.0000
170 B	78.42	1.52	1.51	11.20	7.05	-1.50	.97	1.77224	-24234	0.000000	0.000000	35.2685	4.8193	0.0000	0.0000
171 D	79.16	1.53	1.53	13.56	5.78	-1.71	.76	1.95047	-24234	0.000000	0.000000	38.8128	4.8193	0.0000	0.0000
172 SF	79.16	1.53	1.53	13.56	5.78	-1.63	-.73	1.95047	-23200	0.000000	0.000000	38.8128	4.7154	0.0000	0.0000
173 OS	79.46	1.54	1.54	14.56	5.36	-1.72	.65	2.02007	-23200	0.000000	0.000000	40.2274	4.7154	0.0000	0.0000
174 QF	79.81	1.54	1.55	15.19	5.14	-.03	-.02	2.06088	-00004	0.000000	0.000000	41.0566	-4.0005	0.0000	0.0000
175 QF	80.16	1.54	1.56	14.61	5.40	1.66	-.71	2.02004	-23207	0.000000	0.000000	40.2271	-4.7164	0.0000	0.0000
176 OS	80.46	1.55	1.57	13.64	5.85	1.58	-.79	1.95042	-23207	0.000000	0.000000	38.8121	-4.7164	0.0000	0.0000
177 SF	80.46	1.55	1.57	13.64	5.85	1.65	-.82	1.95042	-24241	0.000000	0.000000	38.8121	-4.8203	0.0000	0.0000
178 D	81.19	1.56	1.58	11.35	7.21	1.45	-1.03	1.77214	-24241	0.000000	0.000000	35.2671	-4.8203	0.0000	0.0000
179 B	82.86	1.59	1.61	7.28	11.37	1.00	-1.45	1.44640	-14908	0.000000	0.000000	28.8112	-2.9530	0.0000	0.0000
180 D	83.59	1.60	1.62	5.96	13.65	.80	-1.65	1.33676	-14908	0.000000	0.000000	26.6395	-2.9530	0.0000	0.0000
181 SD	83.59	1.60	1.62	5.96	13.65	.76	-1.58	1.33676	-14171	0.000000	0.000000	26.6395	-2.8788	0.0000	0.0000
182 OS	83.89	1.61	1.63	5.51	14.62	-.68	-1.65	1.29423	-14171	0.000000	0.000000	25.7759	-2.8788	0.0000	0.0000
183 OD	84.24	1.62	1.63	5.29	15.21	-.00	.00	1.26950	-00000	0.000000	0.000000	25.2730	-4.0000	0.0000	0.0000
184 REFL	158.48	3.25	3.26	17.61	6.38	.00	-.00	-0.04374	-00000	0.000000	0.000000	-4.4258	0.0000	0.0000	0.0000

CIRCUMFERENCE = 503.4538 M THEY(183) = 6.20313638 RAD NUX = 9.73708 DNUX/(DP/P) = .47056
TOS/31/RBY85 = .0028825 M TGAM = (7.58479, 0.00000) NUZ = 9.77853 DNUZ/(DP/P) = .28502
MAXIMA --- BETX(184) = 17.60977 BETY(12) = 17.91103 ETAX(138) = 2.06270 ETAY(184) = 0.00000
MINIMA --- BETX(36) = 4.20509 BETY(48) = 3.32724 ETAX(34) = .00063 ETAY(184) = 0.00000
*** INCR 1 // DP 0.00000 VALUE = -.020000
*** FIN Q 0 // CORE USE SUMMARY MAXIMUM USED UNUSED
STORE (ELEMENT STORAGE) 900 (LMAX) 1911
INFF (ELEMENT DEFINITIONS) 600 (IMAX) 79 7689
321

END OF SYNCH RUN DRSH
15.03.03.WY1111000.HP
15.03.03.JOB CLASS = P3, PRIORITY = HP.
15.03.03.USER,91046.
15.03.03.CHARGE,G112.

APPENDIX E

APPENDIX E

Synch Run

Accumulator Lattice

B O G KINETIC EXTRACTION ORBIT
 7 92767 GEV KINETIC CENTRAL ENERGY
 8 MARCH 83 A. ANDO, DE JOHNSON

*** BRHO = // 294.0756
 *** BO = // 16.8391978
 *** BL = // 0.3048
 *** BL1 = // 1.5240
 *** BL2 = // 3.0480
 *** BL3 = // 4.5720

*** A10 DRF // 0.0
 *** A20 DRF // 0.0

*** LS DRF // 7.946495
 *** LS* DRF // 7.84408
 *** O1 DRF // 0.512413
 *** O2 DRF // 0.960996
 *** O3 DRF // 0.9042
 *** OB3 DRF // 6.42366
 *** O4 DRF // 3.2610
 *** O5 DRF // 7.34776
 *** O6 DRF // 4.18716
 *** O7 DRF // 2.8476
 *** OS7 DRF // 1.29304
 *** OB7 DRF // 0.5080
 *** OB8 DRF // 1.2192
 *** OB6 DRF // 0.5080
 *** O9 DRF // 0.3048
 *** OS9 DRF // 0.6096
 *** OB9 DRF // 0.5080
 *** O10 DRF // 0.5080
 *** OB10 DRF // 0.2919
 *** OS10 DRF // 0.2919
 *** O11 DRF // 0.52102
 *** O12 DRF // 0.2178
 *** OS12 DRF // 0.2178
 *** O13 DRF // 0.49722

SMALL APERTURE DIPOLES

*** B3 MAG // BL1 0.0 BRHO BC \$
 *** B7 MAG // BL2 0.0 BRHO BC \$
 *** B8 MAG // BL3 0.0 BRHO BC \$

LARGE APERTURE DIPOLES

*** B9 MAG // BL3 0.0 BRHO BO \$
 *** B10 MAG // DL3 0.0 BRHO BO \$

SMALL APERTURE QUADRUPOLES
 HALF QUAD LENGTHS LISTED

*** G1 = // 96.6333
 *** G10 = // -97.4126
 *** G1 = // 103.8087
 *** Q1 MAG // 0.32004 GT BRHO
 *** Q2 MAG // 0.655828 -GT BRHO
 *** Q3 MAG // 0.35052 GT BRHO
 *** Q4 MAG // 0.2286 GF BRHO
 *** Q5 MAG // 0.41402 GD BRHO
 *** Q6 MAG // 0.35052 GF BRHO
 *** Q7 MAG // 0.35052 GD BRHO
 *** Q8 MAG // 0.2286 GF BRHO
 *** Q9 MAG // 0.2286 GD BRHO

LARGE APERTURE QUADRUPOLES

*** G10 = // 40.8765
 *** GF1 = // 89.3989
 *** GD1 = // -89.3989
 *** Q10 MAG // 0.2286 G10 BRHO
 *** Q11 MAG // 0.43488 GF1 BRHO
 *** Q12 MAG // 0.3861 GD1 BRHO
 *** Q13 MAG // 0.3861 GD1 BRHO
 *** Q14 MAG // 0.32131 GF1 BRHO

QUADRUPOLES

PDS	S(M)	NOY	NOY	BETAX(M)	BETAY(M)	ETAX(M)	ETAY(M)	ETAS(M)	ALPHA	ALPHAY	BETA	BETAY
0	0.0600	0.0000	0.0000	7.56400	7.26661	00155	0.00000	0.00000	0.00000	0.00000	-0.0000	0.00000
1 A10	0.0000	0.0000	0.0000	7.56400	7.26661	00155	0.00000	0.00000	0.00000	0.00000	-0.0000	0.00000
2 LS	7.9465	12892	13211	15.91233	15.95660	00155	0.00000	0.00000	-1.05057	1.09356	-0.0000	0.00000
3 Q1	8.2665	13210	13519	16.01364	17.27175	00152	0.00000	0.00000	-0.73785	-3.06516	-0.0017	0.00000
4 Q1	8.5866	13536	13795	14.99036	19.97577	00144	0.00000	0.00000	2.42084	-5.48543	-0.0034	0.00000
5 Q1	9.0990	14129	14153	12.62959	26.00603	00126	0.00000	0.00000	-2.18633	-6.28294	-0.0034	0.00000
6 Q2	9.7548	15011	14516	11.68624	30.32147	00113	0.00000	0.00000	-6.67585	-0.03924	-0.0007	0.00000
7 Q2	10.4106	15831	14879	14.58755	25.91321	00117	0.00000	0.00000	-0.96970	-6.33876	-0.0020	0.00000
8 Q2	11.3712	16661	15649	23.27416	15.20161	00136	0.00000	0.00000	-0.07325	4.81223	0.0020	0.00000
9 Q3	11.7218	16887	16055	25.87297	12.59663	00140	0.00000	0.00000	-2.23340	2.72664	0.0002	0.00000
10 Q3	12.0723	17099	16527	26.31581	11.26714	00138	0.00000	0.00000	98833	1.12096	-0.0015	0.00000
11 Q3	12.9765	17665	17927	24.58992	9.40373	00124	0.00000	0.00000	92041	93987	-0.0015	0.00000
12 Q3	14.5005	18708	20947	21.86209	6.94355	06747	0.00000	0.0203	80608	-6.6827	0.0817	0.00000
13 Q3	20.9241	24525	39718	14.70581	6.95470	62745	0.00000	0.0203	32354	-6.6700	0.0817	0.00000
14 Q4	21.1527	24776	40227	14.31239	7.37561	64194	0.00000	0.0203	1.38758	-1.26974	0.0394	0.00000
15 Q4	21.3813	25037	40697	13.45148	8.12909	64542	0.00000	0.0203	2.35686	-1.95720	-0.0899	0.00000
16 Q4	24.6423	33229	44215	3.26194	27.21314	61610	0.00000	0.0203	76780	-3.89501	-0.0899	0.00000
17 Q5	25.0564	35408	44448	2.87570	28.90145	62991	0.00000	0.0203	18270	-1.0537	0.7605	0.00000
18 Q5	25.4704	37700	44680	2.94779	27.38111	67966	0.00000	0.0203	-36012	3.70775	16542	0.00000
19 Q5	32.8181	52344	69382	28.93029	1.97247	1.89516	0.00000	0.0203	-3.17600	2.24974	16542	0.00000
20 Q6	33.1687	52532	72031	29.99143	2.30008	1.91463	0.00000	0.0203	18953	-6.69745	-0.5472	0.00000
21 Q6	33.5192	52721	74184	28.67165	2.97688	1.85705	0.00000	0.0203	3.52486	-1.25931	-2.7267	0.00000
22 Q6	37.7063	57374	81659	7.36233	28.75210	71534	0.00000	0.0203	1.56435	-4.89647	-2.7267	0.00000
23 Q7	38.0569	58180	81845	6.99770	31.04324	63372	0.00000	0.0203	64659	-1.55101	-1.9462	0.00000
24 Q7	38.4074	59043	82024	6.43097	30.86822	57798	0.00000	0.0203	-1.6448	2.50435	1.2451	0.00000
25 Q7	41.2550	65273	83825	8.66271	20.58959	22342	0.00000	0.0203	-6.1925	1.56604	-1.2451	0.00000
26 S7	41.5598	65821	84066	9.05504	19.65051	18547	0.00000	0.0203	-6.6793	1.51493	-1.2451	0.00000
27 Q7	42.8528	67884	85228	11.04937	16.01312	02448	0.00000	0.0203	-8.7443	1.29812	-1.2451	0.00000
28 Q7	45.9008	71351	89247	17.82159	9.29316	-0.08779	0.00000	-0.1127	-1.35874	8.7293	0.5047	0.00000
29 Q8	46.4088	71787	90159	19.24328	8.45519	-0.06215	0.00000	-0.1127	-1.43987	7.7661	0.5047	0.00000
30 Q8	46.6374	71974	90596	19.57382	8.25203	-0.05012	0.00000	-0.1127	0.0223	1.1716	0.5469	0.00000
31 Q8	46.8660	72161	91036	19.24127	8.34682	-0.03722	0.00000	-0.1127	1.44418	-5.3419	0.5798	0.00000
32 Q8	48.0852	73270	93179	15.95816	9.87830	03346	0.00000	-0.1127	1.24866	-7.2194	0.5798	0.00000
33 Q8	52.6572	79843	98624	7.94667	18.80195	89057	0.00000	0.0809	52381	-1.16259	3.2128	0.00000
34 Q8	53.1652	80894	99041	7.45586	20.05379	1.05379	0.00000	0.0809	44235	-1.26213	3.2128	0.00000
35 Q9	53.3938	81386	99221	7.38952	20.23158	1.13658	0.00000	0.0809	-1.5046	2.8603	4.0409	0.00000
36 Q9	53.6224	81873	99403	7.59503	19.75689	1.23907	0.00000	0.0809	-7.5374	1.77849	4.9391	0.00000
37 Q9	53.9272	82492	99655	8.07370	18.69230	1.38961	0.00000	0.0809	-8.1667	1.71427	4.9391	0.00000
38 Q9	54.2320	83075	99922	8.59072	17.66686	1.54016	0.00000	0.0809	-8.7961	1.65004	4.9391	0.00000
39 Q9	54.8416	84137	1.00504	9.73986	15.73343	1.84124	0.00000	0.0809	-1.00547	1.52159	4.9391	0.00000
40 Q9	59.4136	89014	1.08571	23.04733	5.63827	4.66875	0.00000	0.9185	-1.93869	6.1035	7.5721	0.00000
41 Q10	59.9216	89350	1.10084	25.07033	5.08097	5.05342	0.00000	0.9185	-2.04358	4.8669	7.5721	0.00000
42 Q10	60.1502	89493	1.10814	25.82923	4.90713	5.20797	0.00000	0.9185	-1.26816	2.7562	5.9409	0.00000
43 Q10	60.3788	89633	1.11662	26.22433	4.82772	5.32471	0.00000	0.9185	-4.5599	0.7259	4.2664	0.00000
44 Q10	60.8868	89938	1.13244	26.69950	4.80771	5.54144	0.00000	0.9185	-4.7939	-0.03319	4.2664	0.00000
45 Q10	65.4588	92410	1.25367	31.97419	9.12771	8.06492	0.00000	2.67987	-6.8759	-8.7912	6.8995	0.00000
46 Q10	65.7507	92555	1.25862	32.37953	9.65749	8.26631	0.00000	2.67987	-7.0103	-9.3582	6.8995	0.00000
47 Q10	66.0555	92704	1.26350	32.81116	10.24601	8.47661	0.00000	2.67987	-7.1507	-9.9502	6.8995	0.00000
48 Q10	66.3474	92844	1.26790	33.23255	10.84345	8.67801	0.00000	2.67987	-7.2852	-1.05171	6.8995	0.00000
49 Q11	66.7843	93056	1.27394	31.96215	12.47757	8.72598	0.00000	2.67987	3.57995	-2.76080	-4.7140	0.00000

PQS	S(M)	NUX	NUY	BETX(M)	BETAY(M)	L1AX(M)	L1AY(M)	L1AS(M)	ALPHA	ALPHA	BETA	BETAY
50 Q11	67.2212	93289	1.27893	27.21571	15.85689	8.27009	0.00000	2.67987	7.07349	-5.12314	-1.60552	0.00000
51 Q11	67.7422	93641	1.28341	20.35389	21.66177	7.43358	0.00000	2.67987	6.09649	-6.01840	-1.60552	0.00000
52 Q12	68.1283	93977	1.28601	16.72287	25.45541	6.97807	0.00000	2.67987	3.44951	-3.65826	-7.6292	0.00000
53 Q12	68.5144	94370	1.28833	14.86405	27.14243	6.84000	0.00000	2.67987	1.43734	-6.4493	0.4497	0.00000
54 Q12	68.7322	94608	1.28960	14.24773	27.42584	6.84979	0.00000	2.67987	1.39242	-6.5629	0.4497	0.00000
55 S12	69.0370	94959	1.29135	13.41807	27.83076	6.86350	0.00000	2.67987	1.32955	-6.7219	0.4497	0.00000
56 OS12	69.2548	95223	1.29259	12.84871	28.12604	6.87329	0.00000	2.67987	1.28462	-6.8356	0.4497	0.00000
57 Q13	69.6409	95712	1.29479	12.44883	27.39026	7.04712	0.00000	2.67987	-2.3333	2.56037	8.5885	0.00000
58 Q13	70.0270	96195	1.29715	13.22005	24.29020	7.34152	0.00000	2.67987	-1.79422	3.34713	1.71180	0.00000
59 Q13	70.5242	96756	1.30081	15.08319	19.27399	8.39266	0.00000	2.67987	-1.95291	4.74139	1.71180	0.00000
60 Q14	70.8455	97084	1.30366	15.87623	16.90129	8.80845	0.00000	2.67987	-1.48935	2.72016	8.6951	0.00000
61 Q14	71.1668	97407	1.30681	15.69904	15.70432	8.94851	0.00000	2.67987	1.03500	1.04401	0.0000	0.00000
62 LS*	79.0117	1.10180	1.43524	7.57960	7.51415	8.94851	0.00000	2.67987	-0.00000	0.00000	0.0000	0.00000
63 A20	79.0117	1.10180	1.43524	7.57960	7.51415	8.94851	0.00000	2.67987	-0.00000	0.00000	0.0000	0.00000
64 REFL	158.0234	2.20361	2.87048	7.56400	7.26661	.00155	0.00000	5.35974	.00000	.00000	0.0000	0.00000

CIRCUMFERENCE = 474.0703 M THETX = 6.28318533 RAD NUX = 6.61082 DNUX/(DP/P) = -8.47593
 RADIUS = 75.4506 M THETY(63) = 0.00000000 RAD NUY = 8.61144 DNUY/(DP/P) = -12.88242
 (DS/S)/(DP/P) = 0.339174 TGAM = (5.42986, 0.00000)

MAXIMA --- BETX(48) = 33.23255 BETY(23) = 31.04324 ETAX(63) = 8.94851 ETAY(64) = 0.00000
 MINIMA --- BETX(17) = 2.87570 BETY(19) = 1.97247 ETAX(28) = -0.08779 ETAY(64) = 0.00000

*** PAGE **

SETUP/DIE CORRECTIONS

***	KS7	=	//	35.7175	
***	KS9	=	//	-219.5244	
***	KS10	=	//	134.7943	
***	KS12	=	//	-170.5021	
***	S7	SXTP	//	SL	KS7
***	S9	SXTP	//	SL	KS9
***	S10	SXTP	//	SL	KS10
***	S12	SXTP	//	SL	KS12
***		CYC	-3	//	R/6

BRHO
BRHO
BRHO
BRHO

PDS	S(M)	NJA	NUY	BETAX(N)	BETAX(K)	ETAX(M)	ETAX(F)	ETAS(M)	ALPHA	ALPHA	DELTA	DELTA
0	0.0000	0.00000	0.00000	7.56400	7.26661	00155	0.00000	0.00000	0.00000	0.00000	0.00000	0.00000
1 A10	0.0000	0.00000	0.00000	7.56400	7.26661	00155	0.00000	0.00000	0.00000	0.00000	0.00000	0.00000
2 L5	7.7465	12892	13211	15.91233	15.95660	00155	0.00000	0.00000	-1.05057	-1.09396	00000	0.00000
3 Q1	8.2665	13210	13519	16.01364	17.37175	00152	0.00000	0.00000	.73785	-3.06516	00017	0.00000
4 Q1	8.5866	13534	13795	14.99036	19.97577	00144	0.00000	0.00000	2.42084	-5.48543	00034	0.00000
5 Q1	9.0990	14129	14153	12.62959	26.00603	00126	0.00000	0.00000	2.18433	-6.28294	00034	0.00000
6 Q2	9.7548	13011	14516	11.68624	30.32147	00113	0.00000	0.00000	-6.7595	03924	00007	0.00000
7 Q2	10.4106	15831	14879	14.58755	25.91321	00117	0.00000	0.00000	-3.96970	6.33876	00020	0.00000
8 Q2	11.3712	16661	15649	23.27416	15.20161	00136	0.00000	0.00000	-5.07325	4.81223	00020	0.00000
9 Q3	11.7218	16887	16035	25.87297	12.59663	00140	0.00000	0.00000	-2.23340	2.72654	00062	0.00000
10 Q3	12.0723	17099	16527	26.31581	11.26714	00138	0.00000	0.00000	98833	1.12096	-00015	0.00000
11 Q3	12.9765	17665	17927	24.58992	9.40373	00124	0.00000	0.00000	92041	93987	-00015	0.00000
12 Q3	14.3005	18708	20947	21.96209	6.94355	06747	0.00000	00203	80608	66827	08717	0.00000
13 Q3	20.9241	24525	39718	14.70581	6.95470	62745	0.00000	00203	32354	-7.7000	08717	0.00000
14 Q4	21.1527	24774	40227	14.31239	7.39561	64194	0.00000	00203	1.38758	-1.26974	03943	0.00000
15 Q4	21.3813	25037	40697	13.45148	8.12909	64542	0.00000	00203	2.35686	-1.95720	-00899	0.00000
16 Q4	24.6423	33229	44215	3.26194	27.21314	61610	0.00000	00203	-76780	-0.89501	-00899	0.00000
17 Q5	25.0564	35408	44448	2.87570	28.90145	62991	0.00000	00203	18270	-1.10537	07605	0.00000
18 Q5	25.4704	37700	44680	2.94779	27.38111	67966	0.00000	00203	-36012	3.70775	16542	0.00000
19 Q5	32.8181	52344	69382	28.93029	1.97247	1.89516	0.00000	00203	-3.17600	-2.4974	16542	0.00000
20 Q6	33.1687	52532	72031	29.99143	2.30008	1.91463	0.00000	00203	1.8953	-6.9745	-05472	0.00000
21 Q6	33.5192	52721	74184	28.67165	2.97688	1.8547	0.00000	00203	3.92486	-1.25931	-27267	0.00000
22 Q6	37.7063	57374	81659	7.36233	28.75210	71534	0.00000	00203	1.56435	-4.89647	-27267	0.00000
23 Q7	38.0569	58180	81845	6.59770	31.04324	63372	0.00000	00203	64659	-1.55101	-19462	0.00000
24 Q7	38.4074	59043	82024	6.43097	30.86822	57798	0.00000	00203	-1.6448	2.04353	-12451	0.00000
25 Q7	41.2550	65273	83825	8.66271	20.58959	22342	0.00000	00203	-61925	1.56604	-12451	0.00000
26 S7	41.5598	65821	84066	9.05504	19.65051	18547	0.00000	00203	-66793	1.51493	-12451	0.00000
27 Q57	42.8528	67884	85228	11.04937	16.01312	02448	0.00000	00203	-87443	1.29812	-12451	0.00000
28 Q7	45.9008	71351	89247	17.82159	9.29316	-08779	0.00000	-01127	-1.35874	87293	05047	0.00000
29 Q87	46.4088	71787	90159	19.24328	8.45519	-06215	0.00000	-01127	-1.43987	77661	05047	0.00000
30 Q8	46.6374	71974	90596	19.57382	8.25203	-05012	0.00000	-01127	00223	11716	05469	0.00000
31 Q8	46.8660	72161	91036	19.24127	8.34682	-03722	0.00000	-01127	1.44418	-53419	05798	0.00000
32 Q8	48.0852	73270	93179	15.95816	9.87830	03346	0.00000	-01127	1.24866	-72194	05798	0.00000
33 Q8	52.6572	79843	98624	7.94667	18.80195	89057	0.00000	08409	52381	-1.16259	32128	0.00000
34 Q8E	53.1652	80894	99041	7.45586	20.01542	1.05379	0.00000	08409	44235	-1.22613	32128	0.00000
35 Q9	53.3938	81386	99221	7.38952	20.23158	1.13658	0.00000	08409	-15046	28603	40409	0.00000
36 Q9	53.6224	81873	99403	7.59503	19.75689	1.23907	0.00000	08409	-75374	1.77849	49391	0.00000
37 Q9	53.9272	82492	99655	8.07370	18.69230	1.38961	0.00000	08409	-81667	1.71427	49391	0.00000
38 Q9	54.2320	83075	99922	8.59072	17.66686	1.54016	0.00000	08409	-87961	1.65004	49391	0.00000
39 Q99	54.8416	84137	1.00504	9.73986	15.73343	1.84124	0.00000	08409	-1.00547	1.52159	49391	0.00000
40 Q9	59.4136	89014	1.08571	23.04733	5.63827	4.66875	0.00000	91485	-1.93869	61035	75721	0.00000
41 Q89	59.9216	89350	1.10084	25.07033	5.08097	3.05342	0.00000	91485	-2.04358	48669	75721	0.00000
42 Q10	60.1502	89493	1.10814	25.82923	4.90713	3.20797	0.00000	91485	-1.26816	27562	59409	0.00000
43 Q10	60.3788	89633	1.11562	26.22433	4.82772	3.32471	0.00000	91485	-4.5999	07259	42664	0.00000
44 Q10	60.8868	89938	1.13244	26.69950	4.80771	3.34144	0.00000	91485	-4.79939	-03319	42664	0.00000
45 Q10	65.4588	92410	1.25367	31.97419	9.12771	8.06492	0.00000	2.67987	-68759	-87912	68995	0.00000
46 Q810	65.7507	92555	1.25862	32.37953	9.65749	8.26631	0.00000	2.67987	-70103	-93582	68995	0.00000
47 S10	66.0555	92704	1.26350	32.81116	10.24601	8.47661	0.00000	2.67987	-71507	-99502	68995	0.00000
48 Q510	66.3474	92844	1.26790	33.23255	10.84345	8.67801	0.00000	2.67987	-72852	-1.05171	68995	0.00000
49 Q11	66.7843	93056	1.27394	31.96215	12.47757	8.72598	0.00000	2.67987	3.57995	-2.76080	47140	0.00000

PRG	S(M)	NUX	NUY	BETAX(M)	BETAY(M)	ETAX(M)	ETAY(M)	ETAS(M)	ALPHA	ALPHA	BETAX	BETAY
50 G11	67 2212	93289	1 27893	27 21571	15 85280	8 27609	0 00000	2 67987	7 07349	5 12314	-1 60552	0 00000
51 D11	67 7422	93641	1 28341	20 35389	21 66177	7 43358	0 00000	2 67987	6 09649	-6 01840	-1 60552	0 00000
52 G12	68 1283	93977	1 28601	16 72287	25 45541	6 97807	0 00000	2 67987	3 44951	-3 65826	76292	0 00000
53 Q12	68 5144	94370	1 28833	14 86405	27 14243	6 84000	0 00000	2 67987	1 43734	-6 64493	04497	0 00000
54 D12	68 7322	94608	1 28960	14 24773	27 42584	6 84979	0 00000	2 67987	1 39242	-6 65629	04497	0 00000
55 S12	69 0370	94959	1 29135	13 41807	27 83076	6 86350	0 00000	2 67987	1 32955	-6 67219	04497	0 00000
56 DS12	69 2548	95223	1 29259	12 84871	28 12604	6 87329	0 00000	2 67987	1 28462	-6 68356	04497	0 00000
57 Q13	69 6409	95712	1 29479	12 44883	27 39026	7 04712	0 00000	2 67987	-2 33333	2 56037	85885	0 00000
58 Q13	70 0270	96195	1 29715	13 22005	24 29020	7 54152	0 00000	2 67987	-1 79422	5 34713	1 71180	0 00000
59 D13	70 5242	96756	1 30081	15 08319	19 27399	8 39266	0 00000	2 67987	-1 95291	4 74139	1 71180	0 00000
60 Q14	70 8455	97084	1 30366	15 87623	16 90129	8 80845	0 00000	2 67987	-4 8935	2 72016	86951	0 00000
61 Q14	71 1668	97407	1 30681	15 69904	15 70432	8 94851	0 00000	2 67987	1 03500	1 04461	00000	0 00000
62 LS*	79 0117	1 10180	1 43524	7 57960	7 51415	8 94851	0 00000	2 67987	-0 00000	00000	00000	0 00000
63 A20	79 0117	1 10180	1 43524	7 57960	7 51415	8 94851	0 00000	2 67987	-0 00000	00000	00000	0 00000
64 REFL	158 0234	2 20361	2 87048	7 56400	7 26651	00155	0 00000	5 35974	00000	00000	00000	0 00000

CIRCUMFERENCE = 474 0703 M THETA = 6 28318533 RAD NUX = 6 61082 DNUX/(DP/P) = 89856
 RADIUS = 75 4506 M THETY(63) = 0 00000000 RAD NUY = 8 61144 DNUY/(DP/P) = 33310
 (DS/S)/(DP/P) = 0339174 TGAM = (5 42986, 0 00000)

MAXIMA --- BETX(48) = 33 23255 BETY(23) = 31 04324 ETAX(63) = 8 94851 ETAY(64) = 0 00000
 MINIMA --- BETX(17) = 2 87570 BETY(19) = 1 97247 ETAX(28) = - 08779 ETAY(64) = 0 00000

*** PAGE //

INJECTION UNIT
B 00920 GEV KINETIC

// 00930
// V R/6

= PVEC
EXPT 2 -3

DI
V
INJ

DI

1

CALCULATION OF THE EQUILIBRIUM ORBIT AND BETATRON FUNCTIONS OF INJ
 INITIAL REFERENCE RAY DEFINED BY V

X = 0.00000000 DX = 0.00000000 Y = 0.00000000 DY = 0.00000000 DS = 0.00000000 DP/P = 0.09300000 1.00000000

7X/ MATRIX FOR INJ

26824382	8.69314725	0.00000000	0.00000000	0.00000000	-1.15380901	0.0079763
-10675596	26824382	0.00000000	0.00000000	0.00000000	-0.02243921	0.0011637
0.00000000	0.00000000	71018489	-5.07291413	0.00000000	0.00000000	0.00000000
0.00000000	0.00000000	0.9770270	71018489	0.00000000	0.00000000	0.00000000
02243921	15380901	0.00000000	0.00000000	1.00000000	-5.47427891	-0.04757677
0.00000000	0.00000000	0.00000000	0.00000000	0.00000000	1.00000000	0.00000000
0.00000000	0.00000000	0.00000000	0.00000000	0.00000000	0.00000000	1.00000000

EIGENVALUES OF THE 4X4 SUBMATRIX

X... LMD1 = (26824382 .96335105), C(1) = 1.00000000, MU(1) = 1.29922675 RAD, Q(1) = 62033508
 1/LMD1 = (26824382 - .96335105), C(2) = 1.00000000, MU(2) = -1.29922675 RAD, Q(2) = 37966492
 Y... LMD3 = (71018489 .70401522), C(3) = 1.00000000, MU(3) = .78103554 RAD, Q(3) = 37291700
 1/LMD3 = (71018489 - .70401522), C(4) = 1.00000000, MU(4) = -.78103554 RAD, Q(4) = 62708300

EIGENVALUE = (26824382, .96335105), EIGENVECTOR = (3.00397442, -.00000000)
 (.00000000, .33289232)
 (0.00000000, 0.00000000)
 (0.00000000, 0.00000000)

EIGENVALUE = (26824382, -.96335105), EIGENVECTOR = (3.00397442, .00000000)
 (.00000000, -.33289232)
 (0.00000000, 0.00000000)
 (0.00000000, 0.00000000)

EIGENVALUE = (71018489, 70401522), EIGENVECTOR = (0.00000000, 0.00000000)
 (0.00000000, 0.00000000)
 (2.68434129, 0.00000000)
 (0.00000000, -.37253087)

EIGENVALUE = (71018489, -70401522), EIGENVECTOR = (0.00000000, 0.00000000)
 (0.00000000, 0.00000000)
 (2.68434129, -.00000000)
 (0.00000000, 37253087)

	X	DX	Y	DY	DS	DP/P
EQ ORBIT	-.00088124	0.00000000	0.00000000	0.00000000	0.00000000	0.09300000 1.00000000
ETA ORBIT	-.21019162	-.00000000	0.00000000	0.00000000	0.00000000	1.00000000 0.00000000

EIGENVECTORS 1 AND 3 IN POLAR COORDINATES

PKS	X1		X3		DX1		DX3		Y1		Y3		DZ1		DZ3	
	0	1	0	1	0	1	0	1	0	1	0	1	0	1	0	1
0	3.003974	0.000000	0.000000	0.000000	0.332892	1.570796	0.000000	0.000000	0.000000	0.000000	0.000000	0.000000	0.000000	0.000000	0.000000	0.000000
	0.000000	0.000000	0.000000	0.000000	0.000000	0.000000	2.284341	0.000000	0.000000	0.000000	0.000000	0.000000	0.000000	0.372531	-1.570796	0.000000

DEFLECTION FUNCTIONS OF INJ.				EX	BY	AX	AY	EX	EXP	EY	EYP	XCO	VALU	YCO	VALU
FOR	(H)	GX	GY	(H)	(H)			(H)		(H)		(MM)	(MM)	(MM)	(MM)
0		0.00	0.000	0.000	9.0239	7.2057	0.0000	0.0000	-2102	0.0000	0.0000	-8812	0.0000	0.0000	0.0000
1 A10		0.00	0.000	0.000	9.0239	7.2057	0.0000	0.0000	-2102	0.0000	0.0000	-8812	0.0000	0.0000	0.0000
2 LS		7.95	115	133	16.0216	15.6632	-8806	-1.1022	-2102	0.0000	0.0000	-8812	0.0000	0.0000	0.0000
3 Q1		8.27	118	136	16.0160	17.2853	8979	-3.0587	-2065	0.2332	0.0000	0.0000	-8655	0.9981	0.0000
4 Q1		8.59	121	139	14.8994	19.9790	2.5493	-5.4582	-1954	0.458	0.0000	0.0000	-8189	1.926	0.0000
5 Q1		9.10	127	142	12.4189	25.9774	2.2914	-6.2479	-1719	0.458	0.0000	0.0000	-7202	1.926	0.0000
6 Q2		9.75	136	146	11.2940	30.2896	-4.911	-6.0057	-1542	0.090	0.0000	0.0000	-6455	0.379	0.0000
7 Q2		10.41	145	149	13.8403	25.9638	-3.5842	-6.3561	-1599	-0.265	0.0000	0.0000	-6492	-1.110	0.0000
8 Q2		11.37	154	157	21.6493	15.3711	-4.5452	4.7711	-1853	-0.265	0.0000	0.0000	-7758	-1.110	0.0000
9 Q3		11.72	156	161	23.9492	12.7925	-1.9222	2.6906	-1906	-0.034	0.0000	0.0000	-7978	-0.042	0.0000
10 Q3		12.07	159	166	24.2677	11.4897	1.0266	1.0793	-1877	0.197	0.0000	0.0000	-7857	0.832	0.0000
11 Q3		12.98	165	179	22.4805	9.6919	9.9500	9.9089	-1699	0.197	0.0000	0.0000	-7104	0.832	0.0000
12 B3		14.50	176	208	19.7863	7.2965	8.212	-4.566	-0.740	1.062	0.0000	0.0000	0.285	8878	0.0000
13 QB3		20.92	243	387	12.7277	6.9544	2.776	-6.6033	6.085	1.062	0.0000	0.0000	5.7315	8878	0.0000
14 Q4		21.15	245	392	12.3913	7.3627	1.1857	-1.1928	6.276	0.606	0.0000	0.0000	5.8852	4.549	0.0000
15 Q4		21.38	248	397	11.6558	8.0575	2.0135	-1.8639	6.361	0.140	0.0000	0.0000	5.9389	0.143	0.0000
16 Q4		24.64	339	433	3.1350	26.1187	5.995	-3.6746	6.816	0.140	0.0000	0.0000	5.9854	0.143	0.0000
17 Q5		25.06	361	436	2.8752	27.7000	0.397	-0.728	7.066	1.070	0.0000	0.0000	6.1606	8356	0.0000
18 Q5		25.47	384	438	3.0667	26.2348	-3.109	3.5451	7.711	2.061	0.0000	0.0000	6.6839	1.7042	0.0000
19 Q5		32.82	515	684	32.7759	2.0593	-3.5324	-2.549	2.853	2.061	0.0000	0.0000	19.2060	1.7042	0.0000
20 Q6		33.17	516	709	33.9429	2.3906	2.2476	-7.7030	2.3119	-0.549	0.0000	0.0000	19.4165	-5.070	0.0000
21 Q6		33.52	518	730	32.4378	3.0715	3.9864	-1.2651	2.2471	-3.137	0.0000	0.0000	18.8530	-2.6979	0.0000
22 Q6		37.71	559	804	8.1757	28.5098	1.8060	-4.8102	9.336	-3.137	0.0000	0.0000	7.5563	-2.6979	0.0000
23 Q7		38.06	567	806	7.2744	30.7603	7.999	-1.5240	8.416	-2.128	0.0000	0.0000	6.7572	-1.8774	0.0000
24 Q7		38.41	575	808	7.0239	30.5894	-0.754	2.0048	7.834	-1.1203	0.0000	0.0000	6.2314	-1.1328	0.0000
25 Q7		41.25	634	826	8.6144	20.5023	-4.831	1.5375	4.407	-1.203	0.0000	0.0000	3.0057	-1.1328	0.0000
26 S7		41.56	640	828	8.9220	19.5809	-5.259	1.4855	4.041	-1.204	0.0000	0.0000	2.6604	-1.1329	0.0000
27 OS7		42.85	661	840	10.5211	16.0131	-7.109	1.2737	2.484	-1.204	0.0000	0.0000	1.1955	-1.1329	0.0000
28 B7		45.90	698	880	16.1477	9.4111	-1.1448	8.603	1.461	0.530	0.0000	0.0000	2.044	4.793	0.0000
29 OB7		46.41	703	889	17.3478	8.5847	-1.2175	7.663	1.731	0.530	0.0000	0.0000	4.479	4.793	0.0000
30 Q8		46.64	705	893	17.6121	8.3870	0.679	1.036	1.837	0.397	0.0000	0.0000	5.534	4.420	0.0000
31 Q8		46.87	707	897	17.2864	8.4889	1.3487	-5.520	1.912	0.258	0.0000	0.0000	6.494	3.972	0.0000
32 Q8		48.09	720	919	14.2402	10.0634	1.1498	-7.394	2.226	0.258	0.0000	0.0000	1.1337	3.972	0.0000
33 Q8		52.66	794	972	7.1832	19.1305	4.128	-1.1790	9.292	2.866	0.0000	0.0000	8.4140	2.8228	0.0000
34 QB8		53.17	805	976	6.8059	20.3606	3.300	-1.2425	1.0748	2.866	0.0000	0.0000	9.8480	2.8228	0.0000
35 Q9		53.39	811	978	6.7792	20.5816	-2.128	2.819	1.1496	3.691	0.0000	0.0000	10.5797	3.5880	0.0000
36 Q9		53.62	816	980	7.0026	20.1060	-7.702	1.7870	1.2440	4.580	0.0000	0.0000	11.4931	4.4149	0.0000
37 Q9		53.93	823	982	7.4933	19.0360	-8.396	1.7235	1.3836	4.580	0.0000	0.0000	12.8388	4.4149	0.0000
38 S9		54.23	829	985	8.0335	17.9878	-9.334	1.7147	1.5238	4.624	0.0000	0.0000	14.1876	4.4355	0.0000
39 OS9		54.84	840	990	9.2580	15.9787	-1.0753	1.5812	1.8057	4.624	0.0000	0.0000	16.8914	4.4355	0.0000
40 B9		59.42	889	1.072	23.8158	5.4921	-2.1286	6.241	4.4932	7.223	0.0000	0.0000	42.4612	6.8573	0.0000
41 OB9		59.93	893	1.087	26.0383	4.9233	-2.2465	4.956	4.8602	7.223	0.0000	0.0000	45.9447	6.8573	0.0000
42 Q10		60.16	894	1.095	26.8861	4.7443	-1.4513	2.889	5.0079	5.684	0.0000	0.0000	47.3451	5.3879	0.0000
43 Q10		60.39	895	1.103	27.3598	4.6577	-6.143	0.906	5.1198	4.104	0.0000	0.0000	48.4051	3.8798	0.0000
44 Q10		60.90	898	1.120	27.9970	4.6215	-6.399	-0.194	5.3283	4.104	0.0000	0.0000	50.3760	3.8798	0.0000
45 B10		65.48	921	1.246	34.9220	9.0280	-8.680	-9.126	7.7893	6.705	0.0000	0.0000	73.4742	6.3024	0.0000
46 OB10		65.78	923	1.251	35.4330	9.5781	-8.827	-9.719	7.9850	6.705	0.0000	0.0000	75.3138	6.3024	0.0000
47 S10		66.08	924	1.256	35.8605	10.2217	-5.188	-1.1414	8.1764	5.855	0.0000	0.0000	77.1734	5.8997	0.0000
48 OS10		66.37	925	1.260	36.1663	10.9072	-5.291	-1.2072	8.3473	5.855	0.0000	0.0000	78.8955	5.8997	0.0000
49 Q11		66.81	927	1.266	34.5786	12.6845	4.0946	-2.9386	8.3642	-5.088	0.0000	0.0000	79.1914	-4.5516	0.0000

POI	S (M)	GX	GY	BX (M)	BY (M)	AX	AY	EX (M)	EXP	EY (M)	EYP	XCU (MM)	YCU (MM)	ZCU (MM)	STCU (MM)
50 Q11	67.25	929	1.271	29.2765	16.2440	7.7941	-5.3577	7.9062	-1.5744	0.0000	0.0000	74.9526	-14.7424	0.0000	0.0000
51 Q11	67.77	933	1.275	21.7273	22.3234	6.6952	-6.3105	7.0859	-1.5744	0.0000	0.0000	67.2755	-14.7424	0.0000	0.0000
52 Q12	68.15	936	1.278	17.7138	26.3275	3.8634	-3.9148	6.6323	-7871	0.0000	0.0000	63.0567	-7.1923	0.0000	0.0000
53 Q12	68.54	940	1.280	15.5846	28.1845	1.7357	-8.262	6.4743	-6350	0.0000	0.0000	61.6799	0.0000	0.0000	0.0000
54 Q12	68.76	942	1.281	14.8408	28.5473	1.6796	-8.393	6.4667	-6350	0.0000	0.0000	61.6872	0.0000	0.0000	0.0000
55 S12	69.06	945	1.283	13.8872	28.9693	1.4514	-5.440	6.4666	0.345	0.0000	0.0000	61.7483	3.669	0.0000	0.0000
56 OS12	69.28	948	1.284	13.2656	29.2084	1.4027	-5.538	6.4741	0.345	0.0000	0.0000	61.8282	3.669	0.0000	0.0000
57 Q13	69.67	953	1.286	12.7874	28.3381	-1.477	2.7783	6.6318	7865	0.0000	0.0000	63.3642	7.6192	0.0000	0.0000
58 Q13	70.05	957	1.289	13.4975	25.0511	1.7248	5.6189	7.0851	1.5736	0.0000	0.0000	67.7559	15.2150	0.0000	0.0000
59 Q13	70.55	963	1.292	15.2856	19.7849	-1.8712	4.9724	7.8676	1.5736	0.0000	0.0000	75.3211	15.2150	0.0000	0.0000
60 Q14	70.87	966	1.295	16.0256	17.2759	-3.998	2.9069	8.2505	7991	0.0000	0.0000	79.0165	7.7273	0.0000	0.0000
61 Q14	71.19	969	1.298	15.7924	15.9667	1.1211	1.2064	8.3794	-0.0000	0.0000	0.0000	80.2611	-0.0000	0.0000	0.0000
62 LS*	79.04	1.103	1.438	6.9975	6.5028	0.0000	-0.0000	8.3794	-0.0000	0.0000	0.0000	80.2611	-0.0000	0.0000	0.0000
63 A20	79.04	1.103	1.438	6.9975	6.5028	0.0000	-0.0000	8.3794	-0.0000	0.0000	0.0000	80.2611	-0.0000	0.0000	0.0000
64 REFL	158.07	2.207	2.876	9.0239	7.2057	0.0000	-0.0000	-2.102	-0.0000	0.0000	0.0000	-8812	0.0000	0.0000	0.0000

CIRCUMFERENCE = 474.2191 M THETX = 6.28318533 RAD NUX = 6.62034 DNUX/(DP/P) = 2.04842
 RADIUS = 75.4743 M THETY(63) = 0.00000000 RAD NUY = 8.62708 DNUY/(DP/P) = 2.1319
 (DS/S)/(DP/P) = 0.346612 TCAM = (5.37129, 0.00000)

MAXIMA --- BETX(48) = 36.16635 BETY(23) = 30.76032 ETAX(61) = 8.37941 ETAY(64) = 0.00000
 MINIMA --- BETX(17) = 2.87519 BETY(19) = 2.05926 ETAX(2) = -2.1019 ETAY(64) = 0.00000

*** PAGE //

CALCULATION OF THE EQUILIBRIUM ORBIT AND BETATRON FUNCTIONS OF STK

INITIAL REFERENCE RAY DEFINED BY V
 X = 0.00000000 DX = 0.00000000 Y = 0.00000000 DY = 0.00000000 DS = 0.00000000 DP/P = 00165000 1.00000000

4X4 MATRIX FOR STK

28561963	7.47013149	0.00000000	0.00000000	0.00000000	-0.02038452	0.0001813
-12294582	28561963	0.00000000	0.00000000	0.00000000	0.00350820	0.00000312
0.00000000	0.00000000	68819753	-5.27775387	0.00000000	0.00000000	0.00000000
0.00000000	0.00000000	09973640	68819753	0.00000000	0.00000000	0.00000000
0.00350820	0.02038452	0.00000000	0.00000000	1.00000000	-5.38532999	-0.00876629
0.00000000	0.00000000	0.00000000	0.00000000	0.00000000	1.00000000	0.00000000
0.00000000	0.00000000	0.00000000	0.00000000	0.00000000	0.00000000	1.00000000

EIGENVALUES OF THE 4X4 SUBMATRIX

X. LMD1 = (28561963 .95834306), C(1) = 1.00000000, MU(1) = 1.28114340 RAD, Q(1) = 61170091
 1/LMD1 = (28561963 -.95834306), C(2) = 1.00000000, MU(2) = -1.28114340 RAD, Q(2) = 38829909
 Y. LMD3 = (68819753 .72552337), C(3) = 1.00000000, MU(3) = .81179458 RAD, Q(3) = 38760336
 1/LMD3 = (68819753 -.72552337), C(4) = 1.00000000, MU(4) = -.81179458 RAD, Q(4) = 61239664

EIGENVALUE = (28561963, .95834306), EIGENVECTOR = (2.79192419, -0.00000000)
 (0.00000000, -35817591)
 (0.00000000, 0.00000000)
 (0.00000000, 0.00000000)

EIGENVALUE = (28561963, -.95834306), EIGENVECTOR = (2.79192419, 0.00000000)
 (0.00000000, -35817591)
 (0.00000000, 0.00000000)
 (0.00000000, 0.00000000)

EIGENVALUE = (.68819753, .72552337), EIGENVECTOR = (0.00000000, 0.00000000)
 (0.00000000, 0.00000000)
 (2.69711127, 0.00000000)
 (0.00000000, -37076705)

EIGENVALUE = (68819753, -.72552337), EIGENVECTOR = (0.00000000, 0.00000000)
 (0.00000000, 0.00000000)
 (2.69711127, 0.00000000)
 (0.00000000, 37076705)

	X	DX	Y	DY	DS	DP/P
EQ ORBIT	-0.00002178	0.00000000	0.00000000	0.00000000	0.00000000	00165000 1.00000000
ETA ORBIT	-0.02853455	0.00000000	0.00000000	0.00000000	0.00000000	1.00000000 0.00000000

EIGENVECTORS 1 AND 3 IN POLAR COORDINATES

MUR	X1		X3		DX1		DY1		DY3	
	0	1	0	1	0	1	0	1	0	1
0	2.791924	-0.000000	0.358176	0.000000	1.570796	0.000000	0.000000	0.000000	0.000000	0.000000
	0.000000	0.000000	0.000000	0.000000	0.000000	2.697111	0.000000	0.000000	370767	-1.570796

PUC	S (M)	GX	GY	BY (M)	BY (M)	AX	AY	LY (M)	EXP	EY (M)	EYF	XCU (MM)	YCU (MM)	YCU (MM)	LY (MM)
50 Q11	67 23	932	1 277	27.5850	15 8805	7 2030	5 1517	8 2127	-1 6030	0 0000	0 0000	13 5878	-2 6443	0 0000	0 0000
51 Q11	67 75	936	1 282	20.5996	21 7196	6 2041	-6 0553	7 3779	-1 6030	0 0000	0 0000	12 2099	-2 6443	0 0000	0 0000
52 Q12	68 13	939	1 285	16.8993	25 5422	3 5240	-3 6960	6 9219	-7 6880	0 0000	0 0000	11 4585	1 2628	0 0000	0 0000
53 Q12	68 52	943	1 287	14.9917	27 2569	1 4912	-6 778	6 7798	0296	0 0000	0 0000	11 2274	0614	0 0000	0 0000
54 Q12	68 74	945	1 288	14.3523	27 3547	1 4444	-6 895	6 7862	0296	0 0000	0 0000	11 2408	0614	0 0000	0 0000
55 S12	69 04	949	1 290	13.5001	27 9631	1 3521	-6 503	6 7973	0430	0 0000	0 0000	11 2612	0725	0 0000	0 0000
56 OS12	69 26	951	1 291	12.9211	28 2488	1 3064	-6 614	6 8066	0430	0 0000	0 0000	11 2770	0725	0 0000	0 0000
57 Q13	69 65	954	1 293	12.3067	27 4928	-2171	2 5899	6 9777	8463	0 0000	0 0000	11 5613	1 4056	0 0000	0 0000
58 Q13	70 03	961	1 296	13.2664	24 3686	-1 7805	5 3795	7 4651	1 6880	0 0000	0 0000	12 3706	2 8025	0 0000	0 0000
59 Q13	70 53	966	1 299	15 1147	19 3228	-1 9368	4 7686	8 3043	1 6880	0 0000	0 0000	13 7641	2 8025	0 0000	0 0000
60 Q14	70 85	970	1 302	15.8970	16 9338	-4722	2 7438	8 7144	8574	0 0000	0 0000	14 4448	1 4235	0 0000	0 0000
61 Q14	71 17	973	1 305	15 7091	15 7221	1 0509	1 0663	8 8525	-0000	0 0000	0 0000	14 6741	0000	0 0000	0 0000
62 LS*	79 02	1 102	1 435	7 4647	7 3569	0000	-0000	8 8525	-0000	0 0000	0 0000	14 6741	0000	0 0000	0 0000
63 A20	79 02	1 102	1 435	7 4647	7 3569	0000	-0000	8 8525	-0000	0 0000	0 0000	14 6741	0000	0 0000	0 0000
64 REFL	158 03	2 204	2 871	7 7948	7 2744	0000	-0000	-0285	-0000	0 0000	0 0000	-0218	0 0000	0 0000	0 0000

CIRCUMFERENCE = 474.0968 M THETA = 6.28318533 RAD NUJ = 6.61170 DNUJ/(DP/P) = 1.13607
 RADIUS = 75.4549 M THETA(63) = 0.00000000 RAD NUJ = 8.61240 DNUJ/(DP/P) = 31979
 (DS/S)/(DP/P) = 0.340780 TGAM = (5.41705, 0.00000)

MAXIMA --- BETX(48) = 33.75723 BETY(23) = 30.91887 ETAX(61) = 8.85247 ETAY(64) = 0.00000
 MINIMA --- BETX(17) = 2.87575 BETY(19) = 1.98486 ETAX(28) = -0.05199 ETAY(64) = 0.00000

*** PAGE //

5.000 7 006718 GEV KINETIC

// - 00690
//
// V R/6
//

=
PVEC
FAPT

DP
V
CORE

DP

CALCULATION OF THE EQUILIBRIUM ORBIT AND BETATRON FUNCTIONS OF CORE
 INITIAL REFERENCE RAY DEFINED BY

X = 0.0000000 DX = 0.0000000 Y = 0.0000000 DY = 0.0000000 DS = 0.0000000 DP/P = -0.0690000 1.0000000

7X7 MATRIX FOR CORE

28548057	6.43517268	0.00000000	0.00000000	0.00000000	0.66779535	0.0019826
-14273134	28548057	0.00000000	0.00000000	0.00000000	0.1334294	0.0003960
0.00000000	0.00000000	69555851	-5.15560016	0.00000000	0.00000000	0.00000000
0.00000000	0.00000000	10012382	69555851	0.00000000	0.00000000	0.00000000
-0.1334294	-0.66779535	0.00000000	0.00000000	1.00000000	-5.22016486	0.3847210
0.00000000	0.00000000	0.00000000	0.00000000	0.00000000	1.00000000	0.00000000
0.00000000	0.00000000	0.00000000	0.00000000	0.00000000	0.00000000	1.00000000

EIGENVALUES OF THE 4X4 SUBMATRIX

X LMD1 = (28548057 95838450), C(1) = 1.00000000, MU(1) = 1.28128850 RAD, Q(1) = 61177020
 1/LMD1 = (28548057 -95838450), C(2) = 1.00000000, MU(2) = -1.28128850 RAD, Q(2) = 38822980
 Y LMD3 = (69555851 71846946), C(3) = 1.00000000, MU(3) = 80159936 RAD, Q(3) = 38273550
 1/LMD3 = (69555851 -71846946), C(4) = 1.00000000, MU(4) = -80159936 RAD, Q(4) = 61726450

EIGENVALUE = (28548057, 95838450), EIGENVECTOR = (2.59125536, 0.00000000)
 (-0.00000000, 38591334)
 (0.00000000, 0.00000000)
 (0.00000000, 0.00000000)

EIGENVALUE = (28548057, -95838450), EIGENVECTOR = (2.59125536, 0.00000000)
 (-0.00000000, -38591334)
 (0.00000000, 0.00000000)
 (0.00000000, 0.00000000)

EIGENVALUE = (69555851, 71846946), EIGENVECTOR = (0.00000000, 0.00000000)
 (0.00000000, 0.00000000)
 (2.67877020, 0.00000000)
 (-0.00000000, -37330563)

EIGENVALUE = (69555851, -71846946), EIGENVECTOR = (0.00000000, 0.00000000)
 (0.00000000, 0.00000000)
 (2.67877020, 0.00000000)
 (-0.00000000, 37330563)

	X	DX	Y	DY	DS	DP/P
EQ ORBIT	-0.00036225	0.00000000	0.00000000	0.00000000	0.00000000	-0.0690000 1.0000000
ETA ORBIT	0.9348290	0.00000000	0.00000000	0.00000000	0.00000000	1.00000000 0.00000000

DEFLECTION FUNCTIONS OF CORN

POS	S (M)	QY	QY	BX (M)	BY (M)	AX	AY	EX (M)	EXP	EY (M)	EYP	XCU (MM)	DXCU (MM)	YCU (MM)	DYCU (MM)
0	0.00	0.000	0.000	6.7146	7.1758	0.0000	0.0000	0.935	0.000	0.0000	0.0000	-3.622	0.0000	0.0000	0.0000
1 A10	0.00	0.006	0.000	6.7146	7.1758	0.0000	0.0000	0.935	0.000	0.0000	0.0000	-3.622	0.0000	0.0000	0.0000
2 LS	7.95	130	133	16.1190	15.9758	-1.1835	-1.1074	0.935	0.000	0.0000	0.0000	-3.622	0.0000	0.0000	0.0000
3 Q1	8.27	141	136	16.2936	17.3051	-1.6447	-3.0965	0.918	-0.106	0.0000	0.0000	-3.557	0.410	0.0000	0.0000
4 Q1	8.59	145	139	15.3136	20.0367	2.3800	-5.5421	0.867	-0.208	0.0000	0.0000	-3.362	0.804	0.0000	0.0000
5 Q1	9.10	150	143	12.9888	26.1320	2.1570	-6.3532	0.761	-0.208	0.0000	0.0000	-2.930	0.804	0.0000	0.0000
6 Q2	9.75	159	146	12.1482	30.4926	-1.8106	0.466	0.680	-0.042	0.0000	0.0000	-2.637	0.161	0.0000	0.0000
7 Q2	10.41	167	150	15.3387	26.0219	-4.2998	6.4193	0.704	0.118	0.0000	0.0000	-2.733	-0.457	0.0000	0.0000
8 Q2	11.37	175	157	24.7717	15.1840	-5.5202	4.8612	0.817	0.118	0.0000	0.0000	-3.171	-0.457	0.0000	0.0000
9 Q3	11.72	177	161	27.6176	12.5531	-2.4802	2.7591	0.841	0.014	0.0000	0.0000	-3.261	-0.055	0.0000	0.0000
10 Q3	12.07	179	166	28.1488	11.2038	9.868	1.1461	0.827	-0.091	0.0000	0.0000	-3.209	0.350	0.0000	0.0000
11 Q3	12.98	184	180	26.4215	9.3000	9.234	9.594	0.745	-0.091	0.0000	0.0000	-2.893	0.350	0.0000	0.0000
12 B3	14.50	194	211	23.7719	6.7953	8.167	6.780	1.274	0.788	0.0000	0.0000	-4.977	-5.717	0.0000	0.0000
13 OB3	20.92	247	403	16.1731	6.9484	3.662	-7.019	6.341	0.788	0.0000	0.0000	-4.3702	-5.717	0.0000	0.0000
14 Q4	21.15	249	408	15.7332	7.4052	1.3471	-1.3076	6.465	0.300	0.0000	0.0000	-4.4628	-2.372	0.0000	0.0000
15 Q4	21.38	252	413	14.7747	8.1580	2.6215	-2.0043	6.477	-0.193	0.0000	0.0000	-4.4783	1.015	0.0000	0.0000
16 Q4	24.64	328	448	3.3433	27.7703	3.2646	-1.0099	5.846	-0.193	0.0000	0.0000	-4.1474	1.015	0.0000	0.0000
17 Q5	25.06	350	450	2.8710	29.5112	2.784	-1.146	5.935	0.622	0.0000	0.0000	-4.2241	-4.738	0.0000	0.0000
18 Q5	25.47	373	452	2.8645	27.9529	-2.2623	3.8065	6.366	1.473	0.0000	0.0000	-4.5435	-1.0763	0.0000	0.0000
19 Q5	32.82	531	703	26.8640	1.9315	-3.0039	-2.651	1.7191	1.473	0.0000	0.0000	-12.4522	-1.0763	0.0000	0.0000
20 Q6	33.17	533	730	27.8812	2.2710	1.1417	-7.166	1.7353	-0.551	0.0000	0.0000	-12.5747	3.799	0.0000	0.0000
21 Q6	33.52	535	751	26.6706	2.9636	3.2646	-1.2862	1.6807	-2.554	0.0000	0.0000	-12.1877	1.8208	0.0000	0.0000
22 Q6	37.71	585	825	6.9951	29.4367	1.4344	-5.0363	6.115	-2.554	0.0000	0.0000	-4.5638	1.8208	0.0000	0.0000
23 Q6	38.06	593	827	6.3068	31.7902	-5.558	-1.5861	6.341	-1.881	0.0000	0.0000	-4.0150	1.3210	0.0000	0.0000
24 Q7	38.41	602	829	6.1943	31.6002	-2.305	2.1205	4.787	-1.287	0.0000	0.0000	-3.6314	8.755	0.0000	0.0000
25 Q7	41.25	665	847	8.8855	20.9340	-7.146	1.6252	1.122	-1.287	0.0000	0.0000	-1.1382	8.755	0.0000	0.0000
26 Q7	41.56	670	849	9.3370	19.9592	-7.668	1.3729	0.730	-1.287	0.0000	0.0000	-8.714	8.755	0.0000	0.0000
27 Q67	42.86	690	860	11.6042	16.1825	-9.867	1.3479	-0.934	-1.287	0.0000	0.0000	2.607	8.755	0.0000	0.0000
28 Q7	45.90	723	901	19.1536	9.2116	-1.3024	9.033	-2.165	0.475	0.0000	0.0000	1.0722	-3.403	0.0000	0.0000
29 Q7	46.41	727	910	20.7239	8.3448	-1.5888	8.031	-1.924	0.475	0.0000	0.0000	8.994	-3.403	0.0000	0.0000
30 Q8	46.64	728	914	21.0945	8.1289	-0.230	1.470	-1.799	0.617	0.0000	0.0000	8.140	-4.052	0.0000	0.0000
31 Q8	46.87	730	919	20.7447	8.2089	1.3443	-4.990	-1.642	0.748	0.0000	0.0000	7.147	-4.631	0.0000	0.0000
32 Q8	48.09	740	941	17.2216	9.6517	1.3454	-6.845	-0.731	0.748	0.0000	0.0000	1.501	-4.631	0.0000	0.0000
33 Q8	52.66	802	997	8.3864	18.2172	-6.078	-1.1215	8.638	3.400	0.0000	0.0000	-6.0764	-2.2929	0.0000	0.0000
34 Q8B	53.16	812	1.001	7.8111	19.3885	5.249	-1.1844	1.0365	3.400	0.0000	0.0000	-7.2412	-2.2929	0.0000	0.0000
35 Q9	53.39	817	1.003	7.7138	19.5943	-0.970	2.899	1.1236	4.228	0.0000	0.0000	-7.8300	-2.8666	0.0000	0.0000
36 Q9	53.62	821	1.005	7.9008	19.1266	-1.7257	1.7442	1.2304	5.131	0.0000	0.0000	-8.5536	-3.4904	0.0000	0.0000
37 Q9	53.93	827	1.007	8.3611	18.0830	-1.7846	1.6798	1.3868	5.131	0.0000	0.0000	-9.6195	-3.4904	0.0000	0.0000
38 Q9	54.23	833	1.010	8.8512	17.0910	-1.8230	1.5754	1.5426	5.096	0.0000	0.0000	-10.6815	-3.4786	0.0000	0.0000
39 Q9	54.84	843	1.016	9.9250	15.2457	-1.9385	1.4514	1.8533	5.096	0.0000	0.0000	-12.8021	-3.4786	0.0000	0.0000
40 Q9	59.41	892	1.098	22.2238	5.6755	-1.7947	5.767	4.7495	7.756	0.0000	0.0000	-32.6371	-5.3107	0.0000	0.0000
41 Q9	59.92	896	1.113	24.0962	5.1502	-1.8912	4.574	5.1434	7.756	0.0000	0.0000	-35.3349	-5.3107	0.0000	0.0000
42 Q10	60.14	897	1.120	24.7911	4.9901	-1.1396	2.446	5.3016	6.072	0.0000	0.0000	-36.4183	-4.1621	0.0000	0.0000
43 Q10	60.37	899	1.127	25.1337	4.9253	-3.547	0.390	5.4208	4.344	0.0000	0.0000	-37.2355	-2.9830	0.0000	0.0000
44 Q10	60.88	902	1.144	25.5056	4.9382	-3.775	-0.643	5.6414	4.344	0.0000	0.0000	-38.7509	-2.9830	0.0000	0.0000
45 B10	65.44	928	1.260	29.7616	9.4050	-5.795	-8.778	8.1905	7.001	0.0000	0.0000	-56.3225	-4.8146	0.0000	0.0000
46 Q10	65.73	930	1.265	30.1038	9.9335	-5.926	-9.327	8.3949	7.001	0.0000	0.0000	-57.7279	-4.8146	0.0000	0.0000
47 S10	66.04	931	1.270	30.5455	10.4936	-8.572	-9.037	8.6190	7.703	0.0000	0.0000	-59.2321	-5.0550	0.0000	0.0000
48 Q10	66.33	933	1.274	31.0507	11.0359	-8.738	-9.542	8.8438	7.703	0.0000	0.0000	-60.7076	-5.0550	0.0000	0.0000
49 Q11	66.77	935	1.280	30.0168	12.5927	3.1952	-2.6786	8.9183	-4.315	0.0000	0.0000	-61.1298	3.1318	0.0000	0.0000

POS	S	GX	GY	BX	BY	AX	AY	IX	IY	EY	EYP	ZC0	DZC0	YCO	SYC0
	(M)			(M)	(M)			(M)	(M)	(M)	(M)	(MM)	(MM)	(MM)	(MM)
30 Q11	67.20	937	1.285	25.6794	15.9026	6.5318	-5.0407	8.4701	-1.6880	0.0000	0.0000	-57.9977	11.1365	0.0000	0.0000
31 Q11	67.72	941	1.290	19.3346	21.6060	5.6458	-5.9059	7.6323	-1.6880	0.0000	0.0000	-52.1954	11.1365	0.0000	0.0000
32 Q12	68.11	945	1.292	15.9959	25.2987	3.1369	-3.5181	7.1831	-1.7298	0.0000	0.0000	-49.0582	5.1750	0.0000	0.0000
33 Q12	68.50	949	1.294	14.3433	26.8726	1.2093	-4.978	7.0649	1.147	0.0000	0.0000	-48.1683	-5.482	0.0000	0.0000
34 Q12	68.71	951	1.296	13.8247	27.0917	1.1719	-5.079	7.0899	1.147	0.0000	0.0000	-48.2877	-5.482	0.0000	0.0000
35 S12	69.02	955	1.298	13.0914	27.4774	1.2324	-7.7583	7.1155	0.533	0.0000	0.0000	-48.4231	-3.401	0.0000	0.0000
36 OS12	69.24	958	1.299	12.5637	27.8104	1.1905	-7.707	7.1271	0.533	0.0000	0.0000	-48.4972	-3.401	0.0000	0.0000
37 Q13	69.62	963	1.301	12.2270	27.1462	-3.3063	2.4672	7.3121	9.092	0.0000	0.0000	-49.7402	-6.1234	0.0000	0.0000
38 Q13	70.01	967	1.303	13.0493	24.1187	-1.8596	5.2618	7.8340	1.8070	0.0000	0.0000	-53.2617	-12.1873	0.0000	0.0000
39 Q13	70.51	973	1.307	14.9831	19.1801	-2.0295	4.6704	8.7325	1.8070	0.0000	0.0000	-59.3214	-12.1873	0.0000	0.0000
40 Q14	70.83	976	1.310	15.8280	16.8492	-3.5671	2.6540	9.1719	9.180	0.0000	0.0000	-62.2818	-6.1912	0.0000	0.0000
41 Q14	71.15	980	1.313	15.6990	15.6942	9.6643	9.764	9.3199	-0.0000	0.0000	0.0000	-63.2791	0.0000	0.0000	0.0000
42 LS*	78.99	1.102	1.436	8.1182	8.0343	0.0000	-0.0000	9.3199	-0.0000	0.0000	0.0000	-63.2791	0.0000	0.0000	0.0000
43 A20	78.99	1.102	1.436	8.1182	8.0343	0.0000	-0.0000	9.3199	-0.0000	0.0000	0.0000	-63.2791	0.0000	0.0000	0.0000
44 REFL	157.99	2.204	2.872	6.7146	7.1758	0.0000	-0.0000	0.935	-0.0000	0.0000	0.0000	-3.622	0.0000	0.0000	0.0000

CIRCUMFERENCE = 473.9592 M THETA = 6.28318533 RAD NUX = 6.61177 DNUX/(DP/P) = -22134
 RADIUS = 75.4330 M THETA(63) = 0.00000000 RAD NUZ = 8.61726 DNUZ/(DP/P) = 32513
 (DS/S)/(DP/P) = 0.330498 TGAM = (5.50067, 0.00000)

MAXIMA --- BETX(48) = 31.05075 BETY(23) = 31.79018 ETAX(61) = 9.31994 ETAY(64) = 0.00000
 MINIMA --- BETX(18) = 2.86447 BETY(19) = 1.93146 ETAX(28) = -2.1650 ETAY(64) = 0.00000

EXTRACTION ORBIT
8 0 GEV KINETIC

*** U' 00825
*** V // //
*** EXT 2 -3 // //
*** PVEC
*** FXPT 2 -3 // //
*** R/6

DP

CALCULATION OF THE EQUILIBRIUM ORBIT AND BETATRON FUNCTIONS OF EXT

INITIAL REFERENCE RAY DEFINED BY V

X = 0.00000000 DX = 0.00000000 Y = 0.00000000 DY = 0.00000000 DS = 0.00000000 DP/P = 00825000 1.00000000

7X7 MATRIX FOR EXT

27141873	8.50707256	0.00000000	0.00000000	0.00000000	-13191220	00060208
-10888962	27141873	0.00000000	0.00000000	0.00000000	-01971485	00008998
0.00000000	0.00000000	70581336	-5.11973196	0.00000000	0.00000000	0.00000000
0.00000000	0.00000000	09801832	70581336	0.00000000	0.00000000	0.00000000
01971485	13191220	0.00000000	0.00000000	1.00000000	-5.46449632	-04241407
0.00000000	0.00000000	0.00000000	0.00000000	0.00000000	1.00000000	0.00000000
0.00000000	0.00000000	0.00000000	0.00000000	0.00000000	0.00000000	1.00000000

EIGENVALUES OF THE 4X4 SUBMATRIX

X LMD1 = (27141873 .96246136), C(1) = 1.00000000, MU(1) = 1.29592953 RAD, G(1) = 61876077
 1/LMD1 = (27141873 -.96246136), C(2) = 1.00000000, MU(2) = -1.29592953 RAD, G(2) = 38123923
 Y LMD3 = (70581336 .70839784), C(3) = 1.00000000, MU(3) = 78722567 RAD, G(3) = 37587257
 1/LMD3 = (70581336 -.70839784), C(4) = 1.00000000, MU(4) = -78722567 RAD, G(4) = 62412743

EIGENVALUE = (27141873, .96246136), EIGENVECTOR = (2.97302401, -.00000000)
 (.00000000, -.33635786)
 (0.00000000, 0.00000000)
 (0.00000000, 0.00000000)
 EIGENVALUE = (27141873, -.96246136), EIGENVECTOR = (2.97302401, .00000000)
 (.00000000, -.33635786)
 (0.00000000, 0.00000000)
 (0.00000000, 0.00000000)
 EIGENVALUE = (70581336, .70839784), EIGENVECTOR = (0.00000000, 0.00000000)
 (0.00000000, 0.00000000)
 (2.68834497, .00000000)
 (.00000000, -.37197607)
 EIGENVALUE = (70581336, -.70839784), EIGENVECTOR = (0.00000000, 0.00000000)
 (0.00000000, 0.00000000)
 (2.68834497, -.00000000)
 (.00000000, .37197607)

	X	DX	Y	DY	DS	DP/P
EQ ORBIT	-00067869	0.00000000	0.00000000	0.00000000	0.00000000	00825000 1.00000000
ETA ORBIT	-18105351	-00000000	0.00000000	0.00000000	0.00000000	1.00000000 0.00000000

EIGENVECTORS 1 AND 3 IN POLAR COORDINATES

	X1 X2 X3	X1 X2 X3	X1 X2 X3	X1 X2 X3	X1 X2 X3	X1 X2 X3
0	2.873024 0.000000	0.000000 0.000000	336358 0.000000	1.570786 0.000000	0.000000 2.88545	0.000000 371976
						0.000000 1.570786

POS	S	GX	GY	BX	BY	AX	AY	EX	EXF	EY	EYF	XCU	DYCU	YCU	DYCU	
	(M)			(M)	(M)			(M)		(M)		(MM)	(MM)	(MM)	(MM)	
50	011	67.24	930	1.272	29.0478	16.1645	7.7143	-5.3205	7.9519	-1.5793	0.0000	0.0000	66.7010	-13.1008	0.0000	0.0000
51	011	67.76	933	1.276	21.5747	22.2008	6.6290	-6.2631	7.1290	1.5793	0.0000	0.0000	59.8752	13.1008	0.0000	0.0000
52	012	68.15	936	1.279	17.6032	26.1741	3.8176	-3.8790	6.6746	-1.7855	0.0000	0.0000	56.1297	-6.3736	0.0000	0.0000
53	012	68.54	940	1.281	15.5038	28.0094	1.7027	-1.8058	6.5185	-0.2668	0.0000	0.0000	54.9166	0.6559	0.0000	0.0000
54	012	68.75	942	1.282	14.7740	28.3632	1.6480	-1.8186	6.5127	-0.2668	0.0000	0.0000	54.9309	0.6559	0.0000	0.0000
55	012	69.06	946	1.284	13.8340	28.7834	1.4383	-1.5590	6.5140	0.0356	0.0000	0.0000	54.9913	3.304	0.0000	0.0000
56	0512	69.28	948	1.285	13.2180	29.0290	1.3900	-1.5689	6.5218	0.0356	0.0000	0.0000	55.0633	3.304	0.0000	0.0000
57	013	69.66	953	1.287	12.7482	28.1768	-1.1566	2.7465	6.6813	0.7948	0.0000	0.0000	56.4340	6.7962	0.0000	0.0000
58	013	70.05	958	1.290	13.4648	24.9183	-1.7317	5.5755	7.1395	1.5896	0.0000	0.0000	60.3507	13.5685	0.0000	0.0000
59	013	70.55	963	1.293	15.2603	19.6921	-1.8794	4.9353	7.9298	1.5896	0.0000	0.0000	67.0972	13.5685	0.0000	0.0000
60	014	70.87	967	1.296	16.0055	17.2047	-2.4090	2.8783	8.3165	0.072	0.0000	0.0000	70.3927	6.8912	0.0000	0.0000
61	014	71.19	970	1.299	15.7781	15.9122	1.1119	1.1832	8.4467	-0.0000	0.0000	0.0000	71.5027	0.0000	0.0000	0.0000
62	LS*	79.03	1.103	1.437	7.0555	6.6303	0.0000	-0.0000	8.4467	-0.0000	0.0000	0.0000	71.5027	0.0000	0.0000	0.0000
63	A20	79.03	1.103	1.437	7.0555	6.6303	0.0000	-0.0000	8.4467	-0.0000	0.0000	0.0000	71.5027	0.0000	0.0000	0.0000
64	REFL	158.07	2.206	2.875	8.8389	7.2272	0.0000	-0.0000	-1811	0.0000	0.0000	0.0000	-6787	0.0000	0.0000	0.0000

CIRCUMFERENCE = 474.2024 M THETA = 6.28318533 RAD NUX = 6.61876 DNUX/(DP/P) = 1.94317
 RADIUS = 75.4717 M THETA(63) = 0.00000000 RAD NUZ = 8.62413 DNUZ/(DP/P) = 2.3079
 (DS/S)/(DP/P) = .0345932 TGAM = (5.37656, 0.00000)

MAXIMA --- BETX(48) = 35.83982 BETY(23) = 30.73231 ETAX(61) = 8.44668 ETAY(64) = 0.00000
 MINIMA --- BETX(17) = 2.87511 BETY(19) = 2.04719 ETAX(2) = -18105 ETAY(64) = 0.00000

*** PAGE //